Bioanalytical Reviews

Frank-Michael Matysik *Editor*

Trends in Bioelectroanalysis

6
Bioanalytical Reviews

Aims and Scope

Bioanalytical Reviews is the successor of the former review journal with the same name, and it will complement Springer's successful and reputed review book series program in the flourishing and exciting area of the Bioanalytical Sciences.

Bioanalytical Reviews (BAR) publishes reviews covering all aspects of bioanalytical sciences. It therefore is a unique source of quick and authoritative information for anybody using bioanalytical methods in areas such as medicine, biology, biochemistry, genetics, pharmacology, biotechnology, and the like.

Reviews of methods include all modern tools applied, including mass spectrometry, HPLC (in its various forms), capillary electrophoresis, biosensors, bioelectroanalysis, fluorescence, IR/Raman, and other optical spectroscopies, NMR radiometry, and methods related to bioimaging. In particular the series volumes provide reviews on perspective new instrumental approaches as they apply to bioanalysis, and on the use of micro-/nano-materials such as micro- and nanoparticles. Articles on μ-total analytical systems (μ-TAS) and on labs-on-a-chip also fall into this category.

In terms of applications, reviews on novel bioanalytical methods based on the use of enzymes, DNAzymes, antibodies, cell slices, to mention the more typical ones, are highly welcome. Articles on subjects related to the areas including genomics, proteomics, metabolomics, high-throughput screening, but also bioinformatics and statistics as they relate to bioanalytical methods are of course also welcome. Reviews cover both fundamental aspects and practical applications.

Reviews published in BAR are (a) of wider scope and authoratively written (rather than a record of the research of single authors), (b) critical, but balanced and unbiased; (c) timely, with the latest references. BAR does not publish (a) reviews describing established methods of bioanalysis; (b) reviews that lack wider scope, (c) reviews of mainly theoretical nature.

More information about this series at http://www.springer.com/series/11663

Frank-Michael Matysik
Editor

Trends in Bioelectroanalysis

With contributions by

R. Bierl · H. Buck · E. Cortón · M. del Valle · S.H. DuVall · A. Hájková · F.-M. Matysik · S.R. Mikkelsen · G. Nagy · L. Nagy · G. Ocvirk · B. van der Weerd · P. Vatsyayan · V. Vyskočil

Springer

Editor
Frank-Michael Matysik
Institute of Analytical Chemistry
University of Regensburg
Regensburg, Germany

ISSN 1867-2086 ISSN 1867-2094 (electronic)
Bioanalytical Reviews
ISBN 978-3-319-48483-9 ISBN 978-3-319-48485-3 (eBook)
DOI 10.1007/978-3-319-48485-3

Library of Congress Control Number: 2016958447

Printed on acid-free paper

This Springer imprint is published by Springer Nature
The registered company is Springer International Publishing AG
The registered company address is: Gewerbestrasse 11, 6330 Cham, Switzerland

Preface

Since the fundamental studies by Galvani and Ritter in the late eighteenth century, it has been understood that there is a close relationship between electrical and biological phenomena. Currently, bioelectrochemistry is a very active field, with extensive research devoted to studies of biopolymers (DNA, proteins), bioenergetics, biomembranes, and electrochemical applications in medicine or biotechnology. Bioelectroanalysis represents a vital branch of bioanalytical chemistry. According to its interdisciplinary character, electroanalysis integrates aspects of bioelectrochemistry and analytical chemistry. Bioelectroanalytical studies comprise either the incorporation of biological systems and principles into an electrochemical concept or the use of electrochemical methods to generate analytical information regarding biomolecules/biological compartments.

In this third volume of the series *Bioanalytical Reviews*, a selection of trendsetting topics in the field of bioelectroanalysis is presented. Ocvirk and colleagues contribute a comprehensive overview concerning the electrochemical biosensing of glucose for diabetes care. Due to enormous practical importance, this research area has attracted continuous interest for decades. The authors provide a detailed review from an industrial research and development perspective. Cortón and Mikkelsen present a survey of bioassay applications for individually addressable electrochemical arrays, illustrating the significant progress in this field. The focus is on liquid-phase bioanalytical assays. The context of implementation of electrochemical arrays is continued by del Valle who discusses recent advances in the development of electronic tongues based on the use of biosensor arrays coupled with advanced chemometric data analysis. Vyskocil and Hájková summarize novel strategies of DNA biosensor development and corresponding applications for studies of DNA damage. The contribution by Vatsyayan represents the important research area of electrochemistry of redox proteins. Recent trends, including increasing diversity of redox proteins used in electrochemical studies, novel immobilization strategies, and biosensor/biofuel cell applications, are surveyed. The review by van der Weerd et al. provides an overview concerning ongoing developments in the field of

electrochemical sensing of blood gases with advanced sensor concepts. Last, but not least, L. Nagy and G. Nagy address the important aspects of bioelectroanalytical studies with high spatial resolution. Their contribution summarizes recent achievements in bioanalytical applications of scanning electrochemical microscopy. A wide range of applications covering imaging of living cells, studies of metabolic activity, imaging of local enzyme activity, and studies of transport through biolayers are surveyed.

I wish to express my appreciation to all of the authors who contributed to this book project with in-depth review articles illustrating current trends in the research area of bioelectroanalysis. This timely collection of important activities in bioelectroanalytical research directions will be of interest not only for experts in the field but also to students and their teachers in disciplines that include analytical chemistry, biology, electrochemistry, and various interdisciplinary research areas.

Regensburg, Germany
Summer 2016

Frank-Michael Matysik

Contents

BIOREV (2017) 6: 1–102
DOI: 10.1007/11663_2016_3

Published online: 28 June 2016

Electrochemical Glucose Biosensors for Diabetes Care

Gregor Ocvirk, Harvey Buck, and Stacy Hunt DuVall

Abstract Blood glucose monitoring (BGM) is the most successful application of electrochemical biosensor technology and has motivated tremendous improvements in biology, chemistry, measurement, and fabrication methods of biosensors. The performance of electrochemical biosensors used for BGM has improved greatly over the last four decades. Technological advance has allowed to measure blood glucose (BG) over a wide range of glucose concentration, a wide temperature and hematocrit range in the presence of an abundance of interfering substances with ever-increasing accuracy, and precision in minute sample volumes. The use of optimized enzymes, mediators, and electrochemical measurement methods enables this tremendous progress in performance. Continuous glucose monitoring (CGM) systems based on minimally invasive amperometric sensors, inserted into the subcutaneous tissue, have significantly improved over initial offerings over the last 15 years with regard to time of use, accuracy, reliability, and convenience due to a multitude of parallel advances: materials needed for enzyme immobilization, polymeric cover membranes, and biocompatible coatings needed to tackle the response by the complex body interface have been developed; wireless transfer and processing of unprecedented data volume have been established; effortless and painless insertion schemes of ever smaller sensors have been realized in order to overcome the concerns of persons with diabetes (PwDs) to use a minimally invasive sensor; and scalable manufacturing technologies of miniaturized minimally invasive sensors have allowed for ever improved reproducibility and increased production volume. Looking ahead, the demands on blood glucose system performance

G. Ocvirk (✉)
Roche Diabetes Care GmbH, Mannheim, Germany
e-mail: gregor.ocvirk@roche.com

H. Buck and S.H. DuVall
Roche Diabetes Care, Inc., Indianapolis, IN, USA
e-mail: harvey.buck@roche.com; stacy.duvall@roche.com

are expected to grow even as the pressures to lower the cost of systems increase. The drive for the future is to continue to push the limits on system performance under real-life conditions while lowering cost, all while finding ways to provide the best medical value to PwDs and healthcare providers. Technical issues of commercially available CGM sensors remain to be solved which currently impede reliable hypo- and hyperglycemic alarms, safe insulin dosing recommendations, or insulin pump control at any time of use. It is realistic to assume that continuous glucose monitoring (CGM) systems will be adopted in the future by a larger population of PwDs. Yet it is also clear that BGM systems will remain a major choice of the great majority of PwDs on a global scale. This review offers a technical overview about user, system, and major regulatory requirements and available suitable sensor technology and demonstrated performance of electrochemical BGM and CGM systems from an industrial R&D perspective.

Keywords Continuous glucose monitoring • Diabetes care • Electrochemical biosensor • Enzyme electrode • Medical device • Patient with diabetes • Self-monitoring of blood glucose • Sensor coating • System performance • System requirements

Contents

Abbreviations

BGM	Blood glucose monitoring
CGM	Continuous glucose monitoring
FAD-GDH	FAD-dependent glucose dehydrogenase
FBGC	Foreign body giant cell
GOx	Glucose oxidase

HCP	Health care provider
ISF	Interstitial fluid
MARD	Mean absolute relative difference
PARD	Precision absolute relative deviation difference
POC	Point-of-care
PQQ-GDH	Pyrroloquinoline quinone-dependent glucose dehydrogenase
PwD	Person with diabetes
SMBG	Self-monitoring of blood glucose
T1	Type 1 diabetes
T2	Type 2 diabetes
VEGF	Vascular endothelial growth factor

1 Introduction

Glucose measurement has become an essential part of medical diagnostics, particularly for persons with diabetes (PwDs) [1–3]. It is a broad topic, encompassing glucose measurement in different sample matrices, such as blood, plasma, serum, and urine, as well as different settings, for instance, so-called home use (self-monitoring of blood glucose, SMBG), continuous glucose monitoring (CGM), point-of-care blood glucose monitoring (POC), and clinical glucose analyzers.

Over the last 50 years, tremendous advances have been made in glucose biosensing from the first proposal of a glucose measuring device based on glucose oxidase (GOx) and an oxygen-sensing electrode in 1962 [4]. Glucose biosensors encompass the major portion of the biosensor market at approximately 85% of the global market [5]. The success of glucose monitoring, particularly SMBG, is remarkable for both the impact on PwD health and commercialization of the technology. There are several other markers that are useful for diabetes management, for example, HbA_{1c}, ketone bodies, fructosamine, and glycated albumin. While some of these markers are critical for long-term management of diabetes (HbA_{1c}) or immediate medical crisis (ketone bodies), none have had the most wide-reaching utility and benefit for PwDs as reliable glucose measurement [2, 6–11]. Reduction in HbA_{1c} has been shown to be closely tied to effective glycemic control in which glucose monitoring plays an integral role.

For a PwD, the following glucose measurement methodologies may be used; clinical analyzer measurements of plasma or serum levels of blood glucose are used for the diagnosis and treatment of diabetes [2, 12, 13]; POC blood glucose monitors are used for monitoring blood glucose in a hospital or clinic scenario [14, 15]; SMBG is used for monitoring of blood glucose outside of a healthcare setting [16, 17]; and CGM is used to monitor a PwD's glucose profile with high time resolution as an adjunct to SMBG. SMBG and CGM are the focus of this work.

2 General Aspects of Glucose Measurement

2.1 Requirements for Development, Manufacture, and Sale of Glucose Sensors for Diabetes Management

Glucose sensors for diabetes management are either in vitro diagnostic devices (BG) or medical devices (CGM), and as such the development, manufacture, sales, and distribution are strictly regulated by government agencies in all significant markets. In the United States, the Food and Drug Administration (FDA) regulates all aspects of the process and approves devices for sale in the United States. In the European Union (EU), CGM systems need to comply with respective medical device directives (90/385 or 93/42 EC), and the conformity assessment requires the involvement of a notified body. Devices which receive the Conformité Européenne (CE) mark may be sold in all EU countries. Several recent publications provide useful overviews of the requirement of the FDA and in the EU [18–21] and on efforts to standardize and harmonize requirements [22].

In the USA, blood glucose sensors for diabetes management are classified as class II devices, meaning they present a moderate risk of harm to the user in case of device failure. In the USA, sensors used in laboratory settings and sensors for BGM are approved through the process of a 510(k) or premarket notification. In this process, the manufacturer must provide evidence to the FDA that the product is substantially equivalent to a product already marketed, referred to as the predicate device. This initially referred to products marketed at the time of the establishment of the FDA authority over medical devices (1976). In contrast, sensors for CGM are classified as class III devices and therefore have to date been approved through the premarket approval (PMA) process. This is a more stringent evaluation, which requires a reasonable assurance, based on valid scientific evidence, that the device is safe and effective in fulfilling the intended use.

In Europe, sensor systems for in vitro glucose monitoring underlie the in vitro Diagnostic Medical Devices Directive 98/79EC(IVDD), which lists “Essential Requirements” regarding design, production, and labeling, which must be fulfilled prior to marketing the system. Sensor systems for professional use require manufacturer self-certification of conformance with the directive. Personal use systems for BGM require a conformity assessment which includes the involvement of a notified body. The medical device directives 93/42EC (MDD) establish the classification and approval framework for invasive glucose monitoring systems. Sensors for single 7-day use are classified as class IIa devices, presenting low-to-medium risk of harm to the user. CGM sensors used for longer than 7 days are classified as class IIb devices, and require testing to verify biological safety and lack of cytotoxicity. The manufacturer must demonstrate to a Notified Body that the requirements of the MDD have been satisfied. The product is then marked with a CE mark and may be sold within the European Economic Area (EEA).

The regulatory framework for medical devices begins long before the approval for marketing a product with design controls over the development process and the establishment and maintenance of a suitable Quality System according to 21 CFR

820 [23] or ISO 13485. Since single-use devices cannot be tested after manufacture and prior to use, the materials and processes used to produce the devices must be validated to ensure that the resulting product performs according to specification. For the high-volume processes used for production of BGM sensors, this is by far the most time-consuming and costly part of the product development process. Material specifications must be established and validated with analytical procedures and limits testing. Process equipment must be specified, qualified and validated, and limits of all process parameters established and tested. Packaging and labeling is also a significant part of the product and subject to the same standards.

Testing and validating the performance of the sensors requires testing on human subjects, primarily PwDs, both through the development process and to provide data for the required regulatory submissions. These evaluations fall under the regulations which govern the conduct of clinical trials. In the USA, this requires the approval and oversight of the trials by an Institutional Review Board (IRB), development of the appropriate protocols for recruitment of subjects, execution of the study, evaluation and documentation of results, and reporting of adverse events [24]. In Europe the parallel structure requires the approval and monitoring of studies by an Ethics Committee. The documentation overhead significantly increases the development time and cost.

Devices must then be manufactured according to validated processes and records created and maintained to establish that fact. The manufacturer must also maintain a system for documenting and analyzing customer inquiries and complaints. A system for Corrective and Preventive Action (CAPA) must be established and maintained. Reports of problems or product malfunctions must be investigated, and in serious cases, the product might need to be recalled from the market, at great expense. 21 CFR 806 [25] gives detailed instructions for the handling of notifications and product recalls in the USA. Deaths and serious injuries which a device has or may have caused or contributed to and certain device malfunctions must be reported to the responsible regulatory agency. In the USA, a medical device report (MDR) is required to be filed with the FDA. Records of all of these systems and processes must be complete and made available to the agency on request. 21 CFR 803 [26] details the requirements for medical device reporting in the USA. In the EEA, a manufacturer must establish and maintain a systematic procedure to review experience and report to the competent authority any malfunction, failure, or deterioration (see MEDDEV 2.12-1 for further details [27]).

Some practical and commercially important aspects of the development, production, and sale of sensors are not regulated but vital for the commercial success of a product. Production processes are typically scaled for the projected sales quantities, and in the case of BGM sensors, this can be in the billions of sensors per year. While the lower volume processes of the smaller manufacturers can be scaled through parallel replication, this is not economically efficient at the scales required by the major manufacturers. The efficiencies derived from highly automated processes allow the high-volume producers to maintain very high quality at sufficiently low unit production costs. A highly automated process requires significant capital investment in design, installation, and qualification, so the process must be

correctly scaled to the expected volume. Scaled-up production of medical device prototypes is more complex than frequently assumed [28]. Scalable manufacturing methods must be employed early on in the development cycle to ensure production of representative functional test models and prototypes and also in order to ensure that test performance which can be achieved with prototypes can be replicated on a production level. Given the expense of establishing a highly automated and validated process, thorough development of a product design, which meets all performance and handling aspects, must precede investment into particular manufacturing equipment. It was rightly pointed out [29] that an insufficient design cannot be compensated for by good manufacturing practice.

Reliable delivery of product requires suppliers which reliably deliver the materials in the required quantity and quality over product lifetime. Often, second or even third sources for critical reagents and materials must be developed and validated to ensure supply reliability. A material which is used for other purposes than medical device manufacturing can be particularly challenging, as specifications or material property changes which have no impact on most users may significantly impact the medical device manufacturer. For example, a polymeric material which is suitable for nonmedical use may not be applicable for an implanted CGM sensor due to sterilization requirements and subsequent necessity of proving toxicological safety. Materials which can be used in a consumer product may not be able to be combined in a medical device due to material interactions over time of storage which leads to deterioration of performance or even safety.

BGM sensors are rarely shipped directly from the manufacturer to the end user, but typically require a distribution chain of shippers, wholesalers, and retailers. The product must be stable at the conditions required for the time needed to reach the user, which can be up to 18 months, and the storage conditions must be monitored to verify compliance to the product limits. In the case of BGM sensors, which are typically provided in a primary package of 50 sensors, they must also be stable throughout the use time until the package is empty. The package is usually provided with a desiccant, such as silica gel, to maintain a dry environment for the reagent. This package will be opened and closed up to 50 times in the uncontrolled environment of the user. The sensors and desiccant must survive this repeated opening and closing even in challenging environments, such as high temperature and high humidity. Sensors which have been exposed to conditions which might render them inaccurate should be detected in some fashion, and not be allowed to report a value [30].

CGM sensors are currently shipped directly to the user in smaller packages, since they may have shorter expiration dating after sterilization. However, room temperature storage, equally a standard for BGM and CGM sensors, requires robust sensor designs and extensive testing prior to product launch for both applications.

2.2 Glucose Measurement Systems for Different Use Cases

Different use cases in diabetes care require different glucose measurement systems. Three types of setting for glucose measurement can be defined as clinical, healthcare provider (HCP), and patient self-monitoring, including both SMBG and CGM. Each of these settings has different requirements for performance and regulatory approval. In addition, the requirements for regulatory approval are different, depending on the market the product is sold in. The performance and regulatory requirements for SMBG and CGM are discussed in their respective sections.

Glucose measured on clinical systems, which are also called Central Laboratory Systems, are the primary method for diagnosing diabetes mellitus because these instruments are able to provide the high degree of accuracy in glucose measurement needed. These instruments are generally large and perform the glucose measurement under very controlled conditions. The majority of clinical analyzer systems are based on optical measurements. An exception is the 2300 STAT Plus Glucose and Lactate Analyzer, produced by YSI Life Sciences, which is based on an electrochemical method using immobilized GOx [31].

Since lab analyzers are based on a variety of analytical methods, requiring different pre-analytical analytical steps and measurement methodologies, the time required to obtain a glucose measurement varies widely with the type of instrument used. The measurement time to acquire the glucose measurement may range from a little over 1 to 15 min. When sample handing and pre-analytical steps are taken into account, the time from collecting the sample to obtaining a glucose result may take up to 90 min, whereas the time to complete a POC blood glucose measurement is approximately 5 min [32–34]. One consequence of the variability in test time and analytical methodology for clinical analyzers is the significant system-to-system variability, as well as laboratory-to-laboratory variability, in reported glucose values [35, 36]. The trade-off for the potential excellent system performance for clinical analyzers is longer time for a final glucose value.

POC glucose testing is defined as glucose testing which is performed at or near where the patient is located, e.g., in a hospital or in a healthcare provider setting, outside of a clinical laboratory with a portable instrument. POC testing is generally held as separate from SMBG, given the difference in requirements for testing in a POC setting, such as hygiene, system suitability checks, sample type (capillary, venous, and arterial blood), and accuracy. POC systems often have more specialized data management requirements as well, where patient information and test results are tracked in a patient data management system.

CLSI has established guidelines for the use of POC glucose monitoring systems and the controls around such systems through consensus, POCT12-A3 [37] and POCT13 [15]. In these guidelines, practices to ensure proper hygiene, quality control (including training and operator proficiency requirements), performance requirements, and documentation are described. POCT12-A3, for use in acute and chronic care facilities with laboratory support, describes acceptable performance

for POC meters when at least 95% of measured glucose values are within ±12 mg/dL (glucose values below 100 mg/dL) and 12.5% (glucose values at or above 100 mg/dL) of a reference value and when at least 98% of the measured glucose values are within ±15 mg/dL (glucose values below 75 mg/dL) and 20% (glucose values at or above 75 mg/dL). These performance requirements are more stringent than what is required for over-the-counter (OTC) SMBG systems. POCT13, for use in facilities without laboratory support, suggests that the ISO 15197 standard [17] is used for system performance and that the user be aware of limitations for use for the system in use, particularly with respect to interferences. In both guidelines, requirements for an infection control program are suggested as a means of minimizing the risk of blood-borne pathogen transmission when a single device is used with multiple patients, including wearing gloves during the testing procedure and changing gloves between patients, hand washing immediately after glove removal, using a unique lancing device which is assigned for a single patient which is never used for multiple patients, and assigning a BG meter to a particular patient unless a system can be adequately cleaned between uses for multiple patient use.

The FDA has also issued a draft guidance regarding the manufacture and use of blood glucose monitoring systems for POC use [14]. This guidance contains similar information to POCT12-A3 and POCT13, but is geared toward the manufacturer of POC blood glucose devices. The FDA guidance contains more specific and stringent requirements, especially with respect to cleaning and disinfection procedures, as well as performance requirements. Descriptions of performance testing, such as precision, intermediate precision, accuracy in the hands of the intended user with each claimed sample type (e.g., capillary, arterial, venous, or neonate), and interfering substances, are detailed in this guidance. Of particular note, the accuracy requirements are more stringent that what are laid out in ISO15197, 2013, with the requirement that 99% of values are within ±10% of the reference method for glucose values ≥70 mg/dL and ±7 mg/dL for glucose values <70 mg/dL. A further requirement is that no individual glucose measurement may be outside the specified range of ±20% of reference value for glucose values ≥70 mg/dL and ±15 mg/dL for glucose values <70 mg/dL. In addition, the draft guidance states that the system should be able to measure blood glucose accurately over the range of 10–500 mg/dL. The draft guidance has elicited much commentary from both experts and industry, both positive and negative. Some researchers and users applaud the new guidance [38–40]. While it is generally recognized that POC blood glucose monitoring systems should continuously improve performance to improve patient safety, some groups object to the performance requirements in the draft guidance as technically infeasible and will result in the loss of availability or change in device characteristics of POC systems [38, 41, 42].

While most POC blood glucose systems are based on electrochemical measurements, there is an optical system produced by HemoCue, the HemoCue® Glucose 201 system. Examples of electrochemical POC systems include Roche's Accu-Chek® Inform II and Nova Biomedical's StatStrip™.

SMBG and current CGM are "home-use" scenarios, where the PwD is the primary tester and are intended to provide the user with glucose information that

allows them to manage diabetes on a day-to-day basis. While the general testing principal for SMBG and CGM is often the same, i.e., electrochemical methods, the characteristics of the sensors and the frequency that a BG value is produced are very different. SMBG systems are in vitro systems where a single BG value is obtained from a PwD after performing a finger stick by a lancing device, which is a medical device. CGM systems are medical devices which are based on minimally invasive sensors that measure glucose in interstitial fluid with a frequency of minutes and remain implanted from 5 to 14 days. The specific characteristics of electrochemical SMBG and CGM systems are the focus of this review and are discussed in Sects. 3 and 4, respectively.

2.3 Glucose Measurement Technology

The many commercially successful glucose measurement systems available today for diagnosis and monitoring of diabetes all require sampling of a body fluid and involve the use of enzyme-based assays. Attempts to accurately measure glucose, or at least predict its concentration from its effects on the body tissue, without a blood or tissue fluid sample, have been pursued as long as continuous sensor technology. While the promise of noninvasive glucose monitoring [43, 44] remains a strong desire among PwD, the unremarkable spectroscopic characteristics of glucose and interfering physical and chemical properties have to date prevented achievement of the required performance. Nonenzymatic glucose sensors currently find application only in areas where specificity is not required, when no other reducing sugar is present, or when specificity is achieved through some previous process. Nonenzymatic glucose sensors are either based on direct oxidation of glucose on an electrode or on affinity-based glucose assays. Direct oxidation-based approaches have received increased interest due to increased nanomaterials research [45–48]. Arylboronic acid, used for affinity separation of glycoproteins, has frequently been the basis for affinity-based assays coupled with optical or electrochemical detection schemes [49, 50].

Glucose measurement of biological samples in the clinical laboratory is historically primarily based on enzyme-based spectrophotometric assays. The current standard laboratory tests use GOx/peroxidase, hexokinase and glucose-6-phosphate dehydrogenase, or glucose dehydrogenase. These assays are robust, highly specific, and economical. The recent development of assays for biological samples which can be directly traced to NIST reference material [51] has improved the prospects for standardization across different laboratory methods and sites. The first product for decentralized or individual use, the CLINITEST® (still available as the BAYER® CLINITEST®) for reducing substances in urine samples, used Benedicts' reaction employing the chemical reduction of Cu(II) to Cu(I). This test tube and reagent tablet-based assay was followed by Clinistix®, also for urine samples, but now employing the very specific enzyme GOx, along with peroxidase to generate a color change from the hydrogen peroxide produced. The reagents were impregnated in

paper pads laminated to plastic substrates to form the first generation of test strips. [52–54]. Personal diabetes monitoring was greatly advanced by colorimetric test strips for blood glucose measurement, which evolved from the urine test strips. DextroStix® (Ames/Miles/Bayer) and Chemstrip BG® (Boehringer Mannheim/Roche) began the success story of test strips with photometric readout [52] and the currently widespread practice of diabetes self-management [55].

The introduction of the enzyme electrode for medical monitoring by Clark and Lyons [4] led to the development of alternative sensor systems that found application in clinical practice along with ion-selective electrodes. Fundamentally, an enzyme in close association with an electrode surface reacts with a substrate, and a product or co-substrate of the enzyme reaction is measured on the electrode. Clark described an electrode with an adjacent membrane sandwich containing GOx- an FAD-dependent oxidoreductase, which reduces oxygen as a co-substrate. Oxidation of glucose to gluconolactone and subsequent hydrolysis to gluconic acid causes a pH change that is measured with a pH electrode. Alternatively, the decrease of oxygen concentration, which is a consequence of glucose oxidation and reoxidation of the enzyme, can be determined with an oxygen electrode. Updike and Hicks developed a miniaturized oxygen sensor with GOx immobilized in a hydrogel and introduced a differential sensor construction that additionally measured ambient oxygen [56]. Notably, the YSI 23A Glucose Analyzer by Yellow Springs Instruments and the Beckman Glucose Analyzer became popular in clinical laboratories for glucose in plasma or whole blood. The Beckman Glucose Analyzer was introduced into the clinical laboratory in 1968 and used an oxygen electrode to measure the rate of decrease in dissolved oxygen when GOx was added to a sample. The YSI 23A combined the immobilized enzyme electrode with electrochemical hydrogen peroxide detection [31], which was traditionally measured exclusively photometrically using leuco dyes. Derivatives of the YSI 23A instrument remain popular for use as reference methods for evaluating consumer glucose monitoring systems. Disposable single-use sensors, based on electrochemical readout, were first introduced by MediSense (ExacTech), followed by Accu-Chek® Advantage by Boehringer Mannheim and FastTake® by Lifescan. Electrochemical sensors, configured to operate in a "reagent-free" mode [57], avoid reagent leakage and triggered the development of sensors for repeated glucose monitoring. Sensors for continuous (or repeated) glucose monitoring were directly derived from these reusable clinical enzyme sensors. In development almost since Clarke and Lyons' proposal, CGM products were launched successfully by Minimed, Menarini, Dexcom, and Abbott. Roche has a CGM system under development.

Electrochemical biosensor technology for glucose monitoring continues to attract not only the interest of the large commercial manufacturers of sensors but academic and clinical research groups. Many quality reviews of the status and progress of the technology can be found in the literature [58–67]. The details of operation, advantages and shortcomings, and prospects, and commercial considerations will be discussed hereunder. Different generations of electrochemical sensors will be introduced briefly. GOx-oxygen-hydrogen peroxide sensors came to be known as first-generation sensors [68]. The natural availability of ambient oxygen

makes first-generation technology useful for "reagent-free" analysis [57]. However, the low solubility and resultant low concentration of oxygen in biological fluids require measures such as sample dilution, diffusion barriers, or geometric arrangements [69] to maintain analytical performance. GOx can also be reoxidized by artificial electron acceptors, which themselves are reoxidized on an electrode. Organometallic complexes such as ferrocene [70], ferricyanide [71], and osmium complexes [59] are widely used. Small organic molecules, such as phenanthroline quinone and nitrosoaniline [71], have advantages for certain uses. These artificial electron acceptors are termed mediators. Sensors employing artificial mediators are referred to as second-generation sensors. The ability to use a high concentration of mediator improved the performance and manufacturability of sensors to the extent that they became viable consumer products [72]. When used with GOx, mediated sensors are subject to interference from varying concentrations of oxygen in the sample. Thus, glucose dehydrogenases, which are unreactive with oxygen, were introduced. PQQ-GDH, FAD-GDH, and NAD-GDH have all been used in second-generation sensors [71, 73], and significant work in enzyme engineering has gone into optimizing enzymes for specificity and stability [74–77]. The reduced cofactor of glucose-oxidizing enzymes can also be directly oxidized on an electrode surface, sometimes with the aid of surface modifications or small relays. Structured nanomaterials such as metal and metal oxides [63, 65, 78, 79] and carbon structures including graphene and fullerenes [64, 80, 81] have been reported, but are not yet in commercial use. Transfer through the heme group of cytochrome units of enzymes has been reported [82, 83]. Sensors according to this direct electron transfer technology are referred to as third-generation sensors. These generations are a convenient division, but not rigorous. The "wired enzyme" sensor of Heller et al. [59, 84] combines second-generation mediators with immobilization in a 2.5 generation sensor.

3 Self-Monitoring of Blood Glucose (SMBG)

Self-monitoring of blood glucose (SMBG) is the measurement of blood glucose values by a PwD for management of diabetes mellitus. SMBG is based on a "spot monitoring" method, where a singular blood glucose value is collected from a single blood collection, generally a finger stick. SMBG includes systems which are nonintegrated, where a single disposable test strip is used at a time, or somewhat integrated systems, where multiple test strips or test elements are included in a single meter. SMBG has become an essential tool for management of diabetes, especially for the patients using insulin therapy [9, 10, 85–101]. The utility of SMBG has also been established for patients who are not on insulin therapy and are instead using other means to regulate their blood glucose, such as oral or injected medications and regulation of diet/exercise [88, 89, 91–94, 97, 101–114], although there is no clear consensus on how often a PwD who is not using insulin should test [115–120]. The debate around the timing and effectiveness of SMBG for Type

2 (T2) is likely to continue as healthcare costs rise. As shown in the references above, through the monitoring of BG, improved outcomes can be observed with the lowering of HbA_{1c}, PwDs can gain awareness of postprandial blood glucose excursions, and effective behavioral modification and titration of medications can be monitored. SMBG systems, including requirements, system descriptions, measurement principles, sensor manufacturing, and system performance will be discussed in the following sections, concluding with an outlook for SMBG.

3.1 Requirements

3.1.1 Personal User Requirements

PwDs have different testing needs depending on the type of therapy they are undergoing. Generally, diabetes is classified into two categories, Type 1 (T1) and Type 2 (T2). A very general definition of the types is that T1 diabetes, formerly called insulin-dependent diabetes, is where the pancreas produces very little to no insulin to regulate glucose. In T2 diabetes (formerly called non-insulin-dependent diabetes), the PwD's ability to metabolize glucose is changed, either by developing insulin resistance or by reduced production of insulin. Therapy for T2 diabetes may vary significantly based on the progression of the disease in the PwD and ranges from oral medication, non-insulin injectables, and insulin therapy. A PwD who is undergoing insulin therapy will have more extensive testing needs than someone who is not undergoing insulin therapy. There is ever-increasing pressure to reduce the cost of treating diabetes, including the price of blood glucose monitoring supplies. The incidence of diabetes is rising, and the economic impact of diagnosed diabetes, direct and indirect, in the United States has been estimated at $245 billion in 2012, of which diabetes supplies (including testing supplies) are estimated to be 12% of that cost [121]. Consumers and payers are coming to regard diabetes meters and strips as commodity products [122], while the volume of SMBG systems sold has been increasing steadily, the price for SMBG systems has been decreasing. In addition, the lack of consensus of the utility of blood glucose monitoring in certain situations has led to many payers limiting or eliminating coverage of blood glucose monitoring supplies [115, 123]. The cost pressures on reimbursement for blood glucose monitoring systems has been a challenge for manufacturers as they strive to remain profitable and still introduce new technologies. The needs of the PwD have evolved over time beyond analytical performance requirements of the blood glucose measurement, varying with their condition; the needs of a T1 user are different from the needs of a T2 user. Even within the classification of T1 or T2, the type of therapy will also dictate the features that best suit the user.

3.1.2 Healthcare Provider Requirements

HCP requirements can be divided roughly into two categories: managing PwD data generated by SMBG systems during "home" use monitoring and managing systems at the POC. For the first situation, the SMBG system requirements are the same as described above in terms of system performance. For a HCP the ease of data management is more critical for POC systems. While many SMBG manufacturers have software packages that are able to download patient data from the meter, these packages rarely are able to download data from other manufacturer's systems. Consequently third-party systems (e.g., CliniPro®) may be required if a HCP must deal with multiple SMBG systems within a practice. The performance requirements for a POC blood glucose monitoring system for use at a HCPs facility or in a hospital are described in CLSI POCT12-A3 [37], and specifics of performance requirements will be covered in a later section. In addition to requirements around performance, systems for use in a POC setting must meet requirements for infection control and validation of meter cleaning and disinfection. CLSI POCT12-A3 [37], CLSI POCT13 [15], ISO15197:2013 [17], and the FDA draft guidance for POC BG systems [14] offer guidance around infection control and cleaning procedures for POC systems. Since the vast majority of POC meters are used across a certain population of patients, adequate controls around cleaning and disinfection procedures must be clearly defined, validated, and enforced to prohibit the transmission of blood-borne pathogens among the user population.

3.1.3 Payer Requirements

In general, third-party payers for healthcare services, such as governments, public insurers, and private insurers, are motivated to provide treatments to their subscribers that have been determined to be (cost-) effective [124] in comparison to standard care. Furthermore, decision makers do also consider the impact of the respective technology on their budgets.

The use of blood glucose monitoring by PwDs being treated with insulin has been demonstrated to reduce HbA_{1c} and the occurrence and costs of the associated comorbidities and is considered the standard of care for these patients [92, 124, 125]. Blood glucose monitoring for patients being treated only with oral medications can, in fact, facilitate long-term improvement in glycemic status, but only when the following conditions are met: The SMBG regimen is structured (both in timing and frequency) to obtain actionable information about each patient's glucose control. The data are generated and documented in a manner that facilitates analysis and discussion of glycemic patterns between patient and healthcare provider. Both the patient and the healthcare provider are well educated, willing, and skilled to make appropriate treatment decisions based upon the SMBG data. Both the patient and healthcare provider mutually agree upon treatment decisions and modifications.

This position mirrors the International Diabetes Federation's (IDF) guidelines for use of SMBG in non-insulin-treated diabetes. These guidelines recommend that SMBG should be used only when patients and/or their clinicians "have the knowledge, skills and willingness to incorporate SMBG monitoring and therapy adjustment into their diabetes care plan in order to attain agreed treatment goals." Unfortunately, these conditions for appropriate SMBG use are absent from the interventions used in many studies analyzed and summarized systematically by Clar et al. [126].

Structured SMBG as investigated in the STeP study is even more clinically relevant. The STeP study was a large prospective, cluster-randomized, multicenter trial evaluating the use of structured SMBG in 483 poorly controlled ($HbA_{1c} \geq 7.5\%$) insulin-naïve T2DM patients from 34 US primary care practices [127]. The primary endpoint was changed in HbA_{1c} over time. Patients in the structured testing group used a simple paper tool that facilitates collection and interpretation of 7-point glucose profiles over three consecutive days. These patients completed the tool on a quarterly basis, brought to the completed tools to medical visits, and discussed findings with their physicians. Structured testing group patients received training in BG measurement, including instructions for how to identify problematic glycemic patterns and how best to address such problems through changes in physical activity, portion sizes, and/or meal composition; structured testing group physicians received an algorithm describing various pharmacologic/lifestyle treatment strategies that could be used in response to the specific SMBG patterns identified. Active control group patients received enhanced usual care only and were instructed to use their meter following their physicians' recommendations but received no additional SMBG prompting, training, or instruction. At 12 months, intent-to-treat (ITT) analysis revealed that structured testing group patients ($n = 256$) experienced significantly greater improvement in mean HbA_{1c} than active control group patients ($n = 227$): -1.2% vs. -0.9%; $P = 0.04$. Per protocol (PP) analysis revealed an even greater HbA_{1c} reduction (-0.5%) in the experimental ($n = 130$) vs. control ($n = 161$) patient group (-1.3% vs. -0.8%; $P < 0.003$). Further analyses of data from the STeP study have revealed improvements in several other parameters, including clinicians' intensification of treatment, depression and diabetes-related distress, and patient self-efficacy and autonomous motivation in managing their diabetes. Similar findings were seen in a pilot study by Franciosi et al. [128] evaluating the efficacy of a structured SMBG-based intervention with T2DM patients treated with oral agents. Parkin et al. [110] have published a review article that provides more detailed descriptions of these studies. Still, reimbursement varies [129] to a large extent based on varying definitions of the interventions across the relevant studies and questionable assessment criteria by health technology assessment (HTA) agencies, e.g., the "somewhat arbitrary" [126] clinical relevance threshold of 0.5% which is often borrowed from the assessment of pharmaceuticals, but may hinder patients to materialize relevant results. Variability of reimbursement clearly raises similar questions such as clarity, suitability, and transparency of criteria used for reimbursement decisions as expressed recently

by the European Diagnostics Manufacturing Association (EDMA) position paper on health technology assessment for IVDs in the context of market access [130].

3.2 Monitoring Systems

The technology for SMBG is mature. Home-use tests for PwDs have been available in some form since the late 1970s [52, 131]. Early systems were based on testing of the user's urine, with the degree of color on the test strip indicating the glucose level. Today, urine glucose test strips are routinely used for screening both in hospitals and in general practice. The aim of screening is early identification of likely patients by examining large groups of the population. Patients with increased diabetes risk or PwDs can also benefit from urine-based glucose testing for screening purposes [132]. However, urine-based glucose testing is no replacement for blood glucose monitoring for several reasons. Measurements of blood glucose levels is not possible below the renal threshold, which usually corresponds to a plasma glucose level of 11.0 mM (198 mg/dL) [133], which, however, may vary during long-standing diabetes and pregnancy. Consequently no differentiation of hypoglycemia, euglycemia, and even mild hyperglycemia is possible. Further, the time lag between BG and urine levels may be very significant, depending on the time over which urine accumulates in the bladder [52, 134]. Due to these limitations of testing glucose in urine, there was a drive to produce home-use systems which were capable of testing blood and reducing the effect of the user's technique on the blood glucose results. These BG systems relied on photometric determination of blood glucose, which had many advantages over urine glucose monitoring. Electrochemical detection became more common in the 1990s. Improvements in SMBG, ease of use, accuracy, and precision continue to be made for both photometric and electrochemical blood glucose meters.

A SMBG system generally consists of an SMBG meter, disposable strips including a sensor, a lancing device, and one or more control solutions. Diabetes management software may also be included as part of the SMBG system. POC blood glucose monitoring systems designed for use in a clinical setting (hospital, clinic, or HCP facility) include more sophisticated data management, tracking, and transfer capabilities than a consumer system. Currently, the personal user is able to choose from a large number of systems which provide a competitive set of features. Users have come to expect some features as part of a standard user experience, such as small blood volume, fast test time, and some data storage capability. Other features are becoming more common in the competitive blood glucose monitoring market, such as diabetes management tools [135, 136]. The majority of systems currently on the market require sample volumes less than 1 μL, with some systems requiring sample volumes as low as 300 nL. Test time has also decreased significantly since the introduction of consumer SMBG meters. Test times of five seconds are now common. Meters can be differentiated by the availability of additional features, as well as through system performance. One of the most attractive

additional user features is the so-called no code. Instead of the end user having to enter a lot-specific code or insert a code key, the user is able to simply use the strips directly from the vial. Advances in strip manufacturing processes and measurement techniques enable either universal coding, where the strips are produced reproducibly enough to require the same code for all lots, or non-evident coding, where the appropriate code is transferred from the strip packaging or from the strip characteristics. With either method, the end user is not required to input code-specific information into the meter, improving the ease of use of the system and reducing user-induced measurement error [137–139].

Another characteristic which improves ease of use and reduces opportunities of error [140, 141] is the integration of multiple tests into one single container, thus removing the need to handle single strips. A single container may contain 10 to 50 blood glucose tests, depending on the manufacturer of the system. The lancet for this type of system may be integrated into the body of the meter or attached to the body of meter. The advantage of integrated systems is the reduction of the number of steps the PwD must take to complete a blood glucose test, with a possible reduction of errors introduced by multiple handling steps. The Accu-Chek® Mobile is an example of a fully integrated system [140], with a 50-test cassette, attached lancing device with a drum of six lancets, automatic coding, and small required sample size.

Advanced SMBG systems offer features for enhanced diabetes management. The majority of meters currently on the market are able to store multiple BG measurements. More advanced meters will provide average blood glucose measurements at preset intervals. In addition, meters such as the Accu-Chek® Aviva Plus and Accu-Chek® Nano include before and after meal marking, before and after meal BG averages, as well as a customizable hypo indicator, customizable test reminders, and post-meal test reminder. Beyond memory functions, test averaging, and reminders, some meters include features which provide features useful to the insulin-dependent PwD. The Accu-Chek® Aviva Expert BG system provides the user the ability to record events related to diabetes management, such as blood glucose test results, carbohydrate intake, bolus and basal insulin delivery, and significant health events (e.g., exercise, stress, illness). In addition, the Accu-Chek® Aviva Expert and Accu-Chek® Insight systems have a built-in bolus advisor, which provides the user with an insulin dosing or carbohydrate intake recommendation to correct BG levels that are not in the targeted glucose range. Features such as these, especially bolus calculators [142–144], are useful for the insulin-dependent PwD.

Integration of a SMBG system with an insulin pump is the next level of combining SMBG with diabetes management solutions. In these systems, the meter and the remote control for the pump are often the same device. In the Accu-Chek® Combo system, the Accu-Chek® Aviva Combo meter is the remote control for the Accu-Chek® Spirit Combo insulin pump, as well as a BG meter which includes data management features, such as a log book, trending graphs, and reports; other features include event-based reminders and the ability to enter specific data regarding an event (illness, stress, exercise, etc.). The new feature

for bolus advice in the Combo system uses SMBG test results directly from the meter in the bolus calculator, and the user can use the meter/pump remote to deliver the bolus. These features are useful for the PwD ([142] and references contained within), especially for pediatric PwDs [145].

SMBG systems are often coupled to software packages or online tools produced by the manufacturer of the system to allow for more in-depth analysis of SMBG data collected by the user [66, 146, 147]. SMBG data is transferred from the meter to the software package. Both consumers and healthcare providers can use the reports available to help fine-tune therapy and behavior modification for PwDs. These software applications are available on primarily PC systems, although online applications are being introduced. Accu-Chek® 360°, a powerful diabetes management tool, is available for both PC and as a diabetes management app for Android smartphones. Accu-Chek® Connect Online is a web-based diabetes management portal which allows downloading of SMBG data from all Accu-Chek® devices [146]. This product allows for easy sharing of data between PwDs and HCPs/caregivers. The 510(k)-cleared Accu-Chek® Connect Diabetes Management app allows for wireless data transfer from the Accu-Chek® Connect meter to smartphones for data analysis and for bolus calculations.

3.2.1 Measurement Principles

Active Components

Commercially available SMBG systems are based on optical or electrochemical detection schemes. For both schemes, enzymes provide the specificity for glucose. Except for the actual signal transduction, the mechanism for signal generation is very similar for optical and electrochemical systems. Glucose sensors use oxidoreductase enzymes which oxidize glucose to gluconolactone. The commonly used enzymes for SMBG systems are GOx (EC 1.1.3.4), quinoprotein glucose dehydrogenase (PQQ-GDH, EC 1.1.5.2), FAD-dependent glucose dehydrogenase (FAD-GDH, EC 1.1.99.10), and NAD-dependent glucose dehydrogenase (NAD-GDH, EC 1.1.1.47). GOx and FAD-GDH have the same cofactor, flavin adenine dinucleotide, with the native and preferred final electron acceptor for GOx being oxygen. FAD-GDH, unlike GOx, does not use oxygen as the final electron acceptor. PQQ-GDH uses pyrroloquinoline quinone as its cofactor and NAD-GDH nicotinamide adenine dinucleotide. FAD and PQQ are bound to their respective enzymes through strong interactions, while NAD is not bound permanently to NAD-GDH [73]. A generic reaction scheme for electrochemical biosensors is shown below in Fig. 1.

Each of these enzymes has advantages and disadvantages, and the properties of the enzyme will vary with the specific parent organism of the enzyme and depend on potential protein engineering of the enzyme. A brief overview of the enzymes commonly used in SMBG is provided below. An excellent review of enzymes used

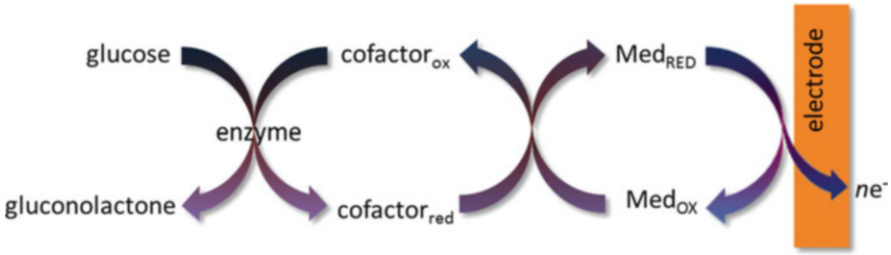

Fig. 1 Generalized working electrode reaction scheme for a SMBG biosensor. "ox" is the oxidized form of the cofactor or mediator, "red" is the reduced form of the cofactor or mediator, and n is the number of electrons (e^-)

for glucose biosensing has been written by Ferri et al. [73]; the reader is referred to that review for more information.

GOx was the first enzyme to find widespread use in glucose sensors [4, 31, 52, 71, 73]. The parent organism for GOx is Aspergillus niger, with the majority of the GOx in use today for glucose sensing produced from this organism. GOx has excellent specificity for glucose, with some interference from 2-deoxy-D-glucose and minimal interference from galactose. These sugars are not generally considered significant for most SMBG use; labeled 2-deoxy-D-glucose may be used for PET-scanning and is not generally encountered by users except in very controlled circumstances [148], and galactose interference is a problem for mainly POC use when galactosemia is present in neonates [33, 149, 150]. Oxygen is the native electron acceptor for GOx, producing hydrogen peroxide as a result of the catalytic reaction. Generally, detection of the hydrogen peroxide produced when oxygen is the electron acceptor is not robust in disposable glucose sensors used for SMBG, making the use of a mediator to transfer electrons to the electrode surface necessary for efficient signal generation. The reduced FADH2 cofactor is fairly tolerant of mediator identity, accepting many metal complexes or organic mediators, as long as the redox potential of the mediator is suitable. When a mediator is used for a GOx-based sensor, oxygen interference becomes a factor and is the main reason why GOx is no longer used for SMBG sensors produced by the main four SMBG manufacturers.

FAD-dependent glucose dehydrogenases, FAD-GDHs, do not use oxygen as its native electron acceptor, unlike GOx. There is variability in the sugar specificity in FAD-GDHs, depending on the parent organism [73]. For FAD-GDH derived from bacteria, an integrated electron acceptor is part of the enzyme in the form of cytochrome c-containing subunit. This FAD-GDH lacks specificity for glucose, with substantial activity for maltose. More commonly used are FAD-GDHs derived from fungal parent organisms. FAD-GDHs from fungi do not have the integrated acceptor, but instead are able to use a wide range of mediators as long as the redox potential of the mediator is suitable. Sugar specificity is, in general, excellent for FAD-GDH derived from fungi; however, there is substantial activity toward

2-deoxy-D-glucose and xylose. Since FAD-GDH does not accept oxygen as an electron acceptor, sensors with FAD-GDH do not experience interference from variations in oxygen partial pressure or have altitude limitations for use as seen in GOx-based systems.

PQQ-GDH (PQQ-dependent glucose dehydrogenase)-based SMBG sensors use soluble PQQ-GDH, derived from *Acinetobacter calcoaceticus*. It has excellent catalytic activity, allowing for fast glucose sensing; however, native PQQ-GDH can have interference from several sugars, including maltose, galactose, and xylose. With protein engineering, mutant forms of PQQ-GDH have been made with excellent glucose specificity, reducing the impact of maltose to the point where significant interference is not observed [73, 151–158]. PQQ-GDH does not have oxygen interference and is able to accept a wide variety of mediators, both organic and inorganic metal complexes.

NAD-dependent glucose dehydrogenase, NAD-GDH, generally has good substrate specificity, but its cofactor is not bound and must be included as part of the strip reagent matrix as an additional component. Also, the number of effective mediators for NAD-GDH-based systems is more limited due the specific requirements for rapid reaction of the mediator with NADH (e.g., quinones and quinoid compounds).

Direct oxidation of the reduced cofactor is not generally possible for GOD, PQQ-, and FAD- dependent enzymes. In theory, NADH could be oxidized directly at an electrode surface; in practice, direct oxidation of NADH often results in incomplete regeneration of active NAD and electrode surface fouling [159–161]. To overcome difficulties with direct electron transfer, all commercially available SMBG systems use a mediator system for transferring the electrons from the reduced cofactor to the electrode surface. The reduced mediator is oxidized at the electrode surface, where the current generated or the charge collected is directly related to the amount of glucose in the sample. FAD- and PQQ-dependent enzymes are relatively tolerant of the mediator choice as long as a mediator with suitable potential is chosen. NAD-dependent enzymes are far "pickier" with respect to effective mediators due to the need for hydride transfer between NADH and the mediator. For this reason, quinones and quinoid compounds, such as quinone diimines, phenazines, and related dyes, are effective mediators for NAD-based systems [162, 163]. Regardless of the identity of the mediator used in SMBG systems, freely diffusing mediators are the norm. Table 1 shows some examples of enzyme and mediator combinations used in SMBG products.

Measurement Methods

The vast majority of electrochemical SMBG systems rely on amperometric detection, with coulometric detection used in a small number of systems [52, 61, 66, 71, 131]. For both of these measurement methods, the general mechanism for signal detection is the same; the reduced mediator produced from the reaction of the reduced cofactor of the glucose-converting enzyme and oxidized mediator must

Table 1 Non-exhaustive list of examples of enzymes and mediators used in SMBG systems

Enzyme	Mediator	Product examples
GOx	Hexacyanoferrate (III)	OneTouch® Ultra®
	Hexaamineruthenium (III)	iBGStar®
FAD-GDH	Hexacyanoferrate (III)	One Touch® Verio®
	Phenothiazine	Bayer Contour® Next
	Osmium based	Abbott FreeStyle Lite®
PQQ-GDH	Not indicated	Nipro TRUE2go®
Mut-Q (engineered PQQ-GDH)	Nitrosoaniline	Roche Accu-Chek® Aviva Roche Accu-Chek® Performa
NAD-GDH	Phenanthroline quinone	Abbott FreeStyle Neo®

diffuse to the test strip working electrode surface, where it is oxidized. The amount of oxidation current or charge collected is directly related to the amount of glucose in the sample. In a classical amperometric experiment, there are three electrodes used in the cell for evaluating the current: a working electrode, where the reaction of interest takes place; a reference electrode, against which the potential applied to the working electrode is set; and a counter electrode, where the current flows between the working and the counter electrode. No current flows through the reference electrode, ensuring that a stable potential is maintained. The most common reference electrode type is a silver/silver chloride reference. This type of electrochemical cell can be expensive and is not often used in SMBG test strips. Instead, most SMBG strips use a two-electrode configuration for the primary electrode set, with a working electrode and a counter electrode. This counter electrode serves as a reference electrode against which a potential difference between the working and counter is applied. The current which flows between the working and the counter electrode is measured. For some SMBG strips, the counter electrode is coated with Ag/AgCl and functions much like a traditional reference electrode, maintaining a stable potential as long as the amount of current passed through the electrode does not disrupt the reference system. More commonly, SMBG strips are configured for use in a "biamperometric" measurement, where the counter electrode reaction also serves as the reference reaction. In this configuration, the absolute potential of the system is not stable and will drift according the properties of the system, in particular, the glucose concentration. The impact of not having a stable reference electrode is accommodated by careful design of the measurement method to ensure that reproducible measurements are made. While the relationship between glucose in the sample and the current produced is, in principle, a very simple and direct relationship, there is considerable variation in the magnitude of the current response due to the influence of temperature on diffusion. The change in diffusion speed is approximately 2% for a 1K change in temperature. Hematocrit also has a large impact on the response, since red blood cells in the sample influence the diffusion of glucose in the sample. Correction of the primary current response for the influence of temperature and hematocrit is accomplished in

different ways, depending on the SMBG system in question. Given the extremely competitive nature of the business of SMBG, different manufacturers strive to keep the exact natures of their measurement methods and correction algorithms confidential. Basic information about the correction mechanisms for BG values can be inferred from product and patent literature. However, the finer details of the compensation algorithms are held as trade secrets.

Temperature correction, in its simplest form, can be achieved by introducing a correction factor based on the measurement of the temperature experienced by the meter. While this type of correction is elegant in its simplicity, BG measurements which have been corrected in this manner can suffer from over- or under- compensation due to differences in the temperature measured by the meter and the temperature of the reaction on the test strip. When a system with a meter-based temperature measurement correction is in a rapidly changing temperature environment, for example, when the meter has been moved from a warm environment to a cool environment and a measurement is made without letting the meter equilibrate to the ambient temperature, a bias in the BG result may occur due to overcompensation for high temperature perceived by the meter. For systems using a meter-based temperature measurement, a waiting time needs to be defined to allow for the system to equilibrate. A more sophisticated temperature compensation scheme relies on the sample properties measured on the test strip, as in the Accu-Chek® Aviva and Accu-Chek® Performa meters. In this compensation method, electrochemical impedance measurements are used to monitor changes in the conductivity in the sample due to temperature in the sample measurement zone. These impedance measurements are used in the correction algorithm to compensate for the impact of sample temperature on the BG response [164, 165].

Compensation for hematocrit is achieved through several methods, again depending on the manufacturer. In the Accu-Chek® Advantage system, hematocrit correction was achieved through monitoring the shape of the current response over time [71]. More current BGM systems use other means of correcting for hematocrit interference; for example, some systems will use a secondary electrode as a hematocrit sensing electrode, using the response of the secondary electrode to correct the primary glucose current measured on the working electrode. Other systems use a technique the manufacturer refers to as "Dynamic Electrochemistry®," where the response of the working electrode to a varied potential input is used to correct for hematocrit [166, 167]. Roche's Accu-Chek® Aviva and Accu-Chek® Performa systems use electrochemical impedance measurements made with the working and counter electrodes of the test strip to measure the impact of hematocrit on the sample conductivity. The impedance measurements used in the correction of temperature are also used to correct for hematocrit interference in that same family of products [164, 165].

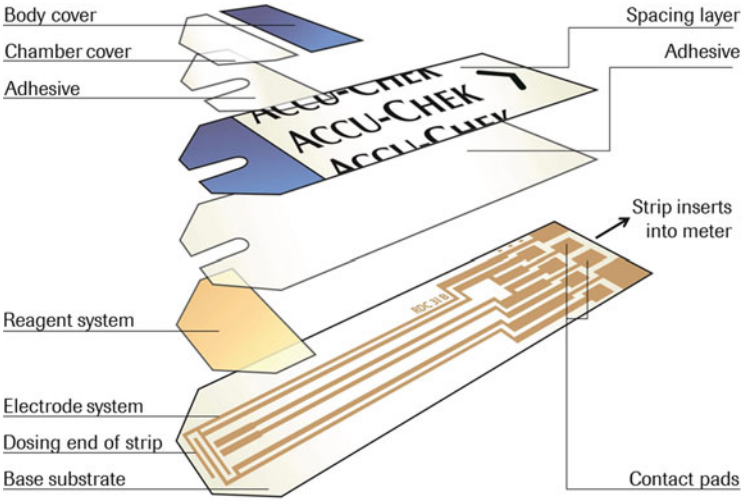

Fig. 2 Accu-Chek® Aviva Test Strip Architecture. Exploded view showing the base film and electrodes, spacer to define the electrode area, and cover layer hydrophilic to define the sample chamber

Correction of other interferences can also be achieved through the measurement method, selection of mediator, or a combination of the two. By choosing the applied potential and/or mediator carefully, interference from some electroactive substances, such as uric acid and acetaminophen, can be avoided [59, 61, 71]. Other methods for reducing endogenous and exogenous interfering substances have been suggested [61]; however, implementing these approaches in inexpensive, disposable SMBG test strips has not been feasible.

3.2.2 Sensor Manufacturing

In the sections below, a brief overview of electrochemical SMBG sensor manufacturing processes is outlined. Since there are a wide variety of SMBG sensors on the market with different sensor architectures, reagents, and manufacturing techniques, an exhaustive review is outside the scope of this description. As an example, a view of the Accu-Chek® Aviva test strip is shown in Fig. 2 [71].

The base film in commercially available SMBG sensors is commonly a thin thermoplastic substrate, usually made of polyester. Depending on the nature of the processing steps, the base film, or "web," may be a large sheet (discrete processing) or a continuous roll (reel-to-reel processing). The benefit of reel-to-reel processing is in the speed inherent in web converting processes, which allows for cost benefits to be derived from large-volume production [59, 61].

The method of forming the electrodes on the base film is dependent on what type of material is used for the electrodes. For systems which use carbon electrodes, the most common method of forming the electrode pattern is through screen printing of carbon inks. If an Ag/AgCl reference electrode is a part of the sensor architecture, the Ag/AgCl ink is also screen printed. The electrodes must be cured before further processing. Since the substrate for the electrodes is a thin plastic web, the inks used for screen printing of electrodes are able to cure at relatively low temperatures. The size of the electrode features is limited by the printing method to approximately 100 μm [168, 169]. It should be noted that for some strips, such as the FreeStyle® Precision Neo (formerly Precision Xtra), the active ingredients (enzyme, cofactor, mediator) are mixed in with the conductive carbon particles and other reagent components to form the electrode ink. For other SMBG sensors, the electrodes are formed from vapor-deposited thin metal layers on the base film. Noble metals, such as gold or palladium, are the electrode materials of choice, and the thickness of the metal layer can be as low as 10 nm. The most common method for patterning the electrodes is to use a laser removal process, either laser scribing or broad-field ablation [170, 171]. The benefit of using broad-field ablation for forming the electrode patterns is the speed of the process, the small size of the electrode features, and the edge quality which can be achieved with this process. Since the electrochemical signal generated in amperometric sensors is directly proportional to the area of the electrode, it is necessary to either control the area of the electrode or correct for variation in the signal due to fluctuations in the electrode area. Control of the electrode area is either through printing of an insulating dielectric ink over the electrodes or by laminating a spacer layer over the electrodes with a controlled-size opening to form the sample chamber [59, 71]. If the electrodes are coplanar, a top covering of the web, generally transparent to provide a view of the sample chamber, is laminated on top of the spacer layer to form the sample chamber. The transparent cover gives the user visual confirmation of successful dosing. When the working and counter electrodes are in a facing configuration, the top layer is formed from one of the electrodes and the sample chamber is confined to the space between the electrodes. With both configurations, the height of the capillary sample chamber is defined by the spacer layer and is a critical dimension for the reproducibility of the signal response. Most electrochemical SMBG test strips include one or more electrodes to indicate when sufficient sample has been introduced into the sensor to perform a reliable method. These fill detection or sample sufficiency electrodes may or may not be part of the working/counter electrode system.

The active ingredients, enzymes, cofactors, and mediators, discussed in the section above, must be included in a reagent formulation which provides a stabilizing matrix for these active ingredients in the dry form [59, 71] and is also conducive to reproducible reagent deposition onto the electrode structures as a wet reagent. These matrix components may include film-forming polymers, buffers to maintain pH, enzyme stabilizers (e.g., trehalose, bovine serum albumin), surfactants, and non-soluble fillers. Reagent formulations are deposited on the electrode structures by a variety of methods. Screen printing [5, 70, 72, 172] is commonly used for depositing regents on electrode structures. Slot-die coating, used in the

Accu-Chek® Aviva and Accu-Chek® Performa product families, is an effective way to coat a narrow reagent stripe over the working and counter electrodes [71, 173, 174]. Use of slot-die coating for reagent deposition ensures a well-controlled, uniformly-thick reagent layer. The properties of the reagent formulation, such as viscosity, solids content, and surface tension, must be formulated to accommodate the specific requirements of the particular reagent deposition method. The drying process must be managed to preserve the active ingredients as well as maintain the quality of the reagent film. Drying should be rapid, so that the enzyme is only exposed to the warm, wet environment which promotes enzyme denaturation for a short period [71]. The optimization of the drying process depends on the properties of the reagent formulation.

The primary packing for most SMBG strips is a desiccant-containing vial. The vial serves to protect the strip reagent from exposure to humidity, which can cause degradation of the active ingredients. The number of strips contained in a vial can vary depending on the stability of the strip components or intended use case (sample packs, kits, or full-count vials), with common strip counts per vial of 10, 25, and 50 strips per vial. Alternative primary packaging was introduced by two competing systems. The Abbott FreeStyle® Optium™ test strip is foil packaged individually. The Ascensia Breeze® system features a foil packaged disk which contains 10 strips.

The manufacture of SMBG systems in the United States is covered by CFR 820 "Quality System Regulation" [23], which includes regulations for establishing a quality policy, design controls, purchasing controls, production and process controls, as well as many other facets of medical device manufacturing. In the EU, manufacturers of SMBG systems must demonstrate that the system meets the requirements in the In vitro Diagnostic Directive in order to place the CE mark on the product [175].

3.3 Performance of Systems Used for SMBG

In order to ensure that SMBG systems provide results suitable for the management of diabetes, standards and guidance documents have been developed to assess the performance and usability of SMBG systems. In the United States, the Food and Drug Administration approves systems for sale. The EU uses the ISO 15197 standard for performance evaluation [17, 175]. The requirements proposed by the FDA [16], as defined in the draft guidance document "Self-Monitoring of Blood Glucose Test Systems for Over-the-Counter Use," and the ISO15197:2013 standard have some commonality, although the FDA guidance document, published in 2014, differs from the ISO15197:2013 in some key areas, such as the evaluation of system accuracy. The FDA has also issued draft guidance for blood glucose monitoring systems used in POC settings, titled "Blood glucose monitoring test systems for prescription POC use" [14]. The draft guidance for POC systems differs in some ways from the FDA draft guidance for SMBG and ISO 15197. The draft guidance

documents from the FDA are currently under revision, and their final form has not been determined; SMBG products are not being cleared according to these draft documents. The ISO 15197 and FDA Draft Guidance documents for SBGM requirements are discussed in the sections below. The inclusion of the draft guidance documents is intended to give the reader an overview of what the FDA requirements may be in the future.

Since SMBG and POC systems may use different enzymes, mediators, materials, and measurement methods, it comes as no surprise that the claim ranges with regard to operating temperature, humidity, hematocrit, interference substances, and shelf-life are unique to each particular system. When comparing performance between systems, one should keep in mind these characteristics in order to make a clear one-to-one comparison of performance.

3.3.1 Reference Methodology

Although SMBG measurements are made on whole blood samples, the preferred method of reporting the BG value is the plasma equivalent [3, 16, 17, 100] to make comparison to plasma clinical analyzer glucose values less confusing [3]. The recommended constant conversion factor of 1.11 is used to convert the whole blood glucose value to the plasma equivalent. This conversion factor is derived from the relationship between activity, molality, and concentration of glucose in sample types and gives the plasma-equivalent result for when the hematocrit and water concentration in the blood sample are normal, i.e., 43% hematocrit. The sample hematocrit, however, may not be the normal 43%. In that case, a correction factor which takes into account the impact of hematocrit can be calculated based on the equation 0,84/(0,93-0,22 * Hct) [176]. While some manufacturers use a conversion factor of 1.11 over the range of samples, others may use a conversion factor that takes the hematocrit into account. When evaluating SMBG performance, it is of critical importance to make sure the plasma-equivalent correction specific to a manufacturer has been applied to BG results in order to avoid bias when comparing to a reference method.

The most common reference methods used in strip performance evaluation are the GOx-based YSI method and the hexokinase method, described briefly below. The commonality of these two methods is that both are traceable to certified reference material where the true glucose value has been determined by the primary NIST glucose reference measurement procedure [177, 178], isotope dilution gas chromatography mass spectrometry (ID/GC/MS). Although ID/GC/MS is the gold standard for determining glucose values, it is unsuitable for the large volume of samples which are processed during product processing and performance evaluation [51].

The hexokinase method for measuring glucose is based on the coupled enzymatic reactions of D-glucose and ATP in the presence of hexokinase to produce glucose-6-phosphate and ADP. The glucose-6-phosphate is then converted to gluconolactate-6-phosphate by NADP-dependent glucose-6-dehydrogenase. By

monitoring the NADPH produced in the second enzymatic step at 340 nm, the concentration of glucose in the sample is determined. Either plasma samples or whole blood samples that have been deproteinized by perchloric acid precipitation may be analyzed by this method. This method is available on many of the Roche Diagnostics Cobas® analyzers. The GOx method, as used in the YSI 2300, is based on the conversion of D-glucose in the presence of oxygen to D-gluconolactone and hydrogen peroxide by GOx immobilized between a polycarbonate membrane and a cellulose acetate membrane. The hydrogen peroxide is detected electrochemically at a platinum electrode. Both plasma and whole blood samples may be analyzed by this method.

The inherent differences in the reference methodology used for evaluation of system accuracy have a direct impact on evaluation of system accuracy. A significant difference in plasma samples is commonly observed between the hexokinase and GOx methods, which can be as great as 8% of the glucose concentration determined by the hexokinase method [36, 179, 180]. If the accuracy of a SMBG system is evaluated using a different reference method than the one used by the strip manufacturer, the apparent performance of the SMBG system may be considerably different than what is reported when using the correct reference method. ISO 15197:2013 defines a reference measurement procedure as an accepted procedure which is fit to assess the measurement trueness of measured quantity values obtained from other measurement procedures for quantities of the same kind. Nevertheless, there is sometimes lack of agreement around what is meant by this definition with regard to sample and accepted measurement method. Commonly, the concentration of glucose is measured in a plasma sample using the hexokinase or YSI methods described above. Schnell et al. call for a more strict definition of reference method [181] to avoid any confusion between the more routine analysis of plasma blood glucose by analyzer for routine laboratory methods and a "true" reference method, where the values determined in the reference method are directly traceable to a reference standard.

3.3.2 Regulatory Guidance

In order to obtain the Conformité Européenne (CE) mark, which is required for launching a product in the EU, the SMBG product must meet the performance and design requirements set out in ISO 15197 [17]. Briefly, ISO 15197 describes the requirements for system accuracy, user performance, measurement precision, interferences, and stability of the materials used in a SMBG system, as well standardized methods for evaluation of these system metrics. ISO 15197 was first published in 2003; the standard published in 2013 reflects the call for better performance for SMBG systems and the advancements in SMBG technology since the publication of the first standard in 2003. While ISO15197:2013 has not yet been harmonized under the IVD directive at the time of this publication, most manufacturers are demonstrating compliance to the 2013 version of this standard in published documents. The FDA guidance for SMBG is still in draft form at the time of this writing

Table 2 Minimum SMBG System Accuracy Criteria according to the ISO 15197 standard in its 2003 and 2013 versions and the FDA draft guidance document from 2014

	ISO 15197:2003		ISO 15197:2013		FDA[a]	
Relative number of results	95%		95%[b]		95%	99%
Within	±15 mg/dL	±20%	±15 mg/dL	±15%	±15%	±20%
At BG concentrations	<75 mg/dL	≥75 mg/dL	<100 mg/dL	≥100 mg/dL	Entire range	
			99% of results within CEG zones A + B			

[a]FDA draft guidance for self-monitoring blood glucose test systems for over-the-counter use, published in 2014 [16]
[b]In ISO 15197:2013, this acceptance criterion is also applied for the user performance evaluation [17]

[16]. One of the major differences between the FDA draft guidance document and ISO 15197:2013 is in how the evaluation of system accuracy is performed. The minimum accuracy criteria require that at least 95% of measurements fall within ±15% and at least 99% fall within ±20% of the reference value across the entire claimed glucose measurement range. Table 2 (adapted from Table 1 in Freckmann et al. [182]) compares the minimum SMBG System Accuracy Criteria from the ISO 15197 Standard (2003 and 2013) with the FDA 2014 Draft Guidance document [16, 182]. The system accuracy requirements as proposed by the FDA are quite stringent, and there is considerable concern among industry and medical experts about the ability of most commercially available systems to meet the criteria.

In addition to minimum SMBG system accuracy performance, ISO 15197 and the FDA 2014 Draft Guidance documents include testing requirements for measurement precision (measurement repeatability and intermediate precision), "influence quantities" (hematocrit and interferences), stability of reagents, and materials. While the types of testing called out in the documents are similar, the specifics of the testing vary between the documents, with the procedure and acceptance criteria being significantly different.

Device performance can be quite different in the hands of a home user when compared to trained laboratory personnel. As part of the ISO standard, "real-world user" testing has been included as one of the criteria for judging system performance. Users are given instruction for using the system and not given any further training or assistance, and their operation of the system is observed by professional personnel. The FDA also has specific requirements for user performance; the system accuracy testing described in Table 2 includes the requirements that three lots of SMBG strips must be used in the testing, with at least 350 users. Of the 350 users, at least 10% must be naive to SMBG systems. If sufficient users are not available to cover the whole glucose range, contrived samples may be used to supplement the user samples in order to extreme set glucose concentrations.

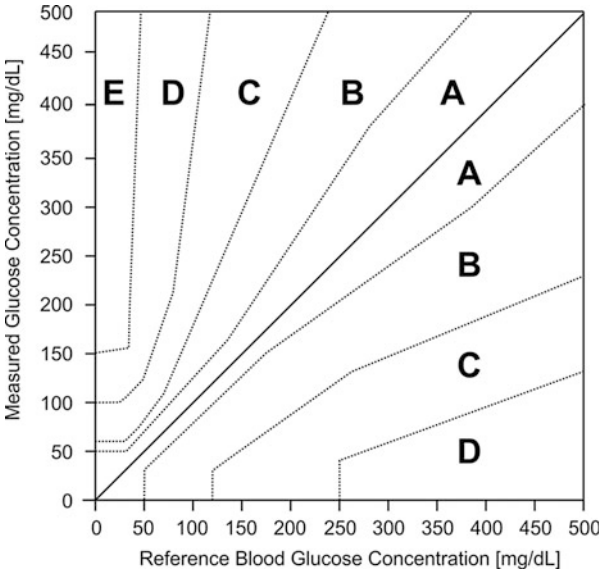

Fig. 3 Consensus Error Grid for Type 1 diabetes management and regulatory purposes. Zones A through E represent areas of clinical risk that may result from error in a measured BG value

3.3.3 Performance Assessment

Consensus Error Grid and Estimation of Clinical Impact

The Clarke Error Grid was developed in 1987 to assess the accuracy of blood glucose meters through the lens of clinical impact of BG error on treatment decisions [183]. In essence, the measured BG value is plotted against the "true" BG value for a particular sample as measured with a reference method. The plot is subdivided into five different risk categories: Region A, where there is no effect of BG error on clinical action; Region B, where the BG error makes little or no impact on clinical action; Region C where the clinical action taken based on the erroneous BG result is likely to have an effect on clinical outcome; Region D, where the BG error results in altered clinical action that carries significant medical risk; and Region E, where the BG error results in altered clinical action that could have "dangerous consequences." One issue that was identified with the Clarke Error Grid is the discontinuity in the regions, where a region where no to little clinical impact would result bordered a region where a decision made on an erroneous BG measurement would have a potentially harmful clinical impact. A more recent modification is the Consensus Error Grid, shown in Fig. 3, developed by Parkes et al. [184], which represents an evolution of the Clarke Error Grid.

Two Consensus Error Grids (EGs) have been prepared: one for Type 1 and a second for Type 2 PwDs on insulin therapy [184]. The difference between the two EGs was based on the opinion of Parkes survey respondents that a T2 insulin-dependent PwD would be able to tolerate BG measurements a larger error than a T1 PwD. However, the creators acknowledge that the T2 EG has not found widespread

use. The T1D Error Grid is widely used to assess meter performance and is what is commonly referred to as the Consensus Error Grid or the Parkes Error Grid and has gained wide acceptance as a tool for assessing glucose meter performance.

Surveillance Error Grid

Against the background of improvements in the clinical accuracy of SMBG systems, expectations around better performance of SMBG systems, new treatment targets for T1 and T2 PwDs, greater use of insulin pumps, and availability of new insulin analogs, the Surveillance Error Grid (SEG) was developed by Klonoff et al. [185, 186], including representatives from the Food and Drug Administration, American Diabetes Association, the Endocrine Society, and the Association for the Advancement of Medical Instrumentation, with these changes in mind. Input from 206 diabetes clinicians in response to a survey where the respondents were asked to evaluate fictitious scenarios and respond with clinical risk associated with errors in measured BG levels. From this input and modeled data that represents the system accuracy of current SMBG system, the SEG was developed. The SEG presents the clinical risk with higher resolution than previous error grids with 15 risk zones and is presented in a color-coded plot that makes it intuitive for the clinician to understand the risk associated with error in BG measurements. The SEG is not intended by its creators for premarket evaluation of SMBG performance, but is intended as a tool for regulatory bodies and manufacturers to monitor SMBG system performance as part of surveillance programs [185, 187].

Other Means of Visualizing SMBG Performance Data

The simplest way to represent performance data is through a regression plot, where the measured BG values are plotted against the reference or comparative method (e.g., YSI or hexokinase value) and regression statistics provided. Reference lines from various standards/guidance documents or user-imposed limits can be included in the plot to aid in evaluation of performance. This method of visualization allows the user a quick overview of the general performance of the data being evaluated. Bland-Altman plots are another useful way to visualize SMBG performance data [188]. This type of plot allows the user to see both the bias and imprecision in a set of SMBG data over the measured glucose range by plotting the difference in the BG result from the comparison method (either as a percent or absolute bias) on the y-axis against the comparison glucose value on the x-axis. Incorporation of reference lines from different guidance documents, such as ISO 15197:2013 or the FDA draft guidance, can be included in modified Bland-Altman plots in aid in visualization of performance [187]. Radar plots are intended to be a more intuitive way of visualizing the same type of data presented in the modified Bland-Altman plots, where the difference between the measured value and reference value for each measurement is plotted using polar coordinates, giving the plots a target-like appearance. Circular

reference lines, representing the 15 mg/dL/15% or 10 mg/dL/10% boundaries, may be included to help the viewer in visualizing system performance [187]. Lastly, Rectangle Target Plots [189, 190] provide a way to compare performance of multiple SMBG systems in an intuitive manner. In this visualization method, the data for one particular system under evaluation (e.g., one lot of test strips) is presented as a single rectangle, where the center point of the rectangle represents the mean bias of the system and the length of the sides of the rectangle represent the tolerance interval for BG levels <100 mg/dL (x-dimension) and ≥100 mg/dL (y-dimension). Thus, the size of the rectangle is an illustration of the measurement variability of the system. Since the system performance is represented by a simple rectangle, multiple systems may be compared on the same plot without the confusion of many data points. Reference rectangles for 15 mg/dL/15% or 10 mg/dL/10% systems can be included to aid in visualization.

Beyond the Regression Line

Other metrics are used to describe SMBG system performance in addition to the methods discussed above. While none of the metrics may be sufficient themselves to describe SMBG system performance, combination of performance metrics allows for a better understanding of system performance.

- Total error (TE) [191] – system error plus user error; difference between the observed glucose value and the true glucose value. A model used for estimating total error can be expressed as [192]

$$\%\mathrm{TE} = \%\mathrm{Bias} + 1.96(\mathrm{CVT}),$$

where %TE is the percent total error, %Bias is the percent average bias, and CVT is the total coefficient of variation due to imprecision. While this model is simple and popular, it can underestimate total error.

- Mean absolute difference (MAD) and mean absolute relative difference (MARD) – MAD and MARD quantify the performance in an entire data set within a single value. MARD is a good metric for comparing multiple systems in a single study, but is not useful itself to describe system quality [187, 193].

$$\mathrm{MAD} = \frac{1}{n}\sum_{i=1}^{n} |\mathrm{Meter}_i - \mathrm{Lab}_i|,$$

$$\mathrm{MARD} = \frac{1}{n}\sum_{i=1}^{n} 100\frac{|\mathrm{Meter}_i - \mathrm{Lab}_i|}{\mathrm{Lab}_i},$$

where Meter is the measured BG value, Lab is the reference value for the sample, and n is the number of blood samples.

- Hematocrit interference factor (HIF) [166, 194] is defined as the largest observed bias above the nominal hematocrit + the largest observed bias below the nominal hematocrit. An HIF <15% for an individual glucose level and a mean HIF over the glucose range <10% has been arbitrarily defined as indicative for no clinically relevant influence of hematocrit on the BG readings [166, 194].

3.3.4 System Performance of SMBG and POC Systems

There is a large body of literature around evaluating the performance of SMBG and POC systems. For SMBG systems, both independent and manufacturer-sponsored evaluations are available. The same is true for POC systems. The reader should be aware that not all studies will follow ISO 15197 guidelines (Table 3); while this does not necessarily make a statement about the quality of a particular study, the reader should take into account different study parameters when comparing performance data presented in the literature. Table 4, shown at the end of this section, summarizes some of the relevant publications from 2012 to present. The list in Table 4 is, by no means, an exhaustive list of the literature that has been published and is meant to provide a sample of what is available. A study stands out for the large number of BG systems assessed at once according to the ISO 15197 standard [195]. Freckmann et al. performed system accuracy evaluation on 43 SMBG systems, both electrochemical and optical, using the reference methodology defined by the manufacturer. Systems assessed include representatives from Roche Diabetes Care, Lifescan, Bayer, and Abbott, as well as smaller manufacturers. One lot of strips per system was tested. This study found that, out of the 34 systems that were assessed completely, only 18 of the systems met the minimum accuracy requirements of ISO 15197:2013. All of the Accu-Chek® products evaluated in this study, Accu-Chek® Active, Accu-Chek® Aviva, Accu-Chek® Aviva Nano, Accu-Chek® Compact Plus, Go, Accu-Chek® Mobile (both the original formulation and maltose-independent formulation), Performa (both the original formulation and maltose-independent formulation), and Accu-Chek® Performa Nano, met the ISO 15197:2013 criteria. A concise plot of the bias for all systems is found in [195] (Fig. 2 therein).

Gijzen et al. evaluated four POC meters (Accu-Chek® Inform II, HemoCue® Glu201DM, Nova StatStrip®, Abbott Precision Xceed Pro™) and one SMBG consumer system (Menarini GlucoCard Memory PC) for use on sample collected from critically ill ICU patients who were under a tight glycemic control (TGC) protocol [196]. Results were compared against the ISO 15197 standard; since this study was published in 2012, the ISO 15197 standard used was not the more stringent ISO 15197:2013. Results were also compared against the Netherlands Organisation for Applied Scientific Research (TNO) quality guidelines (PG/TG/2001.045) and the National Academy of Clinical Biochemistry/American Diabetes Association (NACB/ADA)-2011 guidelines [13]. The NACB/ADA guidelines (greater than 95% results must be within ±15% for values greater than or equal to 100 mg/dL and within ±15 mg/dL for values less than 100 mg/dL) are similar, in

Table 3 Tabular representation of data of the study performed in Gijzen et al. [196], showing the results of 390 paired glucose measurements in 80 ICU patients

	Number	Mean glucose concentration (mM)	Range (mM)	Pearson correlation	% ISO	% TNO	% NACB/ ADA
Abbott	379	8.2 ± 2.1	3.7–17.6	0.94	96.6	94.2	93.4
HemoCue	391	8.3 ± 2.0	3.8–19.1	0.929	95.1	91.0	89.2
Menarini	391	6.9 ± 2.1	2.7–16.2	0.936	63.3	47.7	45.4
Nova	391	7.3 ± 1.9	3.3–15.0	0.964	91.0	81.8	77.9
Roche	389	8.3 ± 2.1	3.1–17.7	0.964	99.5	96.1	95.6
BioSen	389	8.1 ± 2.1	3.5–16.6	0.973	98.7	97.7	97.4
RapidLab	380	7.8 ± 1.9	3.4–16.3	0.986	100	99.2	98.9
DxC-800	390	8.1 ± 2.0	3.6–17.1	–	–	–	–

principle, to ISO 15197:2013. The results are summarized in Table 3. The Accu-Chek® Inform II system met the requirements of all three standards when all available samples were considered. The next-best performing system in this study was the Abbott Precision Xceed Pro™, where that system met the ISO 15197:2003 requirements. When the neonatal samples with low glucose values were considered, again, the Inform II met the requirements of all three standards, the Nova StatStrip meeting the ISO 15197 and TNO requirements. One aspect that should be considered is that the number of neonate samples, $n = 15$, with low glucose values was very small.

3.3.5 Calls for Improved Performance and Postlaunch Monitoring

Despite the tighter system performance criteria introduced in ISO 15197:2013 and proposed in the draft FDA guidance, there are still calls for improved system performance from groups such as the American Association of Clinical Endocrinologist, American Association of Diabetes Educators, and the patient advocacy group Strip Safely [1, 11, 38, 99, 197–199]. The ADA has called for future SMBG systems to be made with an analytic error of 5% [199]. The most pressing concerns, according to these groups, include accuracy of the BGM system at low glucose and the lack of post-marketing surveillance of approved SBGM systems. In 2013, the Diabetes Technology Society held a one-day public meeting of diabetes experts, presided over by its president, David Klonoff, to discuss several questions around SBGM systems and their ability to meet current regulatory standards. Protocols for testing SBGM systems postlaunch are currently being developed [200]. Publications where SMBG systems are evaluated according to ISO15197:2003, ISO15197:2013, FDA draft guidance, and so-called "10/10" and "5/5" criteria are becoming more common [195, 201–204]. The 10/10 criteria require greater that 95% of strip BG values are within 10 mg/dL of the reference result for BG values below 100 mg/dL and 95% of the strip BG values are within 10% of the reference result for BG values above 100 mg/dL. The 5/5 criteria are similarly defined for 5 mg/dL and 5%,

Table 4 Systems additional performance studies and reviews

Ref.	Year	SMBG systems	Sample type	Notes
Sølvik et al. [201]	2015	Accu-Chek® Aviva Accu-Chek® Mobile Ascensia Breeze® 2 Contour® XT DANA DiabeCare® IISG FreeStyle Lite® GlucoMen® LX Mendor Discreet mylife™ Unio™ OneTouch® Verio®	C	System accuracy according to ISO 15197:2004, ISO 15197:2013 and FDA SMBG draft guidance as performed by biomedical laboratory scientists and PwDs Manufacturer's reference method was used for the appropriate system
Link et al. [486]	2015	Accu-Chek® Aviva Contour®XT GlucoCheck XL GlucoMen® LX Plus	C	System accuracy according to ISO 15197:2003, ISO 15197:2013 Manufacturer's reference method was used for the appropriate system
Klaff et al. [487]	2015	Accu-Chek® Aviva Contour® Next FreeStyle Lite® OneTouch® Ultra® Blue OneTouch® Verio® TRUETrack®	C	YSI used as reference method for all systems
Freckmann et al. [488]	2015	Accu-Chek® Aviva Contour® XT GlucoCheck XL GlucoMen® LX Plus	C	System accuracy according to ISO 15197:2003, ISO 15197:2013 Manufacturer's reference method was used for the appropriate system
Dunne et al. [489]	2015	Accu-Chek® Active Accu-Chek® Performa OneTouch® Select Simple FreeStyle Freedom®	C	YSI used as reference method for all systems Consensus Grid analysis
Demircik et al. [490]	2015	Accu-Chek® Aviva Nano Accu-Chek® Performa Contour® XT Contour® Link Freestyle Freedom Lite® mylife™ Pura® MyStar Extra® OneTouch® Verio®	Venous	Hematocrit variation
Pfützner et al. [218, 491]	2012, 2014	Accu-Chek® Aviva BGStar® iBGStar®	C	System accuracy according to ISO 15197:2003, ISO 15197:2013

(continued)

Table 4 (continued)

Ref.	Year	SMBG systems	Sample type	Notes
		FreeStyle Freedom Lite® Contour® OneTouch® Ultra® 2		YSI used as reference method for all systems
Huang et al. [492]	2014	Accu-Chek® Performa Rightest® GM700	C, V	System accuracy according to ISO 15197:2013 Test subject population included persons with and without diabetes, neonates, patients on respiratory therapies, hemodialysis, or peritoneal dialysis
Hsu et al. [493]	2014	Rightest® GM550	C, V	Testing performed by test subjects and technicians HK used as reference method for all systems System accuracy and imprecision according to ISO 15197:2003 Evaluation of autocoding feature
Freckmann et al. [202]	2012	Accu-Chek® Aviva BGStar® Contour® XT GE100 GE200 mylife™ Pura® mylife™ Unio™ GL40 Omnitest® 3 OneTouch® Verio® System x System y	C	System accuracy according to ISO 15197:2003 Manufacturer's reference method was used for the appropriate system System names for x and y not shown due to legal reasons (missed accuracy requirements)
Ramljak et al. [194]	2013	Accu-Chek® Aviva Accu-Chek® Aviva Nano Accu-Chek® Active Contour® Breeze®2 OneTouch® Ultra® 2 OneTouch® Verio® Precision Xceed® Optimum Xceed® FreeStyle Freedom Lite® TaiDoc Fora TD-4227 GlucoMen® LX Plus Glucofix® mio Plus GlucoLab™	V	Hematocrit variation YSI used as reference method for all systems

(continued)

Table 4 (continued)

Ref.	Year	SMBG systems	Sample type	Notes
		GlucoDr. Auto™ On Call® Platinum On Call® Plus NovaMax® Plus NovaMax® Link		
Halldorsdottir et al. [494]	2013	Accu-Chek® Aviva Contour® Next EZ FreeStyle Freedom Lite® OneTouch® Ultra® 2 TRUEtrack®	C	YSI used as reference method for all systems
Brazg et al. [495]	2013	Accu-Chek® Aviva Plus Advocate® Redi-Code Element™ Embrace Prodigy Voice® TRUEbalance™ Wavesense™ Presto®	C	System accuracy according to ISO 15197:2003 Manufacturer's reference method was used for the appropriate system Multiple lots of test strips tested
Pfützner et al. [167]	2013	Accu-Chek® Aviva Accu-Chek® Aviva Nano BGStar® iBGStar® Breeze® Contour® Freestyle Freedom Lite® GlucoMen® LX GlucoCard G+ Precision Xceed® OneTouch® Ultra® 2 OneTouch ®Verio® 2 MediTouch®	V	Hematocrit variation YSI used as reference method for all systems
Teodorczyk et al. [496]	2012	OneTouch® Verio®	V	Hematocrit variation
Tack et al. [497]	2012	FreeStyle Freedom Lite® FreeStyle Lite® OneTouch® UltraEasy® Accu-Chek® Aviva Contour®	C	YSI used as reference method for all systems Test subject performed testing
Baumstark et al. [498]	2012	Accu-Chek® Aviva FreeStyle Lite® GlucoCheck XL mylife™ Pura®	C	System accuracy according to ISO 15197:2003 Manufacturer's reference method was used for the

(continued)

Table 4 (continued)

Ref.	Year	SMBG systems	Sample type	Notes
		OneTouch® Verio® Pro		appropriate system Multiple lots were tested
		POC Systems		
Ceriotti et al. [499]	2015	Accu-Chek® Performa FreeStyle Optium™ StatStrip®	V	Hematocrit variation, interference, and precision
Freckmann et al. [203]	2014	Accu-Chek® Inform II BGStar® BIOSEN C_line HemoCue® Glucose 201+ GLUKOMETERPRO StatStrip®	C	YSI used as comparison method for all systems Trueness and precision assessed following CLSI EP15-A2
Dietzen et al. [500]	2013	Accu-Chek® Inform II Accu-Chek® Performa Accu-Chek® Aviva	N	Multiple lots tested
Zueger et al. [501]	2012	Accu-Chek® Aviva Contour® FreeStyle Lite®	C	HemoCue Glucose 201+ was used as the reference method for all systems
Robinson et al. [502]	2012	Accu-Chek® Performa Contour® TS Nova Max® StatStrip® OneTouch® Ultra®2 Optium Xceed™	C	YSI used as comparison method for all systems

C capillary, *V* venous, *N* neonate

respectively. For comparison, the current ISO 15197:2013 standard calls for strips to meet "15/15" performance criteria, where greater than 95% of strip BG values are within 15 mg/dL of the reference result for BG values below 100 mg/dL and greater than 95% of the strip BG values are within 15% of the reference result for BG values greater than 100 mg/dL. Some systems are also not passing the accuracy standards under which the systems were approved [195, 202, 205, 206]. More pressure has come from professional organizations and diabetes advocate groups for post-market surveillance of SMBG systems [206, 207]. Considerable discussion is ongoing on how to implement as post-market surveillance program with regard to funding, oversight, and reporting of the results of evaluations [200, 208, 209]. Challenges for manufacturers accompany tighter requirements on SMBG systems. Technical challenges for improving system performance may lead to compromises on system design, such as larger devices, larger blood volume required for testing,

and higher costs for the end consumer [38]. There is limited clinical support for improving system performance requirements beyond ISO 15197:2013 [210]. Simulation data based on clinical data from institutions where patients were undergoing tight glycemic control showed that for total allowed system error of 20%, significant insulin dosing errors were predicted to occur where hypoglycemia would result. In contrast, the simulation models for total error of 15% predicted that large insulin dosing errors would occur "very infrequently," with reduced total error of 10% reducing the frequency even more. However, there is more study needed to understand the frequency of dosing errors and the actual clinical impact of such dosing errors [210–214].

As with consumer SMBG systems, there are calls for improvement in POC blood glucose monitoring systems [32, 42, 195, 215]. Tight glycemic control is often a treatment goal for patients in critical care situations to improve outcomes [216, 217]. However, blood glucose measurement error can lead to adverse events. In addition to the measurement error that is due to normal system operation, error due to the influence of extreme sample conditions, such as low or high hematocrit, variation of sodium levels, interference from drug therapies (e.g., icodextrin, intravenously administered ascorbic acid), or oxygen pressure, must be taken into account when evaluating the system performance and use of POC BG systems [191, 218, 219]. Manufacturers endeavor to produce systems that are as robust as possible to interferences and extreme sample conditions to maintain patient safety, and HCPs must be aware of system limitations of the particular POC BG system that is in use in their clinical setting.

3.4 SMBG Outlook

It is undeniable that the performance of SMBG systems has increased tremendously over the last four decades, helping the PwD to achieve better health as part of the day-to-day management of diabetes. Technological advances have allowed systems to be useful over wide temperature, hematocrit, and blood glucose range, while test time and sample size have decreased dramatically [52, 220, 221]. SMBG is part of the necessary toolkit for managing T1 and T2 diabetes. Looking ahead, the demands on SMBG system performance are expected to grow even as the pressures to lower the cost of systems increase. The drive for the future is to continue to push the limits on system performance while lowering cost, all while finding ways to provide the best medical value to PwDs and HCPs.

4 Continuous Glucose Monitoring (CGM)

Continuous Glucose Monitoring (CGM) has generated large research interest over the last decades. Consequently, there are many reviews which allow for a very good overview of employed techniques, results, trends of development, and challenges which remain to be mastered [222–232]. The emphasis of this review is the description of sensor technology which is currently used in CGM systems. We shall therefore focus on the description of minimally invasive electrochemical biosensors and associated systems. Prior to describing technical sensor details from our industry perspective in Sect. 4.2.2, we try to offer a sufficiently detailed overview about published insight concerning the sample matrix, subcutaneous tissue (see Sect. 4.2.1). We hope the reader will excuse the extent of this section after appreciating that subcutaneous tissue constitutes a highly variable, and if one may say so in a scientific context, hostile environment from the sensor's perspective. Since differences between BGM and CGM systems, as we encounter them, are very significant, the reader may find a structured overview in Sect. 4.2. Prior to and during use, the quality of any CGM sensor and CGM system is assessed by the patient, healthcare professional, payers, and regulatory authorities. We thus feel obliged to start this review with requirements (see Sect. 4.1).

4.1 Requirements

4.1.1 Personal User Requirements

PwDs, who rely on insulin therapy and currently utilize SMBG in order to monitor blood glucose levels, have been increasingly using CGM systems for different reasons. Patients on multiple daily insulin injections (MDI) are looking for a system which provides not only glucose concentration but also glucose trend information. Application as well as wear of sensor-patches is expected to be painless and hassle-free, to compare favorably with finger-pricking and blood dosing. SMBG required for CGM sensor calibration should be kept to a minimum; the recorded data is desired to offer the same performance as SMBG systems over a maximum time span of at least 1–2 weeks and should be displayed whenever requested by a separate receiver. Demands on the allowable distance between the patch worn on the body and a receiver, which displays data and which may transfer data to secondary devices, vary largely. Parents and caregivers who want to monitor the glycemic status of a child require long-range communication capabilities in contrast to individual patients who do not transfer data directly to others or may only require read-on-demand data display. Patients who are relying on continuous subcutaneous insulin infusion (CSII) introduce additional demands onto a CGM system targeted toward increased safety and improved control of diabetes. Clearly, reliable alarms, triggered when exceeding set glucose concentration levels or

leaving a defined glucose concentration range need to be implemented, asking for very high accuracy, precision, and reliability of sensor readout. Therefore, long-range communication between the body-worn patch and the receiver needs to be implemented to ensure communication under all relevant circumstances. Constant monitoring of glucose levels, i.e., constant display of the glycemic profile, must be possible in addition to continuous spot and trend information. Insulin bolus recommendation is expected, and ease of data transfer to the HCP is asked for. Patients who are concerned about nocturnal hypoglycemia have been interested in sensor-augmented, automatic pump shutoff (see also Sect. 4.3.1) and predictive alarms in order to feel safe. Improvement in sensor performance has also nurtured interest in more extended control of insulin pump action, i.e., the development of an Artificial Pancreas Device Systems (APDS). Due to the continuous use of insulin catheters, this patient group clearly is interested in integration of insulin dosing and subcutaneous glucose monitoring systems into one patch in order to facilitate use.

Current and soon-to-be launched CGM systems already meet some of the above requirements. Some expectations, however, will need to be adjusted. Sensor performance (see Sect. 4.3.2) has improved considerably, allowing for very good agreement of glycemic profiles derived from CGM data and SMBG reference measurements. Time of wear has been extended to up to 2 weeks [233]. Patch size has become attractively small, allowing for ease of wear. Trend information and alarms are being offered. First steps toward an APDS have been made. In short, patients have been experiencing unprecedented features more recently, which have allowed CGM systems to provide enhanced information about glycemic profiles and providing additional safety. However, CGM performance is inherently limited by physiological time lag between blood and interstitial fluid, in particular during phases of high glycemic variability. Consequently, CGM systems will be incapable to meet current SMBG performance metrics at every point in time (see Sect. 4.3.2 for CGM system accuracy). Also, accuracy will remain dependent on the number and the point in time of SMBG-based calibrations. Patch size will remain dependent on the required use and thus the derived system concept. Battery capacity needed to power measurement, recording, and importantly, data transfer, differs largely depending on measurement, recording frequency, and data transfer frequency, as well as communication range. The integration of insulin dosing and CGM remains challenging for two major reasons. Firstly, insulin catheters and CGM sensors tend to be worn for three days and 7–14 days, respectively. Secondly, the signal of current CGM sensors is influenced by insulin release, asking for spatial separation of insulin catheter and CGM sensor.

Summarizing, a one-size-fits-all CGM application offering ultimate accuracy which allows for insulin dosing, requiring no SMBG-based calibration, a body-worn patch barely larger than a fingernail, extensive and frequent long-distance communication over weeks of use, integrated with an insulin catheter, remains a considerable challenge. Increased adoption of CGM systems by different user groups may thus result in further differentiation of CGM systems in the future.

4.1.2 Healthcare Provider Requirements

CGM system requirements directed to a healthcare provider are greatly dependent on the setting and the use case. The settings can be broadly divided between inpatient and outpatient. The most common outpatient situation is an endocrinologist, diabetes nurse educator (DNE), or general practitioner (GP) managing the diabetes, and perhaps other conditions, of a patient during regular visits [234–236]. The workflow of the office visit demands efficient evaluation of the patient status, needs, and effective delivery of required care. The outpatient may use a professional CGM system or a personal CGM system. The professional CGM system may be a reduced-function system of the Holter Monitor type, which only records data over the use time, or it may be similar to the personal use systems which display calibrated glucose results on a separate device. Critical for the professional system is the ability to clean and disinfect any reusable system component. The outpatient system must meet the same requirements of robustness, ease of use, and convenience as a personal CGM system for the patient. It must also provide easy recovery of the stored continuous glucose data, any associated BGM data, and any auxiliary data collected by the patient over the use interval through transfer to, e.g., PC-based analysis software. The data must be quickly analyzed and formatted to a standard presentation for the HCP and patient. The software may implement rule-based evaluation of the results to guide the HCP in the analysis, recommendations, and education of the patient [237]. The performance required depends on the treatment or education goal of the professional system use [238]. Identification of the undiscovered hypoglycemia is an important goal [235, 239, 240] that is made difficult and less reliable by the performance of the available systems in the hypoglycemic range and the occurrence of signal deviations, or dropouts, especially at night [235]. A personal CGM system may be used by the HCP in the same way as a professional system [241] and must then meet similar requirements for download and evaluation of the saved results. There is no stringent requirement for cleaning and disinfection of any reusable part, however, as long as the system is used as a single patient system and not as a multiple patient system. A significant alternate use case for the outpatient professional continuous monitoring is the dialysis patient, many of whom are diabetic. Continuous glucose monitoring, by providing real-time feedback on the progress of dialysis, can optimize glucose control to prevent hypoglycemia and hyperglycemia during the dialysis procedure [242].

Care of a PwD in an inpatient setting requires managing glucose levels in circumstances which differ greatly from the patient's normal daily routine. Changes in diet, activity level, stress, illness, and other medications all affect the glucose levels and insulin sensitivity of the diabetic patient. In addition, patients without a diagnosis of diabetes frequently experience dysglycemia in an inpatient situation [243]. It has become increasingly clear that effective management of hyperglycemia in the hospital setting improves outcomes, reduces complications and length of stay, and thereby reduces costs [244, 245]. More aggressive management of

hyperglycemia, however, leads to increased risk of hypoglycemia and its associated morbidity [245, 246]. Current standards for managing glycemia [244, 247, 248] rely on POC blood glucose measurements, either with specific professional systems (e.g., Nova Biomedical Stat-Strip®, iStat® by Abbott) or with home-use systems or a hybrid system in which the same disposable is used with a professional meter (e.g., Accu-Chek® Inform II with Accu-Chek® Performa). Measurements are made periodically at 30-min to 6-h intervals, depending on the treatment protocol. The performance of these systems in the POC setting relative to laboratory analysis has been questioned, but the clinical value of the immediate result and treatment seems clear [32]. A CGM system for use in the inpatient environment does not need to have the equivalent ease of use and ergonomic requirements of a system for over-the-counter use, since the application and management of the system is performed by attending medical personnel. However, additional requirements similar to those relevant to the POC BGM systems become relevant, such as connectivity for monitoring and data transfer and periodic performance verification. Use of CGM in the inpatient environment would reduce the testing burden on the HCP and potentially improve the detection of hyper- and hypoglycemia [245, 249]. Clinical trials have been conducted comparing the performance of subcutaneous sensors in inpatient and critical care situations [250, 251]. The current focus is demonstrating equivalent or superior performance to blood monitoring. The performance required for maintaining good glycemic control has been compared with the performance of the current POC methods in simulation and found not to be the critical factor [216]. Performance guidelines for POC BGM are defined by CLSI POCT12-A3 and additionally by CLSI C30A [252]. These standards define performance in terms of pooled deviation of a large number of independent measurements from reference values in absolute or relative limits. Proposed guidance from the FDA has been recently issued that distinguishes requirements for professional POC use from regular over-the-counter (OTC) use systems. The Clarke Error Grid and the Consensus Error Grid define performance in terms of the possible occurrence of an error in the subsequent treatment.

In critical care situations, the benefits and risks of aggressive glucose control are similar to those found in the normal inpatient situation [253–255]. It is considered of such importance to management of all patients (not only PwDs) that integration into standard perioperative monitoring is becoming standard procedure [256]. However, the optimum target range for glucose and best management protocol remains under discussion [257–259]. Further, there is ongoing discussion of the real clinical performance requirements for optimal glucose control [191]. Finally, it has been suggested that the performance of subcutaneous CGM systems may be more influenced by the compromised physical state of a critical care, surgical, or ICU patient [215, 260] than by the action that might be taken based on the result [183, 184].

4.1.3 Payer Requirements

For CGM to receive reimbursement in outpatient use, it should be capable of providing the same or greater utility or significantly improve the standard of care and outcomes. Some currently available CGM products are labeled as adjunctive devices, meaning that the user should not make a significant treatment decision based on the CGM estimate only. Especially in the case of hypoglycemia or rapidly changing glucose concentrations, the user is advised to verify the CGM result with a BGM result.

Reimbursement for CGM for PwDs as an alternative or extension to blood glucose monitoring varies significantly across countries and across healthcare funding organizations [261]. Studies are beginning to show that the use of CGM can result in a reduction of HbA_{1c} in selected patient groups as well as decrease severe hypoglycemia [262, 263]. The American Diabetes Association statement of Standards of Medical Care in Diabetes 2014 indicates that under certain circumstances, CGM can improve the glycemic control of patients with T1 and T2 diabetes, even those under relatively good control [2]. Studies which demonstrate improvements in glycemic control in children are mounting [263, 264]. Nevertheless, many insurance providers limit reimbursement to cases in which specific problems in glycemic control are documented, such as frequent hypoglycemia, hypoglycemic unawareness, and failure to maintain good glycemic control as determined by HbA_{1c} values. Variability of reimbursement clearly raises similar questions, such as clarity, suitability, and transparency of criteria used for reimbursement decisions, as expressed recently by the European Diagnostics Manufacturing Association (EDMA) position paper on Health Technology Assessment for IVDs in the context of market access [130]. Professional use of episodic CGM for the evaluation of the glucose control of PwDs or being at risk of developing or progressing to diabetes is increasing greatly [235, 236, 271]. The development of standardized, automated data analysis and display tools is enabling HCPs to evaluate the status of a patient in a convenient way [272]. Diabetes management education is widely recognized as critical to managing the costly consequences of poor glucose control [124]. Professional CGM has been shown to improve communication and understanding of diabetes management principles. Studies documenting improvements in outcomes or reduction in subsequent costs of care are mounting [234, 271]. For the inpatient and critical care patient, there is adequate evidence to support not only the outcome benefit but the economic benefit of tight glucose control, at least in adult patients [273, 274]. Continuous monitoring must demonstrate satisfactory (equivalent) performance and either a significant improvement in outcome or significant cost or workflow benefit to be accepted as a routine replacement for BGM in the inpatient environment. Current studies are focused on comparing performance, after which improvements in outcome or workflow can be addressed.

4.1.4 Regulatory Requirements

The currently available CGM systems do not meet the performance standards of the BGM systems for regulatory approval (ISO15197). Especially in the hypoglycemic range and in times of rapid glucose change, the results can diverge significantly. Performance metrics equivalent to those for BGM have not yet been issued by regulatory organizations for CGM, but several proposals have been put forth and used in the evaluation of existing products and prototype systems [265–267]. The proposals vary in details, but in general require reference blood glucose values to be compared with time-matched CGM glucose estimates at certain times or in certain circumstances. The CLSI guideline performance metrics for continuous interstitial glucose monitoring (POCT05A) utilizes mean absolute relative deviation (MARD), which is similar to the ISO 15197 criteria in comparing estimated CGM values to reference values. MARD is known to be insufficient and unreliable as indicator of CGM system accuracy [268] due to differences in study protocols, i.e., potentially different numbers and types of study subjects, degree of glycemic variability monitored, duration and conditions of the clinical study, frequency and kind of reference measurements, as well as data analysis methods. Precision absolute relative difference (PARD) compares the results of two CGM devices and has been proposed as a useful method to ensure that the evaluation of sensor performance includes data from all of the use time of the sensor, not just when reference values are available. Error grid analysis of paired CGM and reference values is also discussed, with modifications due to the physiological time lag of the interstitial glucose and the addition of trend information in the CGM results [269, 270].

As previously noted, medical devices are developed and marketed under strict regulatory requirements to ensure safety and efficacy. The transcutaneous nature of the minimally invasive CGM systems on the market and in development creates additional requirements on the materials, processes, packaging, and delivery of the devices. In vitro diagnostic devices are considered to be a subclass of medical devices, and a separate EU regulation (98/79EC) applies. In contrast to in vitro diagnostic devices, medical devices need, e.g., a biocompatibility assessment, and for invasive sensors also sterilization, disinfection requirements apply. As such, the materials used in the construction of the transcutaneous part of the sensor, and the complete sensor itself, must be biocompatible in the sense that the sensor exhibits no toxicity toward the surrounding tissue.

ISO 10993 standard family regulates the testing required for a determination of biocompatibility for tissue contact devices. Cytotoxicity testing is a basic requirement for the biocompatibility assessment. The cytotoxicity assay requires the elution of the sensor with physiological saline and the evaluation of the effect of the eluate on living cells. This can be critical for enzymes which are not properly immobilized, plasticizers in substrates or membrane layers, and the often-used reference electrode material silver/silver chloride. Also relevant for CGM sensors, but not addressed by the elution test, is the effect of the enzymatic reaction in the sensor in the absence of polarization of the sensor. First-generation sensors which

function by oxidation or reduction of hydrogen peroxide at the working electrode may allow hydrogen peroxide to escape into the environment, while the sensor is not polarized. Sensors rely on catalytic materials to react with hydrogen peroxide to reduce the impact of this process by H2O2 disproportionation [275, 276].

Sterilization of the completed sensor which will be inserted into the user can be accomplished with any of the standard sterilization methods, but each has its drawbacks for electrochemical sensors. Radiation sterilization can damage the enzyme reagents as well as electronic components which may be part of the sterilized subsystem. The dosage of radiation must be controlled, and a certain reduction in enzyme activity must be expected. Heat sterilization also deactivates any enzyme-containing reagent. Chemical sterilization via, e.g., ethylene oxide is likewise destructive to the biochemical system, although not the electronics. Current products are sterilized via radiation, e.g., electron beams. The interaction of the sterilization method and other system components must also be considered. Radiation is known to influence the structure and performance of polymers and adhesives and may alter the cytotoxicity of the finished, packaged, and sterilized device [277, 278].

The regulatory requirements for biocompatibility and sterility increase the time and cost of product development for CGM sensors, as all materials and sensors to be used in any experimental programs or clinical trials must be evaluated and satisfy the requirements of the standards.

4.2 Monitoring Systems

Currently, advanced continuous glucose monitoring (CGM) systems differ from BGM systems in several respects. The nature and accessibility of sampling compartments are significantly different. Capillary blood, extracted from the fingertip, is widely used as a sample for BGM systems. Continuous sample extraction is, however, not feasible for CGM systems in an outpatient setting due to the impracticality of blood extraction and due to the difficulty of extracting sufficient volume of ISF over time of use [279]. CGM approaches have therefore relied either on indirect sampling of ISF or on direct measurement of glucose in fatty tissue at different insertion sites. Microdialysis and microperfusion probes have been used for indirect sampling, followed by extracorporeal detection of glucose within the microdialysate or microperfusate [280–284]. Microdialysis and microperfusion-based approaches benefit from using diluted ISF as the sampling matrix, which helps to attenuate the degree of biofouling of electrode surfaces. However, they add to system complexity, size, and cost due to the necessity of providing a high level of fluidic control at very low flow rates [285]. Most commonly, minimally invasive CGM systems utilize disposable so-called needle-type sensors which may seem to resemble miniaturized test strips at first sight yet reveal important differences at more detailed examination.

CGM needle-type sensors tend to be significantly smaller due to the need for implantation. Typical sensor widths and functionalized lengths of CGM needle-type sensors are in the range of 0.2–0.7 mm and 5–10 mm, respectively. CGM needle-type sensors need to prevent any electrode component from leaking into the tissue environment. Unlike in BGM sensors, CGM needle-type sensors may not utilize leachable mediators, enzymes, or electrocatalysts. Further, in contrast to BGM test strips, CGM needle-type sensors need to provide test electrodes whose composition does not change over the total time of measurement. This requirement has proven to be a major obstacle to highly accurate and reliable needle-type glucose sensors over a long time of CGM development and has thus attracted a multitude of research efforts (see Sect. 4.2.2). In the case of extracorporeal CGM flow-through sensors, the flow-system needs to prevent leakage of sensor components which may be toxic or may cause deterioration of sensor performance over time.

Further, there is a fundamental difference between BGM and CGM systems regarding number and nature of functional elements. The measurement of blood glucose fundamentally requires three functional elements: a disposable lancet to extract sample, a disposable test element to receive the sample and to generate a signal based on glucose concentration, and a reusable device to measure glucose concentration and to display its value. Commercialized needle-type sensor-based CGM systems also need to penetrate the skin barrier and need to place the sensor at a defined position within subcutaneous fatty tissue in a painless fashion, followed by extraction of a canula, immobilization via a bodymount which needs to be connected with a measurement and transmission unit which communicates with a separate receiver. Insertion depths of sensors are typically 8 to 10 mm underneath the skin surface, whereas lengths of sensors, which are inserted at an angle of either 45 or 90°, are typically between 8 and 15 mm. Typically a cannula of 0.45 to 1 mm diameter is guided into and out of subcutaneous tissue via an insertion device which can be implemented in a disposable [66] or reusable fashion [286]. Insertion depths of microdialysis, microperfusion catheters, or ultrafiltration probes are somewhat more variable compared with needle-type sensors due to manual insertion. Insertions angles are frequently not defined; however, typically a small angle is used for insertion in a skinfold. Microdialysis catheters as well as microperfusion probes, typically several centimeters long and less than 2 mm in outer diameter [280, 281, 283, 287], tend to be longer and somewhat wider than active sensing areas of implanted sensors.

Detection and calibration methods identified to be suitable for BGM and CGM systems are not identical. BGM systems are based either on photometric [71] or electrochemical [288] detection approaches, whereas CGM systems which have shown advanced clinical performance rely exclusively on electrochemical sensors. While BGM systems routinely rely on factory-based calibration of test element batches, only one continuous glucose measurement system [233] advertises the possibility of renouncing reference-based in vivo calibration measurements. Other CGM systems rely on the daily use of a BGM system for calibration of filtered CGM data [289, 290].

Data quantity per daily application of a BGM and a CGM system varies largely. For example, a frequent BGM user may sample seven times per day, generating seven glucose values which need to be stored in memory. The typical CGM user generates 288–1,440 glucose measurements (1 measurement/minute) which not only need to be stored but typically also require several data processing steps and regular data transfers to a receiving unit prior to displaying the result. The abundance of CGM data further asks for different display options in order to provide access to glycemic profiles as well as derived information, such as trend and forecasting information.

BGM systems need to ensure a reproducible mechanical interface between the measurement device and the test strip over the time of one measurement, which typically takes a few seconds. CGM systems need to do so over a time span of 6 to 14 days, while the system is worn by the patient during his daily routine which asks for different solutions of mechanical coupling and electrical connections. CGM measurement devices need to be attached to the patient's skin via adhesive patches commonly used for transdermal applications [291–293]. BGM test strips do not require sterilization prior to use. CGM probes or CGM sensors need to be sterile prior to use since they are inserted subcutaneously. Materials used for construction of the implants need thus to resist sterilization conditions, and the combination of materials needs to meet ISO 10993 biocompatibility requirements.

Size and weight of BGM and CGM measurement devices vary significantly from each other. In general, the size of BGM measurement devices tends to be determined by the ease to read displayed information and by the ease to perform the coupling of test strip and measurement device. BGM meter size is always balanced against the particular requirement of the respective user group. While BGM meter size has been decreased impressively (see, e.g., the Accu-Chek® Aviva Nano), larger BGM meters have been introduced into the market place [294–296], which integrate the measurement device, the test strip magazine, and the lancing device to allow increased facility of frequent testing. In contrast, CGM measurement devices, which are attached to the human body and require no display function, are designed to be as little and light as technically possible to allow for comfort and safety of discreet wear [66].

4.2.1 Sample Matrix

The immediate surroundings, the matrix, of any sensor affect mass transfer of educts and products from and to the sensor. Also, endogenous and exogenous interferents as well as ambient effects may lead to significant unspecific sensor response. These effects have successfully been tackled by BGM sensors (see, e.g., [297]). CGM sensors, which need to measure glucose continuously over days, have to tackle additional issues which complicate accurate, precise, and reproducible measurement over time. Issues will be listed and discussed in subsequent paragraphs.

1. The sample is typically not whole blood, but interstitial fluid (ISF). ISF glucose levels tend to lag behind blood glucose levels.
2. The ISF containing matrix, which surrounds the sensor, is typically fatty tissue, which is injured during insertion of the biosensor and is subsequently significantly changing its composition after insertion, as described briefly below. The diffusion coefficients of glucose, oxygen, potential interferents, and electrode reaction products may thus change over time. Oxygen itself is known to be present at varying concentration [298–300] and may lead to varying reaction rates at the electrode, depending on the respective sensor measurement technology (see section "Sensor Technology Used in Commercialized Systems").
3. Leakage of sensor components into the surrounding tissue needs to be prevented (see section "Enzyme Electrode").
4. Enzyme and electrocatalyst activity need to be maintained over time of use; electrode fouling [301] needs to be prevented. The choice of membranes and coatings, which shall be highlighted in sections "Diffusional Barrier Membrane" and "Biocompatible Coating", is of paramount relevance.
5. The sensor needs to withstand mechanical stress during time of wear. Integrity of sensor carrier foils or wires, typically 30 to 300 μm in thickness and conductive traces, typically 50 to 500 μm in width, needs to be guaranteed for reliable sensor function and for complete sensor extraction.
6. Artifacts induced by movement of the sensor within the sampling compartment need to be prevented by proper cutaneous immobilization of the sensor base.
7. Biocompatibility requirements which are described in ISO 10993 need to be met.

In general, ISF glucose levels are not identical to venous glucose levels at any time. ISF glucose levels were shown to be almost identical to venous plasma during steady state by microdialysis-based glucose extraction from ISF [302, 303]. It was also shown that ISF glucose levels are lower than plasma glucose levels, which is in agreement with whole blood glucose levels which are typically lower than plasma levels [304]. During times of rapid blood glucose change, levels from alternate sites differ considerably, an effect which was attributed mostly to blood flow variability [305]. Blood flow to the fingertip and the palm is about 5–20 times faster than to the alternate ISF sampling sites such as the forearm. ISF glucose values lag behind blood glucose levels during rapid changes. The rate of glucose transport to ISF will largely depend on the total blood flow to the area, which is determined by the number of capillaries, the permeability of capillary walls which can be changed, e.g., by nerve stimulation [306]. On the other hand, glucose uptake, enhanced by insulin, is determined by the metabolic rate of the cells. A model developed by Steil, Rebrin, and coworkers [307, 308] helps to predict quantitatively the resulting ISF glucose concentration (Fig. 4).

As recently reviewed [309], several groups have measured a time lag of CGM signals and blood glucose levels. In addition to the just-described physiologic component, an instrumental (analytic) component, resulting from the time required

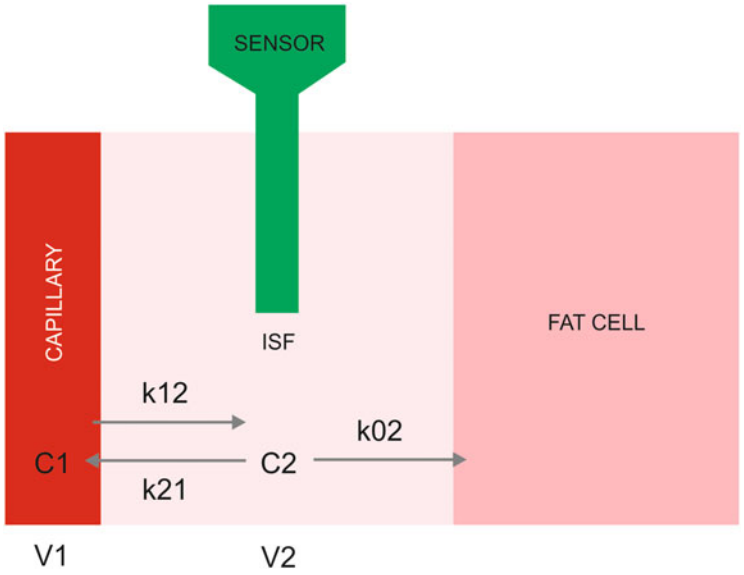

Fig. 4 CGM sampling environment as introduced by Rebrin et al. [308]. Diffusion of glucose from plasma to ISF is in proportion to the concentration in each compartment, whereas ISF glucose is cleared by uptake of the surrounding cell. *C1* glucose concentration in plasma, *C2* ISF glucose concentration, *k12* forward flux rate for glucose transport across the capillary, *k21* reverse flux rate for glucose transport across, *k02* glucose uptake into the subcutaneous tissue, *V1* volume of plasma, *V2* volume of ISF

for analytes to diffuse through sensor elements before signal transduction and a data processing component dependent on signal noise, needs to be taken into account.

Minimally invasive electrochemical sensors typically measure ISF glucose concentration in subcutaneous adipose tissue. The sensor tip, which contains working, counter and reference electrodes, is surrounded by fat cells and interstitial fluid (ISF). ISF serves as the liquid carrier of nutrients, allowing transport through microscopic compartments of ISF, which surrounds the fat cells. Due to capillary walls, protein content in ISF is reported to be about 2/3 lower than in blood plasma, featuring an average albumin/globulin ratio of 1.85 [304]. Subcutaneous adipose tissue is highly vascularized with capillaries of significantly lower wall thickness than found in the dermis [310], thus allowing for relatively fast transfer of nutrients to ISF, to fat cells, and thus also to the sensor which is embedded therein. In contrast, the epidermis is not favored as the sampling compartment since it is an avascular epithelial membrane, containing enzymes which break down glucose [311].

Sensors are typically inserted into the abdominal region, at the back of the upper arm, or at the upper buttock with the help of an inserter, which is applied by the user to the skin surface. The inserter carries the sensor and a cannula surrounding the sensor, which serves to puncture the epidermis and dermis. Commercially available inserters [66] aim to achieve fast and reproducible application of the sensor and

withdrawal of the cannula, resulting in the sensor tip placed typically 7–10 mm under the skin surface and a sensor shaft extending through the subcutaneous tissue, epidermis, and dermis and allowing for an extracutaneous electrical contact canal via a measurement unit. The insertion of a sensor by the cannula leads to a wound healing process whose complexity has been described in detail [see, e.g., [312–314]]. The response to the persistent presence of a sensor, i.e., a non-phagocytosable foreign body, leads to host responses to neutralize this foreign body, followed by reconstitution of the injured tissue by formation of fibroblastic scar tissue [312]. As described by Anderson et al. [312], six different host reactions have been distinguished. Firstly and immediately after sensor insertion, blood proteins adsorb onto the outer coating of the sensor, creating the interface for subsequent host interactions. Secondly during acute inflammation, polymorphonuclear leukocytes (PMNs) accumulate at the site of injury within minutes to days after insertion, resulting in the formation of reactive oxygen species and release of cytokine mediators. Thirdly, monocyte-derived macrophages and lymphocytes determine chronic inflammation, which is reported to extend to typically 2 weeks when using biocompatible materials [312]. Several chemokine and cytokine mediators, IL-1β, IL-6, IL-8, and TNF-α, have been identified during this phase. Macrophage-induced accumulation of fibroblasts and endothelial cells wound healing marks the start of the next wound healing phase, forming granulation tissue prior to scar formation or fibrosis. Granulation tissue is supplied by blood via new capillaries created by angiogenesis. Fibroblasts synthesize collagen, which forms the basis of the fibrous capsule. In a fifth phase, the foreign body reaction takes place during which giant multinucleated cells, so-called foreign body giant cells (FBGCs), are formed by fusion of macrophages. The extent of FBGCs is reportedly [312] dependent on the topography of the sensor surface, whereas smooth surfaces result in a thin layer of macrophages with fibrosis, whereas rough surfaces are reported to result in greater number of macrophages. Clearly, the resulting cell sheath creates a diffusional barrier to reagents and products of electrode processes, subsequently leading to undesirable decrease of local concentration of glucose at the measuring sensor interface and thus to declining sensor sensitivity over time. Finally, the formation of a fibrous capsule, which is reported to attain a thickness of more than 100 μm [301], further isolates the sensor from healthy tissue [100, 314–316] and further decreases influx of reagents and efflux of products. Summarizing, the implanted sensor, which is designed to measure glucose concentration in healthy tissue, ends up to actually sample tissue which has been created as repair tissue after injury.

Since CGM has been gaining more widespread acceptance, multiple subsequent sensor insertions per patient have gained relevance. Consequently, an eventual insertion effect was investigated with multiple sensors carried by one diabetes patient. Single-digit precision absolute relative difference (PARD) points to a small effect of insertion onto sensor performance [266], given that a non-negligible sensor-to-sensor variation needs to be taken into account. A recent study [317] shows that the coefficient of variation of in vivo sensitivity is

significantly higher than for in vitro sensitivity. It was also shown that sensitivity of four sensors worn simultaneously by one subject may vary considerably.

As expected, sensor sensitivity in vitro, measured in aqueous buffered glucose solutions, and in vivo, measured in ISF, may differ significantly from each other. While an effect of the nature of the sensor coating interface to tissue onto the coefficient of in vitro and in vivo sensitivities is expected, it is currently less clear, how large a variation of in vivo sensitivity should be expected when applying sensors of the same architecture material composition and manufacturing a batch to a large population of diabetes patients.

4.2.2 Sensor Technology

Since pioneering academic work introducing an electrochemical implanted glucose biosensor [318–324], there have been very significant industry efforts to make continuous glucose sensing an accessible monitoring tool for the diabetic patient. The requirement of high accuracy, precision, and reliability of reproducible glucose measurement with a miniaturized, implanted sensor over a time of up to 2 weeks has directed research and development toward four main challenges: first, manufacturability of a biosensor with a small footprint (see also Sect. 4.2.3); the challenge of developing a reproducible process for the production of millions of implanted biosensors which are typically less than 1 mm wide and typically 10 to 30 mm long, with tightly controlled electrode size and coating thickness, has frequently been underestimated; second, an enzyme electrode, which offers specific response to glucose over weeks; third, a diffusional barrier which controls mass transfer of glucose, possible interfering species, and oxygen to the enzyme electrode and consequently allows for stable sensor response; and, last, a biocompatible coating, which controls the interface between the sensor surface and the human body and minimizes buildup of protein and cell layers which diminish mass-transfer rates from and to the enzyme electrode. We shall first describe the main challenges and refer to exemplary solutions in sections "Sensor Layout" to "Biocompatible Coating" prior to focusing on technology which is used in CGM systems which is currently commercialized or will be commercialized briefly (see section "Sensor Technology used in commercialized Systems").

Sensor Layout

Three approaches have been pursued, each offering processing advantages in some steps, setbacks in others. First, the traditional wire-based sensor has been pursued and led to the sensor developed by DexCom. At least two electrodes, a working and a reference electrode, are arranged concentrically. A large area of the reference electrode ensures constancy of its potential, eliminating the need of a separate counter electrode. Advantageously, sensor diameters can be small, since the electrode area extends around the entire circumference of the wire. This format

complicates, however, the introduction of a multitude of different electrodes and, second, a planar sensor layout, wherein a working, a counter, and a reference electrode are deposited on one side of a more or less planar, flexible substrate. This approach is very well suited to utilize already established manufacturing processes for electrode deposition and coating. However, very tight manufacturing tolerances are needed when attempting to realize small sensor widths. For example, the current Medtronic Enlite™ sensor [325] is an exemplary embodiment of this sensor layout. The sensor currently developed by Roche [276] is a variant of this approach, shifting one electrode to the backside of a planar sensor substrate. Third, conductive traces connecting electrodes and potentiostat can be assembled on top of each other instead of side by side, allowing for a small footprint (see [326] for a commercialized example). This approach is very well suited to decrease sensor width, yet adds complexity to the manufacturing process.

Enzyme Electrode

The working electrode needs to meet several different demands: provide sufficiently high enzyme activity over time of use to avoid enzyme limitation of sensor response, allow for minimum polarization voltage to execute the redox reaction, adhere strongly to the strip conductor or wire to prevent increase of contact resistance over time, adhere strongly to the barrier membrane deposited on top to avoid increase of sensor sensitivity and leakage of electrode components into the surrounding tissues, and facilitate reproducible deposition. In contrast to BGM systems, CGM sensors have remained GOx based, mostly due to the convenience of using endogenous oxygen as mediator and due to its stability during processing, sterilization, and storage. GOx has been immobilized successfully in different ways to prevent leakage and to minimize enzyme denaturation during processing.

Dispensing GOx containing solutions or suspensions onto electrodes and admixture of GOx into electrode inks or pastes may lead to adhesive immobilization onto electrode components. Also, GOx was modified to decrease the actual diffusion coefficient and to allow for a multitude of anchoring sites [327]. Further, GOx has been encapsulated to allow for glucose and oxygen access [328], yet exclude GOx leakage. Alternatively, GOx has been coupled covalently to electrode components, be it nonselectively via coupling agents such as glutaraldehyde [325] or selectively to the conductor, frequently a carbon component, an electrocatalyst, or a polymeric binder via established linking methods [329]. Clearly, adhesive immobilization of GOx itself, intrigues due to its simplicity, may however suffer from fairly low binding constants which are dependent on the electrode environment. Admixture of GOx is highly attractive if a sufficiently porous electrode can be realized under mild conditions. Encapsulation and covalent linkage are elegant immobilization approaches, which however may significantly lower the total accessible enzyme activity per electrode mass as compared to unmodified GOx.

Currently, all available continuous glucose sensors are based on mediation of electron transfer from the active center of GOx by oxygen or by an immobilized

osmium-based redox polymer. The oxygen-mediated transfer requires fairly high polarization voltage of typically more than 500 mV vs. SCE. Addition of an electrocatalyst such as manganese dioxide lowers the polarization voltage to typically 250–350 mV. The osmium-based redox polymer typically works at polarization voltages of 100 mV vs. SCE or less. While minimization of polarization is desirable in general, its relevance for CGM is somewhat decreased in comparison to BGM for one major reason: concentration of interfering substances, such as acetaminophen, has been reported to be lower in ISF compared to whole blood [330].

Sufficient retainment of GOx typically involves an electrode matrix such as an ink or a paste. In order to ensure sufficient adhesion to the conductive trace, water uptake of the electrode matrix over time has to be limited to avoid partial or complete delamination. To this end, adhesion-promoting layers have been reported. Intimate contact of the diffusion barrier with the working electrode may again strictly rely on sufficient adhesive bonding and utilization of an adhesion-promoting layer or rely on cross-linking of the diffusional barrier on top of the electrode.

Reproducible definition of electrochemically accessible electrode area requires reproducible raw materials, reproducible surface energy of sensor substrate, reproducible dispersion of all electrode components and reproducible viscosity of all media, and transfer of reproducible matrix volumes. Since CGM sensors feature very small electrodes with a typical thickness of 20 μm or less and characteristic electrode dimensions of 500 μm or less, these requirements tend to be more challenging than for BGM sensors.

Diffusional Barrier Membrane

The working electrode of a CGM sensor needs to be covered for two reasons: first, to avoid leaching of electrode components, such as GOx, into the surrounding tissue and second, in order to decrease the mass-transfer rate of glucose toward the electrode. A CGM system relies on the ideally linear response of its amperometric biosensor from 2 to 30 mmol glucose per liter. The mass-transfer rate of glucose through the diffusional barrier needs to be 4 to 5 orders of magnitude smaller than in aqueous solution to avoid limitation of sensor response by enzyme saturation. For oxygen-dependent sensors, oxygen excess is required, introducing a further complication for in vivo applications, since oxygen concentration in subcutaneous tissue is up to 300 times lower than glucose concentration [323, 331–336]. Consequently, the diffusion barrier needs to be selectively oxygen permeable for oxygen-dependent sensors. In vivo use leads to an abundance of additional requirements which need to be met. Sensitivity, i.e., the background corrected sensor current divided by blood glucose concentration, needs to be as constant as possible after insertion. Clearly this requires rapid and reproducible wet-up of the diffusion barrier layer to allow for rapidly achieved constancy of the diffusion coefficients of glucose and oxygen. It also asks for minimum change of background current by endogenous and exogenous substances which change the background current,

asking for a membrane which selectively blocks off interfering substances. It thereby should also minimize reactions of interfering substances with electrode reaction products which may lead to sensitivity changes. Also, glucose-derived sensitivity needs to be held constant over time of use, asking for a membrane which prevents leakage of any electrode components into the surrounding. The membrane should suffer from minimum fouling, i.e., buildup of biological films on its surface. Its high biocompatibility should reduce foreign body response, delaying the buildup of cell barriers and fibrous capsules around the sensor, which reduce mass transfer of glucose to the sensing surface. In addition, the membrane is expected to withstand mechanical stress imposed during manufacturing and during sensor-wear, preventing the formation of cracks which may lead to incremental change of sensitivity over time. Membrane adhesion to the underlying sensor shaft needs to be sufficient to avoid delamination over time. Lastly, the deposition process of polymer membranes needs to be amenable for high-throughput production of sensors with cover layers of tightly controlled thickness. Due to the complexity of this optimization challenge, a multitude of different polymeric coatings and multilayer assemblies have been proposed and implemented in the past. The interested reader is referred to recent specific reviews [67, 313]; polymer coatings employed in sensors shall only be highlighted in this review with particular focus on sensors which are already commercialized or will be commercialized shortly.

The requirement of preferential permeation of oxygen versus glucose is somewhat difficult to obtain with one membrane which consists of one polymer chain of a given hydrophilicity. A trade-off between sufficient linear range and time lag of sensor response needs to be made. Several different routes have been pursued to resolve this challenge. Hydrophobic membranes have been realized [335, 337, 338] which largely decrease glucose permeation. Preferential oxygen permeation between the subcutaneous tissue and the working electrode has been attributed to micropores of the polymer membrane in these approaches, which may be hard to control in a production setting. Alternatively, a multitude of different polymers, such as Nafion [339] and polyurethane, have been studied [340–342], which is appealing due to its relative stability and high mechanical flexibility. In order to meet all requirements, different polymers have been blended to achieve domains of different hydrophilicity [343], wherein hydrophobic and the hydrophilic domains serve to enhance oxygen permeation and to control glucose permeation, respectively. More frequently, copolymers and blends of copolymers have been employed to meet all requirements.

Biocompatible Coating

Given the diverse requirements of the diffusional barrier membrane and a biocompatible sensor-to-tissue interface, a separate biocompatible coating is frequently deposited on top of the diffusional barrier membrane. Two different objectives are pursued: minimization of barrier films in the immediate vicinity and in the extended neighborhood of the sensing surface at each given time point of measurement,

ensuring sufficiently fast glucose transfer from blood capillaries into the fibrous capsule upon its formation. The first objective clearly aims to decrease inflammatory response, delay formation of a fibrous capsule, diminish the density of the inside collagen layer facing the sensing electrode, and thus minimize the diffusional and potentially metabolic barrier which leads to altering glucose mass-transfer rates from interstitial fluid to the sensing surface. The second objective aims at managing the sensing surface after inevitable encapsulation and is thus particularly important for glucose sensors which are implanted several weeks or even months. Importantly, it has been emphasized [314] that wound healing after sensor insertion may well prove to be highly variable from patient to patient, clearly pointing to the necessity of significant clinical studies to evaluate the effect of improved biocompatibility membranes onto glucose sensor performance. A few reviews have summarized the state of development and the direction of research of biocompatible coatings for CGM sensors [68, 313, 314]. Briefly, biocompatible coatings with different chemical surface structures, surface morphologies, and modulus have been suggested and investigated. In addition, drug-eluting coatings have gained interest for long-term use of continuous glucose sensors.

Hydrophilized hydrophobic polymers such as Nafion [344–347] and polyurethane (see, e.g., [348]) were originally used extensively as biocompatible coating. Polyurethane copolymers introducing hydrophilic moieties such as polyethylene oxide into the chain have been described to lead to favorable properties, i.e., decreased encapsulation [348]. In general, more hydrophilic polymers such as phosphorylcholine [315, 349, 350], 2-methacryloxyethyl phosphorylcholine [351–353], PEG [354], cross-linked PEG [355], PEG introduced into a hydroxyethylmethacrylate and ethylene dimethacrylate chain, polyvinyl alcohol [356] and water-rich hydrogels [357] have been reported more recently to reduce protein adsorption on sensor surfaces and thereby mitigate the foreign body reaction. Less frequently, hyaluronic acid [358–361] and humic acid [358] have been utilized in outer biocompatible coatings. Turning to surface morphology, the impact of introducing porosity into biocompatible coatings onto function of implanted glucose sensors has been investigated by several groups [315, 362–367]. Pore size optima were reported with regards to collagen capsule and degree of vascularization in the tissue surrounding the implant [368]. To the best of our knowledge, however, there is currently no published report establishing a clear correlation between pore size and porosity of a particular biocompatible coatings and function of continuous monitoring of human glucose levels. Flexibility and edge definition of CGM sensors may further be optimized to minimize chronic tissue injury by movement of the implanted sensor within the surrounding tissue. Clearly, CGM sensors tend to be based on flexible substrates with rounded edges. The mismatch of moduli of CGM device and the surrounding tissue may however not be negligible (see [316, 369]).

Polymer coatings which elute anti-inflammatory and angiogenic drugs have been considered for long-term CGM sensors [see [313] for an overview of recent publications, i.e. sensors which are designed to be implanted over several weeks over even months]. The integration of anti-inflammatory drugs such as

dexamethasone has been investigated with regard to macrophage concentration adjacent to implants [370] and extent of fibrotic encapsulation of the implant, whereas first studies have been published demonstrating the effect of dexamethasone release upon performance of implanted glucose sensors [371, 372] and microdialysis catheters [373]. It appears that dexamethasone may aid in keeping sensor sensitivity constant over long terms of implantation. However, no clear evidence is available currently. Vascular endothelial growth factor (VEGF), a cytokine, known to promote angiogenesis has been suggested in order to achieve greater capillary density in the capsule surrounding the implanted sensor and consequently ensuring sufficiently rapid transfer of glucose to the sensor surface [374]. While capillary density increase has been demonstrated in rat subcutaneous tissue after implantation over 3 and 4 weeks [375, 376], increased inflammation was reported over the entire four week study. Consequently, studies examining the simultaneous delivery of dexamethasone and VEGF have been conducted [375, 376] with nonuniform results regarding reduction of inflammation and increase of vascularization, which may be attributable to decreased activity of VEGF in the presence of dexamethasone [377–379]. No performance study of implanted glucose sensors with dexamethasone and VEGF containing biocompatible coatings has been published so far. A polyurethane/polydimethylsiloxane coating releasing nitric oxide, and reported to be leading to reduced leukocyte adhesion [380], deposited onto a glucose sensor, was investigated by Gifford [381] for short-term implantation (1–3 days). While drug-releasing polymer coatings for glucose sensors are clearly promising for creating a favorable tissue environment, significant development will still be needed to develop biocompatible coatings which release the respective drugs at the right dosis at the right time after sensor insertion.

Sensor Technology Used in Commercialized Systems

Technology used in CGM systems which are currently commercialized or will be commercialized very soon is exclusively based on electrochemical biosensors which measure glucose concentration in ISF or in an ISF extract over a time of up to 14 days. We shall focus on this technology. Readers who are interested in alternative minimally invasive approaches or noninvasive approaches are referred to extensive reviews [222, 223, 382]. We shall also not focus on the very interesting topic of long-term sensors, i.e., fully implantable sensors, since they are not yet available commercially. The interested reader may be redirected to a recent review [383].

The electrochemical biosensors in commercial use for continuous glucose monitoring are considered amperometric sensors. This means that the working electrode is polarized relative to a reference electrode and the current through the working electrode is measured as the sensor response. Sensors can use either separate reference and counter electrodes (three-electrode sensor) or a single combined reference/counter electrode (two-electrode sensor). A three-electrode sensor places

fewer demands on the reference electrode, at the cost of a more complex electronic control system (potentiostat). A two-electrode sensor requires only that a stable potential difference be applied between the two electrodes. The combined reference/counter electrode must be able to supply the same current as the working electrode, without significant polarization.

Initial first-generation sensors measured the reduction of oxygen on metallic electrodes and were thus polarized at negative potentials relative to an Ag/AgCl reference electrode [56]. In the absence of a mitigating strategy, this method would result in the accumulation of hydrogen peroxide and subsequent loss of GOx activity [53]. Co-immobilization of catalase, which disproportionates hydrogen peroxide into oxygen and water, is one effective strategy for this purpose [322]. Hydrogen peroxide-detecting sensors can either oxidize the hydrogen peroxide produced at a positive potential, thereby regenerating oxygen, or reduce the hydrogen peroxide at a negative potential, forming water. Both methods have found commercial use, though the oxidative approach is more widespread. The platinum group metals are effective catalysts for hydrogen peroxide oxidation. The DexCom sensors utilize a platinum wire at 600 mV vs. Ag/AgCl [384]. The Menarini GlucoDay microdialysis system utilized a platinum electrode at 620 mV vs. Ag/AgCl [385]. The Medtronic sensors utilize electrodeposited platinum black to increase the efficiency and reduce the potential to 535 mV vs. Ag/AgCl [325]. The sensor developed by Roche Diabetes Care sensor utilizes manganese dioxide to increase the effective surface area and reduce the potential further to 350 mV vs. Ag/AgCl [276]. The mediated "Wired Enzyme™" FreeStyle® Navigator™ utilizes an osmium mediator which is reoxidized at 40 mV v. Ag/AgCl, likewise decreasing the occurrence of electrochemical interferences [60]. Hydrogen peroxide reduction has the advantage of a lower applied potential, decreasing the occurrence of electroactive interferences. The updated Menarini GlucoMen® Day utilizes a Prussian blue catalyst to reduce hydrogen peroxide at −20 mV vs. Ag/AgCl [386]. The potential at which an amperometric sensor operated depends on the electrochemically active species, the electrode material and the morphology, and to some extent the desired linearity, sensitivity, and specificity. The traditional in vivo electroactive interfering substances (e.g., bilirubin, uric acid, ascorbic acid) tend to be natural reductants, in that they can be oxidized on an anodically polarized electrode or can react with hydrogen peroxide or oxidized mediator species. Thus, in general, a lower operating potential is advantageous for avoiding interferences. The current generated by these potential interferents depends likewise on the electrode material and any sensor features designed to mitigate the potential effects. When measuring hydrogen peroxide with a platinum electrode at 600 mV vs. Ag/AgCl, an interferent barrier has been placed between the enzyme layer and the electrode surface to limit the contact of alternate reductants [387]. With catalysts to reduce the applied potential [388], with low potential mediators to reoxidize the enzyme [326], or with reductive measurement of hydrogen peroxide [386], no such barrier is required. It should be noted that it cannot be assumed that the common electrochemical interferences in blood are present at the same concentrations as in the interstitial fluid compartment in which the CM

sensors operate. To this date, concentration of electrochemical interferences tested has been derived from BGM system testing [389].

In contrast to the dynamic potential profiles that have become state of the art in single-use electrochemical glucose sensors [390, 391], the commercial amperometric sensors for CGM use a single constant potential for the primary sensor response. Patent literature however describes the application of potential pulses and alternating potentials to interrogate the sensor, to gain information regarding the sensor status, calibration sensitivity, or the immediate environment of the sensor [392–395]. Electrochemical impedance spectroscopy (EIS) is also being used to gain additional information about the sensor, its sensitivity, its status, and the status of the environment in which it is placed. Typically EIS is measured by summing the DC potential applied to the sensor and a small AC potential (10–25 mV) in an appropriate frequency range (e.g., 1 Hz–100 kHz). The resultant AC signal is separated from the sensor DC response and analyzed for magnitude and phase relative to the applied potential. Analysis of the frequency dependence of the impedance (or its inverse, the admittance) provides information on the resistances and capacitances of the sensor. These in turn give information on the status of the sensor components, the environment of the sensor, and changes with time that may affect the sensor calibration sensitivity or reliability. EIS has been used to determine when a sensor is hydrated and ready for the application of the measurement potential [396] and for determining the sensitivity of the sensor, and whether the sensor is still capable of measuring reliably [397–400].

The market leaders in CGM are Medtronic with the Enlite™ Sensor and DexCom with the G4 Platinum® and G5® System. These two CGM systems each command about more than 40% market share worldwide. Remarkably these two market leaders both employ first-generation sensor technology, which is the result of long evolutionary developments. The Abbott Diabetes Care Navigator® [326] and the Menarini GlucoDay® are available only in Europe at this time and share the remaining market share. The newly introduced Abbott FreeStyle® Libre® System seeks to bridge the gap between CGM and spot monitoring, and has generated significant interest since its introduction in 2014. Roche Diabetes Care has published results of a sensor under development [266].

While the details of the production of these commercial products remain confidential, the following general descriptions of the technologies involved can be gleaned from publications and the patent literature. The Medtronic Enlite™ Sensor is the evolutionary development of the MiniMed CGMS® and uses the same basic technology. The electrodes are fabricated on a planar, flexible substrate using lithographic methods originally from the microelectronics industry. A polymeric substrate is sputtered with a conductive gold layer and the layer structured lithographically to produce electrode areas and contact pads joined by conductive traces. The working electrode receives an electrodeposited layer of catalytic platinum black and an overlying layer of GOx in a polymer/protein matrix wherein GOx may be immobilized by cross-linking with glutaraldehyde, carbodiimide [401, 402] disuccinimidyl suberate (DSS), or 1-ethyl-3 (3-dimethylaminopropyl) carbodiimide (EDC) [402]. Embodiments of GOx entrapped in poly(vinyl

alcohol)-styrylpyridinium (PVA-SbQ), which may be UV cross-linked, were described [403]. The reference electrode is electroplated with silver and partially chloridized to silver chloride. The hydrogen peroxide produced by the GOx is catalytically reoxidized on the platinum black working electrode at ca. 535 mV relative to Ag/AgCl to regenerate oxygen and produce an anodic current proportional to glucose concentration [325, 395]. Polymer compositions are described to feature silicone, polyurethane, and polyurea chain elements [404], featuring 4 to 5 times higher diffusion coefficients for oxygen in comparison to glucose. Embodiments of the more recently introduced Medtronic MiniMed Enlite™ sensor [325] are described to additionally use a branched acrylate polymer comprising alkyl, amino, siloxane, and polyethylenoxide (PEO) moieties. Various hydrophilic coatings which show very significant volume increase upon water absorption and do not inhibit glucose permeation have been proposed as interface layer between biological environment and sensor [405]. PEO containing polyurethane has been described as particularly advantageous.

The DexCom Platinum G5® sensor is the evolutionary descendent of the DexCom STS™. The sensor is fabricated from an insulated platinum wire. A section of the insulation is removed, and a series of membrane structures are applied to create the working electrode area. An interference rejection layer, which was described to be based on polyetherurethane [406], is applied first, creating a barrier to the electrooxidation of endogenous reductants such as ascorbic acid. This barrier layer may function through a combination of size exclusion and charge repulsion. A GOx layer consisting of polyurethane latex and glutaraldehyde as a cross linker [406] is applied next followed by polymer layers to reduce glucose flux and increase the relative availability of oxygen. Polymer layers of the previous Seven® sensor's polymer membrane are described [407] to contain two random or ordered block copolymers of differing hydrophilicity, preferably a polyetherurethane-urea/polyetherurethane-urea-block-polyethylene glycol blend wherein polyetherurethane-urea-block-polyethylene glycol constitutes the more hydrophilic component which forms a network of microdomains and controls water uptake and thus glucose transfer to the working electrode. More recent polymer layer embodiments rely on a block copolymer with a hydrophilic and a hydrophobic block wherein the hydrophobic block features segments of repeating hydrophilic and hydrophobic segments [408]. Alternative embodiments are described [409] to contain blends of polyvinylpyrrolidone and polycarbonateurethane solution as hydrophilic and hydrophobic polymers, respectively. Additional bioprotective layers, deposited on top of the barrier layer, have been described (see, e.g., [408, 410]) to aid in defining a biocompatible tissue to sensor interface. In general blends and/or copolymers of polyurethane, such as, e.g., silicone-polycarbonate-polyurethanes with hydrophilic components or segments consisting of PVA, PEG, polyacrylamide, acetates, PEO, PEA, and PVP have been described to be useful in this respect. A chloridized silver wire wrapped around the insulated working electrode or more lately an Ag/AgCl layer deposited onto the insulating working electrode wire serves as the combined counter-reference electrode. Hydrogen peroxide produced by GOx is reoxidized at

the working electrode at 600 mV relative to Ag/AgCl to regenerate oxygen and produce an anodic current [384, 387, 411, 412].

Both of these first-generation sensors must solve the problem of the oxygen deficit. Polymer layers with greater permeability to oxygen than to glucose are used to manage the standing deficit, and materials with greater solubility of oxygen than the aqueous environment manage transient oxygen deficits that exceed the average condition. Measuring hydrogen peroxide by oxidation on the anode requires a relatively high potential, making these sensors subject to electrochemical interferences. The Medtronic sensor uses platinum black to reduce the potential. In both sensors, specific membrane materials act to shield the anode from the endogenous interferences, reducing the degree of interference. The oxidation of hydrogen peroxide serves also to regenerate oxygen, mitigating the oxygen deficit.

Menarini Diagnostics has produced the GlucoMen® Day, the descendent of the GlucoDay™. This product utilizes a small peristaltic pump to drive a dialysis fluid from an external reservoir to a subcutaneous microdialysis fiber. In the fiber, the glucose concentration equilibrates with that in the interstitial space. The continued pumping transports the glucose-enriched fluid to an immobilized enzyme sensor in an extracorporeal monitor. Here, the dialysate impinges on a wall-jet cell containing a screen-printed glucose sensor. The sensor contains a platinum electrode and a catalyst (Prussian Blue, ferric hexacyanoferrate) that catalyzes the reduction of hydrogen peroxide at moderate potential (−40 mV vs. Ag/AgCl) [413, 414]. The electrode is covered with a cellulose acetate membrane for interference rejection, a nylon net carrying immobilized GOx, and a polycarbonate membrane as the barrier layer. This first-generation sensor solves the oxygen-deficit problem by diluting the glucose with the dialysis fluid and providing the sensor with a large, constant concentration of oxygen in the fluid. The catalytic reduction of hydrogen peroxide at low potential eliminates most electrochemical interference [415].

The Roche Diabetes Care sensor is produced by printing electrode areas on a polyimide-based flexible circuit board. Conductive traces are lithographically defined, and the working electrode is distributed in multiple areas along the length of the substrate. A single Ag/AgCl area serves as the reference electrode. A counter electrode is located on the reverse side of the substrate. The working electrode utilizes GOx and oxygen, with a manganese dioxide catalyst to reoxidize the hydrogen peroxide to oxygen at the relatively low potential of 350 mV vs. Ag/AgCl. Polyurethane layers on top of the electrodes [266, 276] limit glucose diffusion; additional coatings enhance biocompatibility. This first-generation sensor design uses a glucose diffusion-limiting membrane as well as the distribution of working electrode area to manage the oxygen deficit. The distributed working electrode area also makes the sensor response more independent of heterogeneity in the tissue and more representative of the overall glucose concentration in the subject (tissue averaging). The manganese dioxide catalyst reduces the potential at which hydrogen peroxide is oxidized, reducing the effect of electrochemical interferences. Additionally, the three-dimensional structure of the manganese dioxide very

efficiently recycles the hydrogen peroxide to oxygen, making the sensor response independent of oxygen concentration.

The Abbott FreeStyle® Navigator™ makes use of the Wired Enzyme™ technology to produce a second-/third-generation sensor. As a mediated sensor, the Navigator does not face the oxygen-deficit problem, but rather the reverse, in which excess oxygen can compete with the immobilized mediator and interfere with the sensor signal. Conductive traces of carbon ink are deposited onto polyester substrate foils which are laminated to form a multilayer assembly. An enzyme mediator hydrogel is deposited on the working electrode. The hydrogel immobilizes the enzyme via epoxy linkages [67] and provides tethered osmium mediators, which transfer electrons from the reduced enzyme to the carbon electrode at a low potential (0 to −100 mV vs. Ag/AgCl). The low potential eliminates most electrochemical interferences, and the lack of reliance on hydrogen peroxide eliminates interference from compounds that react with it. A glucose flux limiting layer and a biocompatible layer cover the working electrode, Ag/AgCl reference electrode, and the carbon counter electrode [59, 60]. The glucose flux limiting layer was described [326] to consist of a poly-(vinylpyridine)–poly(ethylene glycol) copolymer cross-linked using a trifunctional short-chain epoxide. Elegantly, the hydrophilic membrane is described to be the interface to the surrounding tissue. More recent patent literature [416] describes variation of this original layout, adding polystyrene as copolymer to the polymer chain, as well as introducing charge into the side chain by derivatization of pyridine with alkylsulfonates. Advantageously, it is reported that hydration time was decreased due to these polymer compositions, allowing for faster sensor run-in. Additional embodiments of advantageous polymer chains have been described more recently [417]. Cross-linkable polyethylene oxide tetraacrylate has been described as advantageous biocompatible coating covering the sensor in part or in its entity [418].

4.2.3 Sensor Manufacturing

Increasingly, patients who use CGM systems tend to differentiate between CGM systems based on system features which are not directly connected with measurement of glucose per se. Fundamental system performance such as accuracy, precision, and reliability may be receiving different levels of attention depending on the specific user requirements. Pain-free and facile sensor applicators, small and easy-to-wear patches, easy-to-manage receiving units which allow for facile display, and transfer of relevant data and information have become differentiating. This observation translates into a twofold challenge for device manufacturers. For one, the required convenience of system use must be made available at low cost. These requirements ask for intelligent design solutions not only to optimize ease of use but also to minimize manufacturing cost. Manufacturing tolerances, biocompatibility requirements for disposable system components leading to selected materials, suitable manufacturing methods, and manufacturing environment must be reconciled with cost limits to allow for high-volume manufacturing at attractive cost. The

second challenge lies in meeting very high-performance requirements with every single miniaturized sensor, i.e., a sensor, which is typically less than 1 mm in width and just centimeters in length, and which needs to be assembled and sterilized prior to packaging. Briefly, methods shall be highlighted and utilized for manufacturing of flexible sensors, containing (enzyme) microelectrodes, conductive traces leading toward it, insulating, diffusional barrier, and biocompatible layers.

Originally, two different platforms have been used to manufacture minimally invasive, miniaturized glucose sensors. The wire-based approach features an assembly of several conducting wires, which are intertwined or connected via concentric insulation layers [387]. The planar strip approach was originally adapted from BGM test strips by using flexible circuit boards [419, 420] or flexible thermoplastic foil material. Both approaches offer substrates which can be sufficiently flexible and tear-resistant to allow for comfortable and safe wear over extended time of use. Wires are typically made from platinum or alternative noble metals; strip conductors are typically fabricated from noble metals, carbon-based inks or pastes, or combinations thereof and must withstand significant mechanical stress over time of wear. Strip conductors are defined by PCB manufacturing methods, i.e., photolithography and etching processes. Alternatively, masked metal deposition, laser ablation of previously deposited noble metal layers, and several printing methods have been used to define strip conductors, which may be less than 100 μm wide in certain cases. The electrode area has often been defined by a recess of an insulating layer, which is deposited onto the wire or the planar strip. A wide range of insulating layers has been used, as summarized recently [325, 421]; insulating layer recess is typically defined by photolithography and subsequent etching or alternatively by laser-ablation processes. Since sensor sensitivity is directly proportional to electrode area, variability of recess area may have a profound effect onto sensor performance.

Working electrodes, which are deposited on top of wires or strip conductors, frequently consist of carbon- or metal-based polymer dispersions. High resolution of very small working electrodes, typically 50–500 μm in characteristic dimension, asks for uniform dispersion of micro- or even nanoparticles within a suitable matrix. Viscosity of employed dispersions varies widely and depends on the employed deposition method. Low viscosity dispersions are used for electroplating, ink jetting, and coating, e.g., dip coating. Dispersions of higher viscosity are typically used for screen printing or blade coating. Reproducibility of transfer, wettability of the surface to be coated or plated, and reproducible alignment of the working electrode matrix and the underlying conducting feature are necessary to achieve good reproducibility. Continuous deposition of dispersions over extended production time asks for high constancy of composition, i.e., minimization of evaporation, agglomeration, and sedimentation over time. Counter electrodes, employed in three-electrode layouts, have been realized in the same fashion or may simply consist of an extended area of exposed wire or strip conductor. Reference electrodes typically consist of Ag/AgCl which is embedded in a polymer matrix and which is deposited by any of the above-described methods.

High-throughput manufacturing of sensors relies on bulk processing of wire coils, sheet, or roll material. Separation methods to release single sensors are frequently employed prior to the final coating steps. Mechanical methods are very well suited for cuts with modest requirements of edge definition on a microscopic scale, allowing for very high output. Laser-cutting techniques in combination with automated alignment allows for high positional precision and fine control of edge radius. The correct choice of wavelength and pulse width is essential to cut the respective material with small cut widths, minimum heat input, and desired edge profile. Disadvantageously, laser cutting may introduce the need of an additional cleaning step to remove ablation residues, which further decreases output compared to mechanical cutting tools. Water jet cutting may offer an alternative for sensors which withstand the processing conditions.

Diffusional barrier coatings which need to be deposited onto the working electrode and biocompatible coatings which may need to be coated onto the sensor shaft (see sections "Diffusional Barrier Membrane" and "Biocompatible Coating") are frequently deposited from polymer solution. A multitude of coating techniques [422] has been reported, and commercially used sensors are mostly coated by screen printing, blade coating, electropolymerization, or dip or spray coating. Importantly, uniformity of the deposited polymer film and marginal variation of film thickness have to be achieved routinely to assure high reproducibility of sensor readout [407]. Consequently, success in manufacturing highly reproducible films across one sensor lot directly translates into high reproducibility of sensor response time and sensor sensitivity, which is a sine qua non for allowing the use of precalibrated sensors, as promoted more recently [317].

Prior to assembly of the coated sensor, typically after each printing and/or coating step, a suitable drying method needs to ensure reproducible and complete removal of solvents. When using large-scale drying ovens, the drying process is typically not the throughput-limiting step, even if drying time may well exceed a quarter of an hour. Nevertheless, in the interest of increasing output, the number of required printing and coating steps needs to be minimized. Assembling steps depend of course on the respective design. Assembly may already start prior to execution of printing and coating steps in order to facilitate sensor handling.

A controlled environment is typically provided for all manufacturing steps including the final assembly of inserter, cannula, and sensor, if executed by the manufacturer and not by the user. Finally, primary packaging is typically designed to provide a hermetically sealed environment during storage. Radiation sterilization with sufficient dose is used for all commercial CGM systems, since it is compatible with employed sensor chemistry and does not lead to significant change of material properties.

Currently several millions of disposable CGM system units are utilized every year. In the future, this number is expected to grow every year at very significant growth rates due to more widespread adoption of these novel systems. As a consequence, manufacturing methods will be further developed with the aim to meet ever more stringent performance requirements while allowing for significant scale-up of production volume. Simplicity of system design and increased degree of

automation of robust manufacturing methods will be the key to successful rollout of CGM systems on a large scale.

4.2.4 Data

Data Processing

In an amperometric sensor, the potentiostat circuitry maintaining the desired working electrode potential generates a voltage which is proportional to the current passing through the working electrode, and this must be measured, preprocessed, and transferred to the measurement system, where the current values are converted to glucose and rate of change estimates. Because the rate of change of glucose in the body is relatively slow, displayed value does not require very frequent updating. Measuring frequently allows the collection of an excess of data values which may be processed statistically to provide the best estimate of the current over a time interval. However, the process of measuring with digital controllers, data storage, and preprocessing is energy intensive, as is the transmission of an updated value to the external monitoring system, so a compromise is struck between measurement and update frequency and energy use.

The actual processes used for the collection and preprocessing the data in the commercially available systems are proprietary. Standard signal processing methods and information gleaned from publications and patent literature about the commercial systems have been described by Bequette [423] and Rebrin et al. [424]. These include median filters, finite (FIR), and infinite (IIR) impulse response filters, Kalman filters, Wiener filters, Fourier filters, and hybrid approaches such as signal clipping limits and maximum/minimum rejection value combined with averaging. The major trade-off in the data filtering step is between the amount of smoothing of the signal and the delay which is introduced by the filter.

The conversion of a filtered current value into a useful glucose value requires a calibration process. There are several significant issues for subcutaneous glucose sensors that make this calibration process complex. The first is the relationship of the subcutaneous glucose concentration, which is measured by the sensor, and the blood glucose concentration, which is useful to the user and capable of being measured by the user with a BGM system. There has been substantial controversy regarding the steady-state difference between blood glucose and subcutaneous glucose. Estimates of subcutaneous values from ca. 40% of blood values to 100% of blood values have been determined, depending on the method and the site of measurement [308, 425–429]. Comparison of sensor sensitivities in vitro with in vivo further complicates the task, as there are many potential influences on sensor sensitivity in vivo [430]. The standard response has been to calibrate a subcutaneous sensor with blood glucose measurements, on the assumption that, if the values are different, they are at least proportional.

Another complication is the lag time between blood glucose and interstitial glucose. This has been diligently researched and found to vary significantly with measurement method, sensor site, and whether blood glucose is rising or falling [308, 309, 431]. Calibration schemes which incorporate an assumed delay have been proposed, and it is universally recommended that sensors be calibrated when the blood glucose value is relatively stable. Commercial systems will typically reject or underweight a calibration which is made when the sensor signal is changing rapidly. Much work has gone into creating models of glucose kinetics and dynamics to improve sensor calibrations [432–436].

The next complication comes from the zero of the calibration function. Considerable work has been done comparing one-point and two-point calibrations. A two-point calibration requires that reference values be taken at two substantially different concentrations, in order to accurately determine the slope and especially the intercept. This requires complex protocols to manipulate blood glucose levels within safe ranges and is not realized in current products. A one-point calibration with a constant zero level has been determined to improve performance, especially in the hypoglycemic range [437, 438]. An alternative to a population zero value is the use of a blank electrode, which measures a user- and site-specific background current which is subtracted from the active electrode current prior to the application of a sensitivity factor [439]. The reduction of the measurement potential through the use of appropriate mediators is also effective for reducing and stabilizing the background current [60, 440].

Since the sensitivity of the sensors typically changes with time, a strategy of multiple calibrations is required. Initially on insertion, the sensor is in a very dynamic state as the membrane polymers and enzymes absorb water and become hydrated. The insertion site is also in a very dynamic state, as capillaries and small vessels bleed into the insertion site and fluid from disrupted cells collects. A stabilization time is needed until the first calibration can be performed, typically from two to twelve hours. Recalibration is required when the sensor sensitivity changes over the lifetime of the sensor. This may be performed one or several times per day, with the calibrations being statistically combined to generate a new prospective calibration for future measurements. Like the raw data filtering methods, the exact calibration methods used in the commercially available sensors are proprietary, but literature, patent publications, and the operating instructions allow some insight into the methods [423, 441]. The calibration procedure is understood to contribute significantly to the sensor performance, and the manufacturers are making consistent improvements, adapting to the individual characteristics of their sensors [384, 442–445]. To be useful for alerts and alarms, the CGM calibration must use available data and reference values to predict glucose values in the future (prospective calibration). Professional CGM systems can use all of the calibration data retrospectively to optimize the data accuracy [446, 447]. BGM sensors cannot be individually calibrated before use and have long been calibrated at the point of manufacture. More recently, lot-specific calibrations have been replaced with product-specific calibrations or “no-code” products. The product-specific calibration is achieved through control of the materials and processes for

sensor production and sometimes through user-transparent modification of a sensor to allow the measuring device to determine which of several preprogrammed calibration functions should be used with the sensor ("non-evident coding"). A large number of researchers are working to improve the filtering and calibration of the data presented by commercial systems, but the "raw data" with which they work are typically the output data of the system, which have already been preprocessed by the first-stage data filtering and glucose calibration that is carried out in the commercial device. The AP@HOME Consortium has developed the "smart CGM sensor" concept, in which the data stream is processed through a de-noising module (filter), an enhancement module (calibration), and a prediction module, which allows hypoglycemia and hyperglycemia alerts and warning to be given further in advance of the occurrence of the event [435, 448–451]. It has recently been suggested by Hoss et al. that the same process can be adopted for subcutaneous sensors [317]. A recently introduced product, the Abbott Freestyle® Libre™ [452], uses an approach, which does not require BGM measurements for calibration. A recent evaluation of the product [453] suggests similar performance to systems using capillary blood calibration [454].

Data Transfer

A key component of a CGM system is the data transfer link between the body-mounted transmitter and the local receiver. The transmitter polarizes the sensor, measures current, preprocesses the current values, and makes any additional auxiliary measurements. It then transmits, at regular intervals of 1–5 min, the processed data to the local receiver. The local receiver obtains the calibrated data computed from available reference values, the current glucose value, and the direction and rate of change, and displays that information on the local display. The local receiver is responsible for generating any alerts and alarms related to glucose levels. The communication is typically a one-way broadcast, with no acknowledgement from the receiver. This minimizes the energy required by the transmitter, which is thus kept as small and light as possible, but allows data to be lost when the receiver is out of range for an extended time.

The local communication systems in current products have been implemented with proprietary technology. These systems fall under FCC Part 15 in the United States as "unlicensed transmitters" and must not interfere with licensed transmitters and must accept interference from licensed transmitters. They are all approved for use on commercial airlines, though they must be deactivated at the request of airline personnel. Magnetic or X-ray screening may be harmful, and users should request alternative security strategies.

The Medtronic MiniLink® Real-Time Transmitter utilizes 916.5 MHz (NA) or 868.35 MHz (WW). It transmits data every 5 min and has a range of ca. 6 feet (1.8 m). It is powered by a rechargeable battery and has a lifetime of around 14 days between charges. It is paired with the insulin pump prior to use, and the pump then only receives data from the paired transmitter. Interference from other 900 MHz

consumer electronic devices (cordless phones, some cellular phones) may occur when the devices are operating in the vicinity of the sensor, but safety checks on the data ensure that no incorrect data is received [455]. The DexCom G4® Platinum [456] transmitter operates at 2.4 GHz and, with a maximum output power of 1.25 mW, has a range of up to 20 feet. The transmitter is likewise paired with the receiver prior to use, to allow the receiver to accept data only from the paired transmitter. The transmitter is powered by non-replaceable batteries and at the end of battery life must be replaced. The receiver is a stand-alone device with a display for the CGM data, and buttons for setup information, entering calibration values, and responding to alerts and alarms. The G5 Mobile Transmitter uses Bluetooth® technology, which enables compatible mobile devices (currently iOS devices with the G5 Mobile app) to receive data and display trends and warnings. The Freestyle® Navigator™ II [457] transmitter operates at 433.6 MHz with a maximum power of 100 μW. Range is claimed to be up to 3 m (10 feet) through RF-transparent materials and up to 30 m (100 feet) in the absence of RF reflectors. The transmitter is powered by a non-replaceable battery and at the end of battery life must be replaced. The receiver has a display for the CGM data, buttons and a scroll wheel for input and navigation, and a built-in BGM meter for calibration and blood glucose measurements when required. The Abbott FreeStyle® Libre® uses a different model of local data communication, on demand transfer through near-field communication technology (ISO 15693, 13.56 MHz). This is similar to the technology of radio frequency identification (RFID) which is also becoming prevalent in personal devices like smartphones. The reader is brought into the vicinity of the sensor transmitter (ca. 1–3 cm) and current data, and data collected up to the last 8 h are sent to the receiver. The data are processed, displayed, and saved on the reader, which also contains a BGM device. The RFID technology requires no power from the transmitter, thus enabling an even smaller size and weight, but the inability of the transmitter to initiate a data transfer makes real-time alarms impossible [458].

Online data may be repeated to local or remote monitoring systems through an auxiliary device to enable monitoring of CGM users. The Medtronic mySentry® consists of a mySentry® outpost (receiver/transmitter) component that received data from an associated Paradigm® REAL-time Revel® insulin pump and retransmits to a mySentry® monitor unit, which displays the pump status and CGM data. The monitor may be within 50–100 feet of the outpost [459]. The DexCom Share™ extends the range of data sharing by transferring data from the handheld receiver to an associated Internet-connected device, such as a smartphone or tablet, which forward the data to remote servers (“the cloud”). Glucose levels and trends may then be viewed by up to 5 remote Internet-connected devices. It is notable that this type of data sharing is not described as remote monitoring but data sharing, probably due to the lack of assurance of real-time transmission [2]. This is the commercial embodiment of an open-source remote monitoring effort begun by parents of children with diabetes, known as NIGHTSCOUT [460]. The Medtronic MiniMed® Connect has recently been announced and also provides Internet-enabled remote monitoring capabilities through Internet-connected personal electronics. This system requires an additional component that receives status

information and data from the MiniMed 530G or Revel insulin pump and relays to the Internet device via Bluetooth® [461]. The connection of local glucose data capture devices to the Internet mirrors the development of Internet-based data collection, display, and analysis sites for BGM. BG meters with local connections to personal Internet devices send data to Web "portals," which provide the user and his or her healthcare provider tools for using the data to improve the therapy.

Data Display

Data from CGM systems is displayed "online," the data that the user can access directly from the data display unit of the system and focusing on the current value, and, retrospectively, the complete data set from the entire time of wearing the CGM sensor. The online display of CGM data consists of the estimate of the current blood glucose level and usually some indication of the direction and magnitude of the rate of change of the blood glucose over the last minutes, the "trend." The trend information can be displayed as an arrow pointing up, down, or level to indicate the direction of the trend and at different angles to indicate the magnitude of the trend. Alternatively the trend can be inferred from a small graphic display of the most recent glucose values. Alarms or alerts from comparing the current glucose value to preset reference ranges are displayed as text, frequently accompanied by an auditory alarm. Status information related to sensor calibration or sensor use time is displayed through icons. Retrospective evaluation of CGM data is usually accomplished by transferring the data to a PC. Post-processing according to rules-based algorithms and transformation to daily or event-based summaries allow the evaluation of glycemic status and some standardized treatment decisions. Each manufacturer of CGM systems provides software for download and generation of reports. The analysis methods and reports are not consistent and have proven to be a barrier to the professional use of CGM. A graphic of estimated glucose vs. time is the simplest report, with ranges provided for hyper and hypoglycemia. The addition of additional information, such as BGM values, meals, exercise, and insulin, allows a much deeper analysis and understanding of the glucose values. The "modal day" is simply an overlay of all of the estimated glucose values on a single 24-h scale. This allows the assessment of time-based variation in glucose levels, such as identification of overnight hypoglycemia or frequent morning hyperglycemia [235, 237, 462–464]. Various metrics for summarizing the data have been proposed, including simple mean, means within time blocks, area under the curve ("glucose exposure"), and various risk-based calculated values. These are similar to metrics developed for BGM data. The Ambulatory Glucose Profile [465], initially developed to summarize BGM data sets, has since been extended to CGM data and is being suggested as a way to standardize the reporting of retrospective CGM data [272].

4.3 Performance of CGM Systems

CGM systems offer one fundamental advantage over established BGM systems: a glycemic profile based on a previously inconceivably vast number of regularly acquired glucose data points. Clearly this wealth of information, which may be based up to one glucose measurement per second, i.e., 86,400 glucose measurements per day, suggests deep insight into glucose patterns. Also, additional information, such as trend information, and additional device features, such as alarms when exceeding an adjustable threshold glucose concentration or glucose concentration change per time, have become possible and do promise to significantly increase patient safety. Most importantly, the time resolution of glucose measurement is clearly set to be used for improvement of insulin therapy.

Yet advances for the diabetic patient based on CGM systems depend strongly on the analytical quality of the glucose measurement per se. Therapy adjustments, based on retrospectively analyzed glucose patterns, require reliable detection of glycemic extrema; demands on the accuracy of a real-time signal however go far beyond that. Incorrect trend information will reduce, not enhance, patient safety. Incorrect alarm settings, in particular incorrect so-called hypo warnings, will not aid to increase the patient's confidence in technological advance. Incorrect insulin dose recommendations may have fatal, surely negative consequences. In conclusion, sensor performance issues affecting system accuracy, precision, and reliability have been named as main obstacles for widespread complement or even replacement of spot glucose measurements [466, 467]. Demands on accuracy, precision, and reliability required for approval of BGM systems are clearly described by the relevant ISO norm [17] (see Sect. 3.2). ISO 15197:2013 provides regarding accuracy that 95% of meter results shall fall within ±15 mg/dL from a laboratory reference value at a glucose concentration below 100 mg/dL and at maximum by ± 15% at a glucose concentration of 100 mg/dL or higher. Ninety nine percent (99%) of individual glucose results shall fall within zones A and B of the Consensus Error Grid (CEG). The system accuracy evaluation must include data from three different reagent system lots (three test strip lots), each with 100 fresh capillary blood samples.

For several reasons, requirement definition of accuracy, precision, and reliability for continuous glucose measurement systems is more complicated. Firstly, there are fundamental differences in CGM and BGM systems. In contrast to the feasibility of measuring one blood sample at a constant concentration of glucose and selected interfering species with several test strips, as well as with several different measurement systems, the compartment sampled by any CGM system, ISF, is not easily accessible and changes its glucose and interferent concentration over time. A CGM sensor, inserted immediately after removal from its packaging, may not be extracted from the patient to be characterized in vitro prior to reinsertion. It is also impossible to insert several CGM sensors into the exact same environment due to the heterogeneity of the sample compartment. It is thus not feasible to assess accuracy and precision in the same manner as with BGM systems. Secondly, there

is the reliance of CGM system assessment on BGM reference measurements. The accuracy, precision, and timing of BGM reference measurements affect the assessment of the CGM system and thus need to be defined. CGM systems measure glucose concentration of ISF, not blood, which may differ significantly from each other (see Sect. 4.2.1). Thirdly, there is the necessity to assess CGM system performance via clinical studies involving individual subjects with glucose profiles which differ largely from each other. The population of subjects involved in clinical testing thus significantly affects the assessment.

4.3.1 Performance Assessment

Since BGM values are still regarded as the "gold standard," accuracy of CGM systems has frequently been assessed in comparison with blood glucose values. To this avail, the mean absolute relative difference, MARD, as utilized when introducing the first needle-type glucose system [468], has been used very frequently. The clear advantage of this assessment is simplicity. However, it has rightly been pointed out that the evaluation of CGM systems by means of infrequent BG measurements hardly reflects the nature of CGM due to the limited number of paired data points and the inherent physiological difference between the two compartments in which glucose is measured [265, 267]. This simple, MARD-based assessment may also lead to misleading results if case study conditions and details of data evaluation are not taken into account. For example, in case of rapid changes in glycemia, MARD may be quite high. MARD should thus be computed separately for different glucose ranges and for different rate-of-changes to overcome this limitation. Also, the calculation of PARD (paired absolute relative difference) as a means of assessing the deviation of the response of two sensors of identical batch, worn in parallel at identical insertion sites, helps in assessing the precision of any CGM system but also supports the MARD accuracy assessment by distinguishing between physiological time lag and unreproducible readout by only one sensor. PARD has thus also been recommended as an indicator for the overall performance of a CGM system [267].

The selection or omission of performance metrics may affect the overall assessment of CGM systems. In order to derive suitable requirements, the need to standardize experimental conditions for assessment of CGM system performance [267, 469] has been emphasized. Recently, a FDA-recognized consensus guideline, the POCT5-P document [469], has been released, which was developed by the Clinical and Laboratory Standards Institute (CLSI) together with the Diabetes Technology Society. POCT5-P defines requirements and recommendations for methods determining analytical and clinical metrics of CGM systems, which provide the patient with real-time glucose concentration, trend information, direction (stable, increasing, or decreasing), and rate of change ($<$1 mg/dL/min, 1 to 2 mg/dL/min, $>$2 mg/dL/min). Importantly, guidance is given how to present data, how to compare continuous interstitial glucose monitors, and how to compare interstitial glucose monitors with spot blood testing systems.

The FDA has released guidance [470] to provide recommendations to companies which are developing artificial pancreas device systems (APDS), differentiating between three different APDS types: a so-called threshold suspend device system, which may reduce the likelihood or severity of a hypoglycemic event by suspending or reducing insulin delivery temporarily when the sensor value reaches or approaches (reactive or predictive, respectively) a predetermined lower threshold of measured interstitial glucose, a control-to-range (CTR) system that reduces the likelihood or severity of a hypoglycemic or hyperglycemic event by adjusting insulin dosing only if a person's glucose levels reach or approach predetermined higher and lower thresholds, and a control-to-target (CTT) system that sets target glucose levels and tries to maintain these levels at all times. Guidance as to the performance assessment of the CGM component of the APDS refers to the POCT5-P document and details – in addition to BGM performance characteristics – required CGM performance characteristics which need to be established during a pivotal clinical study:

- Accuracy of CGM results, as expressed by the point-to-point agreement between blood glucose reference readings and paired CGM results
- Difference of CGM values from the paired blood glucose reference result (e.g., within 10, 20, 30, 40, or >40 mg/dL), expressed in various glucose concentration bins (e.g., <40, 41–50, 51–60, 61–70, 71–80, 81–120, 121–180, 180–250, 250–325, and 326–400 mg/dL)
- CGM signal bias at various glucose concentrations (according to the blood glucose reference values) of 60, 80, 120, 180, 250, 325, and 400 mg/dL, including 95% confidence intervals
- Point-to-point threshold alarm detection rates (detection rates and false alarm rates), as well as detection rates of hypoglycemic and hyperglycemic event within 15 and 30 min of the event
- Prediction alarm performance. Characterization of detection rates according to whether the CGM detected the predicted hypoglycemic and hyperglycemic glucose level within the horizon setting(s)
- Imprecision observed when sensors are inserted into the same anatomical site and when sensors are inserted into different anatomical sites
- Analytical specificity, including:

– Cross-reactivity with molecular compounds similar to glucose
– Interference by endogenous and exogenous compounds/conditions
– Environmental interference from temperature or water exposure
– Interferences due to medical condition of the patient such as ketoacidosis and fever

4.3.2 Performance of Commercially Available CGM Systems

We shall refrain here from a complete literature review for more than one reason. Clearly, a general trend of improved sensor accuracy as expressed in MARD values and increased percentage of CGM data points in regions A and B of Error Grids, sensor precision as expressed in PARD, and overall system reliability is evident from relevant literature [183, 276, 453, 454, 471–475]. It appears thus most meaningful to focus on the performance of the most recent CGM systems. Comparison based on MARD values only [268] is hardly meaningful given the differences in study protocols as described in Sect. 3.1.3. In spite of the existing Clinical and Laboratory Standards Institute (CLSI) guideline for evaluation of CGM systems [469], the comparison of different CGM systems has remained difficult. Head-to-head sensor comparisons, which are obviously preferable to compare system performance, have remained fairly rare. Finally, it remains difficult to attribute a reported performance improvement to one sole measure, such as sensor layout change, coating change, or algorithm optimization [476]. Consequently, based on published literature, it is thus rarely possible to deduce fundamental advantages associated with one or the other approach. Instead, we choose to describe general system performance of four CGM systems which have either been introduced into the market place or are going to be introduced. Performance of current systems has been ranked as ranging from acceptable to good [467], clearly pointing to potential for improvement.

A recent head-to-head performance study [265] investigated CGM-to-BG differences [(MARD) and sensor-to-sensor differences (PARD)] of 12 subjects with type 1 diabetes, where each subject wore two Abbott FreeStyle® Navigator™, two MiniMed Guardian™ REAL-Time + Enlite™ sensor systems, and two DexCom™ Seven® Plus 3rd-generation (Seven® Plus) sensors. Each sensor was used for the lifetime specified by the manufacturer (5 days, 6 days, and 7 days, respectively). To follow POCT05-A recommendations, glucose excursions were induced on two separate occasions, during which venous and capillary blood glucose (BG) concentrations were obtained every 15 min for five consecutive hours. Capillary BG concentrations were measured at least once per hour during the day and once at night. An overview of performance metrics is given in Table 5. As evident from Table 5, performance in the hypoglycemic range was significantly worse than the overall performance. Overall accuracy did not deteriorate over time of use, as indicated by no increase in MARD over time (see Fig. 5).

A head-to-head comparison [477] of the FreeStyle® Navigator™ (Abbott Diabetes Care), the Seven® Plus™ (DexCom), and the Guardian™ (Medtronic), worn twice simultaneously by 6 Type 1 subjects over 51 h (BGM measurement every 15 min; for 48 h) and until the end of sensor lifetime, confirmed differences in performance characteristics including accuracy, precision, and reliability. The Navigator™ system showed an aggregate mean absolute relative difference (MARD) of all paired points of 11.8 ± 11.1%, an average MARD across all 12 experiments of 11.8 ± 3.8%. The Seven® Plus and Guardian™ produced

Table 5 Performance of overview head-to-head performance study

	MARD (%) overall	MARD (%) hypoglycemic range	MARD during induced glucose excursion (%)	PARD (%)
2× Freestyle Navigator™ (Navigator)	12.1	24.6	14.3	9.6/9.8
2× MiniMed Guardian™ REAL-Time + Enlite™ sensor	16.2	34.9	19.2	16.7/25.5
2× DexCom™ Seven® Plus 3rd generation (Seven® Plus)]	16.3	32.7	15.8	18.1/20.2

FreeStyle Navigator™ (Navigator), MiniMed Guardian™ REAL-Time + Enlite™ sensor, DexCom™ Seven® Plus 3rd generation (Seven® Plus)]
Data extracted from [265]

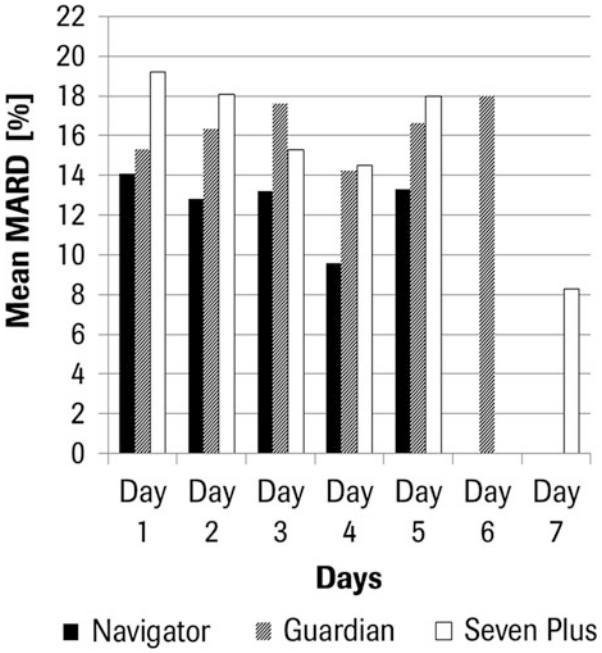

Fig. 5 Mean MARD (%) of three CGM systems in dependence of time of CGM use. Date extracted from [265]

aggregate MARDs of all paired points of 16.5 ± 17.8% and 20.3 ± 18.0%, respectively, and average MARDs across all 12 experiments of 16.5 ± 6.7% and 20.2 ± 6.8%, respectively. Data reporting percentages, a measure of reliability, were 76% for the Seven® Plus and nearly 100% for the Navigator 100% for the Guardian™. Luijf et al. [478] conducted a home study with three CGM systems, the Abbott Diabetes Care FreeStyle® Navigator™ I, the Medtronic Paradigm™ System with Enlite™ Sensor, and the DexCom G4™ version A sensor (G4A), the succeeding system to the Seven® Plus. Twenty patients with type 1 diabetes

mellitus were wearing each system over 4 h, prior to removing one of three systems, selected in a random fashion. Subsequently, two systems were worn until the user lifetime was defined by the manufacturer, thereafter explanted and reinserted to test for long-term performance. BGM measurements were taken every 15 min immediately prior to home use in the clinical phase and less frequently during the home phase. A postprandial glucose peak and nadir were induced intentionally. Prior to phase, overall MARD was measured to be $16.5\% \pm 14.3\%$ for Navigator™ and $16.4\% \pm 15.6\%$ for Enlite™, outperforming G4A at $20.5\% \pm 18.2\%$. During the home study phase, overall MARD was $14.5\% \pm 16.7\%$ for Navigator™, $16.5 \pm 18.8\%$ for DexCom G4A™, and $18.9\% \pm 23.6\%$ for Enlite™. Median time until the end of sensor function was found to amount to 10.0 ± 1.0 days for DexCom G4A™, 8.0 ± 3.5 days for Navigator™, and 8.0 ± 1.5 days for Medtronic MiniMed Enlite™. Overall MARD tends to vary insignificantly for FreeStyle® Navigator™ and DexCom G4A™, while increasing for Enlite™ over time of use. Luijf et al. [478] elucidate the reliability of CGM systems over extended – off-label – use, clarifying that extended use leads to significant reduction of system reliability. Zschornak et al. [266] published data from 30 Type 1 subjects, wearing two identical sensor of a Roche sensor, which is currently in product development, over a time span of 7 days. Glucose excursions were induced on two subsequent study days, 16 capillary blood samples were analyzed every 24 h, whereas one sample was taken and analyzed at night. MARD between CGM readings and paired capillary blood glucose readings and e (PARD), i.e., differences between paired CGM readings, were calculated. An aggregated MARD of 9.2% overall (10.9% during the excursion), an overall aggregated PARD of 7.5% (7.8% during the excursion) were calculated. In the low glycemic range, mean MARD and PARD values of 12.3% and 12.4% were calculated, respectively. Importantly, compared with currently already available CGM systems [265, 290, 475, 477–480], the sensor performance in the hypoglycemic range was remarkably better.

Summarizing, meaningful comparison of CGM systems requires clinical head-to-head comparison. Introduced CGM data as summarized above and as presented very recently [453] for a factory calibrated system show significant improvement in comparison to older studies [468, 472]. Accuracy of CGM systems, in particular in the hypoglycemic range a frequently discussed problem, which limits applicability of CGM systems [481, 482], remains suboptimal for some systems. Constancy of sensor readout over time of use and after different times of storage remains an area of improvement. Efforts to address the root causes of accuracy and reliability issues are well on their way and will – in the opinion of the authors – lead to significant CGM system performance improvement in the near future. The authors nevertheless expect that very high accuracy will still require CGM calibration in the near future.

4.4 CGM System Outlook

CGM systems will be adopted in the future by a larger population of diabetic patients if the advantages outweigh the hassle of using a system which needs to be worn all day. Obviously this asks for increased performance of CGM systems and for largely improved ease of use. Ease-of-use improvements will focus on reduction or even elimination of calibration steps needed, minimization of handling steps, ease of ware, multiple connectivity solutions to allow for communication with well-established receiving devices, and very importantly a self-explanatory user interface which offers ease of control and the depth of information which is required for the particular user. Advantages of a CGM system are weighted differently by different users as described in Sect. 4.1. Lodwig et al. [467] described concisely possible steps toward an artificial pancreas, as defined by the FDA [470], which appeal to patients on continuous subcutaneous insulin infusion (CSII) therapy. Patients who are treated with multiple daily injections (MDI) have identified clearly discernible benefits from CGM use.

Current commercially available CGM systems are significantly improved over initial offerings, but still fall short of user requirements in important areas. Performance, as measured by the accuracy of the estimated blood glucose value, especially in the critical low glucose range [276, 467, 483, 484], is insufficient to exclusively rely on CGM data in all cases. This performance gap is partially due to the physiology of the sample matrix, the subcutaneous tissue space. Especially in circumstances of rapid increase or decrease in blood glucose, the subcutaneous glucose value differs from the blood glucose due to a physiological lag time. The diffusion-limiting membranes of the sensors and the filtering and other signal processing also contribute a technological lag time to the reported glucose estimate [276]. Systems which are calibrated via BGM products also introduce an additional calibration error to the estimate. Systems with no user calibration must accept the within-lot distribution of sensor sensitivities and the between-user and between-sensor site distribution as additional error sources. Precondition to performance improvement is a realistic view of the current CGM sensor performance. Although CGM sensor performance has improved significantly over the last 15 years [467] and time of use has been extended to up to 14 days, there remain significant limitations. Sensor run-in tends to be too long, sensitivity over time of use is not sufficiently constant, artifacts inducible by interferences remain possible, and external influences by changes in pressure and temperature may lead to significant error. Current manufacturing techniques are not optimally suited to produce sensors with largely increased throughput with ever decreased variability of intra- and inter-sensor response. Future transcutaneous CGM sensors, next-generation glucose sensors (NGGS), as coined by Lodwig et al. [467], will need to offer improvements in these aspects.

Inconstant reliability of results is a frequently neglected barrier to the uncritical use of a single CGM estimate for acute treatment. If insulin dosing is to rely on the readout of a CGM system, accuracy at any time of use in contrast to mean accuracy

over total time of use, which is stated frequently, becomes crucially relevant. The well-known "dropouts" or intervals of unusually low estimated glucose values have been described as "tissue compression artifacts" and can sometimes be related to physical pressure on the area of the sensor [485]. Sensors have also been described as being "noisy" at the beginning or especially toward the end of their use period. The physical intrusion of an attached device, especially with an implanted part, remains a barrier to many potential users. Developments in electronic, energy, and communication technology have enabled smaller and lighter external components, and the sensors themselves have become smaller, reducing the intrusion. Reliable attachment of the external component without significant skin irritation is a constant and increasing problem as the duration of use increases.

The lack of general reimbursement and the subsequent out of pocket cost for the user is a significant barrier for broad acceptance. Performance issues motivate especially insulin-dependent users to carry and use a standard BGM system in addition to the CGM. Unless the CGM significantly reduces the number of test strips the user requires, total costs for glucose monitoring are not reduced and may be significantly increased. Reimbursement of CGM systems will require demonstration of improvements in outcomes or reductions in costs due to acute events or long-term complications.

Currently there is no convenient solution for CSII patients due to incompatibility of CGM sensors and insulin infusion catheters regarding time of use and electrode chemistry. Also, the fundamentally limited maximum time of use of transcutaneous CGM sensors remains unclear. Clearly, long-term sensors, extending CGM to a monitoring time of 1 month and longer, will ask for fully implantable solutions. Full implants, however, open up a different set of requirements regarding power management, membranes, and coatings while significantly increasing the cost of clinical trials.

From the authors' perspective, successful improvement of the performance of transcutaneous sensors will allow for therapy adjustments based on CGM sensor signals and consequently for more widespread reimbursement of CGM cost. Development of long-term sensors will continue in parallel to transcutaneous sensors. The development of CGM systems will continue due to the appeal of an easy-to-use CGM system with a highly accurate, highly precise, and highly reliable sensor. The need for significant progress in sensor performance, diverse patient needs asking for different system solutions, increasing cost pressure onto manufacturers, and demanding regulatory environments ask for decisive and rapid progress in the field of CGM system development.

5 Conclusion

Glucose monitoring is the most successful application of biosensor technology and has motivated tremendous improvements in the biology, chemistry, measurement, and fabrication methods of biosensors. The performance of electrochemical

biosensors used for blood glucose measurement has improved greatly over the last four decades. Technological advance has allowed to measure glucose over a wide range of glucose concentration and a wide temperature and hematocrit range in the presence of an abundance of interfering substances with ever-increasing accuracy and precision. The sample volume and time needed to obtain a glucose concentration value have decreased dramatically [52, 72, 220, 221]. The use of optimized enzymes, mediators, and electrochemical measurement methods enable this tremendous progress in performance. Great advances of manufacturing techniques have allowed for a massive scale-up of production which is needed to provide a sufficient number of test strips on a global scale at ever decreasing price. Looking ahead, the demands on blood glucose system performance are expected to grow even as the pressures to lower the cost of systems increase. The drive for the future is to continue to push the limits on system performance while lowering cost, all while finding ways to provide the best medical value to persons with diabetes and healthcare providers. Continuous glucose monitoring promises to provide even greater flexibility and personalized diabetes management, especially for patients who face difficulties to control disease due to extremely variable diet and exercise patterns. CGM systems are significantly improved over initial offerings with regard to convenience and performance. Great progress has been made to achieve effortless and painless insertion of an ever smaller sensor in order to overcome the concerns of some patients to use a minimally invasive sensor. Progress in electronics, power supply, and communication technology has enabled smaller and lighter external components. Further convenience improvements will focus on miniaturization of system size, extension of time of use, reduction or even elimination of calibration steps, minimization of handling steps, ease of ware and combination with insulin catheters, and facile communication with a multitude of established communication devices. Accuracy, precision, and reliability of CGM sensors, which was originally quite poor compared to BGM systems, has been improved greatly by introducing new materials and manufacturing methods, while keeping the amperometric measurement principle. Currently available CGM systems however still fall short of user requirements in important areas. While accuracy of subcutaneously implanted CGM sensors is fundamentally limited by the characteristics of the fatty tissue surrounding the sensor, technical issues of commercially available sensors remain to be solved which currently impede reliable hypo- and hyperglycemic alarms, safe insulin dosing recommendations, or insulin pump control at any time of use. Accuracy tends not be constant over time of use due to sensitivity changes, particularly after sensor insertion and upon extended use. Artifacts inducible by exogenous interfering substances are not negligible due to insufficient specificity. Changes in pressure and temperature may still lead to significant error in some designs. From the authors' perspective, gradual improvement of the currently used amperometric sensing platforms and data evaluation algorithms will keep yielding gradually improved sensor performance. Further advances of material development, manufacturing methods, and the use of advanced measurement methods will allow for improvement of robustness yet also of accuracy. Accuracy gains will translate into improved ease of use (less

BGM calibrations needed) and introduction of artificial pancreas features into the daily routine of Type 1 diabetes patients. Accuracy gains may also allow for therapy adjustments based on CGM sensor signals and – if translated into patient relevant outcomes – consequently for more widespread reimbursement of CGM in the future.

CGM sensors which are fundamentally different from amperometric enzyme-based biosensors will have to compete with comparably mature sensor layouts which have been improved over several decades. Fully implanted long-term sensors may generate the need for alternative glucose sensors. We anticipate that the development of transcutaneous and fully implanted glucose sensors will continue in parallel. The development of CGM systems will continue due to the appeal of an easy-to-use CGM system with a highly accurate, highly precise, and highly reliable sensor. The need for significant progress in sensor performance, diverse patient needs asking for different system solutions, increasing cost pressure onto manufacturers, and demanding regulatory environments ask for decisive and rapid progress in the field of CGM system development.

It is realistic to assume that Continuous Glucose Monitoring (CGM) systems will be adopted in the future by a larger population of diabetic patients. Yet it is also clear that blood glucose monitoring (BGM) systems will remain a major choice of the great majority of persons with diabetes (PwDs) on a global scale who require monitoring but not continuous active management of glucose and insulin levels.

Acknowledgment The authors gratefully acknowledge the contribution of K. Berndt with respect to payer requirements. Further, the authors gratefully acknowledge critical proofreading by N. Carrington, G. Freckmann, R. Heitlinger, A. Rügner, G. Schmelzeisen-Redeker, M. Schoemaker, and D. Urošević.

References

1. Grunberger G, Bailey T, Camacho P, Einhorn D, Garber AJ, Handelsman Y, Mack Harrell R, Lando HM, Law B, Leffert JD, Orzeck EA, Glucose Monitoring Consensus Conference Writing Committee (2015) Proceedings from the American association of clinical endocrinologists and American college of endocrinology consensus conference on glucose monitoring. Endocr Pract 21(5):522–533
2. American Diabetes Association (2014) Standards of medical care in diabetes. Diabetes Care 37(Suppl 1):S14–S80
3. Yoo EH, Lee SY (2010) Glucose biosensors, an overview of use in clinical practice. Sensors 10(5):4558–4576
4. Clark LC Jr, Lyons C (1962) Electrode systems for continuous monitoring in cardiovascular surgery. Ann N Y Acad Sci 102:29–45
5. Turner A (2013) Biosensors, sense and sensibility. Chem Soc Rev 42:3184–3196
6. UKPDS Group (1998) Intensive blood-glucose control with sulphonylureas or insulin compared with conventional treatment and risk of complications in patients with type 2 diabetes (UKPDS 33). Lancet 352(9131):837–853

7. The Diabetes Control and Complications Trial Research Group (1993) The effect of intensive treatment of diabetes on the development and progression of long-term complications in insulin-dependent diabetes mellitus. N Engl J Med 329(14):977–986
8. Li R, Zhang P, Barker LE, Chowdhury FM, Zhang X (2010) Cost-effectiveness of interventions to prevent and control diabetes mellitus: a systematic review. Diabetes Care 33 (8):1872–1894
9. Miller KM, Beck RW, Bergenstal RM, Goland RS, Haller MJ, McGill JB, Rodriguez H, Simmons JH, Hirsch IB (2013) Evidence of a strong association between frequency of self-monitoring of blood glucose and hemoglobin A1C levels in T1D exchange clinical registry participants. Diabetes Care 36(7):2009–2014
10. Ziegler R, Heidtmann B, Hilgard D, Hofer S, Rosenbauer J, Holl R (2011) Frequency of SMBG correlates with HbA1c and acute complications in children and adolescents with type 1 diabetes. Pediatr Diabetes 12(1):11–17
11. Klonoff DC, Blonde L, Cembrowski G, Chacra AR, Charpentier G, Colagiuri S, Dailey G, Gabbay RA, Heinemann L, Kerr D, Nicolucci A, Polonsky W, Schnell O, Vigersky R, Yale JF (2011) Consensus report, the current role of self-monitoring of blood glucose in non-insulin-treated type 2 diabetes. J Diabetes Sci Technol 5(6):1529–1548
12. American Diabetes Association, Standards of Medical Care in Diabetes (2014) Diagnosis and classification of diabetes mellitus. Diabetes Care 37(Suppl 1):S81–S90
13. Sacks DB, Arnold M, Bakris GL, Bruns DE, Horvath AR, Kirkman MS, Lernmark A, Metzger BE, Nathan DM (2011) Guidelines and recommendations for laboratory analysis in the diagnosis and management of diabetes mellitus. Clin Chem 57(6):e1–e47
14. Food and Drug Administration Center for Drugs Evaluation and Research (2014) Blood glucose monitoring test systems for prescription point-of-care use, draft guidance for industry and food and drug administration staff. http://www.fda.gov/downloads/MedicalDevices/DeviceRegulationandGuidance/GuidanceDocuments/UCM380325.pdf
15. CLSI (2015) Glucose monitoring in settings without laboratory support. Clinical and Laboratory Standards Institute, Wayne, p 82
16. Food and Drug Administration Center for Drugs Evaluation Research (2014) Self-monitoring blood glucose test systems for over-the-counter use: Draft Guidance for Industry and Food and Drug Administration Staff Draft Guidance, FDA Maryland
17. ISO 15197:2013 In vitro diagnostic test systems—requirements for blood-glucose monitoring systems for self-testing in managing diabetes mellitus
18. Fouretier A, Bertram D (2014) New regulations on medical devices in Europe, What to expect? Expert Rev Med Devices 11(4):351–359
19. Jarow J, Baxley JH (2015) Medical devices, US medical device regulation. Urol Oncol Semin Orig Investig 33(3):128–132
20. Jyothi G, Venkatesh M, Pramod Kumar T (2013) Regulations of medical devices in regulated countries: a comparative review. Ther Innov Regul Sci 47(5):581–592
21. McCulloch P (2012) The EU's system for regulating medical devices. BMJ 345:e71266
22. Tamura A, Kutsumi H (2014) Multiregional medical device development. Regulatory perspective Clin J Gastroenterol 7(2):108–116
23. Code of Federal Regulations Title 21, Chapter I, Subchapter H, Part 820—PART 820—medical devices; quality system regulation. http://www.ecfr.gov/cgi-bin/text-idx?SID=4f03a00bda668d3977d1260056f8d423&mc=true&node=pt21.8.820&rgn=div5
24. Friedman LM, Furberg CD, DeMets DL, Reboussin DM, Grange CB (2015) Fundamentals of clinical trials. Springer, Heidelberg, pp 519–538
25. Code of Federal Regulations Title 21, Chapter I, Subchapter H, Part 806—medical devices; reports of corrections and removals. http://www.ecfr.gov/cgi-bin/text-idx?SID=4f03a00bda668d3977d1260056f8d423&mc=true&node=pt21.8.806&rgn=div5
26. Code of Federal Regulations Title 21, Chapter I, Subchapter H, Part 803–medical devices; medical device reporting. http://www.ecfr.gov/cgi-bin/text-idx?SID=4f03a00bda668d3977d1260056f8d423&mc=true&node=pt21.8.803&rgn=div5

27. Guidelines on a Medical Devices Vigilance System January 2013 MEDDEV 2.12-1 rev 8. http://ec.europa.eu/DocsRoom/documents/15506/attachments/1/translations/en/renditions/pdf
28. Justiniano J, Gopalaswamy V (2003) Practical design control implementation for medical devices. CRC, Boca Raton
29. Fries RC (2012) Reliable design of medical devices. CRC, Boca Raton
30. Burke DW (2014) Method for determining whether a disposable, dry regent, electrochemical test strip is unsuitable for use. US 8,859,293
31. Chua KS, Tan IK (1978) Plasma glucose measurement with the Yellow Springs Glucose Analyzer. Clin Chem 24(1):150–152
32. Rajendran R, Rayman G (2014) Point-of-care blood glucose testing for diabetes care in hospitalized patients: an evidence-based review. J Diabetes Sci Technol 8(6):1081–1090
33. Heinemann L (2010) Quality of glucose measurement with blood glucose meters at the point-of-care: relevance of interfering factors. Diabetes Technol Ther 12(11):847–857
34. Kiechle FL, Main RI (2000) Blood glucose: measurement in the Point-of-Care Setting. Lab Med 31(5):276–282
35. Stepman HCM, Tiikkainen U, Stoeckl D, Vesper HW, Edwards SH, Laitinen H, Pelanti J, Thienpont LM (2014) Measurements for 8 common analytes in native sera identify inadequate standardization among 6 routine laboratory assays. Clin Chem 60(6):855–863
36. Twomey PJ (2004) Plasma glucose measurement with the Yellow Springs Glucose 2300 STAT and the Olympus AU640. J Clin Pathol 57(7):752–754
37. CLSI (2013) Point-of-Care blood glucose testing in acute and chronic care facilities 2013. Clinical and Laboratory Standards Institute, Wayne
38. American Association of Diabetes Educators AADE analysis on draft guidance for blood glucose monitoring systems, November 2014 http://www.diabeteseducator.org/export/sites/aade/_resources/Advocacy/FDA_BGM_GUIDANCE_COMMENTS_ANALYSIS_2014.pdf
39. Klonoff DC (2014) Point-of-Care blood glucose meter accuracy in the hospital setting. Diabetes Spectr 27(3):174–179
40. Tenderich A (2014) Glucose meter accuracy: FDA's new dual call for tighter standards., http://www.healthline.com/diabetesmine/glucose-meter-accuracy-fdas-new-dual-call-for-tighter-standards#1
41. Hoskins M (2014) Unintended consequences of tighter glucose meter accuary. . .? Diabetes Mine., http://www.healthline.com/diabetesmine/unintended-consequences-of-meter-accuracy#1
42. Klonoff DC, Vigersky RA, Nichols JH, Rice MJ (2014) Timely hospital glucose measurement: here today, gone tomorrow? Mayo Clin Proc 89(10):331–1335
43. Ferrante do Amaral CE, Wolf B (2008) Current development in non-invasive glucose monitoring. Med Eng Phys 30(5):541–549
44. Tura AA, Maran Pacini G (2007) Non-invasive glucose monitoring, assessment of technologies and devices according to quantitative criteria. Diabetes Res Clin Pract 77(1):16–40
45. Chen X, Wu G, Cai Z, Oyama M, Chen X (2014) Advances in enzyme-free electrochemical sensors for hydrogen peroxide, glucose, and uric acid. Microchim Acta 181(7–8):689–705
46. Tian K, Prestgard M, Tiwari A (2014) A review of recent advances in nonenzymatic glucose sensors. Mater Sci Eng C Mater Biol Appl 41:100–118
47. Toghill KE, Compton RG (2010) Electrochemical non-enzymatic glucose sensors, a perspective and an evaluation. Int J Electrochem Sci 5(9):1246–1301
48. Wang G, He X, Wang L, Gu A, Huang Y, Fang B (2013) Non-enzymatic electrochemical sensing of glucose. Microchim Acta 180(3–4):161–186
49. Egawa Y, Seki T, Takahashi S, Anzai J (2011) Electrochemical and optical sugar sensors based on phenylboronic acid and its derivatives. Mat Sci Eng C 31(7):1257–1264
50. Wu Q, Wang L, Yu H, Wang J, Chen Z (2011) Organization of glucose-responsive systems and their properties. Chem Rev 111(12):7855–7875
51. Andreis E, Küllmer K, Appel M (2014) Application of the reference method isotope dilution gas chromatography mass spectrometry (ID/GC/MS) to establish metrological traceability for calibration and control of blood glucose test systems. J Diabetes Sci Technol 8(3):508–515

52. Clarke SF, Foster JR (2012) A history of blood glucose meters and their role in self-monitoring of diabetes mellitus. Br J Biomed Sci J Diabetes Sci Technol 69(2):83–93
53. Dextrostix and Azostix (1968) Drug Ther Bull 6(25):97–99
54. Free AH, Ree AH, Adams EC, Kercher ML, Free HM, Cook MH (1957) Simple specific test for urine glucose. Clin Chem 3(3):163–168
55. McCall AL, Mullin CJ (1986) Home monitoring of diabetes mellitus-A quiet revolution. Clin Lab Med 6(2):215–239
56. Updike SJ, Hicks G (1967) The enzyme electrode. Nature 214(5092):986–988
57. Updike SJ, Hicks G (1967) Reagentless substrate analysis with immobilized enzymes. Science 158(3798):270–272
58. Wang HC, Lee AR (2015) Recent developments in blood glucose sensors. J Food Drug Anal 23(2):191–200
59. Heller A, Feldman B (2008) Electrochemical glucose sensors and their applications in diabetes management. Chem Rev 108(7):2482–2505
60. Heller A, Feldman B (2010) Electrochemistry in diabetes management. Acc Chem Res 43 (7):963–973
61. Wang J (2008) Electrochemical glucose biosensors. Chem Rev 108(2):814–825
62. Wang Y, Xu H, Zhang J, Li G (2008) Electrochemical sensors for clinic analysis. Sensors 8 (4):2043–2081
63. Taguchi M, Ptitsyn A, McLamore ES, Claussen JC (2014) Nanomaterial-mediated biosensors for monitoring glucose. J Diabetes Sci Technol 8(2):403–411
64. Mohd Yazid SNA, Md Isa I, Abu Bakara S, Hashim N, Ab Ghanic S (2014) A review of glucose biosensors based on graphene/metal oxide nanomaterials. Anal Lett 47 (11):1821–1834
65. Chen C, Xie Q, Yang D, Xiao H, Fu Y, Tan Y, Yao S (2013) Recent advances in electrochemical glucose biosensors: a review. RSC Adv 3(14):4473–4491
66. Vashist SK, Zheng D, A-Rubeaan K, Luong JH, Sheu FS (2011) Technology behind commercial devices for blood glucose monitoring in diabetes management: a review. Anal Chim Acta 703(2):124–136
67. McGarraugh G (2009) The chemistry of commercial continuous glucose monitors. Diabetes Technol Ther 11(Suppl 1):S17–S24
68. Vaddiraju S, Burgess DJ, Tomazos I, Jain FC, Papadimitrakopoulos F (2010) Technologies for continuous glucose monitoring, current problems and future promises. J Diabetes Sci Technol 4(6):1540–1562
69. Gough DA, Lucisano JY, Tse HSM (1985) Two-dimensional enzyme electrode sensor for glucose. Anal Chem 57(12):2351–2357
70. Cass AE, Davis G, Francis GD, Hill HA, Aston WJ, Higgins IJ, Plotkin EV, Scott LD, Turner AP (1984) Ferrocene-mediated enzyme electrode for amperometric determination of glucose. Anal Chem 56(4):667–671
71. Hoenes J, Mueller P, Surridge N (2008) The technology behind glucose meters, test strips. Diabetes Technol Ther 10(S1):S-10-S-26
72. Newman JD, Turner AF (2005) Home blood glucose biosensors, a commercial perspective. Biosens Bioelectron 20(12):2435–2453
73. Ferri S, Kojima K, Sode K (2011) Review of glucose oxidases and glucose dehydrogenases, a bird's eye view of glucose sensing enzymes. J Diabetes Sci Technol 5(5):1068–1076
74. Horaguchi Y, Saito S, Kojima K, Tsugawa W, Ferri S (2014) Engineering glucose oxidase to minimize the influence of oxygen on sensor response. Electrochim Acta 126:158–161
75. Horaguchi Y, Saito S, Kojima K, Tsugawa W (2012) Construction of mutant glucose oxidases with increased dye-mediated dehydrogenase activity. Int J Mol Sci 13 (11):14149–14157
76. Tanaka S, Igarashi S, Ferri S, Sode K (2005) Increasing stability of water-soluble PQQ glucose dehydrogenase by increasing hydrophobic interaction at dimeric interface. BMC Biochem 6:1–6

77. Igarashi S, Okuda J, Ikebukuro K, Sode K (2004) Molecular engineering of PQQGDH and its applications. Arch Biochem Biophys 428(1):52–63
78. Rahman MM, Ahammad AJ, Jin JH, Ahn SJ, Lee JJ (2010) A comprehensive review of glucose biosensors based on nanostructured metal-oxides. Sensors 10(5):4855–4886
79. Phan THT, Tran PD, Pham XTT, Dang BTD, NguyenVL TVM, Bui TG, Dang MC, Tong DH (2013) Glucose biosensor based on platinum nanowires, a clinical study. Int J NanoTechnol 10(3–4):166–177
80. Afreen S, Muthoosamy K, Manickam S, Hashim U (2015) Functionalized fullerene (C60) as a potential nanomediator in the fabrication of highly sensitive biosensors. Biosens Bioelectron 63:354–364
81. Zhu Z, Garcia-Gancedo L, Flewitt AJ, Xie H, Moussy F, Milne WI (2012) A critical review of glucose biosensors based on carbon nanomaterials, carbon nanotubes and graphene. Sensors 12(5):5996–6022
82. Kakehi N, Yamazaki T, Tsugawa W, Sode K (2007) A novel wireless glucose sensor employing direct electron transfer principle based enzyme fuel cell. Biosens Bioelectron 22 (9–10):2250–2255
83. Yamazaki T, Okuda-Shimazaki J, Sakata C, Tsuya T, Sode K (2008) Construction and characterization of direct electron transfer-type continuous glucose monitoring system employing thermostable glucose dehydrogenase complex. Anal Lett 41(13):2363–2373
84. Heller A (1992) Electrical connection of enzyme redox centers to electrodes. J Phys Chem 96 (9):3579–3587
85. Bergenstal RM, Gavin JR (2005) The role of self-monitoring of blood glucose in the care of people with diabetes: report of a global consensus conference. Am J Med 118(9):1–6
86. Bismuth E, Laffel L (2007) Can we prevent diabetic ketoacidosis in children. Pediatr Diabetes 8(Suppl 6):24–33
87. Boettcher C, Dost A, Wudy SA, Flechtner-Mors M, Borkenstein M, Schiel R, Weitzel D, Bechtold-Dalla Pozza S, Wolf J, Holl RW (2015) Accuracy of blood glucose meters for self-monitoring affects glucose control and hypoglycemia rate in children and adolescents with type 1 diabetes. Glucose self-monitoring in type 1 diabetes. Diabetes Diabetes Technol Ther 17(4):275–282
88. Dailey G (2007) Assessing glycemic control with self-monitoring of blood glucose and hemoglobin A(1c) measurements. Mayo Clin Proc 82(2):229–236
89. Garg SK (2008) Glucose monitoring, an important tool for improving glucose control and reducing hypoglycemia. Diabetes Technol Ther 10(S1):S-1-S-4
90. Hansen MV, Pedersen-Bjergaard U, Heller SR, Wallace TM, Rasmussen AK, Jørgensen HV, Pramming S, Thorsteinsson B (2009) Frequency and motives of blood glucose self-monitoring in type 1 diabetes. Diabetes Res Clin Pract 85(2):183–188
91. Hirsch IB, Bode BW, Childs BP, Close KL, Fisher WA, Gavin JR, Ginsberg BH, Raine CH, Verderese CA (2008) Self-Monitoring of Blood Glucose (SMBG) in insulin- and non-insulin-using adults with diabetes, consensus recommendations for improving SMBG accuracy, utilization, and research. Diabetes Technol Ther 10(6):419–439
92. Kolb H, Kempf K, Martin S, Stumvoll M, Landgraf R (2010) On what evidence-base do we recommend self-monitoring of blood glucose? Diabetes Res Clin Pract 87(2):150–156
93. Nielsen JK, Christiansen JS (2008) Self-monitoring of blood glucose—epidemiological and practical aspects. Diabetes Technol Ther 10(s1):S-35-S-42
94. Renard E (2005) Monitoring glycemic control, the importance of self-monitoring of blood glucose. Am J Med 118(9):12–19
95. Scaramuzza A, Cherubini V, Tumini S, Bonfanti R, Buono P, Cardella F, d'Annunzio G, Frongia AP, Lombardo F, Monciotti AC, Rabbone I, Schiaffini R, Toni S, Zucchini S, Frontino G, Iafusco D (2014) Recommendations for self-monitoring in pediatric diabetes: a consensus statement by the ISPED. Acta Diabetol 51(2):173–184
96. Subramanian SL, Hirsch IB (2008) The utility and recent advances in self-monitoring of blood glucose in type 1 diabetes. Diabetes Technol Ther 10(s1):S-43-S-50

97. Boutati EI, Raptis SA (2009) Self-monitoring of blood glucose as part of the integral care of type 2 diabetes. Diabetes Care 32(Suppl 2):S205–S210
98. Campbell JA, Walker RJ, Smalls BL, Egede LE (2012) Glucose control in diabetes: the impact of racial differences on monitoring and outcomes. Endocrine 42(3):471–482
99. Molitch ME, Barr J, Callahan PL, Campbell RK, Delahanty LM, Rizza R, Tobin CT, Young DS (1996) Self-monitoring of blood glucose. Diabetes Care 19(Suppl 1):S62–S66
100. Montagnana M, Caputo M, Giavarina D, Lippi G (2009) Overview on self-monitoring of blood glucose. Clin Chim Acta 402(1–2):7–13
101. Naik RG, Ellis SL (2008) Self-monitoring of blood glucose in insulin-requiring type 2 diabetes. Diabetes Technol Ther 10(s1):S-67-S-71
102. Allemann S, Houriet C, Diem P, Stettler C (2009) Self-monitoring of blood glucose in non-insulin treated patients with type 2 diabetes, a systematic review and meta-analysis. Curr Med Res Opin 25(12):2903–2913
103. Bosi E, Scavini M, Ceriello A, Cucinotta D, Tiengo A, Marino R, Bonizzoni E, Giorgino F (2013) Intensive structured self-monitoring of blood glucose and glycemic control in noninsulin-treated type 2 diabetes: the PRISMA randomized trial. Diabetes Care 36:2887–2894
104. Bosi, E et al (2013) Response to comment on: Bosi et al. Intensive structured self-monitoring of blood glucose and glycemic control in noninsulin-treated type 2 diabetes: the PRISMA randomized trial. Diabetes Care (36):2887–2894; Diabetes Care (36):e218
105. Gerich JE, Odawara M, Terauchi Y (2007) The rationale for paired pre- and postprandial self-monitoring of blood glucose: the role of glycemic variability in micro- and macrovascular risk. Curr Med Res Opin 23(8):1791–1798
106. Ipp E, Aquino RL, Christenson P (2005) Point: self-monitoring of blood glucose in type 2 diabetic patients not receiving insulin: the sanguine approach. Diabetes Care 28 (6):1528–1530
107. Klonoff DC, Blonde L, Cembrowski G, Chacra AR, Charpentier G, Colagiuri S, Dailey G, Gabbay RA, Heinemann L, Kerr D, Nicolucci A, Polonsky W, Schnell O, Vigersky R, Yale JF (2011) Consensus report: the current role of self-monitoring of blood glucose in non-insulin-treated type 2 diabetes. J Diabetes Sci Technol 5(6):1534–1548
108. McGeoch G, Derry S, Moore RA (2007) Self-monitoring of blood glucose in type-2 diabetes: what is the evidence? Diabetes Metab Res Rev 23(6):423–440
109. Murata GH, Duckworth WC, Hoffman RM, Wendel CS, Mohler MJ, Shah JH (2004) Hypoglycemia in type 2 diabetes: a critical review. Biomed Pharmacother 58(10):551–559
110. Parkin CG, Hinnen D, Campbell RK, Geil P, Tetrick DL, Polonsky WH (2009) Effective use of paired testing in type 2 diabetes: practical applications in clinical practice. Diabetes Educ 35(6):915–927
111. Pettus J, Stenger P, Schachner HC, Dunne N, Parkes JL, Pardo S, Edelman SV (2014) Testing versus guessing blood glucose values: impact on self-care behaviors in type 2 diabetes. Curr Med Res Opin 30(9):1795–1802
112. Polonsky WH, Fisher L, Hessler D, Edelman SV (2014) What is so tough about self-monitoring of blood glucose? Perceived obstacles among patients with Type 2 diabetes. Diabet Med 31(1):40–46
113. Ruiz Gracia T, García de la Torre Lobo N, Durán Rodríguez Hervada A, Calle Pascual AL (2014) Structured SMBG in early management of T2DM: contributions from the St Carlos study. World J Diabetes 5(4):471–481
114. Szymborska-Kajanek A, Psurek A, Hese R, Strojek K (2009) Self-monitoring of blood glucose in treatment of type 2 diabetes. Diabetes Res Clin Pract 86S:S49–S52
115. Charny M (2014) Reimbursement unravelled: why blood glucose monitoring products are reimbursement anomalies. Clinica Medtech Intelligence 1–2
116. Davidson MB (2005) Counterpoint: self-monitoring of blood glucose in type 2 diabetes patients not receiving insulin: a waste of money. Diabetes Care 28(6):1531–1533

117. Goyder E (2008) Should we stop patients with non-insulin treated diabetes using self monitoring of blood glucose? The implications of the Diabetes Glycaemic Education and Monitoring (DiGEM) trial. Prim Care Diabetes 2(2):91–93
118. Varanauskiene E (2008) Can blood glucose self-monitoring improve treatment outcomes in type 2 diabetes? Diabetes Res Clin Pract 82(Suppl 2):S112–S117
119. Welschen LM, Bloemendal E, Nijpels G, Dekker JM, Heine RJ, Stalman WA, Bouter LM (2005) Self-monitoring of blood glucose in patients with type 2 diabetes who are not using insulin. Diabetes Care 28(6):1510–1517
120. Gomes T, Juurlink DN, Shah BR, Paterson JM, Mamdani MM (2010) Blood glucose test strips: options to reduce usage. CMAJ 182(1):35–38
121. American Diabetes Association (2013) Economic costs of diabetes in the US in 2012. Diabetes Care 36:1033–1046
122. Hughes MD (2009) The business of self-monitoring of blood glucose: a market profile. J Diabetes Sci Technol 3(5):1219–1223
123. Heinemann L, Klonoff DC (2013) Blood glucose meter market: this world is undergoing drastic changes. J Diabetes Sci Technol 7(3):584–586
124. American Diabetes Association (2014) Third-party reimbursement for diabetes care, self-management education, and supplies. Diabetes Care 37(Suppl 1):S118–S119
125. Kesavadev J, Sadikot S, Wangnoo S, Kannampilly J, Saboo B, Aravind SR, Kalra S, Makkar BM, Maji D, Saikia M, Anjana RM, Rajput R, Singh SK, Shah S, Dhruv U, Vishwanathan V (2014) Consensus guidelines for glycemic monitoring in type 1/type 2 & GDM. Diabetes Metab Syndr 8(3):187–195
126. Clar C, Barnard KD, Cummins E, Royle P, Waugh N (2010) Self-monitoring of blood glucose in type 2 diabetes: systematic review. Health Technol Assessment 14(12):1–140
127. Polonsky WH, Fisher L, Schikman CH, Hinnen DA, Parkin CG, Jelsovsky Z, Petersen P, Schweitzer M, Wagner RS (2011) Structured self-monitoring of blood glucose significantly reduces A1C levels in poorly controlled, noninsulin-treated type 2 diabetes – Results from the Structured Testing Program study. Diabetes Care 34(2):262–267
128. Franciosi M, Lucisano G, Pellegrini F, Cantarello A, Consoli A, Cucco L, Ghidelli R, Sartore G, Sciangula L, Nicolucci A, ROSES Study Group (2011) ROSES: role of self-monitoring of blood glucose and intensive education in patients with Type 2 diabetes not receiving insulin. A pilot randomized clinical trial. Diabet Med 28(7):789–796
129. Tunis SL (2011) Cost effectiveness of self-monitoring of blood glucose (SMBG) for patients with type 2 diabetes and not on insulin: impact of modelling assumptions on recent Canadian findings. Appl Health Econ Health Policy 9(6):351–365
130. European Diagnostic Manufacturers Association (2014) Position Paper 27. Health Technology Assessment for IVDs in the context of market access http://www.medtecheurope.org/sites/default/files/2014_10_29_HTA_for_IVDs_in_the_Context_of_Market_Access_PP_PUB%5B1%5D.pdf
131. Moodley N, Ngxamngxa U, Turzyniecka MJ, Pillay TS (2015) Historical perspectives in clinical pathology: a history of glucose measurement. J Clin Pathol 68(4):258–264
132. Roche Diagnostics (2011) Compendium of urinalysis—urine test strips and microscopy. http://www.roche-diagnostics.ch/content/dam/corporate/roche-dia_ch/documents/broschueren/professional_diagnostics/urindiagnostik/12254620001_EN_EA_Compendium-of-urinanalysis_Brosch%C3%BCre_EN.pdf
133. International Diabetes Federation Guideline Development Group (2014) Global guideline for type 2 diabetes. Diabetes Res Clin Pract 104(1):1–52
134. myDr. (2009) Diabetes and urine glucose monitoring. Cirrus Media Pty, Ltd. http://www.mydr.com.au/tests-investigations/diabetes-and-urine-glucose-monitoring
135. Diabetes Forecast Consumer Guide (2015) http://www.diabetesforecast.org/2015/mar-apr/consumer-guide-2015.html
136. Diabetes Forecast (2015) Diabetes devices: what matters most to users. http://www.diabetesforecast.org/2015/mar-apr/diabetes-devices-what-matters-most.html

137. Ginsberg BH (2009) Factors affecting blood glucose monitoring: sources of errors in measurement. J Diabetes Sci Technol 3(4):903–913
138. Raine CH, Schrock LE, Edelman SV, Mudaliar SR, Zhong W, Proud LJ, Parkes JL (2007) Significant insulin dose errors may occur if blood glucose results are obtained from miscoded meters. J Diabetes Sci Technol 1(2):205–210
139. Kristensen GB, Sandberg S (2010) Self-monitoring of blood glucose with a focus on analytical quality: an overview. Clin Chem Lab Med 48(7):963–972
140. Freckmann G, Schmid C, Ruhland K, Baumstark A, Haug C (2012) Integrated self-monitoring of blood glucose system: handling step analysis. J Diabetes Sci Technol 6 (4):938–946
141. Bergenstal R, Pearson J, Cembrowski GS, Bina D, Davidson J, List S (2000) Identifying variables associated with inaccurate self-monitoring of blood glucose: proposed guidelines to improve accuracy. Diabetes Educ 26(6):981–989
142. Colin IM, Paris I (2013) Glucose meters with built-in automated bolus calculator: gadget or real value for insulin-treated diabetic patients? Diabetes Ther 4(1):1–11
143. Barnard K, Parkin C, Young A, Ashraf M (2012) Use of an automated bolus calculator reduces fear of hypoglycemia and improves confidence in dosage accuracy in patients with type 1 diabetes mellitus treated with multiple daily insulin injections. J Diabetes Sci Technol 6(1):144–149
144. Ziegler R, Cavan DA, Cranston I, Barnard K, Ryder J, Vogel C, Parkin CG, Koehler W, Vesper I, Petersen B, Schweitzer MA, Wagner RS (2013) Use of an insulin bolus advisor improves glycemic control in multiple daily insulin injection (MDI) therapy patients with suboptimal glycemic control: first results from the ABACUS trial. Diabetes Care 36 (11):3613–3619
145. Ziegler R, Rees C, Jacobs N, Parkin CG, Lyden MR, Petersen B, Wagner RS (2015) Frequent use of an automated bolus advisor improves glycemic control in pediatric patients treated with insulin pump therapy: results of the Bolus Advisor Benefit Evaluation (BABE) study. Pediatr Diabetes. doi:10.1111/pedi.12290 [Epub ahead of print]
146. Hinnen DA, Buskirk A, Lyden M, Amstutz L, Hunter T, Parkin CG, Wagner R (2015) Use of diabetes data management software reports by health care providers, patients with diabetes, and caregivers improves accuracy and efficiency of data analysis and interpretation compared with traditional logbook data: first results of the Accu-Chek Connect Reports Utility and Efficiency Study (ACCRUES). J Diabetes Sci Technol 9(2):293–301
147. List SM, Starks N, Baum J, Greene C, Pardo S, Parkes JL, Schachner HC, Cuddihy R (2011) Performance evaluation and labeling comprehension of a new blood glucose monitoring system with integrated information management. J Diabetes Sci Technol 5(5):1144–1553
148. Gambhir SS (2002) Molecular imaging of cancer with positron emission tomography. Nat Rev 2:683–693
149. Boren SA, Clarke WL (2010) Analytical and clinical performance of blood glucose monitors. J Diabetes Sci Technol 4(1):84–97
150. Schleis, MS (2007) Interference of maltose, icodextrin, galactose, or xylose with some blood glucose monitoring systems. Pharmacotherapy 27(9):1313–1321
151. Yoshida H, Iguchi T, Sode K (2000) Construction of multi-chimeric pyrroloquinoline quinone glucose dehydrogenase with improved enzymatic properties and application in glucose monitoring. Biotechnol Lett 22(18):1505–1510
152. Dimeski G, Jones BW, Tilley V, Greenslade MN, Russell AW (2010) Glucose meters: evaluation of the new formulation measuring strips from Roche (Accu-Chek) and Abbott (MediSense). Ann Clin Biochem 47(Pt 4):358–365
153. Kelly BN, Haverstick DM, Bruns DE (2012) Interference in a glucose dehydrogenase-based glucose meter revisited. Clin Chim Acta 413(7–8):829–830
154. Ng WY, Tiong CC, Jacob E (2010) Maltose interference-free test strips for blood glucose testing at point-of-care: a laboratory performance evaluation. Diabetes Technol Ther 12 (11):889–893
155. Hamamatsu N, Suzumura A, Nomiya Y, Sato M, Aita T, Nakajima M, Husimi Y, Shibanaka Y (2006) Modified substrate specificity of pyrroloquinoline quinone glucose dehydrogenase

by biased mutation assembling with optimized amino acid substitution. Appl Microbiol Biotechnol 73(3):607–617
156. Boenitz-Dulat M, Beck D, Kratzsch P, Schmuck R, Von Der Eltz H (2007) Improved mutants of Acinetobacter calcoaceticus pyrroloquinoline quinone-dependent soluble glucose dehydrogenase and their use for detection of glucose. WO 2007118647A1
157. Boenitz-Dulat M (2009) Mutants of pyrroloquinoline quinone dependent soluble glucose dehydrogenase. US 20090148874A1
158. Boenitz-Dulat M, Kratzsch P, Schmuck R (2010) Thermostabile mutants of pyrroloquinoline quinone dependent glucose dehydrogenase. US 7,781,196
159. Moiroux J, Elving PJ (1979) Adsorption phenomena in the NAD+/NADH system at glassy carbon electrodes. J Electroanal Chem 102:93–108
160. Moiroux J, Elving PJ (1980) Adsorption phenomena in the NAD+/NADH oxidation of dihydronicotinamide adenine dinucleotide (NADH). J Am Chem Soc 102:6533–6538
161. Nowall WB, Kuhr WG (1995) Adsorption phenomena in the NAD+/NADH of NADH and other anionic molecules of biological significance. Anal Chem 67(19):3583–3588
162. Gorton L, Domínguez E (2000) Adsorption phenomena in the NAD+/NADH-modified electrodes. Rev Mol BioTechnol 82:371–392
163. Prieto-Simon B, Fabregas E (2004) Comparative study of electron mediators used in the electrochemical oxidation of NADH. Biosens Bioelectron 19(10):1131–1138
164. Beaty TA, Kuhn LS, Svetnik V, Burke DW (2003) Meter and method of using the meter for determining the concentration of a component of a fluid. US 6,645,368
165. Burke DW, Surridge NA, Groll H (2014) System and method for analyte measurement. US 8,663,442
166. Musholt PB, Schipper C, Thomé N, Ramljak S, Schmidt M, Forst T, Pfützner A (2011) Dynamic electrochemistry corrects for hematocrit interference on blood glucose determinations with patient self-measurement devices. J Diabetes Sci Technol 5(5):1167–1175
167. Pfuetzner A, Schipper C, Ramljak S, Flacke F, Sieber J, Forst T, Musholt PB (2013) Determination of hematocrit interference in blood samples derived from patients with different blood glucose concentrations. J Diabetes Sci Technol 7(1):170–178
168. Conductive Technologies I, electrochemical sensors. Product brochure. http://www.conductivetech.com/wp-content/uploads/2015/03/CTI-Electrochemical-Sesnors.pdf
169. BI Technologies L Thick film electrodes for sensors. Product brochure. http://www.bitechnologies.com/pdfs/thickfilmelectrodesforsensors.pdf
170. Bhullar RS, Diebold ER, Hill BS, Surridge NA, Walling DP (2006) Method of making a biosensor US 7,073,246
171. Bhullar R, Diebold ER, Hill BS, Surridge N, Walling PD (2013) Biosensor and method of making. US 8,551,308
172. Turner APF, Chen B, Piletsky SA (1999) In vitro diagnostics in diabetes: meeting the challenge. Clin Chem 45(9):1596–1601
173. Burke DW, Marquant M, Zapf U, Fritz M, Mosoiu D, Wilsey C (2011) Reagent stripe for test strip US 7,892,849B2
174. Mosoiu D, Wilsey CD (2009) Method and reagent for producing narrow, homogeneous reagent stripes US 20090162532A1
175. Medical Device Directive 98/79/EC (1998) In vitro diagnostic medical devices. http://ec.europa.eu/growth/single-market/european-standards/harmonised-standards/iv-diagnostic-medical-devices/index_en.htm
176. D'Orazio PD, Burnett RW, Fogh-Andersen N, Jacobs E, Kuwa K, Külpmann WR, Larsson L, Lewenstam A, Maas AHJ, Mager G, Naskalski JW, Okorodudu AO (2006) Approved IFCC recommendation on reporting results for blood glucose. Clin Chem Lab Med 44 (12):1486–1490
177. Chen Y, Liu Q, Yong S, Lee TK (2012) High accuracy analysis of glucose in human serum by isotope dilution liquid chromatography-tandem mass spectrometry. Clin Chim Acta 413 (7–8):808–813

178. Prendergast JL, Sniegoski LT, Welch MJ, Phinney KW (2010) Modifications to the NIST reference measurement procedure (RMP) for the determination of serum glucose by isotope dilution gas chromatography/mass spectrometry. Anal Bioanal Chem 397(5):1779–1785
179. Freckmann G, Schmid C, Baumstark A, Pleus S, Link M, Haug C (2013) In response to Teodorczyk and coauthors: system accuracy of blood glucose monitoring devices according to the current and proposed ISO 15197 standards. J Diabetes Sci Technol 7(6):1659–1660
180. Genter PM, Ipp E (1994) Accuracy of plasma glucose measurements in the hypoglycemic range. Diabetes Care 17(6):595–598
181. Schnell O, Hinzmann R, Kulzer B, Freckmann G, Erbach M, Lodwig V, Heinemann L (2013) Assessing the analytical performance of systems for self-monitoring of blood glucose: concepts of performance evaluation and definition of metrological key terms. J Diabetes Sci Technol 7(6):1585–1594
182. Freckmann G, Schmid C, Baumstark A, Rutschmann M, Haug C, Heinemann L (2015) Analytical performance requirements for systems for self-monitoring of blood glucose with focus on system accuracy: relevant differences among ISO 15197:2003, ISO 15197:2013, and current FDA recommendations. J Diabetes Sci Technol. Epub 2015 Apr 14
183. Clarke WL, Cox D, Gonder-Frederick LA, Carter W, Pohl SL (1987) Evaluating clinical accuracy of systems for self-monitoring of blood glucose. Diabetes Care 10(5):622–628
184. Parkes JL, Slatin SL, Pardo S, Ginsberg BH (2000) A new consensus error grid to evaluate the clinical significance of inaccuracies in the measurement of blood glucose. Diabetes Care 23 (8):1143–1148
185. Klonoff DC, Lias C, Vigersky R, Clarke W, Parkes JL, Sacks DB, Kirkman MS, Kovatchev BJ (2014) The surveillance error grid. Diabetes Sci Technol 8(4):658–672
186. Kovatchev BP, Wakeman CA, Breton MD, Kost GJ, Louie RF, Tran NK, Klonoff DC (2014) Computing the surveillance error grid analysis: procedure and examples. J Diabetes Sci Technol 8(4):673–684
187. Simmons DA (2015) How should blood glucose meter system analytical performance be assessed? J Diabetes Sci Technol 10(1):178–184
188. Bland J, Altman D (1986) Statistical methods for assessing agreement between two methods of clinical measurement. Lancet 8476:307–310
189. Stephan P, Schmid C, Freckmann G, Pleus S, Haug C, Müller P (2015) The rectangle target plot: a new approach to the graphical presentation of accuracy of systems for self-monitoring of blood glucose. J Diabetes Sci Technol. doi:10.1177/1932296815612490
190. Müller P, Hattemer A, Stephan P (2015) Assessing system accuracy of blood glucose monitoring systems using rectangle target plots. J Diabetes Sci Technol 10(2):350–365
191. Krouwer JS, Cembrowski GS (2010) A review of standards and statistics used to describe blood glucose monitor performance. J Diabetes Sci Technol 4(1):75–83
192. Westgard JO, Petersen PH, Wiebe DA (1991) Laboratory process specifications for assuring quality in the U.S. national cholesterol education program. Clin Chem 37(5):656–661
193. Wilmoth DR (2012) The relationships between common measures of glucose meter performance. J Diabetes Sci Technol 6(5):1087–1093
194. Ramljak S, Lock JP, Schipper C, Musholt PB, Forst T, Lyon M, Pfützner A (2013) Hematocrit interference of blood glucose meters for patient self-measurement. J Diabetes Sci Technol 7(1):179–189
195. Freckmann G, Schmid C, Baumstark A, Pleus S, Link M, Haug C (2012) System accuracy evaluation of 43 blood glucose monitoring systems for self-monitoring of blood glucose according to DIN EN ISO 15197. J Diabetes Sci Technol 6(5):1060–1075
196. Gijzen K, Moolenaar DL, Weusten JJ, Pluim HJ, Demir AY (2012) Is there a suitable point-of-care glucose meter for tight glycemic control? Evaluation of one home-use and four hospital-use meters in an intensive care unit. Clin Chem Lab Med 50(11):1985–1992
197. Handelsman Y, Bloomgarden ZT, Grunberger G, Umpierrez G, Zimmerman RS, Bailey TS, Blonde L, Bray GA, Cohen AJ, Dagogo-Jack S, Davidson JA, Einhorn D, Ganda OP, Garber AJ, Garvey WT, Henry RR, Hirsch IB, Horton ES, Hurley DL, Jellinger PS, Jovanovič L,

Lebovitz HE, LeRoith D, Levy P, McGill JB, Mechanick JI, Mestman JH, Moghissi ES, Orzeck EA, Pessah-Pollack R, Rosenblit PD, Vinik AI, Wyne K, Zangeneh F (2015) American Association of Clinical Endocrinologist and American College of Endocrinology – clinical practice guidelines for developing a diabetes mellitus comprehensive care plan. Endocrine Practice 21(Suppl 1):1–87
198. American Association of Diabetes Educators (2013) Survey to gauge knowledge regarding blood glucose meter accuracy. https://www.diabeteseducator.org/docs/default-source/legacy-docs/_resources/advocacy/executive_summary_meter_acc_2014.pdf?sfvrsn=2
199. American Diabetes Association (1994) Self-monitoring of blood glucose. Diabetes Care 17 (1):81–86
200. Klonoff DC, Lias C, Beck S, Parkes JL, Kovatchev B, Vigersky RA, Arreaza-Rubin G, Burk RD, Kowalski A, Little R, Nichols J, Petersen M, Rawlings K, Sacks DB, Sampson E, Scott S, Seley JJ, Slingerland R, Vesper HW (2015) Development of the Diabetes Technology Society Blood Glucose Monitor System Surveillance Protocol. Oct 18. pii: 1932296815614587 [Epub ahead of print]
201. Sølvik UØ, Risa M, Jacobsen CE, Monsen G, Sandberg S (2015) Performance of 10 systems for self-monitoring of blood glucose by trained healthcare professionals and in the hands of users. Clin Chem 61(5):772–774
202. Freckmann G, Baumstark A, Schmid C, Pleus S, Link M, Haug C (2014) Evaluation of 12 blood glucose monitoring systems for self-testing, system accuracy and measurement reproducibility. Diabetes Technol Ther 16(2):113–122
203. Freckmann G, Schmid C, Pleus S, Baumstark A, Link M, Stolberg E, Haug C, Sieber J (2014) System accuracy evaluation of systems for point-of-care testing of blood glucose: a comparison of a patient-use system with six professional-use systems. Clin Chem Lab Med 52 (7):1079–1086
204. Freckmann G, Link M, Schmid C, Pleus S, Baumstark A, Haug C (2015) System accuracy evaluation of different blood glucose monitoring systems following ISO 15197:2013 by using two different comparison methods. Diabetes Technol Ther 17(9):635–648
205. Klonoff DC, Prahalad P (2015) Performance of cleared blood glucose monitors. J Diabetes Sci Technol 9(4):895–910
206. Klonoff DC, Reyes JS (2013) Do Currently available dlood glucose monitors meet regulatory standards? 1-Day public meeting in Arlington, Virginia. J Diabetes Sci Technol 7 (4):1071–1083
207. Klonoff DC (2010) Regulatory controversies surround blood glucose monitoring devices. J Diabetes Sci Technol 4(2):231–235
208. Brookings Institution (2015) Strengthening patient care: building a national postmarket medical device surveillance system. http://www.fda.gov/downloads/AboutFDA/CentersOffices/OfficeofMedicalProductsandTobacco/CDRH/CDRHReports/UCM435112.pdf
209. Levy P (2013) Poor performance of blood glucose monitors prompts call to action. Endocrine Today, Oct. http://www.healio.com/endocrinology/diabetes/news/print/endocrine-today/%7B9119eae5-4781-4c64-a2ac-7476ca45aa98%7D/poor-performance-of-blood-glucose-monitors-prompts-call-to-action
210. Karon BS, Boyd JC, Klee GG (2010) Glucose meter performance criteria for tight glycemic control estimated by simulation modeling. Clin Chem 56(7):1091–1097
211. Virdi NS, Mahoney J (2013) Importance of blood glucose meter and carbohydrate estimation accuracy. J Diabetes Sci Technol 6(4):921–926
212. Karon BS, Boyd JC, Klee GG (2013) Empiric. Diabetes Technol Ther 15(12):996–1003
213. Breton MD, Kovatchev BP (2010) Impact of blood glucose self-monitoring errors on glucose variability, risk for hypoglycemia, and average glucose control in type 1 diabetes: an in silico study. J Diabetes Sci Technol 4(3):562–570
214. Boyd JC, Bruns DE (2001) Quality specifications for glucose meters: assessment by simulation modeling of errors in insulin dose. Clin Chem 47(2):209–214

215. Tirimacco R, Koumantakis G, Erasmus R, Mosca A, Sandberg S, Watson ID, Goldsmith B, Gillery P (2013) Glucose meters – fit for clinical purpose. Clin Chem Lab Med 51 (5):943–952
216. Wilinska ME, Hovorka R (2014) Glucose control in the intensive care unit by use of continuous glucose monitoring: what level of measurement error is acceptable? Clin Chem 60(12):1500–1509
217. Klonoff DC (2011) Intensive insulin therapy in critically Ill hospitalized patients: making it safe and effective. J Diabetes Sci Technol 5(3):755–767
218. Pfuetzner A, Mitri M, Musholt PB, Sachsenheimer D, Borchert M, Yap A, Forst T (2012) Clinical assessment of the accuracy of blood glucose measurement devices. Curr Med Res Opin 28(4):525–531
219. Rebel A, Rice MA, Fahy BG (2012) The accuracy of point-of-care glucose measurements. J Diabetes Sci Technol 6(2):396–411
220. Lee TMH (2008) Over-the-counter biosensors: past, present, and future. Sensors 8 (9):5535–5559
221. McNichols RJ, Coté GL (2000) Optical glucose sensing in biological fluids: an overview. J Biomed Opt 5(1):5–16
222. Fraser DM (1997) Biosensors in the body: continuous in vivo monitoring. Wiley, New York
223. Cunningham DD, Stenken JA (eds) (2010) In vivo glucose sensing. Wiley, Hoboken
224. Gifford R (2013) Continuous glucose monitoring:40 years, what we've learned and what's next. Chem Phys Chem 14(10):2032–2044
225. Tsujino D, Utsunomiya K (2014) Continuous glucose monitoring (CGM). Rinsho byori 62 (1):53–59
226. Mauras N, Fox L, Englert K, Beck RW (2013) Continuous glucose monitoring in type 1 diabetes. Endocrine 43(1):41–50
227. Heo YJ, Takeuchi S (2013) Towards smart tattoos: implantable biosensors for continuous glucose monitoring. Adv Healthc Mater 2(1):43–56
228. Kim HS, Shin JA, Chang JS, Cho JH, Son HY, Yoon KH (2012) Continuous glucose monitoring: current clinical use. Diabetes Metab Res Rev 28(Suppl 2):73–78
229. Sparacino G, Zanon M, Facchinetti A, Zecchin C, Maran A, Cobelli C (2012) Italian contributions to the development of continuous glucose monitoring sensors for diabetes management. Sensors (Switzerland) 12(10):13753–13780
230. Joubert M, Reznik Y (2012) Personal continuous glucose monitoring (CGM) in diabetes management: review of the literature and implementation for practical use. Diabetes Res Clin Pract 96(3):294–305
231. Skyler JS (2009) Continuous glucose monitoring: an overview of its development. Diabetes Technol Ther 11(Suppl 1):S5–S10
232. Oliver NS, Toumazou C, Cass AEG, Johnston DG (2009) Glucose sensors: a review of current and emerging technology. Diabet Med 26(3):197–210
233. Hoss U, Budiman ES, Liu H, Christiansen M (2013) Continuous glucose monitoring in the subcutaneous tissue over a 14-day sensor wear period. J Diabetes Sci Technol 7 (5):1210–1219
234. Leinung M, Nardacci E, Patel N, Bettadahalli S, Paika K, Thompson S (2013) Benefits of short-Term professional continuous glucose monitoring in clinical practice. Diabetes Technol Ther 15(9):744–747
235. Jensen MH, Christensen TF, Tarnow L, Mahmoudi Z, Johansen MD, Hejlesen OK (2013) Professional continuous glucose monitoring in subjects with type 1 diabetes, retrospective hypoglycemia detection. J Diabetes Sci Technol 7(1):135–143
236. Pepper GM, Steinsapir J, Reynolds K (2012) Effect of short-term iPRO continuous glucose monitoring on hemoglobin A1c levels in clinical practice. Diabetes Technol Ther 14 (8):654–657
237. Hammond P (2012) Continuous glucose monitoring: the clinical picture. How to interpret and use the data. Pract Diabetes 29(9):364–368

238. Hirsch IB (2009) Realistic expectations and practical use of continuous glucose monitoring for the endocrinologist. J Clin Endocrin Metabol 94(7):2232–2238
239. Kenny C (2014) When hypoglycemia is not obvious, diagnosing and treating under-recognized and undisclosed hypoglycemia. Prim Care Diabet 8(1):3–11
240. Dunn TC, Hayter GA, Doniger KJ, Wolpert HA (2014) Development of the Likelihood of Low Glucose (LLG) algorithm for evaluating risk of hypoglycemia A new approach for using continuous glucose data to guide therapeutic decision making. J Diabetes Sci Technol 8 (4):720–730
241. Bonomo M, Grassi G, Di Bartolo P, Maran A (2015) Real-time continuous glucose monitoring in adult outpatients. In: Bruttomesso D, Grassi G (eds) Technological advances in the treatment of type 1 diabetes, vol 24, Front diabetes. Karger, Basel, pp 110–127
242. Gai M, Merlo I, Dellepiane S, Cantaluppi V, Leonardi G, Fop F, Guarena C, Grassi G, Biancone L (2014) Glycemic pattern in diabetic patients on hemodialysis, Continuous Glucose Monitoring (CGM) analysis. Blood Purif 38(1):68–73
243. Evans CH, Lee J, Ruhlman MK (2015) Optimal glucose management in the perioperative period. Surg Clin North Am 95(2):337–354
244. Moghissi ES, Korytkowski MT, DiNardo M, Einhorn D, Hellman R, Hirsch IB, Inzucchi SE, Ismail-Beigi F, Kirkman MS, Umpierrez GE (2009) American association of clinical endocrinologists and American diabetes association consensus statement on inpatient glycemic control. Diabetes Care 32(6):1119–1131
245. Pichardo-Lowden AR (2015) Management of hyperglycemia in hospitalized patients: noncritical care setting. In: Bruttomesso D, Grassi G (eds) Technological advances in the treatment of type 1 diabetes, vol 24, Front diabetes. Karger, Basel, pp 31–46
246. Brutsaert E, Carey M, Zonszein J (2014) The clinical impact of inpatient hypoglycemia. J Diabetes Complications 28(4):565–572
247. Savion I, Khoury K, Alkoken G, Raz I, Leibovitz G, Eldor R, Toren O (2010) Glucose management by registered nurses for adult patients hospitalized in medical wards, Structured guidelines (protocol) and working process. Diabetes Spectr 23(4):268–271
248. Mathioudakis N, Golden SH (2015) A comparison of inpatient glucose management guidelines, implications for patient safety and quality. Curr Diabetes Rep 15(3):1–11
249. Fahy BG, Coursin DB (2008) An analysis, hyperglycemic intensive care patients need continuous glucose monitoring-easier said than done. J Diabetes Sci Technol 2(2):201–204
250. Gomez AM, Umpierrez GE (2014) Continuous glucose monitoring in insulin-treated patients in non-ICU settings. J Diabetes Sci Technol 8(5):930–936
251. Bridges BC, Preissig CM, Maher KO, Rigby MR (2010) Continuous glucose monitors prove highly accurate in critically ill children. Crit Care 14:R176
252. National Committee for Clinical Laboratory Standards (NCCLS) (2002) Point-of-care blood glucose testing in acute and chronic care facilities. Approved guideline—2nd edn NCLLS document C30-A2
253. Wan Sulaiman WA, Hashim HZ, Che Abdullah ST, Hoo FK, Basri H (2014) Managing post stroke hyperglycaemia, moderate glycaemic control is better? An update. EXCLI J 13:825–833
254. Todi S, Bhattacharya M (2014) Glycemic variability and outcome in critically ill. Indian J Crit Care Med 18(5):285–290
255. Srinivasan V, Agus MSD (2014) Tight glucose control in critically ill children – a systematic review and meta-analysis. Pediatr Diabetes 15(2):75–83
256. Poljakova I, Elsikova E, Chlup R, Kalabus S, Hasala P, Zapletalova J (2013) Glucose sensing module – is it time to integrate it into real-time perioperative monitoring? An observational pilot study with subcutaneous sensors. Biomed Papers 157(4):346–357
257. Minakata K, Sakata R (2013) Perioperative control of blood glucose level in cardiac surgery. Gen Thorac Cardiovasc Surg 61(2):61–66
258. Krinsley JS (2014) Should guidelines for glycemic control of the critically ill be individualized? Weighing the evidence from randomized and observational investigations. Hosp Pract 42(2):14–22

259. Jeschke MG (2013) Clinical review, glucose control in severely burned patients – current best practice. Crit Care 17(4):1–8
260. Rabiee A, Andreasik V, Abu-Hamdah R, Galiatsatos P, Khouri Z, Gibson BR, Andersen DK, Elahi D (2009) Numerical and clinical accuracy of a continuous glucose monitoring system during intravenous insulin therapy in the surgical and burn intensive care units. J Diabetes Sci Technol 3(4):951–959
261. Heinemann L, Franc S, Phillip M, Battelino T, Ampudia-Blasco FJ, Bolinder J, Diem P, Pickup J, Hans Devries J (2012) Reimbursement for continuous glucose monitoring. A European view. J Diabetes Sci Technol 6(6):1498–1502
262. Heinemann L, Devries JH (2014) Evidence for continuous glucose monitoring sufficient for reimbursement? Diabet Med 31(2):122–125
263. Battelino T, Dovč K, Bratina N (2015) Real-time continuous glucose monitoring in children and adolescents. Front Diabet 99–109
264. Dovč K, Bratina N, Battelino T (2015) A new horizon for glucose monitoring. Horm Res Paed 83(3):149–156
265. Freckmann G, Pleus S, Link M, Zschornack E, Klötzer HM, Haug C (2013) Performance evaluation of three continuous glucose monitoring systems comparison of six sensors per subject in parallel. J Diabetes Sci Technol 7(4):842–853
266. Zschornack E, Schmid C, Pleus S, Link M, Klötzer HM, Obermaier K, Schoemaker M, Strasser M, Frisch G, Schmelzeisen-Redeker G, Haug C, Freckmann G (2013) Evaluation of the performance of a novel system for continuous glucose monitoring. J Diabetes Sci Technol 7(4):815–823
267. Obermaier K, Schmelzeisen-Redeker G, Schoemaker M, Klötzer HM, Kirchsteiger H, Eikmeier H, del Re L (2013) Performance evaluations of continuous glucose monitoring systems: precision absolute elative deviation is part of the assessment. J Diabetes Sci Technol 7(4):824–832
268. Kirchsteiger H, Freckmann G, Heinemann L, Lodwig V, Schmelzeisen-Redeker G, Schoemaker M, del Re L (2015) Performance comparison of CGM systems: MARD values are not always a reliable indicator of cgm system accuracy. J Diabetes Sci Technol 9 (5):1030–1040
269. Klonoff DC (2012) The need for clinical accuracy guidelines for blood glucose monitors. J Diabetes Sci Technol 6(1):1–4
270. Kovatchev BP, Gonder-Frederick LA, Cox DJ, Clarke WL (2004) Evaluating the accuracy of continuous glucose-monitoring sensors continuous glucose–error grid analysis illustrated by TheraSense Freestyle Navigator data. Diabetes Care 27(8):1922–1928
271. Miele A, Weiland K, Dungan KM (2012) Clinical outcomes associated with referral-based continuous glucose monitoring using a central standardized interpretation strategy. Diabetes Technol Ther 14(9):765–771
272. Bergenstal RM, Ahmann AJ, Bailey T, Beck RW, Bissen J, Buckingham B, Deeb L, Dolin RH, Garg SK, Goland R, Hirsch IB, Klonoff DC, Kruger DF, Matfin G, Mazze RS, Olson BA, Parkin C, Peters A, Powers MA, Rodriguez H, Southerland P, Strock ES, Tamborlane W, Wesley DM (2013) Recommendations for standardizing glucose reporting and analysis to optimize clinical decision making in diabetes the ambulatory glucose profile (AGP). Diabetes Technol Ther 15(3):198–211
273. Hilleman DE (2006) Cost considerations with tight glycemic control in the acute care setting. Semin Thorac Cardiovasc Surg 18(4):359–365
274. Macrae D, Grieve R, Allen E, Sadique Z, Betts H, Morris K, Pappachan VJ, Parslow R, Tasker RC, Baines P, Broadhead M, Duthie ML, Fortune PM, Inwald D, McMaster P, Peters MJ, Schindler M, Guerriero C, Piercy D, Slavik Z, Snowdon C, Van Dyck L, Elbourne D (2014) A clinical and economic evaluation of control of hyperglycaemia in paediatric intensive care the CHiP randomised controlled trial. Health Technol Assess 18(26):1–210
275. Mang A, Pill J, Gretz N, Kränzlin B, Buck H, Schoemaker M, Petrich W (2005) Biocompatibility of an electrochemical sensor for continuous glucose monitoring in subcutaneous tissue. Diabetes Diabetes Technol Ther 7(1):163–173

276. Schmelzeisen-Redeker G, Staib A, Strasser M, Müller U, Schoemaker M (2013) Overview of a novel sensor for continuous glucose monitoring. J Diabetes Sci Technol 7(4):808–814
277. Shintani H (1996) Formation and elution of toxic compounds from sterilized medical products Toxic compound formation from irradiated products. Rad Phys Chem 47 (1):139–148
278. Brookman RS (1991) A new PVC based polymer for medical applications. J Vinyl Addit Techn 13(4):191–194
279. Haar HP, List H, Meacham GBK (2006) Direct monitoring of interstitial fluid composition. US 20060,122,536A1
280. Pfeiffer EF (1994) The "Ulm Zucker Uhr System" and its consequences. Horm Metab Res 26 (11):510–514
281. Trajanoski Z, Brunner GA, Schaupp L, Ellmerer M, Wach P, Pieber TR, Kotanko P, Skrabal F (1997) Open-flow microperfusion of subcutaneous adipose tissue for on-line continuous ex vivo measurement of glucose concentration. Diabetes Care 20(7):1114–1121
282. Schoemaker M, Schwaninger R, Wittmann U, Rinne H, Kontschieder H, Strohmeier W, Andreis E, Röper J, Kotulla R, Lodwig V, Obermaier K, Stephan P, Reuschling W, Rutschmann M (2003) The SCGM1 system: subcutaneous continuous glucose monitoring based on microdialysis technique. Diabetes Technol Ther 5(4):599–608
283. Ricci F, Moscone D, Palleschi G (2008) Ex vivo continuous glucose monitoring with microdialysis technique: the example of GlucoDay. IEEE Sens J 8(1):63–70
284. Nielsen JK, Freckmann G, Kapitza C, Ocvirk G, Koelker KH, Kamecke U, Gillen R, Amann-Zalan I, Jendrike N, Christiansen JS, Koschinsky T, Heinemann L (2009) Glucose monitoring by microdialysis: performance in a multicenter study. Diabet Med 26(7):714–721
285. Ocvirk G, Hajnsek M, Gillen R, Guenther A, Hochmuth G, Kamecke U, Koelker K-H, Kraemer U, Obermaier K, Reinheimer C, Jendrike N (2009) The clinical research tool: a high-performance microdialysis-based system for reliably measuring interstitial fluid glucose concentration. J Diabetes Sci Technol 3(3):468–477
286. Medtronic Enlite Serter User Guide
287. Rosdahl LL, Millgard J, Lithell H, Ungerstedt U, Henriksson J (1998) Effect of physiological hyperinsulinemia on blood flow and interstitial glucose concentration in human skeletal muscle and adipose tissue studied by microdialysis. Diabetes 47:1296–1301
288. Kuhn L (1998) Biosensors blockbuster or bomb? Electrochemical biosensors for diabetes monitoring. Electrochem Soc Interface. 26–31
289. Bailey TS, Ahmann A, Brazg R, Christiansen M, Garg S, Watkins E, Welsh JB, Lee SW (2014) Accuracy and acceptability of the 6-day enlite continuous subcutaneous glucose sensor. Diabetes Technol Ther 16(5):277–283
290. Pleus S, Schmid C, Link M, Zschornack E, Klötzer HM, Haug C, Freckmann G (2013) Performance evaluation of a continuous glucose monitoring system under conditions similar to daily life. J Diabetes Sci Technol 7(4):833–841
291. Kulichikhin VG, Antonov SV, Zadymova NM (2009) In: Benedek I, Feldstein MF (eds) Skin contact pressure-sensitive adhesives in applications of pressure-sensitive products. CRC, Boca Raton
292. Cilurzo F, Gennari CG, Minghetti P (2012) Adhesive properties: a critical issue in transdermal patch development. Expert Opin 9(1):33–45
293. Kandavilli S, Nair V, Panchagnula R (2002) Polymers in transdermal drug delivery systems. Pharm Technol 5:62–80
294. Roche diagnostics GmbH (2007) Accu-Chek® Compact Plus Gebrauchsanleitung. https://www.accu-chek.de/download/info/downloadcenter/Accu-Chek-Compact-Plus-Gebrauchsanweisung-komplett.pdf
295. Sachse D, Bolstad N, Jonsson M, Sæves I, Johansson CB, Delezuch W, Hagve M, Hardang IM, Isaksson HS, Ivarsson A, Lehto L, Keikkala E, Mattsson N, Ranta JK, Stavelin A, Sudmann AA, Varsi K (2012) The Accu-Chek Mobile blood glucose monitoring system used under controlled conditions meets ISO 15197 standards in the hands of diabetes patients. Scand J Clin Lab Invest 72(5):374–379

296. Overland J, Abousleiman J, Chronopoulos A, Leader N, Molyneaux L, Gilfillan C (2014) Improving self-monitoring of blood glucose among adults with type 1 diabetes: results of the Mobile™ study. Diabetes Ther 5(2):557–565
297. Roche diagnostics (2011) Evaluation report: Accu-Chek® Aviva test strips with advanced chemistry. https://www.accu-chek.ch/documents/Accu-Chek_Aviva_Evaluation_Report.pdf
298. Jensen JA, Goodson WH, Hopf HW, Hunt TK (1991) Cigarette smoking decreases tissue oxygen. Arch Surg 126:1131–1134
299. Sheffield CW, Sessler DI, Hopf HW, Schroeder M, Moayeri A, Hunt TK, West JM (1997) Centrally and locally mediated thermoregulatory responses alter subcutaneous oxygen tension. Wound Repair Regen 4:339–345
300. Carreau A, El Hafny-Rahbi B, Matejuk A, Grillon C, Kieda C (2011) Why is the partial oxygen pressure of human tissues a crucial parameter? Small molecules and hypoxia. J Cell Mol Med 15(6):1239–1253
301. Wisniewski N, Moussy F, Reichert WM (2000) Characterization of implantable biosensor membrane biofouling. Fresenius J Anal Chem 366:611–621
302. Lönnroth P, Jansson A, Smith U (1987) A microdialysis method allowing characterization of intercellular water space in humans. Am J Physiol 253:E228–E231
303. Jensen BM, Bjerring P, Christiansen JS, Orskov H (1995) Glucose content in human skin: relationship with blood glucose levels. Scand J Clin Lab Invest. 55427–55432
304. Cengiz E, Tamborlane WV (2009) A tale of two compartments interstitial versus blood glucose monitoring. Diabetes Technol Ther 11(Suppl 1):S11–S16
305. Jungheim K, Koschinsky T (2001) Risky delay of hypoglycemia detection by glucose monitoring at the arm. Diabetes Care 24:1303–1306
306. Koschinsky T, Heinemann L (2001) Sensors for glucose monitoring technical and clinical aspects. Diabetes Metab Res Rev 17:113–123
307. Steil GM, Rebrin K, Hariri F, Jinagonda S, Tadros S, Darwin C, Saad MF (2005) Interstitial fluid glucose dynamics during insulin-induced hypoglycaemia. Diabetologia 481:833–1840
308. Rebrin K, Steil GM, van Antwerp W, Mastrototaro JJ (1999) Subcutaneous glucose predicts plasma glucose independent of insulin implications for continuous monitoring. Am J Physiol 277:E561–E571
309. Ward WK, Engle JM, Branigan D, El Youssef J, Massoud RG, Castle JR (2012) The effect of rising vs. falling glucose level on amperometric glucose sensor lag and accuracy in Type1 diabetes. Diabet Med 29(8):1067–1073
310. Braverman IM, Keh-Yen A (1981) Ultrastructure of the human dermal microcirculation. III. The vessels in the mid- and lower dermis and subcutaneous fat. J Invest Dermatol 77:297–304
311. Schure NY, Elias M (1991) The biochemistry and function of stratum corneum lipids. Adv Lipid Res 24:27–56
312. Anderson JM, McNally AK (2011) Biocompatibility of implants: lymphocyte/macrophage interactions. Semin Immunopathol 33:221–233
313. Nichols S, Koh A, Storm WL, Shin JH, Schoenfisch MH (2013) Biocompatible materials for continuous glucose monitoring devices. Chem Rev 113(4):2528–2549
314. Frost M, Meyerhoff ME (2006) In vivo chemical sensors, tackling biocompatibility. Anal Chem 78(21):7370–7377
315. Sharkawy AA, Klitzman B, Truskey GA, Reichert WM (1997) Engineering the tissue which encapsulates subcutaneous implants. I. Diffusion properties. J Biomed Mater Res A (37):401–412
316. Helton KL, Ratner BD, Wisniewski NA (2011) Biomechanics of the sensor-tissue interface-effects of motion, pressure, and design on sensor performance and the foreign body response-part I: theoretical framework. J Diabetes Sci Technol 5:632–646
317. Hoss U, Budiman ES, Liu H, Christiansen M (2014) Feasibility of factory calibration for subcutaneous glucose sensors in subjects with diabetes. J Diabetes Sci Technol 8(1):89–94
318. Bessmas S, Schultz RD (1973) Prototype glucose-oxygen sensor for the artificial pancreas. Trans Am Soc Artif Intern Organs 19:361–364

319. Soeldner JS, Chang KW, Aisenberg S, Hiebert JM (1973) Progress towards an implantable glucose sensor and an artificial beta cell. In: Temporal aspects of therapeutics—volume 2 of the series ALZA conference series. Plenum Press, New York, pp 181–207
320. Kondo T, Ito K, Ohkura K, Ito K, Ikeda S (1982) A miniature glucose sensor, implantable in the blood stream. Diabetes Care 5(3):218–221
321. Updike SJ, Shults M, Ekman B (1982) Implanting the glucose enzyme electrode problems, progress, and alternative solutions. Diabetes Care 5(3):207–212
322. Gough DA, Leypoldt JK, Armour JC (1982) Progress toward a potentially implantable enzyme based glucose sensor. Diabetes Care 5(3):190–198
323. Clark LC Jr, Duggan CA (1982) Implanted electroenzymic glucose sensors. Diabetes Care 5 (3):174–180
324. Wilkins E, Wilkins MG (1983) Implantable glucose sensor. J Biomed Eng 5(4):309–315
325. Pesantez DE (2014) Microarray electrodes useful with analyte sensors and methods for making and using them. US 20140163346
326. Feldman B, Brazg R, Schwartz S, Weinstein R (2003) A continuous glucose sensor based on Wired Enzyme™ technology – results from a 3-day trial in patients with type 1 diabetes. Diabetes Technol Ther 5(5):769–779
327. Staib A, Mischler R, Hajnsek M, Buck H, Jernigan W (2013) Amperometric sensor and method for its manufacturing. US8527024B2
328. Salimi A, Compton RG, Hallaj R (2004) Glucose biosensor prepared by glucose oxidase encapsulated sol–gel and carbon-nanotube-modified basal plane pyrolytic graphite electrode. Anal Biochem 333(1):49–56
329. Ocvirk G, Gaessler-Dietsche C (2012) Enzyme stabilization in electrochemical sensors. EP 2,251,432 B1
330. Linn JH (2006) Tissue distribution and pharmacodynamics: a complicated relationship. Curr Drug Metab 7(1):39–65
331. Fischer U, Hidde A, von Woedtke H, Rebrin K, Abel P (1989) Oxygen tension at the subcutaneous implantation site of glucose sensors. Biomed Biochim Acta 48:965–971
332. Abel P, Fischer U, Brunstein E, Ertle R (1988) The GOD-H2O2-electrode as an approach to implantable glucose sensors. Horm Metab Res Suppl Ser 20:26–29
333. Clark LC, Noyes LK, Spokane RB, Sudan R, Miller ML (1988) Long-term implantation of voltammetric oxidase/peroxide glucose sensors in the rat peritoneum. Methods Enzymol 137:68–89
334. Gough DA (1988) Issues related to in vitro operation of potentially implantable enzyme electrode glucose sensors. Horm Metab Res Suppl Ser 20:30–33
335. Shaw GW, Claremont DJ, Pickup JC (1991) In vitro testing of a simply constructed, highly stable glucose sensor suitable for implantation in diabetic patients. Biosens Bioelectron 6:401–406
336. Wilson GS, Zhang Y, Reach G, Moatti-Sirat D, Poitout V, Thevenot DR, Lemonnier F, Klein JC (1992) Progress toward the development of an implantable sensor for glucose. Clin Chem 38:1613–1617
337. Bindra DS, Zhang Y, Wilson GS, Sternberg R, Thevenot DR, Moatti D, Reach G (1991) Design and in vitro studies of a needle-type glucose sensor for subcutaneous monitoring. Anal Chem 63:1692–1696
338. Shichiri M, Yamasaki Y, Nao K, Sekiya M, Ueda N (1988) In vivo characteristics of needle-type glucose sensor-measurements of subcutaneous glucose concentrations in human volunteers. Horm Metab Res Suppl Ser 20:17–20
339. Moussy F, Harrison DJ, Rajotte RV (1994) A miniaturized nafion-based glucose sensor, In vitro and in vivo evaluation in dogs. Int J Artif Organs 17:88–94
340. Zhang Y, Wilson GS (1993) In vitro and in vivo evaluation of oxygen effects on a glucose oxidase based implantable glucose sensor. Anal Chim Acta 281:513–520
341. Yu B, Moussy Y, Moussy F (2005) Coil-type implantable glucose biosensor with excess enzyme loading. Front Biosci 10:512–520

342. Yu B, Long N, Moussy Y, Moussy F (2006) A long-term flexible minimally-invasive implantable glucose biosensor based on an epoxy-enhanced polyurethane membrane. Biosens Bioelectron 21:2275–2282
343. Boock R, Rixman M (2011) Silicone based membranes for use in implantable glucose sensors. US 8,543,184B2
344. Harrison DJ, Turner RF, Baltes H (1988) Characterization of perfluoro-sulfonic acid polymer coated enzyme electrodes and a miniaturized integrated potentiostat for glucose analysis in whole blood. Anal Chem 60(19):2002–2007
345. Moussy F, Harrison DJ, O'Brien DW, Rajotte RV (1993) Performance of subcutaneously implanted needle-type glucose sensors employing a novel trilayer coating. Anal Chem 65 (15):2072–2077
346. Galeska I, Chattopadhyay D, Moussy F, Papadimitrakopoulos F (2000) Calcification-resistant Nafion/Fe3+ assemblies for implantable biosensors. Biomacromol 1(2):202–207
347. Galeska I, Chattopadhyay D, Papadimitrakopoulos F (2002) Application of polyanion/Fe3 multilayered membranes in prevention of biosensor mineralization. J Macromol Sci Pure Appl Chem 39(10):1207–1222
348. Ward WK, Slobodzian EP, Tiekotter KL, Wood MD (2002) The effect of microgeometry, implant thickness and polyurethane chemistry on the foreign body response to subcutaneous implants. Biomaterials 23(21):4185–4192
349. Yang Y, Zhang SF, Kingston MA, Jones G, Wright G, Spencer SA (2000) Glucose sensor with improved haemocompatibilty. Biosens Bioelectron 15:221–227
350. Wisniewski N, Reichert M (2000) Methods for reducing biosensor membrane biofouling. Colloid Surf B 18:197–219
351. Zhang S, Benmakroha Y, Rolfe P, Shinobu T, Kazuhiko I (1996) Development of a haemocompatible pO2 sensor with phospholipid-based copolymer membrane. Biosens Bioelectron 11:1019–1029
352. Yajima S, Sonoyama Y, Suzuki K, Kimura K (2002) Ion-sensor property and blood compatibility of neutral-carrier-type poly(vinyl chloride) membranes coated by phosphorylcholine polymers. Anal Chim Acta 463:31–37
353. Ishihara K, Nakabayashi N, Nishida K, Sakakida M, Shichiri M (1994) New biocompatible polymer, application for implantable glucose sensor. Diag Biosens Polymer 556:194–210
354. Hetrick EM, Schoenfisch MH (2006) Reducing implant-related infections: active release strategies. Chem Soc Rev 35:780–789
355. Quinn CAP, Connor RE, Heller A (1997) Biocompatible, glucose-permeable hydrogel for in situ coating of implantable biosensors. Biomaterials 18:1665–1670
356. Deitzel JM, Kleinmeyer J, Harris DEA, Tan NCB (2001) The effect of processing variables on the morphology of electrospun nanofibers and textiles. Polymer 42:261–272
357. Suri JT, Cordes DB, Cappuccio FE, Wessling RA, Singaram B (2003) Continuous glucose sensing with a fluorescent thin-film hydrogel. Angew Chem Int Ed Engl 42(47):5857–5859
358. Praveen SS, Hanumantha R, Belovich JM, Davis BL (2003) Novel hyaluronic acid coating for potential use in glucose sensor design. Diabetes Technol Ther 5:393–399
359. Yu B, Ju Y, West L, Moussy Y, Moussy F (2007) An investigation of long-term performance of minimally invasive glucose biosensors. Diabetes Technol Ther 9:265–275
360. Tipnis R, Vaddiraju S, Jain F, Burgess DJ, Papadimitrakopoulos F (2007) Layer-by-layer assembled semipermeable membrane for ampero-metric glucose sensors. J Diabetes Sci Technol 1(2):193–200
361. Galeska I, Hickey T, Moussy F, Kreutzer D, Papadimitrakopoulos F (2001) Characterization and biocompatibility studies of novel humic acids based films as membrane material for an implantable glucose sensor. Biomacromol 2(4):1249–1255
362. Dungel P, Long N, Yu B, Moussy Y, Moussy F (2008) Study of the effects of tissue reactions on the function of implanted glucose sensors. J Biomed Mater Res A 85A:699–706

363. Koschwanez HE, Reichert WM, Klitzman B (2010) Intravital microscopy evaluation of angiogenesis and its effects on glucose sensor performance. J Biomed Mater Res A 93A:1348–1357
364. Koschwanez HE, Yap FY, Klitzman B, Reichert WMJ (2008) In vitro and in vivo characterization of porous poly-L-lactic acid coatings for subcutaneously implanted glucose sensors. J Biomed Mater Res A 87A:792–807
365. Sharkawy AA, Klitzman B, Truskey GA, Reichert WMJ (1998) Engineering the tissue which encapsulates subcutaneous implants. II. Plasma–tissue exchange properties. J Biomed Mater Res 40:586–597
366. Sharkawy AA, Klitzman B, Truskey GA, Reichert WMJ. (1998) Engineering the tissue which encapsulates subcutaneous implants. III. Effective tissue response times. J Biomed Mater Res (40):598–605
367. Updike SJ, Shults MC, Gilligan BJ, Rhodes RK (2000) A subcutaneous glucose sensor with improved longevity, dynamic range, and stability of calibration. Diabetes Care 23:208–214
368. Marshall AJ, Irvin CA, Barker T, Sage EH, Hauch KD, Ratner BD (2004) Biomaterials with tightly controlled pore size that promote vascular in-growth. ACS Polym Prepr 45:100–101
369. Subbaroyan J, Martin DC, Kipke DR (2005) A finite-element model of the mechanical effects of implantable microelectrodes in the cerebral cortex. J Neural Eng 2:103–113
370. Ward WK, Hansen JC, Massoud RG, Engle JM, Takeno MM, Hauch KD (2010) Controlled release of dexamethasone from subcutaneously-implanted biosensors in pigs: localized anti-inflammatory benefit without systemic effects. J Biomed Mater Res A 94A:280–287
371. Klueh U, Kaur M, Montrose DC, Kreutzer DL (2007) Inflammation and glucose sensors: use of dexamethasone to extend glucose sensor function and life span in vivo. J Diabetes Sci Technol 1:496–504
372. Ju YM, Yu BZ, West L, Moussy Y, Moussy FJ (2010) A dexamethasone-loaded PLGA microspheres/collagen scaffold composite for implantable glucose sensors. J Biomed Mater Res A 93A:200–210
373. Mou X, Lennartz MR, Loegering DJ, Stenken JAJ (2011) Modulation of the foreign body reaction for implants in the subcutaneous space: microdialysis probes as localized drug delivery/sampling devices. J Diabetes Sci Technol 5:619–631
374. Klueh U, Dorsky DI, Kreutzer DL (2005) Enhancement of implantable glucose sensor function in vivo using gene transfer-induced neovascularization. Biomaterials 26:1155–1163
375. Patil SD, Papadmitrakopoulos F, Burgess DJ (2007) Concurrent delivery of dexamethasone and VEGF for localized inflammation control and angiogenesis. J Control Release 117:68–79
376. Norton LW, Koschwanez HE, Wisniewski NA, Klitzman B, Reichert WM (2007) Vascular endothelial growth factor and dexamethasone release from nonfouling sensor coatings affect the foreign body response. J Biomed Mater Res A (81A):858–869
377. Edelman JL, Lutz D, Castro MR (2005) Corticosteroids inhibit VEGF-induced vascular leakage in a rabbit model of blood-retinal and blood-aqueous barrier breakdown. Exp Eye Res 80:249–258
378. Machein MR, Kullmer J, Ronicke V, Machein U, Krieg M, Damert A, Breier G, Risau W, Plate KH (1999) Differential downregulation of vascular endothelial growth factor by dexamethasone in normoxic and hypoxic rat glioma cells. Neuropathol Appl Neurobiol 25:104–112
379. Wu WS, Wang FS, Yang KD, Huang CC, Kuo YRJ (2006) Dexamethasone induction of keloid regression through effective suppression of VEGF expression and keloid fibroblast proliferation. J Invest Dermatol 126:1264–1271
380. Carreau A, Kieda C, Grillon C (2011) Nitric oxide modulates the expression of endothelial cell adhesion molecules involved in angiogenesis and leukocyte recruitment. Exp Cell Res 317:29–41
381. Gifford R, Batchelor MM, Lee Y, Gokulrangan G, Meyerhoff ME, Wilson GS (2005) Mediation of in vivo glucose sensor inflammatory response via nitric oxide release. J Biomed Mater Res A (75A):755–766

382. Heise HM, Marbach R, Koschinsky T, Gries FA (1994) Noninvasive blood glucose sensors based on near-infrared spectroscopy. Artif Organs 18(6):439–447
383. Renard E (2008) Implantable continuous glucose sensors. Curr Diabetes Rev 4(3):169–174
384. Brauker JH (2015) Transcutaneous analyte sensor. US 8,989,833
385. Poscia A, Mascini M, Moscone D, Luzzana M, Caramenti G, Cremonesi P, Valgimigli F, Bongiovanni C, Varalli M (2003) A microdialysis technique for continuous subcutaneous glucose monitoring in diabetic patients (part 1). Biosens Bioelectron 18(7):891–898
386. Lucarelli F, Ricci F, Caprio F, Valgimigli F, Scuffi C, Moscone D, Palleschi G (2012) GlucoMen day continuous glucose monitoring system A screening for enzymatic and electrochemical interferents. J Diabetes Sci Technol 6(5):1172–1181
387. Brister MC (2015) Transcutaneous analyte sensor. US 7,494,465
388. Schachl K, Alemu H, Kalcher K, Ježkova J, Švancara I, Vytřas K (1997) Amperometric determination of hydrogen peroxide with a manganese dioxide-modified carbon paste electrode using flow injection analysis. Analyst 122(9):985–989
389. McEnroe RJ, Burritt MF, Powers DM, Rheinheimer DW, Wallace BH (2005) Interference testing in clinical chemistry. Approved Guideline, 2nd edn. Clinical and Laboratory Standards Institute, Wayne
390. Wu H (2015) Rapid-read gated amperometry devices. US 9,034,160B2
391. Cardosi M (2012) Systems and methods for determining a substantially hematocrit independent analyte concentration. US 8,293,096
392. Hayter G, Doniger KJ, Budiman ES, Zhang S, Mazza JC (2014) Method and system for providing calibration of an analyte sensor in an analyte monitoring system. US 8,376,945
393. Goode Paul V (2014) Systems and Methods for replacing signal artifacts in a glucose sensor data stream. US 8,010,174
394. Buck HB (2010) Electrochemical Sensor and method for continuous analyte monitoring. US 7,731,835
395. Rose J (2015) Method and apparatus for continuous analyte monitoring. US 9,008,744
396. Wang L, Shah, R, Cooper KW, Yoon, RK, Lee H (2011) Method and system for detecting age, hydration, and functional states of sensors using electrochemcial impedance spectroscopy. US 7,985,330B2
397. Buck HB (2010) System and method for operating an electrochemical analyte sensor. US 7,751,864
398. Yang N (2013) Application of electrochemcial impedance spectroscopy in sensor systems, devices, and related methods. WO 2013184,416A2
399. Telson SA, Gifford R, Fei J, Reynolds JS (2011) Electrochemical impedance spectroscopy enabled continuous glucose monitoring system. US 20110,040,163A1
400. Varsavsky A (2015) Use of electrochemical impedance spectroscopy (EIS) in intelligent diagnostics. US 20150,164,387
401. Shah R, Gottlieb RK (2014) Method of making a sensor with layered electrodes. US 8,850,688B2
402. Gottlieb RK, Grovender EA, Hoss U, Pendo SM, Shah R, Soundararajan G (2010) Biosensors and Methods for making and using them. US 7,813,780B2
403. Li X, Shah R, Yang Q, Li Y, Pham B (2013) Layered enzyme compositions for use with analyte sensors. US 8,608,921B2
404. Van Antwerp W (1996) Homogeneous polymer compositions containing silicone for biosensor membranes. EP 0,817,809B1
405. Vachon David J (2002) Anti-inflammatory biosensor for reduced biofouling and enhanced sensor performance. US 7,153,265B2
406. Shults MC, Updike SJ, Rhodes RK, Gilligan, BJ, Tapsak MA (2014) Device and method for determining analyte levels. US 8,923,947B2
407. Tapsak MA, Rhodes RK, Rathbun K, Shults MC, McClure JD (2007) Techniques to improve polyurethane membranes for implantable glucose sensors. US 7,226,978

408. Boock RJ, Rixman MA, Zhang H, Estes MJ, Lawrence K (2015) Polymer membranes for continuous analyte sensors. US 8,954,128B2
409. Brauker JH, Shults M, Tapsak MA (2014) Membrane for use with implantable devices. US 8,840,552
410. Brauker JH, Tapsak MA, Shults M, Carr-Brendel V, Fisher JC, Seare WJ, Neale V (2005) Implantable analyte sensor. US 20050245799
411. Boock RJ (2015) Polymer Membrane for continuous analyte sensors. US 8,954,128
412. Petisce JR (2014) Oxygen enhancing membrate system for implantable devices. US 8,909,314
413. Ricci F, Caprio F, Poscia A, Valgimigli F, Messeri D, Lepori E, Dall'Oglio G, Palleschi G, Moscone D (2007) Toward continuous glucose monitoring with planar modified biosensors and microdialysis study of temperature, oxygen dependence and in vivo experiment. Biosens Bioelectron 22(9–10):2032–2039
414. Ricci F, Moscone D, Tuta CS, Palleschi G, Amine A, Poscia A, Valgimigli F, Messeri D. (2005) Novel planar glucose biosensors for continuous monitoring use. Biosens Bioelectron 20(10 Spec Iss):1993–2000
415. Valgimigli F, Lucarelli F, Scuffi C, Morandi S, Sposato I (2010) Evaluating the clinical accuracy of GlucoMen® day, a novel microdialysis-based continuous glucose monitor. J Diabetes Sci Technol 4(5):1182–1192
416. Mao F, Cho H (2005) Biosensor membranes composed of polymers containing heterocyclic nitrogens. US 6,932,894
417. Feldman BJ, Ouyang T, Cho B (2014) Heterocyclic Nitrogen containing polymers coated analyte monitoring device and methods of use. US 8,808,515
418. Heller A, Pishko MV (1997) Subcutaneous glucose electrode. US 5,593,852
419. Johnson KW, Mastrototaro JJ, Howey DC, Brunelle RL, Burden-Brady L, Bryan NA, Andrew CC, Rowe HM, Allen DJ, Noffke BW, McMahan WC, Morff RJ, Lipson D, Nevin RS (1992) In vivo evaluation of an electroenzymatic glucose sensor implanted in subcutaneous tissue. Biosens Bioelectron 7:709–714
420. Mastrototaro JJ, Johnson KW, Molt RJ, Lipson D, Andrew CC, Allen DJ (1991) An electroenzymatic glucose sensor fabricated on a flexible substrate. Sens Actuators B 5:139–144
421. Allen CT, Khan TS (2009) Method and system for producing thin film biosensors. US20090294277A1
422. LaPorte RJ (1997) Considerations for development and manufacture. In: Hydrophilic polymer coatings for medical devices. CRC, Boca Raton
423. Bequette BW (2010) Continuous glucose monitoring. Real-time algorithms for calibration, filtering, and alarms. J Diabetes Sci Technol 4(2):404–418
424. Rebrin K, Sheppard NF, Steil GM (2010) Use of subcutaneous interstitial fluid glucose to estimate blood glucose revisiting delay and sensor offset. J Diabetes Sci Technol 4 (5):1087–1098
425. Thomas K, Kiwit M, Kerner W (1998) Glucose concentration in human subcutaneous adipose tissue: comparison between forearm and abdomen. Exp Clin Endocrin Diabet 106 (6):465–469
426. Schmidt FJ, Sluiter WJ, Schoonen AJM (1993) Glucose concentration in subcutaneous extracellular space. Diabetes Care 16(5):695–700
427. Meyerhoff C, Mennel FJ, Bischof F, Sternberg F, Pfeiffer EF (1994) Combination of microdialysis and glucose sensor for continuous on line measurement of the subcutaneous glucose concentration Theory and practical application. Horm Metabol Res 26(11):538–543
428. Pickup JC, Claremont DJ, Shaw GW (1993) Responses and calibration of amperometric glucose sensors implanted in the subcutaneous tissue of man. Acta Diabetol 30(3):143–148
429. Tiessen RG, Kaptein WA, Venma K, Korf J (1999) Slow ultrafiltration for continuous in vivo sampling. Application for glucose and lactate in man. Anal Chim Acta 379(3):327–335

430. Moatti-Sirat D, Capron F, Poitout V, Reach G, Bindra DS, Zhang Y, Wilson GS, Thévenot DR (1992) Towards continuous glucose monitoring in vivo evaluation of a miniaturized glucose sensor implanted for several days in rat subcutaneous tissue. Diabetologia 35 (3):224–230
431. Kamath A, Mahalingam A, Brauker J (2009) Analysis of time lags and other sources of error of the dexcom seven continuous glucose monitor. Diabetes Technol Ther 11(11):689–695
432. Facchinetti A, Sparacino G, Cobelli C (2010) Enhanced accuracy of continuous glucose monitoring by online extended kalman filtering. Diabetes Technol Ther 12(5):353–363
433. Leal Y, Garcia-Gabin W, Bondia J, Esteve E, Ricart W, Fernández-Real JM, Vehí J (2010) Real-time glucose estimation algorithm for continuous glucose monitoring using autoregressive models. J Diabetes Sci Technol 4(2):391–403
434. Facchinetti A, Del Favero S, Sparacino G, Castle JR, Ward WK, Cobelli C (2014) Modeling the glucose sensor error. IEEE Trans Biomed Eng 61(3):620–629
435. Sparacino G, Facchinetti A, Zecchin C, Cobelli C (2014) Algorithmically smart continuous glucose sensor concept for diabetes monitoring. IFMBE Proc 41:1543–1546
436. Schiavon M, Dalla Man C, Dube S, Slama M, Kudva YC, Peyser T, Basu A, Basu R, Cobelli C (2015) Modeling plasma-to-interstitium glucose kinetics from multitracer plasma and microdialysis data. Diabetes Technol Ther 17(11):825–831
437. Mahmoudi Z, Johansen MD, Christiansen JS, Hejlesen O (2014) Comparison between one-point calibration and two-point calibration approaches in a continuous glucose monitoring algorithm. J Diabetes Sci Technol 8(4):709–719
438. Choleau C, Klein JC, Reach G, Aussedat B, Demaria-Pesce V, Wilson GS, Gifford R, Ward WK (2002) Calibration of a subcutaneous amperometric glucose sensor implanted for 7 days in diabetic patients Part 2 Superiority of the one-point calibration method. Biosens Bioelectron 17(8):647–654
439. Brister MC (2015) Dual Electrode system for a continuous analyte sensor. US 7,831,287
440. Schmidtke DW, Heller A (1998) Accuracy of the one-point in vivo calibration of "Wired" glucose oxidase electrodes implanted in jugular veins of rats in periods of rapid rise and decline of the glucose concentration. Anal Chem 70(10):2149–2155
441. Rossetti P, Bondia J, Vehí J, Fanelli CG (2010) Estimating plasma glucose from interstitial glucose. The issue of calibration algorithms in commercial continuous glucose monitoring devices. Sensors 10(12):10936–10952
442. McGarraugh G, Brazg R, Weinstein R (2011) FreeStyle navigator continuous glucose monitoring system with TRUstart algorithm, a 1-hour warm-up time. J Diabetes Sci Technol 5(1):99–106
443. Keenan DB, Cartaya R, Mastrototaro JJ (2010) Accuracy of a new real-time continuous glucose monitoring algorithm. J Diabetes Sci Technol 4(1):111–118
444. Keenan DB, Mastrototaro JJ, Zisser H, Cooper KA, Raghavendhar G, Lee SW, Yusi J, Bailey TS, Brazg RL, Shah RV (2012) Accuracy of the enlite 6-day glucose sensor with Guardian and Veo calibration algorithms. Diabetes Technol Ther 14(3):225–231
445. Hayter GA (2013) Method and system for dynamically updating calibration parameters for an analyte sensor. US 7,618,369
446. Del Favero S, Facchinetti A, Sparacino G, Cobelli C (2015) Retrofitting of continuous glucose monitoring traces allows more accurate assessment of glucose control in outpatient studies. Diabetes Technol Ther 17(5):355–363
447. Del Favero S, Facchinetti A, Sparacino G, Cobelli C (2014) Improving accuracy and precision of glucose sensor profiles retrospective fitting by constrained deconvolution. IEEE Trans Biomed Eng 61(4):1044–1053
448. Facchinetti A, Sparacino G, Cobelli C (2010) An online self-tunable method to denoise CGM sensor data. IEEE Trans Biomed Eng 57(3):634–641
449. Facchinetti A, Sparacino G, Cobelli C (2011) Online denoising method to handle intraindividual variability of signal-to-noise ratio in continuous glucose monitoring. IEEE Trans Biomed Eng 58(9):2664–2671

450. Facchinetti A, Sparacino G, Cobelli C (2013) Signal processing algorithms implementing the "smart sensor" concept to improve continuous glucose monitoring in diabetes. J Diabetes Sci Technol 7(5):1308–1318
451. Garcia A, Rack-Gomer AL, Bhavaraju NC, Hampapuram H, Kamath A, Peyser T, Facchinetti A, Zecchin C, Sparacino G, Cobelli C (2013) DexCom G4AP: an advanced continuous glucose monitor for the artificial pancreas. J Diabetes Sci Technol 7 (6):1436–1445
452. Abbott Diabetes Care Ltd. (2014) Freestyle Libre Flash glukose Messsystem Benutzerhandbuch
453. Bailey T, Bode BW, Christiansen MP, Klaff LJ, Alva S (2015) The performance and usability of a factory-calibrated flash glucose monitoring system. J Diabetes Sci Technol 17 (11):787–794
454. Bailey TS, Chang A, Christiansen M (2015) Clinical accuracy of a continuous glucose monitoring system with an advanced algorithm. J Diabetes Sci Technol 9(2):209–214
455. Medtronic MiniMed (2014) Minilink real time transmitter user guide. https://www.medtronicdiabetes.com/sites/default/files/library/download-library/user-guides/minilink_user_guide.pdf
456. DexCom, Inc. (2015) DexCom G4 platinum with share user guide. http://www.dexcom.com/sites/dexcom.com/files/dexcom-g4-platinum/ifu/dexcom-g4-platinum-ifu.pdf
457. Abbott Diabetes Care Ltd (2015) FreeStyle Navigator II Expertenanleitung. https://www.abbott-diabetes-care.de/uploads/tx_products/FreeStyleNavigatorII_Expertenanleitung_PW.pdf
458. Abbott Diabetes Care (2015) https//abbottdiabetescare.co.uk/our-products/freestyle-libre. https//abbottdiabetescare.co.uk/our-products/freestyle-libre
459. Medtronic Diabetes (2010) mySentry™ user guide. https://www.medtronicdiabetes.com/sites/default/files/library/download-library/user-guides/MP6025332-011_j+FINALUser+Guide_Rx Only.pdf
460. Nightscout (2016), Nightscout. http//www.nightscout.info/
461. Medtronic Diabetes (2015) MiniMed® Connect. http//www.medtronicdiabetes.com/products/minimed-connect
462. Kohnert KD, Heinke P, Fritzsche G, Vogt L, Augstein P, Salzsieder E (2013) Evaluation of the mean absolute glucose change as a measure of glycemic variability using continuous glucose monitoring data. Diabetes Technol Ther 15(6):448–454
463. Mazze RS, Strock E, Wesley D, Borgman S, Morgan B, Bergenstal R, Cuddihy R (2008) Characterizing glucose exposure for individuals with normal glucose tolerance using continuous glucose monitoring and ambulatory glucose profile analysis. Diabetes Technol Ther 10 (3):149–159
464. Rodbard D (2009) Display of glucose distributions by date, time of day, and day of week New and improved methods. J Diabetes Sci Technol 3(6):1388–1394
465. Mazze RS, Strock E, Wesley D, Borgman S, Morgan B, Bergenstal R, Cuddihy R (1987) Ambulatory glucose profile representation of verified self-monitored blood glucose data. Diabetes Care 10(1):111–117
466. Kovatchev B (2015) Assessing sensor accuracy for non-adjunct use of continuous glucose monitoring. Diabetes Technol Ther 17(3):1–10
467. Lodwig V, Kulzer B, Schnell O, Heinemann L (2014) What are the next steps in continuous glucose monitoring? J Diabetes Sci Technol 8(2):397–402
468. Mastrototaro J (2000) The MiniMed continuous glucose monitoring system. Diabetes Technol Ther 2(S1):S13–S18
469. Clinical and Laboratory Standards Institute (CLSI) (2008) Performance metrics for continuous interstitial glucose monitoring. Approved guideline. POCT 05-A
470. Guidance for Industry and Food and Drug Administration Staff (2012) The content of investigational device exemption (IDE) and premarket approval (PMA)—applications for

artificial pancreas device systems. http://www.fda.gov/downloads/medicaldevices/deviceregulationandguidance/guidancedocuments/ucm259305.pdf
471. Wentholt IM, Hoekstra JB, DeVries JH (2007) Continuous glucose monitors the long-awaited watch dogs? Diabetes Technol Ther 9(5):399–409
472. Zisser HC, Bailey TS, Schwartz S, Ratner RE, Wise J (2009) Accuracy of the SEVEN continuous glucose monitoring system comparison with frequently sampled venous glucose measurements. J Diabetes Sci Technol 3(5):1146–1154
473. Bailey T, Zisser H, Chang A (2009) New features and performance of a next-generation SEVEN-day continuous glucose monitoring system with short lag time. Diabetes Technol Ther 11(12):749–755
474. Pickup JC, Freeman SC, Sutton AJ (2011) Glycaemic control in type 1 diabetes during real time continuous glucose monitoring compared with self monitoring of blood glucose meta-analysis of randomised controlled trials using individual patient data. BMJ 343:d3805
475. Zijlstra E, Heise T, Nosek L, Heinemann L, Heckermann S (2013) Continuous glucose monitoring quality of hypoglycaemia detection. Diabetes Obes Metab 15(2):130–135
476. Lodwig V, Kulzer B, Schnell O, Heinemann L (2014) Current trends in continuous glucose monitoring. J Diabetes Sci Technol 8(2):390–396
477. Damiano ER, El-Khatib FH, Zheng H, Nathan DM, Russell SJ (2013) A comparative effectiveness analysis of three continuous glucose monitors. Diabetes Care 36(2):251–259
478. Luijf YM, Mader JK, Doll W, Pieber T, Farret A, Place J, Renard E, Devries JH (2013) Accuracy and reliability of continuous glucose monitoring systems. A head-to-head comparison. Diabetes Technol Ther 5(8):722–727
479. Garg SK, Smith J, Beatson C, Lopez-Baca B, Voelmle M, Gottlieb A (2009) Comparison of accuracy and safety of the SEVEN and the navigator continuous glucose monitoring systems. Diabetes Technol Ther 11(2):65–72
480. Weinstein RL, Schwartz SL, Brazg RL, Bugler JR, Peyser TA, McGarraugh GV (2007) Accuracy of the 5-day FreeStyle Navigator Continuous Glucose Monitoring System comparison with frequent laboratory reference measurements. Diabetes Care 30(5):1125–1130
481. Hermanides J, Phillip M, DeVries JH (2011) Current application of continuous glucose monitoring in the treatment of diabetes pros and cons. Diabetes Care 34(Suppl 2):S197–S201
482. Ramchandani N, Arya S, Ten S, Bhandari S (2011) Real-life utilization of real-time continuous glucose monitoring the complete picture. J Diabetes Sci Technol 5(4):860–870
483. Kropff J, Bruttomesso D, Doll W, Farret A, Galasso S, Luijf YM, Mader JK, Place J, Boscari F, Pieber TR, Renard E, DeVries JH (2015) Accuracy of two continuous glucose monitoring systems. A head-to-head comparison under clinical research centre and daily life conditions. Diabetes Obes Metab 17(4):343–349
484. Bay C, Kristensen PL, Pedersen-Bjergaard U, Tarnow L, Thorsteinsson B (2013) Nocturnal continuous glucose monitoring: accuracy and reliability of hypoglycemia detection in patients with type 1 diabetes at high risk of severe hypoglycemia. Diabetes Technol Ther 15(5):371–377
485. Mensh BD, Wisniewski NA, Neil BM, Burnett DR (2013) Susceptibility of interstitial continuous glucose monitor performance to sleeping position. J Diabetes Sci Technol 7 (4):863–870
486. Link M, Schmid C, Pleus S, Baumstark A, Rittmeyer D, Haug C, Freckmann G (2015) System accuracy evaluation of four systems for self-monitoring of blood glucose following ISO 15197 using a glucose oxidase and a hexokinase-based comparison method. J Diabetes Sci Technol 9(5):1041–1050
487. Klaff LJ, Brazg R, Hughes K, Tideman AM, Schachner HC, Stenger P, Pardo S, Dunne N, Parkes JL (2015) Accuracy evaluation of contour next compared with five blood glucose monitoring systems across a wide range of blood glucose concentrations occurring in a clinical research setting. Diabetes Technol Ther 17(1):8–15
488. Freckmann G, Pleus S, Link M, Baumstark A, Schmid C, Högel J, Haug C (2015) Accuracy evaluation of four blood glucose monitoring systems in unaltered blood samples in the low

glycemic range and blood samples in the concentration range defined by ISO 15197. Diabetes Technol Ther 17(9):625–634
489. Dunne N, Viggiani MT, Pardo S, Robinson C, Parkes JL (2015) Accuracy evaluation of CONTOURPLUS compared with four blood glucose monitoring systems. Diabetes Ther 6 (3):377–388
490. Demircik F, Ramljak S, Hermanns I, Pfützner A, Pfützner A (2015) Evaluation of hematocrit interference with MyStar extra and seven competitive devices. J Diabetes Sci Technol 9 (2):262–267
491. Pfuetzner A, Hengesbach C, Demircik F, Schipper C, Forst T, Musholt PB (2014) Performance of blood glucose meters in compliance with current and future clinical ISO15197 accuracy criteria. Curr Med Res Opin 30(2):185–190
492. Huang TY, Chang HW, Tsao MF, Chuang SM, Ni CC, Sue JW, Lin HC, Hsu CT (2014) Evaluation of accuracy of FAD-GDH- and mutant Q-GDH-based blood glucose monitors in multi-patient populations. Clin Chim Acta 433:28–33
493. Hsu CT, Wu MH, Kuo CY, Zen JM (2014) Testing quality of a self-monitoring blood glucose sensor with an auto-coding mechanism when used by patients versus technicians. Clin Chim Acta 437:62–65
494. Halldorsdottir S, Warchal-Windham ME, Wallace JF, Pardo S, Parkes JL, Simmons DA (2013) Accuracy evaluation of five blood glucose monitoring systems: the North American comparator trial. J Diabetes Sci Technol 7(5):1294–1304
495. Brazg R, Klaff LJ, Parkin CG (2013) Performance variability of seven commonly used self-monitoring of blood glucose systems: clinical considerations for patients and providers. J Diabetes Sci Technol 7(1):144–152
496. Teodorczyk M, Cardosi M, Setford S (2012) Hematocrit compensation in electrochemical blood glucose monitoring systems. J Diabetes Sci Technol 6(3):648–654
497. Tack C, Pohlmeier H, Behnke T, Schmid V, Grenningloh M, Forst T, Pfützner A (2012) Accuracy evaluation of five blood glucose monitoring systems obtained from the pharmacy: a European multicenter study with 453 subjects. Diabetes Technol Ther 14(4):330–337
498. Baumstark A, Pleus S, Schmid C, Link M, Haug C, Freckmann G (2012) Lot-to-lot variability of test strips and accuracy assesment of systems for self-monitoring of blood glucose according to ISO 15197. J Diabetes Sci Technol 6(5):1076–1086
499. Ceriotti F, Kaczmarek E, Guerra E, Mastrantonio F, Lucarelli F, Valgimigli F, Mosca A (2015) Comparative performance assessment of point-of-care testing devices for measuring glucose and ketones at the patient bedside. J Diabetes Sci Technol 9(2):268–277
500. Dietzen DJ, Wilhite TR, Rasmussen M, Sheffield M (2013) Point-of-care glucose analysis in neonates using modified quinoprotein glucose dehydrogenase. Diabetes Technol Ther 15 (11):923–928
501. Zueger T, Schuler V, Stettler C, Diem P, Christ ER (2012) Assessment of three frequently used blood glucose monitoring devices in clinical routine. Swiss Med Wkly 142:w13631
502. Robinson C, Sharp P (2012) Tighter accuracy standards within point-of-care blood glucose monitoring: how six commonly used systems compare. J Diabetes Sci Technol 6(3):547–554

BIOREV (2017) 6: 103–142
DOI: 10.1007/11663_2016_4

Published online: 28 June 2016

Electrochemical Arrays for Bioassay Applications

Eduardo Cortón and Susan R. Mikkelsen

Abstract This chapter presents a survey of developments and bioassay applications of individually addressable electrochemical arrays covering the past two decades and including over 90 references. Many different array designs have been fabricated, from macroscopic devices that have two to four sensing elements to ultramicroelectrode arrays containing as many as 12,000 individually addressable micrometer-sized working electrodes. Some inexpensively fabricated arrays are intended for single sample analysis and are disposable, while others are encapsulated for incorporation into reusable microfluidic systems. Devices and assays are grouped according to the types of modifications done to the sensing elements, and sections are included to consider unmodified elements as well as modifications with enzymes, antibodies or antigens, nucleic acids, in addition to viable cells and tissues. Some trends have been identified, and possible future directions are suggested.

Keywords Amperometry • Bioassays • Electrochemical arrays • Impedimetry • Individually addressable • Microfluidics • Multielectrode • Ultramicroelectrodes • Voltammetry

Contents

E. Cortón
Facultad de Ciencias Exactas y Naturales, and IQUIBICEN-CONICET, Department of Biological Chemistry, University of Buenos Aires, Buenos Aires, Argentina

S.R. Mikkelsen (✉)
Department of Chemistry, University of Waterloo, Waterloo, ON, Canada
e-mail: susan.mikkelsen@uwaterloo.ca

Abbreviations

ACV	Alternating current voltammetry
Ag/AgCl	Silver/silver chloride reference electrode
BRCA1	Gene indicator of breast cancer predisposition
CCD	Charge coupled device camera
CE	Counter electrode
CFUs	Colony forming units (viable cells)
CMOS	Complementary metal oxide semiconductor chip
DNA	Deoxyribonucleic acid
ECL	Electrochemiluminescence
ELISA	Enzyme-linked immunosorbent assay
HLA	Human leukocyte antigen
IgG	Immunoglobulin G
ITO	Indium-tin oxide
LED	Light-emitting diode
MEMS	Microelectromechanical system
PC12	Cell line derived from rat adrenal medulla
PCB	Printed circuit board
PCR	Polymerase chain reaction
PDMS	Polydimethylsiloxane
RE	Reference electrode
RGDS	Arginine-glycine-aspartic acid-serine peptide
RNA	Ribonucleic acid
rRNA	Ribosomal ribonucleic acid
$Ru(bpy)_3^{2+}$	Tris(2,2′-bipyridine) ruthenium ion
SDC	Sigma-delta converter (analog to digital converter)
SECM	Scanning electrochemical microscopy
SEM	Scanning electron microscopy
SNPs	Single nucleotide polymorphisms
SU-8	Insulating photoresist film
UV	Ultraviolet light
VACNF	Vertically aligned carbon nanofibers
WE	Working electrode

1 Introduction

This chapter concerns arrays of electrodes, or electrochemical cells, that have been applied to bioanalytical assays. These arrays are orderly arrangements of elements, with a minimum of two, that are uniquely and individually addressable. Ensemble electrodes, in which all of the exposed macro-, micro-, or nano-sized sensing elements are connected to a single source of stimulus and measurement of response, are not considered, nor are electrode arrays that are used for electrical stimulation (for example, arrays used for cochlear implant stimulation) without measurement of an analyte-selective response.

Figure 1 shows a number of possible planar array geometries. The array elements in the figure may be amperometric, potentiometric, or impedimetric working electrodes, and each element may consist of a complete electrochemical cell. The most widely reported devices contain metallic amperometric or voltammetric working electrode arrays that employ common counter and reference electrodes that may be coplanar or external. Reported element dimensions vary from the mm scale down to tens of nm. Many reports describe arrays that have been encapsulated into microfluidic chips, and some have specialized external electronic and software systems to allow multiplexed sequential or simultaneous data acquisition from all elements.

Figure 2 demonstrates possible element complexities for amperometric, voltammetric, and impedimetric measurements at individual array elements. Amperometric and voltammetric measurements may be performed using either two- or three-electrode electrochemical cells, and the reference/counter electrode (s) may be components of the fabricated arrays. Impedimetric measurements require two electrodes per element, and these are often interdigitated comb-type electrodes.

Following an initial discussion of focused review articles, in which information has been grouped according to analyte or measurement method, primary research reports have been organized according to the types of surface modifications on the sensing electrode elements.

A more traditional approach to the organization of this material would likely involve sections about array fabrication methods, element numbers and dimensions, and multiplexed instrument control and data acquisition strategies. Our approach, however, is application-oriented: what are the analytes, what biorecognition agents might be available for these, and what kinds of arrays have been fabricated using these types of agents? For this reason, our chapter has been organized according to the surface modifications of array elements. We hope that this “opposite direction” approach might inspire bioanalytical and life science researchers to consider applications of electrochemical arrays in their areas of expertise.

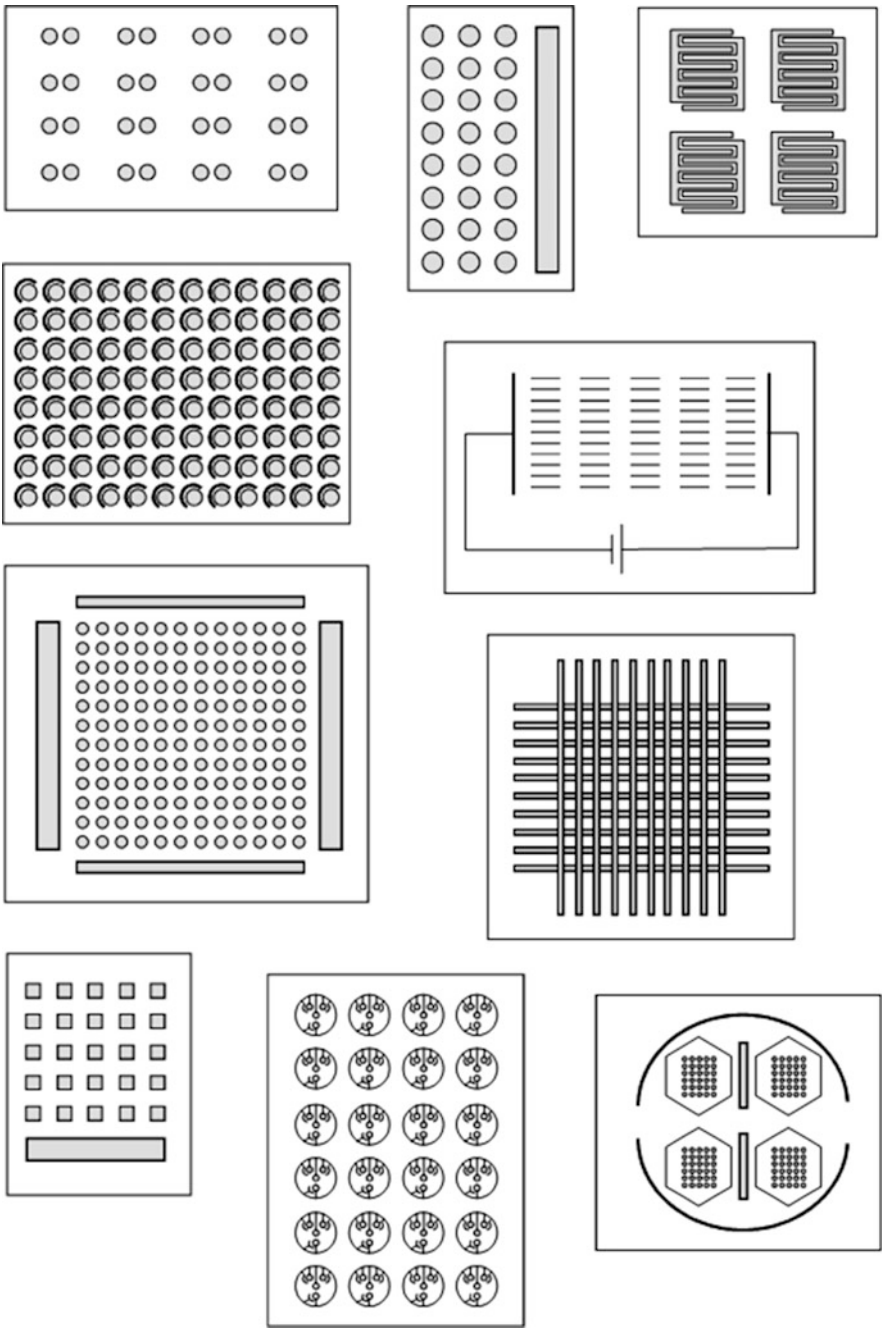

Fig. 1 Various reported geometries for individually addressable, planar electrochemical arrays

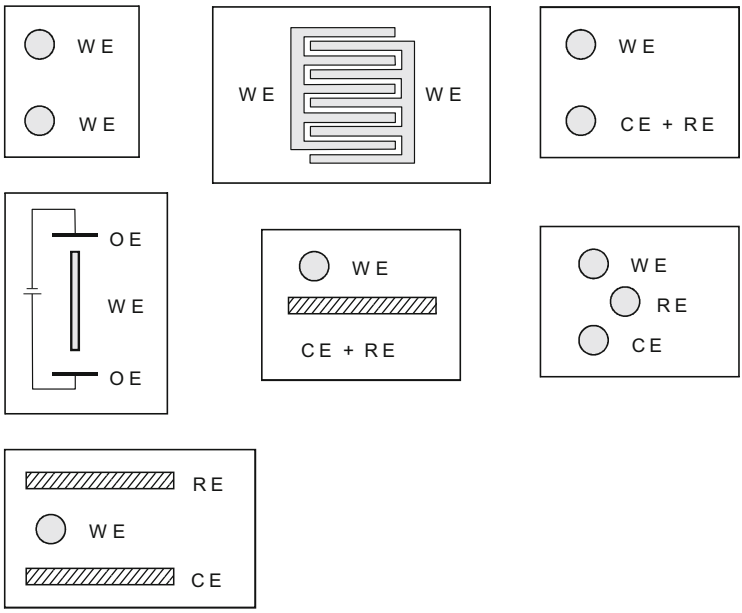

Fig. 2 Illustration of various reported array element complexities. *WE* working electrode, *CE* counter electrode, *RE* reference electrode, *CE+RE* pseudoreference electrode, *OE* other electrodes. Striped band WE, RE, and CE+RE are shared by several WE

2 Specialized Reviews of Principles and Practices

Tomčik has reviewed fundamental aspects of array performance when arrays are fabricated with very closely spaced microelectrode elements [1]. Array elements of micrometer dimensions, separated by very small gaps, have overlapping diffusion layers, and allow interactions between adjacent elements. Theoretical studies and basic applications of affected phenomena, in comparison with isolated array elements, include collection efficiency and redox cycling. The detection of catecholamines is considered.

An older general review by Stefan et al. [2] considers mathematical modeling for data processing (including a variety of chemometric methods such as linear and nonlinear partial least squares, fuzzy neural networks, and multivariate analysis of variance), designs for electrochemical sensor arrays as well as applications in environmental, food and clinical analysis. Arrays of potentiometric ion-selective electrodes, piezoelectric crystal sensors, and voltammetric biosensors, as well as the "electronic nose" gas-phase sensor arrays are reviewed.

An older but very comprehensive review is focused on modification of conductive supports with layered redox proteins [3]. Modification of individual array elements for applications in various bioelectronic devices is discussed, leaning toward amperometric and voltammetric transducers and including

photoelectrochemical and photoswitchable devices. Applications to electrochemical arrays are considered with various bioanalytical components and analytes.

A review of biochips and microarrays [4] considers requirements for biochemical and medical diagnostic applications, focusing on silicon manufacturing technology coupled with magnetic beads, nucleic acid recognition, and enzyme catalysis. This review includes optical as well as electrochemical measurement methods.

A more recent and very useful review [5] considers voltammetric/amperometric microelectrode arrays, their construction techniques, and various approaches to surface modification. This review includes disk and band microelectrodes with regular or random spacings between array elements. Several bioanalytical applications, including nucleic acid and protein detection, are included.

A review of chemical sensors and arrays [6] focuses on conducting polymers: as inherent receptors, the modification of conducting polymers with receptors, the use of conducting polymers as transducers as well as some applications in combinatorial and high-throughput assays. Fundamental aspects of redox-related conductivity and pH-sensitive conductivity are included, and applications to chemical- and enzyme-based biosensors are summarized based on analyte. A variety of detection methods (electrical, electrochemical, and optical) are surveyed.

Protein analytes are the topic of a review of electrochemical biochips [7]. Both assays and sensors are considered, using antibodies or nucleic acid aptamers for analyte recognition. Consideration of "parallelization" or array construction for biochips, by integration of these recognition agents onto single device elements, forms a significant summary.

An interesting recent review focuses on immunoassays that employ amperometric array elements that have been coupled with magnetic separation principles [8]. Magnetic beads are suitably modified and used as a readily separated solid phase for antibody–antigen reactions, and electrodes modified with bioaffinity ligands provide array element-specific interactions and detection that, when individually addressed, allow the acquisition of unique signals for different analytes present in mixtures.

Electrochemical biosensors for applications to food pathogens and toxins is the topic of another review [9]. While the main content of this review involves individual, single-analyte sensors, their integration into lab on a chip devices is also considered. Amperometric, potentiometric, and impedimetric biosensor examples are included.

An excellent review of earlier developments in DNA biosensors that employ electrochemical and piezoelectric transduction includes specific emphasis on those that have been, or can be, implemented in array formats [10]. The design of recognition materials, probe immobilization methods, hybridization conditions, signal trandsuction, and amplification methods have been considered.

A short review [11] summarizes applications of one commercially available device, the ElectraSense^{TM} microarray and reader, to the detection of RNA and DNA in viral and bacterial pathogens. The microarray consists of 12,544 individual platinum electrodes onto which probe nucleic acids are robotically spotted. Target

nucleic acids are labeled with biotin prior to hybridization, and this is followed by incubation with a peroxidase–streptavidin reagent to allow amperometric detection. The reader interrogates all array elements in about 25 s, with each element being read in less than 2 ms.

A recent review of bipolar electrochemistry focuses on the basic principles of controlling solution, rather than electrode potentials, and includes many demonstrated and possible applications [12]. The potential gradient generated across the bulk solution covering the electrode arrays controls the anode-to-cathode potential difference, which drives electrochemical reactions to generate optically detectable anodic products. Various wireless bipolar electrode array configurations and applications are considered.

3 Unmodified Electrochemical Array Elements

This section includes unmodified electrodes as well as those modified by electrochemical or chemical pretreatments to allow rapid electrochemical kinetics for measurements. Electrode modifications with biomolecular recognition agents are considered in following sections.

Recent developments in this area include instrumental advances, such as those described in Rothe et al. [13]. The connection of rapid electrochemical data acquisition with elements of large arrays remains a challenge that has resulted in some creative approaches. In this report, a 32×32 array of Pt disc working electrodes (1,024 elements) with a center-to-center distance of 100 μm have been investigated in a systematic study of disc diameters from 5 to 50 μm, for amperometric or voltammetric measurements with spatial and temporal imaging. Up to 90 frames per second can be acquired, with currents in the pA range. Results with this device, shown in Fig. 3, demonstrate a significant instrumental advance that may inspire many potentially useful bioanalytical applications.

The microplate model has often been used as a starting platform for electrochemical array development. In a report from Tang et al. [14], a multichannel array consisting of eight channels of Pt electrodes, fitted to the dimensions of standard microplate wells, has been developed, with the required multichannel potentiostat for amperometric detection of the product of an enzymatic immunoassay label. Alkaline phosphatase was used as the model immunoassay label in a model rabbit/anti-rabbit IgG study, where the second IgG is labeled with enzyme. The enzyme product provided the amperometric signal with a detection limit in the low pM range.

Reiter et al. [15] have reported a multielectrode system that is compatible with the format of standard 96-well microplates. The system, housed in a Faraday cage, is capable of sequentially monitoring, by cyclic or differential pulse voltammetry, the contents of 16 wells, using three-electrode cells with Pt working electrodes. The authors used this system to optimize conditions for redox modification of pyrroquinolinequinone-dependent glucose dehydrogenase with a ruthenium complex for enhanced electrochemical properties.

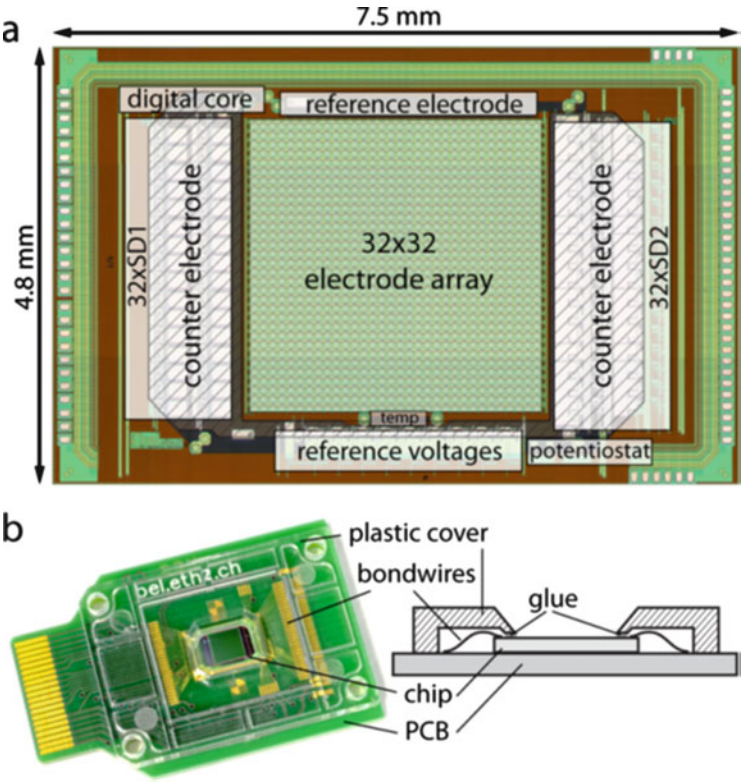

Fig. 3 (**a**) Micrograph of the CMOS chip with the main circuit blocks indicated. The platinum is patterned on top of the CMOS circuits; the SDCs thus are below the counter electrodes. (**b**) Picture and schematic cross-section of the packaged CMOS chip. Only the electrode array and counter and reference electrodes are exposed. The electric contacts and wire bonds are protected by an injection molded polycarbonate cover glued on the chip and PCB (Reproduced with permission from Rothe et al. [13])

The DOX-96 system, compatible with standard 96-well microplates, has 96 three-electrode electrochemical cells with disposable electrodes [16]. Using a multipotentiostat, it applies a fixed potential to each electrochemical cell to monitor current from the reduction of dissolved oxygen in a continuous and real-time manner. The authors demonstrated the utility of this system for the evaluation of antimicrobial susceptibilities both qualitatively and quantitatively (through minimum inhibitory concentrations) for a variety of aerobically respiring bacterial isolates in both clear and turbid samples. Good agreement with broth microdilution results was obtained for both sample types.

The DOX-96 system has been applied to aerobic respiratory activity measurements to monitor the interactions of isoflavonoids with A549 lung adenocarcinoma cells [17]. These compounds inhibit cellular respiratory activity, resulting in decreased consumption of dissolved oxygen. The authors report a detection limit,

for fully respiring cells, of 1×10^4 cells per well, compared to values of 2×10^2 and 6×10^3 cells per well for the accepted MTT and fluorescence assays, respectively.

The DOX-96 oxygen-sensing array has also been applied, using pattern recognition methods, to the detection, classification, and differentiation of oxygen-consuming bacteria based on their different and characteristic responses to the presence of antibiotics [18]. The system has been further applied, in conjunction with pattern recognition, to detection and identification of aerobically respiring bacteria [19]. The time-dependent oxygen consumption was measured for pure cultures during growth, in the presence of different, low concentrations of three broad-spectrum antibiotics. Sufficiently distinct data were obtained for five bacterial species to allow their discrimination.

An interesting approach to thin-layer electrochemical arrays, involving conversion of electrochemical current to light using light-emitting diodes, has been introduced but not yet applied to bioanalytical assays [20]. The measurement of LED light intensity was shown to correlate with concentration for detection of an inorganic ruthenium complex, and in a comparison with electrogenerated chemiluminescence coupled to light intensity detection, an improvement in the efficiency and stability of electron-to-photon conversion was observed.

Two ensemble working electrodes, each consisting of 37 microdiscs of 50 μm diameter, as components of two electrochemical cells have been microfabricated and characterized by voltammetry and electrochemical impedance spectroscopy [21]. The authors have designed this implantable two-electrode wireless biochip as a step toward continuous in vivo monitoring of glucose and lactate in an animal trauma model, and compared characterization results with a corresponding device containing 5,184 microdiscs.

Small microelectrode arrays consisting of two, three, and seven working electrodes have been constructed using 5 μm diameter carbon fibers sealed in multibarrel glass capillaries that were pulled at one end, beveled and polished to produce individually addressable working electrodes [22]. Conducting epoxy was used at the open ends of the capillary barrels to individually connect the carbon fibers to tungsten rods, and four connected bipotentiostats were used to control and monitor all array elements. Spatial resolution of neurotransmitter exocytosis from single pheochromocytoma cells was observed using the seven-electrode array.

A reusable microplate-compatible biamperometric electrochemical array, with 48 elements, has been reported and characterized using small organic reductants as well as the glucose oxidase-catalyzed quantitation of glucose [23]. Since biamperometry requires no reference electrode, simple construction of the array involved two platinum wires per cell (96 total), designed so that the array is lowered into half of the wells of a standard microplate, as shown in Fig. 4. Independent control of each array element allowed simultaneous quantitative data collection from 48 microplate wells in 2 min.

An electrochemical array consisting of electrode pairs separated by micrometer- to nanometer-sized gaps, with the gaps bridged by the conducting polymer polyaniline, has been reported [24]. Each electrode pair can be monitored amperometrically or conductometrically, either separately or simultaneously. The

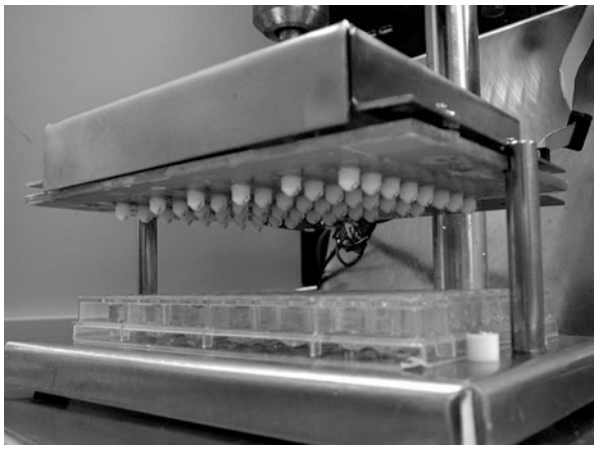

Fig. 4 Photograph of 48-channel biamperometry array (Reproduced with permission from Mann et al. [23])

combination of the two detection methods allows significant selectivity improvements over the use of one or the other method on its own; this was demonstrated by the selective detection of dopamine in the presence of a 1,000-fold excess of the interferant ascorbic acid.

Arrays consisting of four platinum microelectrodes fabricated on glass microscope coverslips have been used to electrochemically image the opening of exocytotic fusion pores in single chromaffin cells from bovine adrenal glands [25]. These fusion pores release single vesicles containing catecholamine neurotransmitters that are amperometrically detected at each of four 3 μm wide electrodes located at the corners of a 10 μm × 10 μm window. A common external reference/counter electrode immersed in the electrolyte bath completed the circuit, and a four-channel potentiostat allowed rapid data acquisition for high temporal resolution of exocytotic events. Locations and magnitudes were measured for the current spikes that occurred during exocytosis.

Exocytotic events from neural cells have also been followed using a microelectrode array system designed for monitoring the effects of drugs on neurotransmitter release [26]. An excellent detection limit for dopamine (40 nM) and linear calibration over two orders of magnitude were demonstrated. The effects of K^+ and L-3,4-dihydroxyphenylalanine concentrations and incubation times on dopamine release were examined.

The electrochemical microplate model has also been used in an array for *Salmonella enterica* detection in meat, using immunomagnetic beads [27]. -Antibody-modified magnetic beads allow rapid bacterial capture and are readily separated and rinsed prior to incubation with a second, enzyme-labeled antibody. Amperometric detection of the product of the enzyme reaction allowed excellent detection limits of 1–10 CFU (viable cells) per 25 g meat sample.

Microbial fuel cells are attracting increasing interest because they promise an alternative "green energy" source. While earlier studies demonstrated principles, sufficiently efficient bacterial species have yet to be discovered. A new microbial

fuel cell array has been reported for the discovery of electrochemically active microbes, to compare species and strains for selection and practical use [28]. The array consists of 24 integrated chambers, each containing an anode and a cathode, and allows separate examinations of 24 miniature samples to quantitate and compare microbial power outputs. The use of the array was demonstrated using isolates of *Shewanella* species that showed distinct strain differences in power output.

The search for efficient electrochemically active bacteria for use in fuel cells has been expanded with a high-throughput voltage-based screening assay [29]. This assay uses a four- to nine-well prototype anode array and a universal cathode compartment. Measurement of open-circuit voltages and currents occurred during bacterial growth; results correlated well with known bacterial doubling times, and several different organic electron donors were examined.

Screen-printing methods have been used to fabricate a 16-electrode microwell array of carbon electrodes [30]. The polycarbonate-supported conducting tracks were sandwiched between a solid lower block and an upper block of teflon that was drilled to create microwells above each of the 16 electrodes. A silver wire, anodized in chloride, was inserted from the top to allow amperometric/coulometric measurements. This array was applied to antibiotic susceptibility testing with one strain of *E. coli*, using bacterial respiratory activity changes to compare responses to 17 antibiotics. The use of ferricyanide reduction (and detection by oxidation of ferrocyanide) rather than oxygen consumption as an indicator of respiratory activity allows this method to be used with bacteria that do not respire aerobically.

An interesting approach to electrochemical array design uses facing, orthogonal band electrodes, made of platinum, photolithographically deposited on glass substrates [31]. An array of ten "row" and ten "column" electrodes produced 100 individually addressable intersection points for the detection of redox cycling, as shown in Fig. 5. The use of the array was demonstrated using a multiplexed bipotentiostat and both the ferri-/ferrocyanide redox couple and an alkaline phosphatase assay with *p*-aminophenyl phosphate as substrate.

An analytically underdeveloped electrochemical phenomenon, wireless bipolar electrochemistry, has resulted in a significant development in electrochemical array design [12, 32]. The principle behind the generation of electrochemical reactions at disconnected microband electrodes involves control of the solution potential, particularly the potential gradient across the solution adjacent to, and along the length of the microband. Since the potential of the electrode itself is constant, the gradient of solution potential can drive an anodic reaction at one end of the microband and a cathodic reaction at the other, analogous to a biamperometric reaction in which both an oxidizable and a reducible species must be present and reactive within a small potential window (the solution potential difference between the ends of the band). An array of 1,000 gold electrodes, each 500 μm long and 50 μm wide, separated horizontally by 200 μm and vertically by 50 μm (as in rows and columns) were microfabricated on glass slides. A single fluid reservoir sealed and covered the array, allowing the introduction of one solution as well as the two stainless steel plate electrodes used to generate the solution potential gradient. Application of

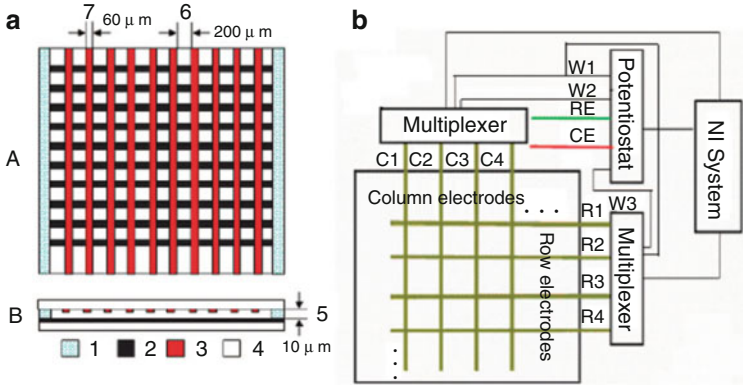

Fig. 5 (**a**) Scheme of the working area of the device and (**b**) addressable microelectrode array detection system. *A* Top view, *B* side view, *1* double-sided adhesive paper, *2* row electrode, *3* column electrode, *4* glass substrate, *5* gap of the substrate, *6* gap between the two microelectrodes, *7* width of the microelectrode (Reproduced with permission from Lin et al. [31])

85 V across 18 mm distance between the plates resulted in an anode-to-cathode potential difference of about 2 V at each electrode.

Demonstration of the phenomenon employed an electrochemiluminescent reaction at the anodes and oxygen reduction at the cathodes, allowing photographic capture of signals, as shown in Fig. 6. This array design has subsequently been applied to nucleic acid detection and is discussed further in a following section of this chapter.

4 Electrode Arrays Modified with Enzymes

Electrochemical arrays are often composed of multiple sensing and detection strategies, with some elements modified by enzymes for amperometric detection (typically for glucose and/or lactate analytes) and others being either potentiometric or modified with other recognition agents. In this section, arrays that contain enzyme-modified elements are considered.

A sensor array for monitoring indicators of mammalian cell metabolic status has been reported by Pemberton et al. [33], and is based on both enzyme-modified elements and chemical sensors for temperature, pH, and dissolved oxygen. The array, fabricated in a silicon platform using MEMS technology, consists of five-well sensor strips with a multipotentiostat to switch between potentiometric and amperometric measurement modes. Screen-printed biosensors for glucose and lactate were grafted onto two of the wells. The authors envision applications to cell culture and cytotoxicity studies.

The characterization of wastewater samples was the objective of a study of small screen-printed amperometric enzyme biosensor arrays [34]. This study considered

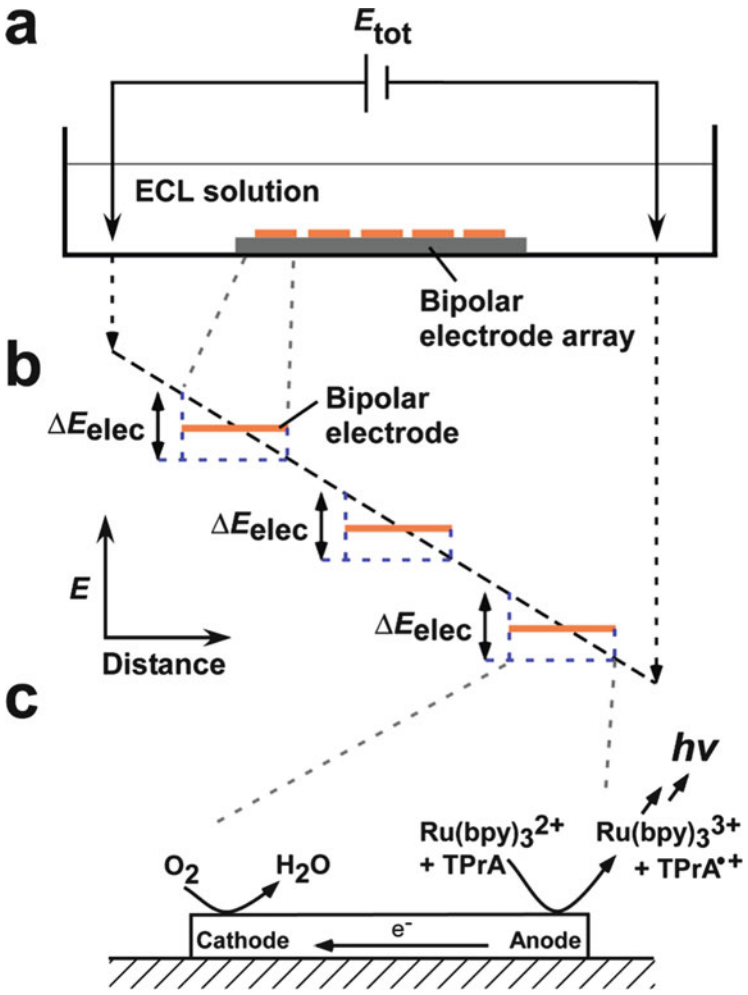

Fig. 6 (**a**) Illustrates how these principles are exploited in a microarray. A voltage applied between two driving electrodes (E_{tot}) creates a linear potential gradient through the solution above the bipolar electrodes. Each bipolar electrode floats to an equilibrium potential whose value is governed by the potential gradient in solution (**b**). The potential difference at the electrode/solution interface will vary across the length of the electrode according to the potential gradient applied to the solution. For a linear potential gradient, the potential difference across each electrode (ΔE_{elec}) will be identical, and both anodic and cathodic overpotentials will exist on a single electrode. (**c**) When the anodic and cathodic overpotentials are larger than the onset potentials for the oxidation and reduction of species in solution, then both reactions will occur simultaneously at the ends of the bipolar electrode. Due to charge neutrality, an electrochemical process at one pole of the bipolar electrode must be accompanied by an equal and opposite process at the other pole (Reproduced with permission from Chow et al. [32])

the compatibility of different enzymes, on different array elements, with common solution conditions that include pH, cosubstrates, and product and/or substrate inhibition, when all array elements are exposed to the same analyte solution. The model for investigation included tyrosinase with horseradish peroxidase and tyrosinase with cholinesterase, and these were studied in batch and flow injection modes.

Microelectrode arrays may also have a single enzyme immobilized on multiple array elements, such as in the work reported by Stephens et al. [35] for in vivo monitoring of glutamate in living animal subjects. These arrays are ceramic-based, with glutamate oxidase cross-linked to platinum electrode surfaces, for real-time amperometric detection and designed for in vivo applications. Ultimately, the research is designed to provide an implantable device to provide alerts for human ischemia or seizure as well as for human neurosurgical monitoring.

An earlier application of in vivo glucose oxidase-based biosensors employed a 3×3 array consisting of glucose and dissolved oxygen measurement elements, employed to map epileptic focus during surgery [36]. The authors report that, during seizure in rats, oxygen levels decreased slightly while extracellular glucose levels showed a biphasic response.

Another creative approach to enzyme electrode arrays, with minimization or elimination of crosstalk between elements by cosubstrates or products, has been reported by Kanungo et al. [37]. This group employed three different immobilized enzyme systems in which the enzymes were immobilized during electrosynthesis of poly(styrenesulfonate)-polyaniline composite films on track-etched polycarbonate membranes. Good activity retention as well as large dynamic ranges and fast response times were reported for the measurement of glucose, urea, and triglycerides.

Four different enzyme modifications were used in an array designed for wastewater quality determination [38]. Tyrosinase, horseradish peroxidase, acetylcholinesterase, and butyrylcholinesterase were used on an eight-element Pt electrode amperometric array, with principal component analysis and signal drift correction. Samples included untreated, variously treated, and pure water samples. Interestingly, the most useful signals were obtained from the horseradish peroxidase and unmodified Pt electrode array elements. Various forms of standard assessment (including total organic carbon, chemical and biochemical oxygen demand, inhibition of nitrification and respiration as well as several biotoxicity assays) provided correlative data for the biosensor array signals.

Screen-printed, four-element gold electrode arrays were investigated using tyrosinase (polyphenol oxidase) loaded into an osmium-loaded redox hydrogel for surface modifications [39]. Two arrays were investigated that differed in design and insulating layer as well as working electrode composition and construction with respect to coatings over the gold layer. Characterization employed catechol as a model substrate, and its direct electrochemistry (without enzyme) did not interfere with the amperometric sensor responses. Good sensitivity and mechanical stability are reported, along with stability up to 6 months. Detection limits for catechol were below 1 μM.

Another approach to enzyme-based biosensor arrays has been reported by Moser et al. [40]. This flow-based detector, produced with a sealed glass-plate gold-modified counter electrode, has a total internal volume of less than 10 μL, and includes glass-supported elements for the quantitation of glucose, lactate, glutamine, and glutamate in whole blood samples or fermentation broths. Crosstalk and stability issues were successfully addressed.

A very specialized application of enzyme-based biosensor arrays has been reported for the resolution of pesticide mixtures containing dichlorvos and methylparaoxon, with a three-element array and a flow injection system [41]. The screen-printed, amperometric electrode array was modified with three acetylcholinesterase enzyme variants, one from electric eel and two from *Drosophila* (fruit fly) mutants, and were used to measure signal inhibition in conjunction with an artificial neural network. Good results down to the low nM range of pesticide concentrations were reported.

Another small array for pesticide determination, based on amperometric enzyme electrodes, using tyrosinase, peroxidase, acetylcholinesterase and butyrylcholinesterase, and measuring enzyme inhibition, has been reported [42]. This report expands on an earlier paper that describes preliminary work using the same enzyme combination for wastewater monitoring [38]. Key optimizations were performed, specifically for enzyme substrates and compatibility regarding crosstalk of esterases and oxidoreductases. Pesticides, heavy metals, phenols, and other chemicals were examined using the array in flow and steady-state modes. Nanomolar detection limits for several common pesticides were achieved in the steady-state mode.

Research involving enzyme-based biosensor arrays for pesticide determination has apparently been dominated by northern European groups. An English collaboration to develop a screen-printed enzyme-based biosensor array for organophosphate pesticide determination, using six acetylcholinesterase variants along with a neural network program, has resulted in a significant practical development [43]. Matrix effects were examined and field studies were conducted to quantitate organophosphates in the nM to μM concentration range, with no false positive or false negative results. The total assay time was less than 6 min.

A recent report of an in vivo flexible strip microelectrode sensor array for glutamate and lactate monitoring in tissue represents an advance [44]. The polyimide substrate was patterned with platinum microelectrodes in addition to epoxy and dry film insulations to produce amperometric, enzyme-based sensors. An on-chip reference electrode and a perm-selective layer, with hydrogel membranes or direct cross-linking for enzyme immobilization, provided stable devices with good performance and allowed a demonstration of in vivo application to glutamate monitoring in rat brain.

A very interesting bioelectrochemical array development has been reported from a collaborative effort in Japan [45]. This team has developed a model 400-element array that uses four measurement modes (open circuit, potentiometric, and two amperometric modes with different applied potentials). This was designed as a platform for electrochemical imaging of biochemical and biological samples.

Preliminary reported studies include oxidation of ferrocenemethanol as well as enzyme-modified array elements, with an osmium-polyvinylpyridine gel containing horseradish peroxidase. The results demonstrate promise for the reported device in further bioanalytical applications.

5 Array Elements Modified with Antibodies or Antigens

A 16-element gold electrode array, fabricated with 200 nm wide N-shaped array elements, operates on a signal inhibition principle for antigen detection [46]. Lipid vesicles functionalized with ferrocene and biotin derivatives are delivered to the microwells, followed by a streptavidin-protein G conjugate, followed by capture antibody. This prepared surface is exposed to the antigen analyte. Voltammetric signals from ferrocene oxidation are measured before and after antigen exposure. One element of the array, before and after exposure to vesicles, is shown in Fig. 7. Very significant signal decreases occur upon binding of human serum albumin, a model antigen, to the capture antibody. Control experiments indicate good selectivity, and the authors suggest a rearrangement of the surface-bound structure upon antigen binding, to inhibit ferrocene oxidation.

An eight-element, screen-printed array of two-electrode electrochemical cells consisting of carbon working and Ag/AgCl counter electrodes has been designed for microfluidic applications and functions in a sealed multichannel microfluidic chip with amperometric detection [47]. A conducting polymer layer consisting of poly(pyrrole propylic acid), coating the carbon working electrodes, allowed covalent immobilization of capture antibody for a sandwich-type immunoassay. The

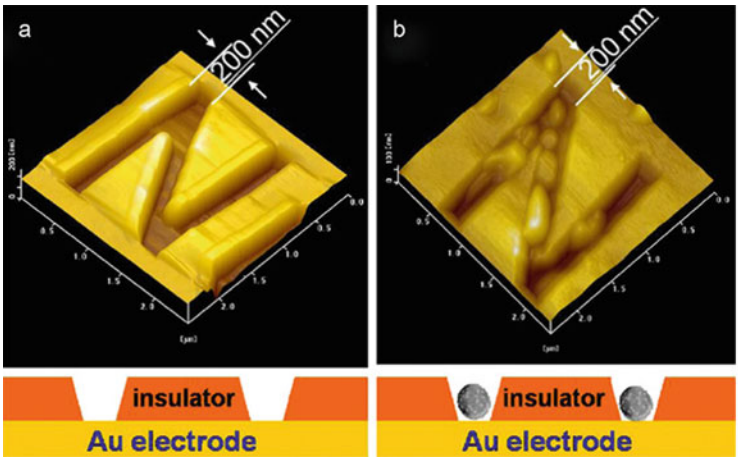

Fig. 7 AFM topographic images of N-inscription-nanosized geometrics before (**a**) and after (**b**), immobilization of functionalized lipid vesicles, which show 200-nm-sized wells (Reproduced with permission from Lee et al. [46])

second antibody, conjugated to alkaline phosphatase, allowed electrochemical detection of the product of the *p*-aminophenyl phosphate hydrolysis product. With mouse IgG as the target analyte and two anti-mouse IgGs for capture and detection, a dynamic range of 100 ng/mL to 10 μg/mL was demonstrated. Selectivity was tested using immobilized anti-goat IgG instead of the anti-mouse antibody, with good results.

Another sandwich-type immunoassay device, with four elements designed for impedance measurements, has been reported [48]. Individual elements consist of electrode arrays constructed from gold-modified pencil graphite onto which anti-human IgG was chemically immobilized. Capture of the analyte, human IgG, was followed by incubation with the sandwich antibody, another anti-human IgG, modified with 15 nm gold nanoparticles. Binding of the sandwich antibody, occurring only when human IgG was present, resulted in a very significant decrease in impedance. A very wide linear response range was achieved, from 50 pg/mL to 100 ng/mL human IgG.

An eight-element array consisting of iridium oxide working electrodes, an iridium counter and a Ag/AgCl reference electrode has been used for amperometric multianalyte sandwich immunoassay with an enzyme label on the second antibody [49]. Each planar array element, patterned on a glass substrate, has an area of 0.78 mm^2. Simultaneous detection of four model analytes (goat, mouse, human, and chicken antibodies) occurred without amperometric crosstalk between adjacent elements, with 3 ng/mL detection limits.

The microplate model for immunoassays has been successfully adapted for electrochemical measurements, with a 96-well screen-printed carbon microplate system [50], shown in Fig. 8. The well bottoms form the sensing surfaces with carbon working electrodes and Ag/AgCl counter electrodes. The system employs intermittent pulse amperometry at fixed pulse potentials for detection. In this report, aflatoxin B_1 was the analyte, and a spiked corn matrix was chosen for examination of extraction efficiencies and matrix effects in a competitive enzyme-linked

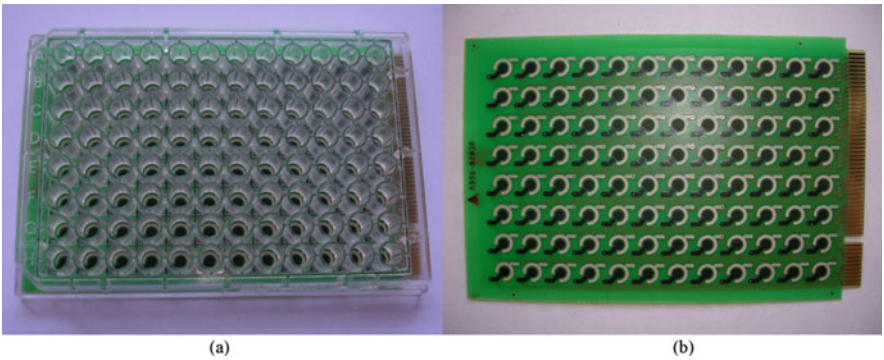

Fig. 8 Picture of a complete 96-well microplate (**a**) and of the support where the 96 sensors are printed (carbon and Ag/AgCl) (**b**) showing also the comb-type connections (on the right site) (Reproduced with permission from Piermarini et al. [50])

immunoassay format with alkaline phosphatase as the enzyme label. The use of this enzyme allowed comparison of the electrochemical results (with naphthyl phosphate as substrate) with traditional optical detection (using *p*-nitrophenyl phosphate). With an immobilized polyclonal antibody preparation, selectivity for aflatoxin B_1 was excellent with the exception of interference from aflatoxin G_1. A working range of 50 pg/mL to 2 ng/mL was obtained with the electrochemical microplate system. A fivefold improvement in detection limit, in comparison with the spectrophotometric assay, was demonstrated.

The quantitation of a different aflatoxin (aflatoxin M_1 in bovine milk) was the subject of another competitive, enzyme-linked electrochemical immunoassay report [51]. Photolithographic methods were used to prepare a 35-element array of gold microelectrodes with 20 μm × 20 μm dimensions and 200 μm edge-to-edge spacings. On-chip reference and counter electrodes were included. A competitive immunoassay format was selected, and horseradish peroxidase was used with tetramethylbenzidine/hydrogen peroxide substrates to generate the amperometrically detectable product. Following optimization, a dynamic detection range of 10–100 ng/mL aflatoxin M_1 in undiluted milk was achieved.

A novel antibody immobilization method, using diazonium-functionalized anti-cytokine antibodies for use in a sandwich-type immunoassay with horseradish peroxidase labels, was used on a three-element array of gold disk electrodes [52]. Despite close spacing of the three 0.5 mm diameter working electrodes, crosstalk was insignificant when three different antibodies (to different cytokines) were immobilized on the three elements. The assay was presented as a yes/no type of multianalyte assay, using blank or 10 ng/mL solutions of the cytokines.

A four-element screen-printed graphite voltammetric array has been used in an inhibition mode, with sol–gel containing gold nanoparticles modified with peroxidase-labeled antibodies to detect protein biomarkers for cancer diagnostics [53]. Binding of the soluble antigen to the immobilized antibody caused inhibition of the peroxidase-catalyzed production of detectable species, indicated by significantly decreased voltammetric peak heights. Antigen interaction with the surface-bound antibody was facilitated by electrokinetic transport of negatively charged antigen using a 2 min, 0.5 V incubation step orthogonal to the electrode surfaces. The total analysis time of 5 min allowed clinically relevant concentrations of carcinoma, carbohydrate, and carcinoembryonic antigens to be determined. Previous work in this area, leading to the four-element array, has been published [54, 55] and a following paper with the same four-element array, including improved validation results, is also available [56].

Exposure to *Bacillus anthracis* involves detection of an antibody to the microbe's protective antigen in serum and whole blood. For this purpose, a novel 8 × 3 microwell array has been developed, in which each well contains three electrodes to allow capture of the antibody and electrochemical detection using a second antibody labeled with alkaline phosphatase, using *p*-aminophenylphosphate as its substrate [57]. A layer-by-layer fabrication approach on silicon substrates, using alternating gold and insulating layers, followed by reactive ion etching to produce wells, resulted in a well-bottom disk electrode and two well-wall ring

electrodes in each of the 24, 50 μm diameter wells that are about 8 μm deep and have about 16 pL volumes. The *B. anthracis* protective antigen was immobilized on the bottom disk electrode as a capture agent, to which the antibody, if present, would bind. A second antibody, labeled with enzyme, forms the sandwich for this noncompetitive immunoassay, and its product, *p*-aminophenol, is detected using the two well-wall electrodes and an 8-channel multipotentiostat. The device and assay scheme are shown in Fig. 9. Results showed excellent differentiation between antibody-spiked and blank whole blood samples from different ethnic groups and both genders.

A nine-electrode array has been reported for use in simultaneous protein and nucleic acid detection on a single sample [58]. Bias-assisted assembly of probes onto individual elements was employed with carboxyphenyldiazonium immobilization chemistry. Simultaneous detection of DNA related to the breast cancer BRCA1 gene and the cytokine interleukin-12 was demonstrated.

An array of sixteen 1×1 mm^2 gold electrodes, with each sandwiched between a 0.2×1 mm^2 gold counter and 0.2×1 mm^2 silver pseudoreference electrodes, has been incorporated into a planar packaged microfluidic device for the detection of

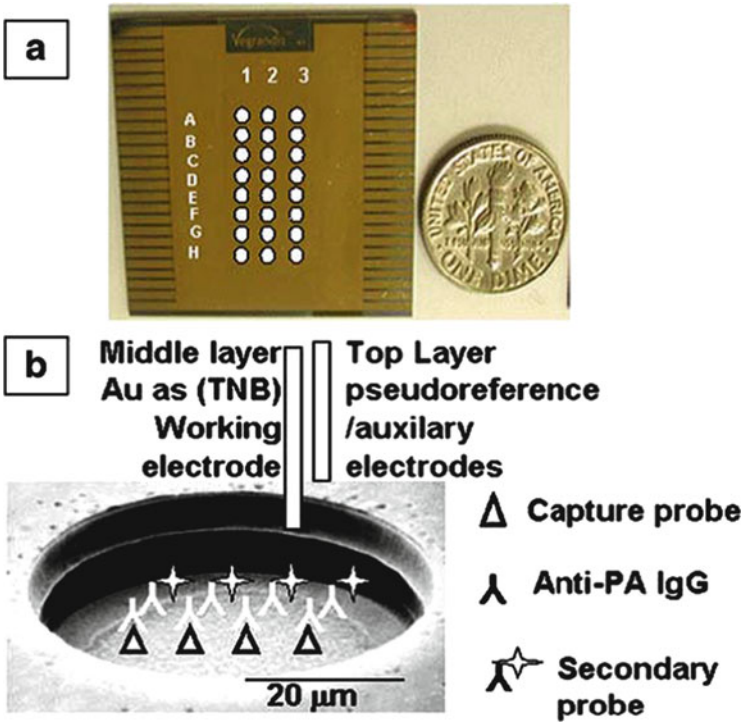

Fig. 9 (**a**) The VEG8X1™ microcavity array chip with a schematic of the cavities. (**b**) The immunoassay on a self-assembled monolayer of the 50-μm-diameter cavity (Reproduced with permission from Aguilar and Sirisena [57])

cancer biomarkers [59]. Derivatization of the electrode surfaces using thiolated antibodies or short DNA probes allowed the detection of various tumor markers on a single chip. Effective and rapid measurement of recognition was accomplished using impedimetric and voltammetric methods.

An interesting approach to static electrochemical immunoassay arrays that employs microcontact printing has been reported [60]. In this work, the authors printed hydrophilic patterns onto a hydrophobic poly(dimethylsiloxane) substrate to create "virtual beakers" to allow spatial separation of aqueous solutions. A demonstration of the device employed anti-dinitrophenyl-galactose oxidase as a model, and the galactose oxidase product hydrogen peroxide was detected by fixed potential amperometry.

Immunoassay methods for cancer markers have been the topic of a recent report involving detection of electrogenerated chemiluminescence [61]. This work combines microfluidics with the electrochemical array, and detection with a CCD camera to allow simultaneous, multiplexed analysis of responses in 30 microwells. Each microwell contains a dense forest of single-walled carbon nanotubes, decorated with the capture antibody. Protein analyte capture is followed by incubation with a second antibody bound to Ru(bpy)-loaded silica nanoparticles to form the sandwich. Detection by CCD camera, following reagent addition, completed the procedure. Assays required 36 min and detection limits were 10–100 fg/mL for four general prostate cancer biomarkers. Very good correlations were obtained with single protein ELISA analyses of sera from human prostate cancer patients.

6 Electrochemical Nucleic Acid Arrays

An array of nine individually addressable working electrodes, made of vertically aligned ensembles of carbon nanofibers grown on 100 nm Ni dots and spaced 1 μm apart, was used for the detection of DNA targets from *E. coli* O157:H7 [62]. The multistep 3×3 element array fabrication was followed by DNA immobilization, with probes labeled with cyanine dyes and amine-terminated. Scanning electrochemical microscopic images of these arrays, at various stages of fabrication, are shown in Fig. 10. Guanine bases in the immobilized probe were substituted with an electroinactive moiety. Immobilization employed a carbodiimide/*n*-hydroxysuccinimide formation of an amide bond to surface carboxylic acid groups. The chosen DNA targets had an oligo(dG) tail, and AC voltammetry was employed with a solution containing $Ru(bpy)_3^{2+}$. Both guanine and the ruthenium complex are oxidized near 1 V (SCE), but the guanine oxidation is irreversible. The difference in peak heights between the first and second ACV scans was used to determine the signal for comparison with positive and negative control elements. The authors state that fabrication of larger arrays of up to 10×10 elements is possible with their fabrication method.

Commercially available arrays of 16 three-electrode amperometric elements, with gold electrodes deposited onto a plastic substrate, and overall array dimensions

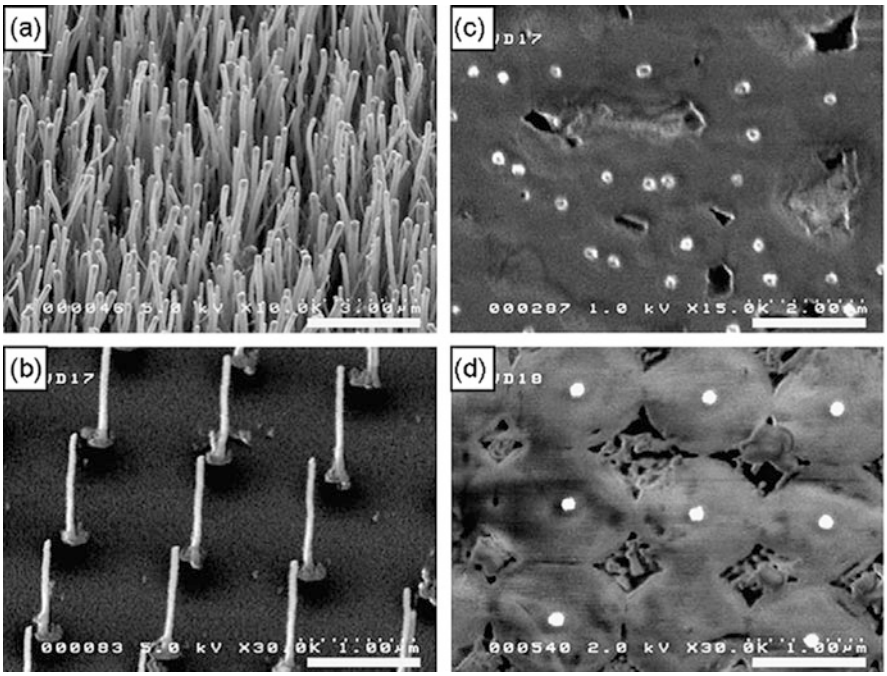

Fig. 10 SEM images of (**a**) as-grown forest-like VACNFs, (**b**) as-grown patterned VACNF arrays on 100 nm diameter Ni spots using e-beam lithography, (**c**) the surface of a polished VACNFs embedded in SiO_2 matrix, and (**d**) the surface of a polished patterned VACNF array embedded in SiO_2 matrix. (**a** and **b**) are 30° perspective views while (**c** and **d**) are top views. The scale bars in (**a**)–(**d**) are 3, 2, 1, and 1 μm, respectively (Reproduced with permission from Arumugam et al. [62])

of 2.5 cm × 7.5 cm, have been used to identify uropathogenic bacteria based on rRNA detection [63]. A single, short sample processing step, involving the lysis of bacteria to release the 16S rRNA fragments, was required. Thiol-terminated capture DNA probes were self-assembled onto the working electrodes. Capture of the (longer) target was followed by incubation with a detection probe consisting of a fluorescein-labeled complementary DNA sequence. A further incubation with a peroxidase-labeled anti-fluorescein antibody allowed the tetramethylbenzidine/peroxide reaction to provide amperometrically measured products, indicating the presence of the bacterial rRNA in the examined sample. Samples included pure cultures, inoculated urine, and clinical urine samples. Each of the 78 clinical samples was examined in duplicate on the 16-element array, using seven probe pairs and one negative control pair of elements. Correct identification of 98% of gram-negative bacteria, for which species-specific probes were available, was accomplished in 45 min from the beginning of sample processing. The same array was used in a following clinical examination of 109 urine samples with comparison to standard urine culture results [64]. Excellent results for identification

of 20 different organisms in the 74% of positive cases within a point of care time frame were reported.

Most electrochemical DNA sensor arrays are used to detect products of the polymerase chain reaction (PCR), which increases the concentration of the sequence of interest in the sample. Goto et al. [65] have reported a microfabricated DNA chip that they applied to both bacterial and viral nucleic acid detection. The chip consists of 40 gold working electrodes of 200 μm diameter along with common reference and counter electrodes. Thiol-terminated DNA probes were self-assembled onto individual working electrodes in the array elements. Incubation of the chip elements with PCR products, and with the redox-active intercalating dye Hoescht 33258 was followed by voltammetric detection of responses at the individual elements. The immobilization, hybridization, and detection steps are illustrated schematically in Fig. 11. One strain of *Clostridium*, two of *Helicobacter* as well as the nucleocapsid protein gene of mouse hepatitis virus were successfully and quantitatively detected.

A 16-element array of square gold working electrodes with widths/lengths of 100 μm, 90 μm, 80 μm, and 70 μm (four working electrodes of each size, to study area effects on signals) has been employed for the detection of a model target DNA sequence from human retinoblastoma cells [66]. Each row of four working electrodes shares a common counter electrode, and the chip dimensions are 5 mm × 3 mm. Integrated electronics allow voltammetric detection. Immobilized thiol-terminated DNA probes were hybridized with ferrocene-labeled targets, and ferrocene oxidation provided voltammetric peaks, the areas under which were integrated to provide analytical signals. This system allowed real-time monitoring of the hybridization of ferrocene-labeled DNA targets to the immobilized probes.

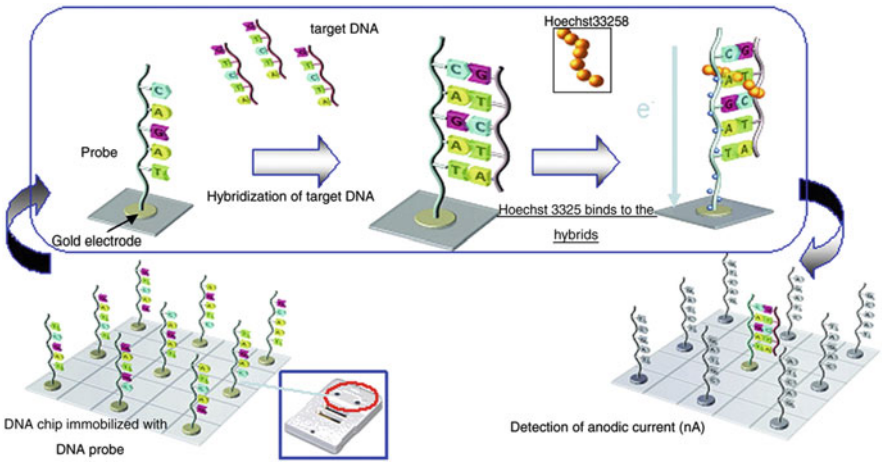

Fig. 11 Principles of the DNA detection strategy using a 40-working-electrode gold array system (Reproduced with permission from Goto et al. [65])

Results suggest a target DNA detection limit of 50 pM. Possibly, a competitive assay could be developed for unlabeled target DNA.

An interesting application of scanning electrochemical microscopy (SECM) to DNA detection on a 48-electrode array has been reported for the detection of *Salmonella* spp. [67]. Both 10 and 25 μm gold electrodes were tested with thiol-modified, self-assembled DNA probes; the approach to chemisorption employed four-thiol groups on each DNA strand, spaced with adenine residues, to reduce steric hindrance for hybridization and enzyme labeling. The soluble targets were biotin-labeled. An avidin-alkaline phosphatase enzyme label was then used and, with the redox cycling of the *p*-aminophenylphosphate hydrolysis product *p*-aminophenol with its quinoneimine, inherent in the measurement technique, a two-stage signal amplification was possible. Femtomolar detection limits for the target sequences were obtained without redox cycling. Approach curves demonstrated a 3.6-fold signal amplification due to redox cycling with the SECM tip positioned very close to the electrode surfaces.

Arrays containing three gold sensing elements, each 900 μm × 900 μm, one counter and one reference electrode were fabricated on glass substrates and sealed into reusable microfluidic devices for DNA detection in PCR-amplified samples [68]. Gold–thiol self-assembled monolayer immobilization chemistry was used for gold working electrode modification with probes complementary to human (H1N1) and avian (H5N1) viral PCR amplicons. All assay steps, including electrochemical addressing and immobilization, sequence-specific detection, and sensing element regeneration were accomplished in situ, within the sealed device. The use of oxidative desorption at one sensing element allowed arrays with different probe/capture sequences on different elements to be sequentially constructed. The immobilized probe sequences were labeled with electrochemically detectable methylene blue, while target sequences were not labeled. Characterization experiments used 400 nM solutions of target DNA and 25 min hybridization times. Scanning voltammetry was used for detection, by measurement of peak heights, with significantly smaller peaks observed following hybridization.

Gold–thiol immobilization was also employed using the same commercially available 16-element array that was used in the work described for the detection of urinary tract infections [63, 64], but in this case was used to demonstrate the detection of single nucleotide polymorphisms (SNPs) which result in a single mismatched base in a probe-target hybrid [69]. In this work, each element is modified with a different capture probe. Following analyte sequence capture, a biotin-labeled detection probe is ligated to the immobilized DNA using a ligase enzyme that functions only in the absence of base-pairing mismatches. A single-base mismatch was efficiently recognized by the ligase, and the detection probe was not ligated. An avidin-peroxidase conjugate, with tetramethylbenzidine was used for amperometric signal generation.

A different array design, with six gold working electrodes of reproducible area (0.030 ± 0.002 cm^2), and common gold counter and Ag/AgCl reference electrodes, has been fabricated and applied to the simultaneous detection of HIV-1 and HIV-2 oligonucleotides [70]. Thiolated hairpin DNA probes were used, with

immobilization by self-assembly, and methylene blue was used as a hybridization indicator. The single-stranded hairpin capture probes associated more strongly with methylene blue than did the hybridized DNA, and square wave voltammetry showed significant signal decreases upon successful hybridization. Detection limits were reported as 0.1 nM target DNA, using a 6 h self-assembly time and a 1 h hybridization time.

Another approach to electrochemical detection of DNA hybridization on electrode arrays involves the exploitation of unpaired guanine residues on the immobilized capture probe [71]. This work used a 5×3 array of planar, square gold electrodes of 1 mm^2 area each (note that in this reference, 1 cm^2 is reported in their materials section (2.1) while 1 mm^2 is reported in their methods section (2.2.1); given the reported signal amplitudes, the latter is likely the correct value). Measurements used common platinum counter and Ag/AgCl wire reference electrodes. The model target was a 107-base amplicon of lymphotoxin-α, which is a diagnostic indicator of breast cancer predisposition through the BRCA1 gene. A 20 base capture probe was immobilized on working electrode surfaces using thiol groups tethered to the 5′ ends with hexamethylene spacers. Control experiments used an immobilized 21 base capture probe corresponding to exon 13 on the BRCA1 gene. Differential pulse voltammetry was used for the reduction of methylene blue, and results showed significantly increased peak currents for hybridized probes in comparison with controls. The different mechanisms of interaction of methylene blue, with unpaired guanine bases, by electrostatic interaction, and by intercalation, were discussed with respect to other reports, with different experimental conditions, of signal decreases following hybridization. A detection limit of 20 nM target was reported.

An eight-element array has been constructed using silicon technology to produce interdigitated gold electrode pairs at each array element; redox cycling may occur between the two electrodes if different poised potentials are employed [72]. The interdigitated elements are constructed with an overall circular pattern of radius 200 μm with a 250 μm gap between elements, as shown in Fig. 12. The interdigitated fingers on each element have submicrometer widths and gaps. The array is sealed and used in a flow system with an external Ag/AgCl reference electrode and a 16-channel multipotentiostat. Used for the detection of *p*-aminophenol, the hydrolysis product of *p*-aminophenylphosphate by alkaline phosphatase, with each anode at +350 mV and each anode at −50 mV, redox cycling of the aminophenol/quinoneimine couple was observed. Self-assembly of hexanethiol-modified capture DNA probes was used for electrode modification. Two elements were used for each of the cytomegalovirus, Epstein Barr virus, and herpes simplex virus DNA sequences, and the two remaining elements were used for positive and negative controls. Target PCR products with biotin labels were hybridized, and an avidin-alkaline phosphatase conjugate was bound. After introduction of substrate, flow was stopped and currents due to product redox cycling were measured. Target concentrations of 2 nM were selectively detected, and the entire procedure was complete within 50 min.

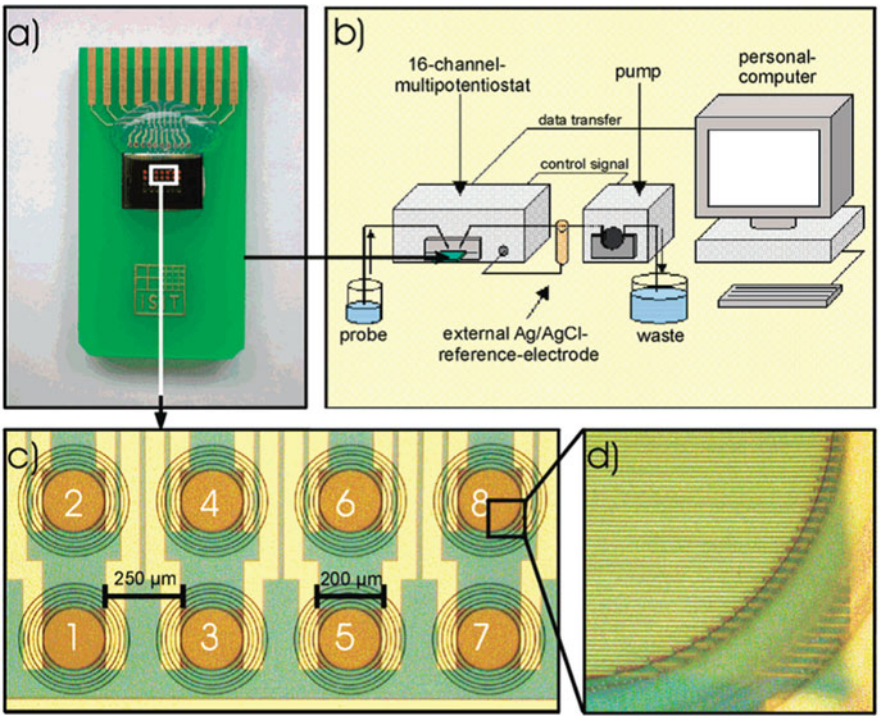

Fig. 12 Photograph of the electrical biochip and a scheme of the measuring system: (**a**) chip on printed circuit board; (**b**) 16-channel multipotentiostat with chip and flow-through cell connected to the reference electrode, pump, and computer; (**c**) details of the eight used chip positions; (**d**) details of the submicrometer interdigitated electrode fingers and the three-dimensional polymeric ring structures (Reproduced with permission from Nebling et al. [72])

A ten-element potentiometric microelectrode array, with iridium oxide electrodeposited onto 20 µm planar gold disks, has been used to selectively capture and monitor acidification with single, viable mammalian cells using DNA-modified electrode surfaces and complementary DNA-modified cells [73]. The iridium oxide surface was silanized using an aldehyde silane for amine-terminated capture DNA immobilization. Cell surfaces were modified with *N*-hydroxysuccinimide-terminated DNA sequences at exposed primary amine groups. The encapsulated array employed a syringe-based flow system to introduce pure or mixed cultures of healthy primary T cells and Jurkat T lymphoma cells. Acidification due to single captured cells was monitored on individual array elements using potentiometric measurements with respect to an external Ag/AgCl reference electrode. Results demonstrate that the cancerous Jurkat cells acidify at a significantly greater rate than the healthy T cells.

An eight-working electrode array with common counter and reference electrodes has been fabricated by screen printing, using conducting graphite ink followed by an insulating ink layer to define a 3 mm diameter electrochemical cell [74]. Each of

the working electrodes has an approximate area of 780 μm^2 and the eight graphite electrodes are positioned around central common ring reference and disk counter electrodes. Carbodiimide/*N*-hydroxysuccinimide immobilization of amine-terminated DNA probes onto surface carboxylic acid groups was used to immobilize three different probes on different elements: a 20-base sequence targeting codon 273 in exon 8 of the *p53* gene (related to esophageal adenocarcinoma), a noncomplementary sequence, and a single-base mismatched sequence. Measurements of faradaic impedance showed large shifts upon hybridization and allowed detection of complementary targets at concentrations of 1–200 nM, without labeling. Hybridization conditions were optimized for easy discrimination between complementary, noncomplementary, and single-base mismatch targets.

Another planar, circular array produced by screen-printing consists of eight radially distributed gold working electrodes around a larger, central, common Ag/AgCl counter electrode [75]. Thiolated capture DNA probes were immobilized on all eight 1.5 mm diameter working electrodes. Following hybridization to the longer, purified PCR amplicon target, four different biotin-labeled signaling sequences were used with sequences complementary to different regions of the target. Avidin-alkaline phosphatase was then used, with α-naphthyl phosphate as substrate, and detection was performed by differential pulse voltammetry. Target detection limits of 0.1 and 0.3 nM were obtained for two hazelnut allergen sequences. Commercially available foods were comparatively tested against the accepted ELISA tests, with very good agreement.

A 16-element electrochemical array, consisting of a linear arrangement of 16 gold working electrodes (1.5 mm diameter) next to a coplanar common counter/reference band electrode, has been fabricated on a device similar in total size to a glass microscope slide [76]. The goal of the work was to examine the rRNA of phytoplankton communities for the detection of toxic algae. Thiolated capture probes were immobilized on the working electrode surfaces, and hybridization mixtures contained a digoxigenin-labeled signaling probe that was subsequently incubated with anti-digoxigenin-peroxidase. Amperometric detection of the product of the 4-aminophenylamine substrate occurred for 10 s at −147 mV with respect to the Ag/AgCl counter electrode.

An array of interdigitated electrode pairs has been reported for the redox-cycling detection of the alkaline phosphatase reaction product *p*-aminophenol, used as a label for hybridization detection of unamplified uropathogenic bacterial 16S rRNA [77]. Sixteen interdigitated electrode pairs, with 800 nm finger widths and 400 nm gaps, and a 500 μm circular interdigitation diameter, formed the 16-element electrode pair array. Thiolated capture probes, specific to the individual bacteria, were spotted onto the gold array elements and a common signaling/detection probe, labeled with biotin, employed a sequence complementary to a region of the rRNA that was identical in all of the five bacterial species. Avidin-alkaline phosphatase was used for product and signal generation. All of the hybridization, rinsing and detection steps were fully automated in a multiport flow system with automated detection system that provides results for all elements in 8 s. Potentials of +350 and −150 mV were used for the anodic and cathodic components of each element,

respectively, controlled against an external Ag/AgCl reference electrode. Supporting oligonucleotides were also used to promote efficient target capture at the array elements. Excellent selectivities were achieved for discrimination of the five bacterial species, and an *E. coli* detection limit for total RNA was reported as 0.5 ng/μL.

The ElectraSense™ electrode array platform, containing 12,544 individually addressable platinum working electrodes, is shown in Fig. 13. It has been applied to genotyping and gene expression assays [78]. The CombiMatrix system for synthesis of immobilized DNA probes was used to compare fluorescence detection of hybridization with the cyanine dye Cy5 to amperometric measurements, using biotin-labeled targets followed by streptavidin-peroxidase labeling and tetramethylbenzidine product detection. Influenza genotyping assays for H3N2 and H15N5 subtypes were compared for fluorescence and electrochemical detection methods, and detection limits of 1.5 pM and 0.75 pM were reported, respectively. A number of bacterial pathogens were also included in this large, comparative study.

A demonstration of a wireless bipolar electrode array for DNA detection, using only three array elements (but almost infinitely scalable) has been reported [79]. The electrochemical principle involves controlling the potential of the solution across the electrode, rather than the potential of the individual electrode elements of the array. Anodic and cathodic plate electrodes are immersed in buffer covering the parallel-aligned, disconnected electrodes to generate a solution potential gradient. Gold electrode elements were modified with thiol-terminated 25-base capture probes. Target DNA was labeled with 4 nm Pt nanoparticles. Once hybridized, an electrochemiluminescent reaction occurs at the anodic ends of the elements due to the oxidation of $Ru(bpy)_3^{2+}$ and tri-*n*-propylamine, while Pt nanoparticle-catalyzed oxygen reduction occurs at the cathodic ends. To demonstrate the principle, optical micrography was used to capture emitted light. A schematic and photographic demonstrations of results are shown in Fig. 14.

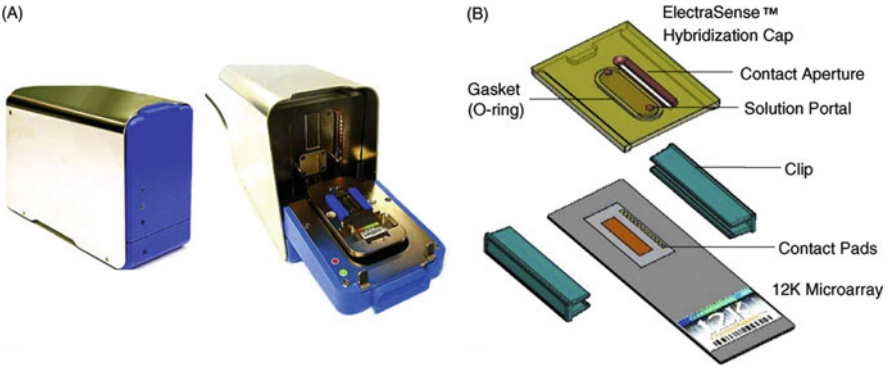

Fig. 13 ElectraSense™ Reader (**a**) and ElectraSense™ 12K microarray with hybridization cap (**b**) (Reproduced with permission from Ghindilis et al. [78])

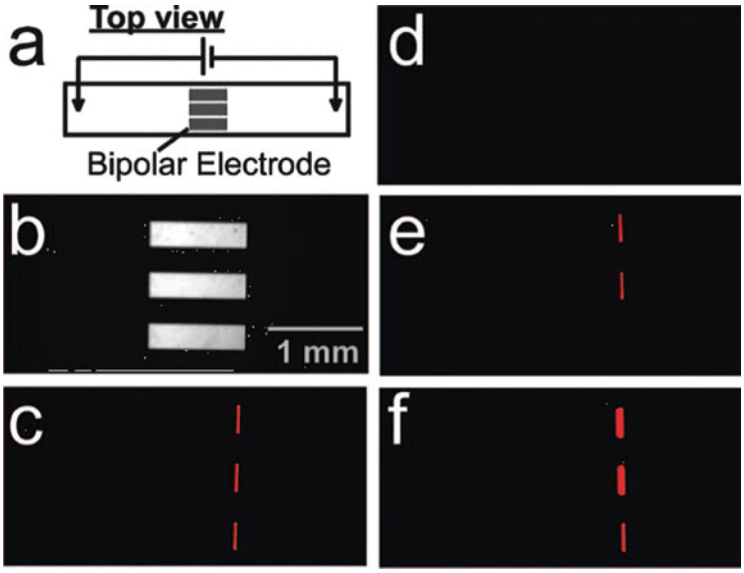

Fig. 14 (**a**) Top-view schematic illustration of the microdevice. (**b**) Optical micrograph of the bipolar electrode configuration used to obtain the data in the other panels of this figure. False-color luminescence micrographs showing (**c**) the ECL emitted at $E_{tot} = 16.0$ V when complementary target DNA functionalized with Pt-NPs is hybridized to probe DNA present on the electrode surface; (**d**) no ECL emitted at 16.0 V prior to hybridization; (**e**) the ECL emitted at 16.0 V when only the top two electrodes of the device are exposed to the labeled target; and (**f**) the ECL emission at $E_{tot} = 22.0$ V for the device in (**e**) (Reproduced with permission from Chow et al. [79])

A 15-element thin-layer platform, consisting of two 5×3 element gold primary electrodes modified with thiol-terminated DNA, separated by a teflon spacer from a top 5×3 array of secondary electrodes has been reported [80]. The electrodes are 1 mm diameter disks embedded in teflon blocks. The immobilization method employs click chemistry, with azide-terminated thiol spacers initially immobilized on the primary electrodes, and ethynyl-labeled DNA probe duplexes covalently bound via catalysis by an electrochemically reduced copper complex (demonstrating element-specific immobilization). Methylene blue oxidation, with regeneration from ferrocyanide, allows detection at the aligned and opposite secondary electrodes. The authors report the detection of femtomoles of target DNA from transcription factors TATA-binding protein and CopG.

Another application of a sandwich hybridization assay, using immobilized capture and soluble reporter probes, has been reported for the detection of PCR-amplified DNA sequences associated with celiac disease [81]. A 4×4 planar array of 1 mm^2 gold working electrodes was used with shared, coplanar counter, and reference electrodes and was sealed into a microfluidic housing. A reporter probe with a common sequence was premodified with a terminal peroxidase label, and the tetramethylbenzidine oxidation product was detected using a multiplexed potentiostat for sequential addressing of the 16 elements. Good agreement was found in comparison with standard clinical HLA typing methods.

7 Electrode Arrays Modified with Cells or Tissues

A four-element array, with four working electrodes and common counter and reference electrodes, has been fabricated using screen printing and applied to the capture of cells for surface glycan detection [82]. Carbon working electrodes were modified with peptide-functionalized single-walled carbon nanotubes. The arginine-glycine-aspartic acid-serine peptide (RGDS) was chosen because it has very high affinity for cell surface integrins, to allow capture of viable cells on the working electrode surfaces. With cells immobilized, each working electrode was exposed to a different lectin-peroxidase conjugate. The four lectins (concanavalin A, *Dolichos biflorus* agglutinin, peanut agglutinin, and wheat germ agglutinin) were chosen because of their different oligosaccharide-binding selectivities. Voltammetric detection of the peroxidase reaction products allowed discrimination of human leukemic K562 cells before and after treatment with a drug, 3′-azido-3′-deoxythymidine, that induces changes in cell surface glycosylation. Good agreement with fluorimetric flow cytometry results was observed.

Thin-film platinum ultramicroelectrode arrays, with subcellular-sized working electrode elements, have been used for spatial resolution of single vesicle release from cultured PC12 cells from rat adrenal medulla [83]. Three array types, with 4×4 (4 μm element width), 5×5 (3 μm), and 6×6 (2 μm) approximately square, planar working electrodes, were fabricated. All arrays were designed to fit within a 30×30 μm square, to allow examination of single cells or small cell clusters. Nine working electrode arrays were constructed on each glass wafer. PDMS wells were created over the arrays, which formed the well bottoms. The arrays were coated with dilute collagen, and PC12 cells were then cultured on the array surface. The arrays with cells attached, and signals for dopamine release, are shown in Fig. 15. The release of dopamine from individual cells was monitored simultaneously at each of the 16 elements in the 4×4 array, with a multichannel potentiostat and an external Ag/AgCl counter electrode. Very high temporal resolution and rapid data acquisition were achieved. Over total acquisition times of about 2 min, many individual transients, corresponding to exocytosis, were observed when cells were located on one or more of the array elements. The effects of reserpine and L-dopa on release events was examined using this array.

A thorough characterization of a multi-working-electrode amperometric array, fabricated and proposed for the measurement of nitric oxide and peroxynitrite released from cells, has been reported [84]. Each array element contains seven short-circuited 50 μm diameter, planar, circular gold ultramicroelectrodes positioned at the corners and center of a hexagonal element with 500 μm interelectrode spacings. These seven coplanar elements, with similar hexagonal geometry, were located next to one element containing 61 short-circuited elements of the same size and separation. Common coplanar ring counter and band Ag/AgCl reference electrodes were used. The complete array contains eight addressable elements, allowing simultaneous measurements at 7, 49, or 110 individual ultramicroelectrodes. Elements coated with poly(eugenol) and poly(phenol) layers were

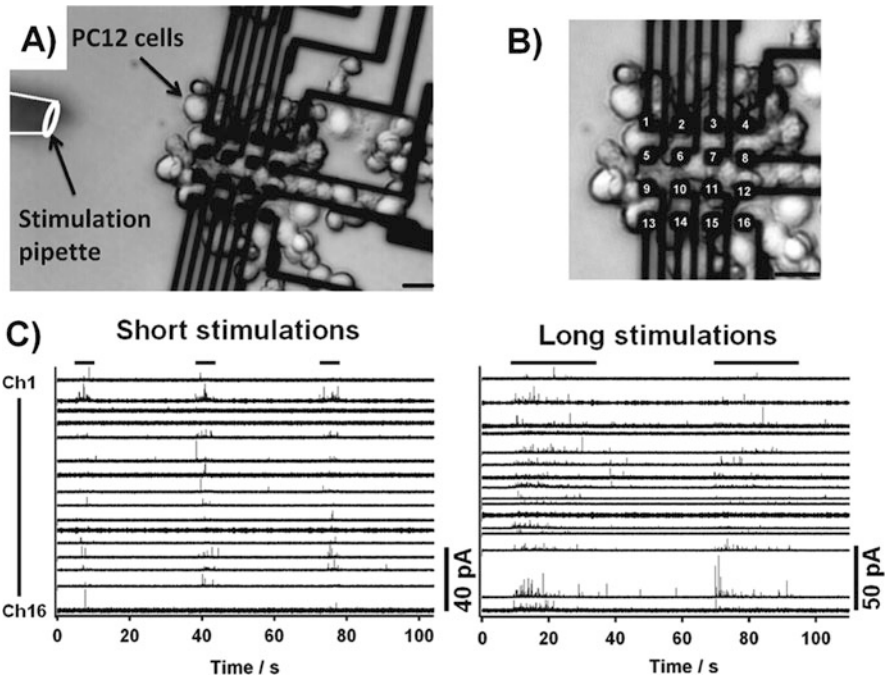

Fig. 15 Electrochemical imaging of a PC12 layer for short (5 s) and long (25 s) K^+ stimulations. (**a**) Micrograph showing the 16-electrode array covered by a population of PC12 cells and the stimulation pipet positioned on the left of the picture. (**b**) Blow-up of the electrode array, showing the cell population and the labeling of the electrodes (scale bar, 10 μm). (**c**) Amperometric traces obtained for short or long stimulations of the cell layer. In both cases, the stimulations are indicated by a *black bar* at the top of the graph (Reproduced with permission from Wang et al. [83])

used for selective NO detection at +0.8 V, while uncoated gold elements were used for the detection of $ONOO^-$ at −0.1 V. Excellent interference rejection for common biochemical species was observed, and simultaneous measurements of nitric oxide and peroxynitrite were demonstrated. The authors state their intention to expand applications to viable cell cultures.

Spatial sensing of three-dimensional cell aggregates and constructs in a gelatin matrix has been proposed using a four-chamber reservoir, with each reservoir containing eight platinum rod electrodes for directional impedance measurements [85]. Two electrodes were located on each of the sides of each square chamber. For each measurement, four electrodes are used: two to carry current and two to measure voltage. Different combinations of electrode locations allow acquisition of spatially resolved impedance. Demonstrations included gelatin-encapsulated HepG2 cells (derived from a liver hepatocellular carcinoma), molded into cylinders and placed at different locations inside the reservoirs, which were then filled with blank crosslinked gelatin. Results demonstrate the possibility of applications to tissue engineering processes.

8 Other Modifications of Electrochemical Array Elements

Four-element electrochemical transistor arrays, encapsulated in a microfluidic device, with gate voltages controlled by solution composition and drain-source currents providing analytical signals, have been fabricated [86]. Source and drain electrodes are connected by a 300 μm diameter channel coated with poly (3,4-ethylenedioxythiophene) doped with poly(styrenesulfonate), which is a conductive coating, filled with electrolyte solution. The Pt electrode gates are in contact with the solutions separating the gates from the conducting source-drain channels. Multianalyte detection was demonstrated using reference, glucose oxidase, lactate oxidase, and combined glucose and lactate oxidase enzyme assays. Due to the patterning of hydrophilic and hydrophobic coatings, no external pumps or electrophoretic flow control is needed to fill the channels, and sample volumes of 5 μL are adequate.

The microplate model for electrochemical arrays has been applied to 24-well cell culture plates, for the measurement of nitric oxide and superoxide in cultured cells [87]. In this work, the authors used screen-printed carbon electrodes, modified with electrodeposited nickel tetrasulfonated phthalocyanine, coated with a Nafion® film, for NO detection. Superoxide detection used the gold array elements, modified first by a thiol-succinimide reagent and subsequently exposed to cytochrome c for its covalent attachment. Each well contained, at the well bottom, three 1 mm diameter electrodes (two gold and one carbon) with individual Ag/AgCl counter electrodes. The device is shown in Fig. 16. Measurements employed a two-channel potentiostat, with applied potentials of +100 mV for superoxide and +750 mV for nitric oxide, for acquisition of chronoamperometric data. Wells were seeded

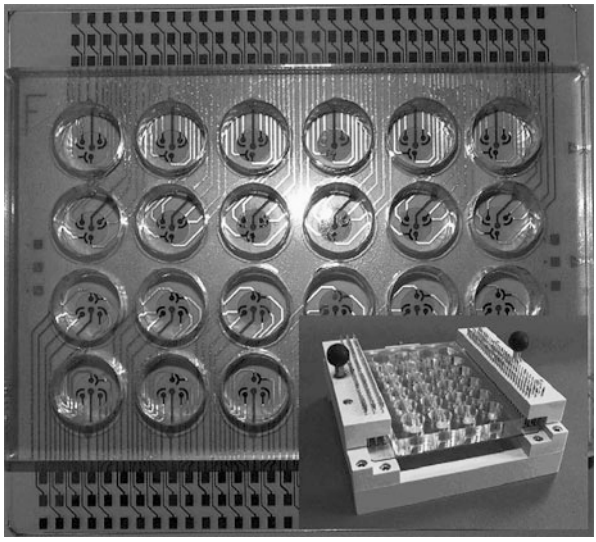

Fig. 16 Amperometric sensor array in a standard 24-well cell culture plate format, the fabrication details of which are given in Sect. 2. The *inset* shows the array mounted in a specially constructed connection system (Reproduced with permission from Chang et al. [87])

with different quantities of A172 human glioblastoma cells, and signals for both superoxide and nitric oxide increased with cell numbers. Simultaneous recording of both signals following cell stimulation was demonstrated. The authors propose the use and expansion of this platform for the screening of compounds designed to inhibit NO synthase or to inhibit superoxide free radical production.

Four-element arrays, with each element consisting of three Pt electrodes (one modified 30 μm × 30 μm square working, one counter and one Pt pseudo-reference), have been fabricated on glass substrates for the detection of the anabolic steroid albuterol, which is a doping concern in athletics and has been used as a food supplement for farm animals [88]. The arrays are based on working electrode modification with a molecularly imprinted polymer that is selective for albuterol over clenbuterol and terbutaline, two closely related compounds. The arrays are reusable (at least 20 times) and linear responses, as differential pulse voltammetric peak currents, for the oxidation of phenolic hydroxyl groups at about +0.45 V, occur over the 1–50 μM concentration range of albuterol. The molecularly imprinted polymer electrode films allow discrimination over similarly functionalized interferants.

A new polymer has been developed to modify the surfaces of ElectraSense™ platinum electrode arrays, to allow general immobilizations on porous, hydrophilic surfaces [89]. Surface modification of the electrodes with an initial layer of polymethacrylate block copolymer with poly4-bromostyrene was followed by spin coating the array with a new diblock copolymer that, after UV irradiation, produced a porous cross-linked polymer coating with 20 nm pores. The new polymer both protects the electrode surfaces from fouling and also allows immobilization of biorecognition agents. On both the 1,024 and 12,544 microelectrode/cm^2 prototypes, consistent coating was observed and optically detectable markers were immobilized.

The integration of different kinds of proteins into electrochemical arrays has been the subject of a recent report involving an alkali ion-channel protein and alcohol dehydrogenase [90]. A scalable 2 × 2 array of 1 mm^2 radius gold disk working electrodes was fabricated, with each pair separated by a Ag/AgCl reference band on a CMOS chip. Immobilization of a bilayer membrane containing the ion channel protein on one element, and alcohol dehydrogenase on the other electrode, using gold–thiol chemistry, provided the two detection elements. Both sensors performed well using voltammetric detection (dehydrogenase) and impedimetric detection (for K^+) of about 2 mM.

Bovine adrenal chromaffin cells were used to demonstrate a new multi-microwell array, shown in Fig. 17, with tiny indium-tin oxide semitransparent disk working electrodes at the bottoms, and with the wells suitably sized to house single cells and monitor quantal exocytosis of dopamine [91]. Disk electrodes 20 μm in diameter were recessed from the surface of an insulating film (SU-8) laminated to a microscope slide glass substrate. Polylysine modification of the ITO surfaces allowed the size-selective capture of individual cells facilitated by gravity. Poly(ethylene glycol) was used to coat the outer surfaces with a hydrophilic,

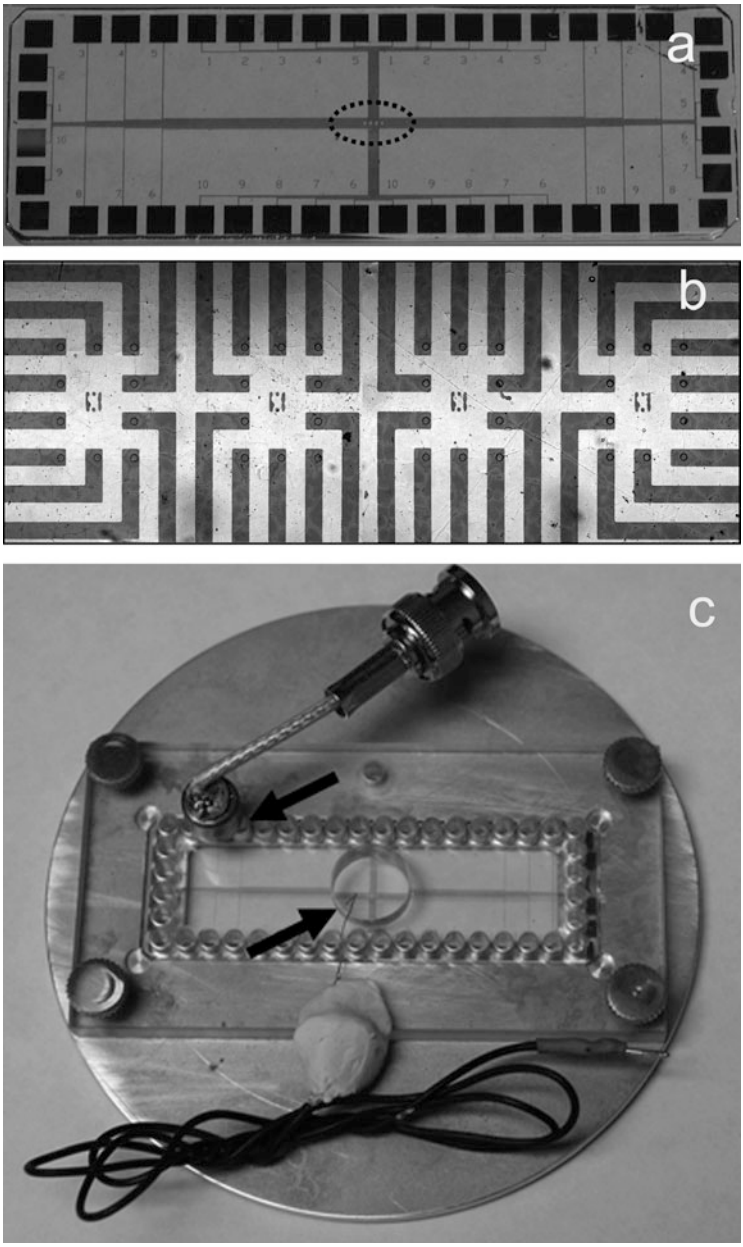

Fig. 17 Photos of device and chip holder. (**a**) Photo of device on glass slide substrate. The 40 squares around the perimeter are connection pads whereas the working electrodes are in the center (*dashed oval*). (**b**) Expanded view of the 40 working electrodes, which are arranged in 4 sets of 10. Each conductive trace is 60 μm wide. (**c**) Photo of chip holder. The removable plastic cover has 40 holes to facilitate connection of amplifier to the connection pads (*upper arrow*). Cells and solutions are placed in the center of the device as is a Ag/AgCl reference electrode (*lower arrow*). The round aluminum bottom inserts into the microscope stage to allow viewing of cells (Reproduced with permission from Liu et al. [91])

nonadherent layer. An external Ag/AgCl wire reference electrode was used for amperometric measurements at +700 mV. Very rapid data acquisition allowed well-resolved transient peaks to be observed from single cells in individual wells, corresponding to quantal exocytosis of dopamine. Reusability of the devices was demonstrated.

9 Conclusions and Future Directions

The past two decades have seen enormous progress in the fundamentals and applications of electrochemical arrays with individually addressable elements. We have considered applications to liquid-phase bioanalytical assays and sensors in this chapter; however, many other applications exist. The timeline of array element density is nonlinear: in some cases, particularly diagnostic screening, inexpensive, targeted analyte detection/quantitation is desired, and paper (cellulose) substrates have been introduced. In other applications, such as genomics or proteomics, arrays with very large numbers and high densities of tiny elements are very beneficial. Many arrays may be considered adaptations and/or miniaturizations of common macroscopic high-throughput methods (e.g., multiwell microplate ELISAs), but many are uniquely designed and fabricated with novel applications providing creative impetus. Current and future array developments must consider the intended applications of the devices, to determine the fabrication method(s), the materials, the kinds of surface modifications of individual elements, any requirements for microfluidic and/or specialized instrument interfacing, and the reusability or disposable nature of the ultimate devices. These considerations are all important for the determination of capital (instrumentation) and disposable or reusable (array) component expenses for complete assay systems, and are largely driven by assay multiplexing requirements. The introduction of commercially available electrochemical arrays has been a limiting factor in the application of electrochemical measurement techniques to biochemical and biological assays, and this is now being alleviated with both smaller (e.g., 16 element) and much larger (e.g., 12,544 element) arrays with their associated signal measurement devices. The authors of this chapter are optimistic that the ready availability of inexpensive electrochemical array systems will allow strong competition for bioassay applications in comparison with other common readout technologies (e.g., absorbance or fluorescence) that require much more expensive components.

Acknowledgements The assistance of Dr Mehdi Rahimi is gratefully acknowledged for a preliminary collection of array references. The authors also acknowledge support from colleagues and the institutions of the University of Waterloo, Department of Chemistry (SM) as well as the Universidad de Buenos Aires, Departamento de Química Biológica (EC), and the IQUIBICEN-CONICET of Argentina (EC).

References

1. Tomčik P (2013) Microelectrode arrays with overlapped diffusion layers as electroanalytical detectors: theory and basic applications. Sensors 13:13659–13684
2. Stefan R-I, van Staden JF, Aboul-Enein HY (1999) Electrochemical sensor arrays. Crit Rev Anal Chem 29:133–153
3. Willner I, Katz E (2000) Integration of layered redox proteins and conductive supports for bioelectronic applications. Angew Chem Int Ed 39:1180–1218
4. Albers J, Grunwald T, Nebling E, Piechotta G, Hintsche R (2003) Electrical biochip technology – a tool for microarrays and continuous monitoring. Anal Bioanal Chem 377:521–527
5. Huang X-J, O'Mahoney AM, Compton RG (2009) Microelectrode arrays for electrochemistry: approaches to fabrication. Small 5:776–788
6. Lange U, Roznyatovskaya NV, Mirsky VM (2008) Conducting polymers in chemical sensors and arrays. Anal Chim Acta 614:1–26
7. Warsinke A (2008) Electrochemical biochips for protein analysis. Adv Biochem Eng 109:155–193
8. Laschi S, Centi S, Mascini M (2011) Electrochemical arrays coupled with magnetic separators for immunochemistry. Bioanal Rev 3:11–25
9. Palchetti I, Mascini M (2008) Electroanalytical biosensors and their potential for food pathogen and toxin detection. Anal Bioanal Chem 391:455–471
10. Lucarelli F, Tombelli S, Minunni M, Marrazza G, Mascini M (2008) Electrochemical and piezoelectric DNA biosensors for hybridization detection. Anal Chim Acta 609:139–159
11. Merlos Rodrigo MA, Zitka O, Krejcova L, Hynek D, Masarik M, Kynicky J, Heger Z, Adam V, Kizek R (2014) Electrochemical microarray for identification pathogens: a review. Int J Electrochem Sci 9:3431–3439
12. Fosdick SE, Knust KN, Scida K, Crooks RM (2013) Bipolar electrochemistry. Angew Chem Int Ed 52:10438–10453
13. Rothe J, Frey O, Stettler A, Chen Y, Hierlemann A (2014) Fully integrated CMOS microsystem for electrochemical measurements on 32 x 32 working electrodes at 90 frames per second. Anal Chem 86:6425–6432
14. Tang T-C, Deng A, Huang H-J (2002) Immunoassay with a microtiter plate incorporated multichannel electrochemical detection system. Anal Chem 74:2617–2621
15. Reiter S, Eckhard K, Blöchl A, Schuhmann W (2001) Redox modification of proteins using sequential-parallel electrochemistry in microtiter plates. Analyst 126:1912–1918
16. Kitahara T, Koyama N, Matsuda J, Hirakata Y, Kamihira S, Kohno S, Nakashima M, Sasaki H (2003) Evaluation of newly developed oxygen meters with multi-channels and disposable oxygen electrode sensors for antimicrobial susceptibility testing. Biol Pharm Bull 26:1229–1234
17. Andreescu S, Sadik OA, McGee DW, Suye S-I (2004) Autonomous multielectrode system for monitoring the interactions of isoflavonoids with lung cancer cells. Anal Chem 76:2321–2330
18. Karasinski J, Andreescu S, Sadik OA, Lavine B, Vora MN (2005) Multiarray sensors with pattern recognition for the detection, classification, and differentiation of bacteria at subspecies and strain levels. Anal Chem 77:7941–7949
19. Karasinski J, White L, Zhang Y, Wang E, Andreescu S, Sadik OA, Lavine B, Vora M (2007) Detection and identification of bacteria using antibiotic susceptibility and a multi-array electrochemical sensor with pattern recognition. Biosens Bioelectron 22:2643–2649
20. Sun L, Crooks RM (2005) Photonic reporting of electrochemical reactions using light-emitting diodes. J Electrochem Soc 152(11):E371–E377
21. Abdur Rahman AR, Justin G, Guiseppi-Elie A (2009) Towards an implantable biochip for glucose and lactate monitoring using microdisc electrode arrays (MDEAs). Biomed Microdevices 11:75–85

22. Zhang B, Adams KL, Luber SJ, Eves DJ, Heien ML, Ewing AG (2008) Spatially and temporally resolved single-cell exocytosis utilizing individually addressable carbon microelectrode arrays. Anal Chem 80:1394–1400
23. Mann TS, O'Hagan L, Ertl P, Sparkes DI, Mikkelsen SR (2008) Microplate-compatible biamperometry array for parallel 48-channel amperometric or coulometric measurements. Anal Chem 80:2988–2992
24. Forzani ES, Li X, Tao N (2007) Hybrid amperometric and conductometric chemical sensor based on conducting polymer nanojunctions. Anal Chem 79:5217–5224
25. Hafez I, Kisler K, Berberian K, Dernick G, Valero V, Yong MG, Craighead HG, Lindau M (2005) Electrochemical imaging of fusion pore openings by electrochemical detector arrays. Proc Natl Acad Sci U S A 102:13879–13884
26. Chen Y, Guo C, Lim L, Cheong S, Zhang Q, Tang K, Reboud J (2008) Compact microelectrode array system: tool for in situ monitoring of drug effects on neurotransmitter release from neural cells. Anal Chem 80:1133–1140
27. Delibato E, Volpe G, Romanazzo D, De Medici D, Toti L, Moscone D, Palleschi G (2009) Development and application of an electrochemical plate coupled with immunomagnetic beads (ELIME) array for *Salmonella enterica* detection in meat samples. J Agric Food Chem 57:7200–7204
28. Hou H, Li L, Cho Y, de Figueiredo P, Han A (2009) Microfabricated microbial fuel cell arrays reveal electrochemically active microbes. PLoS One 4:e6570
29. Biffinger J, Ribbens M, Ringeisen B, Pietron J, Finkel S, Nealson K (2008) Characterization of electrochemically active bacteria utilizing a high-throughput voltage-based screening assay. Biotechnol Bioeng 102:436–444
30. Mann TS, Mikkelsen SR (2008) Antibiotic susceptibility testing at a screen-printed carbon electrode array. Anal Chem 80:843–848
31. Lin Z, Takahashi Y, Kitagawa Y, Umemura T, Shiku H, Matsue T (2008) An addressable microelectrode array for electrochemical detection. Anal Chem 80:6830–6833
32. Chow K-F, Mavré F, Crooks JA, Chang B-Y, Crooks RM (2009) A large-scale, wireless electrochemical bipolar electrode microarray. J Am Chem Soc 131:8364–8365
33. Pemberton RM, Cox T, Tuffin R, Drago GA, Griffiths J, Pittson R, Johnson G, Xu J, Sage IC, Davies R, Jackson SK, Kenna G, Luxton R, Hart JP (2014) Fabrication and evaluation of a micro(bio)sensor array chip for multiple parallel measurements of important cell biomarkers. Sensors 14:20519–20532
34. Sapelnikova S, Dock E, Solná R, Skládal P, Ruzgas T, Emnéus J (2003) Screen-printed multienzyme arrays for use in amperometric batch and flow systems. Anal Bioanal Chem 376:1098–1103
35. Stephens ML, Pomerleau F, Huettl P, Gerhardt GA, Zhang Z (2010) Real-time glutamate measurements in the putamen of awake rhesus monkeys using an enzyme-based human microelectrode array prototype. J Neurosci Methods 185:264–272
36. Dalbasti T, Kilinc E, Erdem A, Ozsoz M (1998) Multielectrode array for simultaneous recording of glucose, oxygen and electrocorticography from cerebral cortex in experimental focal epilepsy. Biosens Bioelectron 13:881–888
37. Kanungo M, Kumar A, Contractor AQ (2003) Microtubule sensors and sensor array based on polyaniline synthesized in the presence of poly(styrene sulfonate). Anal Chem 75:5673–5679
38. Tønning E, Sapelnikova S, Christensen J, Carlsson C, Winther-Nielsen M, Dock E, Solna R, Skladal P, Nørgaard L, Ruzgas T, Emnéus J (2005) Chemometric exploration of an amperometric biosensor array for fast determination of wastewater quality. Biosens Bioelectron 21:608–617
39. Sapelnikova S, Dock E, Ruzgas T, Emnéus J (2003) Amperometric sensors based on tyrosinase-modified screen-printed arrays. Talanta 61:473–483
40. Moser I, Jobst G, Urban GA (2002) Biosensor arrays for simultaneous measurement of glucose, lactate, glutamate and glutamine. Biosens Bioelectron 17:297–302

41. Valdés-Ramírez G, Gutiérrez M, del Valle M, Ramírez-Silva MT, Fournier D, Marty J-L (2009) Automated resolution of dichlorvos and methylparaoxon pesticide mixtures employing a flow injection system with an inhibition electronic tongue. Biosens Bioelectron 24:1103–1108
42. Solná R, Sapelnikova S, Skládal P, Minther-Nielsen M, Carlsson C, Emnéus J, Ruzgas T (2005) Multienzyme electrochemical array sensor for determination of phenols and pesticides. Talanta 65:349–357
43. Crew A, Lonsdale D, Byrd N, Pittson R, Hart JP (2011) A screen-printed, amperometric biosensor array incorporated into a novel automated system for the simultaneous determination of organophosphate pesticides. Biosens Bioelectron 26:2847–2851
44. Weltin A, Kieninger J, Enderle B, Gellner A-K, Fritsch B, Urban GA (2014) Polymer-based, flexible glutamate and lactate microsensors for *in vivo* applications. Biosens Bioelectron 61:192–199
45. Inoue KY, Matsudaira M, Nakano M, Ino K, Sakamoto C, Kanno Y, Kubo R, Kunikata R, Kira A, Suda A, Tsurumi R, Shioya T, Yoshida S, Muroyama M, Ishikawa T, Shiku H, Satoh S, Esashi M, Matsue T (2015) Advanced LSI-based amperometric sensor array with light-shielding structure for effective removal of photocurrent and mode selectable function for individual operation of 400 electrodes. Lab Chip 15:848–856
46. Lee HY, Lee BK, Park JW, Jung HS, Kim JM, Kawai T (2008) Self-organized functional lipid vesicle array for sensitive immunoassay chip. Ultramicroscopy 108:1325–1327
47. Dong H, Li C-M, Zhang Y-F, Cao X-D, Gan Y (2007) Screen-printed microfluidic device for electrochemical immunoassay. Lab Chip 7:1752–1758
48. Zhang Y, Wang H, Nie J, Zhang Y, Shen GYR (2009) Individually addressable microelectrode arrays fabricated with gold-coated pencil graphite particles for multiplexed and high sensitive impedance immunoassays. Biosens Bioelectron 23:34–40
49. Wilson MS, Nie W (2006) Electrochemical multianalyte immunoassays using an array-based sensor. Anal Chem 78:2507–2513
50. Piermarini S, Michele L, Ammida NHS, Palleschi G, Moscone D (2007) Electrochemical immunosensor array using a 96-well screen-printed microplate for aflatoxin B_1 detection. Biosens Bioelectron 22:1434–1440
51. Parker CO, Lanyon YH, Manning M, Arrigan DWM, Tothill IE (2009) Electrochemical immunochip sensor for aflatoxin M_1 detection. Anal Chem 81:5291–5298
52. Polsky R, Harper JC, Wheeler DR, Dirk SM, Arango DC, Brozik SM (2008) Electrically addressable diazonium-functionalized antibodies for multianalyte electrochemical sensor applications. Biosens Bioelectron 23:757–764
53. Wu J, Yan Y, Yan F, Ju H (2008) Electric field-driven strategy for multiplexed detection of protein biomarkers using a disposable reagentless electrochemical immunosensor array. Anal Chem 80:6072–6077
54. Wu J, Yan F, Tang J, Zhai C, Ju H (2007) A disposable multianalyte electrochemical immunosensor array for automated simultaneous determination of tumor markers. Clin Chem 53:1495–1502
55. Wu J, Zhang Z, Fu Z, Ju H (2007) A disposable two-throughput electrochemical immunosensor chip for simultaneous multianalyte determination of tumor markers. Biosens Bioelectron 23:114–120
56. Wu J, Yan F, Zhang X, Yan Y, Tang J, Ju H (2008) Disposable reagentless electrochemical immunosensor array based on a biopolymer/sol-gel membrane for simultaneous measurement of several tumor markers. Clin Chem 54:1481–1488
57. Aguilar ZP, Sirisena M (2007) Development of automated amperometric detection of antibodies against *Bacillus anthracis* protective antigen. Anal Bioanal Chem 389:507–515
58. Harper JC, Polsky R, Wheeler DR, Dirk SM, Brozik SM (2007) Selective immobilization of DNA and antibody probes on electrode arrays: simultaneous electrochemical detection of DNA and protein on a single platform. Langmuir 23:8285–8287

59. Henry OY, Fragoso A, Beni V, Laboria N, Acero Sánchez JL, Latta D, Von Germar F, Drese K, Katakis I, O'Sullivan CK (2009) Design and testing of a packaged microfluidic cell for the multiplexed electrochemical detection of cancer markers. Electrophoresis 30:3398–3405
60. Jeon SI, Hong JW, Yoon HC (2006) A new immunosensing method by galactose oxidase-mediated electrocatalysis using a virtual beaker array. Biotechnol Lett 28:1401–1408
61. Kadimisetty K, Malla S, Sardesai NP, Joshi AA, Faria RC, Lee NH, Rusling JF (2015) Automated multiplexed ECL immunoarrays for cancer biomarker proteins. Anal Chem 87:4472–4478
62. Arumugam PU, Chen H, Siddiqui S, Weinrich JAP, Jejelowo A, Li J, Meyyappan M (2009) Wafer-scale fabrication of patterned carbon nanofiber nanoelectrode arrays: a route for development of multiplexed, ultrasensitive disposable biosensors. Biosens Bioelectron 24:2818–2824
63. Liao JC, Mastali M, Gau V, Suchard MA, Møller AK, Bruckner DA, Babbit JT, Li Y, Gornbein J, Landaw EM, McCabe ERB, Churchill BM, Haake DA (2006) Use of electrochemical DNA biosensors for rapid molecular identification of uropathogens in clinical urine specimens. J Clin Microbiol 44:561–570
64. Mach KE, Du CB, Phull H, Haake DA, Shih M-C, Baron EJ, Liao JC (2009) Multiplex pathogen identification for polymicrobial urinary tract infections using biosensor technology: a prospective clinical study. J Urol 182:2735–2741
65. Goto K, Horiuchi H, Shinohara H, Motegi K, Hashimoto K, Hongo S, Gemma N, Hayashimoto N, Itoh T, Takakura A (2007) Specific and quantitative detection of PCR products from *Clostridium piliforme*, *Helicobacter bilis*, *H. hepaticus*, and mouse hepatitis virus infected mouse samples using a newly developed electrochemical DNA chip. J Microbiol Methods 69:93–99
66. Levine PM, Gong P, Levicky R, Shepard KL (2009) Real-time, multiplexed electrochemical DNA detection using an active complementary metal-oxide-semiconductor biosensor array with integrated sensor electronics. Biosens Bioelectron 24:1995–2001
67. Neugebauer S, Zimdars A, Liepold P, Gębala M, Schuhmann W, Hartwich G (2009) Optimization of an electrochemical DNA assay by using a 48-electrode array and redox amplification studies by means of scanning electrochemical microscopy. ChemBioChem 10:1193–1199
68. Pavlovic E, Lai RY, Wu TT, Ferguson BS, Sun R, Plaxco KW, Soh HT (2008) Microfluidic device architecture for electrochemical patterning and detection of multiple DNA sequences. Langmuir 24:1102–1107
69. Wan Y, Zhang J, Liu G, Pan D, Wang L, Song S, Fan C (2009) Ligase-based multiple DNA analysis by using an electrochemical sensor array. Biosens Bioelectron 24:1209–1212
70. Zhang D, Peng Y, Qi H, Gao Q, Zhang C (2010) Label-free electrochemical DNA biosensor array for simultaneous detection of the HIV-1 and HIV-2 oligonucleotides incorporating different hairpin-DNA probes and redox indicator. Biosens Bioelectron 25:1088–1094
71. Henry OY, Acero Sanchez JL, Latta D, O'Sullivan CK (2009) Electrochemical quantification of DNA amplicons via the detection of non-hybridised guanine bases on low-density electrode arrays. Biosens Bioelectron 24:2064–2070
72. Nebling E, Grunwald T, Albers J, Schäfer P, Hintsche R (2004) Electrical detection of viral DNA using ultramicroelectrode arrays. Anal Chem 76:689–696
73. Douglas ES, Hsiao SC, Onoe H, Bertozzi CR, Francis MB, Mathies RA (2009) DNA-barcode directed capture and electrochemical metabolic analysis of single mammalian cells on a microelectrode array. Lab Chip 9:2010–2015
74. Marquette CA, Lawrence MF, Blum LJ (2006) DNA covalent immobilizatiton onto screen-printed electrode networks for direct label-free hybridization detection of p53 sequences. Anal Chem 78:959–964
75. Bettazzi F, Lucarelli F, Palchetti I, Berti F, Marrazza G, Mascini M (2008) Disposable electrochemical DNA-array for PCR amplified detection of hazelnut allergens in foodstuffs. Anal Chim Acta 614:93–102

76. Diercks S, Metfies K, Medlin LK (2008) Development and adaptation of a multiprobe biosensor for the use in a semi-automated device for the detection of toxic algae. Biosens Bioelectron 23:1527–1533
77. Elsholz B, Wörl R, Blohm L, Albers J, Feucht H, Grunwald T, Jürgen B, Schweder T, Hintsche R (2006) Automated detection and quantitation of bacterial RNA by using electrical microarrays. Anal Chem 78:4794–4802
78. Ghindilis AL, Smith MW, Schwartzkopf KR, Roth KM, Peyvan K, Munro SB, Lodes MJ, Stőver AG, Bernards K, Dill K, McShea A (2007) CombiMatrix oligonucleotide arrays: genotyping and gene expression assays employing electrochemical detection. Biosens Bioelectron 22:1853–1860
79. Chow K-F, Mavré F, Crooks RM (2008) Wireless electrochemical DNA microarray sensor. J Am Chem Soc 130:7544–7545
80. Furst AL, Hill MG, Barton JK (2015) A multiplexed, two-electrode platform for biosensing based on DNA-mediated charge transport. Langmuir 31:6554–6562
81. Joda H, Beni V, Willems A, Frank R, Höth J, Lind K, Strömbom L, Katakis I, O'Sullivan CK (2015) Modified primers for rapid and direct electrochemical analysis of coeliac disease associated HLA alleles. Biosens Bioelectron 73:64–70
82. Cheng W, Ding L, Ding S, Yin Y, Ju H (2009) A simple electrochemical cytosensor array for dynamic analysis of carcinoma cell surface glycans. Angew Chem Int Ed 48:6465–6468
83. Wang J, Trouillon R, Lin Y, Svensson MI, Ewing AG (2013) Individually addressable thin-film ultramicroelectrode array for spatial measurements of single vesicle release. Anal Chem 85:5600–5608
84. Quinton D, Girard A, Kim LTT, Raimbault V, Griscom L, Razan F, Griveau S, Bedioui F (2011) On-chip multi-electrochemical sensor array platform for simultaneous screening of nitric oxide and peroxynitrite. Lab Chip 11:1342–1350
85. Canali C, Mazzoni C, Larsen LB, Heiskanen A, Martinsen OG, Wolff A, Dufva M, Emneus J (2015) Analyst 140:6079–6088
86. Yang SY, DeFranco JA, Sylvester YA, Gobert TJ, Macaya DJ, Owens RM, Malliaras GG (2009) Integration of a surface-directed microfluidic system with an organic electrochemical transistor array for multi-analyte biosensors. Lab Chip 9:704–708
87. Chang S-C, Pereira-Rodrigues N, Henderson JR, Cole A, Bedioui F, McNeil CJ (2005) An electrochemical sensor array system for the direct, simultaneous in vitro monitoring of nitric oxide and superoxide production by cultured cells. Biosens Bioelectron 21:917–922
88. Huang H-C, Huang S-Y, Lin C-I, Lee Y-D (2007) A multi-array sensor via the integration of acrylic molecularly imprinted photoresists and ultramicroelectrodes on a glass chip. Anal Chim Acta 582:137–146
89. Hu L, Bartels JL, Bartels JW, Maurer K, Moeller KD (2009) A new porous reaction layer for developing addressable molecular libraries. J Am Chem Soc 131:16638–16639
90. Huang Y, Liu Y, Hassler BL, Worden RM, Mason AJ (2013) A protein-based electrochemical biosensor array platform for integrated microsystems. IEEE Trans Biomed Circuits Systems 7:43–51
91. Liu X, Barizuddin S, Shin W, Mathai CJ, Gangopadhyay S, Gillis KD (2011) Microwell device for targeting single cells to electrochemical microelectrodes for high-throughput amperometric detection of quantal exocytosis. Anal Chem 83:2445–2451

BIOREV (2017) 6: 143–202
DOI: 10.1007/11663_2016_2

Published online: 28 June 2016

Bioelectronic Tongues Employing Electrochemical Biosensors

Manel del Valle

Abstract This chapter presents recent advances concerning work with electronic tongues that employ electrochemical biosensors, that is, bioelectronic tongues. (Bio)electronic tongues represent a new methodological use of (bio)sensors; they start by the use of biosensor arrays and assume the coupling of the obtained complex response with advanced chemometric data treatment; the goal is improving performance of existing sensors. Most of the bioelectronic tongues reported employ enzyme biosensors, essentially based on potentiometric or voltammetric/amperometric transduction. This report is organized considering the different forms to incorporate biosensors, i.e. considering the number of biosensors in the array, the number of different enzymes used, if the determination is aimed to substrates or inhibitors, etc. Significant applications in real problem-solving, mainly in the food and clinical or environmental fields, are commented.

Keywords Amperometry • Artificial neural networks • Biosensor arrays • Electronic tongues • Enzyme biosensors • Potentiometry • Voltammetry

Contents

M. del Valle (✉)
Sensors and Biosensors Group, Chemistry Department, Universitat Autònoma de Barcelona, 08193 Bellaterra, Barcelona, Spain
e-mail: manel.delvalle@uab.es

Abbreviations

AA	Arachidic acid
AChE	Acetylcholinesterases
ADH	Alcohol dehydrogenase
AFM	Atomic force microscopy
ANN	Artificial neural network
AOx	Alcohol oxidase
AuNP	Gold nanoparticles
BChE	Butyrylcholinesterase
BioET	Bioelectronic tongue
BOD	Biological oxygen demand
BSA	Bovine serum albumin
CDH	Cellobiose dehydrogenase
CE	Capillary electrophoresis
COD	Chemical oxygen demand
CPE	Carbon paste electrodes
CV	Cyclic voltammetry
DAO	Diamino oxidase
ET	Electronic tongue
FC	Folin–Ciocalteu (index)
FFT	Fast Fourier transform
FIA	Flow-injection automated analysis
GOX	Glucose oxidase
GPCRs	G-protein-coupled receptor
HPLC	High-performance liquid chromatography
HRP	Horseradish peroxidase
hTAS1R2	Human taste receptor type 1, receptor 2
hTAS1R3	Human taste receptor type 1, receptor 3
ISE	Ion-selective electrode
ITO	Indium tin oxide
K-NN	K-nearest neighbours
LB	Langmuir–Blodgett
LDA	Linear discriminant analysis

MAO	Monoamine oxidase
MC	Microcystins
MCR	Multiple component regression
MDC	Multiplicative drift correction
MEA	Microelectrode arrays
MWCNT	Multiwalled carbon nanotubes
PCA	Principal component analysis
PCR	Principal component regression
PEG	Poly(ethylene glycol)
PLS	Partial least squares
PP1, PP2A	Protein phosphatases
PRM	Partial robust M regression model
Pt	Platinum
SBP	Soybean peroxidase
SEM	Scanning electron microscopy
SIA	Sequential injection automated analysis
SPE	Screen-printed electrodes
SVM	Support vector machines
TAO	Tyramine oxidase
TOC	Total organic carbon
TTF	Tetrathiafulvalene
TYR	Tyrosinase

1 Introduction

ETs or electronic tongues are based on the usage of an array of sensors with low-selectivity and/or cross-response features in order to obtain some added value in the generated analytical information; the latter normally coupled with advanced chemometric tools that allow the interpretation and extraction of meaningful data from the complex readings [1]. Thus, ETs represent a different progress line in sensor research; instead of focusing on finding highly selective sensors, ETs are inspired and try to mimic the sense of taste in animals: in these, a few receptors can respond to a large variety of substances, thanks to the combinatorial principles used, and the obtained information be later processed by the brain [2]. Hence, ETs prefer using low-selective sensors and extracting the sought information by use of advanced data treatment. This coupling of chemometrics and electrochemical sensors was already identified as one of the best ways to improve sensor performance and already suggests a consolidated line of research in the electroanalysis field [3].

In this chapter, I will focus on presenting advances concerning work with ETs that employ electrochemical biosensors, that is, bioelectronic tongues (BioETs). BioETs represent, in their turn, a new methodological use of biosensors; although biosensors are supposedly highly selective, then providing easily the direct

measurement, this case is largely utopian, and there are different distorting situations. Among these we can list the group specificity that widens the range of responses, the interfering effect of other compounds or of the sample matrix, or the different forms of activation and inhibition by third substances. The idea of BioETs is then to couple existing biosensors with advanced chemometric treatment, with the goal of improving biosensor performance, per example coping with the inconveniences above. Most of the bioelectronic tongues reported employ enzyme biosensors, essentially based on potentiometric or voltammetric/amperometric transduction, although there are some few cases involving per example microbial sensors, or protein receptors. When designing this chapter, there appeared different ways to organize the existing research. There was a trivial, immediate way, which was to use the transduction technique to present works done, but this was not practical, as there is not much variety in use, as we will see later. There was a second way to classify accordingly the enzyme/biological element used, but again this was too straightforward to extract useful recommendations, with the risk of long lists of essentially the same application and very little variants in between. There was also the possibility of the type of application: i.e. identification/classification of samples, prediction of concentration of certain compounds, etc. This way could be useful, and variety and scope of applications may be interesting enough, although this would be more indicated for an application type report; it could be an organization sharing its scheme also with the chemometric tools employed, what would provide their double association, application/chemometric tool. At the end, the way to organize the set or recorded works is by how the biosensor element(s) is incorporated in the sensor array, in what it could be translated into array complexity. As such, it was considered a way directly related to the experimental plan underlying the research and can be very useful to show how a certain experimental configuration may be used for different purposes and can help the reader in preparing and developing new research with BioETs. In this way, there is the first section dedicated to extraction of extra information when a single biosensor is used, as the first instance showing most simplicity. This case, although not directly pertaining to the BioET definition (a single biosensor is used), can be extrapolated into when the biosensor generated a high dimensional signal, as this is the case with enzyme voltammetric biosensors, wherever the complete voltammogram is used to extract multivariate information. Next in complexity, the second considered case is the use of one biosensor together with other sensors not of the biosensor type, in general, a case where certain substrate(s) is determined with high precision from the enzyme biosensor, and the rest of ordinary sensors are used to counterbalance any interfering effect from the sample matrix of other species present. The most complex situation corresponds to the use of different biosensors, probably with different biological elements, and is the class with most interest and with the largest amount of different application cases registered. Last, as a subclass of the latter worth mentioning, there is the case of inhibition ET, where a set of different inhibitors are identified or resolved according to different inhibition degrees produced into a number of different biosensors used.

One reflection to be done when introducing the concepts and principles used by BioETs is how this approach is biomimetic [4]. Nature clearly inspires these approaches, and the combinatorial way of providing receptor diversity in the senses of olfaction or taste (or even tactile) is the approach found by Nature to cope with the immense need of differentiating thousands or even more situations. Biomimetic principles are therefore used in electronic noses and electronic tongues, as the total picture generated by the different (bio)sensors in the array is processed in parallel, as our brain would do, to define a certain identification/perception. And although there are attempts in which research is directed towards mimicking as close as possible functioning and performance of human senses, I consider this, although interesting and licit, a limited case goal, nevertheless being many other applications to be imagined and attempted, specially from the bioanalysis focus.

It is clear there is the demand for fast and accurate identification and analysis methods, specially to help in the development and quality control of food and beverages. It is in this sole application where BioETs can be a clear alternative to most of nowadays used analytical methods, as it is suggested in a recent insight article in *Nature* journal [5]. Systems can be developed to specifically mimic the human sensory experience or to reproduce the expert quality faster; for this aim, the use of biosensors may provide more accurate signals than with the use of the simplest sensors (e.g. pH, redox potential or conductivity), and these signals may be translated in an automated system capable of a more objective, intensive and tireless use. Such BioET systems may be of great help for food producers and commercializers, to assure its quality and to provide its standardization. And this may be possible for human-consumed products but also for pet food or animal feed, also in search of better products, where the important point is still to gather together the accumulated experience of the specialist.

It is also a must reminding the reader that initial approaches within the field, i.e., all the conceptual generation of ETs, is now a couple of decades old, even, the employ of biosensors is quite younger. All the initial developments and evolution in the field can be extracted from different review papers from the main laboratories doing research within the field, as there are around 600 important published works to comment. As such, there is one of the founding groups, that of Legin, in St. Petersburg, mainly working with potentiometric sensors [6], or the group from Wroblewski in Warsaw, also mastering work with potentiometric sensors, specially in flow-injection (FIA) systems [7]. It is worth mentioning also a group now in different laboratories in Brazil, specially dedicated to micro-/nanotechnologically engineered sensors [8], or the group from Tokyo in Japan, mainly devoted to the artificial taste developments [9]. In the case of our laboratory in Barcelona, we are widely known for our versatility and variety of options. Displaying previous successful background for some decades in the work with different technologies of electrochemical sensors and biosensors, we can take advantage of the experience with potentiometric, voltammetric, impedimetric sensing and biosensing, providing in this way most of the available technology to develop ETs and BioETs [10].

Concerning the term bioelectronic tongue (BioET) [11], we can cite the first usage in the work by Tønning et al., where an array of different amperometric

biosensors were used to characterize type of wastewaters [12], and a contribution from our laboratory [13], where we performed the multivariate analysis of a mixture of phenolic compounds from the voltammetric response of a tyrosinase enzyme biosensor, both in 2005. As already defined, the idea behind the BioET is to use biosensors in a multiplex mode, with each biosensor recognizing one analyte or a certain group of analytes, and then use advanced computational methods in order to get an accurate characterization of the sample.

In our laboratory, the first ideas of BioETs were later expanded to multicomponent resolution of diverse ions plus urea in the food/clinical application by use of potentiometric urease biosensor [14]. The ions resolved were the ones that would be interfering in the potentiometric urea biosensor, chosen for transduction, e.g. NH_4^+, Na^+ and K^+. This application signified a complement of existing research in the field; apart from searching for methods to physically separate interfering species away from the biosensors, which were the general trend, the idea was to measure all species intervening and mathematically compensating its presence. Also, a very significant contribution from our laboratory in the research with enzyme containing sensor arrays has been the resolution of compounds, in this case pesticides from different families and from different inhibition patterns shown by enzymes with slightly differentiated activity, depending from their natural source and natural variability or by artificial intervention, e.g. using enzymes genetically engineered [15, 16].

1.1 Types of Biosensors Used in the Array

The total number of works in the literature that employ one or several biosensors in the array in order to operate like an ET is slightly below one hundred (search performed on July 2015), whereas there are approximately 600 works related to the more generic one. From these, practically all of them employ electrochemical techniques as transduction variant, and also, practically all of them use enzyme elements in the design of the biosensor.

When the types of sensors used are scrutinized in more detail, one finds a curious peculiarity (see Fig. 1). In the generic field of electronic tongues (ETs), most of the works collected (ca. 50%) use potentiometric sensors, that is, ion-selective electrodes (ISEs), to design the analysis system. This share is followed by ETs using voltammetric and conductimetric (bio)sensors, while other transduction principles like optical or gravimetric sensing are minoritary. Curiously, this scenery changes completely in the case of BioETs, showing a maximum contribution by voltammetric (bio)sensors, followed by potentiometric and mostly a testimonial presence of other transduction schemes. Obviously this global pattern is mainly determined by the preferred choice of enzyme-modified electrodes with voltammetric transduction principle, as the most preferred biosensor for its incorporation in BioETs. Probably this choice is also justified by the wide diffusion and knowledge of amperometric enzyme sensors and also by preferred usage of redox

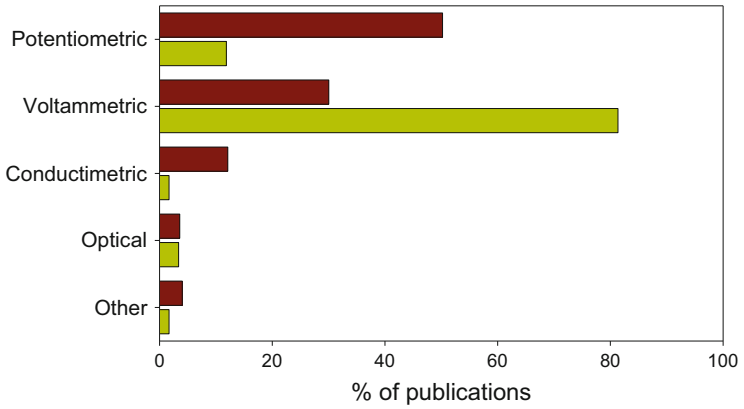

Fig. 1 Share of the transduction technique used for the sensors forming the BioET (*clear bars*) versus the situation in normal ET systems (*dark bars*). Data obtained from the literature search on the period 1996–2015 using SCOPUS database (Elsevier)

enzymes in their construction, given they are the ones directly converting turnover into current, i.e. directly observable analytical signal.

In any case, when observing the evolution timeline, first works that are worth mentioning are potentiometric sensors, and only after first attempts with ion-selective electrodes and enzymatically converting systems are voltammetric types found. This progression also follows the timeline of ETs, as there were the ones using the potentiometric sensors the ones first proposed and developed, and only after a few years, the first voltammetric electronic tongue was reported [17].

1.1.1 Potentiometric Biosensors

It was down to 2002 that Magalhaes proposed, within the Machado laboratory in Porto, Portugal, the use of an array of potentiometric sensors to alkaline ions together with two creatinine biosensors for the determination of potassium and creatinine in urine [18]. The biosensors used creatinine iminohydrolase enzyme (E.C. 3.5.4.21), a hydrolytic enzyme that converts creatinine into ammonium, and transduction was achieved through detection of the formed ammonium through an ammonium ISE. Interferents to the latter, both any ammonium initially present or alkaline ions, were counterbalanced through measurement from ISEs to ammonium, sodium, potassium and calcium. Estimation of concentrations was achieved through partial least squares (PLS) calculation. Although it will be commented in more depth in Sect. 2, it should be mentioned that PLS is a multivariate linear regression method, in which only a part of transformed original variables are used.

Later, the same idea was applied to determine urea in blood serum [19]. The system was formed by two urea biosensors, obtained by immobilization of urease enzyme (EC 3.5.1.45) onto ammonium-selective membranes, plus ISEs for

ammonium, sodium and potassium, which were the most interfering species in the considered case. Our laboratory contributed with complete application research examples, first in the determination of urea [14] and next with two-enzyme biosensors, urease for urea and iminohydrolase for creatinine [20]. The first potentiometric BioET in Barcelona was then designed employing an array formed by two urea biosensors based on urease enzyme covalently linked to carboxylated PVC, along with ISEs for H^+, K^+, Na^+, NH_4^+ and cationic generic response. Biosensors were optimized in detail, in order to get the maximum stability of response, and this was obtained through covalent immobilization onto carboxylated PVC, a polymeric matrix also employed for the ammonium ion transducer. In this example, we used artificial neural networks (ANNs) to build the response model, as the preferred chemometric tool in our laboratories. An ANN is a massively parallel data processing technique, very much resembling an animal brain. ANNs are composed by processing elements called nodes or neurons, plus their interconnections (known as weights), and have been shown to be especially effective for modelling complex nonlinear problems. Response models were also built employing partial least squares (PLS) for comparison purposes, showing slightly better prediction capabilities for ANNs, especially at the lower concentration limits. This result is particularly significant due to the better performance of the ANN modelling at the nonlinear response regions, given PLS is more dependent on the linearity of the data. Figure 2 depicts how to build the quantitative response model using the ANN, with the data from the ISEs as departure point; the concentrations of the sought species are provided, together with the concentrations of the interferent species that were measured and modelled. With this array, it was possible to determine urea in clinical samples without the need to separate endogenous ammonium or the interfering ions sodium and potassium, all them normally present in clinical samples. In the same progress line, the system was enlarged with an additional potentiometric biosensor employing creatinine iminohydrolase to determine urea, creatinine and alkaline interferents. Such a BioET is ready at the moment for its clinical application in studies of renal function or the monitoring of haemodialysis processes.

1.1.2 Voltammetric Biosensors

The voltammetric technique which measures a current intensity originated by a redox process at an electrode polarized at a certain potential is an interesting analytical technique for identification and determination of chemical species, whose only condition is that they must be electroactive. The exact potential applied, and the form it is done (through linear sweep, AC, square wave, differential pulse, etc.), determines the analytical signal that is generated. Depending also on the nature of the electrode utilized, different electroactive compounds may get oxidized or reduced with a certain current, which can vary significantly when catalytic processes appear within the electrode surface or, alternatively, when overpotential comes out. Normally, voltammetry shows high sensitivity, being able to detect compounds below the ppm level; however, the selectivity is not so good, as many

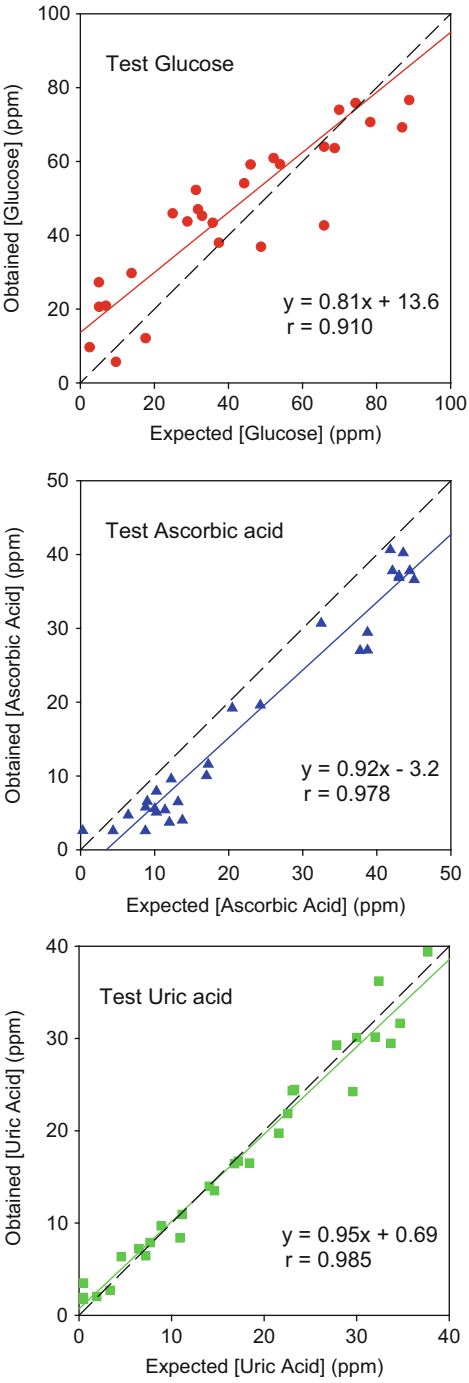

Fig. 2 Scheme of electronic tongue multicomponent determination of the two compounds A and B from the readings of an array formed by potentiometric sensors

electroactive compounds will react if the potential applied is sufficiently extreme. A second positive feature for our bioanalytical interests is that voltammetry can utilize easily redox enzymes as catalysts in electrode processes, obtaining in this way enzyme biosensors of the voltammetric type (when the technique utilizes a scan of polarization potential) or of the amperometric one (where the difference is that the applied potential is kept constant at certain fixed value). One existing objection may be that current measured at a certain potential is due to the sum of all the compounds present that are electrochemically active below the applied potential; this drawback degrades the overall selectivity of the technique but also assures the cross response needed for the ET concept. On the other hand, an important characteristic of ETs using voltammetric sensors is that their measured information is normally a vector for each sensor used, what converts the data treatment in a highly dimensioned calculation, which can be difficult to overcome.

First voltammetric ETs were devised at Linköping laboratories in Sweden, by Prof. Winquist and coworkers [17]. They essentially built arrays by joining a number of disc electrodes made of different metals, mostly of the noble family. Pieces of metal wire of ca. 1 mm diameter, made of gold, iridium, platinum, palladium, rhenium, rhodium or other metals, were then encased in a single body and formed a multiple channel voltammetric cell, together with an auxiliary and reference electrode. Applied potential was a second factor to originate different signals in a certain application, and experimenters may vary this from a single linear sweep, cyclic voltammetry, normal pulse, differential pulse, square wave, etc. Especially for the latter waveforms applied, recorded signals may be extremely complex, with important information contained in the time transients recorded. Apart, a high dimensionality situation is normally originated, as any voltammogram is formed by a vector with a large number of measures. Even, taking into account that several voltammetric sensors will be used in a given application, a multiway dimension problem originates, in which a 3-D data matrix (current x electrode x potential) is generated. Solutions to cope with this problem pertain to the chemometric part, to be commented in the next section.

Our laboratory also contributed in these aspects of ET research, first by chemometric analysis of linear sweep signals originated at a carbon electrode, where ANNs were the preferred tool for signal treatment [21]. Figure 3 sketches the signal processing approach, applied per example to resolve mixtures of phenols with environmental relevance: *o*-cresol, *p*-chlorophenol and 4-chloro-3-methylphenol. Quickly we realized that interesting applications could be derived from existing voltammetric biosensors, in order to improve the analytical features of determination. With this idea, a tyrosinase biosensor was prepared immobilizing enzyme in an equivalent epoxy–graphite biocomposite, and the multicomponent determination of phenol, catechol and *m*-cresol was achieved at the μM level [13] with better detection limits, linearity and recoveries vs. the ET.

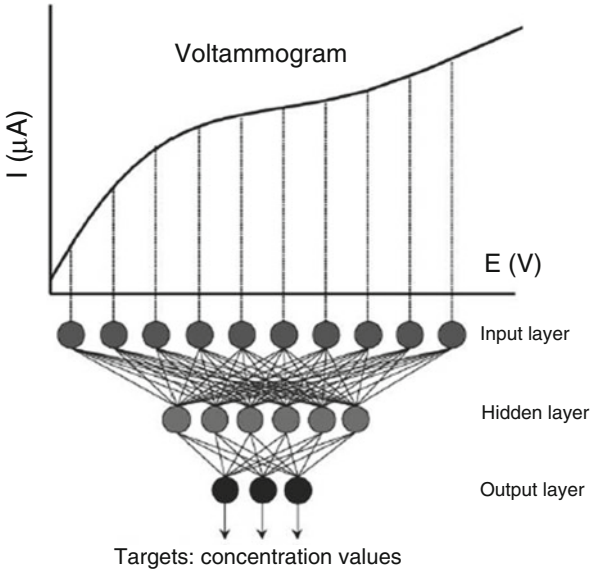

Fig. 3 Simple scheme of the voltammetric electronic tongue, processing a whole voltammogram and performing a multicomponent determination of three compounds sought. From [13], with permission from Elsevier

1.1.3 Other Sensors

Other electrochemical biosensors may be utilized for the design of BioETs; mainly one can think of using conductimetric and/or impedimetric enzyme-based biosensors that might be utilizable as the others above. However, there remain the fields of optical sensing and gravimetric sensing (employing quartz crystal microbalance, bulk or surface acoustic wave devices), two fields rarely used up to now in conjunction with biosensors. [10]

1.2 Chemometric Tools

As Pravdova already stated in his review paper [22], nowadays it is rather straightforward the possibility of working with multivariate data in electroanalysis. Modern potentiostats generate easily voltammograms with different electroanalytical variants; electrochemical detection coupled to high-performance liquid chromatography (HPLC) or capillary electrophoresis (CE) provides without much effort 1-D and 2-D data. And the bioinspired way to do this is by the use of an array of non-specific sensors, responding to primary ions and interferents, coupled with the multivariate chemometric treatment of the complex data to extract the different components present, the ET approach. In these conditions, there is a need for data treatment methods, especially of multivariate data analysis. Chemometric methods used are essentially identical to the methods already used for artificial olfaction or electronic nose systems [23]. The purpose of the processing tool differs depending

on the application, as this can be from identifying a chemical species or determining its concentration without having to eliminate interferences to quantifying them at all. Key points are that the multidimensional generated data have to comprise the needed information about the system and that the high-order data have no colinearity (thanks to the cross-sensitivity assumption). In cross-response conditions, practically all the sensors used in the array may respond to all analytes; the amount of generated data can be large and highly complex, which must be processed using a multivariate calibration approach. Especially, if each individual sensor generates high dimensional data (e.g. a vector in the case of a voltammetric sensor), final data to process can be multiway; that is, a 3-D matrix (or tensor) of (current *x* sensor *x* potential) that must have in correspondence the identification of a variety, or the estimation of the concentration of chemical species. Chemometrics is in charge then for the extraction of significant features and for the transformation of these into the sought information. Curiously, this is in coincidence with nowadays trend of finding hidden trends in current data, forming consumer habits to forecast new trends, what has already been named big data analysis. In fact the tools for finding these hidden trends, or to identify specific situations, are also in common with those used in ETs; in a way, BioETs perhaps may be explained like a big data treatment of biosensor measurements.

Researchers in the field have presented, in specific reviews, the state of the art of chemometric methods amenable to be used with ET systems (or BioETs). [24]. Obviously , chemometrics still form a significant part of ET research [25], particularly when the issues involved are artificial intelligence, among others the work with ANNs, or the multiway data treatment in the cases of highest dimensionality [26, 27]. As already commented, 3-D data can be easily generated (e.g. in multichannel voltammetry, current *x* sensor *x* potential); even systems with 4-D data can be already envisaged (transient response in flow systems or in HPLC, current *x* sensor *x* time *x* potential), which poses greater requirements to the data processing in ET and BioET applications.

Figure 4 summarizes the most frequently used chemometric tools in the development of BioETs in comparison with those mostly used for generic ET systems. This comparison is made by scrutinizing the data treatment details of the different articles found in a literature search by SCOPUS. Curiously, the tools most frequently used in BioETs are somewhat more sophisticated (e.g. ANNs) than those in ETs, where a simple principal component analysis (PCA) or linear discriminant analysis (LDA) might be sufficient. This also suggests that applications related with BioETs can be more elaborated in average and may be conducted by more experienced laboratories than those of ETs, normally simpler in design, in the sensing elements and also in the data treatment.

About the different data processing tools used with electronic tongue systems, albeit being one of their chief parts, a detailed description is out the scope of this paper, but they will be just mentioned here; a proper exposition can be consulted in specific reviews [23, 24]. Basically, for readers not familiar with chemometrics, it can be stated that certain processing algorithms are more indicated to identification/classification purposes, such as principal component analysis (PCA), and are

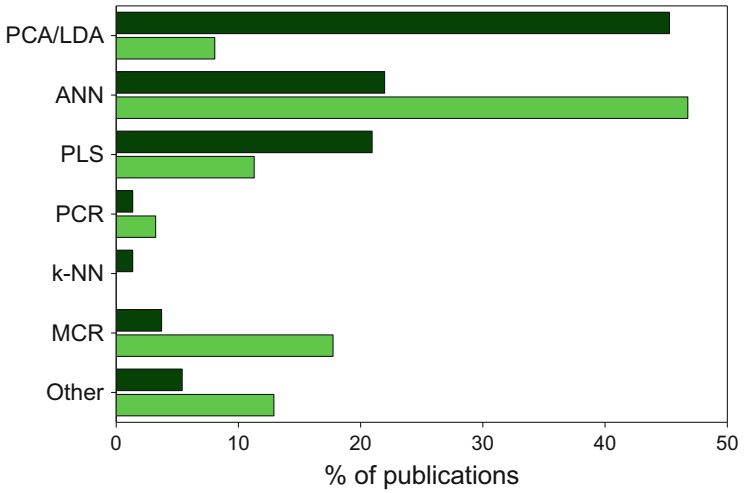

Fig. 4 Different chemometric tools used in the development of BioETs (*clear bars*) in comparison with those mostly used for generic ET systems (*dark bars*). *PCA* principal component analysis, *LDA* linear discriminant analysis, *ANN* artificial neural network, *PLS* partial least squares, *PCR*: principal component regression, *k-NN* k-nearest neighbours, *MCR* multiple component regression. Data obtained from the literature search on the period 1996–2015 using SCOPUS database (Elsevier)

therefore used for qualitative applications. Other procedures, for example, regression using partial least squares (PLS), are specially devised for quantification purposes and mainly used for multidetermination applications.

Most of the mentioned chemometric variants are conventional pattern recognition techniques, mainly linear in nature, which can be somehow limited if the sensors considered show nonlinear response trends. In our experience, we are specially in favour on the use of ANNs, which is a massively parallel computing technique, especially suited to nonlinear sensor responses and very much related to human pattern recognition. ANNs can be devised for quantitative modelling and also as classifiers in pattern recognition applications. An interesting chemometric tool of recent use in electronic nose/electronic tongue applications is support vector machines, a radically different type of "machine learning algorithm" with high identification/classification capability.

An additional stage in the data treatment can be the data pretreatment, which is a necessary step in the high dimensional case. Voltammograms, for example, can be compressed to facilitate their treatment by Fourier transforms, or Wavelet transform, even by simple PCA, in order to extract significant information prior to modelling, in a procedure similar to MP3 compression of digital audio. Data reduction is accomplished through domain transform, in a way that only significant information is kept and original content can be reduced to ca. 10% or less of data space, in a step that also can be useful to reduce the data dimensionality. If the latter is to be faithfully preserved, recent multiway methods may be also applied in the ET

data treatment, such as PARAFAC in the qualitative applications or nPLS in quantitative modelling. Particularly useful for researchers in the field are some comparative studies in which different methods may be contrasted to see which one may show better performance [28].

One of the problems that may occur in the development of the classification rule or the response model is called overfitting. All these chemometric algorithms need a first learning stage normally named training, in which a number of known calibration samples are used to deduct the rule or the model. Overfitting occurs when the model developed is forced to reproduce the training set to its minimum details, but when new data is presented to the model, large errors are obtained. The overfitting concept means that the model/the rule has been forced to a limit where it has memorized the training examples, but the generalization to new situations is incorrect. In practice, the recommended method to avoid overfitting is to use additional subsets of data, so any bias or corrupt learning can be detected and avoided. This subdivision of data is sketched in Fig. 5: the first subset is used for calibrating or training the model, the second (validation set) is used to check if overfitting is taking place (detected as an increase in the validation error) and the third (the external test set, or the prediction set) is used only to compare performance between different models. This is known as cross-validation and it is the recommended way to compare the performances of different predictive modelling procedures. Cross validation involves subdivision of the data into complementary subsets, obtaining the model from one subset (called the training set) and validating the prediction ability on the other subsets (which can be the validation set or the external test set). In this way, an unbiased verification of the generalization capability is obtained. To assure independence of results from subdivision of the data, multiple rounds of cross validation can be performed using different partitions and validation results are averaged over the rounds. Latest recommendation in the field suggests also that a fourth data subset for optimizing the model configuration should be used, so the final selection of the model is completely independent of training, validating, or even fine-tuning of their characteristics. All these precautions produce high experimental requirements in generating/acquiring big amounts

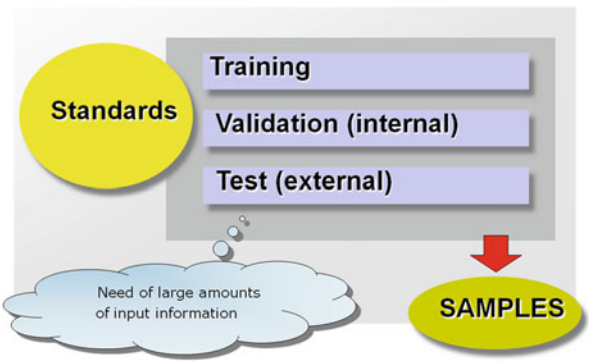

Fig. 5 Subdivision of the sample set in the different subsets recommended to prepare the training process of an ANN model

of data, the only way to assure completely unbiased results, a must especially for biomedical applications.

These precautions can be highly demanding especially when working with ANNs, as a second recommendation to avoid overfitting is to use a large number of samples to develop the model, at least 5 times the number of connecting weights, according to experts in the field [29]. This is in analogy to curve fitting of a polynomial of grade n, in which results are statistically significant only if there are more than $(n+1)$ points available. All this poses a high demand in the gathering of samples, as quickly the number of desirable samples may rise to one hundred or more, a limiting situation for many applications and a precaution rarely followed by researchers nor reproached by reviewers. Generating the complete set is done by experimental design schemes, viz., a factorial design or others, or by complete random generation of values for the calibration samples. When working with ETs of sample varieties (juices, wines, an intermediate industrial product, etc.), it will be needed to bring some reference value (the target or a parallel analytical determination) in order to build the training set, or a set of examples generated by accumulated microadditions of certain standards in a predefined background.

1.3 Type of Applications

The use of sensors in array mode is becoming every day more usual, as it leads to certain advantages. First, using sensor in arrays provides multicomponent data at almost nil effort. Other laboratory stages can be shared together, and finally the only need is to bring the prepared sample to the different sensors and to get a multiplex analyte determination. This is easy task when the sensors used are selective and no interaction is present. If the latter is manifest, a multicomponent data processing can be applied which will make possible the interpretation of complex compositions, the resolution of mixtures, the deconvolution of the contributions from primary species and their interferents, to counterbalance any matrix effect or, even, to distinguish between spurious responses and the true ones. It may be easy, or it may be extremely complex, but with enough and rich biosensor information, and the proper chemometric treatment, all these demands can be fulfilled. An additional reason for the popularization of sensor arrays may be due to the availability of multichannel electrochemical instrumentation, probably installed in a laboratory PC, making the storage, visualization and processing of complex data easier each day. Even we may envisage a personal use of such systems, relying on the ubiquitous cell phone, with adequate transduction capabilities and enough computing power to make possible a handheld analysis for identification or diagnostic purposes.

Concerning the type of applications that can be performed with (bio)sensor arrays, there are different types, and these may be closely related to the experimental procedure on how are the biosensors arranged. If the array is formed by equal sensors, the type of functionality we may obtain is to gain confidence by redundancy, or to map a certain species in concentration taking profit of the spatial resolution provided.

These two applications are specific when equal sensing elements are used, positioned in a single point or distributed in space. Mapping can be at micrometric or geographical region scale, depending on how the sensors are deployed.

As for other enzyme electrodes, let's consider the glucose biosensor as one of the frequent case examples. In it, the lack of specificity for glucose limits its practical applications. This is normally caused by the fact that voltammetric signal is observed at quite high potential; then other oxidizable species present in the sample may be interfering in the final voltammetric signal. The use of the glucose biosensor in conjunction with additional sensor elements may constitute a way to counterbalance these matrix effects. Then, the first potential use of biosensor arrays is the coupling of one biosensor with additional sensors, (i.e. all the sensors in the array do not need to be necessarily biosensors); the goal, counteracting interfering effects from other components present (which need to be also measurable) or from a matrix effect. In fact, prior to the BioET concept, this strategy was simply the use of differential measurements to counterbalance any effect not unique to the employed biosensor.

Coupling biosensor responses with chemometric tools can be used to solve complex analytical signals from mixtures of species with similar properties; in the case of biosensors, particularly this makes possible the determination of group specificity substrates – resolution of mixtures of compounds, for which the biosensor presents a slightly differentiated response, or, alternatively, the estimation of global indexes. Examples of this situation are the possible differentiation of different alcohols of short carbon chain from alcohol dehydrogenases or oxidases; the second is the oxidation of different phenolic compounds catalysed by tyrosinase (or laccase) enzyme biosensors. This type of application may be developed by multicomponent analysis of a single biosensor signal, if this is of high dimensionality; this may be the case of chemometric treatment of a voltammogram obtained from a single biosensor. Although this may not be exactly a BioET, as only one sensing device is used, all the remaining parts of the application are in common.

Some typical applications in the ET or BioET field consist of the identification or qualitative differentiation of types of samples that can rely on the cross response exhibited by using different (bio)sensors in parallel, or even in their specific measurement. Identification of food varieties, especially beverages, is a typical application in this subsection: wines, beer, juices, honey, milk, etc., can be the target of the determination. Also the qualification/classification of polluted waters and wastewaters is another recurring case.

These systems can be extrapolated to an interesting possibility, which can be termed the *software sensor*. In this situation, there is a need of information from certain species or condition whose sensor is unavailable; in the absence of any other possibility, one can combine the information from a number of (bio)sensors and try to correlate the generated information with the target needed to be detected. This indirect methodology that may succeed or not can be suited for complex analytical determinations (e.g. organic matter) or for those of general nature, such as toxicity, caducity, degree of maturity, etc., and obviously is forced by the need of a quick, automated generation of chemical information to diagnose or forecast important situations (e.g. an algal bloom).

Table 1 Application of different enzymes of analytical use in BioET systems

Enzyme	One single biosensor	One-enzyme biosensor in the array	Several enzyme biosensors in the array	Inhibition BioET
PPO	X		X	
Laccase	X		X	
Tyr	X		X	
GOx	X	X	X	
Creatinine iminohydrolase		X	X	
Urease		X	X	
Amine oxidases			X	X
Mutarotase			X	
Invertase			X	
β-Galactosidase			X	
Peroxidase			X	
AChE			X	X
BChE			X	X
CDE			X	
ADH			X	
AOx			X	
Phosphotriesterase				X
Sarcosine oxidase				X
PPE				X

Finally, if the biosensor considered experiences inhibition by a substance or group of substances, and a cross-response condition can be achieved, the multicomponent resolution of the set of considered compounds might be devised. For this objective, one may rely on the use of slightly different inhibited enzymes depending on the natural variability of different animal or vegetal species. Or, alternatively, one may use genetically engineered enzymes, in which specific changes on activity or inhibition have been procured.

On Table 1, I have summarized the type of usage of the biosensor in a BioET, cross-linking this information with exact enzyme used in the bioanalytical approach. Apart of serving as a quick glance on the variety of biosensors considered, it also will permit visualizing how the most habitual enzyme biosensors in diagnostics and analysis, (such as glucose oxidase, GOx, or urease), are also the ones showing more variants in their use in arrays and in BioET systems.

2 Systems Using a Single Biosensor

Although the use of a single biosensor would not form a true bioelectronic tongue, it can be the case (when the biosensor used is voltammetric type) that the high dimension (vector) of the measured signal may make possible the use of

multicomponent data treatment; this can be considered completely a precursor of the considered BioETs. Initially, we would be considering a multivariate determination of a number of substrates of a wide-specificity enzyme system, whereas the departure information would be the voltammogram. Typical chemometric procedures to develop the multivariate response model would be PCR, PLS and even ANNs.

In a first research, again originated in our laboratory, we planned the resolution of phenolic compounds from the information-rich voltammogram originating in an amperometric biosensor using polyphenol oxidase (tyrosinase) enzyme, as it has a characteristic that shows differentiated response for different diphenols [13]. The idea came after performing equivalent research but using a non-enzymatic voltammetric sensor, and the resolving of the three compounds mixture was attempted using ANNs.

The use of ANNs in phenolic compound quantification had been reported [30], but this is still a hard problem to be solved. This kind of determination commonly uses enzymatic reactions combined with amperometric detection of the resulting product. For phenolic compound determination, polyphenol oxidase (also known as tyrosinase) is used as the enzymatic recognition element [31]. This enzyme catalyses the oxidation of phenolic compounds into the corresponding *o*-quinones. This is accomplished in a two-reaction scheme, as long as tyrosinase first oxidizes phenols into the corresponding catechols, and afterwards, these catechols are reoxidized into *o*-quinones. Amperometric reduction of the generated quinones is then used as the quantification method, by simply applying reduction potentials. Reduction potentials for this process are close to 0V, a great advantage, as few substances interfere at this potential. Nevertheless, and because of the similarity in the produced quinones, amperometric signal overlapping in the reduction voltammograms is high. This fact transforms the quantification problem into a chemometric case study that ANNs can solve. Our performed work consisted in the quantification of mixtures of three phenolic compounds, viz., phenol, catechol and m-cresol, and the use of ANN in order to deconvolve the contribution of each analyte in the voltammogram. The resulting calibration permits the development of a BioET capable of quantifying these three pollutants in waters of environmental concern. The performance achieved with the BioET system can be observed in Fig. 6, where the predicted

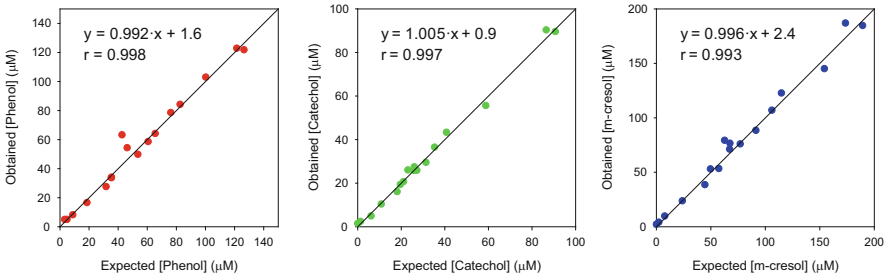

Fig. 6 Modelling ability of the ANN model to predict the three phenolic compounds from the voltammogram recorded using a single tyrosinase biosensor. From [13], with permission from Elsevier

values were compared against the expected ones, for the external test subset, those samples not intervening at all in the training of the ANN model.

The same idea has been subsequently reproduced in determining polyphenolic compounds in olive oil mill wastewater, as the generic index [32], or in the resolution of majoritarian compounds, caffeic acid and catechol [33], in this case from the similar behaviour shown by laccase enzyme, in its response to the group of compounds.

A related electrochemical biosensor based on the immobilization of laccase on magnetic core-shell (Fe_3O_4-SiO_2) nanoparticles was combined with ANNs for the determination of catechol concentration in compost bioremediation of municipal solid waste. Catechol concentration could be determined between 0.75 μM and 0.44 mM [34].

In another biosensor construction variant, an enzyme electrode based on tyrosinase immobilized with ordered mesoporous carbon-Au (OMC-Au), L-lysine membrane and Au nanoparticles (tyrosinase/OMC-Au/L-lysine/Au) was combined with ANNs for the simultaneous determination of catechol and hydroquinone in compost bioremediation of municipal solid waste [35]. Limits of detection achieved were below 1 μM, demonstrating this is an appropriate tool for the quantitative study of a composting system.

As a variant to these ideas, a different work related to the use of a glucose biosensor and the chemometric treatment of the whole voltammogram to correct the effect of interfering species was developed by Torrecilla and coworkers. They reported an amperometric glucose biosensor based on a colloidal gold – cysteamine – gold disc electrode with the enzyme GOx and a redox mediator, tetrathiafulvalene (TTF), co-immobilized atop the modified electrode that was used for the simultaneous determination of glucose and its common interferences, ascorbic acid and uric acid, in three-component mixtures [36]. The redox mediator TTF was used to improve selectivity by decreasing the potential of detection. Analytical data obtained from cyclic voltammograms generated with the biosensor were processed using ANNs, and the separate quantification of the analytes over a range of 0.1–1 mM each was performed without any sample pretreatment. Achieved predicted errors for the three analytes were below 2%. The referred example illustrates how the BioET approach allows for a more accurate determination of the sought component, and that with the same effort, it allows also for the determination of the interfering species.

To summarize these ideas, the different examples mentioned have been incorporated in Table 2, where the different enzymes used and analytes determined can be quickly visualized.

Table 2 Extract of significant applications recorded for systems that employed a single voltammetric biosensor, in the resolution of mixtures of different compounds. Applications recorded a long time

Author	Enzymes used	Type of biosensors	Analytes determined/concentration level			Type of sample	References
Trojanowicz et al.	Tyrosinase	Voltammetric	Phenol/100 μM	Catechol/50 μM	*m*-cresol/50 μM	Waters	[30]
Gutés et al.	Tyrosinase	Voltammetric	Phenol/25 μM	Catechol/25 μM	*m*-cresol/25 μM	Waters	[13]
Torrecilla et al.	Laccase	Voltammetric	Total phenol index/	2.5 μM	–	Wastewater	[32]
Torrecilla et al.	Laccase	Voltammetric	Caffeic acid/2.5 μM	Catechol/2.5 μM	–	Wastewater	[33]
Tang et al.	Laccase	Voltammetric	Catechol/1 μM	–	–	Compost	[34]
Zhou et al.	Tyrosinase	Voltammetric	Hydroquinone 25 μM	Catechol/25 μM	–	Compost	[35]
Torrecilla et al.	Glucose oxidase	Voltammetric	Glucose/0.5 mM	Ascorbic acid/ 0.5 mM	Uric acid/ 0.5 mM	Laboratory standards	[36]

3 Biosensor Arrays Incorporating One Enzyme

In the next step of complexity, and also in the proper conceptual idea of BioETs, I will include the design of analysis systems with biosensor arrays incorporating one-enzyme biosensor and, as the rest of sensors in the array, conventional type potentiometric or voltammetric sensors. With this conceptual design, the application normally performed is the determination of a specific substrate or group of substrates in presence of interferents.

For the case of potentiometry, one has to remind that biosensors rely on an enzyme converting substrate into a measurable ion, next detected by the appropriate ISE. The disappearing of a particular ion involved in a catalytic enzyme process might be useful also as the measure principle, only there is not any case to consider here.

For the case of voltammetry, the normal case is a substrate directly consumed in the enzyme reaction or, alternatively, a product, any of the two electroactives; then its appearance (or disappearance, depending on the case) can be related to the enzyme activity.

3.1 Potentiometric Systems

The typical potentiometric BioET utilizes a sensor array with one-enzyme biosensor, and additionally it incorporates ion ISEs to counterbalance interference presented by related ions.

The first system, devised in the University of Porto, Portugal, was a sensor array for the measurement of creatinine in urine [18]. It consisted of a creatinine iminohydrolase enzyme immobilized by entrapment using a chitosan membrane onto a nonactin ISE. Catalytic hydrolysis by the enzyme generated ammonium ion which was then directly detected. The system was completed with ISEs for ammonium, potassium, sodium and calcium which allowed to correct for any endogenous ammonium (by the first ISE) or for alkaline and alkaline-earth interference in the ammonium-based biosensor (the other three). Linear response ranges were between 0.1 and 10 mM, what permitted the resolution of the multicomponent determination by PLS method. Comparison with reference Jaffé method showed a satisfactory correlation, although the slope of obtained vs. reference values was rather low; the obtained value was 0.87, whereas theoretical value should be 1.0.

In a second system reported by the same laboratory, a sensor array incorporating a urea biosensor was proposed for the determination of urea in blood serum [19]. Similarly to the previous case, the urease enzyme was immobilized employing BSA and glutaraldehyde onto an ammonium ISE, taking profit of the appearance of ammonium product after the enzyme hydrolysis of urea. As before, the array was complemented by ISEs for K^+, Na^+ and NH_4^+ with the idea of counterbalancing any interference by alkaline ions. Authors achieved correct prediction of urea and potassium, not sodium or ammonium initially present. Correlation and prediction

errors were satisfactory in front of results from the clinical analysis laboratory when calculations were performed by PLS.

This idea was retaken later in our laboratory in a four species multidetermination approach [14]. First, we studied in detail different methods and performance for urea biosensors, selecting a covalent immobilization of urease enzyme onto carboxylated PVC, which also acted as polymer matrix to form the ISE membrane. The array was completed with ISEs selective to NH_4^+, K^+ and Na^+ plus H^+ and one ISE of generic response to alkaline ions. The determination of the four species was attempted by PLS and by ANN, which provided slightly better results, especially at the lower concentrations. The method was applied and validated in multiple analyses in urine, at concentrations down to 0.1 mM and without the necessity of eliminating the alkaline interferences or compensating endogenous ammonium. Figure 7 schematizes the approach followed for the four-analyte multidetermination performed with the potentiometric BioET in urine.

This topic is of evident interest, given these are frequent analyses specially in clinical laboratory and in patients related with renal malfunction. Other authors have been doing similar contributions, having in mind an easy and efficient analytical approach during haemodialysis [37].

3.2 Voltammetric Systems

The BioET formed by voltammetric biosensors starts with the idea of using an array of electrode biosensors formed by different catalysts and different modifiers with the same enzyme. The different catalysts/modifiers introduce the differentiated response of each electrode; in this case, all of them will present signal for the primary substrate, only with different shapes or appearing at different potentials, depending on the catalysis or modification of the electroanalytical signal. With this idea, our laboratory contributed with a first work in which different biosensors incorporating glucose oxidase (GOx) were prepared with different metallic catalysts, as platinum microparticles or mixture of gold/platinum microparticles, as the way to induce a differentiated response [38]. In Fig. 8, an image of the biosensing device integrating the three epoxy–graphite containing GOx biosensors can be appreciated. The device was tested in the joint determination of glucose and its frequent interferents in biological fluids, ascorbic acid and uric acid, with usage integrated in an automated SIA system for proper automation of operation. Figure 9 displays the achieved performance with the external test set, where the predicted values are compared against the expected ones, and satisfactory behaviour, with a fitted comparison line with 1.0 slope and 0.0 intercept, demonstrates successful performance.

The way to obtain the cross response is through the different catalysts that modify the voltammograms by different mechanisms producing slightly varying signals. Of course, for the proper functioning of the approach, the underlying condition is that signals used must not be co-linear, that is, must not be proportional one from the other. If this were the case, the system would be ill-behaved, in the

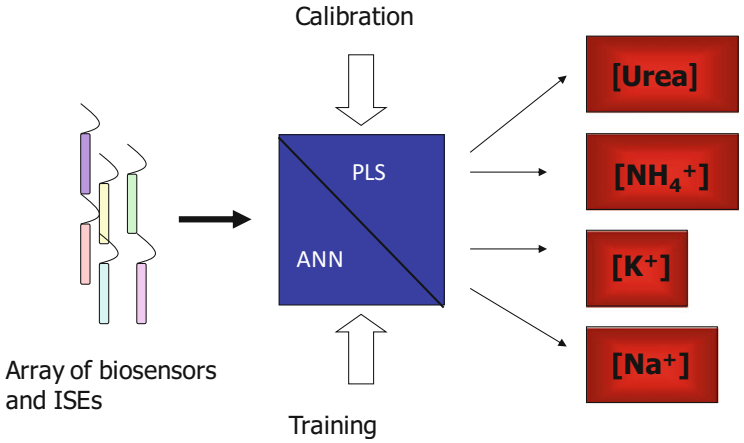

Fig. 7 Conceptual scheme of the BioET to determine urea in presence of endogenous ammonia and alkaline ions, as interferents in the multidetermination application in clinical samples

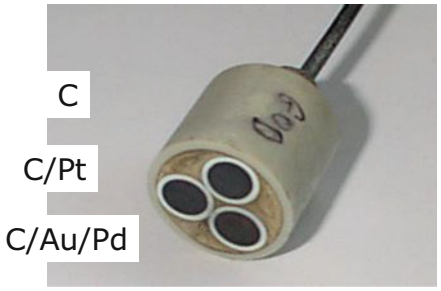

Fig. 8 Image of the three-sensor array with GOX and different modifiers/catalysts as a simple mean to induce differentiated response

manner as in the resolution of a linear system of equations; in there, as we know from university algebra, if one equation is linearly dependent from the others, then the system cannot be solved. Equivalently, if the signals produced by the sensor array are linearly dependent, because one sensor is then producing duplicated, non-original information, therefore the possibility of resolving the system is jeopardized. As a recommendation for the reader interested in diagnosing when such a situation is present, the recommended way is to check the trilinearity of the data; for this, first, it is recommended to unfold the three-space data matrix into conventional *row* × *column* matrix and to check the singular value decomposition after normalization [39]. This has to provide equivalent number of significant factors to describe the data, independently of the direction chosen to unfold the data (row, column or third direction).

This idea with GOX was retaken recently by Al-Issa et al. [40]; in their work, they prepared a BioET immobilizing the enzyme over Au or Pt disc electrodes. The

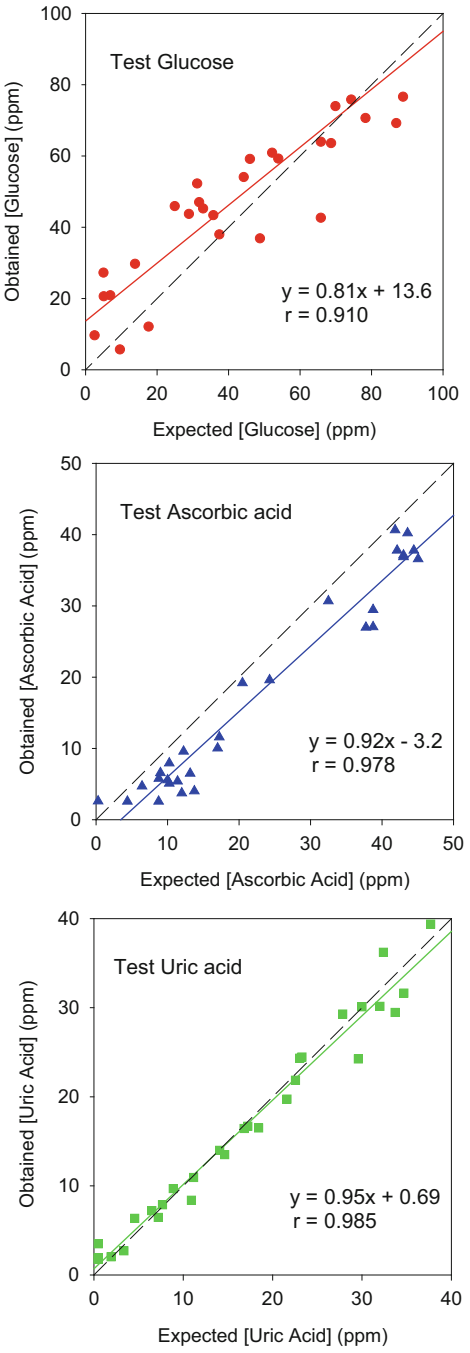

Fig. 9 Correlations between obtained and expected concentrations for glucose analyte (*top*) and ascorbic acid (*middle*) and uric acid (*bottom*) interfering species, obtained in the ANN modelling. *Dashed lines* correspond to the theoretical $y = x$ line

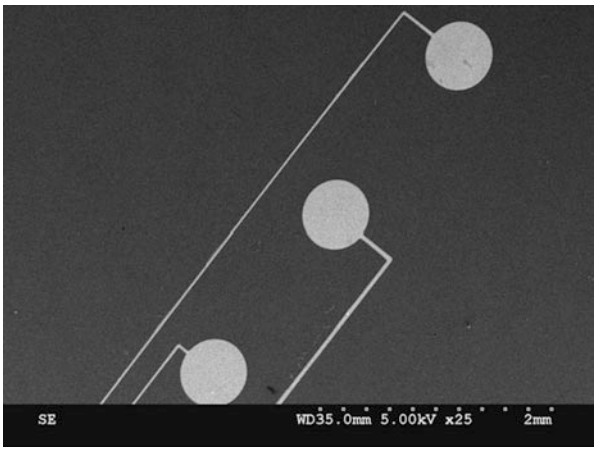

Fig. 10 Redundant glucose biosensor array devised for the interstitial determination of this sugar. Reprinted from [42], with permission from Wiley

determination of glucose in the presence of their common interferents, ascorbic acid and uric acid, could be successfully determined at the 1 mM level, while interfering species were quantified at no extra effort.

In 2012, in a work from the laboratory of Mari Luz Rodriguez-Mendez in Valladolid, they conceived an array of biosensors for measuring phenolic compounds, in which the differentiated response was derived from an array of tyrosinase electrodes, furnished each one with a different metallic phthalocyanine catalyst. This system was applied for the evaluation of changes that occur during the aging of beers. The features extracted from the cyclic voltammograms were used to perform principal component analysis (PCA) and linear discriminant analysis (LDA). Data have revealed a clear discrimination among the beer classes in the aging process [41].

Searching the scientific literature, one can find also the use of biosensor arrays formed by the same enzyme electrode, in this case intended for redundant analysis of certain compound. Redundant microsensor arrays for glucose sensing were fabricated using photopolymerization of poly(ethylene glycol) diacrylate (PEG-DA) with 2-hydroxy-2-methyl phenyl-propanone as photoinitiator to encapsulate the enzyme glucose oxidase. Silicon microfabrication technologies were used to fabricate microelectrode sensor arrays on flexible polyimide sheets. These microarray sensors were individually addressable as observed using square-wave voltammetry. Redox polymer, poly[4-vinylpyridine Os(bipyridine)2Cl]-co-ethylamine, was first immobilized on the electrode surface and then GOx was entrapped in PEG-DA hydrogels. The redox polymer was found to exchange electrons with glucose oxidase in biocompatible PEG-DA hydrogels. The entrapped GOx was found to respond linearly to glucose in solution (0–20 mM) as determined using square-wave voltammetry. The array of devices, as it can be observed on the image of Fig. 10, was then used for concentration mapping of glucose, in this case to study its distribution in tissues, with special interest in resolving interstitial concentrations from the intravascular values [42].

Table 3 Extract of significant examples recorded for BioETs that employs a single enzyme in the resolution of mixtures of different compounds. Applications recorded a long time

Author	Enzymes used	Type of biosensors	Analytes determined/concentration level			Type of sample	References
Magalhães and Machado	Creatinine iminohydrolase	Potentiometric	Creatinine/ 1 mM	–	–	Urine	[18]
Correia et al.	Urease	Potentiometric	Urea/1 mM	Potassium/ 3 mM	–	Blood serum	[19]
Gutés et al.	Glucose oxidase	Voltammetric	Glucose/ 0.5 mM	Ascorbic acid/ 20 mM	–	Laboratory standards	[38]
Gutiérrez et al.	Urease	Potentiometric	Urea/1 mM	Ammonium/ 0.1 mM	Potassium/0.1 mM Sodium/ 1 mM	Urine	[14]
Correia et al.	Urease	Potentiometric	Urea/1 mM	Potassium/ 0.25 mM	–	Blood serum	[37]
Al-Issa et al.	Glucose oxidase	Voltammetric	Glucose/ 0.5 mM	Ascorbic acid/ 0.1 mM	Uric acid/0.1 mM Acetamino-phen/0.1 mM	Laboratory standards	[40]

A table has been prepared summarizing these ideas, where the different BioET examples using biosensors devised with only one enzyme plus other sensors or modifiers of response are indicated (Table 3). Application details, with analytes determined, its concentration level and the type of sample have been added.

4 Biosensor Arrays Employing Several Enzymes

Next in the conceptual progress in the work with BioETs, it is the turn of the design of sensor arrays incorporating different enzymes; these will be normally devised to determine one single substrate or closely related substances, whose sum will be defining one general index or one group of substances somehow related to a certain chemical compound or certain sample generic feature.

4.1 Determining One Substrate

When revising the scientific literature in search of biosensors used in an array mode, a very interesting anticipative work was that of Lange and Wittmann, in which with the use of a three-enzyme voltammetric array, they attempted the resolution of different biogenic amines, an important issue in food analysis; this analysis is interesting by the quantification of individual amines by themselves, or in their sum as a direct indicator of spoilage of food products. In the work of Lange (2002) [43], an enzyme sensor array for the simultaneous determination of the three biogenic amines (histamine, tyramine and putrescine) is described by pattern recognition using an ANN response model and its application to different food samples. The work used an array of a monoamine oxidase, MAO (EC 1.4.3.6); a tyramine oxidase, TAO (EC 1.4.3.4); and a diamine oxidase, DAO from pea seedlings (EC 1.4.3.6) (with specific activities sufficient for rapid detection), immobilized each on a separate screen-printed thick-film electrode via cross-linking with transglutaminase and glutaraldehyde. Figure 11 shows the cross-sensitivity found to selected biogenic amines by the different amine-degrading enzyme biosensors, where a satisfactory departure point seems to exist: TAO biosensors show higher sensitivity to tyramine, MAO biosensors to histamine and DAO to putrescine, which makes feasible the three species multidetermination approach. The lower detection limits achieved were 10 mg/kg for histamine and tyramine and 5 mg/kg for putrescine. The application area of this BioET was tested from fish to meat products, sauerkraut, beer, dairy products, wine and further fermented foods and compared with the data of conventional LC analyses (the mean correlation coefficient of the obtained vs. reference values was $r = 0.854$).

Continuing this topic, three-enzyme-based amperometric biosensors incorporating different amine oxidases were applied for meat spoilage monitoring. With diamine oxidase (EC 1.4.3.6), the total biogenic amine content was measured.

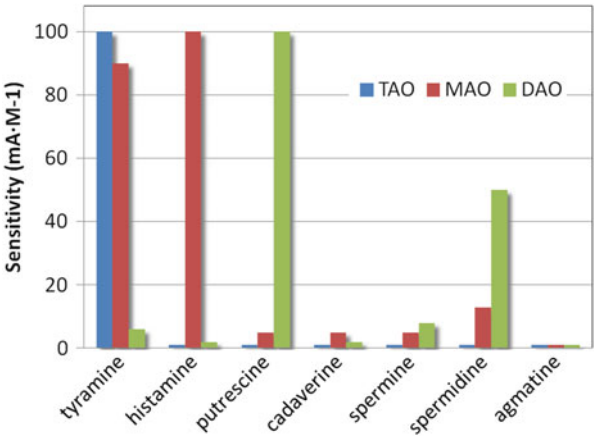

Fig. 11 Cross-sensitivity to selected biogenic amines shown by amine-degrading enzyme biosensors. *TAO* tyramine oxidase, *MAO* monoamine oxidase, *DAO* diamino oxidase. Adapted from data in [43]

Monoamine oxidase A (EC 1.4.3.4) was used for determination of tyramine, tryptamine and phenylethylamine content. Putrescine was selectively detected with putrescine oxidase (EC 1.4.3.10). The enzymes were separately co-immobilized on graphite electrodes with peroxidase and Os mediator (PVI7-dme-Os). A fast extraction method using special centrifugal separator was applied for pork and fish samples stored at different conditions. Although partial extraction was achieved, the results correlated well with total biogenic amine content measured by HPLC method [44]. An equivalent determination has been reported very recently from the bi-amperometric measurement of a double enzyme biosensor using histamine dehydrogenase and putrescine oxidase [45] that performs the specific determination of histamine and putrescine, working simply at two fixed potentials of +130 and +300 mV, respectively, in this case, without the need of any chemometric contribution.

A similar case study has been intended as a simple voltammetric electronic tongue, this time with the use of an array of modified electrodes, in particular carbon electrodes modified with different phthalocyanines as different catalysts to induce differentiated response. The method involved the global detection of biogenic amines, spoilage products resulting from the degradation of fish. The performance of an array of screen-printed electrodes (SPE) was compared with that of an array formed by classic carbon paste electrodes (CPE). The sensors have shown good sensitivity towards model solutions of biogenic amines (ammonia, dimethylamine, trimethylamine, cadaverine and histamine). It was evidenced that the electroactivity and basic character of amines influenced considerably the electrochemical behaviour of each electrode. The pattern of responses provided by the array was successfully used to evaluate fish freshness and to determine the post-mortem period. An increase of the signals associated to biogenic amines and other spoilage products was observed with increasing storage days. Signals provided by classical CPE were better resolved and showed better sensor-to-sensor reproducibility than SPE. However, the SPE modification enabled simple mass production of

low-cost and miniaturized sensing units with good sensitivity and repeatability. The capability of discrimination demonstrated by PCA and the capability of prediction of fish freshness calculated by partial least squares-discriminant analysis (PLS-DA) were similar in both cases [46].

Another interesting example is the estimation of total organic load, a pollution parameter especially important in the environmental field. In this case, highly related to the enzyme type biosensor, respirometric microbial sensors have been proposed to be used in an array mode to estimate biochemical oxygen demand (BOD). BOD as a parameter illustrates the amount of organic compounds susceptible to biochemical degradation in the water. The standard BOD test lasts for at least 5–7 days or even up to 21 days. An incubation time this long is not acceptable for monitoring purposes or system control. In order to shorten the BOD measurement time, a multitude of biosensors have been proposed. Unfortunately, BOD biosensors have several limitations, such as short lifetime, limited substrate range, precision, etc. Some of those limitations can be overcome by using microbial sensor arrays. Such BioETs can achieve the much wider substrate range usually attributed to multiculture sensors and still maintain the long lifetime of a single culture sensor. This is achieved by separating different cultures from each other in the array and using the signals of separate sensors to produce global information via statistical analysis. Although a waiting period of up to days has no practical use, by proper training of the BioET, accurate estimation of the final value can be made in much shorter times [47].

In the particular study, seven respirometric biosensors based on different semi-specific and universal microorganisms were constructed for biochemical oxygen demand (BOD) measurements in various synthetic industrial wastewaters [48]. Microorganisms used were chosen according to different affinities for different substrates like fat, phenol, lactose or cellulose. All biosensors were calibrated using OCDE synthetic wastewater, and the resulting calibration curves were used in the calculations of the sensor-BOD values for all biosensors. In addition, the output signals of all biosensors were analysed as a BioET, and comprehensive multivariate data analysis was applied to extract qualitative and quantitative information from the samples. In the case of individual biosensor measurements, most accurate result was gained when semi-specific biosensor was applied to analyse sample specific to that biosensor. Universal biosensors or biosensors semi-specific to other samples underestimated the BOD7 of the samples up to 10–25%. A PLS regression method was used for the multivariate calibration of the biosensor array. The calculated sensor-BOD values differed from BOD7 less than 5.6% in all types of samples, as shown in Fig. 12, where the correlation of predicted vs. reference values demonstrates the satisfactory comparison. By applying PCA and using three first principal components, adding up to a 99.66% of explained variance, it was possible also to differentiate samples by their compositions.

In a final exemplary study, toxicity as a relevant environmental parameter was also attempted employing sensor arrays. Toxicity is a key parameter of water quality and is normally evaluated as a response of living beings (as their mobility, fertility, death rate, etc.) to water quality; therefore, toxicity can only be assessed

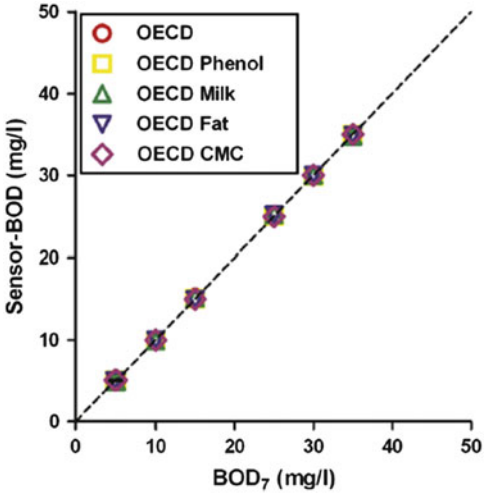

Fig. 12 Obtained results in the comparison of reference BOD7 with BioET-estimated BOD, showing the satisfactory comparison between both methodologies. Reprinted from [48] , with permission from Elsevier

with the help of these living beings. This imposes certain restrictions on toxicity bioassay as an analytical method: biotest organisms must be properly bred, fed and kept under strictly regulated conditions and duration of tests can be quite long (up to several days), thus making the whole procedure the prerogative of the limited number of highly specialized laboratories. The specified report describes an original application of potentiometric multisensor system (ET system) where the set of electrochemical sensors was calibrated against *Daphnia magna* death rate in order to perform toxicity assessment of urban waters without immediate involvement of living creatures, hereby extracting bioassay information from the sensor array and correlating with the bioassay [49]. PRM (partial robust M) and PLS (projections on latent structures) regression models based on the data from this multisensor system allowed for prediction of toxicity of unknown water samples in terms of biotests but in the fast and simple instrumental way. Typical errors of water toxicity predictions were below 20% in terms of *Daphnia* death rate which can be considered as a good result taking into account the complexity of the task. Figure 13 displays final results in the comparison of predicted and reference values of toxicity, in this case when using the PLS model.

When thinking about the different combinations of enzyme biosensors in arrays and the possible determinations associated, there is one case that is not covered, and then, it seems nobody attempted the idea. This is to use different enzyme biosensors related to a certain substrate and to perform its determination, probably improving the analytical performance, taking profit of the redundancy used, or of the different interferences that may interact, or of the different environmental factors affecting the determination. Possible examples are sugar determinations, e.g. combining oxidase and dehidrogenase enzymes, a case also applicable, for example, to alcohols; in the case of phenolic compounds, the coupling of laccase and tyrosinase biosensors has curiously been attempted in different manners, together in the same device, or separately, as it will be described below.

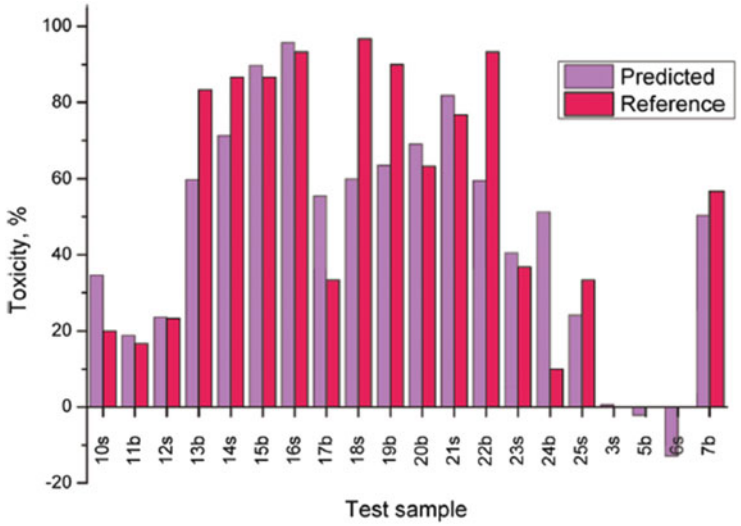

Fig. 13 Obtained results in the comparison of toxicity reference test using Daphnia Magna and data extracted from BioET, when using PLS model, showing a satisfactory comparison between both methodologies. Reprinted from [49], with permission from Elsevier

4.2 Coupling Different Enzymes in the Same Sensing Device

A curious experimental procedure is the proposal made in the 1990s to co-immobilize two different enzymes reacting with the same substrate(s) in order to increase the final signal and the variety of compounds that may show response [50]. In any case, this approach may be useful when the final goal of the analysis is to obtain the general indicator of certain group of compounds, or when a total content or general index is the information sought.

Specifically, this interesting work suggested the combined use of tyrosinase and laccase for the overall detection of phenolic compounds relevant as environmental pollutants. The idea is not so strange, given tyrosinase is mainly responding to generic phenols, which are first converted to *o*-diphenols and then oxidized to the corresponding quinones and laccase which reacts preferently with *o*- and *p*-diphenols; obviously, the coupling of the two is in search of a more equilibrated response towards the different phenolic compounds than with the use of a single enzyme. As an illustration, these concepts are presented in Fig. 14, showing how the cross response may be easily achieved; as it can be seen in there, laccase may show increased response for caffeic acid or catechol, both being *o*-diphenols, or phenol will show large signal increment by coupling the two enzymes. This idea was later retaken by El-Kaoutit et al. to evaluate main polyphenols present in beer and to estimate total polyphenol index in beer samples [51]. Final results obtained are summarized in Fig. 15, where comparison of calculated and reference values shows

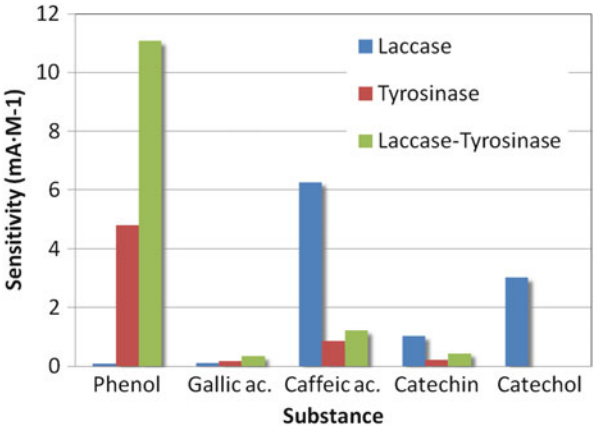

Fig. 14 Cross-sensitivity to selected phenolic compounds shown by phenol-degrading enzymes used in biosensors alone or associated in pair. Adapted from data in [52]

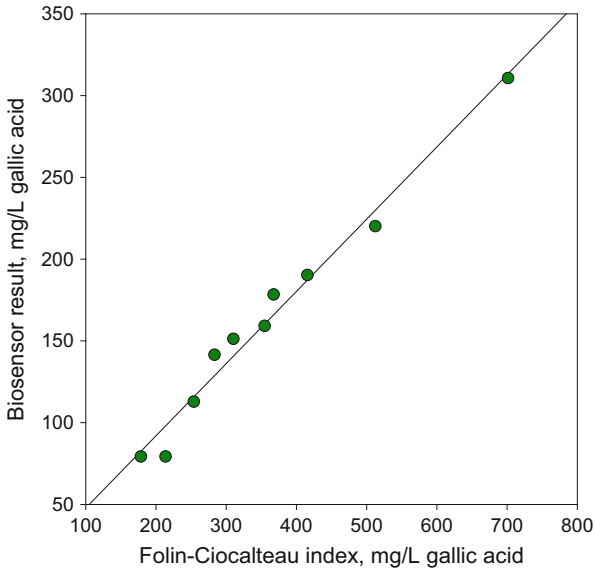

Fig. 15 The use of the sensor array as key concept in the development of an electronic tongue analysis system. Adapted from the data in [51], with permission from American Chemical Society

satisfactory behaviour. In there, the correlation is highly significant (correlation coefficient $r = 0.9894$), although the slope is only a fraction of the theoretical one (slope = 0.44), indicating that even a clear correspondence is present, both methods are measuring different forms of phenolics.

This idea of coupling the two laccase and tyrosinase enzymes has been repeatedly used in the literature by different authors. For example, a tyrosinase/laccase bienzyme biosensor for amperometric determination of phenolic compounds was constructed by immobilizing enzymes in titania gel matrix. The obtained biosensor could be used for determination of 2,6-dimethoxyphenol, 4-tertbutylcatechol,

4-methylcatechol, 3-chlorophenol and catechol, with relative responses between the 12.7% for 4-tertbutylcatechol and 100% (max) for catechol [53].

Polyphenols are a group of naturally occurring compounds that can be found in fruits and vegetables or beverages like tea or wine. Most of these compounds are powerful antioxidants with great health benefits. In this sense, beer and wine contain a wide variety of polyphenolic compounds. Although content values for each of the single polyphenols are rather low, these compounds play an important role in flavour (bitterness, astringency and harshness), colour and stability of these beverages. Given its control is of clear interest, several methods to quantify total phenols and polyphenols have been described in the literature. Among these, biosensors provide an alternative solution to the determination of polyphenols for their low cost and simple use, which make them ideal tools for analyses on field. Applicability of electrochemical biosensors to the analysis of antioxidant compounds, including polyphenols, is promising, and there is a growing interest in the development of such devices. An amperometric biosensor for the detection of polyphenols in wine was developed, immobilizing the two enzymes tyrosinase and laccase on graphite screen-printed electrodes modified with ferrocene. The biosensor gave good results when employed for wine analysis, showing a good agreement with the spectrophotometric data obtained with the Folin–Ciocalteu test, the official method for polyphenol analysis in wine [52].

In a recent work, a bienzymatic sensor for the determination of polyphenols was presented. An ITO electrode was modified with multiwalled carbon nanotubes, and the enzymes laccase and tyrosinase were co-entrapped into a chitosan matrix. The resulting biosensor was calibrated at −50 mV (vs. the Ag/AgCl reference electrode) using rosmarinic acid, caffeic acid and gallic acid as the substrates. The new biosensor resulted in a 10.7-fold increase in response sensitivity and a considerable improvement of the detection limit (42 nM for rosmarinic acid). The sensor was used to evaluate the total phenolic content from plant extracts of *Salvia officinalis* and cultures of *Basilicum callus* [54].

4.3 Determining Several Substrates

In this section we will describe the multiplex determination of a number of substrates departing from a biosensor array formed by different enzyme biosensors incorporating different enzymes. In this definition class, there can be two extreme variants, when each associated enzyme biosensor is employed for its own substrate, just relying on the specificity of each biosensor, and when there is the cross-response condition, and some extra ability to resolve the exact compounds involved is therefore obtained.

There are the first examples, the ones referred to a multiplex multi-specificity case. Per example in a work from the group of Soldatkin, in Ukraine, an array of conductimetric enzyme biosensors for simultaneous determination of carbohydrates maltose, lactose, sucrose and glucose were developed [55]. Several enzyme

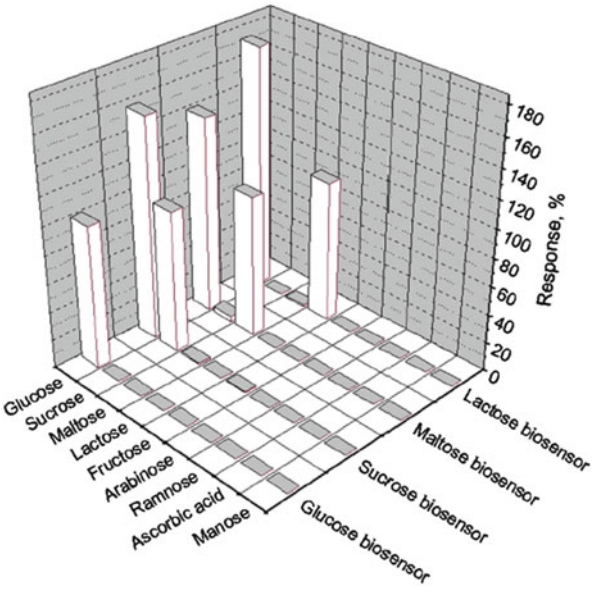

Fig. 16 Selectivity of the biosensors in the array for determination of glucose, sucrose, maltose and lactose – concentration of carbohydrates measured, 0.5 mM. Reprinted from [55], with permission from Elsevier

systems selective to lactose, maltose, sucrose and glucose were immobilized on the surface of four conductimetric transducers and served as bio-recognition elements of the biosensor array. Direct enzyme analysis carried out by the developed biosensors was highly sensitive to the corresponding substrates. GOx, mutarotase and suitable glycosidase (invertase, β-galactosidase and α-glucosidase, respectively) were immobilized by cross-linking with 1:1 BSA and glutaraldehyde in 1:1 ratio, and then each mixture was deposited onto the pair of electrodes considered (differential measurement vs. a membrane not containing the enzyme). The analysis lasted 2 min and determinations span concentration values from 0.001 to 1.0 mM. First, the sensor array stability was studied, and effect by the solution pH, ionic strength and buffer capacity on the biosensors responses was investigated; the conditions of simultaneous operation of all biosensors were optimized. The data on cross response of the different enzymes used to the considered substrates were obtained and was presented in Fig. 16; in there one can observe how carbohydrate oxidizing enzymes are quite specific, only there is certain secondary response of lactose, maltose and sucrose biosensors, in all cases, to glucose present. The developed biosensor array showed good signal reproducibility and storage stability. The biosensor array demonstrated its utility for the simultaneous, quick, simple and selective determination of maltose, lactose, sucrose and glucose.

In an additional closely related work, specific enzyme systems were devised to detect analytes comprising markers of the stage of maturity and quality in selected fruits of economic importance to tropical countries, like mangoes or pineapples [56]. Analytes detected were β-D-glucose, total D-glucose, sucrose and ascorbic acid. Enzyme principles used were: the GOx reaction, mutarotase and GOx for total

D-glucose and the three-enzyme system GOx, mutarotase and invertase for sucrose estimation. A common format was adopted to facilitate design and operation, in this case immobilization method, the fact that all enzymes used were oxidases and that a common detection principle, reoxidation of H_2O_2 generated product, was chosen (except for ascorbic acid which was estimated directly). Pectin, a natural polysaccharide present in plant cells, was used as a novel matrix to enhance enzyme entrapment and stabilization in the sensors. Interferences related to electrochemically active compounds present in fruits under study were significantly reduced by inclusion of a suitable cellulose acetate membrane diffusional barrier or by enzymatic inactivation with ascorbate oxidase. Enzyme sensors demonstrated expected response with respect to their substrates, on analyte average concentration of 5 mM.

In the two examples above, o cross response of biosensors was considered, and then no advanced data treatment was employed. All analytes were estimated from direct measurements performed, whereas the simple analysis of generated data would have provided improved results, if only by correction of any cross response or interference between considered species.

After the first potentiometric BioET in our laboratory, the one using potentiometric sensors to determine urea [14], progress in this line culminated in a bioanalytical system to simultaneously determine urea and creatinine aimed to application cases such as patients with renal failure [20].

Urea and creatinine biosensors based on urease and creatinine iminohydrolase, respectively, covalently immobilized onto ammonium-selective electrodes were included in an array together with sensors sensitive to ammonium, potassium and sodium. Generic sensors to alkaline ions were also included. All the sensors used were of all-solid-state type, employing polymeric membranes and having rather non-specific response characteristics. Carboxylated PVC matrix was employed as material with double functionality, to form the ammonium potentiometric membrane and to provide anchoring points for the covalent immobilization of the enzyme using the carbodiimide reaction. A response model based on ANNs was built and tested for the simultaneous determination of the five species urea, creatinine, ammonium, potassium and sodium. The results show that it is possible to obtain a good multivariate calibration model with the employment of feedforward 5-output ANNs. In this way, the developed bioelectronic tongue was successfully applied to multidetermination of the five species in raw and spiked urine samples. Predicted concentrations showed a good agreement with reference methods of analysis, allowing a simple direct method for determining urea and creatinine in real samples. At the same time, this method permitted to obtain the concentrations of the alkaline interferences (endogenous ammonium, potassium and sodium) without the need of eliminating them.

In an interesting work by Skladal, a four-electrode biosensor based on immobilization of laccase (*Coriolus hirsutus*), peroxidase (horseradish) and tyrosinase (mushroom) in a same screen-printed array was developed for generic monitoring of phenols [57]. The enzymes were immobilized onto a self-assembled monolayer (4-mercapto-1-butanol)-modified gold surface via covalent attachment by epichlorohydrin coupling. The experimental conditions for simultaneous operation of the

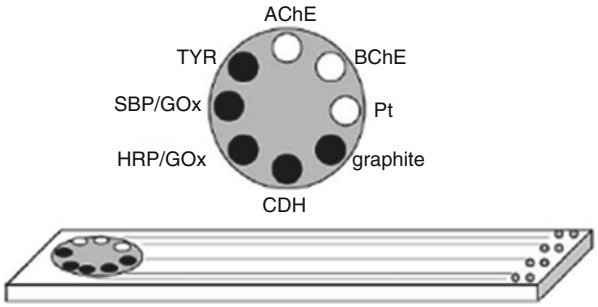

Fig. 17 Screen-printed biosensor array used for estimation of water quality. *TYR* Tyrosinase, *AChE* Acetylcholinesterase, *BChE* Butyrylcholinesterase, *Pt* Platinum, *CDH* cellobiose dehydrogenase, *HRP* Horseradish peroxidase, *GOX* glucose oxidase, *SBP* Soybean peroxidase. Reprinted from [58], with permission from Elsevier

three enzymes were optimized based on catechol determination. The sensors were further applied for the amperometric detection of several substituted phenolic compounds, carried out using a single-line flow-injection system. Hydrogen peroxide served as co-substrate for peroxidase. The limits of detection for phenols in aqueous solutions were in the micromolar range and each assay was completed in less than 5 min. The preliminary studies showed that the compatibility of the above-mentioned enzyme array enabled the multielectrode biosensor to be applied to real samples including industrial wastewaters and surface waters.

In a closely related work, amperometric screen-printed biosensor arrays for the generic detection of pesticides (organophosphates and carbamates) and phenols were developed [58]. Cholinesterases (AChE and BChE), tyrosinase (TYR), peroxidases (from soybean, SBP, and horseradish, HRP) and cellobiose dehydrogenase (CDH) were combined on the same array consisting of one Ag/AgCl reference electrode surrounded by eight radially distributed working electrodes of either carbon or platinum, to form a complete 8-channel voltammetric cell as it is depicted on Fig. 17. Cross-linking with glutaraldehyde was employed for enzyme immobilization. The substrates for the enzymes were acetylthiocholine for cholinesterases (ChEs), cellobiose for CDH and hydrogen peroxide for peroxidases. Hydrogen peroxide was generated in the presence of glucose by co-immobilized glucose oxidase (GOx). All measurements were performed in an electrochemical steady-state system specially constructed for eight-channel screen-printed electrode arrays. The achieved relative standard deviation values calculated for different enzyme substrates (10 measurements) were typically below 7%, and one assay was completed within less than 10 min. The detection limits for pesticides and phenols were in the nanomolar and micromolar ranges, respectively. The developed biosensor array was evaluated on wastewater samples. To simplify interpretation of results, the measured data were treated with multivariate analysis – principal component analysis (PCA), which permitted to identify the origin of a wastewater, e.g. if from a pesticide industry or from a paper and pulp industry (see Fig. 18).

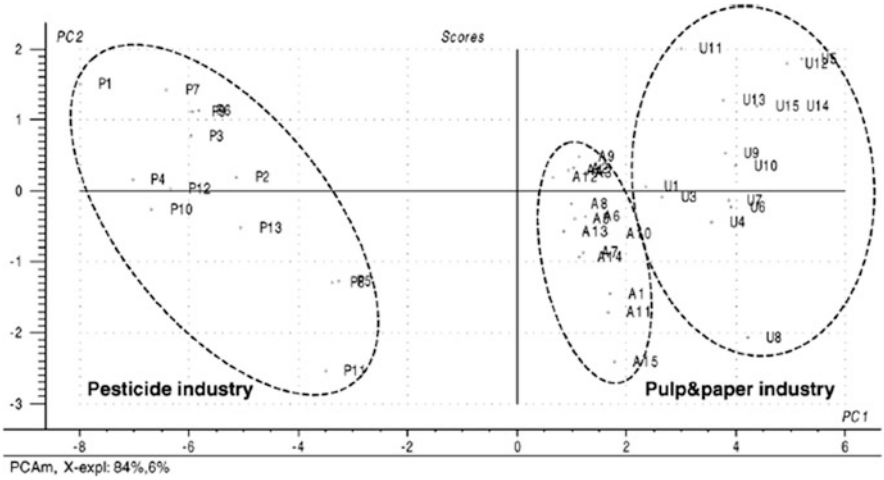

Fig. 18 Example of PCA score plot for the first two principal components, showing the clustering of the samples according to its origin. Reprinted from [58], with permission from Elsevier

Later, these principles were studied in more detail by the same laboratories involved, in what it seemed a consortium from a EU project [12]. Four wastewater samples of different treatment qualities, untreated, alarm, alert and normal, from a Swedish chemi-thermo-mechanical pulp mill and pure water were investigated using an amperometric BioET. The aim was to explore the ability of the enzymatically modified screen-printed amperometric sensors for the discrimination of wastewater quality and to counteract inherent drifts appearing in long-term use of the devices. Seven out of eight platinum electrodes on the array were modified with four different enzymes: tyrosinase, horseradish peroxidase, acetyl cholinesterase and butyryl cholinesterase. At a constant potential, the current intensity on each sensor was measured for 200 s, 100 s before injection and 100 s after injection of the sample. The dynamic biosensor response curves from the eight sensors were used for PCA identification of the four sample classes. A simple baseline and sensitivity correction equivalent to multiplicative drift correction (MDC), using steady-state intensities of reference sample (catechol) recordings, was employed. A clear pattern emerged in perfect agreement with prior knowledge of the samples explaining 97% of the variation in the data by two principal components (PCs). The first PC described the treatment quality of the samples and the second PC described the difference between treated and untreated samples. Horseradish peroxidase and pure platinum sensors were found to be the determinant sensors, while the rest did not contribute much to the discrimination. The wastewater samples were characterized by the chemical oxygen demand (COD), biological oxygen demand (BOD), total organic carbon (TOC), inhibition of nitrification, inhibition of respiration and toxicity towards *Vibrio fischeri* using Microtox®, the freshwater alga *Pseudokirchneriella subcapitata* and the freshwater crustacean *Daphnia magna*. Exploration of the predictive capabilities of the BioET for the determination of

toxicity, BOD, COD and TOC, a key factor important for the development of chemometrically stabilized commercial wastewater sensors was initiated, but with non-conclusive results. An equivalent system has been further applied in a very recent work to urban and industrial wastewaters from a paper mill [59], where the eight-sensor screen-printed electrode was operated in a flow-injection system and where different pollution index related to organic load (COD, BOD, TOC and toxicity) was successfully estimated through PLS regression. Simultaneous determination of several global environmental parameters characterizing wastewaters is possible with this kind of biosensor array, in particular because it was possible to establish the correspondence between the sensor responses and the biological effect onto the ecosystem into which the wastewater is to be released.

Although a classic example in enzyme analysis textbooks, and also explored from the point of view of kinetic analysis, there is only one single case study appearing in the literature performing the quantification of different short chain alcohols from biosensors' differentiated activities of alcohol-degrading enzymes. Such an analysis system would have interesting applications in the spirit industry for the control of alcohol distillates. A bienzymatic analytical system was developed then for the chronoamperometric analysis of methanol–ethanol mixtures [60]. The system consisted of two biosensors, one based on alcohol dehydrogenase (ADH) that responds only to the ethanol and the second one based on alcohol oxidase (AOx) that responds to both methanol and ethanol. The transducers were screen-printed electrodes (SPEs) modified with mediators: Meldola blue for ADH and Co-phthalocyanine for AOx. The calibration graph of the ADH biosensor resulted linear between 0.3 and 8 mmol/L of ethanol. The AOx biosensor was able to quantify both analytes in mixtures that contained methanol between 3 and 70 mmol/L and ethanol ranging from 15 to 110 mmol/L. Interferences due to non-specific oxidations from common oxidizable compounds like gallic acid and ascorbic acid were smaller in the case of transducer based on Meldola blue. The analytical system was tested on real samples with success: non-alcoholized beer spiked with ethanol or methanol and a counterfeit rosé wine

One of the most recurrent case studies for the demonstration of the operation and possibilities offered by BioET is that of the determination of phenolic compounds, by phenol-degrading enzymes tyrosinase and laccase. Departing from these measurements, there can be developed different applications: (1) to perform the identification/classification of types of samples, (2) to estimate general indexes and (3) to resolve the presence of specific phenolic compounds. And many different specific applications can be developed to estimate polyphenolic compounds in wine, beer, juices, teas, coffee, fruits, etc., or to estimate polluting load in wastes originated in this type of industries.

Among the first works to resolve mixtures of phenolic substances was that of the laboratory from Kubota, in Brazil. A simple and reliable method for rapid evaluation of mixtures phenol/chlorophenol was described that used a dual amperometric biosensor, that is, a two-biosensor array [61]. The approach was based on the difference of sensitivities for laccase and tyrosinase biosensors and the different phenolic compounds tested, which is in essence the application of the BioET

principles. A multichannel potentiostat was used to monitor simultaneously the response originated at the two biosensors, and the data were treated using PLS to quantify concentrations of the compounds involved. For example, in the phenol/chlorophenol mixture, the determination of individual species in a concentration ranging from 1 to 10 μM obtaining relative standard deviations of 3.5 and 3.1% for phenol and chlorophenol, respectively, was studied. The excellent correlation between the estimated and the real concentrations was also observed by the correlation coefficients (0.9958 and 0.9981 for phenol and chlorophenol, respectively). Other pair mixtures that could be resolved successfully were catechol/phenol, cresol/chlorocresol and phenol/cresol. These results showed that the methodology could be successfully employed to the simultaneous determination of phenolic compounds in mixtures, even in diluted solutions.

The development of BioETs employing phenol-degrading enzymes has been a case study extensively considered in our laboratory. In a first BioET devised for analysis of phenols in wine samples that was developed in our laboratory, both the estimation of polyphenol content in wine and the identification of the different individual phenolics were attempted [62]. The approach used an array of enzyme biosensors capable of giving a wide and complete response of the analysed species, plus a chemometric processing tool able to interpret the chemical signals and extract meaningful data from the complex readings. In our case, the proposed BioET was formed by an array of four voltammetric enzymatic biosensors based on epoxy–graphite composites, one blank electrode and the other three bulk modified with tyrosinase and laccase on one side and copper nanoparticles on the other: these modifiers were used in order to incorporate differentiated or catalytic response to different polyphenols present in wine and aimed to the determination of its total polyphenol content value. The use of Cu nanoparticles is inspired in observing some catalytic effect, given both laccase and tyrosinase are Cu-containing enzymes. The obtained voltammetric responses were preprocessed employing the fast Fourier transform (FFT); this was used to compress the relevant information whereas the obtained coefficients were input to an ANN model that accomplished the quantification of the total polyphenol content. For comparison purposes, obtained polyphenol content was compared against the one assessed by two different reference methods: Folin–Ciocalteu and UV polyphenol index (I_{280}); good prediction ability was attained with correlation coefficients higher than 0.949 when comparing against the reference methods. The obtained comparison of calculated vs. reference values can be observed in Fig. 19, where comparison data for the train subset and for the external test subset have been split up. Apart from excellent correlation, the comparison slopes are indistinguishable from one (0.993 ± 0.008 for the train subset and 1.027 ± 0.033 for the external test subset). Additionally, a singular effort was made to provide some uncertainties associated to the prediction made. In this case, the ANN prediction model was retrained several number of times (ca. 30) with random distribution of samples used for training and samples used for testing. Learning algorithm used was Bayesian regularization, and as such, no internal validation was needed, given the possibility of overfitting is controlled in some other ways. By grouping the repeated cases, each sample was

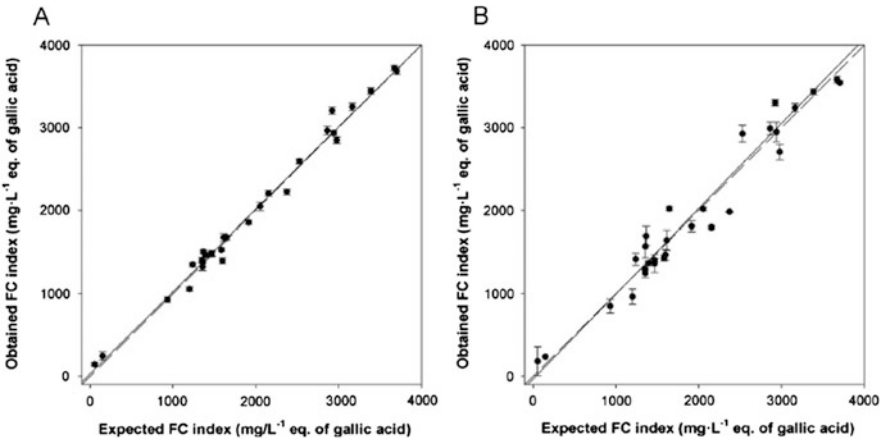

Fig. 19 Modelling ability of the optimized FFT–ANN. Sets adjustments of expected vs. obtained concentrations for Folin–Ciocalteu index, both for (**a**) training and (**b**) testing subsets. *Dashed line* corresponds to theoretical diagonal line. Reprinted from [62], with permission from Elsevier

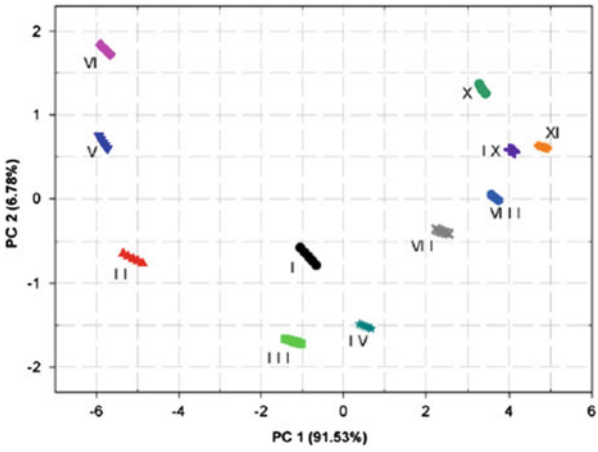

Fig. 20 Example of PCA score plot for the first two principal components, corresponding to wine sample matrix (I) spiked with typical phenolic compounds that may be present in wine. The *graph* demonstrates how the different phenolic compounds are discriminated. Reprinted from [62], with permission from Elsevier

used for training and for external test; average values and standard deviations could be calculated, which is the information provided in the figure; this illustrates how the final result is dependent on the precise choice of which samples are used for what function.

Qualitative identification of individual polyphenols found in wine was also assessed by means of PCA which allowed the discrimination of the individual polyphenols under study. Pure chemicals were spiked onto a control wine, and voltammograms were recorded and FFT processed. After PCA transformation, samples are grouped together in clear clusters, as can be seen in Fig. 20. This fact permitted differentiating phenol-related compounds present in wine like gallic acid,

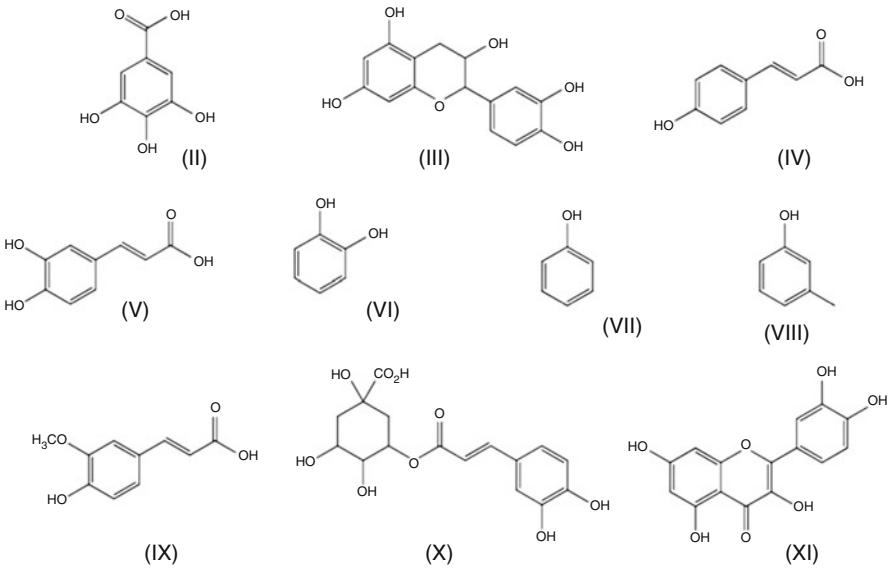

Fig. 21 Some of the most abundant polyphenols present in wine matrix (I) wine, (II) gallic acid, (III) (7) catechin, (IV) *p*-coumaric acid, (V) caffeic acid, (VI) catechol, (VII) phenol, (VIII) *m*-cresol, (IX) ferulic acid, (X) chlorogenic acid and (XI) quercetin

catechin, *p*-coumaric acid, caffeic acid, catechol, phenol, *m*-cresol, ferulic acid, chlorogenic acid and quercetin. Even more, closely related phenolics appear in close vicinity (like ferulic acid (IX), chlorogenic acid (X) and quercetin (XI), all of them flavonoids). To visualize the relation of all these phenolic compounds, their structures have been depicted in Fig. 21.

Later, in the continuing work in our laboratory, the same system was applied to a more demanding application of a BioET system. In this case, the array made from different enzymatic biosensors in the analysis of polyphenols was focused on the quantitative determination of the major polyphenols found in wine [63]. For this purpose, the biosensor array was formed by a set of epoxy–graphite biosensors, bulk modified with different redox enzymes (tyrosinase and laccase) and copper nanoparticles, aimed at the simultaneous determination of different polyphenols. One blank epoxy–graphite electrode was also included as control channel. Departure information for the BioET was the set of voltammograms generated with the biosensor array, selecting some characteristic features in order to reduce the data for the ANN quantitative model. Finally, the optimized ANN model was used for the resolution and quantification of three majoritary phenolic compounds in wine. Catechol, caffeic acid and catechin formed the three-analyte case study resolved in the work. Good prediction ability was attained, therefore allowing the separate quantification of the three phenols with predicted vs. expected slope better than 0.970 for the external test set ($n = 10$) (see Fig. 22). Finally, the BioET was also

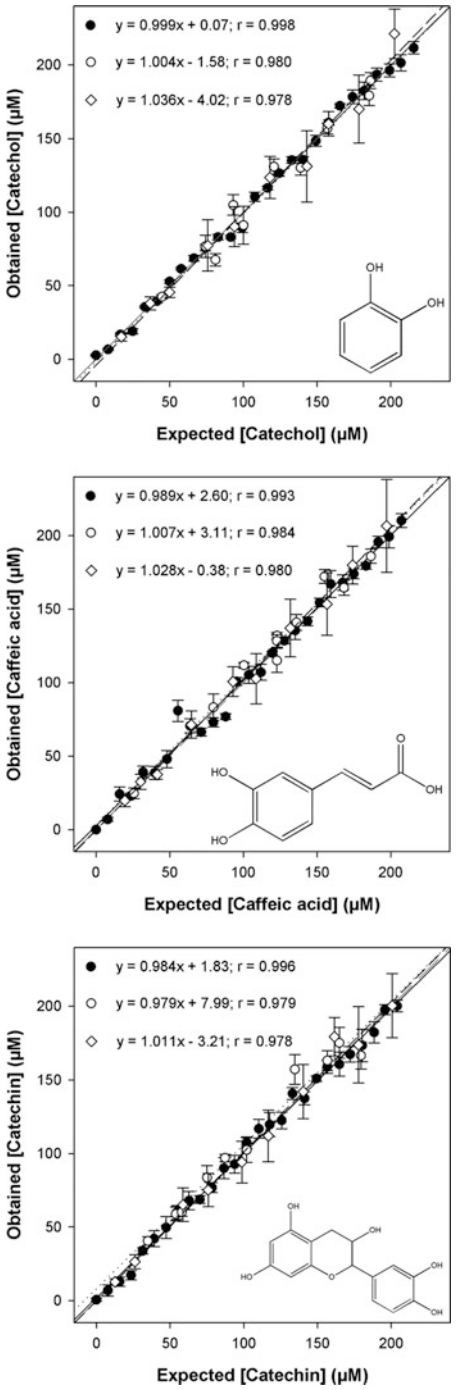

Fig. 22 Modelling ability of the optimized ANN for the multicomponent determination of phenolic compounds present in wine. Training (*filled circles*), external test (*empty circles*) and spiked wine samples (*empty diamonds*) set adjustments of the expected concentration vs. obtained concentrations for (*top*) catechol, (*middle*) caffeic acid and (*bottom*) (±)-catechin. *Dashed lines* correspond to theoretical diagonal line. *Error bars* correspond to five different retrainings with random reinitialization of weights for the final architecture. Polyphenolic structures attached to the graphs and fitted regression lines for the three subsets stated on top of each plot. Adapted from [63], with permission from the Royal Society

evaluated with spiked wine samples displaying satisfactory recovery yields (values of 104%, 117% and 122% for catechol, caffeic acid and catechin, respectively).

The same system was later applied to the analysis of specific type of sparkling wines produced in our Catalonia region. A BioET based on a sensor array comprising four voltammetric enzyme-modified (bio)sensors plus pattern recognition and multivariate calibration data processing tools was applied towards the analysis of rosé cava wines [64]. A total of 20 different samples from different producers were analysed using cyclic voltammetry without any sample pretreatment. Obtained responses were preprocessed employing the windowed slicing integral method in order to compress and extract significant features from the recorded voltammogram. Extracted coefficients were then evaluated by means of PCA to visualize some initial patterns, like producing region, or aging degree. The quantification of different phenolic indexes was achieved by an ANN model. In this manner, correlations were attempted between (bio)sensor responses and three different classical indexes related to total phenolic content (i.e. I_{280}, I_{320} and Folin–Ciocalteu index) plus two other indexes related to other specific phenolic features, like total tannins, related to astringency and body perception of the wine, and anthocyanins content, related to intensity of the red colour.

In a close related work, the BioET was applied to the determination of the three major phenolic compounds found in beer, namely, ferulic, gallic and sinapic acids [65]. The proposed BioET was formed by an array of four epoxy–graphite-modified voltammetric biosensors, with marked mix response towards the involved compounds. The array comprised one blank electrode, a laccase biosensor, a tyrosinase biosensor and one electrode bulk modified with copper nanoparticles; these modifiers were selected in order to incorporate differentiated or catalytic response towards different polyphenols present in beers and aimed to their simultaneous resolution. Departure information was the set of voltammograms generated with the biosensor array, which were preprocessed employing the windowed slicing integral method in order to reduce the complexity of the input signal while preserving the relevant information. Then, the obtained coefficients were input to an ANN model able to extract meaningful data from the complex readings, overcoming signal overlapping, and who carried out the quantification. Finally, after optimization of the ANN model, it was applied to the quantification of ferulic, gallic and sinapic acid mixtures both in synthetic and spiked beer samples. Good prediction ability was attained, therefore permitting the individual quantification of the three phenols, with good recovery yields for the spiked beer samples.

The laboratory of Prof. Rodriguez-Mendez in Valladolid completed recently a BioET system for the analysis of grapes, in which they combined sensor principles based on voltammetric biosensors employing phenol oxidases (tyrosinase and laccase) and rare-earth phthalocyanines as redox mediators [66]. The enzymes were incorporated into a Langmuir–Blodgett (LB) film onto an electrode, formed of Arachidic acid (AA) plus lutetium bisphthalocyanine (LuPc2) which was introduced in the films to act as electron mediator. The incorporation of the enzymes into the floating layers to form Tyr/AA/LuPc2 and Lac/AA/LuPc2 films was confirmed by examining pressure isotherms and by atomic force microscopy (AFM) images.

The cyclic voltammetric response towards six phenolic compounds, vanillic acid (one monophenol,), catechol, caffeic acid, hydroquinone, (three *o*-diphenols) and gallic acid and pyrogallol (two triphenols), demonstrated the performance of the biosensors that resulted from a preserved activity of the tyrosinase and laccase combined with the electron transfer activity of LuPc2. A PCA score plot demonstrated that the multisensor system was able to discriminate phenols according to the number of phenolic groups attached to the structure (1, 2 or 3). Biosensors show improved detection limits for concentrations below 1 μM. The array formed by three biosensors AA/LuPc2, Tyr/AA/LuPc2 and Lac/AA/LuPc2 was employed to discriminate phenolic antioxidants of interest in the food industry by exposing it to musts prepared from grapes of different varieties (diluted 50% in water). The system was also able to discriminate grapes of different varieties (Tempranillo, Garnacha, Cabernet, Mencia or PrietoPicudo) according to their phenolic content.

In a derived work made in our laboratory, the above concepts were extended to environmental field, when we reported the use of a BioET for the monitoring of the photodegradation of phenolic compounds [67]. Phenolic compounds are widely used in industry as antioxidants, chemical intermediates, additives to lubricants and gasoline, disinfectants, tanning agents and photographic developers or in the production of drugs and pesticides, between others. However, despite its extensive usage, some of them are known to possess well-known adverse health effects and are consequentially regulated as priority pollutants, by both the US Environmental Protection Agency (EPA) and the European Union (EU). Therefore, removal and control of these compounds from industrial waste, where they act as recalcitrant pollutants, is a critical issue.

Current official analytical methods for phenolic compound detection imply separation steps (liquid–liquid extraction or solid-phase extraction for liquid samples and Soxhlet extraction for solid samples) followed by chromatography using different detection devices, where they may require also a derivatization step. Unfortunately, these methods may require expensive and hazardous organic solvents, which are undesirable for health and disposal reasons; in addition, the analysis is labour intensive and takes long time. Hence, there is a general trend to find alternatives that may also be utilizable for on-site analyses.

The work reported the applicability of a voltammetric BioET to the monitoring of different phenolic pollutants present in wastewaters. Voltammetric responses obtained from an array of bulk-modified (bio)sensors, containing enzymes such as tyrosinase and laccase, were combined with chemometric tools such as ANNs for building the quantitative prediction model. The four voltammetric electrodes prepared consisted in one blank electrode plus three (bio)composite electrodes modified with tyrosinase, tyrosinase+laccase and Cu nanoparticles. This choice was intended as to maximize the response of the (bio)sensor array towards phenolic compounds. That is, on one side, tyrosinase and laccase were chosen as they are extensively used for the development of amperometric biosensors aimed to the detection of phenolic compounds; on the other side, copper nanoparticles were also considered due to the well-known catalytic properties of nanoparticles and the importance of copper in the two enzymes used. To fully exploit all the information

Fig. 23 Screen-printed array of 16 electrodes, suitable for modification of each surface and obtaining a BioET, materials available from Dropsens S.L., http://www.dropsens.com, Oviedo, Spain

obtained from each voltammogram and to prevent the underdetermination problem encountered with an oversized ANN with excessively complex data (i.e. when too few data points are available compared with the number of adjustable parameters), a compression step was performed to decrease the dimensionality of the electrochemical signatures. In our case, compression of voltammetric data was achieved by means of fast Fourier transform (FFT), while ANNs were chosen as the modelling tool to achieve the individual quantification of each of the compounds. In this manner, each voltammogram was compressed down to 32 coefficients without any significant loss of information, and obtained coefficients were then used as inputs to the ANN model. The response model was built employing a set of standards prepared based on a factorial design; afterwards, and once validated, it was applied to the monitoring of the mineralization of three phenol pollutants, catechol, *m*-cresol and guaiacol, during a UV-assisted photo-Fenton advanced oxidation process. The procedure also permitted to characterize the kinetics of the degradation process for each of the three phenolic compounds tested.

A part from the wide usage of phenol-degrading enzymes in relation to the determination of phenolics, these can be further associated with sugar estimating enzymes (i.e. GOx), in order to obtain mixed info data related to phenolics and sugars and estimate better properties, varieties, grades, etc., especially for applications in the food field. Disposable screen-printed sensors were modified with enzymes and used to form a BioET dedicated to the discrimination between different grape varieties [68]. The multisensory system combined screen-printed electrodes modified with inks of carbon, platinum, gold, graphene, Prussian blue and nickel oxide nanoparticles (M-SPE) covered with glucose oxidase (M-GOx-SPE) or tyrosinase (M-Tyr-SPE). The M-GOX-SPE and M-Tyr-SPE sensors produced a variety of responses due to different behaviours of the electron mediators of the six screen-printed materials used for the electrocatalysis of the glucose and phenols by means of glucose oxidase and tyrosinase. This variety of responses, together with the capability of the sensors to detect glucose or phenols, allowed the developed BioET to discriminate between the juices obtained from

different varieties of grape. PLS multivariate calibration of electrochemical data was successfully applied to the simultaneous determination of glucose and polyphenols in musts. The discrimination capability shown by this array of cheap and single-use sensors was similar to that found in other complex bioelectronic tongues. The lower price, ease of use and portability of the modified screen-printed electrode system make the bioelectronic tongue developed here an alternative tool that can be used in situ in the vineyard block. The technologies described permit to envisage multisensing devices, in which a common auxiliary and reference electrode is used in a single screen-printed device to permit the BioET development; for this purpose, only a separate, individually controllable deposit or formation of the enzyme layer is needed, in order to get easily 8-sensing or 16-sensing devices, as shown in Fig. 23.

As previously, it is elaborated in Table 4 to help in sketching different case studies related to the use of several enzymes into the BioET. The different analytes that can be resolved, together with the order of magnitude of the concentration determined and the type of samples analysed, are indicated.

5 Inhibition Electronic Tongues

The conceptual idea behind an inhibition BioET is the fact that inhibitory effect may present differences depending on the exact form of a certain enzyme, that is, depending on its exact animal or plant source, or if it has been altered by genetic engineering. If there exists a different pattern of responses from different enzymes towards different inhibitors, then it is obvious that the exact inhibitor(s) present and their concentrations may be extracted.

Although the case of analysis of activators would be essentially equivalent to inhibition, as both rely on equivalent principles (the change of enzymatic activity through a third substance), there are few enzyme cases applicable in analysis, and even, there is no example in the literature related to BioETs.

From the different cases related to inhibition, the most in-depth studied case is that of pesticides, mainly as inhibitors of cholinesterase enzymes; other cases involve inhibition of sarcosine oxidase that allows determining carboxylic acids or inhibition of protein phosphatases, attempted for the resolution of microcystin types. Inhibition of aminooxidases also opens a way for determination of amount and effects of modern antidepressants.

5.1 Determination of Pesticides

The case most studied in the literature has been that of the determination of pesticides using their inhibitory effect on the hydrolysis reaction by neurotransmitter-degrading enzyme acetylcholinesterase (AChE). The inhibition

Table 4 Extract of significant examples recorded for BioETs that employs several enzyme biosensors in the resolution of mixtures of different compounds. Applications recorded a long time

Author	Enzymes used	Type of biosensors	Analytes determined/concentration level			Type of sample	References
Lange and Whitmann	Monoamine oxidase, tyramine oxidase and diamine oxidase	Voltammetric	Histamine / 1 μmol kg^{-1}	Tyramine/ 1 μmol kg^{-1}	Putrescine/ 1 μmol kg^{-1}	Food products	[43]
Freire et al.	Laccase and tyrosinase	Voltammetric	Phenol/ 1 μM	*p*-Chlorophenol/ 1 μM	–	Water	[61]
Jawaheer et al.	Glucose oxidase, mutarotase and invertase	Voltammetric	Glucose/ 1 mM	Sucrose/1 mM	Ascorbic acid/ 10 mM	Fruits	[56]
Solna and Skladal	Laccase, peroxidase and tyrosinase	Voltammetric	Catechol/ 10 μM	–	–	Wastewater	[57]
Bucur et al.	Alcohol dehydrogenase and alcohol oxidase	Voltammetric	Methanol/ 1 mM	Ethanol/0.25 mM	–	Alcoholic beverages	[60]
Gutiérrez et al.	Urease and creatinine iminohydrolase	Potentiometric	Urea/1 mM	Creatinine/1 mM	Ammonium/1 mM Potassium/1 mM Sodium /1 mM	Urine	[20]
Bóka et al.	Diamine oxidase, monoamine oxidase A and putrescine oxidase	Voltammetric	Histamine / 1 μmol kg^{-1}	Tyramine/ 1 μmol kg^{-1}	Putrescine/ 1 μmol kg^{-1}	Meat, Fish	[44]
Cetó et al.	Tyrosinase and laccase	Voltammetric	Total phenol content/5 mM gallic acid equivalents			Wine	[62]
Cetó et al.	Tyrosinase and laccase	Voltammetric	Catechol/ 50 μM	Caffeic acid / 50 μM	(±)-Catechin/ 10 μM	Wine	[63]
Cetó et al.	Tyrosinase and laccase	Voltammetric	Ferulic acid/ 50 μM	Gallic acid/50 μM	Sinapic acid/50 μM	Beer	[65]
Raud and Kikas	Seven microorganism respirometric sensors	Amperometric	Biochemical oxygen demand, 10 mg $O_2 l^{-1}$			Wastewater	[48]
Soldatkin et al.	Glucose oxidase, mutarotase, invertase and β-Galactosidase	Conductimetric	Maltose/ 1 mM	Lactose/1 mM	Sucrose/1 mM, Glucose/1 mM	Laboratory solutions	[55]
Cetó et al.	Tyrosinase and laccase	Voltammetric	Total phenol content	Tannins	Anthocyanins	Cava wine	[64]

(continued)

Table 4 (continued)

Author	Enzymes used	Type of biosensors	Analytes determined/concentration level			Type of sample	References
Cetó et al.	Tyrosinase and laccase	Voltammetric	Catechol/ 0.1 mM	*m*-cresol/0.1 mM	Guaiacol/0.1 mM	Wastewater	[67]
Henao-Escobar et al.	Histamine dehydrogenase and putrescine oxidase	Amperometric	Histamine/ 10 µM	Putrescine/10 µM	–	Food	[45]
Czolkos et al.	Cellobiose dehydrogenase, soybean peroxidase, tyrosinase, horseradish peroxidase, butyryl cholinesterase and acetyl cholinesterase	Voltammetric	Toxicity index	Chemical oxygen demand	Biochemical oxygen demand	Wastewater	[59]

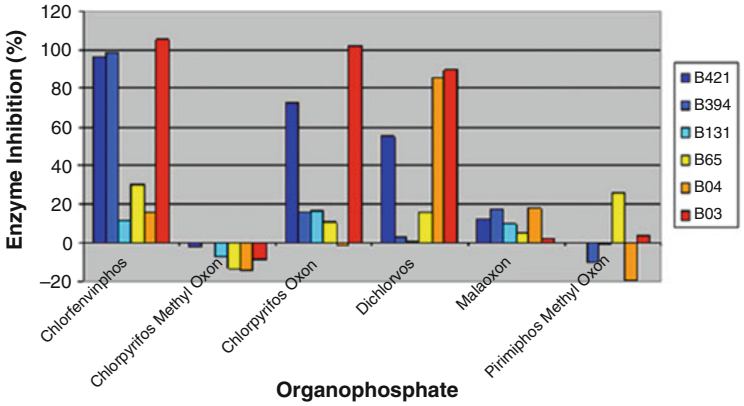

Fig. 24 Inhibition profiles obtained from the inhibition of each considered enzyme by the six organophosphate pesticides included in the study. Reprinted from [58], with permission from Elsevier

of this enzyme, which is observable at concentration levels of 10^{-10} M and below, is extraordinarily useful for the determination of these compounds at concentration levels of environmental relevance.

Per example, in the paper by Crew et al. [69], the cross response of six genetically modified AChEs (B03, B04, B65, B131, B394 and B421) was evaluated against six organophosphate pesticides. Figure 24 shows pictorially the different patterns of inhibition presented by each AChE enzyme evaluated, clearly displaying the different patterns by each pesticide and announcing that the resolution of pesticide mixtures is possible.

Inhibition biosensors are normally used in a generic way, given they provide a result that combines the sum of all inhibitors present. One biosensor by itself is not capable of discriminating presence of particular inhibitor. But the use of biosensors in array mode to form BioET makes possible this interesting application, a methodology with performance only equivalent to that supplied by the state-of-the-art GC-MS instrumentation.

An important particularity with inhibition assays is that when this is an irreversible inhibition, it forces the use of disposable biosensors that may be prepared, e.g. by screen-printing technology, and the whole application relies then on the reproducibility of manufacture of different devices [70].

The first work in the literature named as inhibition BioET was a collaborative work between our laboratory and a French laboratory commanding pesticide analysis. In this work, the BioET was developed, employing an array of inhibition biosensors and ANNs [15]. The array of biosensors was formed by three amperometric pesticide biosensors that used different AChE enzymes: the wild type from electric eel (EE) and two different genetically modified enzymes (B1 and B394). The system was employed for the simultaneous determination and/or resolution of mixtures of two pesticides, dichlorvos and carbofuran, with mean values of

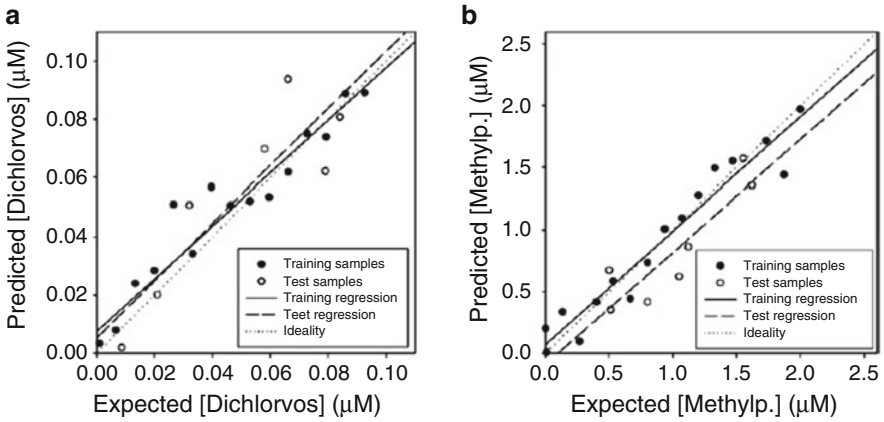

Fig. 25 Correlation results between expected and obtained concentration for (**a**) dichlorvos and (**b**) methylparaoxon. Reprinted from [16], with permission from Elsevier

concentration of 0.8 and 4 nM for each pesticide, respectively. This work was soon extended to a similar one, with a system using wild electric-eel AChE, B394 AChE and a two-enzyme (AChE + phosphotriesterase) biosensor, employed to resolve mixtures of chlorpyrifos and chlorfenvinfos pesticides at the nM level [71].

Later, these concepts were translated into an automated flow-injection system, now using dichlorvos and methylparaoxon pesticide mixture, a more difficult to resolve mixture than the previous ones, given both pesticides are from the same family of organophosphates [16]. Figure 25 displays the performance of the developed device, where it can be observed how dichlorvos can be determined down to the 10 nM level and methylparaoxon down to 200 nM level, both with satisfactory comparison between calculated and expected values (especially for the external test set).

The concept was further extended by the French researchers to three-pesticide mixtures, chlorpyrifos-oxon (CPO), chlorfenvinphos (CFV) and azinphos methyl-oxon (AZMO) [72]. The array of biosensors was designed using only two acetylcholinesterases from *Drosophila melanogaster* (wild type and genetically modified) and used the dynamic component of the inhibition profiles and an ANN to solve mixtures of CPO, CFV and AZMO insecticides at the 1–10 nM level.

Analogously, paraoxon, dichorlvos and carbofuran could be determined by combining response of AChEs from electric eel and from the fly *Drosophila melanogaster* [73]; alternatively chlorpyrifos-oxon or paraoxon could be determined in milk down to the 1 nM level [74]. To clarify and systematize all the different variants registered in the literature, the enzymes used, the insecticides resolved and the order of concentrations determined have been gathered together in Table 5, where a quick view of advances in the field can be readily discerned.

To finish, it is just left to say that the possibility to resolve up to mixtures formed by six pesticides has been postulated, although no clear results have been provided [69]. This may be possible, but important efforts on the reproducibility of

Table 5 Different variants recorded for inhibition BioETs employed in the resolution of mixtures of pesticides. Applications recorded a long time

Author	Enzymes used	Resolved pesticides/concentration (nM)			References
Cortina et al.	3 AChEs, wild electric eel and genetically engineered B1, B394	Dichlorvos/ 0.8 nM	Carbofuran/ 4 nM	–	[15]
Istambouile et al.	2 AChEs, wild electric eel and B394 + phosphotriesterase	Chlorpyrifos/ 0.5 nM	Chlorfenvinfos/ 100 nM	–	[71]
Valdes et al.	3 AChEs, wild electric eel and genetically engineered B1, B394	Dichlorvos/ 0.8 nM	Methylparaoxon/ 500 nM	–	[16]
Alonso et al.	1 AChE and B131	Chlorpyrifos/ 10 nM	Chlorfenvinfos/ 10 nM	Azinphos methyl-oxon/10 nM	[77]
Crew et al.	6 AChEs, B02, B04, B65, B394 and B421	Chlorpyrifos/ malaoxon	Chlorfenvinfos/ dichlorvos	Chlorpyrifos/ pirimiphos methyl-oxon	[69]
Alonso et al.	2 AChEs from *Drosophila melanogaster*, wild and genetically modified B394	Chlorpyrifos/ 10 nM	Chlorfenvinfos/ 1 nM	Azinphos methyl-oxon/5 nM	[72]
Alonso et al.	2 AChEs from electric eel (wild) and genetically modified from *Drosophila melanogaster* (B131)	Paraoxon/ 500 nM	Dichlorvos/ 10 nM	Carbofuran/50 nM	[73]
Mishra et al.	2 AChEs genetically modified from electric eel (B4 and B394)	Chlorpyrifos/ 0.5 nM	Malaoxon/ 0.5 nM	–	[74]

manufacture of disposable biosensors and on the operation, for example, by the use of automated FIA or SIA systems probably will be necessary.

5.2 Other Inhibition Systems

In a research line by Czech laboratory from Prof. Skládál, the inhibitory effect of carboxylic acids on the activity of sarcosine oxidase has been examined in detail. A flow-through amperometric biosensor was firstly presented, based on two sensor layers that are deposited on a platinum electrode. The inner layer served to eliminate interferences by limiting diffusion of electrochemically active substances such as ascorbic acid. This layer is electro-polymerized using an equimolar mixture of *o*-phenylenediamine and resorcinol. The outer layer was prepared by cross-linking the enzyme sarcosine oxidase and bovine serum albumin using glutaraldehyde. The formation of enzymatically produced hydrogen peroxide by this oxidase is monitored at 600 mV vs. an Ag/AgCl reference electrode. The addition of carboxylic acids caused competitive inhibition of the enzyme and a decrease in signal. The assay was optimized for determination of carboxylic acids in wine samples. Following tenfold dilution, most samples contain 1–10 mM individual carboxylic acids, and thus a 5 mM concentration of sarcosine was chosen as being optimal for competition. In case of real samples, the biosensor measured the sum of all carboxylic acids, which serves as a parameter describing the quality of wines. Results from testing several wine samples are reported [75]. In a very recently published work during the writing of this chapter, the idea was put into practice, coupling amperometric biosensors based on lactate oxidase, sarcosine oxidase and mixture of fumarase and sarcosine oxidase that were used for monitoring of organic acids like tartaric, malic and lactic in wine samples [76], with correct comparison against standard HPLC methods.

In a recent work in J. L. Marty Laboratory in Perpignan, France, a BioET system was conceived to determine high-priority pollutants, LR and YR microcystins, based on inhibition of protein phosphatases [78]. Microcystins (MC) are generated during algal blooms of toxic cyanobacteria (blue-green algae) representing a serious problem because of the potent toxins that can be released. Microcystins (MCs) are produced by cyanobacteria present in lakes, ponds, reservoirs and rivers with low turbidity flow regimes. The enzymatic test is based on the toxicity mechanism of MCs: these toxins specifically inhibit protein phosphatase PP2A and PP1 activities. The inhibition characteristics of three different protein phosphatases by three MC variants, MC-LR, MC-YR and MC-RR, were studied. The corresponding inhibition constant for each enzyme-MC couple was calculated. The toxicity of MC varies in the following order: MC-LR>MC-YR>MC-RR. The sensitivity of the enzymes increased in the following order: mutant PP2A<mutant PP1<natural PP2A. The lowest limit of detection obtained was 21.2 pM for MC-LR using the most sensitive enzyme. Figure 26 displays the cross-response features shown by the protein phosphatases considered in the study, where the minimum inhibitory effect is experienced by MC-RR on PP2A, or the more balanced

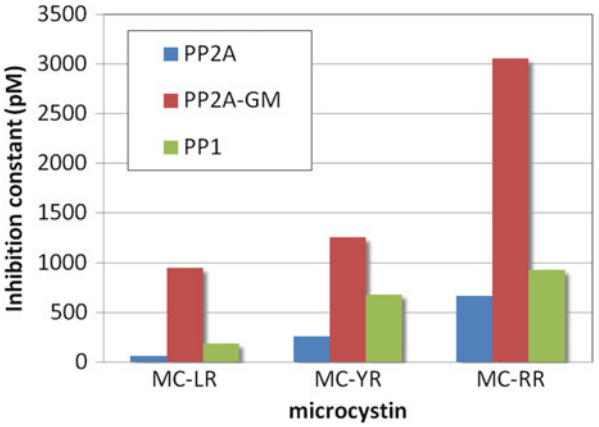

Fig. 26 Cross-response features use of protein phosphatases included in the study towards microcystins LR, YR and RR. Adapted from data in [78]

inhibitory effect of YR-microcystin on the three enzymes evaluated shows that the case of resolution of different microcystins could be feasible. An ANN model was used to discriminate MC variants – LR and YR – using the differences in inhibition percentages measured with mutant PP1 and natural PP2A at the 100 pM level.

In a third example case, β-carbolines are inhibitors of monoamine oxidases (MAO-A and MAO-B) and can be found in foods, hallucinogenic plants or certain plant drugs. The referred article described a fast analysis method for β-carbolines based on the inhibition of MAO [79]. The MAO-A is inhibited by all three tested β-carbolines (harmane, norharmane and harmaline), while MAO-B is inhibited only by norharmane. The presence of norharmane in mixtures of β-carbolines can be identified based on the difference between the cumulative inhibition of MAO-A by all β-carbolines and MAO-B inhibition. The enzymes were immobilized on screen-printed electrodes modified with a stabilized film of Prussian blue that contain also copper. Benzylamine was used as substrate for the enzymatic reaction and the hydrogen peroxide formed was measured amperometrically at −50 mV. The developed biosensors were used for food analysis. The detection limits obtained were 5.0 μM for harmane and 2.5 μM for both harmaline and norharmane.

In a closed related idea, amperometric biosensors based on planar screen-printed graphite electrodes modified with multiwall carbon nanotubes (MWCNTs) and immobilized monoamine oxidase enzyme (MAO) have been proposed for the determination of antidepressants (imipramine, afobazole and phenazepam) [80]. The operation of the proposed biosensors is based on the inhibiting ability of antidepressants on the considered enzymes. Monoamine oxidase is an enzyme that catalyses reactions of the oxidative deamination of monoamines: serotonin, dopamine, tyramine and also adrenalin and noradrenalin. The analytical capabilities of the proposed devices have been compared to those of biosensors based on the unmodified electrodes. The proposed biosensors are shown to be used for the control of both residual amounts of drug substances in biological fluids (urine) and the active ingredient in dosage forms and to adjust the exact dose of medication for a given patient, a goal very delicate and important to fulfil. On the other hand, this case study remains open for interesting studies, in this case in environmental

field, in the determination of emerging pollutants as it can be inhibitors of serotonin uptake receptors, that is, the new antidepressants Prozac and related drugs.

6 Concluding Remarks

To summarize, here we have presented, in the form of organizing the biosensing part, or in the procedural part, but always with the application pursued goals in mind, the gathering of literature papers and our own work in Barcelona laboratories dealing with work on BioETs. I hope it could be highlighted how limitations in the work with bioanalytical reagents or in the work with biosensors can be tackled in this new procedural way that makes the bioanalytical chemist think multicomponent way and opts for complementing traditional responses with additional complementary ones. These integration possibilities envisage highly valuable applications of unthought performance, like concentration mapping at the micro and the macro scales, enhanced reliability of sensor operation, correction of interferent effects or matrix effects or multidetermination at the level of most complex existing hyphenated technologies.

Although not described in detail here, there are BioETs designed specifically for replication of taste [4], in a search to reproduce human sense of taste. That is, in a purely bioinspired design, the intention is to mimic primary perceptions of salty, sour, sweet, bitter and *umami* (the fifth oriental basic taste, standing for "deliciousness"). This goal has been attempted by two different means. The first was reproducing, by usage of conventional potentiometric sensors, as it is the case with commercial instruments Astree (from Alpha-MOS) [81] and Insent [82]. On the other hand, the most recent attempts to replicate taste have been done by designing BioETs that employ as sensing elements sensing proteins and receptors originally intervening in the sense of taste, therefore doing a complete translation of physiology into a biosensing instrument [83].

A first work that can be listed here is the one using taste buds in a microelectrode array and pertain to the variety of stochastic sensing [85]. In the referred work [84], extracted biological tissue from specific points in human palate is coupled with microchips to establish a novel BioET system, in this case devised for salty detection. Before experiment, a computational model of action potential in salt taste receptor cell is established, simulating the responsive results to natural salt stimuli of NaCl solution with various concentrations. A 36-channel microelectrode array (MEA) with electrode diameter of 30 μm was fabricated on glass substrate, and taste epithelium was stripped from rat and fixed on MEA. When stimulated by the salty stimuli, electrophysiological activities of taste receptor cells in taste buds were measured through a multichannel recording system. Both simulation and experiment results showed a dose-dependent increase in NaCl-induced spike potentials of taste receptor cells, in amplitude and frequency, which indicated good applications in salt measurements. The multichannel analysis demonstrated that different groups of MEA channels were activated during stimulations, by recording

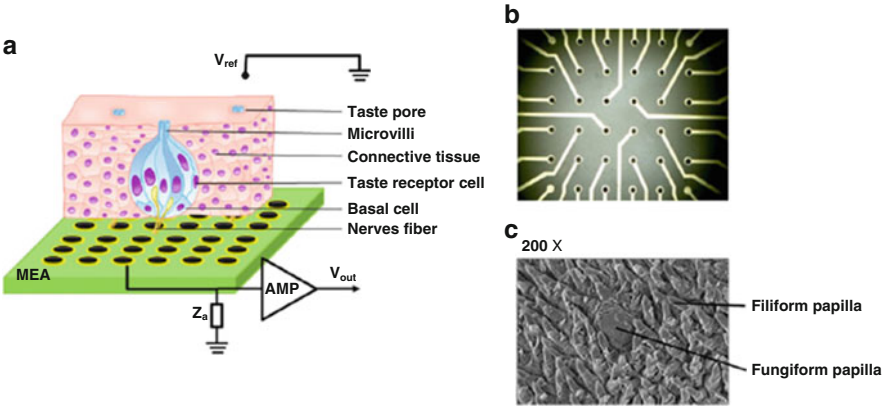

Fig. 27 The recording extracellular potentials of taste receptor cells in taste buds by microelectrodes.(**a**) Schematic diagram of the biosensor. (**b**) The pattern of 30 μm electrodes in 36 channel arrays.(**c**) Fungiform papillae of the taste epithelium observed by SEM. Reprinted from [84], with permission from Elsevier

the nerve spikes and indicating nonoverlapping populations of receptor cells in taste buds involved in salt taste perception. As illustrated above, Fig. 27 displays the involved biosensor platform and how the protein taste receptors might be deployed and transduced through a microfabricated electrode substrate.

In a related nanobiotechnological work, a BioET was designed using human sweet taste receptors for the detection and discrimination of sweeteners with human-like performance. For this purpose, single-walled carbon nanotube field-effect transistors were functionalized with nanovesicles containing human sweet taste receptors and used to detect the binding of sweeteners to the taste receptors [86]. Protein receptors used were heterodimeric G-protein-coupled receptors (GPCRs) composed of human taste receptor type 1 member 2 (hTAS1R2) and human taste receptor type 1 member 3 (hTAS1R3), which have multiple binding sites and allow a human tongue-like broad selectivity for the detection of sweeteners. This nanovesicle-based BioET demonstrated to be a powerful tool for the detection of sweeteners as an alternative to labour-intensive and time-consuming cell-based assays and the sensory evaluation panels used in the food and beverage industry. Furthermore, this study also allows the artificial sensor to exam the functional activity of dimeric GPCRs.

Obviously, as it can be deduced from the conceptual depth and interesting applications covered, BioETs have already been constituted as a consolidated research line with the purpose of improving performance, applicability and proper results for existing biosensors.

Acknowledgements Financial support from the European Commission (Grant Agreement number 264772 – ITN CHEBANA) and from the Spanish Ministry of Economy and Innovation, MINECO (Madrid), through project CTQ2013-41577-P is gratefully acknowledged. Manel del Valle thanks the support from programme ICREA Academia. Many thanks are also debt to PhD

students that completed their formation in our laboratories in the research line of BioETs: Albert Gutés, Montserrat Cortina, Manuel Gutiérrez Capitán, Xavier Cetó, Andrea Cipri and Andreu González-Calabuig.

References

1. Vlasov Y, Legin A, Rudnitskaya A, Di Natale C, D'Amico A (2005) Nonspecific sensor arrays ("electronic tongue") for chemical analysis of liquids (IUPAC Technical Report). Pure Appl Chem 77(11):1965–1983
2. del Valle M (2011) Bioinspired sensor systems. Sensors 11(11):10180–10186
3. Lavine BK, Workman J (2002) Chemometrics. Anal Chem 74:2763
4. Toko K (2000) Biomimetic sensor technology. Cambridge University Press, Cambridge
5. Savage N (2012) Technology: the taste of things to come. Nature 486(7403):S18–S19
6. Vlasov YG, Ermolenko YE, Legin AV, Rudnitskaya AM, Kolodnikov VV (2010) Chemical sensors and their systems. J Anal Chem 65(9):890–898
7. Ciosek P, Wroblewski W (2007) Sensor arrays for liquid sensing – electronic tongue systems. Analyst 132(10):963–978
8. Riul A Jr, Dantas CAR, Miyazaki CM, Oliveira ON Jr (2010) Recent advances in electronic tongues. Analyst 135(10):2481–2495
9. Tahara Y, Toko K (2013) Electronic tongues-a review. IEEE Sens J 13(8):3001–3011
10. del Valle M (2010) Electronic tongues employing electrochemical sensors. Electroanalysis 22 (14):1539–1555
11. Zeravik J, Hlavacek A, Lacina K, Skladal P (2009) State of the art in the field of electronic and bioelectronic tongues – towards the analysis of wines. Electroanalysis 21(23):2509–2520
12. Tønning E, Sapelnikova S, Christensen J, Carlsson C, Winther-Nielsen M, Dock E, Solna R, Skladal P, Nørgaard L, Ruzgas T, Emnéus J (2005) Chemometric exploration of an amperometric biosensor array for fast determination of wastewater quality. Biosens Bioelectron 21 (4):608–617
13. Gutes A, Cespedes F, Alegret S, del Valle M (2005) Determination of phenolic compounds by a polyphenol oxidase amperometric biosensor and artificial neural network analysis. Biosens Bioelectron 20(8):1668–1673
14. Gutierrez M, Alegret S, del Valle M (2007) Potentiometric bioelectronic tongue for the analysis of urea and alkaline ions in clinical samples. Biosens Bioelectron 22 (9-10):2171–2178
15. Cortina M, del Valle M, Marty J-L (2008) Electronic tongue using an enzyme inhibition biosensor array for the resolution of pesticide mixtures. Electroanalysis 20(1):54–60
16. Valdes-Ramirez G, Gutierrez M, del Valle M, Ramirez-Silva MT, Fournier D, Marty JL (2009) Automated resolution of dichlorvos and methylparaoxon pesticide mixtures employing a Flow Injection system with an inhibition electronic tongue. Biosens Bioelectron 24 (5):1103–1108
17. Winquist F (2008) Voltammetric electronic tongues – basic principles and applications. Microchim Acta 163(1–2):3–10
18. Magalhães JMCS, Machado AASC (2002) Array of potentiometric sensors for the analysis of creatinine in urine samples. Analyst 127(8):1069–1075
19. Correia DPA, Magalhães JMCS, Machado AASC (2005) Array of potentiometric sensors for simultaneous analysis of urea and potassium. Talanta 67(4):773–782
20. Gutierrez M, Alegret S, del Valle M (2008) Bioelectronic tongue for the simultaneous determination of urea, creatinine and alkaline ions in clinical samples. Biosens Bioelectron 23(6):795–802

21. Gutes A, Ibanez A, Cespedes F, Alegret S, del Valle M (2005) Simultaneous determination of phenolic compounds by means of an automated voltammetric "electronic tongue". Anal Bioanal Chem 382(2):471–476
22. Pravdová V, Pravda M, Guilbault GG (2002) Role of chemometrics for electrochemical sensors. Anal Lett 35:2389–2399
23. Scott SM, James D, Ali Z (2006) Data analysis for electronic nose systems. Microchim Acta 156:183
24. Richards E, Bessant C, Saini S (2002) Multivariate data analysis in electroanalytical chemistry. Electroanalysis 14:1533
25. Oliveri P, Casolino MC, Forina M (2010) Chemometric brains for artificial tongues. Adv Food Nutr Res 61(61):57–117
26. Cartas R, Mimendia A, Legin A, del Valle M (2011) Multiway processing of data generated with a potentiometric electronic tongue in a SIA system. Electroanalysis 23(4):953–961
27. Rudnitskaya A, Kirsanov D, Blinova Y, Legin E, Seleznev B, Clapham D, Ives RS, Saunders KA, Legin A (2013) Assessment of bitter taste of pharmaceuticals with multisensor system employing 3 way PLS regression. Anal Chim Acta 770:45–52
28. Ceto X, Cespedes F, del Valle M (2013) Comparison of methods for the processing of voltammetric electronic tongues data. Microchim Acta 180(5-6):319–330
29. Despagne F, Massart DL (1998) Neural networks in multivariate calibration. Analyst 123 (11):157R–178R
30. Trojanowicz M, Jagielska A, Rotkiewicz P, Kierzek A (1999) Flow injection determination of phenols with tyrosinase amperometric biosensor and data processing by a neural network. Chem Anal Warsaw 44:865–878
31. Serra B, Jiménez S, Mena ML, Reviejo AJ, Pingarrón JM (2002) Composite electrochemical biosensors: a comparison of three different electrodes matrices for the construction of amperometric tyrosinase biosensors. Biosens Bioelectron 17:217–226
32. Torrecilla JS, Mena ML, Yanez-Sedeno P, Garcia J (2007) Application of artificial neural network to the determination of phenolic compounds in olive oil mill wastewater. J Food Eng 81(3):544–552
33. Torrecilla JS, Mena ML, Yañez-Sedeno P, Garcia J (2007) Quantification of phenolic compounds in olive oil mill wastewater by artificial neural network/laccase biosensor. J Agric Food Chem 55(18):7418–7426
34. Tang L, Zeng G, Liu J, Xu X, Zhang Y, Shen G, Li Y, Liu C (2008) Catechol determination in compost bioremediation using a laccase sensor and artificial neural networks. Anal Bioanal Chem 391(2):679–685
35. Zhou Y, Tang L, Zeng G, Zhang Y, Li Z, Liu Y, Chen J, Yang G, Zhou L, Zhang S (2014) Simultaneous determination of hydroquinone and catechol in compost bioremediation using a tyrosinase biosensor and artificial neural networks. Anal Methods 6(7):2371–2378
36. Torrecilla JS, Mena ML, Yanez-Sedeno P, Garcia J (2008) A neural network approach based on gold-nanoparticle enzyme biosensor. J Chemometr 22(1-2):46–53
37. Correia DPA, Magalhaes JMCS, Machado AASC (2008) Array of potentiometric sensors for multicomponent analysis of blood serum. Microchim Acta 163(1-2):131–137
38. Gutes A, Ibanez AB, del Valle M, Cespedes F (2006) Automated SIA e-tongue employing a voltammetric biosensor array for the simultaneous determination of glucose and ascorbic acid. Electroanalysis 18(1):82–88
39. Massart DL, Vandeginste LMC, Buydens LMC, de Jong S, Lewi PJ, Smeyers-Verbeke J (1997) Handbook of chemometrics and qualimetrics, vol A. Elsevier, Amsterdam
40. Al-Issa Y, Njagi J, Schuckers SC, Suni II (2015) Amperometric bioelectronic tongue for glucose determination. Sens Bio-Sens Res 3:31–37
41. Ghasemi-Varnamkhasti M, Luz Rodriguez-Mendez M, Mohtasebi SS, Apetrei C, Lozano J, Ahmadi H, Razavi SH, Antonio de Saja J (2012) Monitoring the aging of beers using a bioelectronic tongue. Food Control 25(1):216–224

42. Mugweru A, Clark BL, Pishko MV (2007) Electrochemical redundant microsensor arrays for glucose monitoring with patterned polymer films. Electroanalysis 19(4):453–458
43. Lange J, Wittmann C (2002) Enzyme sensor array for the determination of biogenic amines in food samples. Fresenius J Anal Chem 372(2):276–283
44. Bóka B, Adányi N, Virág D, Sebela M, Kiss A (2012) Spoilage detection with biogenic amine biosensors, comparison of different enzyme electrodes. Electroanalysis 24(1):181–186
45. Henao-Escobar W, del Torno-de Román L, Domínguez-Renedo O, Alonso-Lomillo MA, Arcos-Martínez MJ (2016) Dual enzymatic biosensor for simultaneous amperometric determination of histamine and putrescine. Food Chem 190:818–823
46. Rodriguez-Mendez ML, Gay M, Apetrei C, De Saja JA (2009) Biogenic amines and fish freshness assessment using a multisensor system based on voltammetric electrodes. Comparison between CPE and screen-printed electrodes. Electrochim Acta 54(27):7033–7041
47. Pitman K, Raud M, Kikas T (2015) Biochemical oxygen demand sensor arrays. Agronomy Res 13(2):382–395
48. Raud M, Kikas T (2013) Bioelectronic tongue and multivariate analysis: a next step in BOD measurements. Water Res 47(7):2555–2562
49. Kirsanov D, Legin E, Zagrebin A, Ignatieva N, Rybakin V, Legin A (2014) Mimicking Daphnia magna bioassay performance by an electronic tongue for urban water quality control. Anal Chim Acta 824:64–70
50. Yaropolov AI, Kharybin AN, Emnéus J, Marko-Varga G, Gorton L (1995) Flow-injection analysis of phenols at graphite electrode modified with co-immobilised laccase and tyrosinase. Anal Chim Acta 308:137–144
51. ElKaoutit M, Naranjo-Rodriguez I, Temsamani KR, De La Vega MD, De Cisneros JLHH (2007) Dual laccase – tyrosinase based sonogel-carbon biosensor for monitoring polyphenols in beers. J Agric Food Chem 55(20):8011–8018
52. Montereali MR, Seta LD, Vastarella W, Pilloton R (2010) A disposable Laccase-Tyrosinase based biosensor for amperometric detection of phenolic compounds in must and wine. J Mol Catal B Enzym 64(3-4):189–194
53. Kochana J, Nowak P, Jarosz-Wilkołazka A, Bieroń M (2008) Tyrosinase/laccase bienzyme biosensor for amperometric determination of phenolic compounds. Microchem J 89 (2):171–174
54. Diaconu M, Litescu SC, Radu GL (2011) Bienzymatic sensor based on the use of redox enzymes and chitosan-MWCNT nanocomposite. Evaluation of total phenolic content in plant extracts. Microchim Acta 172(1):177–184
55. Soldatkin OO, Peshkova VM, Saiapina OY, Kucherenko IS, Dudchenko OY, Melnyk VG, Vasylenko OD, Semenycheva LM, Soldatkin AP, Dzyadevych SV (2013) Development of conductometric biosensor array for simultaneous determination of maltose, lactose, sucrose and glucose. Talanta 115:200–207
56. Jawaheer S, White SF, Rughooputh SDDV, Cullen DC (2003) Development of a common biosensor format for an enzyme based biosensor array to monitor fruit quality. Biosens Bioelectron 18:1429–1437
57. Solná R, Skládal P (2005) Amperometric flow-injection determination of phenolic compounds using a biosensor with immobilized laccase, peroxidase and tyrosinase. Electroanalysis 17 (23):2137–2146
58. Solná R, Dock E, Christenson A, Winther-Nielsen M, Carlsson C, Emnéus J, Ruzgas T, Skládal P (2005) Amperometric screen-printed biosensor arrays with co-immobilised oxidoreductases and cholinesterases. Anal Chim Acta 528:9–19
59. Czolkos I, Dock E, Tønning E, Christensen J, Winther-Nielsen M, Carlsson C, Mojzíková R, Skládal P, Wollenberger U, Nørgaard L, Ruzgas T, Emnéus J (2016) Prediction of wastewater quality using amperometric bioelectronic tongues. Biosens Bioelectron 75:375–382
60. Bucur B, Radu GL, Toader CN (2008) Analysis of methanol-ethanol mixtures from falsified beverages using a dual biosensors amperometric system based on alcohol dehydrogenase and alcohol oxidase. Eur Food Res Technol 226(6):1335–1342

61. Freire RS, Ferreira MMC, Durán N, Kubota LT (2003) Dual amperometric biosensor device for analysis of binary mixtures of phenols by multivariate calibration using partial least squares. Anal Chim Acta 485(2):263–269
62. Cetó X, Cespedes F, del Valle M (2012) BioElectronic Tongue for the quantification of total polyphenol content in wine. Talanta 99:544–551
63. Cetó X, Céspedes F, Isabel Pividori M, Manuel Gutiérrez J, del Valle M (2012) Resolution of phenolic antioxidant mixtures employing a voltammetric bio-electronic tongue. Analyst 137 (2):349–356
64. Cetó X, Capdevila J, Minguez S, del Valle M (2014) Voltammetric BioElectronic Tongue for the analysis of phenolic compounds in rose cava wines. Food Res Int 55:455–461
65. Cetó X, Cespedes F, del Valle M (2013) Assessment of individual polyphenol content in beer by means of a voltammetric bioelectronic tongue. Electroanalysis 25(1):68–76
66. Medina-Plaza C, de Saja JA, Rodriguez-Mendez ML (2014) Bioelectronic tongue based on lipidic nanostructured layers containing phenol oxidases and lutetium bisphthalocyanine for the analysis of grapes. Biosens Bioelectron 57:276–283
67. Cetó X, González-Calabuig A, del Valle M (2015) Use of a bioelectronic tongue for the monitoring of the photodegradation of phenolic compounds. Electroanalysis 27(1):225–233
68. Medina-Plaza C, Garcia-Hernandez C, de Saja JA, Fernandez-Escudero JA, Barajas E, Medrano G, Garcia-Cabezon C, Martin-Pedrosa F, Rodriguez-Mendez ML (2015) The advantages of disposable screen-printed biosensors in a bioelectronic tongue for the analysis of grapes. Lwt-Food Sci Technol 62(2):940–947
69. Crew A, Lonsdale D, Byrd N, Pittson R, Hart JP (2011) A screen-printed, amperometric biosensor array incorporated into a novel automated system for the simultaneous determination of organophosphate pesticides. Biosens Bioelectron 26:2847–2851
70. Crew A, Hart JP, Wedge R, Marty JL, Fournier D (2004) A Screen-printed, amperometric, biosensor array for the detection of organophosphate pesticides based on inhibition of wild type, and mutant acetylcholinesterases, from *Drosophila melanogaster*. Anal Lett 37 (8):1601–1610
71. Istamboulie G, Cortina-Puig M, Marty J-L, Noguer T (2009) The use of artificial neural networks for the selective detection of two organophosphate insecticides: Chlorpyrifos and Chlorfenvinfos. Talanta 79(2):507–511
72. Alonso GA, Istamboulie G, Noguer T, Marty J-L, Muñoz R (2012) Rapid determination of pesticide mixtures using disposable biosensors based on genetically modified enzymes and artificial neural networks. Sens Actuators B Chem 164(1):22–28
73. Alonso GA, Muñoz R, Marty J-L (2013) Automatic electronic tongue for on-line detection and quantification of organophosphorus and carbamate pesticides using enzymatic screen printed biosensors. Anal Lett 46(11):1743–1757
74. Mishra RK, Alonso GA, Istamboulie G, Bhand S, Marty J-L (2015) Automated flow based biosensor for quantification of binary organophosphates mixture in milk using artificial neural network. Sens Actuators B Chem 208:228–237
75. Zeravik J, Lacina K, Jilek M, Vlcek J, Skládal P (2010) Biosensor for determination of carboxylic acids in wines based on the inhibition of sarcosine oxidase. Microchim Acta 170 (3–4):251–256
76. Zeravik J, Fohlerova Z, Milovanovic M, Kubesa O, Zeisbergerova M, Lacina K, Petrovic A, Glatz Z, Skládal P (2016) Various instrumental approaches for determination of organic acids in wines. Food Chem 194:432–440
77. Alonso GA, Dominguez RB, Marty J-L, Muñoz R (2011) An approach to an inhibition electronic tongue to detect on-line organophosphorus insecticides using a computer controlled multi-commuted flow system. Sensors 11(4):3791–3802
78. Covaci OI, Sassolas A, Alonso GA, Muñoz R, Radu GL, Bucur B, Marty JL (2012) Highly sensitive detection and discrimination of LR and YR microcystins based on protein phosphatases and an artificial neural network. Anal Bioanal Chem 404(3):711–720

79. Radulescu MC, Bucur MP, Bucur B, Radu GL (2015) Biosensor based on inhibition of monoamine oxidases A and B for detection of β-carbolines. Talanta 137:94–99
80. Medyantseva EP, Brusnitsyn DV, Varlamova RM, Beshevets MA, Budnikov HC, Fattakhova AN (2015) Capabilities of amperometric monoamine oxidase biosensors based on screen-printed graphite electrodes modified with multiwall carbon nanotubes in the determination of some antidepressants. J Anal Chem 70(5):535–539
81. Alpha Mos, Toulouse, France. http://wwww.alpha-mos.com
82. Insent Co., Japan. http://www.insent.co.jp/english/top.htm
83. Ha D, Sun Q, Su K, Wan H, Li H, Xu N, Sun F, Zhuang L, Hu N, Wang P (2015) Recent achievements in electronic tongue and bioelectronic tongue as taste sensors. Sens Actuators B Chem 207:1136–1146
84. Liu Q, Zhang F, Zhang D, Hu N, Wang H, Hsia KJ, Wang P (2013) Bioelectronic tongue of taste buds on microelectrode array for salt sensing. Biosens Bioelectron 40(1):115–120
85. Bayley H, Cremer PS (2001) Stochastic sensors inspired by biology. Nature 413 (6852):226–230
86. Song HS, Jin HJ, Ahn SR, Kim D, Lee SH, Kim U-K, Simons CT, Hong S, Park TH (2014) Bioelectronic tongue using heterodimeric human taste receptor for the discrimination of sweeteners with human-like performance. ACS Nano 8(10):9781–9789

BIOREV (2017) 6: 203–222
DOI: 10.1007/11663_2015_5002

Published online: 1 March 2016

Novel Electrochemical DNA Biosensors as Tools for Investigation and Detection of DNA Damage

Vlastimil Vyskočil and Andrea Hájková

Abstract Supramolecular interactions of various organic xenobiotic compounds with deoxyribonucleic acid (DNA) are among the most important aspects of biological studies in clinical analysis, drug discovery, and pharmaceutical development processes. In recent years, there has been a growing interest in the electrochemical investigation of interactions between a studied analyte and DNA. Observing the pre- and post-electrochemical signals of DNA or monitoring its interaction with xenobiotics provides good evidence for the interaction mechanism to be elucidated. Such interaction can also be used for sensitive determination of these compounds. This short review summarizes our results obtained during the last 5 years in the field of novel electrochemical DNA biosensors utilizing carbon-based transducers as substrates for immobilization of DNA. It should provide evidence that the electrochemical approach (employing simple, fast, sensitive, and inexpensive DNA biosensors as tools for investigation and detection of DNA damage) brings new insight into human health protection or rational drug design and leads to further understanding of the interaction mechanism between xenobiotic compounds and DNA.

Keywords Carbon electrodes • Chemical carcinogens • DNA biosensors • DNA damage detection • Drugs • Oxidative stress • Review • Supramolecular chemistry

V. Vyskočil (✉) and A. Hájková
Charles University in Prague, Faculty of Science, University Research Centre UNCE "Supramolecular Chemistry", Department of Analytical Chemistry, UNESCO Laboratory of Environmental Electrochemistry, Hlavova 2030/8, 12843 Prague 2, Czech Republic
e-mail: vlastimil.vyskocil@natur.cuni.cz; andrea.hajkova@natur.cuni.cz

Contents

Abbreviations

AA	2-Aminoanthracene
Ag/AgCl	Silver/silver chloride reference electrode
CFE	Microcrystalline natural graphite–polystyrene composite film-modified electrode
CV	Cyclic voltammetry
DNA	Deoxyribonucleic acid
DPV	Differential pulse voltammetry
dsDNA	Double-stranded deoxyribonucleic acid
EIS	Electrochemical impedance spectroscopy
GCE	Glassy carbon electrode
IARC	International Agency for Research on Cancer
NTMA	4-Nitro-3-(trifluoromethyl)aniline
PB	Phosphate buffer
phen	1,10-Phenanthroline
RNS	Reactive nitrogen species
ROS	Reactive oxygen species
RSS	Reactive sulfur species
SPCE	Screen-printed carbon electrode
SWCNT	Single-walled carbon nanotube
SWV	Square-wave voltammetry

1 Introduction

In the last decade, increasing attention has been paid to the binding of small organic molecules to nucleic acids. Such in vitro studies have a key importance for a detailed understanding to these supramolecular interactions, especially in terms of damage to deoxyribonucleic acid (DNA) caused by various xenobiotic compounds [1]. A variety of small molecules are known to interact reversibly with double-stranded DNA (dsDNA) through one of the following three modes: (1) electrostatic interactions with the negatively charged nucleic sugar–phosphate structure, (2) groove binding interactions, or (3) intercalations between the stacked base pairs of dsDNA [2–4].

Analysis of the interfacial biomolecular interaction between DNA-targeted drugs and immobilized DNA probes has a particular role in the rational design of novel DNA-binding drugs and to the drug screening. Interactions of anticancer drugs with nucleic acids have been studied by numerous physical and biochemical techniques. UV–vis absorption spectrophotometry, fluorescence spectroscopy, vibrational spectroscopy (Fourier transform infrared spectroscopy and Raman spectroscopy), polarized light spectroscopies (linear and circular dichroism), fluorescence anisotropy or resonance, surface plasmon resonance, nuclear magnetic resonance, viscometry, and gel or capillary electrophoresis have been applied to provide insight into binding modes, DNA affinity, and base pair selectivity of DNA-binding drugs [5]. However, these techniques mostly address the issues of the binding mechanisms and structural analysis (e.g., DNA base sequence selectivity, correlation of structure–activity relationships, linkages between the geometry and thermodynamic properties, or influences of substituent modifications on the physical, chemical, and biological properties of the drug–DNA complex formed) [6].

Nucleic acid layers combined with electrochemical transducers have produced a new kind of affinity biosensor capable of rapidly recognizing and monitoring DNA-binding organic compounds [1]. Electrochemical biosensors have been successfully used for a number of applications including monitoring DNA damage, studies of the interactions of DNA with various genotoxic agents (carcinogens, mutagens, toxins, drugs, etc.), and also for the detection of specific mutations in DNA sequences [7]. Thus, they potentially offer fast and inexpensive alternative to traditional methods of measuring analyte–DNA interactions [8–10].

Recently, various reviews of electrochemical DNA biosensors have been reported [1, 11–20]. The present review will focus on the most widely used strategies in the technology of electrochemical DNA biosensors, with the special emphasis placed on their construction and application in the field of DNA damage detection and investigation of supramolecular interactions between xenobiotic compounds and DNA. Our results, obtained during the last 5 years in the field of novel electrochemical DNA biosensors utilizing carbon-based transducers as substrates for immobilization of DNA, will serve as illustrative examples.

2 Electrochemical DNA Biosensors for Detection of DNA Damage

DNA belongs to main biological macromolecules that undergo serious structural changes such as oxidation of the DNA bases and sugar moieties and release of the bases, as well as strand breaks caused by chemical systems generating so-called reactive oxygen (ROS), reactive nitrogen (RNS), or reactive sulfur (RSS) species [21, 22] or caused by other classes of genotoxic substances [23]. Thus, one of the main application areas for DNA biosensors is the detection of damage to DNA.

ROS are formed either endogenously (during normal aerobic metabolism and under various pathological conditions) or exogenously (e.g., upon the exposure to UV light, ionizing radiation, or environmental mutagens and carcinogens). About ten thousands to millions of DNA damage events occur to a cell per day [23]. Accumulation of oxidative DNA lesions is associated with aging and with a variety of human diseases including cancer and neurodegeneration.

Altered chemical, physicochemical, and structural properties of damaged DNA are reflected in its redox behavior which is utilized in numerous techniques of DNA damage detection. Electrochemical DNA biosensors have been used not only to detect but also to induce and control DNA damage at the electrode surface via electrochemical generation of the damaging (usually radical) species [24]. In this way, chemical carcinogens and drugs (e.g., nitro derivatives of polycyclic aromatic hydrocarbons [25], adriamycin [26], niclosamide [27], or nitrofurazone [28]) have been investigated.

2.1 Construction of Biosensors

DNA biosensors are integrated receptor–transducer devices that use DNA as a biomolecular recognition element to measure specific binding processes with DNA, usually by electrical, thermal, or optical signal transduction [12]. Compared with other transducers, electrochemical ones received particular interest due to a rapid detection and great sensitivity. Among the electrochemical transducers, carbon-based electrodes (e.g., glassy carbon electrode (GCE), pyrolytic graphite electrode, pencil lead electrode, carbon composite electrodes, carbon paste electrodes, carbon film electrodes, screen-printed carbon electrodes (SPCEs), boron-doped diamond electrodes [29, 30], chemically modified carbon electrodes, or carbon nanoparticle-modified electrodes) exhibit several unique properties [12]. The wide electrochemical potential window in the positive direction allows sensitive electrochemical detection of oxidative damage caused to DNA by monitoring the appearance of oxidation peaks of DNA bases [31].

In the last 5 years, our attention has been paid to the development of novel electrochemical DNA biosensors based on carbon-based transducers as substrates for immobilization of DNA. Among others, following four electrodes exhibited the best properties for these purposes: GCE (supplied by Metrohm, Herisau, Switzerland), microcrystalline natural graphite–polystyrene composite film-modified electrode (CFE), SPCE (supplied by Food Research Institute, Bratislava, Slovakia), and SPCE modified with single-walled carbon nanotubes (SWCNTs).

The newly developed CFE [32] (Fig. 1a), formed by covering a classical solid working electrode with a conductive carbon film, represents a very promising alternative to electrode surfaces modified by several carbon nanoparticles with profitable electrocatalytic properties (nanotubes, graphene, etc.). The smallest particles of micronized natural graphite (type CR 2 995, Graphite Týn, Týn nad Vltavou, Czech Republic) reach the size around 1,000 nm [33], which is very close

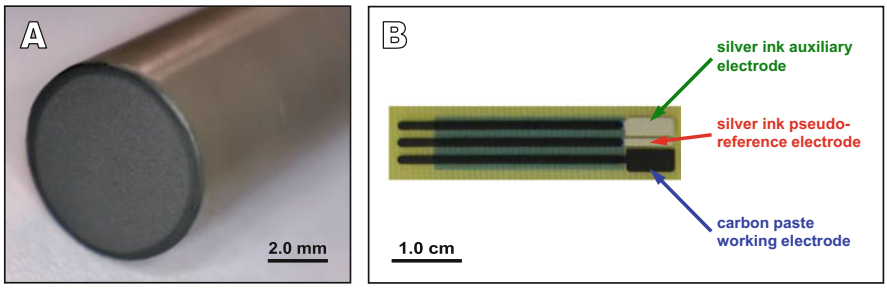

Fig. 1 Detailed pictures of the CFE (**a**) and the SPCE (**b**)

to dimensions of carbon nanoparticles commonly used in modern electroanalytical applications. However, the price of this electrode material is incomparably lower (about 1 euro cent per 1 g) than that of commercially available carbon nanoparticles. Therefore, it is more applicable for electroanalytical practice. Moreover, the CFE represents a suitable alternative to the commercially available disposable SPCEs [34]. Its simple, fast, and inexpensive preparation (the surface of a classical solid working electrode in a plastic electrode body is covered with a carbon ink suspension and left to evaporate to dryness), simple mechanical renewal of the electrode surface (by wiping off the old film with filter paper and forming a new one), good reproducibility of measurements, elimination of problems connected with "electrode history", and simple chemical modification are the main advantages.

The SPCE assembly (Fig. 1b) [25] consisted of a carbon paste working electrode, a silver ink pseudo-reference electrode, and a silver ink auxiliary electrode and was fabricated using a typical screen-printing equipment. The SPCE modified with carboxylated SWCNTs (SWCNTs/SPCE) was prepared as described in [35].

Adsorption is the simplest method to immobilize DNA on an electrode surface. It does not require reagents or special modifications in the DNA structure. There are many reports on DNA immobilization using a potential applied to GCEs, carbon paste electrodes, or SPCEs [1, 36–38]. The polished surface of the carbon electrode is usually pretreated by applying a positive potential (ca. 1.5–1.8 V vs. silver/silver chloride reference electrode (Ag/AgCl)) for a certain time. This pretreatment of the carbon surface increases its roughness and hydrophilicity [39, 40]. Afterward, the electrochemical adsorption of DNA is realized using a stirred solution at a potential of 0.5 V vs. Ag/AgCl for a preset time that depends on DNA concentration. This potential enhances the stability of the immobilized DNA through the electrostatic attraction between the positively charged carbon surface and the negatively charged hydrophilic sugar–phosphate backbone [24].

We used this immobilization approach in the development of a novel electrochemical DNA biosensor utilizing low molecular weight dsDNA isolated from salmon sperm as a biorecognition layer immobilized onto a GCE surface [41]. Such a biosensor was used for the high-throughput detection of dsDNA damage caused by various organic xenobiotic compounds [41–43]. The whole

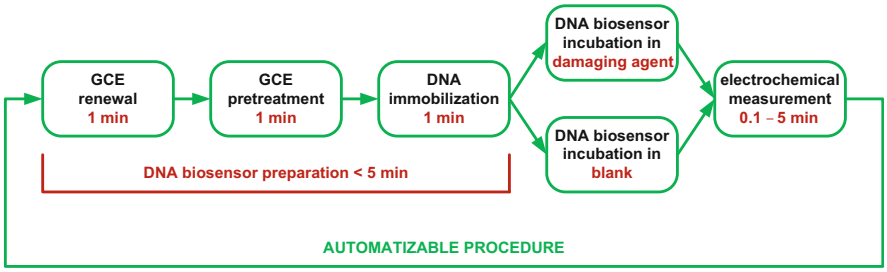

Fig. 2 Working procedure diagram for the automatization of measurement using the DNA-modified glassy carbon electrode (GCE)

preparation of this biosensor (involving removal of the previous dsDNA layer, pretreatment of the regenerated electrode surface, and deposition of the new dsDNA layer) takes no more than 5 min. This represents a significant shortening of the preparation time in comparison to procedures employing the air-drying of a DNA solution on the electrode surface [42]. Moreover, it allows an automatization of measurement and processing of experimental data (Fig. 2) if the electrochemical removal (desorption in a stirred solution at a potential of −0.5 V vs. Ag/AgCl) of the previous dsDNA layer is used.

Another way to immobilize DNA by adsorption on an electrochemical transducer has been described [44, 45]. In this case, the DNA biosensor was prepared by dipping a GCE in a DNA solution and leaving the electrode to dry. This sensor was then used to preconcentrate nitroimidazole [44] or mitoxantrone [45] on the surface and to study the interaction mechanism of these drugs with DNA by means of cyclic voltammetry (CV), differential pulse voltammetry (DPV), and square-wave voltammetry (SWV).

A different approach for immobilization of DNA is based on evaporation of a small volume of DNA solution on the GCE surface [46]. We used this approach during the preparation of the DNA-modified CFE [32], SPCEs [25, 47], or SWCNTs/SPCEs [35]. Similarly, an electrochemical DNA biosensor has been developed [48], based on DNA adsorbed on a polished basal plane pyrolytic graphite electrode. An adsorptive method to immobilize DNA on the gold electrode has also been reported [49, 50]. The gold electrode was modified by dropping a small volume of DNA on its surface, followed by air-drying overnight and rinsing to remove unabsorbed DNA.

On the other hand, DNA-modified mercury electrodes can be prepared easily by immersing a hanging mercury drop electrode or a mercury film electrode into a drop of the DNA solution. This approach requires less amount of DNA for analysis [51–53]. DNA bases and nucleosides are strongly adsorbed at mercury electrodes. Nucleosides possess an extraordinary ability of self-association (two-dimensional condensation) at the surface of mercury electrodes and can form monomolecular compact films. At high positive potentials, all DNA bases can react with mercury electrodes, forming sparingly soluble compounds.

Nanostructured interfaces between the bare electrode and DNA, formed by various nanomaterials such as gold nanoparticles and carbon nanomaterials (e.g., SWCNTs, multi-walled carbon nanotubes, carbon nanofibers, graphene, and graphene oxide nanosheets) [54–63], represent another approach to the enhancement of the biosensor response due to inherent electroactivity, effective electrode surface area, etc. [35, 64]. Nanometer scale complex films of DNA, enzymes, polyions, and redox mediators were suggested for tests of genotoxic activity of various chemicals [65].

2.2 Detection Techniques

Voltammetric (especially CV, DPV, and SWV (Fig. 3a)) and chronopotentiometric detection modes are most frequently used [31]. Together with them, electrochemical impedance spectroscopy (EIS) (Fig. 3b) becomes to be very popular in the field of DNA-based biosensors [67]. According to electrochemically active species,

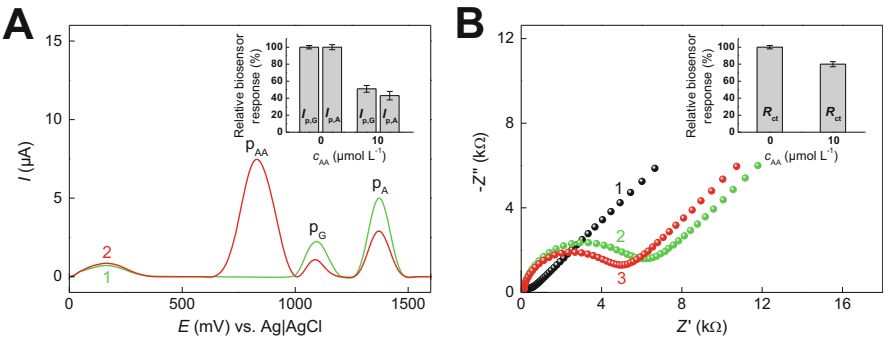

Fig. 3 (**a**) Baseline-corrected square-wave voltammograms recorded in 0.1 mol L^{-1} acetate buffer of pH 4.8. Legend: (*1*) measured at a DNA-modified GCE after 5 min incubation of the biosensor in 0.1 mol L^{-1} phosphate buffer (PB) of pH 7.0 and (*2*) measured at a DNA-modified GCE after 5 min incubation of the biosensor in 0.1 mol L^{-1} PB of pH 7.0 containing 1×10^{-5} mol L^{-1} 2-aminoanthracene (AA); p_G peak of a guanine moiety, p_A peak of an adenine moiety, p_{AA} peak of intercalated AA. Experimental conditions: polarization rate 3 V s^{-1}, pulse amplitude 0.04 V, frequency 200 Hz, potential step 0.015 V. *Inset*: the relative biosensor responses to DNA damage caused by AA, evaluated from the changes in the height of the guanine ($I_{p,G}$) and adenine ($I_{p,A}$) moiety peaks; the *error bars* are constructed for the significance level of 0.05 ($n = 3$) [66]. (**b**) Nyquist plots in the presence of 1×10^{-3} mol L^{-1} $[Fe(CN)_6]^{4-/3-}$ in 0.1 mol L^{-1} PB of pH 7.0. Legend: (*1*) measured at a bare GCE, (*2*) measured at a DNA-modified GCE after 5 min incubation of the biosensor in 0.1 mol L^{-1} PB of pH 7.0, and (*3*) measured at a DNA-modified GCE after 5 min incubation of the biosensor in 0.1 mol L^{-1} PB of pH 7.0 containing 1×10^{-5} mol L^{-1} AA. Experimental conditions: polarization potential 0.21 V vs. Ag/AgCl, potential amplitude 0.01 V, frequency range 0.1–5,000 Hz (51 frequency steps). *Inset*: the relative biosensor responses to DNA damage caused by AA, evaluated from the changes in the charge transfer resistance (R_{ct}) values; the *error bars* are constructed for the significance level of 0.05 ($n = 3$) [66]

which responses are evaluated at the detection of damage to DNA, the experimental techniques can be classified as follows [12]:

(a) Label-free and often reagent-less techniques which represent the work with no additional chemical reagents (redox indicators, mediators, enzyme substrates, etc.) needed to generate measured response
(b) Techniques which employ redox indicators either non-covalently bound to DNA (groove binders, intercalators, anionic or cationic species interacting with DNA electrostatically) or present in the solution phase (e.g., hexacyanoferrate anions ($[Fe(CN)_6]^{4-/3-}$))
(c) Techniques which employ electrochemically active labels (nanomaterials, enzymes, etc.) covalently bound to DNA (not frequently used in fundamental investigations of DNA damage)

Combination of these principles allows obtaining more complex information on DNA changes and damaging supramolecular interactions, as well [35, 68].

The first group of techniques utilizes surface activity or redox activity of DNA itself [69]. The electrochemical activity is based on the presence of redox active sites at nucleobases and sugar residues. Only DNA bases can undergo redox processes at carbon and mercury electrodes. Deoxyribose and phosphate groups are not electroactive. Electrochemical oxidation on carbon-based electrodes [70–72] showed that all bases (guanine, adenine, thymine, and cytosine) can be oxidized, following a pH-dependent mechanism. Electrochemical preconditioning of the GCE enabled a better peak separation and an enhancement of the current of the oxidation peaks for all four DNA bases in phosphate buffer (PB) of pH 7.4 (value close to physiological pH) used as the supporting electrolyte [71].

Electrochemical reduction of natural and biosynthetic nucleic acids at a dropping mercury electrode [1, 3, 73] showed that adenine and cytosine residues, as well as guanine residues in a polynucleotide chain, are reducible. The CV of DNA at a hanging mercury drop electrode showed a cathodic peak due to irreversible reduction of cytosine and adenine moieties. The reduction of the guanine moiety occurs at very negative potentials, but a peak due to the oxidation of the reduction product of the guanine moiety (7,8-dihydroguanine moiety) could be detected in the reverse scan [3].

As both the electrochemical reduction and oxidation of DNA bases are irreversible, measurements cannot be performed repeatedly. Initial increase in the anodic guanine moiety response after short-time incubation of the biosensor in damaging agents can indicate opening of the original dsDNA structure, while decrease in this response (Fig. 3a) is an evidence for the deep DNA degradation [68]. Decrease of the anodic guanine moiety peak height or area relative to that yielded by intact DNA was suggested as a measure representing degree of damage to this nucleobase and proposed as a screening test for environmental pollutants present in water or wastewater samples [9]. Some products of the DNA damage exhibit characteristic electrochemical signals (e.g., anodic peaks of 8-oxo-7,8-dihydroguanine [25, 74] and 2,8-dihydroxyadenine [75] moieties) which can be evaluated with better sensitivity than the change in the original guanine moiety response.

The second group of techniques employs electroactive compounds added to the measured system and interacting with DNA non-covalently as its indicators (cationic indicators, intercalators, and groove binders). Decrease in the intercalator or groove binder response indicates strand breaks and helix destruction. The redox indicators may be also used as diffusionally free species present in the solution phase. For instance, the $[Fe(CN)_6]^{4-/3-}$ anions indicate the presence of DNA layer on the electrode surface on the basis of electrostatic repulsion between the indicator anion and the negatively charged DNA backbone (Fig. 3b) [76, 77].

Moreover, the investigated xenobiotic compound itself can serve as a redox indicator. While its peak potential is shifted in the positive direction when the analyte binds to DNA by intercalation between the stacked base pairs of dsDNA, the peak potential is shifted in the negative direction when the interaction with DNA occurs by electrostatic attraction (interaction with the negatively charged nucleic sugar–phosphate structure) [78]. Such approach was used in our recent study [41] where the interaction between genotoxic 2-aminofluoren-9-one and dsDNA was investigated by DPV (performed at the bare GCE when both dsDNA and 2-aminofluoren-9-one were present in the measured solution). The intercalation of 2-aminofluoren-9-one between the dsDNA base pairs was the predominant supramolecular interaction observed.

2.3 Investigated Xenobiotic Compounds

There are thousands of organic compounds that bind and interact with DNA and can cause serious human diseases. The factors that determine affinity and selectivity in binding molecules to DNA need to be explained, because a quantitative understanding of the reasons that determine selection of DNA reaction sites is useful in designing sequence-specific DNA-binding molecules for application in chemotherapy and in explaining the mechanism of action of genotoxic compounds [31].

DNA damage induced by environmental pollutants (a lot of them are marked as chemical carcinogens) (Table 1) is a major endogenous toxicity pathway in biological system [84]. Most of organic pollutants may not directly cause DNA damage but their metabolized products by enzyme reactions are genotoxic and may cause DNA lesions [25, 85]. Electrochemical DNA biosensors enabling detection of such DNA damage could serve as a basis for in vitro genotoxicity screening for new organic chemicals at an early stage of their commercial development. For example, styrene is one of the most widely used industrial chemicals and itself shows little genotoxicity [86]. However, after being metabolized by liver cytochrome P450 enzymes, its oxidized product styrene oxide can induce DNA damage by formation of DNA adducts [87–89]; styrene oxide is classified by the International Agency for Research on Cancer (IARC) as a probable human carcinogen (group 2A) [90].

In our paper [25], an electrochemical DNA biosensor based on an SPCE with an immobilized layer of calf thymus dsDNA was used for in vitro investigation of the

Table 1 A survey of compounds investigated in the UNESCO Laboratory of Environmental Electrochemistry using various electrochemical DNA biosensors in connection with DNA damage

Xenobiotic compound	Detection technique	Transducer	Type of damage	References
Chemical carcinogens				
2,7-Diaminofluorene	DPV, SWV	GCE	Intercalation	[79]
	SWV	SPCE	Intercalation	[80]
2,7-Dinitrofluorene	CV, DPV, SWV	SPCE	Intercalation	[25]
2-Acetylaminofluorene	DPV, SWV	GCE	Intercalation	[79]
2-Aminoanthracene	SWV, EIS	GCE	Intercalation	[42]
2-Aminofluorene	DPV, SWV	GCE	Intercalation	[79]
	CV, SWV	CFE	Intercalation	[32]
	CV, EIS	CFE	Intercalation	[81]
	SWV	SPCE	Intercalation	[80]
2-Aminofluoren-9-one	DPV, SWV	GCE	Intercalation	[41]
2-Nitrofluorene	CV, EIS	GCE	Intercalation	[43]
	CV, DPV, SWV	SPCE	Intercalation	[25]
Anthracene	SWV, EIS	GCE	Intercalation	[42]
Fluorene	CV, EIS	CFE	Intercalation	[81]
Fluoren-9-one	SWV	SPCE	Intercalation	[80]
Drugs				
Ellipticine	CV	CFE	Intercalation	[82]
Flutamide	SWV, EIS	GCE	No damage detected	[42]
NTMA	SWV, EIS	GCE	No damage detected	[42]
Thioridazine	CV, SWV, EIS	SWCNTs/SPCE	Intercalation	[35]
Reactive radical species				
ROS (hydroxyl radicals)	CV, SWV, EIS	CFE	Oxidative damage	[83]
	CV, SWV, EIS	SWCNTs/SPCE	Oxidative damage	[35]
RNS (nitro radical anions)	SWV	SPCE	Oxidative damage	[25]

interaction between genotoxic nitro derivatives of fluorene (namely, 2-nitrofluorene and 2,7-dinitrofluorene) and DNA. Two types of DNA damage were detected at the DNA-modified SPCE: (1) caused by direct association of the nitrofluorenes, for which an intercalation association was found using the known dsDNA intercalators $[Cu(phen)_2]^{2+}$ and $[Co(phen)_3]^{3+}$ (phen stands for 1,10-phenanthroline) as competing agents, and (2) caused by short-lived radicals generated by electrochemical reduction of the nitro group (observable under specific conditions only).

Similar investigation was performed in our study [32] where a novel voltammetric DNA biosensor based on the CFE in the role of a transducer was used for investigation of the interaction between model carcinogenic substance

2-aminofluorene (one of the most extensively studied examples of the aromatic amine class of carcinogens) and calf thymus dsDNA. The layer of dsDNA immobilized at the electrode surface was utilized as a biocomponent responsive interface. The biosensor was characterized regarding the detection of DNA damage (induced by direct interaction with 2-aminofluorene) using SWV responses of the guanine and adenine moieties and CV responses of the anionic redox indicator $[Fe(CN)_6]^{4-/3-}$ present in solution. The obtained results confirmed that the interaction of dsDNA with 2-aminofluorene caused dsDNA damage, leading to the formation of strand breaks and desorption of DNA fragments from the electrode surface.

A number of aromatic compounds induce oxidative DNA damage through the generation of ROS. ROS produced in vivo react with DNA and its precursors modifying them thus giving rise to the so-called oxidative stress. It is thought that the modification of DNA (DNA lesions) leads to the formation of incorrect base pairs (changes in the genetic information), which induces mutagenesis and carcinogenesis. Therefore, there is a deep interest in identifying free radical scavengers or antioxidants that inhibit oxidative DNA damage. Owing to their polyphenolic nature, flavonoids (compounds found in rich abundance in all land plants) often exhibit strong antioxidant properties [91–95]. Initially, flavonoids were investigated as potential chemopreventive agents against certain carcinogens. Previous intake of a large quantity of flavonoid inhibited the incidence of ROS produced damages to DNA. In sharp contrast with their commonly accepted role, there is also considerable evidence that flavonoids themselves are mutagenic and have DNA-damaging ability [31, 92, 93].

In agriculture, farmers use numerous pesticides to protect crops and seeds before and after harvesting. Pesticide residues may enter into the food chain through air, water, and soil. They affect ecosystems and cause several health problems to animals and humans. Pesticides can be carcinogenic and cytotoxic. They can produce bone marrow and nerve disorders, infertility, and immunological and respiratory diseases [96]. Recently, an electrochemical DNA biosensor was developed to study DNA damage caused by several pesticides such as atrazine, 2,4-dichlorophenoxyacetic acid, glufosinate ammonium, carbofuran, paraoxon-ethyl, and difluorobenzuron [97]. A biotinylated DNA probe was immobilized on a streptavidin-modified electrode surface. This DNA probe was hybridized with biotinylated complementary DNA target analyte. Streptavidin labeled with ferrocene was further attached to the hybridized biotinylated DNA. The close proximity of ferrocene to the electrode surface induced a current signal. The presence of pesticides caused an unwinding of the DNA and thus a decrease of the ferrocene oxidation current observed in voltammetric experiments. Paraoxon-ethyl and atrazine caused the fastest and most severe damage to DNA [97].

The interaction of DNA with drugs (Table 1) is among the important aspects of biological studies in drug discovery and pharmaceutical development processes [98]. There are several types of interactions associated with drugs that bind to DNA. These include intercalation, non-covalent groove binding, covalent binding (formation of DNA adducts), DNA cleaving, or nucleoside analog incorporation. Consequences of these binding interactions involve changes to both the DNA and

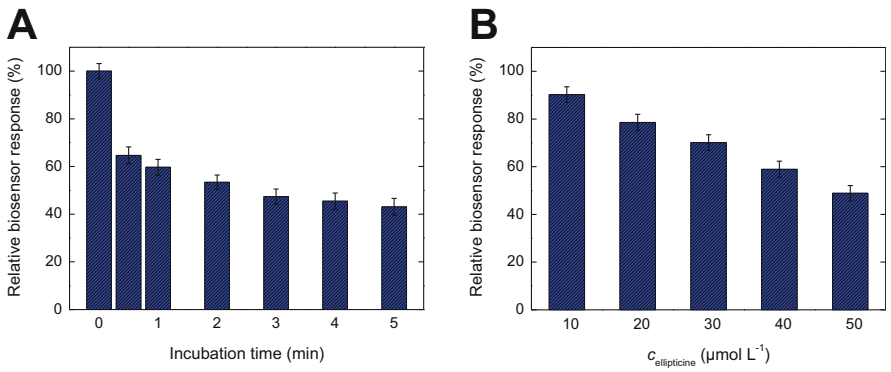

Fig. 4 (**a**) The relative biosensor responses to DNA damage caused by ellipticine, evaluated from the changes in the height of the anodic CV peak of 1×10^{-3} mol L^{-1} $[Fe(CN)_6]^{4-/3-}$ in 0.1 mol L^{-1} PB of pH 7.2 before and after incubation of the DNA-modified CFE in 0.1 mol L^{-1} PB of pH 7.2 containing 5×10^{-5} mol L^{-1} ellipticine for various times. (**b**) The relative biosensor responses to DNA damage caused by ellipticine, evaluated from the changes in the height of the anodic CV peak of 1×10^{-3} mol L^{-1} $[Fe(CN)_6]^{4-/3-}$ in 0.1 mol L^{-1} PB of pH 7.2 before and after 5 min incubation of the DNA-modified CFE in 0.1 mol L^{-1} PB of pH 7.2 containing various concentrations of ellipticine. For both (**a**) and (**b**), the *error bars* are constructed for the significance level of 0.05 ($n = 3$) [82]

drug molecules to accommodate complex formation. In many cases, changes to the structure of the DNA duplex result in altered thermodynamic stability and are manifested as changes in the functional properties of DNA [99]. Our study can serve as an example [82] where the damaging effect of an anticancer drug ellipticine was studied using CV performed at the DNA biosensor based on the CFE in the role of a transducer. The observed extent of dsDNA damage increased with the time of incubation of the biosensor in the solution containing ellipticine, as well as with the concentration of ellipticine present in the incubation solution (Fig. 4).

On the other hand, the investigated drug itself can successfully serve as a redox indicator in the detection of DNA damage. In our paper [35], simple electrochemical DNA biosensors composed of the SPCE and low molecular weight dsDNA recognition layer were reported and applied to the detection of damage to DNA by UV-C radiation and ROS produced by the Fenton-type reaction in model water samples, as well as in mineral water samples with additives. Complex DNA biosensor response was based on (1) SWV intrinsic signals of the guanine moiety, as well as that of the intercalative indicator thioridazine (an antipsychotic drug belonging to the phenothiazine drug group), (2) CV responses of the $[Fe(CN)_6]^{4-/3-}$ indicator in solution, and (3) EIS responses of the same redox indicator. For the last two types of measurements, the biosensor was also used with an interface between the SPCE and dsDNA formed by a composite of carboxylated SWCNTs and chitosan to enhance the transducer conductivity. Individual electrochemical/electrical signals

depended on the time of the biosensor incubation in a cleavage medium and their profiles characterized process of deep dsDNA degradation.

Also specific fraction of organic dyes (acridine, anthraquinone, etc.) belongs to the group of DNA intercalators (compounds able to interact with DNA through insertion of molecules with planar aromatic ring systems between DNA base pairs). For instance, acridine dyes have demonstrated to present mutagenic, carcinogenic, antibacterial, and antiviral properties [100]. Their similarity to several antibiotics, such as daunomycin or actinomycin, makes them interesting model systems for studying a variety of biophysicochemical problems [101]. Acridine derivatives initially bind (prior their intercalation between base pairs) to the minor groove of dsDNA through counterion displacement [102, 103].

Electrochemical DNA biosensors can be successfully used not only for the investigation of mutual interactions between xenobiotic compounds and DNA but also for the development of highly sensitive analytical methods utilizing a spontaneous accumulation of the analyte into the DNA structure (intercalation between the dsDNA base pairs) to increase the sensitivity of the determination [104]. Such a method was developed also in our laboratory for the DPV determination of genotoxic anthracene [105]: the limit of quantification of anthracene at the bare GCE was 2.2 μmol L^{-1}, while the limit of quantification of 0.15 μmol L^{-1} was reached at the DNA-modified GCE. The applicability of the method was furthermore successfully verified on model samples of gravel and sand, with the added/found recoveries of 98% and 96%, respectively.

3 Conclusions

It has been shown in this chapter that the DNA-modified electrodes (electrochemical DNA biosensors) already represent very effective and, at the same time, simple, fast, inexpensive, miniaturized, and mass-producible analytical devices for evaluation and classification of modes of genotoxic effects of individual xenobiotic compounds (e.g., chemical carcinogens, pesticides, drugs, dyes, or reactive radical species), as well as for prescreening of new drugs and newly synthesized chemicals. Moreover, the evaluation of DNA protection capacity of various natural and synthetic chemical substances (antioxidants) is also possible using the detection of DNA damage caused by prooxidants.

It can be expected that, in a near future, complex biorecognition layers utilizing various supramolecular interactions will be suggested to detect potentially risky compounds and to improve further abilities of biosensors to detect damage to DNA. The advanced level of medical and clinical diagnosis will be largely dependent on the successful development and implementation of new materials and technologies envisaging the fabrication of state-of-the-art biosensors. Attractive properties of electrochemical devices are thus extremely promising for improving the efficiency of environmental screening, diagnostic testing, and therapy monitoring.

For instance, one of the most important directions in the prospective development of DNA biosensors successfully applicable in practice can be seen in the investigation of protective membranes, which prevent the biosensor surface from unwanted fouling and interferences. One such an example is shown in our paper [47] where novel electrochemical DNA-based biosensors with outer-sphere Nafion and chitosan protective membranes were prepared for the evaluation of antioxidant properties of beverages (beer, coffee, and black tea) against prooxidant hydroxyl radicals.

Acknowledgments This publication originated in the framework of the Specific University Research (SVV). V.V. thanks the Grant Agency of the Czech Republic (Project GP13-23337P), and A.H. thanks the Grant Agency of the Charles University in Prague (Project GAUK 430214/2014/B-CH/PrF) for the financial support.

References

1. Paleček E, Bartošík M (2012) Electrochemistry of nucleic acids. Chem Rev 112 (6):3427–3481. doi:10.1021/cr200303p
2. Palecek E, Fojta M (2001) Detecting DNA hybridization and damage. Anal Chem 73 (3):74A–83A. doi:10.1021/ac0123936
3. Fojta M (2002) Electrochemical sensors for DNA interactions and damage. Electroanalysis 14(21):1449–1463. doi:10.1002/1521-4109(200211)14:21<1449::aid-elan1449>3.0.co;2-z
4. Erdem A (2007) Nanomaterial-based electrochemical DNA sensing strategies. Talanta 74 (3):318–325. doi:10.1016/j.talanta.2007.10.012
5. Rauf S, Gooding JJ, Akhtar K, Ghauri MA, Rahman M, Anwar MA, Khalid AM (2005) Electrochemical approach of anticancer drugs–DNA interaction. J Pharm Biomed Anal 37 (2):205–217. doi:10.1016/j.jpba.2004.10.037
6. Erdem A, Muti M, Papakonstantinou P, Canavar E, Karadeniz H, Congur G, Sharma S (2012) Graphene oxide integrated sensor for electrochemical monitoring of mitomycin C–DNA interaction. Analyst 137(9):2129–2135. doi:10.1039/c2an16011k
7. Fojta M (2005) Detecting DNA damage with electrodes. In: Paleček E, Scheller F, Wang J (eds) Electrochemistry of nucleic acids and proteins – towards electrochemical sensors for genomics and proteomics. Elsevier, Amsterdam, pp 385–431
8. Wang J, Rivas G, Cai X, Palecek E, Nielsen P, Shiraishi H, Dontha N, Luo D, Parrado C, Chicharro M, Farias PAM, Valera FS, Grant DH, Ozsoz M, Flair MN (1997) DNA electrochemical biosensors for environmental monitoring. A review. Anal Chim Acta 347(1–2):1–8. doi:10.1016/s0003-2670(96)00598-3
9. Mascini M, Palchetti I, Marrazza G (2001) DNA electrochemical biosensors. Fresenius J Anal Chem 369(1):15–22. doi:10.1007/s002160000629
10. Gooding JJ (2002) Electrochemical DNA hybridization biosensors. Electroanalysis 14 (17):1149–1156. doi:10.1002/1521-4109(200209)14:17<1149::aid-elan1149>3.0.co;2-8
11. Tosar JP, Brañas G, Laíz J (2010) Electrochemical DNA hybridization sensors applied to real and complex biological samples. Biosens Bioelectron 26(4):1205–1217. doi:10.1016/j.bios.2010.08.053
12. Labuda J, Oliveira-Brett AM, Evtugyn G, Fojta M, Mascini M, Ozsoz M, Palchetti I, Paleček E, Wang J (2010) Electrochemical nucleic acid-based biosensors: concepts, terms, and methodology (IUPAC technical report). Pure Appl Chem 82(5):1161–1187. doi:10.1351/pac-rep-09-08-16

13. Šimková D, Labuda J (2011) Electrochemical DNA biosensors and flow-through analysis. A review. Curr Anal Chem 7(1):2–7. doi:10.2174/157341111793797662
14. Chang HX, Wang Y, Li JH (2011) Electrochemical DNA sensors: from nanoconstruction to biosensing. Curr Org Chem 15(4):506–517. doi:10.2174/138527211794474500
15. Kimmel DW, LeBlanc G, Meschievitz ME, Cliffel DE (2012) Electrochemical sensors and biosensors. Anal Chem 84(2):685–707. doi:10.1021/ac202878q
16. Ozsoz M (2012) Electrochemical DNA biosensors. Pan Stanford, Singapore. doi:10.4032/9789814303989
17. Vyskočil V, Blašková M, Hájková A, Horáková E, Krejčová Z, Stávková K, Wang J (2012) Electrochemical DNA biosensors – useful diagnostic tools for the detection of damage to DNA caused by organic xenobiotics (a review). In: Kalcher K, Metelka R, Švancara I, Vytřas K (eds) Sensing in electroanalysis, vol 7. University Press Centre, Pardubice, pp 141–162
18. Labuda J, Vyskocil V (2014) DNA/electrode interface: detection of damage to DNA using DNA-modified electrodes. In: Kreysa G, Ota K, Savinell RF (eds) Encyclopedia of applied electrochemistry. Springer, New York, pp 346–350. doi:10.1007/978-1-4419-6996-5_259
19. Abu-Salah KM, Zourob MM, Mouffouk F, Alrokayan SA, Alaamery MA, Ansari AA (2015) DNA-based nanobiosensors as an emerging platform for detection of disease. Sensors 15 (6):14539–14568. doi:10.3390/s150614539
20. Fojta M, Daňhel A, Havran L, Vyskočil V (2015) Recent progress in electrochemical sensors and assays for DNA damage and repair. Trends Anal Chem. doi:10.1016/j.trac.2015.11.018
21. Cooke MS, Evans MD, Dizdaroglu M, Lunec J (2003) Oxidative DNA damage: mechanisms, mutation, and disease. FASEB J 17(10):1195–1214. doi:10.1096/fj.02-0752rev
22. Barzilai A, Yamamoto KI (2004) DNA damage responses to oxidative stress. DNA Repair 3 (8–9):1109–1115. doi:10.1016/j.dnarep.2004.03.002
23. Friedberg EC (2003) DNA damage and repair. Nature 421(6921):436–440. doi:10.1038/nature01408
24. Paleček E, Fojta M, Tomschik M, Wang J (1998) Electrochemical biosensors for DNA hybridization and DNA damage. Biosens Bioelectron 13(6):621–628. doi:10.1016/S0956-5663(98)00017-7
25. Vyskočil V, Labuda J, Barek J (2010) Voltammetric detection of damage to DNA caused by nitro derivatives of fluorene using an electrochemical DNA biosensor. Anal Bioanal Chem 397(1):233–241. doi:10.1007/s00216-010-3517-y
26. Oliveira-Brett AM, Vivan M, Fernandes IR, Piedade JAP (2002) Electrochemical detection of in situ adriamycin oxidative damage to DNA. Talanta 56(5):959–970. doi:10.1016/s0039-9140(01)00656-7
27. Abreu FC, Goulart MOF, Oliveira-Brett AM (2002) Detection of the damage caused to DNA by niclosamide using an electrochemical DNA-biosensor. Biosens Bioelectron 17 (11–12):913–919. doi:10.1016/s0956-5663(02)00082-9
28. Ni YN, Wang P, Kokot S (2012) Voltammetric investigation of DNA damage induced by nitrofurazone and short-lived nitro-radicals with the use of an electrochemical DNA biosensor. Biosens Bioelectron 38(1):245–251. doi:10.1016/j.bios.2012.05.034
29. Weng J, Zhang J, Li H, Sun L, Lin C, Zhang Q (2008) Label-free DNA sensor by boron-doped diamond electrode using an AC impedimetric approach. Anal Chem 80 (18):7075–7083. doi:10.1021/ac800610z
30. Švorc Ľ, Jambrec D, Vojs M, Barwe S, Clausmeyer J, Michniak P, Marton M, Schuhmann W (2015) Doping level of boron-doped diamond electrodes controls the grafting density of functional groups for DNA assays. ACS Appl Mater Interfaces 7(34):18949–18956. doi:10.1021/acsami.5b06394
31. Diculescu VC, Paquim AMC, Oliveira-Brett AM (2005) Electrochemical DNA sensors for detection of DNA damage. Sensors 5(6–10):377–393. doi:10.3390/s5060377
32. Vyskočil V, Barek J (2012) Voltammetric DNA biosensor based on a microcrystalline natural graphite–polystyrene composite transducer. Procedia Chem 6:52–59. doi:10.1016/j.proche.2012.10.130

33. Šmejkalová H, Vyskočil V (2014) Large-surface carbon film electrode – a simple sensor for voltammetric determination of electrochemically reducible organic compounds. Chem Listy 108(3):264–270
34. Yosypchuk B, Barek J, Fojta M (2006) Carbon powder based films on traditional solid electrodes as an alternative to disposable electrodes. Electroanalysis 18(11):1126–1130. doi:10.1002/elan.200503488
35. Hlavata L, Benikova K, Vyskocil V, Labuda J (2012) Evaluation of damage to DNA induced by UV-C radiation and chemical agents using electrochemical biosensor based on low molecular weight DNA and screen-printed carbon electrode. Electrochim Acta 71:134–139. doi:10.1016/j.electacta.2012.03.119
36. Lucarelli F, Marrazza G, Turner APF, Mascini M (2004) Carbon and gold electrodes as electrochemical transducers for DNA hybridisation sensors. Biosens Bioelectron 19 (6):515–530. doi:10.1016/s0956-5663(03)00256-2
37. Kerman K, Kobayashi M, Tamiya E (2004) Recent trends in electrochemical DNA biosensor technology. Meas Sci Technol 15(2):R1–R11. doi:10.1088/0957-0233/15/2/r01
38. Zima J, Švancara I, Barek J, Vytřas K (2009) Recent advances in electroanalysis of organic compounds at carbon paste electrodes. Crit Rev Anal Chem 39(3):204–227. doi:10.1080/10408340903011853
39. Wang J, Cai XH, Jonsson C, Balakrishnan M (1996) Adsorptive stripping potentiometry of DNA at electrochemically pretreated carbon paste electrodes. Electroanalysis 8(1):20–24. doi:10.1002/elan.1140080105
40. Wang J, Cai XH, Rivas G, Shiraishi H, Dontha N (1997) Nucleic-acid immobilization, recognition and detection at chronopotentiometric DNA chips. Biosens Bioelectron 12 (7):587–599. doi:10.1016/s0956-5663(96)00076-0
41. Hájková A, Barek J, Vyskočil V (2015) Voltammetric determination of 2-aminofluoren-9-one and investigation of its interaction with DNA on a glassy carbon electrode. Electroanalysis 27(1):101–110. doi:10.1002/elan.201400427
42. Blašková M, Vyskočil V (2014) Simple electrochemical biosensor for comprehensive detection of DNA damage by chemical carcinogens. Chem Listy 108(S4):S211–S215
43. Stávková K, Vyskočil V (2014) Electrochemical research on supramolecular interactions of DNA with genotoxic 2-nitrofluorene. Chem Listy 108(S4):S262–S265
44. Oliveira-Brett AM, Serrano SHP, Gutz I, La-Scalea MA, Cruz ML (1997) Voltammetric behavior of nitroimidazoles at a DNA-biosensor. Electroanalysis 9(14):1132–1137. doi:10.1002/elan.1140091419
45. Oliveira-Brett AM, Macedo TRA, Raimundo D, Marques MH, Serrano SHP (1998) Voltammetric behaviour of mitoxantrone at a DNA-biosensor. Biosens Bioelectron 13 (7–8):861–867. doi:10.1016/s0956-5663(98)00053-0
46. Labuda J, Bučková M, Vaníčková M, Mattusch J, Wennrich R (1999) Voltammetric detection of the DNA interaction with copper complex compounds and damage to DNA. Electroanalysis 11(2):101–107. doi:10.1002/(sici)1521-4109(199902)11:2<101::aid-elan101>3.0.co;2-v
47. Hlavatá L, Vyskočil V, Beníková K, Borbélyová M, Labuda J (2014) DNA-based biosensors with external Nafion and chitosan membranes for the evaluation of the antioxidant activity of beer, coffee, and tea. Cent Eur J Chem 12(5):604–611. doi:10.2478/s11532-014-0516-4
48. Hashimoto K, Ito K, Ishimori Y (1994) Novel DNA sensor for electrochemical gene detection. Anal Chim Acta 286(2):219–224. doi:10.1016/0003-2670(94)80163-0
49. Pang DW, Abruña HD (1998) Micromethod for the investigation of the interactions between DNA and redox-active molecules. Anal Chem 70(15):3162–3169. doi:10.1021/ac980211a
50. Wang SF, Xie F, Hu RF, Cai HC (2006) The determination of nonelectroactive anticancer drug 6-thioguanine on DNA-modified gold electrode. Anal Lett 39(6):1041–1052. doi:10.1080/00032710600620328

51. Paleček E, Boublíková P, Jelen F (1986) Cyclic voltammetry of nucleic acids and determination of submicrogram quantities of deoxyribonucleic acids by adsorptive stripping voltammetry. Anal Chim Acta 187:99–107. doi:10.1016/s0003-2670(00)82902-5
52. Paleček E (1996) From polarography of DNA to microanalysis with nucleic acid-modified electrodes. Electroanalysis 8(1):7–14. doi:10.1002/elan.1140080103
53. Fojta M, Paleček E (1997) Supercoiled DNA-modified mercury electrode: a highly sensitive tool for the detection of DNA damage. Anal Chim Acta 342(1):1–12. doi:10.1016/s0003-2670(96)00551-x
54. Wang J (2005) Carbon-nanotube based electrochemical biosensors: a review. Electroanalysis 17(1):7–14. doi:10.1002/elan.200403113
55. Wang J (2005) Nanomaterial-based amplified transduction of biomolecular interactions. Small 1(11):1036–1043. doi:10.1002/smll.200500214
56. Trojanowicz M (2006) Analytical applications of carbon nanotubes: a review. Trends Anal Chem 25(5):480–489. doi:10.1016/j.trac.2005.11.008
57. Balasubramanian K, Burghard M (2006) Biosensors based on carbon nanotubes. Anal Bioanal Chem 385(3):452–468. doi:10.1007/s00216-006-0314-8
58. Kim SN, Rusling JF, Papadimitrakopoulos F (2007) Carbon nanotubes for electronic and electrochemical detection of biomolecules. Adv Mater 19(20):3214–3228. doi:10.1002/adma.200700665
59. Guo SJ, Wang EK (2007) Synthesis and electrochemical applications of gold nanoparticles. Anal Chim Acta 598(2):181–192. doi:10.1016/j.aca.2007.07.054
60. Pumera M, Sánchez S, Ichinose I, Tang J (2007) Electrochemical nanobiosensors. Sens Actuators B 123(2):1195–1205. doi:10.1016/j.snb.2006.11.016
61. Shao YY, Wang J, Wu H, Liu J, Aksay IA, Lin YH (2010) Graphene based electrochemical sensors and biosensors: a review. Electroanalysis 22(10):1027–1036. doi:10.1002/elan.200900571
62. Kuila T, Bose S, Khanra P, Mishra AK, Kim NH, Lee JH (2011) Recent advances in graphene-based biosensors. Biosens Bioelectron 26(12):4637–4648. doi:10.1016/j.bios.2011.05.039
63. Pumera M (2011) Graphene in biosensing. Mater Today 14(7–8):308–315. doi:10.1016/S1369-7021(11)70160-2
64. Galandova J, Ziyatdinova G, Labuda J (2008) Disposable electrochemical biosensor with multiwalled carbon nanotubes–chitosan composite layer for the detection of deep DNA damage. Anal Sci 24(6):711–716. doi:10.2116/analsci.24.711
65. Rusling JF (2005) Sensors for genotoxicity and oxidized DNA. In: Paleček E, Scheller F, Wang J (eds) Electrochemistry of nucleic acids and proteins – towards electrochemical sensors for genomics and proteomics. Elsevier, Amsterdam, pp 433–450
66. Blašková M (2012) Novel electrochemical biosensor for the detection of DNA damage caused by chemical carcinogens. B.Sc. thesis, Charles University in Prague, Prague
67. Guan JG, Miao YQ, Zhang QJ (2004) Impedimetric biosensors. J Biosci Bioeng 97(4):219–226. doi:10.1016/s1389-1723(04)70195-4
68. Ziyatdinova G, Labuda J (2011) Complex electrochemical and impedimetric evaluation of DNA damage by using DNA biosensor based on a carbon screen-printed electrode. Anal Methods 3(12):2777–2782. doi:10.1039/c1ay05403a
69. Paleček E, Jelen F (2005) Electrochemistry of nucleic acids. In: Paleček E, Scheller F, Wang J (eds) Electrochemistry of nucleic acids and proteins – towards electrochemical sensors for genomics and proteomics. Elsevier, Amsterdam, pp 74–174
70. Oliveira-Brett AM, Matysik FM (1997) Voltammetric and sonovoltammetric studies on the oxidation of thymine and cytosine at a glassy carbon electrode. J Electroanal Chem 429(1–2):95–99. doi:10.1016/S0022-0728(96)05018-8
71. Oliveira-Brett AM, Piedade JAP, Silva LA, Diculescu VC (2004) Voltammetric determination of all DNA nucleotides. Anal Biochem 332(2):321–329. doi:10.1016/j.ab.2004.06.021

72. Švorc Ľ, Kalcher K (2014) Modification-free electrochemical approach for sensitive monitoring of purine DNA bases: simultaneous determination of guanine and adenine in biological samples using boron-doped diamond electrode. Sens Actuators B 194:332–342. doi:10.1016/j.snb.2013.12.104
73. Paleček E (2002) Past, present and future of nucleic acids electrochemistry. Talanta 56 (5):809–819. doi:10.1016/s0039-9140(01)00649-x
74. Oliveira-Brett AM, Piedade JAP, Serrano SHP (2000) Electrochemical oxidation of 8-oxoguanine. Electroanalysis 12(12):969–973. doi:10.1002/1521-4109(200008)12:12<969::aid-elan969>3.0.co;2-o
75. Oliveira SCB, Corduneanu O, Oliveira-Brett AM (2008) In situ evaluation of heavy metal–DNA interactions using an electrochemical DNA biosensor. Bioelectrochemistry 72 (1):53–58. doi:10.1016/j.bioelechem.2007.11.004
76. Galandová J, Ovádeková R, Ferancová A, Labuda J (2009) Disposable DNA biosensor with the carbon nanotubes–polyethyleneimine interface at a screen-printed carbon electrode for tests of DNA layer damage by quinazolines. Anal Bioanal Chem 394(3):855–861. doi:10.1007/s00216-009-2740-x
77. Labuda J, Ovádeková R, Galandová J (2009) DNA-based biosensor for the detection of strong damage to DNA by the quinazoline derivative as a potential anticancer agent. Microchim Acta 164(3–4):371–377. doi:10.1007/s00604-008-0068-4
78. Carter MT, Rodriguez M, Bard AJ (1989) Voltammetric studies of the interaction of metal chelates with DNA. 2. Tris-chelated complexes of cobalt(III) and iron(II) with 1,10-phenanthroline and 2,2′-bipyridine. J Am Chem Soc 111(24):8901–8911. doi:10.1021/ja00206a020
79. Hájková A, Vyskočil V (2014) Novel voltammetric biosensor for the detection of DNA damage caused by amino derivatives of fluorene. In: Hrouzková S, Májek P (eds) Analytical chemistry in practice 2014, Bratislava, 1–4 June 2014, pp 75–76
80. Vyskočil V, Labuda J, Barek J (2009) Damaging effects of genotoxic fluorene derivatives on DNA detected voltammetrically using an electrochemical DNA biosensor. In: Hudská V (ed) Prague–Dresden electrochemical seminar, Červený Hrádek, Jirkov, 23–25 Nov 2009, pp 32–33
81. Jurečková Z (2013) Novel electrochemical biosensor for the detection of DNA damage based on a large-surface carbon film electrode. B.Sc. thesis, Charles University in Prague, Prague
82. Hrochová Z (2013) Novel voltammetric DNA biosensor for the detection of the DNA damage caused by oncological drugs. B.Sc. thesis, Charles University in Prague, Prague
83. Jurečková Z (2015) Detection of oxidative stress using electrochemical DNA biosensors. M. Sc. thesis, Charles University in Prague, Prague
84. Schärer OD (2003) Chemistry and biology of DNA repair. Angew Chem Int Ed 42 (26):2946–2974. doi:10.1002/anie.200200523
85. Turesky RJ (2002) Heterocyclic aromatic amine metabolism, DNA adduct formation, mutagenesis, and carcinogenesis. Drug Metab Rev 34(3):625–650. doi:10.1081/dmr-120005665
86. Speit G, Henderson L (2005) Review of the in vivo genotoxicity tests performed with styrene. Mutat Res Rev Mutat Res 589(1):67–79. doi:10.1016/j.mrrev.2004.10.001
87. Zhang Y, Hu NF (2007) Cyclic voltammetric detection of chemical DNA damage induced by styrene oxide in natural dsDNA layer-by-layer films using methylene blue as electroactive probe. Electrochem Commun 9(1):35–41. doi:10.1016/j.elecom.2006.08.032
88. Liao TL, Wang YF, Zhou XB, Zhang Y, Liu XH, Du J, Li XJ, Lu XQ (2010) Detection of DNA damage induced by styrene oxide in dsDNA layer-by-layer films using adriamycin as electroactive probe. Colloids Surf B 76(1):334–339. doi:10.1016/j.colsurfb.2009.11.016
89. Zu Y, Hu NF (2009) Electrochemical detection of DNA damage induced by in situ generated styrene oxide through enzyme reactions. Electrochem Commun 11(10):2068–2070. doi:10.1016/j.elecom.2009.08.055
90. Vodicka P, Koskinen M, Arand M, Oesch F, Hemminki K (2002) Spectrum of styrene-induced DNA adducts: the relationship to other biomarkers and prospects in human

biomonitoring. Mutat Res Rev Mutat Res 511(3):239–254. doi:10.1016/s1383-5742(02)00012-1
91. Rice-Evans CA, Miller NJ, Paganga G (1996) Structure-antioxidant activity relationships of flavonoids and phenolic acids. Free Radic Biol Med 20(7):933–956. doi:10.1016/0891-5849(95)02227-9
92. Ohshima H, Yoshie Y, Auriol S, Gilibert I (1998) Antioxidant and pro-oxidant actions of flavonoids: effects on DNA damage induced by nitric oxide, peroxynitrite and nitroxyl anion. Free Radic Biol Med 25(9):1057–1065. doi:10.1016/s0891-5849(98)00141-5
93. Johnson MK, Loo G (2000) Effects of epigallocatechin gallate and quercetin on oxidative damage to cellular DNA. Mutat Res DNA Repair 459(3):211–218. doi:10.1016/s0921-8777(99)00074-9
94. Labuda J, Bučková M, Heilerová L, Šilhár S, Štepánek I (2003) Evaluation of the redox properties and anti/pro-oxidant effects of selected flavonoids by means of a DNA-based electrochemical biosensor. Anal Bioanal Chem 376(2):168–173. doi:10.1007/s00216-003-1884-3
95. Korbut O, Bučková M, Labuda J, Gründler P (2003) Voltammetric detection of antioxidative properties of flavonoids using electrically heated DNA modified carbon paste electrode. Sensors 3(1):1–10. doi:10.3390/s30100001
96. Sassolas A, Prieto-Simón B, Marty JL (2012) Biosensors for pesticide detection: new trends. Am J Anal Chem 3(3):210–232. doi:10.4236/ajac.2012.33030
97. Nowicka AM, Kowalczyk A, Stojek Z, Hepel M (2010) Nanogravimetric and voltammetric DNA-hybridization biosensors for studies of DNA damage by common toxicants and pollutants. Biophys Chem 146(1):42–53. doi:10.1016/j.bpc.2009.10.003
98. Erdem A, Ozsoz M (2002) Electrochemical DNA biosensors based on DNA–drug interactions. Electroanalysis 14(14):965–974. doi:10.1002/1521-4109(200208)14:14<965::aid-elan965>3.0.co;2-u
99. Graves DE, Velea LM (2000) Intercalative binding of small molecules to nucleic acids. Curr Org Chem 4(9):915–929. doi:10.2174/1385272003375978
100. Belmont P, Bosson J, Godet T, Tiano M (2007) Acridine and acridone derivatives, anticancer properties and synthetic methods: where are we now? Anticancer Agents Med Chem 7(2):139–169. doi:10.2174/187152007780058669
101. Wheate NJ, Brodie CR, Collins JG, Kemp S, Aldrich-Wright JR (2007) DNA intercalators in cancer therapy: organic and inorganic drugs and their spectroscopic tools of analysis. Mini Rev Med Chem 7(6):627–648. doi:10.2174/138955707780859413
102. Crenshaw JM, Graves DE, Denny WA (1995) Interactions of acridine antitumor agents with DNA: binding energies and groove preferences. Biochemistry 34(41):13682–13687. doi:10.1021/bi00041a050
103. Farias PAM, Wagener ADR, Castro AA, Bastos MBR (2005) Adsorptive stripping voltammetric behavior of acridine orange at the static mercury drop electrode. Anal Lett 38(10):1601–1610. doi:10.1081/al-200065796
104. Ferancová A, Bucková M, Korgová E, Korbut O, Gründler P, Wärnmark I, Štepán R, Barek J, Zima J, Labuda J (2005) Association interaction and voltammetric determination of 1-aminopyrene and 1-hydroxypyrene at cyclodextrin and DNA based electrochemical sensors. Bioelectrochemistry 67(2):191–197. doi:10.1016/j.bioelechem.2004.06.007
105. Blašková M, Hájková A, Vyskočil V (2015) Voltammetric determination of anthracene using a DNA-modified glassy carbon electrode. Chem Listy 109(3):235–240

BIOREV (2017) 6: 223–262
DOI: 10.1007/11663_2015_5001

Published online: 1 March 2016

Recent Advances in the Study of Electrochemistry of Redox Proteins

Preety Vatsyayan

Abstract Redox proteins constitute a diverse class of proteins that facilitate the chemical and biological processes which are otherwise thermodynamically challenging. Efficient catalysis, diversity of biotransformation, potent redox centres and fast electron transport kinetics make these redox proteins an interesting target for electrochemical investigation for both theoretical and practical implications. The first and foremost requirement for electrochemical studies of redox proteins is to create an environment where they could interact with the electrodes either directly or via electron transport mediators. The last few years have seen a tremendous development in this field ranging from the increase in diversity of redox proteins that could possibly be studied electrochemically to their efficient immobilisation in a variety of matrices especially nanomatrices. Major advances have also been made in the area of characterisation of fabricated bioelectrodes by using different spectroscopic and microscopic techniques supplementing the electrochemical findings. This chapter will focus mainly on the aforementioned recent developments in the field of electrochemical studies of redox proteins and their applications for studies of redox mechanism or as biosensors or biofuel cells.

Keywords Biofuel cell • Biosensor • Immobilisation • Protein structure–function • Redox proteins

Contents

P. Vatsyayan (✉)
Institute of Analytical Chemistry, Chemo- and Biosensors, University of Regensburg, 93053 Regensburg, Germany
e-mail: preety.vatsyayan@chemie.uni-regensburg.de

Abbreviations

ACNTs	Aligned carbon nanotubes
AFM	Atomic force microscopy
ArO	Arsenite oxidase
AuNPs/NWs	Gold nanoparticles/nanowires
Az	Azurin
CAT	Large catalase
cbo3	Cytochrome bo3
CcO	Cytochrome c oxidase
ChOx	Cholesterol oxidase
CV	Cyclic voltammetry
CYP	Cytochrome P450
cyt c	Cytochrome c
D/ET	Direct/electron transfer
DDAB	Didodecyldimethylammonium bromide
EFCs	Enzymatic fuel cells
EIS	Electrochemical impedance spectroscopy
FAD	Flavin adenine dinucleotide
FT/IR	Fourier transform/infrared
GCE	Glassy carbon electrode
GOx	Glucose oxidase
Hb	Haemoglobin
HRTEM	High-resolution transmission electron microscopy
hSO	Human sulphite oxidase
k_s/k_{ET}	Electron transfer rate constant
M/SWCNTs	Multi/single-walled carbon nanotubes
MP-11	Microperoxidase-11
MW	Molecular weight
NADH	Nicotinamide adenine dinucleotide
NapAB	Nitrate reductase
NF	Nafion®
PANI-NTs	Polyaniline nanotubes
PEI	Polyethyleneimine

PFV	Protein film voltammetry
PGE	Pyrolytic graphite edge
QCM	Quartz crystal microbalance
R_{ct}	Charge transfer resistance
SAM	Self-assembled monolayer
SCE	Saturated calomel electrode
SEM	Scanning electron microscopy
SHE	Standard hydrogen electrode
SPR	Surface plasmon resonance
tBLMs	Tethered bilayer membranes

1 Introduction

Redox proteins are a class of biological molecules responsible for many important functions in living organisms. They act as mediators for electron flow to cover the energy gap between source and sink in respiratory or photosynthetic chains, e.g. cytochromes, plastoquinones, etc. [1]. Some of them act as biological catalysts facilitating oxidation and reduction of a substrate or a group of substrates with the addition or removal of a proton (H^+) or electron (e^-). Enzymes mostly included in this class are dehydrogenases, oxidases, peroxidases, etc. which carry out reactions ranging from oxidation of glucose to detoxification of xenobiotics inside the living cells [2]. Another group of redox proteins is involved in transfer of O_2 inside the blood and muscles (e.g. haemoglobin and myoglobin). Thus redox proteins constitute a diverse class of proteins that facilitate the chemical and biological processes that are otherwise thermodynamically challenging. Most of these proteins contain metals especially first-row transition metals alone or in a prosthetic group as their redox-active centres, e.g. iron in cytochromes, copper in cupredoxins, zinc in nucleases and transcription factors, etc. to name a few [3]. Sometimes they require cofactors such as flavins or quinones as their redox partners, e.g. glucose oxidase (GOx) and plastoquinone, respectively. Efficient catalysis, diversity of biotransformation, potent redox centres and fast electron transport kinetics make these redox proteins an interesting target for electrochemical investigation for both theoretical and practical implications [4–7].

The first and foremost requirement for electrochemical studies of redox proteins is to create an environment where they could interact with the electrodes either directly or via electron transport mediators. This could be achieved either in solution or by confinement of proteins onto electrodes by immobilisation or wiring. Although, electrochemical studies of redox proteins in solution are relatively simple and have been practised since the 1970s [8, 9], they are mostly limited by various factors, e.g. the tendency of proteins to adsorb and denature at electrode surfaces, their diffusional limitation because of their large sizes compared to other chemical molecules in the solution, slower in and out electron flow due to the deeply buried redox centres inside the protein matrices and their dilution in solution

compared to when they are confined to electrode surfaces. Immobilisation of redox proteins for electrochemical studies is normally done to overcome the limitations faced in solution studies. The immobilisation of proteins over electrodes also paves the way towards their miniaturisation for practical applications such as biosensors or biofuel cells. The recent studies related to electrochemistry of redox proteins largely focus on their immobilisation in suitable matrices or wiring over the electrode surfaces to maintain their structural integrity and orientation for stable and efficient electron transfer [10, 11].

The field of electrochemical studies of redox proteins from its theory to application has been extensively reviewed and documented since its inception in 1970s [4–7, 12–19]. The last few years have seen a tremendous development in this field ranging from the diversity of proteins (small to large, monomeric to multimeric, cytoplasmic to membrane bound, simple to complex) that could possibly be studied electrochemically to their efficient immobilisation in a variety of matrices especially nanomatrices. Major advances have also been made in the areas of characterisation of fabricated bioelectrodes and their applications for studies of redox mechanism or as biosensors or biofuel cells. This chapter will focus mainly on the aforementioned recent developments in the field of electrochemical studies of redox proteins with a brief discussion over the theory and instrumentation required to understand the context.

2 Instrumentation/Theory

Electrochemical study of redox proteins starts with the selection of an electrode/transducer surface that can act as a source/sink for electrons in the redox cycle. It also provides a surface for capturing redox proteins in protein film voltammetry (PFV) or for modification by different techniques of protein immobilisation. The electrode material should be chemically inert, non-toxic to biological processes and conductive to support efficient electron transfer. The commonly used electrodes for protein electrochemical studies are either metallic (Au, Pt, Ag) or made up of carbon (graphite, glassy carbon, etc.) [12, 20]. Metal surfaces especially gold are frequently used on which a monolayer of adsorbate can easily be self-assembled (SAM). The adsorbates are usually bifunctional molecules such as $X\text{-}(CH_2)_n\text{-}Y$, where X is a substituent that anchors the molecule on the metal electrode surface (e.g. a thiol) and Y is a functional group (typically carboxyl for basic proteins like cytochrome c or amine for acidic proteins such as plastocyanin or ferredoxins) which forms amide bonds with proteins via carbodiimide coupling. Other metals such as platinum, silver and sometimes nickel are also used as electrode materials. Graphite is also among the most frequently used electrode materials on which rapid and reversible electrochemistry of redox proteins is often observed even without surface modifications. One such graphite electrode is pyrolytic graphite (PG) which is formed by the deposition of carbon from the vapour phase and has a crystalline structure. It provides two highly distinctive types of surfaces depending upon the

plane along which it is cleaved – edge or basal. Edge or basal plane PG electrodes provide surfaces for hydrophilic or hydrophobic interactions, respectively. The electrode surfaces can also be modified to provide other functional groups for protein cross-linking or adsorption.

The electrochemical experiments of redox proteins are usually carried out using an electrochemical analyser or potentiostat in conjunction with the cell. The cell consists of mainly three electrodes: reference, working and auxiliary or counter electrode. The analyser measures the current registered in response to the potential that is applied. In general, the potential of the working electrode (vs. the reference electrode) is modulated (e.g. in a linear sweep), and the current between the working electrode and the counter electrode is recorded. It is the working electrode where the redox protein is immobilised and/or its redox properties are studied.

Cyclic voltammetry (*CV*) is the most popular method for studying redox protein electrochemistry. The electrode potential is swept forward and backward with a scan rate (in units of V s^{-1}), and a voltammogram is generated which is a plot of current against electrode potential. CV is extensively used to evaluate the electron transfer properties of redox proteins for their thermodynamic, kinetic and mechanistic information. Ideally at slow scan rates for thin film of proteins over the electrode, the CVs are predicted to have symmetric oxidation and reduction peaks with both peak potentials at the formal potential ($E^{\circ\prime}$), and the oxidation–reduction peak separation (ΔE_p) equals to zero. The surface coverage (Γ) of redox protein over the electrode is described by the equation, $\Gamma = Q/nFA$, where Q is charge obtained by integrating the peak current area, n is number of electrons transferred, F is Faraday's constant and A is the electrode area. When the ideal thin-layer protein film model is followed, results of ΔE_p vs. scan rate can be used to estimate the surface electron transfer rate constant k_s (s^{-1}) [16, 20, 21].

Electrochemical impedance spectroscopy (*EIS*) is a valuable tool for characterising surface modifications during immobilisation of biomolecules over the transducer surface [22]. The biological component is generally immobilised on the working electrode with layer/s of immobilisation matrix. This alters the resistive or capacitive properties of the electrode. For EIS studies, a low-amplitude *AC* potential is applied through the cell, and the interaction of modified electrode with a redox analyte in the solution is measured over a wide range of frequencies to generate an impedance spectrum. The data can be plotted in different forms such as Nyquist plot, Cole–Cole plot, etc. The immobilisation layers over the working electrode result in a well-defined charge transfer resistance R_{ct} or impedance Z, e.g. a blocking layer will cause increase in R_{ct} and vice versa.

Catalytic protein voltammetry and chronoamperometry are generally used to characterise the electrochemical activity of redox proteins [16, 20]. In the absence of substrate and at sufficiently high surface coverage, a redox protein immobilised onto an electrode gives peak-like signals resulting from the reversible transformation of its redox centres. However, upon addition of substrate, the non-turnover peaks are transformed to sizeable catalytic waves. Reaction with substrate transforms the active site, which is regenerated by electron exchange with the electrode in a succession of catalytic cycles. The magnitude of the current is proportional to

electroactive coverage and to turnover rate, and so the relationship between potential and catalytic activity is traced in a single voltammetric experiment. Alternatively, in an experiment called chronoamperometry, the electrode potential is held at a fixed value, and the current is recorded as a function of time with increasing/decreasing substrate/inhibitor concentrations.

Besides above-mentioned classical electrochemical techniques, many other microscopic and spectroscopic techniques are routinely used for bioelectrode characterisation which help to fortify the electrochemical findings. Microscopic techniques especially atomic force microscopy (AFM), scanning electron microscopy (SEM), transmission electron microscopy (TEM), etc. are largely used to image surface topography of electrodes after immobilisation of redox proteins in different matrices [23–25]. Electronic absorption spectroscopy has been used for long time to study redox protein interactions with immobilisation matrices [26, 27]. Recently different forms of vibrational spectroscopy such as infrared (IR), Raman, etc. are used frequently to characterise immobilisation matrices and to study their interactions with redox proteins [25, 26]. With the onset of the use of nanomaterials such as gold nanoparticles (AuNPs), it is now possible to characterise the AuNP-modified redox proteins or electrodes with surface plasmon resonance (SPR) [28]. Gravimetric technique like quartz crystal microbalance (QCM) is used to calculate the surface coverage of immobilised redox proteins over the electrode by measuring the change in frequency of crystal [24]. Elaborating on the principles of all these techniques is out of context for this chapter, but their usages for bioelectrode characterisation or as supporting evidence for electrochemical studies have been included wherever applicable in the following sections.

3 Immobilisation of Redox Proteins

Proteins being biological macromolecules are highly sensitive to rapid denaturation once isolated from the natural environment/living cells and have a small shelf life in solution at room temperature. The effect of immobilisation on improvement of enzyme activity, stability and selectivity has long been established for industrial applications and has been reviewed [29]. For electrochemical studies also immobilisation of redox proteins over electrode surfaces helps to overcome many of the limitations faced in solution studies. Many a times, immobilising a redox protein on an electrode is the only way to study them electrochemically. Besides, immobilisation of proteins also enhances the probability of electrodes to act as their redox partners for direct electron transfer (DET) which helps in better understanding of protein electrochemistry. Although, it adds additional steps to find suitable matrices and to develop strategies for immobilisation of different proteins that provide maximum stability and efficiency over the electrode surfaces, the benefits achieved later make it worth pursuing. Most of the immobilisation techniques discussed here facilitate direct electron transfer between redox proteins and electrodes.

3.1 To Mimic the Natural Environment

Immobilisation of proteins in suitable matrices sometimes mimics their natural environment and enhances their structural and functional stability. Membrane-associated proteins form a large class of redox proteins and are frequently involved in respiratory electron transport chains and photosystems besides other functions in living cells. They are usually large in size with hydrophobic patches and tend to lose their structural integrity and activity once brought into the solution [30]. As a result, the electrochemical studies with membrane proteins especially integral membrane proteins have made significantly less progress compared to globular proteins.

Lipid films are widely used to mimic the bilayer structure of membrane over the electrodes for immobilisation of membrane-associated redox proteins. They impart structural stability and also preserve the conformational freedom of macromolecules for their function [31, 32]. Besides, lipid films also protect the solid support from undesirable interferences and thus minimise redox processes at the electrode surface. The power of lipid films was realised long back when a reversible electrochemistry for cytochrome P450cam was observed for a month with only 10% decrease in activity after immobilisation in dimyristoylphosphatidylcholine (DMPC) films [33]. In solution the activity degraded completely in less than a day. The redox proteins can be incorporated into the lipid films either by dissolution of the protein molecules in the lipid solution from which the film is prepared or by immobilisation of the protein on the lipid film surface.

A recent review by Khan et al. [34] provides detailed insight into the engineering of lipid bilayers over different electrode materials for protein immobilisation and their electrochemical studies. Jeuken [31] summarised different strategies for bilayer assembly over metal (gold and silver) or graphite electrodes for electrochemical studies of cytochrome c oxidase (CcO), a representative protein for integral membrane-bound proteins. CcO was incorporated either into a hybrid bilayer membrane (consisting of SAM of alkane thiols over a metal electrode and a phospholipid monolayer) or in a pure phospholipid bilayer. The pure phospholipid bilayer was either directly adsorbed on the electrode or tethered to the electrode surface with lipid thiols (tethered bilayer membranes, tBLMs). In another approach, histidine-tagged CcO was tethered to the electrode by Ni–nitrilotriacetic acid (thiol modified) affinity system, and then the phospholipid bilayer was reconstituted around the tethered protein. In hybrid bilayer and directly adsorbed lipid bilayer, the thin water layer between electrode and bilayer was not sufficient to prevent direct interaction of transmembrane proteins with electrode surface resulting in their direct adsorption at the electrode and denaturation [34]. In case of tBLMs, the space between the electrode and the lower leaflet of lipid bilayer was used for the incorporation of a hydrophilic spacer. The spacer in turn avoided the direct interaction of proteins with the electrode surface and their subsequent denaturation.

The tBLM approach was successfully used to immobilise cytochrome bo3 (cbo3), a ubiquinol oxidase from *Escherichia coli* [35]. The tBLM was formed on gold surface functionalised with cholesterol tethers which inserted itself into the

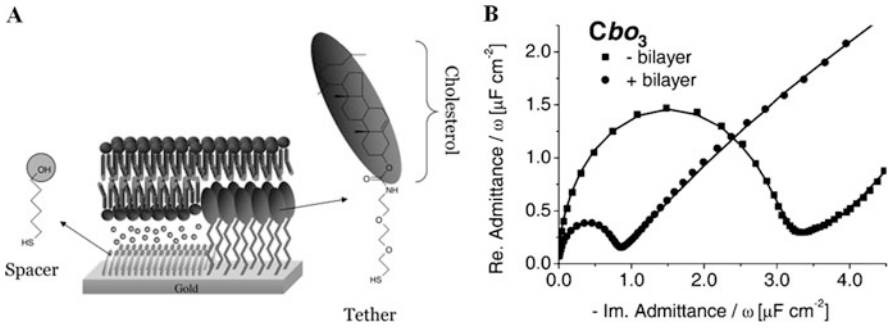

Fig. 1 (**A**) Schematic representation of a tBLM formed on a mixed self-assembled monolayer of tether (cholesterol) and spacer molecules (6-mercaptohexanol). (**B**) Cole–Cole plots for cbo3 before and after formation of a tBLM measured at 0 V vs. SCE. Adapted with permission from [35]. Copyright (2006) American Chemical Society

lower leaflet of the membrane (Fig. 1A). 6-Mercaptohexanol was used as the hydrophilic spacer. The planar membrane architecture was formed by self-assembly of proteoliposomes, and its structure was characterised electrochemically by EIS. Normally, the double-layer capacitance of an ideal phospholipid bilayer should be around 0.5 μF cm^{-2}. A drastic increase in the capacitance is generally caused by some disorder or defect in the bilayer. Incorporation of a protein also increases the capacitance values, as a result of the higher dielectric constant and disorder in the bilayer. As shown in Fig. 1B, the double-layer capacitance of the tBLMs on gold electrode was around 0.7–0.8 μF cm^{-2} which was only slightly larger than that of the ideal and was almost the same both in the absence (figure not shown) and presence of cbo3. These results showed that the inclusion of cbo3 had almost no effect on the double-layer capacitance of the tethered membrane and did not induce large defects in the tethered bilayer. The functionality of tBLM-immobilised cbo3 was investigated by CV and was confirmed by catalytic reduction of O_2.

Surfactant cast films are also one of the frequently used immobilisation techniques for membrane-bound redox proteins. Surfactants are surface-active agents with a charged or polar head group and a nonpolar tail similar to naturally occurring lipids. Stable films can be cast from surfactants that are insoluble in water and do not form micelles. Molecules fulfilling these requirements have ionic or zwitterionic head groups and two or more hydrocarbon tails of 12 carbons or longer, e.g. didodecyldimethylammonium bromide (DDAB), dihexadecylphosphate (DHP), sodium dodecyl sulphate (SDS), etc. Similar to the incorporation of protein in lipid films, the redox protein is either taken up by the surfactant film already casted on the electrode or a mixture of protein and surfactant is co-casted on the electrode.

The discussion over electrochemical studies of membrane-bound redox proteins is incomplete without a mention of cytochrome P450 (CYP). CYP is one of the most important redox proteins which needs to be studied electrochemically for both

theoretical and practical applications. It is a class of monooxygenase enzymes which are used for synthesis of industrially important compounds as well as for detoxification of drugs and xenobiotics [36]. Thus it has both industrial and pharmaceutical applications. However, multiple attempts to replicate this enzyme system in vitro have been only marginally successful owing to the structural instability of CYP after membrane solubilisation and the intricate electron transfer machinery required for its catalysis. Although, the electrochemical methods are perhaps the simplest way of providing reducing equivalents to the catalytic cycle of CYP [37], the immobilisation of CYP over electrodes to retain its functional activity still remains tricky. Udit et al. [26] reported electrochemical measurements of CYP BM3 (from *Bacillus megaterium*) in DDAB surfactant films on basal plane graphite electrodes. At slow scan rates, a well-defined, chemically reversible redox couple centred at −260 mV (vs. saturated calomel electrode, SCE) was observed. This redox couple was assigned to the heme $Fe^{III/II}$ process. Thus, DDAB films facilitate electronic coupling between heme proteins and electrodes for direct electrochemistry. However, electrode-driven oxidative substrate catalysis was not observed, possibly due to conversion of P450 into P420 like structures in DDAB films. Recently, the same group used DDAB films for the electrochemical studies of full-length mammalian microsomal CYP 2B4 [27]. The studies of CYP BM3 and CYP 2B4 provide a great insight into understanding the redox behaviour of heme proteins inside the DDAB films.

3.2 To Impart Operational Stability

The shelf life of proteins in solution is short as their stability is affected by various factors once they are isolated from the living cell. The major factors affecting protein stability in solution are aeration, pH, ionic strength, temperature, proteolysis or denaturation by exposure of protein to unsterile surfaces, etc. During electrochemical studies the protein in solution is exposed to many such physical and chemical denaturants. These factors cause rapid denaturation of proteins in solution and their reusability is further limited. It has been shown by many researchers that immobilisation of proteins in suitable matrices over electrodes reduces such effects and contributes towards the stability of proteins and their reusability [29].

Mesoporous or macroporous matrices often provide a suitable environment for immobilisation of proteins over electrodes. They are highly ordered porous thin films coated over the electrodes with pore sizes ranging from micrometres (macroporous) to few nanometres (mesoporous) where protein could either be adsorbed or cross-linked. Immobilisation of redox proteins into these pores provides them with much desired mechanical stability besides hindering their direct interaction with some of the physical denaturants such as gas bubbles, unsterile surfaces, etc. One of the important characteristics of porous materials is their high surface area/volume ratio that provides more loading space for proteins compared to flat electrode surfaces. Large surface area also favours the interaction with

external reagents. Electrically conducting porous materials (metals, carbon) contribute to increase the electroactive surface by several orders of magnitude thereby increasing the sensitivity of the resulting device. Semiconducting or non-conducting materials, such as metal oxides or organically modified ceramics or silica, are also attractive, especially in combining the mechanical stability of a rigid inorganic matrix with desired chemical reactivity.

Different strategies are used to generate such organised porous films on electrode surfaces. One strategy involves the use of nanomaterials as the building blocks and their self-assembly over electrodes. The other strategy is the generation of continuous nanostructured phases by a template route. Walcarius and Kuhn [38] reviewed the strategies involved in the generation of highly ordered mesoporous and macroporous thin films via template formation. The templates for the deposition of these films are made up of silica, latex or surfactants. Silica or latex templates over electrodes are formed either by self-assembly after evaporation of solvents or by dipping them in the solution so that a film could form over time. A derivative of Langmuir–Blodgett technique is also used where the micelles are first formed at the air–water interface of solution which are then transferred onto the electrodes. Once formed they are filled with conducting materials like carbon, metal or polymers by electrodeposition or electropolymerisation. The templates are later dissolved by HF or organic solvents to leave highly ordered, interconnected mesoporous or macroporous films over the electrodes where the redox proteins are then immobilised. Surfactant templates are generally prepared by sol–gel method where the metal, metal oxide or silica precursors are dissolved in surfactant–solvent mixture and are then deposited on the electrode either by evaporation (evaporation-induced self-assembly, EISA) or by electrodeposition (electro-assisted self-assembly, EASA) to produce mesoporous thin films.

For biological applications requiring protein immobilisation, macroporous structures are favoured as they correlate well with the protein dimensions. Proteins could be easily immobilised over the walls of the pores and would not block the connections and thus the flow of analytes and reagents. However, in mesoporous structures which have few nm pore dimensions, the immobilisation of proteins (which are usually bigger than the size of these pores or interconnections) would clog them causing the obstruction for the analyte flow and conductivity. Szamocki et al. [23] used macroporous gold electrodes for immobilisation of GOx and glucose dehydrogenase (GDH) for glucose sensing. The silica templates were built by Langmuir–Blodgett technique on flat cysteamine-modified gold electrodes. After electrodeposition of gold, the silica template was dissolved by 5% HF. The enzymes were then immobilised into the pores of the macroporous gold electrode either by glutaraldehyde cross-linking or by incorporation in an electrodeposition paint. Figure 2A and B shows the hexagonal arrangement of pores in the macroporous gold electrode. For the modification with biomolecules, especially proteins, it is very important that the interconnections between the pores are big enough to allow the large molecules to enter the pores where they can be immobilised. Earlier experiments with CV of similar substrate showed that the active surface area is highly increased compared to the geometrical surface area of

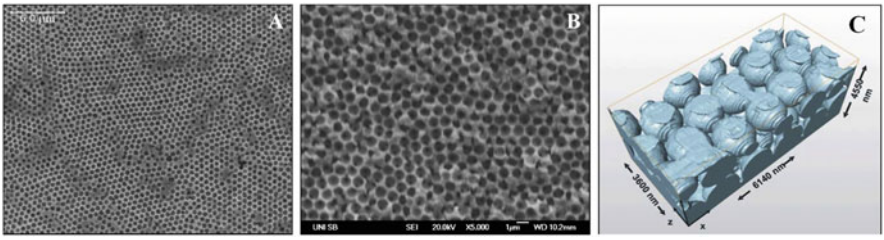

Fig. 2 (**A**) SEM image of a macroporous electrode (*top view*) with a pore diameter of 680 nm and a thickness of the porous gold of 3½ pore layers. (**B**) Magnification of the locally ordered domains. (**C**) FIB tomography of a macroporous electrode with a diameter of 1,100 nm and a thickness of the porous gold of 1½ pore layers. The 3D image has been obtained by the reconstruction of the air-filled zones in a series of SEM images cut by a focussed ion beam every 50 nm. The substrate oriented view is shown. Adapted with permission from [23]. Copyright (2007) Elsevier

the electrode [39]. Although this provided an indirect evidence for the interconnections, to establish this fact directly and to characterise the pore dimensions, focused ion beam tomography (FIB) was used. A real 3D structure (Fig. 2C) was obtained by the reconstruction of the structure from a series of SEM images of slices cut by a focused ion beam. The figure clearly shows that every pore is connected to the neighbouring pores. From this reconstruction, it was possible to quantitatively determine the distribution of diameters of the pores and their interconnections. For a macroporous electrode with a pore diameter of 1,100 nm, the average diameter of interconnection was about 300 nm with a minimum of 200 nm. Since enzymes have a typical diameter of 20 nm, these interconnections were large enough to allow a good penetration of the enzyme and the entire internal surface to be electrochemically active.

In the same work, the effect of pore layers on sensitivity of glucose detection was also established. It was shown that for electrodes with a higher number of pore layers, thus with higher active surface area but equal geometrical area, the signal for any glucose concentration was higher. This led to higher saturation current for the electrode that could easily be increased by two orders of magnitude. This behaviour was based on the fact that on a porous electrode more glucose receptors per square centimetres were available and therefore saturation was reached only at higher concentrations. The signal difference for concentration steps in the low concentration region was higher for electrodes with a higher number of pore layers, and thus the sensitivity and the lower detection limit were also improved. When compared to a flat electrode, for an electrode with 5½ pore layers, the saturation current increased from 2.42 to 46.5 μA, the apparent Michaelis–Menten constant increased from 4.9 to 9.4 mM and the sensitivity increased from 107 μA mol^{-1} cm^{-2} to 1.85 mA mol^{-1} cm^{-2}. The so prepared glucose sensors also showed a higher storage and operational stability when compared to the flat electrodes. The signal for glucose sensing was observed for a month with a gradual decrease of around 30% over a period of 7 days when stored at 4°C in Tris buffer.

In another work, a direct electron transfer of haemoglobin (Hb) was achieved by adsorbing the protein in the pores of a similarly synthesised highly ordered macroporous gold electrode prepared via silica template [40]. Its interconnected macroporous structure, containing AuNPs, significantly enhanced the amount of adsorbed Hb molecules at the monolayer level with an observed surface coverage of 88.1%. The uniform, three-dimensional macroporous gold also provided superior conductivity and higher stability to protein by providing a good microenvironment for retaining the biological activity of the adsorbed protein.

Ionic polymer films are one of the frequently used matrices for immobilisation of redox proteins over the electrodes. The ionic interactions of polymer films with proteins and electrodes stabilise the protein inside the matrix over the electrode surface, thereby increasing the operational stability of the resulting device. Such ionic interactions facilitate direct electron transfer between protein and electrode and also their interaction with reaction analytes. Some of the ionic polymers used for film formation are polyethyleneimine (PEI), polydiallyldimethylamine (PDDA), polystyrene sulphonate (PSS), etc. Stable polyionic polymer-protein films are constructed by the layer-by-layer electrostatic adsorption method [41]. The layer-by-layer method involves alternately adsorbing ionic macromolecules of different charges onto a surface, so that at each adsorption step, the outer layer has excess charge density enabling subsequent adsorption of a new layer of the opposite charge, thereby stabilising the whole matrix ionically. Most enzymes in these films retain high activity. This method is general and versatile and allows the film architecture to be controlled according to desired specifications. Most of the earlier electrochemical experiments with redox proteins used cytochrome c (cyt c, molecular weight, MW ~12 kDa) or other small-sized proteins as their model compounds because of their ease of handling and possibility for DET with the electrode. Electrochemical studies with bulky proteins with deeply buried redox centres were consciously avoided for their anticipated inability to interact directly with the electrodes. However, with the onset of development of various efficient immobilisation techniques lately, it is now possible to successfully study the electrochemistry of such bulky proteins too. In one such attempt, layer-by-layer electrostatic assembly technique was used for the immobilisation of large catalase (CAT, subunit MW ~90 kDa), a bulky tetrameric heme enzyme isolated and purified from *Aspergillus terreus* MTCC 6324 [42]. Figure 3A shows a schematic representation of the steps involved in the assembly of the bioelectrode, where CAT was adsorbed over multi-walled carbon nanotube/Nafion® (MWCNT/NF) nanocomposite coated on a glassy carbon electrode (GCE). Polycationic polymer PEI was used to encapsulate the assembly. The resulting bioelectrode was characterised by EIS (Fig. 3B). The spectra were presented in the form of Nyquist plots (where Z_{re} is the real and Z_{im} is the imaginary part of impedance) and were overlaid to pinpoint the differences in R_{ct} with subsequent modification layers. Interestingly, the addition of PEI layer decreased the overall R_{ct} of GCE/MWCNTs-NF/CAT assembly from about 500 to 280 Ω. As shown in the scheme (Fig. 3A), the PEI layer neutralised the negative charge density developed by the composite MWCNTs-NF/CAT (pI 4.2) and thereby reduced the charge repulsion between

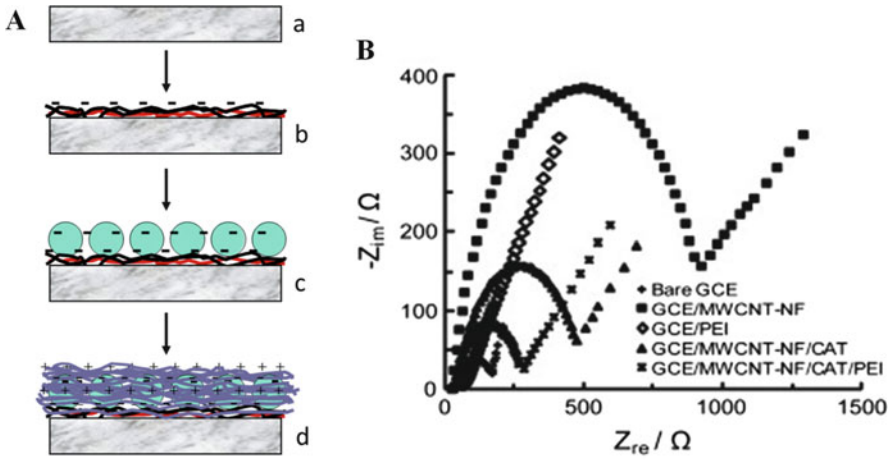

Fig. 3 (**A**) Schematic representation (*a*) bare GCE, (*b*) GCE/MWCNT-NF, (*c*) GCE/MWCNTs-NF/CAT and (*d*) GCE/MWCNTs-NF/CAT/PEI and (**B**) EIS for layer-by-layer fabrication of CAT bioelectrode. Adapted with permission from [42]. Copyright (2010) Elsevier

the negatively charged NF and CAT resulting in decrease of the overall R_{ct} of the bioelectrode. The ionic interactions of PEI layer also facilitated the direct electron transfer between the enzyme and the electrode as shown by CV experiments (not shown here). A pair of nearly reversible CV peaks for $Fe^{III/II}$ couple with $E^{\circ\prime}$ of about −0.45 V (vs. Ag/AgCl electrode at pH 7.5) was obtained for the CAT. In the same work, the effect of encapsulating layer of PEI on the stability of CAT bioelectrode was also accessed. A considerably high storage and operational stability were recorded for PEI-coated bioelectrode. The CAT activity was completely lost within 48 h without PEI compared to 75% of residual activity when encapsulated with PEI. The ionic interactions and encapsulation provided by PEI stabilised the charge density on enzyme nanocomposite assembly and prohibited the leaching of surface-bound enzyme in solution.

3.3 To Enhance the Electron Transfer Efficiency

Most of the redox proteins have their active centre deeply buried inside the protein matrix which slows down or sometimes insulates the transfer of electrons from protein to the electrode. As per the classical Marcus theory for the monolayer redox couple [Eq. (1)] [16, 43, 44], k_{ET} decreases exponentially with the distance of electron transfer, d, where k_0 is the electron transfer rate constant at the distance of closest contact d_0:

$$k_{ET} = k_0 \exp[\beta(d - d_0)] \quad (1)$$

Since, in redox protein electrochemistry, electrode and the protein redox centre are usually considered as a donor–acceptor pair, the distance or spatial separation of the protein redox centre from the electrode by means of the protein shell prohibits the direct electrical communication between the redox site and the electrode.

Mediated electrochemistry by wiring of redox proteins to electrodes via soluble mediators, redox metallopolymer hydrogels or conducting polymers are extensively used to overcome electron transfer barrier between redox proteins and electrodes. Mediators which could diffuse inside the protein matrix such as ferrocene derivatives, quinones, synthetic or semi-synthetic cofactors (NADH, microperoxidases, etc.), organic salts and metal bipyridine complexes have been used to shuttle electrons from proteins to electrodes [9]. Redox metallopolymers are also used as electron bridges between electrodes and redox centres of enzymes. The redox polymers are usually soluble in water and contain hydrophobic, charged or hydrogen-bonding domains, so that they can form complex with the protein and penetrate deeply into the buried redox cofactor centre to facilitate electron transfer. In addition, the polymers are also able to achieve a three-dimensional network that allows rapid diffusion of the substrate and fast charge transport. $Os^{III/II}$ redox hydrogels such as poly(vinylpyridine)-[bis(2,2′-bipyridine)chloroosmium]$^{+/2+}$, poly(vinylimidazole) complex of [bis(2,2′-bipyridine)chloroosmium]$^{+/2+}$, polyvinyl imidazole complex of [(Os-4,4-dimethyl-2,2-bipyridine)Cl]$^{2+/+}$, poly (allylamine) with attached ferrocene (PAA–Fc), poly(*N*-isopropylacrylamide-co-vinylferrocene) polymer, etc. were used extensively to mediate GOx and peroxidase electrochemistry [16, 41]. In one of the recent studies, Plumeré et al. [45] immobilised an O_2-sensitive hydrogenase in the viologen-functionalised redox hydrogel film on the electrode surface. Under pure H_2 atmosphere, the polymer/hydrogenase-modified electrodes displayed stable catalytic currents. The catalytic wave for H_2 oxidation was centred on viologen redox couple ($E_{V++/V+\bullet} = -0.3$ V vs. standard hydrogen electrode, SHE), demonstrating that the viologen moieties were exclusively responsible for ET from the hydrogenase to the electrode. Interestingly, the integration of the O_2-sensitive hydrogenase into the viologen-based redox polymer film also protected the enzyme from O_2 damage and high-potential deactivation thereby increasing the operational stability of the enzyme. Electron transfer between the polymer-bound viologen moieties controlled the potential applied to the active site of the hydrogenase and thus insulated the enzyme from excessive oxidative stress. Under catalytic turnover, electrons provided from the H_2 oxidation reaction induced viologen-catalysed O_2 reduction at the polymer surface, thus providing self-activated protection from O_2. The advantages of this tandem protection were demonstrated using a single-compartment biofuel cell based on an O_2-sensitive hydrogenase anode and H_2/O_2 mixed feed. Conductive polymers such as polypyrrole (PPy), polyaniline (PANI), polythiophene and polyindole are also used to wire redox proteins to the electrodes for their electrochemical studies. They can be grown on electrode surfaces by electrochemical polymerisation. Film

thickness can be controlled by the amount of charge consumed during electropolymerisation. The resulting polymers sometimes also exhibit low interference in sensor applications resulting from size exclusion. Redox proteins can be entrapped into the polymer network during electropolymerisation. The high inherent electron conductivity of these polymers has fostered their use as molecular wires to shuttle electrons between the redox-active sites of the proteins and electrodes. Recently many authors have extensively reviewed the use of conducting polymers for electrochemical studies of redox proteins directed towards their biosensing applications [46–48]. Although the different mediators discussed so far have been successful in establishing ET communication between the redox centres and electrodes, the bioelectrocatalytic features of the resulting enzyme electrodes represent the collective properties of numerous configurations of enzyme molecules of variable degrees of loading with electron mediator groups that reach a variety of orientations in respect to the conductive support. These difficulties limit the ET communication of the biocatalysts and the conductive supports, as compared to the ET efficiency between the enzyme redox sites and their natural ET substrates or cofactors. Besides, mediated electrochemistry suffers from its own limitations where the electrochemistry of mediators usually predominates and provides only indirect information about the protein electrochemistry or its electrocatalytic activity.

Reconstitution of redox proteins over their natural cofactors wired to the electrode via different approaches provides an interesting alternative for enhancing the electron transfer efficiency between redox proteins and electrodes. Willner and co-workers [17, 49] have extensively worked and reviewed this approach for both the fundamental understanding of electron transfer and their applications for biosensor and biofuel cell. The reconstitution method involves the exclusion of the native active centre from the protein, for example, an ion or a cofactor, to yield the respective apoprotein (or hollow protein). The redox-active ion or cofactor is then wired on the electrode. The reconstitution of apoprotein around wired cofactors allows the direct electrical contact of protein to the electrode. A volume of work has been done mainly with GOx and iron-containing proteins by first removing their flavin adenine dinucleotide (FAD) cofactor or heme prosthetic group, respectively, and then wiring them to the electrode via a molecular relay, conducting polymer or some nanotechnological means and reconstituting the apoprotein around them.

In one of the representative work, Patolsky et al. [24] demonstrated the reconstitution of apo-GOx on FAD cofactor electrically contacted to the electrode via single-walled carbon nanotubes (SWCNTs), which act as conductive nanoneedles that electrically wire the enzyme redox-active site to the transducer surface (Fig. 4A). Before immobilisation, the commercially obtained SWCNTs were chemically shortened by treatment with strong acids. The formation of carboxylic (and phenolic) groups at the nanotube ends (and sidewall defect sites) as a result of acid treatment allowed the covalent immobilisation of the SWCNTs on thioethanol/cysteamine-modified Au electrode in the presence of the coupling reagent 1-ethyl-3-(3-dimethylaminopropyl)carbodiimide hydrochloride (EDC) as depicted in Fig. 4A. The incorporation of 2-thioethanol in the mixed monolayer prevented

the nonspecific (as well as horizontal) adsorption of the surfactant-protected SWCNTs onto the electrode surface. The amino derivatives of the FAD cofactor were then coupled to the carboxyl groups at the free edges of the standing SWCNTs (after wall protection in the presence of surfactants Triton X-100 and PEG, MW = 10,000). Apo-GOx was then reconstituted on the FAD units linked to the ends of the standing SWCNTs. The pretreatment of the SWCNT monolayer with a mixture of the surfactants prior to the binding of FAD units and reconstitution with apo-GOx was found to be an essential step to generate a bioelectrocatalytically active interface, with the enzyme specifically coupled to the SWCNTs' FAD-modified ends. The reconstitution of the apo-GOx units on the FAD units linked to the ends of the SWCNTs was supported by AFM measurements (Fig. 4B). Figure 4C shows the high-resolution TEM image (HRTEM) of a SWCNT modified with two GOx units (negatively stained with uranyl acetate) at the edges of the tube. Voltammetric experiments revealed that FAD units were electrically connected with the electrode surface with a quasi-reversible CV ($E^{\circ\prime} = -0.45$ V vs. SCE at pH 7.4). The bioelectrocatalytic oxidation of glucose was observed at $E > 0.18$ V vs. SCE, and the electrocatalytic anodic current increased with increasing concentrations of glucose with a saturation at 60 μA. The modification of the electrode surface with the reconstituted GOx units was further characterised by means of microgravimetric QCM and electrochemical experiments. From the frequency changes of the crystals in QCM and the CVs of the FAD units, the surface coverage of the SWCNTs and of the GOx units were calculated to be 4×10^{-11} mol cm^{-2} (3–4 FAD units per SWCNT) and 1×10^{-12} mol cm^{-2}, respectively. Thus, the turnover rate of 4,100 s^{-1} was calculated for electrons transferred from reconstituted GOx to the electrodes. This value is about six fold higher than the turnover rate of electrons from the active site of GOx to its natural O_2 electron acceptor (700 s^{-1}) proving the enhanced electrocatalytic efficiency of reconstituted GOx after wiring of FAD to the electrode.

The electron pumping from reconstituted GOx to the electrode via FAD wiring was further established in another work by Lioubashevski et al. [28]. Apo-GOx was reconstituted on FAD cofactor-functionalised AuNPs (1.4 nm) linked to the bulk Au electrode via dithiol monolayer. Although the reconstituted GOx/AuNP hybrid system exhibited electrical communication between the enzyme redox cofactor and the AuNPs [50], an overpotential (0.4 V) was recorded for bioelectrocatalytic oxidation of glucose by the hybrid system. This positive potential shift was attributed to the tunnelling barrier introduced by the dithiolate spacer that bridged the AuNPs to the bulk electrode. To establish this observation, the GOx/AuNP hybrid was linked to the bulk Au electrode by a short dithiol, 1,4-benzenedithiol, or a long dithiol, 1,9-nonanedithiol, monolayer. Because the thiol monolayers provided a barrier for electron tunnelling, the electron transfer occurring upon the biocatalytic oxidation of glucose resulted in AuNPs charging. The charging of AuNPs altered the plasma frequency and dielectric constant of AuNPs, which led to the changes in the dielectric constant of the interface. The effects were reflected in pronounced shifts of the plasmon angle, θ_p, in the SPR spectra. In case of the GOx/AuNP system bridged to Au support by the long dithiol monolayer, a shift of θ_p (39′) was

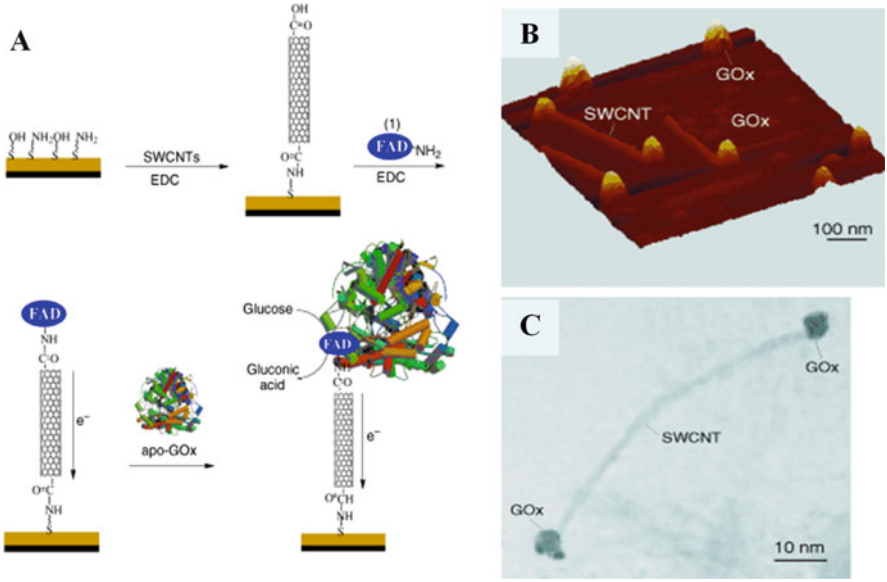

Fig. 4 (**A**) Assembly of the SWCNT electrically contacted GOx electrode. (**B**) AFM image of SWCNTs reconstituted at their ends with GOx units. (**C**) HRTEM image of a SWCNT modified at its ends with GOx units. Adapted with permission from [24]. Copyright (2004) WILEY-VCH Verlag GmbH & Co.

observed before and after addition of glucose. Whereas, in analogous system, which was bridged with the short dithiol monolayer, a smaller change θ_p (27′) was observed before and after addition of glucose. Thus, the changes in the plasmon angles were more pronounced in the long dithiol system, as compared to the short dithiol system. Charging of the AuNPs associated with the interface also resulted in changes of the double-layer capacitance. The potentials of the aligned GOx/AuNP-modified electrodes, prior to the addition of glucose, were close to the zero-charge potential values and thus provided the minimum values of C_{dl}. Upon addition of 100 mM of glucose, the capacitance increased from ca. 2.1 to 3.6 μF cm^{-2} (ΔC_{dl} ~80%) for longer dithiol monolayer. In contrast, the change was lesser for shorter dithiols from ca. 19 to 24.7 μF cm^{-2} (ΔC_{dl} ~22%). These results were consistent with the larger shift of θ_p observed in the SPR measurements in the presence of the long dithiol linker as compared to the changes observed with shorter dithiol. The long dithiol linker yielded a densely packed monolayer which provided an effective tunnelling barrier for the transport of electrons from the AuNPs to the bulk Au electrode. This resulted in the effective charging of the AuNPs reflected by the significant changes of the interfacial capacitance. In contrast, the short dithiol linker allowed the leakage of electrons from the AuNPs to the bulk Au electrode, resulting in diminished charging of the AuNPs. As a result only moderate changes in the capacitance values of the interface were observed. A control for GOx/AuNP hybrid where GOx was unspecifically linked to AuNPs did not show significant changes in

plasmon angle or capacitance after addition of glucose. The studies showed that the electrocatalytic efficiency of GOx reconstituted over electrically connected FAD was considerably enhanced when compared to a non-aligned assembly.

Protein engineering has long been used to alter the native protein structures to acquire desired functions which could be exploited for their electrochemical applications. These desired functions could be increased sensitivity of engineered redox proteins towards their substrate, ease of their immobilisation over the electrode surface with added stability and/or enhanced electron transfer efficiency [51]. Different approaches are used for redox protein engineering [11]. Rational design is one of the commonly used approach where the existing extensive knowledge of protein structure–function and computational modelling are combined together either to chemically synthesise de novo proteins with desired functionalities or to accurately modify native protein structure (either by controlled digestion of amino acids or by point mutations to alter amino acid sequence) to tune the redox (or other desired) properties of proteins. In contrast to this approach, directed evolution does not require the prior knowledge of protein structural data and the relationship between sequence, structure and mechanism for generation of mutants. Instead, a library of variants is created by iterative rounds of mutagenesis of the target gene that are then selected and screened till the desired functions are acquired. Molecular "lego" is another approach to engineer redox proteins where the proteins with desired properties are fused together [52]. The molecular lego mimics the natural molecular evolution which is proceeded by modular assembly of genes/DNA segments. The key domains or building blocks are selected to assemble artificial redox chains with the desired properties, ultimately capable of communicating with the electrodes. The link between protein domains can be achieved by a peptide linker or by a disulphide bridge between the two domains. To ensure efficient electron transfer between the two domains and ultimately with the electrode, the position and length of the linkers are chosen in such a way that the association complexes are favoured, allowing optimal electron transfer.

One of the most popular examples of rational design approach to engineer a redox protein for its electrochemical application was trimming of cyt c by controlled enzymatic digestion to yield microperoxidase-11 (MP-11). The heme redox centre in cyt c was exposed in MP-11 for better electron coupling with the electrode. The approach of rational design has also been used to selectively modify protein surface structure for ease of immobilisation over electrode surface (e.g. introduction of surface-exposed histidine or cysteine for cross-linking or self-assembly over electrode, respectively) [53]. In another example, Willner and co-workers [17] reconstituted a de novo synthesised four-helix bundle with Fe^{III} protoporphyrin IX moiety wired over the functionalised Au electrode and explored its electrochemical properties. The reconstituted helical protein showed efficient electron transfer with the electrode and acted as an artificial heme cofactor that substituted cyt c in activating cyt c-dependent enzymes like nitrate reductase (from *E. coli*). In one of the recent studies, Marshall et al. [54] predictably and rationally tuned the $E^{\circ\prime}$ of cupredoxin azurin (Az) to the full range 706 ± 3 mV at pH 4 for N47S/F114N/M121L Az variant to -2 ± 13 mV at pH 9 for F114P/M121Q Az

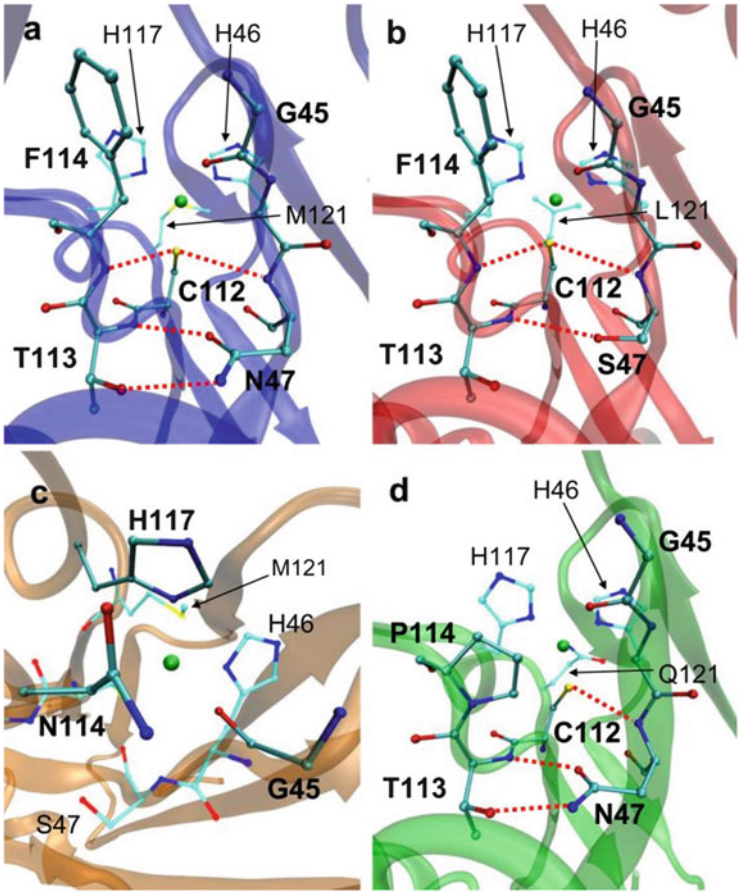

Fig. 5 X-ray structures of Az and selected variants. (**a**) Native Az (PDB 4AZU). (**b**) N47S/M121L Az: N47S affects the rigidity of the copper binding site and, probably, the direct hydrogen bonds between the protein backbone and Cys 112. (**c**) N47S/F114N Az: introducing a hydrogen bond donor at position 114 perturbs hydrogen bonding near the copper binding site, possibly disrupting donor–acceptor interactions to His 117 or ionic interactions between the copper and the carbonyl oxygen of Gly 45. (**d**) F114P/M121Q Az: F114P deletes a direct hydrogen bond to Cys 112 resulting in a lower redox potential. In all panels copper is shown in *green*, carbon in *cyan*, nitrogen in *blue*, oxygen in *red* and sulphur in *yellow*. Hydrogen-bonding interactions are shown by *dashed red lines*. Adapted with permission from [54]. Copyright (2009) Nature Publishing Group

variant surpassing the highest and lowest reduction potentials reported for any mononuclear cupredoxin. This unprecedented level of control over an electron transfer protein was achieved by mapping out major interactions in protein structure followed by their selective modification, an approach that could be extended to all other redox proteins (Fig. 5). Such proteins with wide redox potential and pH ranges are useful as biosensor or biofuel cell catalysts. Other attempts at protein

engineering involved directed evolution to enhance the catalytic efficiency and stability and to modify substrate specificity in CYP variants from different sources [55, 56]. The manyfold increased sensitivity towards various environmental pollutants and drugs makes these variants a potential target for biosensor applications.

3.4 To Aid in Miniaturisation of Bioelectrochemical System

The combination of biological molecules and novel nanomaterial components is of great importance in the process of developing new nanoscale devices for future biological, medical and electronic applications. Recent studies show a tremendous increase in the use of nanomaterials for bioelectrochemical applications. The reasons are high surface to volume ratio provided by these nanomaterials over the transducer surface (aiding in the increased protein loading that results in higher sensitivity and lower detection limit), their fast electron transfer efficiency, their specific electronic and optical properties and their ease of availability. A lot of research has been published lately exploring the utility of nanomaterials for electrochemical studies of redox proteins and their applications in biosensing and biofuel cells.

Nanotubes and nanowires are extensively used immobilisation matrices for electrochemical studies of redox proteins. The group includes mostly carbon, silicon, conducting polymer, metallic (Au, Pt, Ni) and semimetallic (TiO_2 [57], ZnO [58]) nanotubes or nanowires. They are also termed as one-dimensional (1-D) nanostructures because of a high ratio of their length (μm) to their diameter (nm). Synthesis, characterisation and alignment of these 1-D structures for their biosensor applications have been extensively reviewed [59, 60]. Since most of these nanowires are commercially available, a detailed description of synthesis and characterisation are either consciously avoided or only briefly discussed in the context of examples in this section. However, there are many research groups which focus on synthesising these nanowires for their tailor-made applications.

Among 1-D structures, carbon nanotubes (CNTs) are the most popular ones. The physical and catalytic properties make CNTs ideal for use in sensors. Most notably, CNTs display high electrical conductivity, chemical stability and mechanical strength. The two main types of CNTs are single-walled CNTs and multi-walled CNTs. SWCNTs are sp^2-hybridised carbon in a hexagonal honeycomb structure that is rolled into a hollow tube morphology. MWCNTs are multiple concentric tubes encircling one another. SWCNTs can be classified as either semiconducting or metallic allotropes, depending on the chirality. CNTs are primarily synthesised by three main techniques: arc discharge, laser ablation/vaporisation and carbon vapour deposition (CVD). Most commercially available CNTs are formed by CVD. After synthesis, CNTs may be treated to functionalise their surfaces. The most common treatment with strong acids removes the end caps and may also shorten the length of the CNTs. Acid treatment also adds oxide groups, primarily carboxylic acids, to the tube ends and defect sites. Further chemical reactions can be performed

at these oxide groups to functionalise with groups such as amides, thiols or others. Altering the nanotube surface strongly affects solubility properties, which can affect the ease of fabrication of CNT-based sensors. A recent review by Jacobs et al. [61] compiled detailed accounts of CNT-based electrochemical sensors for biomolecule detection. A large number of studies have focused on immobilisation of GOx in nanocomposite films of SWCNTs/MWCNTs dispersed in chitosan/NF/PPy for fast and sensitive electrochemical detection of glucose. Besides GOx, other enzymes such as lactate oxidase, lactate dehydrogenase, galactose oxidase, cholesterol oxidase, alcohol dehydrogenase, etc. have also been immobilised in CNT nanocomposite for the detection of biologically important molecules. CNTs are also frequently used as immobilisation matrix for heme-containing proteins. Yang et al. [25] developed a method to directly bind Hb to diazonium-modified aligned CNTs (ACNTs) via carbodiimide chemistry. The aligned nanotube forest resulted in greater surface coverage ($\Gamma = 2.7 \times 10^{-9}$ mol cm^{-2}) for Hb resulting in higher catalytic current when compared to immobilisation in random tangled webs of CNTs. SEM and FTIR spectroscopy were used to characterise the ACNTs and Hb-ACNTs (Fig. 6A and B). The ACNTs showed partially opened tip and uniform, straight and smooth sidewalls with average outer diameter of ca. 50 nm (Fig. 6A, a, b, c). Figure 6A, d, e, f shows the ACNT arrays after diazonium reaction and covalent immobilisation of Hb molecules. Sidewall roughness and closed tips showed that the Hb was immobilised both on sidewalls and the tips of ACNTs (Fig. 6A, e, f). The FTIR spectrum for Hb-ACNT showed (Fig. 6B, d) two typical peaks at 1,656 and 1,546 cm^{-1}, which contributed to the C=O stretching vibration of amide I band and the combination of N–H bending and C–N stretching vibration of amide II band, respectively. The bands showed only a slight redshift after immobilisation on ACNTs when compared to the natural Hb peaks at 1,652 and 1,540 cm^{-1} (Fig. 6B, c), indicating that the interaction of Hb with diazonium-ACNTs did not destroy the native secondary structure of Hb. The Hb film on the diazonium-ACNTs electrode showed well-defined redox peaks with $E^{\circ\prime}$ at −312 mV (vs. Ag/AgCl) and good electrocatalytic activity for H_2O_2 reduction. The Hb-ACNTs electrode exhibited high sensitivity, long-term stability and wide concentration range from 40 μM to 3 mM for the amperometric detection of H_2O_2. The fact that vertically aligned nanotube forests had better kinetics for direct electron detection was further established by Esplandiu et al. [62]. They immobilised myoglobin over vertical ACNTs to detect either H_2O_2 or O_2 separately. CNT forests showed superior kinetics when compared to nanocomposite epoxy-incorporated SWCNTs/myoglobin sensors. A higher limit of detection of ~50 nM was recorded for H_2O_2, superior to other previously reported random and aligned nanotube methods.

Among metallic nanowires, gold nanowires (AuNWs) are fast gaining ground in the biosensing applications due to their high chemical and thermal stability, biocompatibility and excellent electrical conductivity [63, 64]. Their ease of self-assembly over thiol-modified transducer surfaces provides a stable matrix for biomolecule assembly. The self-assembled AuNWs can then be functionalised to acquire free amino or carboxyl groups for protein cross-linking. While a number of

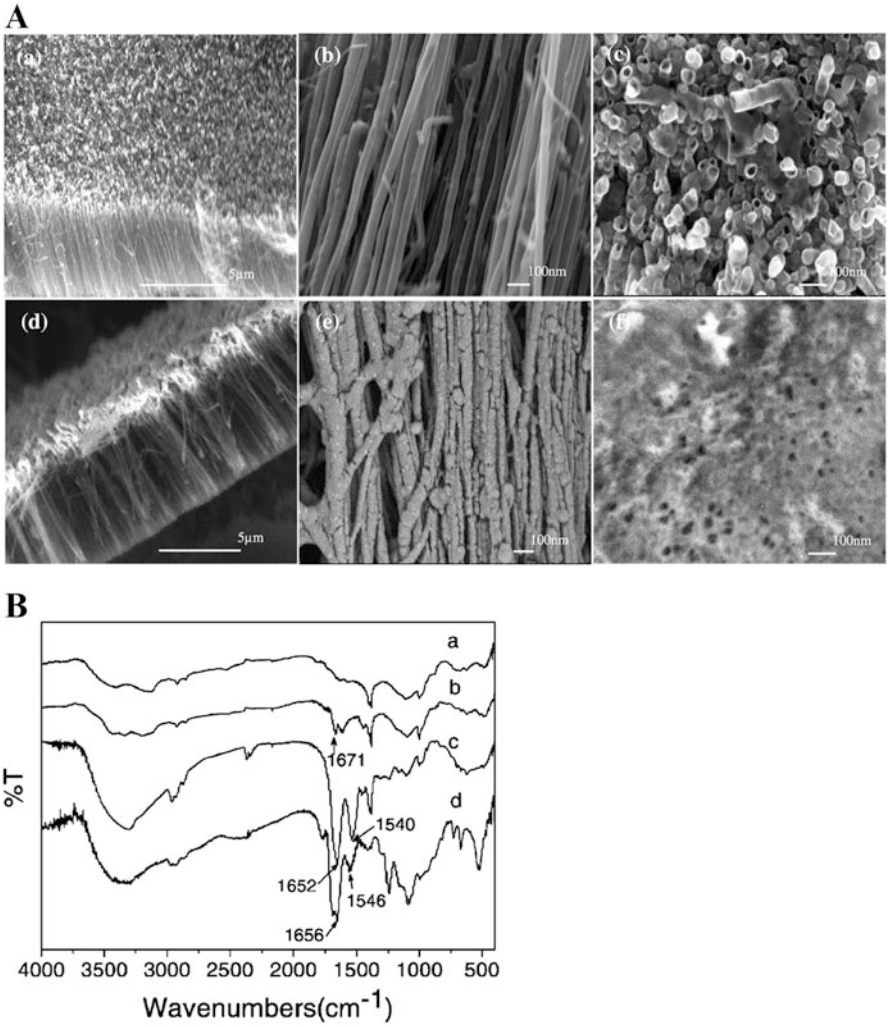

Fig. 6 (**A**) SEM images of ACNTs (*a*, *b*, *c*) and Hb-ACNTs (*d*, *e*, *f*). (**B**) IR spectra of (*a*) ACNTs, (*b*) diazonium-ACNTs, (*c*) Hb and (*d*) Hb-ACNTs film. Adapted with permission from [25]. Copyright (2009) WILEY-VCH Verlag GmbH & Co.

techniques for AuNWs fabrication have been reported, electron beam lithography [64] and electrodeposition in alumina template [65] are frequently used. Sometimes they are fused together with platinum or nickel to change the functionality [65].

Recent trends suggest increasing use of conducting polymer nanowires such as PPy, PANI and poly(ethylene dioxythiophene) (PEDOT) and their functionalised derivatives as immobilisation matrix for redox proteins. Ease of synthesis of conducting polymer nanowires and their in-built functional groups give them an edge over other inorganic nanowires where addition of functional groups for redox

protein immobilisation is always an additional step. Among the methods used for fabrication of conducting polymer nanowires are template-assisted synthesis, photolithography and e-beam lithography, dip-pen nanolithography, hydrodynamic focusing and direct electrochemical synthesis [66]. Wang et al. [67] reported an amperometric glucose biosensor based on the direct electron transfer of GOx by electrochemically entrapping GOx onto the inner wall of highly ordered PANI nanotubes (PANI-NTs). PANI-NTs were synthesised using anodic aluminium oxide (AAO) membrane as a template. Figure 7A shows SEM images of highly ordered PANI-NTs with the outer diameter of 250–300 nm and the inner diameter of ~150 nm. Inset of the Fig. 7A is the top view showing the open ends of these nanotubes. The PANI-NTs thus provided an ideal size of channel to entrap GOx. The immobilised GOx is shown as small and uniformly distributed island-like nanostructures with the size of ~50 nm adhered on the inner wall of PANI-NTs (Fig. 7B). Figure 7B also shows that PANI-NTs retain the nanotube structure after GOx immobilisation, an important characteristic to enable free and fast diffusion of substrates and products inside the nanotubes. GOx immobilised in PANI-NTs showed a pair of well-defined and nearly symmetrical redox peaks in CV with the anodic and cathodic peak potentials at −390 and −420 mV, respectively, with $\Delta E_p = 30$ mV. The apparent k_s was estimated to be $5.8 \pm 1.6\ s^{-1}$. In addition, the GOx/PANI-NTs/Pt electrode showed higher sensitivity ($97.18 \pm 4.62\ \mu A\ mM^{-1}\ cm^{-2}$), lower detection limit ($0.3 \pm 0.1\ \mu M$) and faster response time (~3 s) with considerable stability when compared to other reported glucose biosensors.

Nanoparticles and microparticles constitute a diverse class of materials frequently used for immobilisation of redox proteins. The commonly used are metallic nanoparticles (Au, Ag, Pt), conducting polymer nanoparticles, silica microparticles, etc. The obvious advantages are high surface to volume ratio, thus allowing higher protein loading and aiding miniaturisation besides their efficient conductivity and stability as a matrix for protein immobilisation. Metallic nanoparticles, especially AuNPs are increasingly being used for protein electrochemical studies. Similar to

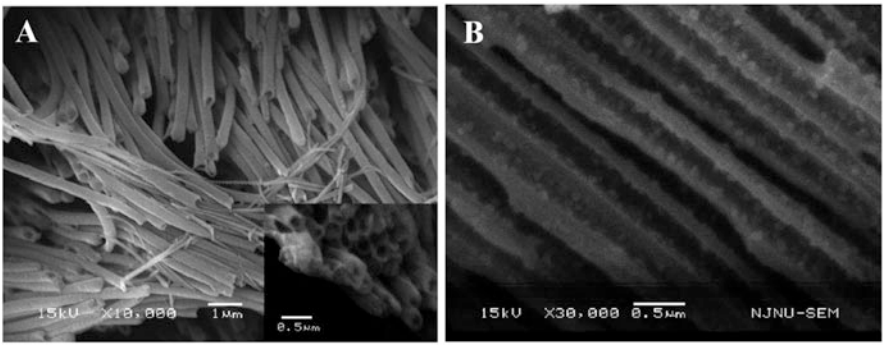

Fig. 7 (**A**) SEM images of PANI-NTs obtained by etching away the AAO membrane. (**B**) The cross-sectional image of the PANI-NTs after loading GOx on the inner wall of the nanotubes. Adapted with permission from [67]. Copyright (2009) American Chemical Society

AuNWs, the ability of AuNPs to self-assemble over a thiol-modified surface provides a stable matrix for protein immobilisation. Furthermore, because of their efficient electron conductivity, they permit direct electron transfer between redox proteins and bulk electrode, thus allowing electrochemical sensing to be performed without the need of electron transfer mediators. AuNPs have also demonstrated to constitute useful interfaces for the electrocatalysis of redox processes of molecules such as H_2O_2, O_2 or NADH involved in many significant biochemical reactions. One recent review by Pingarron et al. [68] provides a detailed account on the use of AuNPs for immobilisation and electrochemical studies of various proteins including GOx, horseradish peroxidase, Hb, myoglobin, etc. In an interesting approach, Melin et al. [69] compared the effect of size of AuNPs on electrochemistry of cbo3. AuNPs of sizes 15, 38 and 56 nm were drop casted on a series of gold electrode surfaces, and their surface areas were compared electrochemically by integration of the Au–O reduction peak at 1.1 V. Although the overall surface area increased with AuNP layer, it decreased with increasing size of AuNPs from 15 to 5.5 and 2.5 cm^2, respectively. The electrocatalytic peak potential of cbo3 also shifted towards more negative values with increasing nanoparticle size, meaning smaller AuNPs apparently allowed faster electron exchange rates with this enzyme.

Recently, nanoparticles with magnetic properties have also been used for protein immobilisation and their electrochemical studies [70, 71]. They usually contain a metal or metal oxide core of iron or cobalt. The magnetic core is often stabilised by an outer inorganic or organic shell, such as silica [71], carbon [70], etc. where the redox proteins are directly adsorbed. It is possible to further modify these magnetic nanoparticles by anchoring different functional groups to their outer shell to serve specific functions. For example, addition of charged polymers such as PEI increases the solubility of these magnetic nanoparticles in aqueous solutions [72]. Besides, they also provide additional functional groups that can be used for protein cross-linking.

Graphene is also among one of the important carbon materials used for the electrochemical studies of redox proteins. The unique properties of graphene (fast electron transportation, high thermal conductivity, excellent mechanical flexibility and good biocompatibility) provide it with potential applicability in electrochemical biosensors as summarised by Kuila et al. [73] in one of their recent reports.

4 Applications

The efficient confinement of the redox proteins over the transducer surfaces opens the way for their various electrochemical applications with high precision and reproducibility.

4.1 Study of Mechanism

Applications of electrochemical methods in investigation of mechanism of redox protein catalysis have greatly increased in the past few years, as confidence has grown in their ability to provide alternative new insight into complex electron transfer processes [4, 74]. Electrochemical studies of redox proteins have contributed a lot towards understanding enzyme kinetics, substrate binding and structure–function relationships in proteins. Some of the recent examples are elaborated in this section to understand the contributions. As discussed before, CYP is an enzyme whose electrochemical investigation has a huge application potential. However, catalytic cycle of CYP is quite complex which makes its electrochemical investigation quite intriguing [75]. Hagen et al. [27] investigated the CYP 2B4 electrochemistry in DDAB films. The variation of $E^{\circ\prime}$ with a range of temperature from 18°C to 40°C was used to measure the entropy and enthalpy changes that accompany heme reduction in CYP 2B4 to understand the nuclear reorganisation of the enzyme. Reduction of six-coordinate water-ligated Fe^{III} yields five-coordinate Fe^{II} and expulsion of the axial water ligand [74]. The corresponding changes in entropy (ΔS°) and enthalpy (ΔH°) values were -151 J mol^{-1} K^{-1} and -46 kJ mol^{-1}, respectively. To further probe the effect of dehydration, on entropy and enthalpy changes, similar electrochemical experiments with CYP 2B4-DDAB films in the presence of imidazole in solution were performed. Imidazole replaces water as the heme axial ligand and remains bound to the heme in both Fe^{III} and Fe^{II} oxidation states, unlike water which dissociates upon reduction. The values for ΔS° and ΔH° were calculated to be -59 J mol^{-1} K^{-1} and -18 kJ mol^{-1}, respectively, significantly smaller than the water-ligated CYP 2B4. This dramatic difference was explained with the likely structural rearrangements that accompanied these two redox reactions. Reduction of a six-coordinate axially aquated heme triggered water dissociation, whereas reduction of an imidazole-bound heme produced no change in coordination, thus causing minimal nuclear reorganisation resulting in small entropy and enthalpy changes.

Lately, electrochemical studies of redox enzymes are frequently being used to gain significant insight into the enzyme kinetics. They add a new dimension called potential (V) to the familiar substrate concentration ([s]) and time (t) dimensions in the usual enzyme kinetics. The enzyme kinetic studies by electrochemical methods have also benefited from the ability of these methods to utilise extremely small quantities of enzyme sample on an electrode [74]. Fourmond et al. [76] used PFV to examine the kinetics of nitrate reduction by periplasmic nitrate reductase (NapAB) from *Rhodobacter sphaeroides*. The enzyme reversibly interconverts between active and inactive states. In their study, protein film voltammetry proved invaluable for detecting these states and determining the conditions under which they are produced. NapAB was adsorbed on pyrolytic graphite edge (PGE) electrode, and a fast and direct electrochemistry was observed with the activity detected as a negative current with peak potential at -100 mV (Fig. 8a, A). However, the catalytic voltammograms recorded with higher nitrate concentrations exhibited a

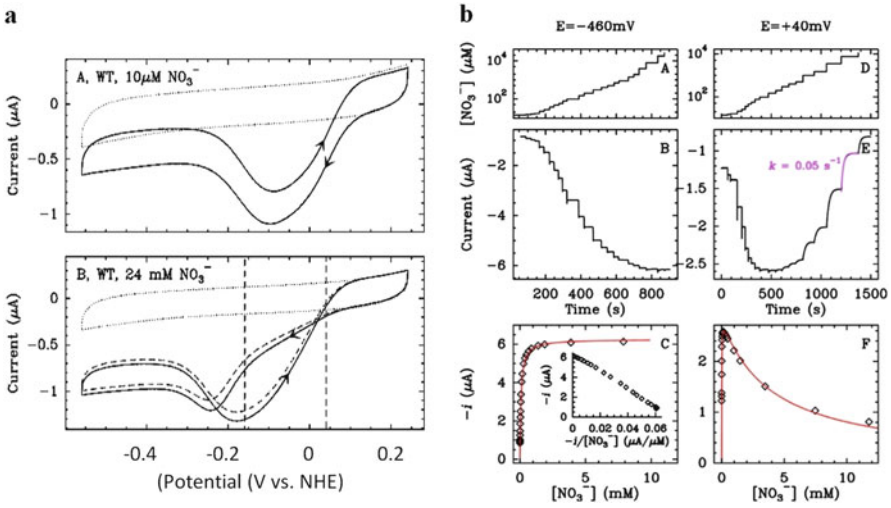

Fig. 8 (**a**) CVs of NapAB adsorbed on a rotating disc PGE electrode, at pH 6, 25°C, a scan rate of 20 mVs^{-1} and an electrode rotation rate of 5 krpm. *Panel A* shows the usual steady-state catalytic response obtained in the presence of 10 μM nitrate (*plain line*); the *dotted line* is a blank recorded with no adsorbed enzyme. The *arrows* indicate the direction of the sweep. *Panel B*: a large hysteresis is visible at high nitrate concentration (24 mM). The *dashed line* is the scan following immediately the *solid line*; the only difference is a decrease in the amplitude of the signal due to film loss. (**b**) Dependence of the rate of nitrate reduction on nitrate concentration. The left- and right-hand sides correspond to a redox poise at −460 and +40 mV vs. SHE, respectively. Conditions: pH 6; 25°C; 5 krpm. *Panels A* and *D* show the evolution of nitrate concentration against time, when the concentration is stepwise increased by adding aliquots of a stock solution of potassium nitrate (note the logarithmic Y scale). *Panels B* and *E* show the resulting change in catalytic current. *Panels C* and *F* show the catalytic current reached at the end of each step as a function of nitrate concentration. The fit of the data in *panel C* to the Michaelis–Menten equation gives $K_m = 85$ μM. The *inset* shows an Eadie–Hofstee plot. The *red line* in *panel F* is the best fit to an equation accounting for substrate inhibition, with $K_m = 10$ μM and $K_i = 4$ mM. Adapted with permission from [76]. Copyright (2010) American Chemical Society

pronounced hysteresis above −200 mV (Fig. 8a, B), and the current measured during the forward scan (towards negative potentials) was smaller than that during the return scan. Chronoamperometric experiments were carried out to understand this phenomenon by stepwise varying the substrate concentration at two different potentials, and the resulting change in activity was monitored as a change in current (Fig. 8b). At very low electrode potential ($E = -460$ mV) (Fig. 8b, A, B, C), the catalytic activity increased with increasing nitrate concentration and followed Michaelis–Menten kinetics. However, under less reductive condition ($E =$ +40 mV) (Fig. 8b, D, E, F), high concentrations of nitrate inhibited the enzyme. The experiments showed that reduction activated NapAB irreversibly, whereas at moderately reducing potentials, high nitrate concentrations reversibly inhibited the enzyme.

Chronoamperometry allows for the study of enzyme kinetics with great temporal resolution which is useful for the study of reactions involving substrate (especially gaseous substrates) binding and depletion with time. Hydrogenases, which catalyse H_2 to H^+ conversion as part of the bioenergetic metabolism of many microorganisms, are among the metalloenzymes for which the existence of a gas-substrate tunnel is already reported (by crystallography and molecular dynamics methods). However, the correlation between protein structure and gas diffusion kinetics remains unexplored. Leroux et al. [77] used chronoamperometry to resolve the kinetics of binding and release of the competitive inhibitor CO in structurally characterised mutants of a NiFe hydrogenase (Fig. 9a and b). As shown in Fig. 9a, the mutations L122M-V74M (MM) and L122F-V74I (FI) significantly narrow the tunnel near the entrance of the catalytic centre. Since CO substitutes for H_2 at the active site of NiFe hydrogenase in a competitive manner, PFV was used to monitor H_2 oxidation to measure the rates of binding and release of the competitive inhibitor CO with high temporal resolution. In the wild-type (WT) enzyme at room temperature, binding of CO was fast (Fig. 9b, A); it is just below the diffusion limit of $10^8\ s^{-1}\ M^{-1}$ [$\sim 10^5\ s^{-1}$ atm $(CO)^{-1}$; the solubility of CO is 0.96 mM atm^{-1}]. The two double mutations induced spectacular delays in both binding and release of CO (Fig. 9b, B and C). The rate constants for both forward and backward CO transport decreased by more than two orders of magnitude in MM mutant, whereas the double FI mutant had an intermediate phenotype. Since the mutations affect the rates of CO binding and release in approximately the same

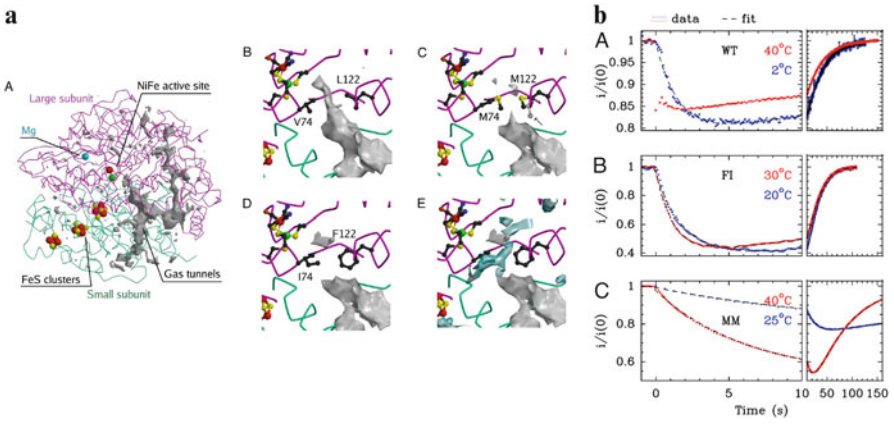

Fig. 9 (**a**) Structural models of the three enzymes. *A* is an overview of the tunnel network; *B* is a close-up of the tunnel near the active site in the WT. *C*, *D* and *E* are close-ups of the MM and FI mutants, as indicated. In *C*, an arrow points to the second conformation of M122. A conserved hydrophilic cavity is shown in *blue* in *E*. (**b**) Comparison of the kinetics of CO inhibition of H_2 oxidation in PFV experiments. The current (i) has been normalised by its value i_0, measured before CO was added. *Left* shows the short-term change in current, whereas the end of the relaxation is shown on *Right*. The dimensionless volumic fractions of solutions saturated under 1 atm of CO at 25°C and injected at time 0. Electrode rotation rate 2 krpm, pH 7. Adapted with permission from [77]. Copyright (2008) PNAS

manner, they had a smaller effect on the binding affinity, which is the ratio of the two. This was expected for a mutation that affects the channel for CO access, but not the free energy of binding at the active site. Thus electrochemical studies established the effect of mutations affecting the molecular structure of substrate tunnels in hydrogenase enzyme. In fact, electrochemical studies of redox proteins are now fast becoming an inevitable tool to establish or support structure–function findings [78–80].

4.2 Biosensors

Biosensors are the most practical and important applications where developments in electrochemical studies of redox proteins have played a major role. In the last decade, a substantial part of these studies were directed towards biosensing applications. However, most of these biosensing devices were of lab scale that are yet to be optimised for real-world applications. Sensors in general are devices that register a physical, chemical or biological change and convert them into a measurable signal. They usually contain a recognition element which detects the analyte of interest, a transducer that produces the signal and a processor that collects, amplifies and displays the signal. Electrochemical biosensors are a class of sensors that combine the sensitivity and selectivity of biological components (especially enzymes) with low detection capabilities of electrochemical transducers ($\sim 10^{-12}$ A current). The biosensor performance is usually evaluated on the basis of its selectivity, sensitivity, limit of detection (LOD), reproducibility, response time, operational and storage stability, ease of use and portability. With the onset of electrochemical biosensors in 1960s and subsequent development of glucose biosensors for blood glucose analysis, a volume of literature has been published in last 50 years. Some of the recent reviews have covered the details about the enzymatic biosensors including their working principal, design, selection of biocatalyst and immobilisation strategies for biocatalysts over electrodes followed by their usage and performance for clinical, environmental and industrial applications [5, 81–86].

Electrochemical biosensors have found their potential applications in clinical diagnostics. The substrate specificity (selectivity) and sensitivity of enzymatic biosensors avoid a great deal of sample preparation when analysing complex biological fluids such as blood or urine. In Sect. 3, we have already seen that many of the immobilisation strategies were directed towards the development of glucose biosensor for blood glucose analysis. However, the studies on glucose biosensors are consciously eluded here in this section as this book contains an independent chapter focused on glucose biosensors. After glucose, cholesterol is one among the important analytes in blood that requires frequent monitoring. It is an important biomarker in the diagnosis of many diseases, such as hypertension, coronary heart disease, arteriosclerosis, lipid metabolism dysfunction, etc. This has led to an increased interest in the development of various kinds of cholesterol biosensors [87]. Saxena et al. [88] developed a cholesterol oxidase (ChOx)

bioelectrode and established its potential as biosensor for total cholesterol determination in human serum samples. ChOx was immobilised on AuNP-modified gold electrode. The nanoparticle film on the electrode surface provided an environment for the enhanced electrocatalytic activity of ChOx and thus resulted in enhanced analytical response. The resulting bioelectrode exhibited a linear response to cholesterol in the range of 0.04–0.22 mM with a detection limit of 34.6 μM and a high sensitivity of 9.02 μA mM^{-1} at a working potential of 0.46 V. A high operational (6 h, 30 measurements) and storage stability (~95% residual activity after 1 month of storage) was reported for this ChOx-based biosensor. A recent report by Saxena and Das [89] summarised the progress in designing and fabrication of cholesterol biosensors using nanomaterials and their importance in clinical studies.

In addition to clinical diagnostic applications [84, 85], enzymatic biosensors have also made a lot of progress in environmental applications [81, 86] such as for detection of various pollutants, pesticides, heavy metal contaminations of groundwater, etc. to name a few. The monitoring of arsenite, the major contributor of groundwater arsenic contamination, is among one of the major environmental concerns that requires immediate attention. Arsenite oxidase (ArO), a molybdenum-containing enzyme, is responsible for arsenite utilisation in a large number of microorganisms, e.g. *Rhizobium* sp. str. NT-26, *Alcaligenes faecalis*, etc. The arsenite utilisation pathways in these organisms make use of arsenite as the electron donor and molecular oxygen as the terminal electron acceptor. Despite having a huge potential for biosensor applications for one of the most dreaded pollutants of water, ArO was largely ignored in terms of its electrochemical studies. The reason could again be attributed to the enzyme being dimeric and bulky (heterologous subunits: molybdenum-containing Aro A, MW ~90 kDa, and Rieske-type Fe–S-containing Aro B, MW ~15 kDa) [90]. However, a biosensor for arsenite was developed using ArO (from *Rhizobium* sp. str. NT-26) that oxidises arsenite to arsenate. ArO was galvanostatically deposited onto the active surface of a MWCNT-modified GCE. The resulting biosensor showed a linearity up to 500 ppb and a detection limit of 1 ppb for arsenite at 0.3 V electrode potential. A low response time (~10 s) and excellent reproducibility were reported for the ArO biosensor. The biosensor was used for repeated analysis of spiked arsenite in tap water, river water and commercial mineral water. River water from the St. Lawrence River was analysed using the ArO biosensor (Fig. 10). The results implied that arsenite was not present in the river water, since the current signal (~17 nA) for curve b was very similar in the presence or absence of ArO (Fig. 10A and B). The results were later confirmed by other established methods for arsenite determination.

Enzymatic biosensors also have potential applications in the food industry to detect the analytes which should be in permissible levels, e.g. peroxides, sulphites, etc. Sulphite is used as an additive in food and beverages to prevent oxidation and bacterial growth and to control enzymatic reactions during production and storage. The level of sulphite is the subject of legislation because it can cause asthmatic attacks and allergic reactions to hypersensitive people. Wollenberger and

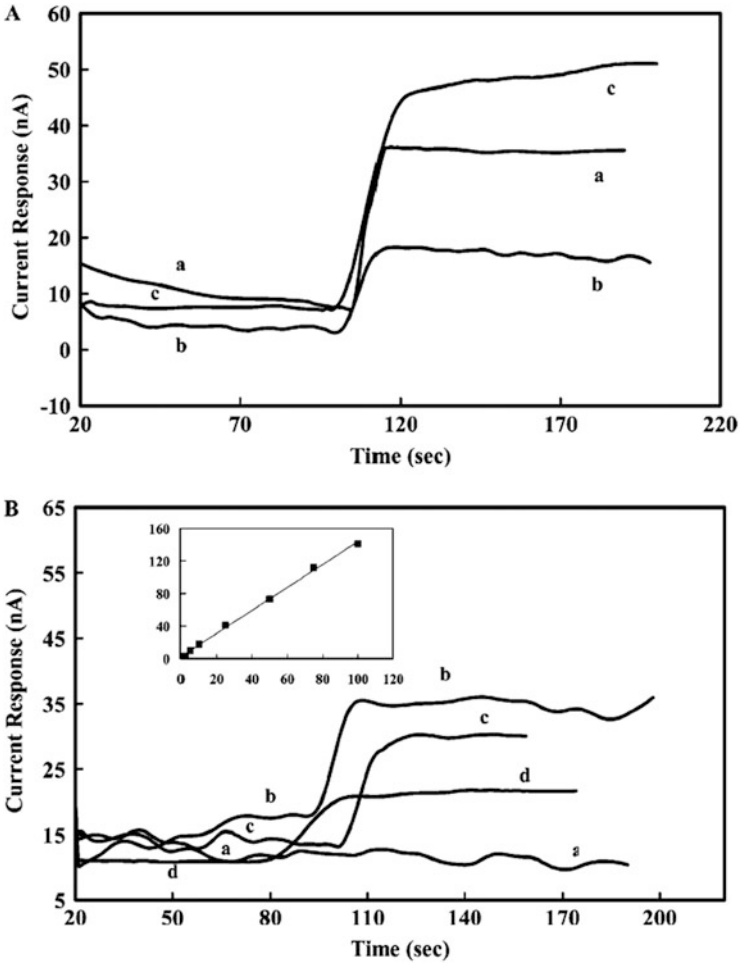

Fig. 10 (**A**) St. Lawrence River water analysis with MWCNTs/ArO/GCE (*a*) 20 ppb arsenite, (*b*) St. Lawrence River water alone and (*c*) St. Lawrence River water spiked with arsenite to give 20 ppb after mixing. (**B**) St. Lawrence River water analysis with MWCNTs/GCE (*a*) 20 ppb arsenite, (*b*) St. Lawrence River water alone, (*c*) river water spiked with arsenite to give 20 ppb after mixing and (*d*) 10 ppm humic acid. The *inset* shows a calibration curve for arsenite in the presence of the St. Lawrence River water. Adapted with permission from [90]. Copyright (2007) American Chemical Society

co-workers [91] developed sulphite biosensor using human sulphite oxidase (hSO) enzyme, a metalloprotein containing the molybdenum cofactor and a cytochrome b5-type heme. In a layer-by-layer assembly method, the hSO was co-immobilised with cyt c in polyaniline sulphonic acid. A 17-bilayer electrode showed a linear range between 1 and 60 μM sulphite with a sensitivity of 2.19 mA M^{-1} sulphite and a response time of 2 min. The multilayer electrode was used for determination of sulphite in unspiked and spiked samples of red and white wine.

The recent developments in electrochemical studies of redox enzymes have opened a whole new horizon for biosensor development for a variety of analytical applications. However, a lot of research is still required to find potential biocatalysts for a number of analytes that need constant monitoring and to make electrochemical biosensors commercially successful bioanalytical device.

4.3 Biofuel Cells

In addition to biosensors, biofuel cells are another important devices benefitting from the recent progress in electrochemical studies of redox proteins. With the increasing energy demand and depleting non-renewable energy resources, it is important to shift our focus to utilise renewable resources. Biofuel cells provide one such alternative, where microbes or isolated enzymes are used to utilise fuels such as glucose, fructose, lactose, ethanol, methanol, H_2, etc. for energy generation. Microbial fuel cells provide certain advantages over enzymatic fuel cells (EFCs), e.g. longer lifetime, capability of complete oxidation of fuel, etc. They are however limited by low power densities and lack of substrate specificities which necessitate the use of membrane separator in microbial fuel cells. EFCs are used to overcome the shortcomings of microbial fuel cells by providing better substrate specificity and higher power densities. EFCs also provide certain edge over inorganic catalyst-based chemical fuel cells, e.g. the overpotential of EFCs is usually close to zero, they have the ability to scavenge fuel and oxidant from ambient environment (even when they are present in trace concentrations) and they are feasible to be used in disposable and completely biodegradable devices. However, EFCs drastically lag behind the chemical fuel cells in the amount of power produced and their shelf life. The time and cost of isolation and purification of enzymes, their poor stability and restricted pH and temperature optima for functioning and difficulty in achieving good electronic coupling with the electrode are other serious limitations of EFCs. The focussed research towards finding novel biocatalysts from natural resources or engineering the available enzymes to generate improved biocatalysts combined with the efficient immobilisation strategies of biocatalysts over electrodes has a potential to solve few of the above-mentioned problems. Some of the recent reviews [6, 7, 92–96] have detailed the developments in the field of EFCs from selection of biocatalysts and their immobilisation strategies to the design and characterisation of EFCs for their theoretical and practical applications. A wide variety of redox proteins have been employed to create unique biofuel cells that can be used in applications such as implantable power sources, energy sources for small electronic devices, self-powered sensors and bioelectrocatalytic logic gates.

Like other chemical fuel cells, EFCs have cathode-receiving oxidant and anode-receiving reductant or fuel. For most EFCs, O_2 is the oxidant of choice because it is freely available and has a high reduction potential, thus maximising the voltage output of the cell. The enzymes commonly used for O_2 reduction at cathode are blue copper oxidases such as laccase or bilirubin oxidase. Peroxidases containing iron

porphyrins are also used at cathode for reduction of H_2O_2. The enzymes commonly used at anode are oxidases, dehydrogenases or hydrogenases which use sugar, alcohol or H_2 as fuel. Some of the hydrogenases use proton as an oxidant and reduce it to produce H_2 at cathode. This concept is useful in identifying possible ways for renewable H_2 production [6]. In one of the examples, the [FeFe]-hydrogenase from *Clostridium acetobutylicum* attached to a carbon electrode was shown to be a very good catalyst for H^+ reduction, and this property was further demonstrated in a device in which light-dependent H_2 production was observed when this hydrogenase electrode was coupled to a TiO_2 photoanode with NADH as electron donor [97].

Habrioux et al. [98] developed a concentric glucose/O_2 biofuel cell. The device constituted two carbon tubular electrodes, one in the other, and combined the glucose electrooxidation at the anode and O_2 electroreduction at the cathode (Fig. 11A). The anodic catalyst was GOx co-immobilised with the mediator 8-hydroxyquinoline-5-sulphonic acid hydrate, and the cathodic catalyst was bilirubin oxidase co-immobilised with the mediator 2,20-azinobis(3-ethylbenzothiazoline-6-sulphonate) diammonium salt. Both enzymes and mediators were entrapped at the surface of the tubular electrodes by an electrogenerated PPy polymer. The concept of the concentric configuration was to compartmentalise the anode and cathode electrodes and to supply dissolved O_2 separate from the electrolyte in order to avoid secondary reactions. The dissolved O_2 circulated through the inside of the cathode tube and diffused from the inner to the external surface of the tube to react directly with the immobilised bilirubin oxidase. The assembled biofuel cell was studied at 37°C in phosphate buffer pH 7.4 (Fig. 11B). They further studied the influence of the thickness of the PPy polymer on the electrochemical activity of the bioelectrodes. As the enzymes were mainly adsorbed on the electrode surface of the tube rather than within the polymer film (which acted as conductive matrix to avoid enzyme linkage and the loss of mediator, Fig. 11A), the decrease in PPy thickness led to higher current density for the biocathode, whereas no real effect was observed on the catalytic electrooxidation of glucose at the anode. They also demonstrated the effect of the chemical reticulation of the enzymes by glutaraldehyde within the polymer on the performances of the bioelectrodes. In this case the bioanode showed increase in current density. The maximum power density delivered by the assembled glucose/O_2 biofuel cell reached 42 μW cm^{-2}, at a cell voltage of 0.3 V with 10 mM glucose. The results demonstrated that the concentric design of the EFC based on compartmented electrodes is a promising architecture for further development of microelectronic devices.

To overcome the limitations of partial oxidation of fuel by EFCs and to enhance their power output, Minteer and co-workers [99–101] immobilised multiple enzymes of citric acid cycle or enzymes for complete oxidation of glycerol on respective anodes. In one of the examples [101], they developed the enzymatic bioanode for complete oxidation of pyruvate, where the bioanode contained the enzymes of the Kreb's cycle (Fig. 12A). Representative power curves for the five biofuel cells containing different numbers of dehydrogenase enzymes are shown in

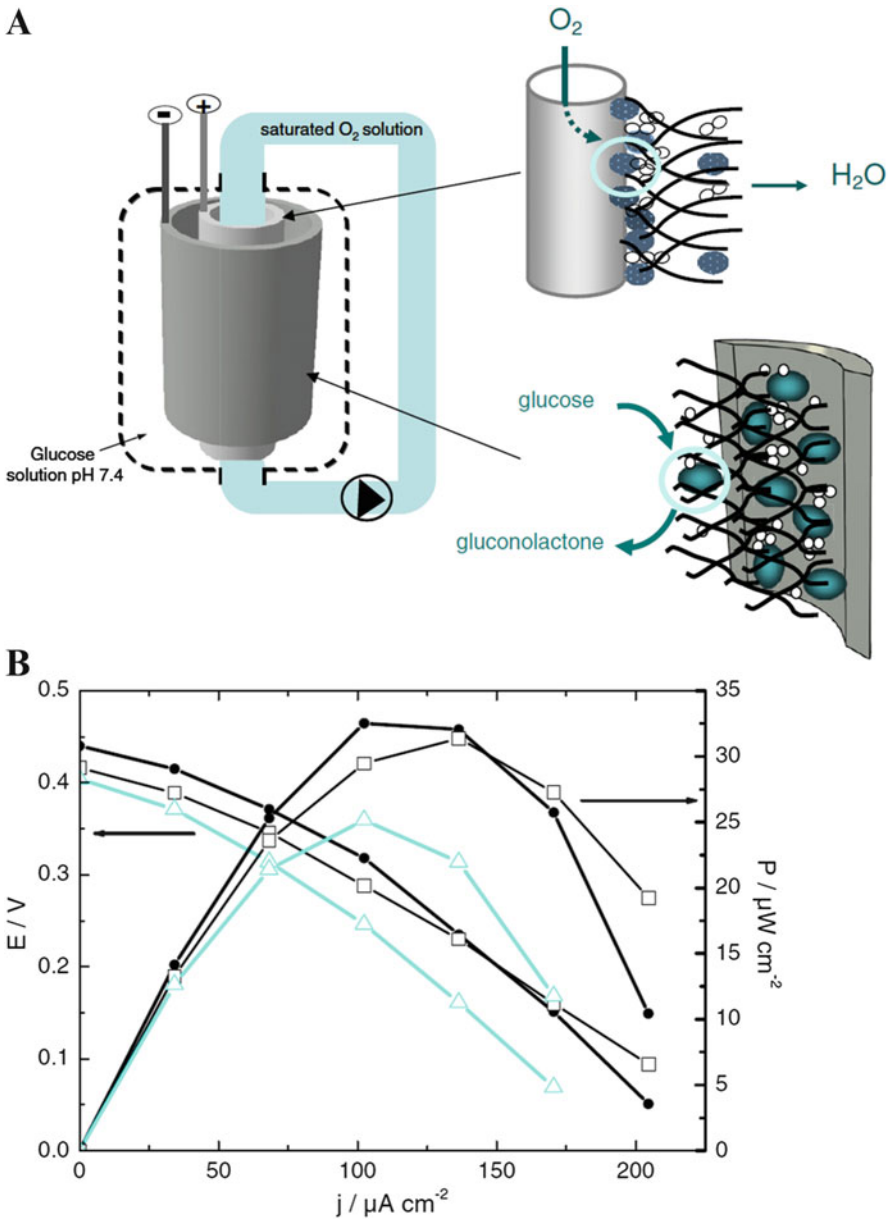

Fig. 11 (**A**) Schematic configuration of the EFC prototype working from glucose and O_2 as fuel and oxidant, respectively. (**B**) Fuel cell performances obtained with the biocathode and the bioanode in a phosphate-buffered solution (pH 7.4) containing 10 mM glucose at 37°C. A saturated O_2 solution circulates in the interior of the inner cathode tube. (–●–) initial performances; (–□–) after 3 operating hours; (–Δ–) after 3 operating hours and 2 days of storage at 4°C. Adapted with permission from [98]. Copyright (2008) Elsevier

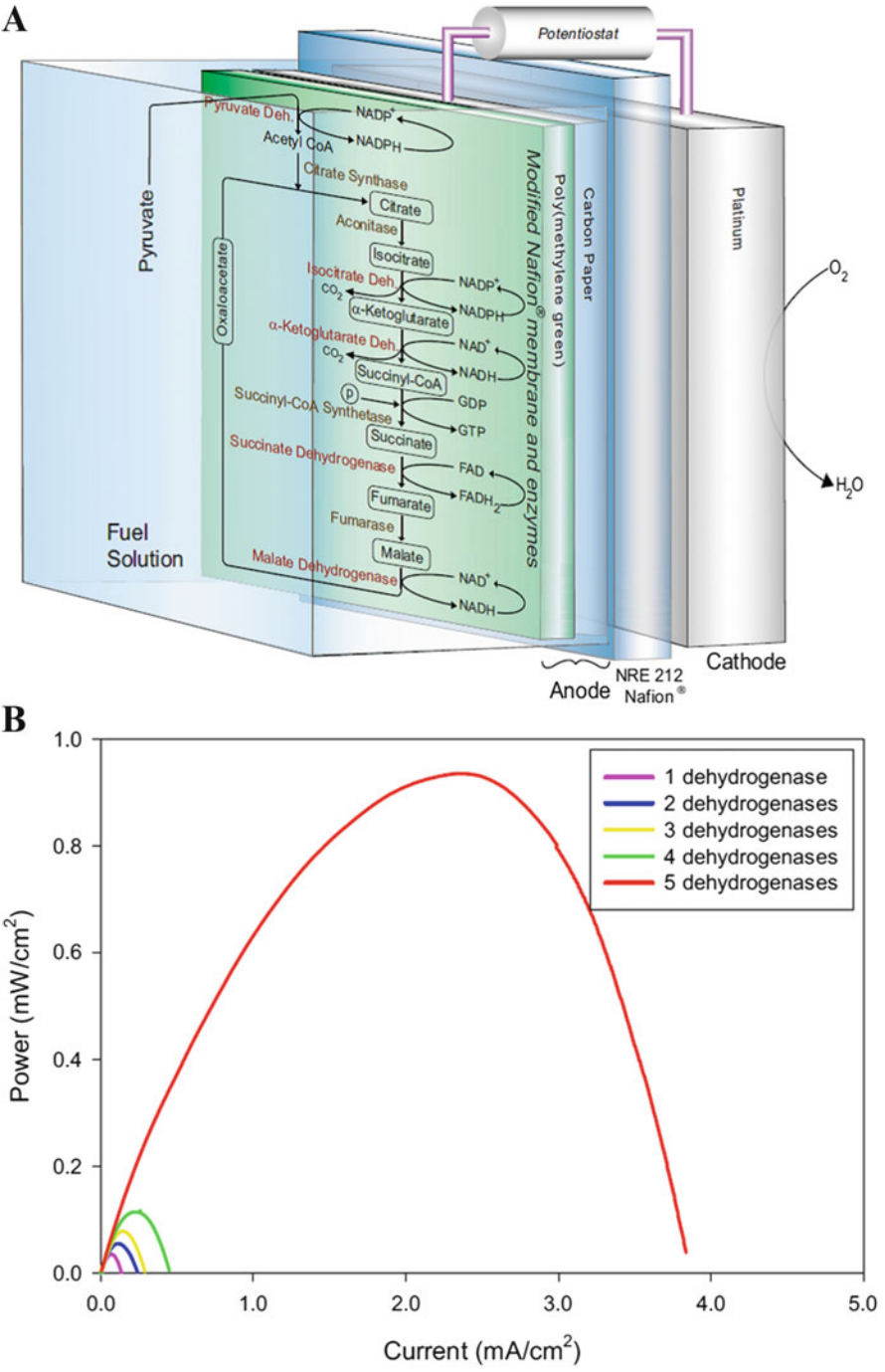

Fig. 12 (**A**) Schematic of the chemistry occurring at the pyruvate/air biofuel cell. (**B**) Representative power curves for pyruvate/air biofuel cells in 100 mM sodium pyruvate fuel solution at room temperature. Adapted with permission from [101]. Copyright (2009) Electrochemical Society

Fig. 12B. As the number of dehydrogenase enzymes increased, the current and power density increased from 0.0298 ± 0.0082 mW cm^{-2} to 0.931 ± 0.091 mW cm^{-2} with 31.2-fold overall increase in power output. An overall 4.6-fold power density increase was observed using individual Kreb's cycle enzymes when compared to the intact mitochondria. These results showed that the complete oxidation of fuel could increase the power output of EFCs drastically.

5 Conclusions

Electrochemical studies of redox proteins have made tremendous progress in the last decade which is reflected in the literature published so far. A wide range of proteins are now being studied electrochemically, and these studies have become an integral part of protein characterisation and their structure–function studies. The constant research work dedicated towards improving the immobilisation strategies of redox proteins over electrodes for their maximum stability and electron transfer efficiency has made these studies more feasible and reproducible. Discovery and synthesis of novel materials including a variety of nanomaterials have only fuelled this progress. Recent development and use of different spectroscopic and microscopic techniques have made it possible to visualise the details at molecular level thus complementing the findings obtained by electrochemical analysis and making them more reliable. All these developments combined with the constant efforts towards improvement in stability, biocompatibility and miniaturisation of bioelectrochemical systems have established biosensors as a promising bioanalytical device for monitoring analytes of clinical, environmental and industrial importance. In addition to biosensors, the research work on enzymatic biofuel cells has also benefitted a lot from the recent progress in electrochemical studies of redox proteins. A considerable progress in stability, performance and overall power output of EFCs has been achieved. Although they still lag behind the chemical fuel cells in their power output, they are promising towards fuelling small portable and disposable devices. Thus electrochemical studies of redox proteins have become quite an interdisciplinary field of research which requires constant attention of researchers for their various theoretical and practical implications.

Acknowledgements I am thankful to Alexander von Humboldt Foundation for the financial support.

References

1. Nelson DL, Cox MM (2008) Oxidative phosphorylation and photophosphorylation. In: Lehninger principles of biochemistry, 5th edn. W. H. Freeman, New York

2. Gamenara D, Seoane G, Méndez PS, Domínguez de María P (2012) Redox biocatalysis: fundamentals and applications. Wiley, Hoboken
3. Messerschmidt A, Bode W, Cygler M (eds) (2004) Handbook of metalloproteins. Wiley, Chichester
4. Léger C, Bertrand P (2008) Direct electrochemistry of redox enzymes as a tool for mechanistic studies. Chem Rev 108:2379–2438
5. Newman JD, Setford SJ (2006) Enzymatic biosensors. Mol Biotechnol 32:249–268
6. Cracknell JA, Vincent KA, Armstrong FA (2008) Enzymes as working or inspirational electrocatalysts for fuel cells and electrolysis. Chem Rev 108:2439–2461
7. Minteer SD, Liaw BY, Cooney MJ (2007) Enzyme-based biofuel cells. Curr Opin Biotechnol 18:228–234
8. Bowden EF, Hawkridge FM, Blount HN (1985) Electrochemical aspects of bioenergetics. In: Srinivasan S, Chizmadzhev YA, Bockris JOM, Conway BE, Yeager E (eds) Comprehensive treatise of electrochemistry, vol 10. Plenum, New York, pp 297–346
9. Armstrong FA (1990) Probing metalloproteins by voltammetry. In: Bioinorganic chemistry, vol 72, Structure and bonding. Springer, Berlin, pp 137–221
10. Sarma AK, Vatsyayan P, Goswami P, Minteer SD (2009) Recent advances in material science for developing enzyme electrodes. Biosens Bioelectron 24:2313–2322
11. Prabhulkar S, Tian H, Wang X, Zhu J-J, Li C-Z (2012) Engineered proteins: redox properties and their applications. Antioxid Redox Signal 17:1796–1822
12. Hill HAO, Moore CB, NabiRahni DMA (1997) Electrochemistry of redox proteins. In: Lenaz G, Milazzot G (eds) Bioelectrochemistry of biomacromolecules. Birkhauser, Basel
13. Armstrong FA, Wilson GS (2000) Recent developments in faradaic bioelectrochemistry. Electrochim Acta 45:2623–2645
14. Habermüller K, Mosbach M, Schumann W (2000) Electron-transfer mechanisms in amperometric biosensors. Fresenius J Anal Chem 366:560–568
15. Ferapontova EE, Shleev S, Ruzgas T, Stoica L, Christenson A, Tkac J, Yaropolov AI, Gorton L (2005) Direct electrochemistry of proteins and enzymes. Perspectives in bioanalysis 1:517–598
16. Rusling JF, Wang B, Yun S (2008) Electrochemistry of redox enzymes. In: Bartlett PN (ed) Bioelectrochemistry, fundamentals, experimental techniques and applications. Wiley, Hoboken
17. Willner I, Katz E (eds) (2005) Bioelectronics from theory to applications. Wiley, Weinheim
18. Zhang W, Li G (2004) Third-generation biosensors based on the direct electron transfer of proteins. Anal Sci 20:603–609
19. Roger M, de Poulpiquet A, Ciaccafava A, Ilbert M, Guiral M, Giudici-Orticoni MT, Lojou E (2014) Reconstitution of supramolecular organization involved in energy metabolism at electrochemical interfaces for biosensing and bioenergy production. Anal Bioanal Chem 406:1011–1027
20. Léger C (2012) Direct electrochemistry of proteins and enzymes: an introduction
21. Laviron E (1979) General expression of the linear potential sweep voltammogram in the case of diffusionless electrochemical systems. J Electroanal Chem 101:19–28
22. Lisdat F, Schäfer D (2008) The use of electrochemical impedance spectroscopy for biosensing. Anal Bioanal Chem 391:1555–1567
23. Szamocki R, Velichko A, Mücklich F, Reculusa S, Ravaine S, Neugebauer S, Schuhmann W, Hempelmann R, Kuhn A (2007) Improved enzyme immobilization for enhanced bioelectrocatalytic activity of porous electrodes. Electrochem Commun 9:2121–2127
24. Patolsky F, Weizmann Y, Willner I (2004) Long-range electrical contacting of redox enzymes by SWCNT connectors. Angew Chem Int Ed 43:2113–2117
25. Yang J, Xu Y, Zhang R, Wang Y, He P, Fang Y (2009) Direct electrochemistry and electrocatalysis of the hemoglobin immobilized on diazonium-functionalized aligned carbon nanotubes electrode. Electroanalysis 21:1672–1677

26. Udit AK, Hagen KD, Goldman PJ, Star A, Gillan JM, Gray HB, Hill MG (2006) Spectroscopy and electrochemistry of cytochrome p450 BM3-surfactant film assemblies. J Am Chem Soc 128:10320–10325
27. Hagen KD, Gillan JM, Im S-C, Landefeld S, Mead G, Hiley M, Waskell LA, Hill MG, Udit AK (2013) Electrochemistry of mammalian cytochrome P450 2B4 indicates tunable thermodynamic parameters in surfactant films. J Inorg Biochem 129:30–34
28. Lioubashevski O, Chegel VI, Patolsky F, Katz E, Willner I (2004) Enzyme-catalyzed bio-pumping of electrons into Au-nanoparticles: a surface plasmon resonance and electrochemical study. J Am Chem Soc 126:7133–7143
29. Mateo C, Palomo JM, Fernandez-Lorente G, Guisan JM, Fernandez-Lafuente R (2007) Improvement of enzyme activity, stability and selectivity via immobilization techniques. Enzyme Microb Technol 40:1451–1463
30. Kotyk A, Janacek K, Koryta J (1988) Biophysical chemistry of membrane function. Wiley, Chichester
31. Jeuken LJC (2009) Electrodes for integral membrane enzymes. Nat Prod Rep 26:1234–1240
32. Melin F, Hellwig P (2013) Recent advances in the electrochemistry and spectroelectrochemistry of membrane proteins. Biol Chem 394:593–609
33. Rusling JF (1998) Enzyme bioelectrochemistry in cast biomembrane-like films. Acc Chem Res 31:363–369
34. Khan MS, Dosoky NS, Williams JD (2013) Engineering lipid bilayer membranes for protein studies. Int J Mol Sci 14:21561–21597
35. Jeuken LJC, Connell SD, Henderson PJF, Gennis RB, Evans SD, Bushby RJ (2006) Redox enzymes in tethered membranes. J Am Chem Soc 128:1711–1716
36. Beilen JB, Funhoff EG (2005) Expanding the alkane oxygenase toolbox: new enzymes and applications. Curr Opin Biotechnol 16:308–314
37. Udit AK, Gray HB (2005) Electrochemistry of heme-thiolate proteins. Biochem Biophys Res Commun 338:470–476
38. Walcarius A, Kuhn A (2008) Ordered porous thin films in electrochemical analysis. Trends Anal Chem 27:593–603
39. Szamocki R, Reculusa S, Ravaine S, Bartlett PN, Kuhn A, Hempelmann R (2006) Tailored mesostructuring and biofunctionalization of gold for increased electroactivity. Angew Chem Int Ed Engl 45:1317–1321
40. Wang CH, Yang C, Song YY, Gao W, Xia XH (2005) Adsorption and direct electron transfer from hemoglobin into a three-dimensionally ordered macroporous gold film. Adv Funct Mater 15:1267–1275
41. Rusling JF, Forster RJ (2003) Electrochemical catalysis with redox polymer and polyion–protein films. J Colloid Interface Sci 262:1–15
42. Vatsyayan P, Bordoloi S, Goswami P (2010) Large catalase based bioelectrode for biosensor application. Biophys Chem 153:36–42
43. Marcus RA, Sutin N (1985) Electron transfers in chemistry and biology. Biochim Biophys Acta 811:265–322
44. Henstridge MC, Laborda E, Rees NV, Compton RG (2012) Marcus–Hush–Chidsey theory of electron transfer applied to voltammetry: a review. Electrochim Acta 84:12–20
45. Plumeré N, Rüdiger O, Oughli AA, Williams R, Vivekananthan J, Pöller S, Schuhmann W, Lubitz W (2014) A redox hydrogel protects hydrogenase from high-potential deactivation and oxygen damage. Nat Chem 6:822–827
46. Malhotra BD, Chaubey A, Singh SP (2006) Prospects of conducting polymers in biosensors. Anal Chim Acta 578:59–74
47. Ahuja T, Mir IA, Kumar D, Rajesh (2007) Biomolecular immobilization on conducting polymers for biosensing applications. Biomaterials 28:791–805
48. Rahman MA, Kumar P, Park D-S, Shim Y-B (2008) Electrochemical sensors based on organic conjugated polymers. Sensors 8:118–141

49. Willner B, Katz E, Willner I (2006) Electrical contacting of redox proteins by nanotechnological means. Curr Opin Biotechnol 17:589–596
50. Xiao Y, Patolsky F, Katz E, Hainfeld JF, Willner I (2003) Plugging into enzymes: nanowiring of redox enzymes by a gold nanoparticle. Science 299:1877–1881
51. Campàs M, Prieto-Simón B, Marty J-L (2009) A review of the use of genetically engineered enzymes in electrochemical biosensors. Semin Cell Dev Biol 20:3–9
52. Sadeghi SJ, Meharenna YT, Fantuzzi A, Valetti F, Gilardi G (2000) Engineering artificial redox chains by molecular "lego". Faraday Discuss 116:135–153
53. Wong TS, Schwaneberg U (2003) Protein engineering in bioelectrocatalysis. Curr Opin Biotechnol 14:590–596
54. Marshall NM, Garner DK, Wilson TD, Gao Y-G, Robinson H, Nilges MJ, Lu Y (2009) Rationally tuning the reduction potential of a single cupredoxin beyond the natural range. Nature 462:113–117
55. Kumar S, Chen CS, Waxman DJ, Halpert JR (2005) Directed evolution of mammalian cytochrome P450 2B1, mutations outside of the active site enhance the metabolism of several substrates, including the anticancer prodrugs cyclophosphamide and ifosfamide. J Biol Chem 280:19569–19575
56. Axarli I, Prigipaki A, Labrou NE (2005) Engineering the substrate specificity of cytochrome P450 CYP102A2 by directed evolution: production of an efficient enzyme for bioconversion of fine chemicals. Biomol Eng 22:81–88
57. Sarauli D, Riedel M, Wettstein C, Hahn R, Stib K, Wollenberger U, Leimkühler S, Schmuki P, Lisdat F (2012) Semimetallic TiO_2 nanotubes: new interfaces for bioelectrochemical enzymatic catalysis. J Mater Chem 22:4615–4618
58. Pradhan D, Niroui F, Leung KT (2010) High-performance, flexible enzymatic glucose biosensor based on ZnO nanowires supported on a gold-coated polyester substrate. ACS Appl Mater Interfaces 2:2409–2412
59. Wanekaya AK, Chen W, Myung NV, Mulchandani A (2006) Nanowire-based electrochemical biosensors. Electroanalysis 18:533–550
60. Kumar AM, Jung S, Ji T (2011) Protein biosensors based on polymer nanowires, carbon nanotubes and zinc oxide nanorods. Sensors 11:5087–5111
61. Jacobs CB, Peairs MJ, Venton BJ (2010) Review: carbon nanotube based electrochemical sensors for biomolecules. Anal Chim Acta 662:105–127
62. Esplandiu MJ, Pacios M, Cyganek L, Bartroli J, del Valle M (2009) Enhancing the electrochemical response of myoglobin with carbon nanotube electrodes. Nanotechnology 20:355502
63. Cusmà A, Curulli A, Zane D, Kaciulis S, Padeletti G (2007) Feasibility of enzyme biosensors based on gold nanowires. Mater Sci Eng C 27:1158–1161
64. Dawson K, Baudequin M, O'Riordan A (2011) Single on-chip gold nanowires for electrochemical biosensing of glucose. Analyst 136:4507–4513
65. Mayorga-Martinez CC, Guix M, Madrid RE, Merkoci A (2012) Bimetallic nanowires as electrocatalysts for nonenzymatic real-time impedancimetric detection of glucose. Chem Commun 48:1686–1688
66. Travas-Sejdic J, Aydemir N, Kannan B, Williams DE, Malmström J (2014) Intrinsically conducting polymer nanowires for biosensing. J Mater Chem B 2:4593–4609
67. Wang Z, Liu S, Wu P, Cai C (2009) Detection of glucose based on direct electron transfer reaction of glucose oxidase immobilized on highly ordered polyaniline nanotubes. Anal Chem 81:1638–1645
68. Pingarron JM, Yanez-Sedeno P, Gonzalez-Cortes A (2008) Gold nanoparticle-based electrochemical biosensors. Electrochim Acta 53:5848–5866
69. Melin F, Meyer T, Lankiang S, Choi SK, Gennis RB, Blanck C, Schmutz M, Hellwig P (2013) Direct electrochemistry of cytochrome bo3 oxidase at a series of gold nanoparticles-modified electrodes. Electrochem Commun 26:105–108

70. Yu D, Renedo OD, Blankert B, Sima V, Sandulescu R, Arcos J, Kauffmann J-M (2006) A peroxidase-based biosensor supported by nanoporous magnetic silica microparticles for acetaminophen biotransformation and inhibition studies. Electroanalysis 18:1637–1642
71. Nowicka AM, Kowalczyk A, Donten ML, Donten M, Bystrzejewski M, Stojek Z (2014) Carbon-encapsulated iron nanoparticles as ferromagnetic matrix for oxygen reduction in absence and presence of immobilized laccase. Electrochim Acta 126:115–121
72. Kainz QM, Fernandes S, Eichenseer CM, Besostri F, Koerner H, Mueller R, Reiser O (2014) Synthesis of functionalized, dispersible carbon-coated cobalt nanoparticles for potential biomedical applications. Faraday Discuss 175:27–40
73. Kuila T, Bose S, Khanra P, Mishra AK, Kim NH, Lee JH (2011) Recent advances in graphene-based biosensors. Biosens Bioelectron 26:4637–4648
74. Armstrong FA (2005) Recent developments in dynamic electrochemical studies of adsorbed enzymes and their active sites. Curr Opin Chem Biol 9:110–117
75. Honeychurch M, The direct electrochemistry of cytochrome P450. What are we actually measuring? m.honeychurch@uq.edu.au
76. Fourmond V, Sabaty M, Arnoux P, Bertrand P, Pignol D, Leger C (2010) Reassessing the strategies for trapping catalytic intermediates during nitrate reductase turnover. J Phys Chem B 114:3341–3347
77. Leroux F, Dementin S, Burlat B, Cournac L, Volbeda A, Champ S, Martin L, Guigliarelli B, Bertrand P, Fontecilla-Camps J, Rousset M (2008) Experimental approaches to kinetics of gas diffusion in hydrogenase. Proc Natl Acad Sci U S A 105:11188–11193
78. Almeida MG, Silveira CM, Guigliarelli B, Bertrand P, Moura JJG, Moura I, Leger C (2007) A needle in a haystack: the active site of the membrane-bound complex cytochrome c nitrite reductase. FEBS Lett 581:284–288
79. Lautier T, Ezanno P, Baffert C, Fourmond V, Cournac L, Fontecilla-Camps JC, Soucaille P, Bertrand P, Meynial-Salles I, Leger C (2011) The quest for a functional substrate access tunnel in FeFe hydrogenase. Faraday Discuss 148:385–407
80. Liebgott P-P, Leroux F, Burlat B, Dementin S, Baffert C, Lautier T, Fourmond V, Ceccaldi P, Cavazza C, Meynial-Salles I, Soucaille P, Fontecilla-Camps JC, Guigliarelli B, Bertrand P, Rousset M, Léger C (2010) Relating diffusion along the substrate tunnel and oxygen sensitivity in hydrogenase. Nat Chem Biol 6:63–70
81. Rodriguez-Mozaz S, Lopez de Alda MJ, Marco MP, Barcelo D (2005) Biosensors for environmental monitoring A global perspective. Talanta 65:291–297
82. Grieshaber D, MacKenzie R, Vörös J, Reimhult E (2008) Electrochemical biosensors – sensor principles and architectures. Sensors 8:1400–1458
83. Ronkainen NJ, Halsall HB, Heineman WR (2010) Electrochemical biosensors. Chem Soc Rev 39:1747–1763
84. Yoo E-H, Lee S-Y (2010) Glucose biosensors: an overview of use in clinical practice. Sensors 10:4558–4576
85. Vaddirajua S, Tomazos I, Burgess DJ, Jain FC, Papadimitrakopoulosa F (2010) Emerging synergy between nanotechnology and implantable biosensors: a review. Biosens Bioelectron 25:1553–1565
86. Sassolas A, Prieto-Simón B, Marty J-L (2012) Biosensors for pesticide detection: new trends. Am J Anal Chem 3:210–232
87. Arya SK, Datta M, Malhotra BD (2008) Recent advances in cholesterol biosensor. Biosens Bioelectron 23:1083–1100
88. Saxena U, Chakraborty M, Goswami P (2011) Covalent immobilization of cholesterol oxidase on self-assembled gold nanoparticles for highly sensitive amperometric detection of cholesterol in real samples. Biosens Bioelectron 26:3037–3043
89. Saxena U, Das AB (2016) Nanomaterials towards fabrication of cholesterol biosensors: key roles and design approaches. Biosens Bioelectron 75:196–205
90. Male KB, Hrapovic S, Santini JM, Luong JHT (2007) Biosensor for arsenite using arsenite oxidase and multiwalled carbon nanotube modified electrodes. Anal Chem 79:7831–7837

91. Spricigo R, Dronov R, Lisdat F, Leimkühler S, Scheller FW, Wollenberger U (2009) Electrocatalytic sulfite biosensor with human sulfite oxidase co-immobilized with cytochrome c in a polyelectrolyte-containing multilayer. Anal Bioanal Chem 393:225–233
92. Bullen RA, Arnot TC, Lakeman JB, Walsh FC (2006) Biofuel cells and their development. Biosens Bioelectron 21:2015–2045
93. Davis F, Higson SPJ (2007) Biofuel cells—recent advances and applications. Biosens Bioelectron 22:1224–1235
94. Ivanov I, Vidaković-Koch T, Sundmacher K (2010) Recent advances in enzymatic fuel cells: experiments and modelling. Energies 3:803–846
95. Meredith MT, Minteer SD (2012) Biofuel cells: enhanced enzymatic bioelectrocatalysis. Annu Rev Anal Chem 5:157–179
96. Rasmussen M, Abdellaoui S, Minteer SD (2016) Enzymatic biofuel cells: 30 years of critical advancements. Biosens Bioelectron 76:91–102
97. Hambourger M, Gervaldo M, Svedruzic D, King PW, Gust D, Ghirardi M, Moore AL, Moore TA (2008) [FeFe]-hydrogenase-catalyzed H_2 production in a photoelectrochemical biofuel cell. J Am Chem Soc 130:2015–2022
98. Habrioux A, Merle G, Servat K, Kokoh KB, Innocent C, Cretin M, Tingry S (2008) Concentric glucose/O_2 biofuel cell. J Electroanal Chem 622:97–102
99. Sokic-Lazic D, Minteer SD (2008) Citric acid cycle biomimic on a carbon electrode. Biosens Bioelectron 24:939–944
100. Arechederra RL, Minteer SD (2009) Complete oxidation of glycerol in an enzymatic biofuel cell. Fuel cells 9:63–69
101. Sokic-Lazic D, Minteer SD (2009) Pyruvate/air enzymatic biofuel cell capable of complete oxidation. Electrochem Solid-State Lett 12:26–28

BIOREV (2017) 6: 263–280
DOI: 10.1007/11663_2016_1

Published online: 28 June 2016

Trends in Electrochemical Sensing of Blood Gases

Bastiaan van der Weerd, Rudolf Bierl, and Frank-Michael Matysik

Abstract The monitoring of partial pressures of the blood gases carbon dioxide (pCO_2) and oxygen (pO_2) is of great importance in clinical diagnostics. The measure of pCO_2 and pO_2 provides essential information about the patient's metabolism, gas exchange, ventilation, and acid–base homeostasis. The conventional electrochemical methods for clinical blood gas analysis are based on the potentiometric Severinghaus sensor for carbon dioxide and the amperometric Clark sensor for oxygen. These techniques are well established and are only shortly discussed in this overview. However, in recent years a variety of modifications of these classical sensor concepts and new approaches of electrochemical sensing of pCO_2 and pO_2 have been introduced. This review summarizes recent developments in this field and discusses the potential for future applications in clinical blood gas analysis.

Keywords Blood gas analysis • Clinical analysis • CO_2 sensor • Electrochemical sensor • Noninvasive blood gas sensor • O_2 sensor

Contents

B. van der Weerd, R. Bierl, and F.-M. Matysik (✉)
Institute of Analytical Chemistry, Chemo- and Biosensors, University of Regensburg, Universitätsstr. 31, 93053 Regensburg, Germany
e-mail: frank-michael.matysik@chemie.uni-r.de

Abbreviations

ABG	Arterial blood gas analysis
AIROF	Anodically grown iridium oxide film
ARDS	Acute respiratory distress syndrome
CBG	Arterialized capillary blood gas analysis
ECMO	Extracorporeal membrane oxygenation
Hb	Hemoglobin
ISE	Ion-selective electrode
ISFET	Ion-selective field-effect transistor
LIX	Liquid ion exchanger
MEMS	Microelectromechanical systems
p_aCO_2	Arterial partial pressure of carbon dioxide
p_aO_2	Arterial partial pressure of oxygen
pBDD	Polycrystalline boron-doped diamond
pCO_2	Partial pressure of carbon dioxide
PDMS	Polydimethylsiloxane
$p_{et}CO_2$	End-tidal partial pressure of carbon dioxide
pO_2	Partial pressure of oxygen
$p_{tc}CO_2$	Transcutaneously determined partial pressure of carbon dioxide
$p_{tc}O_2$	Transcutaneously determined partial pressure of oxygen
VBG	Venous blood gas analysis
τ_{90}/τ_{95}	Time to approach 90%/95% of the steady-state signal

1 Physiological Background

The blood gases oxygen (O_2) and carbon dioxide (CO_2) play an essential role in the human organisms. The exchange of respiratory gases into and out of blood occurs in pulmonary alveoli by diffusion through alveolar and capillary walls. After the dissolution of oxygen in the blood plasma, it diffuses into red blood cells (erythrocytes) containing hemoglobin (Hb), which is used as a carrier for oxygen. The protein hemoglobin contains four heme groups of which each group binds one oxygen molecule in form of an iron complex. Therefore, hemoglobin transports up to four oxygen molecules through the blood vessels. The oxygen is released if the oxygenated hemoglobin accomplishes tissue structures with lower pO_2 (partial pressure of O_2) levels. Carbon dioxide is formed as a product of the metabolism and dissolves partly in the blood plasma. The main part of CO_2 is bound covalently as bicarbonate to the NH_2 group of hemoglobin [1].

The determination of arterial blood gases is very important to monitor the gas exchange in critically ill patients. It provides valuable information about the patient's metabolism, gas exchange, ventilation, and acid–base homeostasis [2]. A reliable way for blood gas determination is the direct analysis of an arterial blood sample by point-of-care blood gas analyzers with implemented Clark and Severinghaus sensors to measure pO_2 and pCO_2, respectively [3].

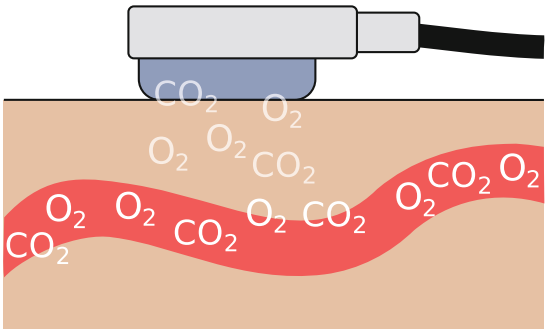

Fig. 1 Schematic representation of a transcutaneous blood gas measurement. Both blood gases (CO_2 and O_2) diffuse through the skin of the patient and penetrate into the sensor

Besides common direct measurements, indirect methods for blood gas determination are as follows: capnometry (only pCO_2), transcutaneous blood gas measurement [1, 4], and the pCO_2 [5] and pO_2 [6] determination at the gas outlet of a membrane oxygenator during extracorporeal membrane oxygenation (ECMO). However, these methods cannot replace the invasive blood gas analysis because of a number of limitations and the risk of artifacts. Typical problems are the patients' disease pattern, age, the entire health condition, etc [4, 7, 8]. Nevertheless, these noninvasive alternatives for the monitoring of arterial blood gases have been applied, e.g., during cardiopulmonary bypass [5].

The transcutaneous blood gas measurement enables the measurement of pO_2 and pCO_2 through the skin of the patient. The principle of this sensing strategy is illustrated in Fig. 1. Blood gases diffuse from the cutaneous capillary bed directly into the sensor. This process is facilitated by means of a heating system inside the sensor leading to elevated temperatures up to 42–45°C. This temperature level results in a reduced vascular tension associated with slacked arterioles and the penetration of arterial blood into the capillary bed (arterialization) [1]. Several related studies have been published comparing arterial blood gas measurements with transcutaneous ones [9–11]. The main reason for the underestimation of transcutaneously measured pO_2 ($p_{tc}O_2$) is the oxygen consumption by superficial tissues. In contrast, the overestimation of transcutaneously measured pCO_2 ($p_{tc}CO_2$) is caused by cellular metabolic production. Further artifacts affecting the accuracy of transcutaneous blood gas measurements are the temperature-dependent shift of the oxygen–hemoglobin binding curve as well as the shift of the chemical equilibrium of dissolved CO_2 and bound CO_2, which occur with increasing temperature [1]. Despite the differences between $p_{tc}O_2/p_{tc}CO_2$ and p_aO_2/p_aCO_2, commercially available systems usually guarantee acceptable correlations ($r > 0.8$). The transcutaneous analysis of blood gases requires long integration times as the measurement is mainly determined by the time-consuming gas diffusion through the skin. In this context, there is actually no need for a fast responding CO_2 sensor element inside the transcutaneous sensor body. However, the sensor should exhibit stable function for a period of 8–12 h [12] without any signal drift because there is no possibility for any recalibration.

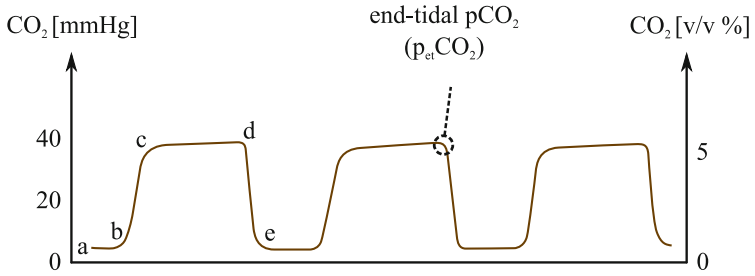

Fig. 2 Normal capnogram. (**a**, **b**) Beginning of exhalation. Gas is exhaled from the physiological dead space. (**b**, **c**) Steep rise of the CO_2 level, from the lower airways. (**c**, **d**) Alveolar plateau. CO_2 concentration of the expired alveolar gas. (**d**) End-tidal pCO_2. (**d**, **e**) Inspiration. Adapted from [1] with permission

Capnometry is a continuous measurement of CO_2 in the respiratory gas. The CO_2 profile during normal respiration, which has a characteristic waveform, is shown in Fig. 2. Low CO_2 signals during inspiration reflect the fact that the ambient air contains very low CO_2 concentrations. At the beginning of the expiration, the signal increases rapidly, and subsequently it flattens and increases slightly until it reaches the maximum CO_2 value, the end-tidal pCO_2 ($p_{et}CO_2$), at the end of exhalation. This end-tidal CO_2 level represents the alveolar CO_2 concentration, which correlates clearly with the p_aCO_2 [1]. However, the accuracy of $p_{et}CO_2$ is not comparable to direct arterial blood gas determinations due to the alveolar dead space. Several studies have estimated a mean difference of approximately 2–5 mmHg between p_aCO_2 and $p_{et}CO_2$. This bias varies by age, pulmonary disorders, reduced cardiac output, hypervolemia, and anesthesia [10, 13]. The oscillation of the capnometric CO_2 signal is caused by the alternating inspiration and expiration. A typical respiration rate of 10 to 30 breaths per minute results in measurement times in the seconds range. A suitable sensing device for capnometric CO_2 determinations should therefore have short response times within one second or in a few hundred milliseconds. Hence, commercially available capnometers are typically based on spectroscopic or time-of-flight ultrasound methods.

Pros and cons of different pCO_2 monitoring techniques are summarized in Table 1.

Another possibility for continuous blood gas analysis can be realized during extracorporeal membrane oxygenation. Extracorporeal membrane oxygenation (ECMO) is a mature clinical treatment for acute respiratory distress syndromes (ARDS). ECMO is applied to patients with severe lung failure. It can be understood as an artificial lung realizing oxygenation and carbon dioxide elimination. A schematic representation of a typical setup is illustrated in Fig. 3. Venous blood is pumped through a membrane oxygenator before the oxygenated blood flows back into the patient's vein [14]. Blood penetrates through thousands of membrane capillaries inside the membrane oxygenator. At the outer side of the membranes, the respiration gas passes and equilibrates with the blood (oxygenation and CO_2 elimination). The pCO_2 and pO_2 of the exhaust gas should be equal to both the

Table 1 Primary clinical applications for various pCO_2 monitoring techniques

Clinical application	ABG	CBG	VBG	Capnometric CO_2	Transcutaneous CO_2
Intensive care unit setting	+	–	–	+	–
Emergency department	+	–	+	–	–
Acute respiratory failure	+	–	–	–	–
Chronic respiratory failure	+	+	–	–	+
Invasive mechanical ventilation	+	+	–	–	–
Noninvasive mechanical ventilation	+	+	–	–	+
General anesthesia	+	–	–	+	–

Meaning of symbols: + advantage, – disadvantage
ABG arterial blood gas analysis, *CBG* arterialized capillary blood gas analysis, *VBG* venous blood gas analysis
Adapted from [4] with permission

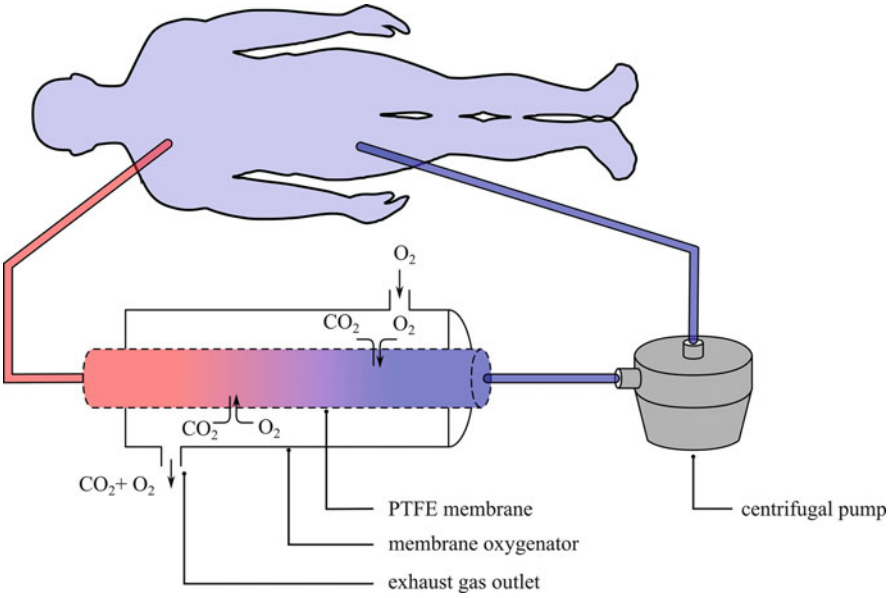

Fig. 3 Scheme of an extracorporeal membrane oxygenation (ECMO) combining a membrane oxygenator and a centrifugal pump. Oxygen diffuses into the blood (oxygenation) and carbon dioxide diffuses out of the blood (CO_2 elimination)

arterial pCO_2 (p_aCO_2) and the arterial pO_2 (p_aO_2), provided that the respiration gas is completely equilibrated with the blood. As a consequence, blood gases can indirectly be determined at the exhaust gas outlet of a membrane oxygenator of an ECMO system. Different studies have validated the correlation between the exhaust gas concentrations and the corresponding blood gas values. Exhaust gas monitoring has been used for p_aCO_2 monitoring with a good correlation between

corrected exhaust gas and blood gas values with a standard deviation of 4% [5]. Studies concerning continuous pO_2 exhaust gas monitoring and the correlation with p_aO_2 have been reported [6].

2 Conventional Blood Gas Sensors

2.1 Clark Sensor

A common configuration of a conventional two-electrode sensor system for pO_2 determination is shown in Fig. 4. This electrochemical probe is based on the sensing principle first reported by Clark [16]. It consists of a platinum or gold working electrode and an Ag/AgCl electrode serving as reference and counter electrode. A thin semipermeable membrane separates the internal electrolyte (KCl solution) from the blood sample. Suitable membrane materials are polyethylene or polytetrafluoroethylene (PTFE). The spacing between the platinum cathode and the membrane should range in the micrometer region in order to guarantee fast response characteristics [17].

This sensor principle is based on the electrochemical reduction of oxygen at the cathode. For a typical working electrode potential setting of −0.6 V vs. Ag/AgCl/0.1 M KCl, the following cathodic reaction occurs under transport-controlled conditions:

$$O_2 + 2H_2O + 4e^- \rightarrow 4OH^-$$

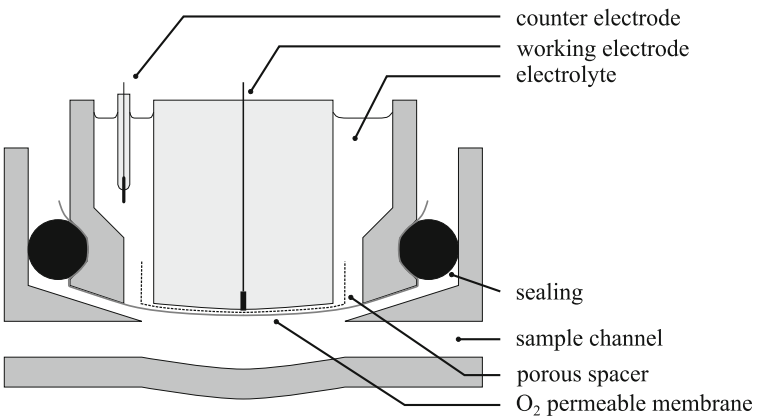

Fig. 4 Sectional drawing through a Clark sensor. Adapted from [15] with permission

2.2 Severinghaus Sensor

In 1954, the first pCO_2 sensor was introduced by Stow and Randall [18]. Severinghaus and Bradley [19] have optimized this sensing concept and published a CO_2 sensor suitable for routine laboratory use one year later. These Severinghaus-type probes are still the sensors of choice for pCO_2 monitoring in modern blood gas analyzers.

Figure 5 shows a scheme of a typical Severinghaus sensor for pCO_2 measurements in blood. The major components of this sensor are a pH-sensitive combination glass electrode, a thin electrolyte layer (bicarbonate solution), and a polymer membrane permeable for CO_2 [20]. If a flowing solution of blood sample passes the sample channel, CO_2 permeates the membrane and dissolves in the thin electrolyte layer of bicarbonate solution. In this way the following equilibrium is influenced:

$$CO_2 + H_2O \leftrightarrow HCO_3^- + H^+$$

The CO_2 diffusing into the internal electrolyte results in a pH change recorded with the combination glass electrode. The pH change correlates with the pCO_2. Theoretically calculated pH values as a function of pCO_2 with different $NaHCO_3$ concentrations of the electrolyte solution are shown in Fig. 6.

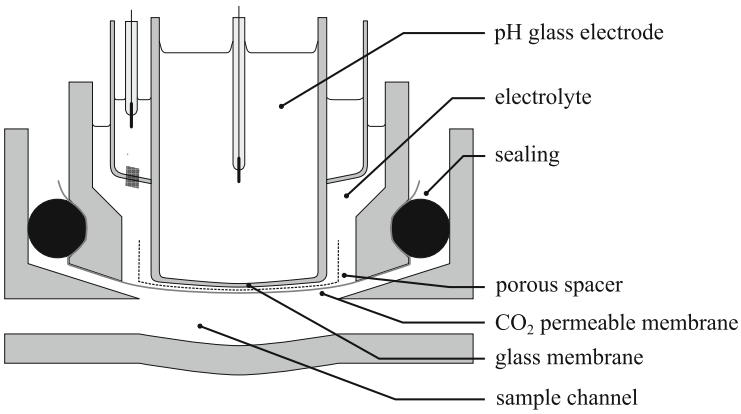

Fig. 5 Sectional drawing through a Severinghaus sensor. Adapted from [16] with permission

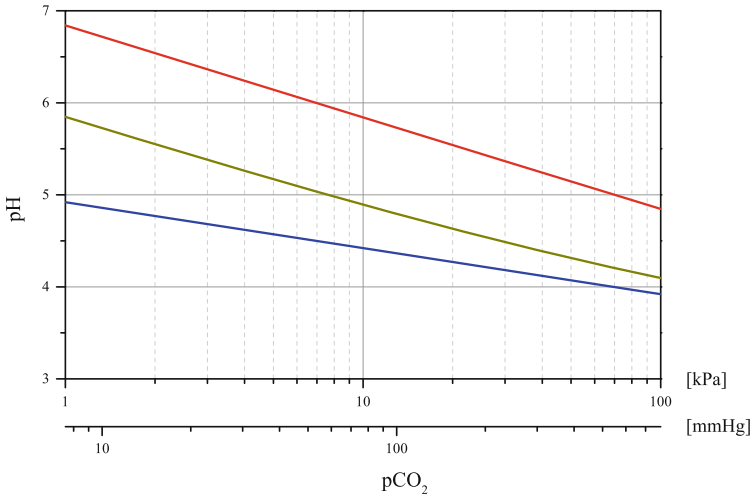

Fig. 6 Sensitivities of a Severinghaus CO_2 sensor with different $NaHCO_3$ concentrations of the electrolyte. Calculated according to [21]. *Blue*, $[NaHCO_3] = 0$ mol/l; *green*, $[NaHCO_3] = 10^{-4}$ mol/l; *red*, $[NaHCO_3] = 10^{-3}$ mol/l

3 New Trends in Direct and Indirect Blood Gas Analysis

3.1 Oxygen

The electrochemical reduction of oxygen has been investigated for a number of novel electrode materials under various conditions. Polycrystalline boron-doped diamond (pBDD) is presently one of the most promising electrode materials because of its wide potential window in aqueous solution, low background current, corrosion consistency, high temperature stability, and resistance to fouling [22]. Hutton et al. [22] have studied a membraneless chronoamperometric oxygen sensor based on a platinum nanoparticle-modified pBDD electrode. The characteristics of the composite sensor have been determined in 0.1 M KNO_3 solution with varying oxygen concentrations. The sensor shows a well-defined linear behavior between peak current and dissolved oxygen. Another chronoamperometric oxygen sensing concept has been suggested by Preidel et al. [23]. In this study a pulsed electrochemical determination of oxygen is applied which reduces the oxygen consumption at the cathode surface drastically. Consequently, this approach enables the direct oxygen measurements in tissue without affecting the oxygen concentration. The authors have investigated the sensor behavior in different environments, for example, bovine serum, a shunt measurement of a mini pig, and a direct subcutaneous measurement of a cat.

Modifications of miniaturized polydimethylsiloxane (PDMS)-based oxygen sensors have been reported as relevant alternatives to conventional transcutaneous pO_2 devices [24–27]. Koley et al. [24] presented a flexible amperometric prototype

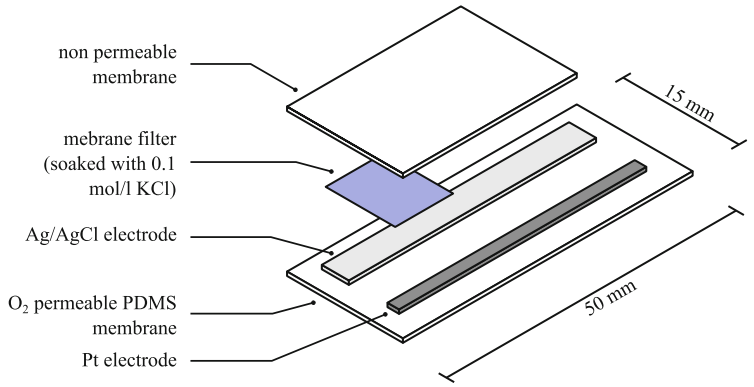

Fig. 7 Flexible transcutaneous polydimethylsiloxane (PDMS)-based oxygen sensor described by Koley et al. [24]. Adapted from [24] with permission

sensor consisting of three layers, an oxygen permeable PDMS membrane (30 μm), a membrane filter soaked with KCl as an electrolyte layer, and an electrode layer in the form of Pt and Ag/AgCl film electrodes. A schematic setup is shown in Fig. 7. In 2007 Kudo et al. [25] published a transcutaneous oxygen measurement at the forearm by means of the described sensor type combined with a thermistor and a commercially available skin heater. The results show a linear dependency of dissolved oxygen concentrations in the physiological range from 0 to 7 mg/l on the output current. Due to the small dimensions and the flexible character of the sensor, this device is promising for continuous transcutaneous oxygen measurements.

3.2 Carbon Dioxide

3.2.1 *Miniaturized Severinghaus Sensors*

As described in Sect. 2.2, Severinghaus sensors still dominate the known sensing principles in the sector of electrochemical CO_2 probes. Despite the fact that the Severinghaus sensor can be considered as a gold standard for clinical CO_2 blood gas analysis, a few drawbacks of this sensor concept are still hard to overcome. One of the major problems consists of the relatively long response time which typically is longer than 1 min. This is due to the rather slow CO_2 diffusion through the membrane and the equilibration time to establish a stable signal at the pH glass electrode.

The construction of the pH electrode can be seen as the main factor in terms of miniaturizing a Severinghaus sensor. It should be a small component of the overall sensor design exhibiting fast and reliable response characteristics. Known CO_2 microsensors use pH electrodes with a liquid ion exchanger (LIX) membrane

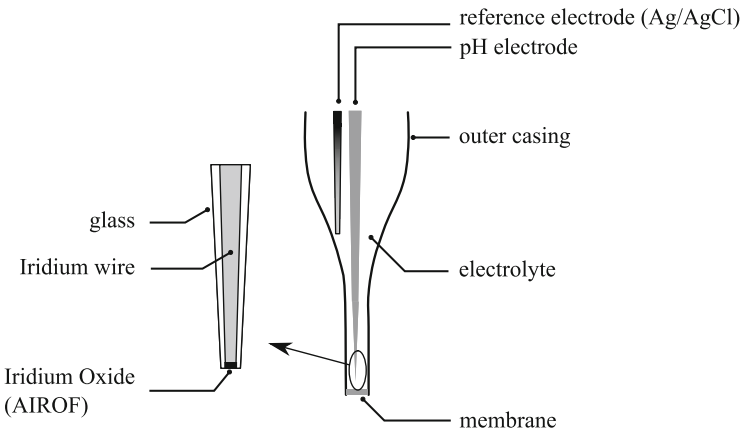

Fig. 8 Anodically grown iridium oxide film (AIROF)-based Severinghaus microsensor. Adapted from [28] with permission

[29, 30]. However, these LIX-based sensors suffer from drift problems and short lifetimes which are both related to a leakage of the LIX into the sensor body. An alternative to overcome these weaknesses of the pH electrode is the use of an anodically grown iridium oxide film (AIROF). AIROF-based pH electrodes respond fast to pH changes and have a low signal drift and a long lifetime [31]. Beyenal et al. [28] reported an improved Severinghaus-type carbon dioxide microsensor for an application in biofilms using an AIROF as an internal pH electrode. The sensor setup can be seen in Fig. 8. The authors could demonstrate a significant improvement of the sensitivity and long-term stability of the sensor compared to previously described CO_2 microsensors based on LIX pH membranes. The CO_2 microsensors have been calibrated in distilled water with various CO_2/N_2 mixtures and were afterward applied to measure carbon dioxide concentration profiles in biofilms of *Staphylococcus aureus*. Miniaturized Severinghaus-type microsensors are not only an adequate tool for CO_2 determinations in biofilms but also a promising solution for CO_2 blood gas analysis. The high integration factor and tip diameters in the low micrometer range enable a minimally invasive pCO_2 measurement.

3.2.2 *Trends in Electrochemical CO_2 Sensing*

A traditional approach for CO_2 determinations during ECMO is a sensor based on electrolytic conductivity. This principle was first described by Kempen and Kreuzer [32] in 1975. Gaseous CO_2 penetrates through a semipermeable polymer membrane and dissolves in a defined water volume. The change of electrolytic conductivity depends on the CO_2 concentrations. Compared to other sensor principles where humidity is a limiting factor, in this case a high humidity level is required in order to ensure the formation of a stable water film to prevent long-term drifts.

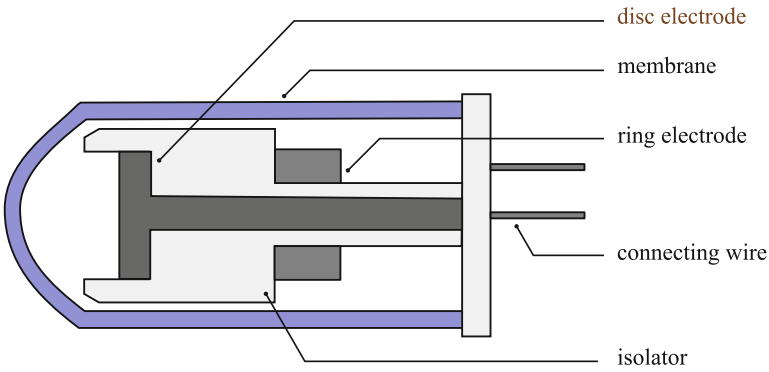

Fig. 9 Cylindrically shaped conductivity-based CO_2 sensor for biosensor applications. Adapted from [33] with permission

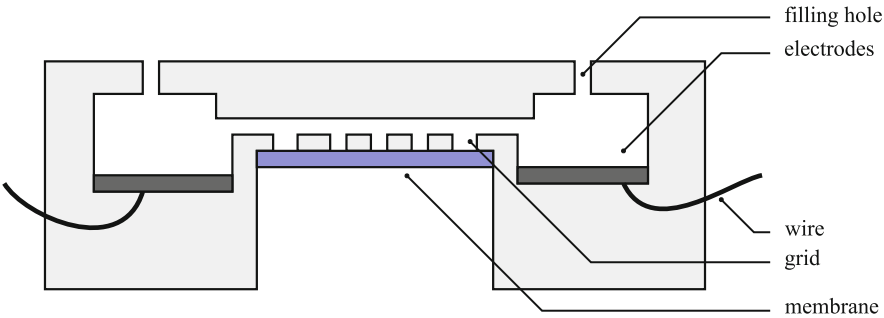

Fig. 10 Planar conductivity sensor for biomedical CO_2 measurements. Adapted from [33] with permission

Further promising trends in CO_2 sensing have been reported during the last decades which are of particular interest in terms of indirect CO_2 blood gas monitoring by capnometry or by ECMO exhaust monitoring. Two different configurations of conductivity-type CO_2 sensors have been reported. One is the conventional setup with a two- or four-electrode system determining the impedance by a cell-dependent measuring frequency. Mirtaheri et al. [33] have fabricated a cylindrical (Fig. 9) and a planar sensor (Fig. 10). Studies by the same group [34] resulted in a miniaturized cylindrically shaped cell configuration. They have presented an ex vivo measurement in a small latissimus dorsi muscle flap of a pig. This conductivity-based sensor showed similar results as a Severinghaus microsensor. The other configuration is based on differential conductivity measurement [35]. Water flows continuously through a microfluidic system where it passes the inner side of a polymer membrane. The conductivity of the water volume is measured before (upstream cell) and after the diffusion zone (downstream cell). The difference of conductivity depends on the water flow, the gas flow across the membrane, and the gaseous CO_2 concentration. An advantage of this sensing

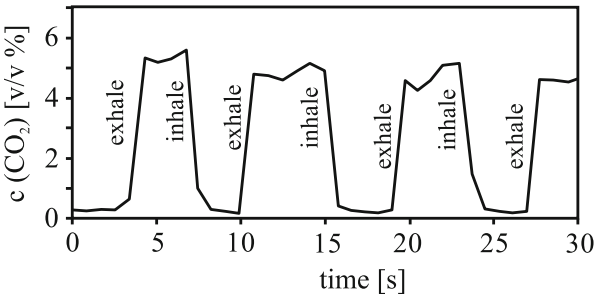

Fig. 11 Capnometric CO_2 signal recording using a solid-state sensor during respiration. Adapted from [36] with permission

strategy is the attractive response behavior as there is a constant CO_2 gradient across the membrane.

There are various reports on solid-state-based CO_2 sensors. Preferred sensor materials are Li_3PO_4 combined with a Li_2CO_3 sensing electrode [36] or Nasicon in combination with a Li_2CO_3 | $BaCO_3$ sensing electrode [37]. A solid-state potentiometric CO_2 sensor with fast response characteristics was proposed by Wiegärtner et al. [37] in 2014. The electrochemical sensor of the type CO_2, O_2, Au, Li_2CO_3-$BaCO_3$|Nasicon|$Na_2Ti_6O_{13}$-TiO_2, Au, O_2, CO_2 was fabricated in thick film technology and could be an alternative to the conventional infrared-based capnometer. The sensor showed a well-defined Nernst behavior according to calibration results with different CO_2 concentrations in the range of 0–5 v/v%. Figure 11 shows a capnometric measurement in human breathing air illustrating the CO_2 concentration during inspiration and expiration.

Another planar potentiometric CO_2 sensor was described by Shin et al. [38]. They developed a microchemical pCO_2 sensor based on both pH-sensitive and CO_2-permeable membranes sensing in a differential arrangement. Figure 12 shows a cross-sectional view of the sensor configuration. In this case, two Ag/AgCl electrodes are embedded in a buffered and an unbuffered hydrogel layer and backfilled with a pH-sensitive polymeric membrane. Different CO_2 concentrations result in corresponding pH changes inside the unbuffered hydrogel layer. As the pH of the buffered hydrogel layer is not affected by different CO_2 levels, the CO_2 concentrations determine a defined potential difference between the two pH-sensitive membrane electrodes. Carbonic anhydrase was added into the unbuffered hydrogel in order to catalyze the hydration and dehydration of CO_2. This leads to a significant acceleration of the reaction rate and consequently to shorter response times. Continuous measurements with two solutions for calibration, four prepared control samples, and a whole blood sample showed good results compared to a commercially available blood gas analyzer. A long-term experiment showed that the pCO_2 electrode can be operated with good stability for at least 80 days without any loss in sensitivity.

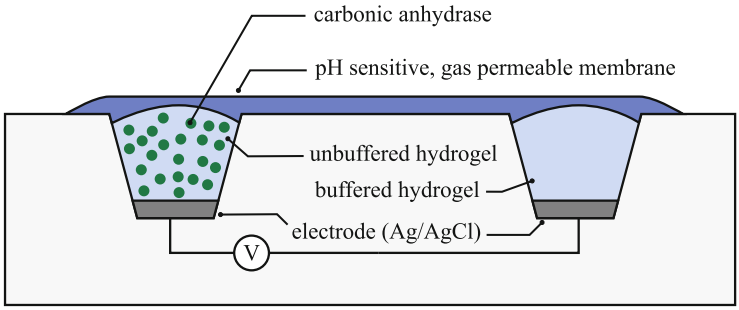

Fig. 12 Planar differential CO_2 sensor based on buffered and unbuffered pH membrane electrodes. Adapted from [38] with permission

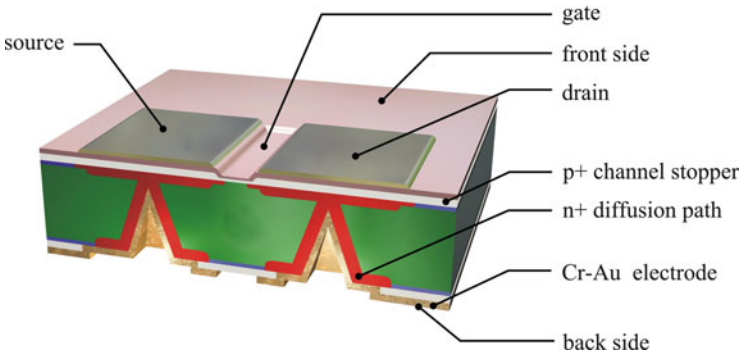

Fig. 13 Scheme of an ISFET blood gas sensor described by Ekwinska et al. Adapted from [39] with permission

A promising concept for simultaneous sensing of pCO_2 and pO_2 is based on the use of ion-selective field-effect transistors (ISFETs). A scheme of a typical ISFET configuration is illustrated in Fig. 13. The first ISFET sensor was reported by Bergveld [40] in 1970. The fabrication in MOS technology provides a high miniaturization or integration level of these sensors. Various ISFET-based sensors for CO_2 and O_2 in the context of blood gas sensing can be found in the literature [41–44]. In 2011, Ekwinska et al. [39] published an optimized electrochemical sensor configuration for a noninvasive determination of the p_aCO_2 by means of a transcutaneous measurement. The sensor element contains a highly integrated CO_2 ISFET embedded in a plastic housing with heating element, Ag/AgCl reference electrode, thermistor, and a polymer membrane.

A different concept based on amperometry was described by Fasching et al. [45]. They have developed a miniaturized amperometric sensor for CO_2 in liquids for applications in clinical blood gas analysis. The detection principle is based on the pH-dependent dissociation of copper complexes. Different CO_2 concentrations result in corresponding pH shifts of the internal hydrogel electrolyte. These pH variations lead to certain dissociation levels of the copper complexes

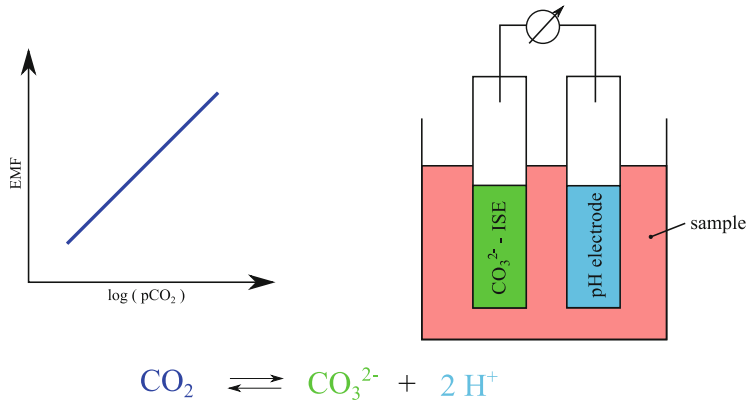

Fig. 14 Setup of a novel potentiometric non-Severinghaus concept. The pCO_2 is determined by the potential difference between a carbonate ISE and a pH electrode. Both electrodes are directly immersed in the sample solution without the use of a separating membrane. Adapted from [46] with permission

which can be measured in terms of an amperometric signal. This sensor was miniaturized down to 100 µm and showed a chemically stable behavior. The sensor response to different CO_2 concentrations was investigated in a computer-controlled test bench using defined mixing ratios of CO_2 and argon both dissolved in water. Successful applications of CO_2 measurements in blood serum were demonstrated. An advantage of this sensor is its compatibility with advanced MEMS production techniques.

An interesting novel approach to carbon dioxide sensing was reported by Xie and Bakker [46]. This concept is based on the measurement of the potential difference between a pH glass electrode and a carbonate-selective electrode. Figure 14 illustrates this electrode configuration. Both electrodes are directly immersed into the sample solution which is in clear contrast to Severinghaus-type sensors implementing a membrane in order to separate the internal electrolyte from the sample. In this configuration, the pH of the sample is measured vs. the carbonate ion-selective electrode (ISE). There is no need for a separate liquid junction reference electrode. The sensor response to varying CO_2 concentrations is shown in Fig. 15. A good sensitivity was found even for low pCO_2 (see Fig. 15 left diagram). The response time was much faster compared to the Severinghaus sensor due to the elimination of diffusion processes into the internal sensor compartment. A $\tau_{95\%}$ response time of 5 s was reported [46]. A combination of this electrode arrangement with a classical reference electrode enabled the determination of pH, pCO_2, and carbonate.

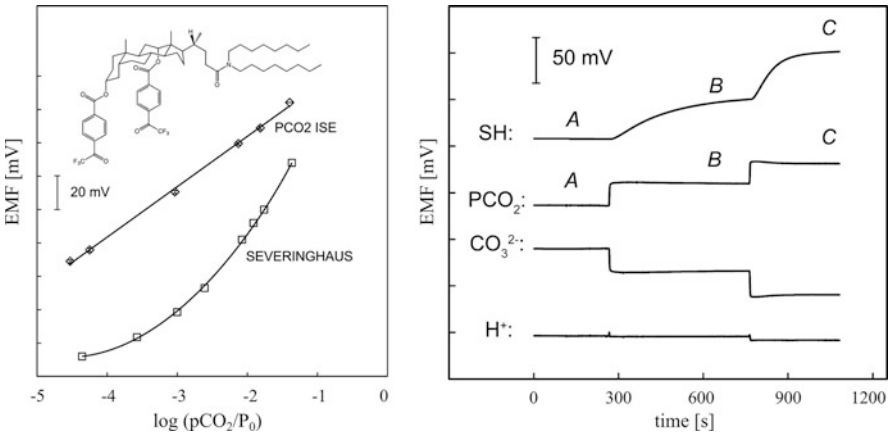

Fig. 15 *Left*: Calibration curve of a conventional Severinghaus sensor (SH) and a novel non-Severinghaus sensor measuring the potential difference between a pH glass electrode and a carbonate ISE as a function of $\log(pCO_2/p_o)$ [46]. Reproduced from [46] with permission. *Right*: Comparison of the response characteristics of both CO_2 sensors – the SH and the new pCO_2 electrode arrangement. Measured in 0.1 M Tris-H_2SO_4, pH 8.0 buffer solution for the following pCO_2: (*A*) 0.0004 atm, (*B*) 0.0066 atm, (*C*) 0.0655 atm [46]

3.3 Combined Oxygen and Carbon Dioxide Sensors

Integrated sensors allowing the simultaneous determination of pCO_2 and pO_2 have a high potential for the development of miniaturized sensors for applications in clinical analysis [47]. Anjos and Hahn [48] have reported an innovative sensor which is promising for applications in the field of direct blood gas analysis. The miniaturized sensor reduces both oxygen and carbon dioxide simultaneously at two different potentials. Both blood gas concentrations can be measured simultaneously by means of potential step chronoamperometry. Two types of gold microelectrode arrays were investigated; the first one containing 37 electrodes (20 µm in diameter) and the second one containing 256 microelectrodes (5 µm in diameter) were employed for this measuring concept. The use of gold microelectrode arrays in combination with very short potential steps could reduce all cross interferences between O_2 and CO_2. The calibration behavior of the two prototype sensors was studied with various mixtures of CO_2 in N_2 or O_2 in N_2. The analytical performance of the sensor could further be improved by reducing the electrode diameter.

Another integrated module for the determination of pO_2, pCO_2, and pH has been developed by Suzuki et al. [41]. A planar electrochemical microchip system was fabricated by ordinary processes of photolithography and micromachining. Miniaturized Clark-type and Severinghaus-type electrodes were implemented. The amperometric signal showed a linear dependence on pO_2. For a step change of the oxygen concentration, a $\tau_{90\%}$ response time of 20 s was found. The integrated miniaturized Severinghaus sensor element exhibited the typical potentiometric sensor characteristics. However, a rather slow response behavior characterized by $\tau_{90\%}$ between 150 s (increasing step) and 210 s (decreasing step) was obtained.

References

1. Hieronymi U, Kramme R, Kronberg H (2011) Respiratory monitoring and pulse oximetry. In: Kramme R, Hoffmann K-P, Pozos RS (eds) Springer handbook of medical technology. Springer, Berlin-Heidelberg, pp 973–984
2. Crocetti J, Diaz-Abad M, Krachman SL (2010) Blood gas sampling. In: Criner GJ, Barnette RE, D'Alonzo GE (eds) Critical care study guide, 2nd edn. Springer, New York, pp 38–50
3. Cristalli C, Manzoni A (1999) Basics of blood gas instrumentation. In: Bronzino JD (ed) The biomedical engineering handbook, 2nd edn. Boca Raton, CRC
4. Huttmann SE, Windisch W, Storre JH (2014) Techniques for the measurement and monitoring of carbon dioxide in the blood. Ann ATS 11(4):645–652
5. Hogetveit JO, Kristiansen F, Pedersen TH (2006) Development of an instrument to indirectly monitor arterial pCO_2 during cardiopulmonary bypass. Perfusion 21:13–19
6. Hogetveit JO, Kristiansen F, Roislien J (2009) A novel method for indirectly monitoring arterial pO_2 during cardiopulmonary bypass. J Med Eng Technol 33(7):567–574
7. Zaugg M, Lucchinetti E, Zalunardo MP, Zumstein S, Spahn DR, Pasch T, Zollinger A (1998) Substantial changes in arterial blood gases during thoracoscopic surgery can be missed by conventional intermittent laboratory blood gas analyses. Anesth Analg 87:647–653
8. Ganter M, Zollinger A (2003) Continuous intravascular blood gas monitoring: development, current techniques, and clinical use of a commercial device. Brit J Anaesth 91(3):397–407
9. Rosner V, Hannhart B, Chabot F, Polu JM (1999) Validity of transcutaneous oxygen/carbon dioxide pressure measurement in the monitoring of mechanical ventilation in stable chronic respiratory failure. Eur Respir J 13:1044–1047
10. Sanders MH, Costantino JP, Strollo PJ, Coates JA (1994) Accuracy of end-tidal and transcutaneous pCO_2 monitoring during sleep. Chest 106(2):472–483
11. Stücker M, Memmel U, Altmeyer P (2000) Transkutane Sauerstoffpartialdruck- und Kohlendioxidpartialdruckmessung – Verfahrenstechnik und Anwendungsgebiete. Phlebologie 29:81–91
12. Restrepo RD, Hirst KR, Wittnebel L, Wettstein R (2012) AARC Clinical practice guideline: transcutaneous monitoring of carbon dioxide and oxygen: 2012. Resp Care 57(11):1955–1962
13. Hinkelbein J, Floss F, Denz C, Krieter H (2008) Accuracy and precision of three different methods to determine pCO_2 (p_aCO_2 vs. $p_{et}CO_2$ vs. $p_{tc}CO_2$) during interhospital ground transport of critically ill and ventilated adults. J Trauma 65(1):10–18
14. Müller T, Lubnow M, Bein T, Philipp A, Pfeifer M (2009) Extrakorporale Lungenunterstützungsverfahren beim ARDS des Erwachsenen: eine Standortbestimmung. Intensivmed 46:109–119
15. D'Orazio P, Meyerhoff ME (2008) Electrochemistry and chemical sensors. In: Sawyer BG (ed) Fundamentals of clinical chemistry, 6th edn. Saunders, Missouri, pp 84–101
16. Clark LC (1956) Monitor and control of blood and tissue oxygen tension. ASAIO Trans 2(1): 41–48
17. Linek V (1988) Measurement of oxygen by membrane-covered probes: guidelines for applications in chemical and biochemical engineering. Ellis Horwood, Chichester; Halsted, New York
18. Stow RW, Randall BF (1954) Electrical measurement of pCO_2 of blood. Am J Physiol 179: 678–681
19. Severinghaus JW, Bradley AF (1958) Electrodes for blood pO_2 and pCO_2 determination. J Apply Phys 13(3):515–520
20. Lewenstam A (2007) Clinical analysis of blood gases and electrolytes by ion-selective sensors. In: Alegret S, Merkoci A (ed) Compr Anal Chem, vol 49. Elsevier, Oxford, pp 5–24
21. Zosel J, Oelßner W, Decker M, Gerlach G, Guth U (2011) The measurement of dissolved and gaseous carbon dioxide concentration. Meas Sci Technol 22(072001):1–45

22. Hutton L, Newton ME, Unwin PR, Macpherson JV (2009) Amperometric oxygen sensor based on a platinum nanoparticle-modified polycrystalline boron doped diamond disk electrode. Anal Chem 81(3):1023–1032
23. Preidel W, Rao JR, Mund K, Schunck O, David E (1995) A new principle for an electrochemical oxygen sensor. Sens Actuators B 28:71–74
24. Koley G, Liu J, Nomani MW, Yim M, Wen X, Hsia T-Y (2009) Miniaturized implantable pressure and oxygen sensors based on polydimethylsiloxane thin film. Mater Sci Eng C 29: 685–690
25. Kudo H, Iguchi S, Yamada T, kawase T, Saito H, Otsuka K, Mitsubayashi K (2007) A flexible transcutaneous oxygen sensor using polymer membranes. Biomed Microdevices 9:1–6
26. Mitsubayashi K, Wakabayashi Y, Murotomi D, Yamada T, Kawase T, Iwagaki S, Karube I (2003) Wearable and flexible oxygen sensor for transcutaneous oxygen monitoring. Sens Actuators B 95:373–377
27. Iguchi S, Mitsubayashi K, Uehara T, Ogawa M (2005) A wearable oxygen sensor for transcutaneous blood gas monitoring at the conjunctiva. Sens Actuators B 108:733–737
28. Beyenal H, Davis CC, Lewandowski Z (2004) An improved Severinghaus-type carbon dioxide microelectrode for use in biofilms. Sens Actuators b 97:202–210
29. Lewandowski Z, Beyenal H (2003) Use of microsensors to study biofilms. In: Lens P, O'Flaherty V, Moran AP, Stoodley P, Mahony T (eds) Biofilms in medicine, industry and environmental biotechnology. IWA, London, pp 375–412
30. Hanstein S, de Beer D, Felle HH (2001) Miniaturised carbon dioxide sensor designed for measurements within plant leaves. Sens Actuators B 81:107–114
31. Bezbaruah AN, Zhang TC (2002) Fabrication of anodically electrodeposited iridium oxide film pH microelectrodes for microenvironmental studies. Anal Chem 74:5726–5733
32. van Kempen LHJ, Kreuzer F (1975) The CO_2 conductivity electrode, a fast-responding CO_2 microelectrode. Respir Physiol 24(1):89–106
33. Mirtaheri P, Grimnes S, Martinsen OG, Tonnessen TI (2004) A new biomedical sensor for measuring pCO_2. Physiol Meas 25:421–436
34. Mirtaheri P, Omtveit T, Klotzbuecher T, Grimnes S, Martinsen OG, Tonnessen TI (2004) Miniaturization of a biomedical gas sensor. Physiol Meas 25:1511–1522
35. Zosel J, Wex K, Gambert R, Oeßner W (2004) Kohlendioxidsensor. DE 10 2004 058 135 A1, Dec 2004
36. Lee I, Akbar SA (2014) Potentiometric carbon dioxide sensor based on thin Li_3PO_4 electrolyte and Li_2CO_3 sensing electrode. Ionics 20:563–569
37. Wiegärtner S, Kita J, Hagen G, Schmaus C, Kießig A, Glaser E, Bolz A, Moos R (2014) Development and application of a fast solid-state potentiometric CO_2-Sensor in thick-film technology. Procedia Eng 87:1031–1034
38. Shin JH, Lee JS, Choi SH, Lee DK, Nam H, Cha GS (2000) A planar pCO_2 sensor with enhanced electrochemical properties. Anal Chem 72(18):4468–4473
39. Ekwinska MA, Jaroszewicz B, Domanski K, Grabiec P, Zaborowski M, Tomaszewski D, Palko T, Przytulski J, Lukaski W, Dawgul M, Pijanowska D (2012) A transcutaneous blood capnometry sensor head based in a back-side contacted ISFET. In: Jablonski R, Brezina T (eds) Mechatronics. Springer, Berlin-Heidelberg, pp 607–614
40. Bergveld P (1970) Development of an ion-sensitive solid-state device for neurophysiological measurements. IEEE T Bio-Med Eng 17(1):70–71
41. Suzuki H, Hirakawa T, Sasaki S, Karube I (2000) An integrated module for sensing pO_2, pCO_2 and pH. Anal Chim Acta 405:57–65
42. Tsukada K, Miyahara Y, Shibata Y, Miyagi H (1990) An integrated chemical sensor with multiple ion and gas sensors. Sens Actuators B 2:291–295
43. Shoji S, Esashi M (1992) micro flow cell for blood gas analysis realizing very small sample volume. Sens Actuators B 8:205–208
44. Arquint P, van den Berg A, van der Schoot BH, de Rooij NF, Bühler H, Morf WE, Dürselen LFJ (1993) Integrated blood-gas sensor for pO_2, pCO_2 and pH. Sens Actuators B 13:340–344

45. Fasching R, Kohl F, Urban G (2003) A miniaturized amperometric CO_2 sensor based on dissociation of copper complexes. Sens Actuators B 93:197–204
46. Xie X, Bakker E (2013) Non-Severinghaus potentiometric dissolved CO_2 sensor with improved characteristics. Anal Chem 85:1332–1336
47. Guth U, Vonau W, Zosel J (2009) Recent developments in electrochemical sensor application and technology – a review. Meas Sci Technol 20(042002):1–14
48. Anjos TG, Hahn EW (2008) The development of a membrane-covered microelectrode array gas sensor for oxygen and carbon dioxide measurement. Sens Actuators B 135:224–229

BIOREV (2017) 6: 281–340
DOI: 10.1007/11663_2016_5

Published online: 22 July 2016

Application of Scanning Electrochemical Microscopy in Bioanalytical Chemistry

Lívia Nagy and Géza Nagy

Abstract For more than six decades electroanalytical microsensors have been employed in experimental life sciences for investigation of physiological processes. Researchers have been able to assess concentration of different species with good temporal and spatial resolution at the vicinity or inside of biologic objects. In the eighties of the last century a remarkable technique, the so-called probe microscopy, has been developed for studying the microworld. It is named scanning probe microscopy. Scanning tunneling microscopy (STM) and the atomic force microscopy (AFM) were the first probe microscopy methods. Soon after these the electrochemical version of the probe microscopy, the scanning electrochemical microscopy (SECM) appeared, resulted by the pioneering work of Bard and Engstrom. One of the most promising application fields of SECM is the bioanalysis. The availability of sophisticated, easy to use scanning probe instruments and the development of theoretical background boosted the popularity of electrochemical microscopy in biosciences. SECM uses high precision three-dimensional positioning devices, electrochemical microsensor tip and computer controlled measuring, evaluating and image formation algorithm; voltammetric, potentiometric, and conductance measuring methods have been successfully employed for studying biological objects or processes. Accordingly miniaturized voltammetric working electrodes, ion selective potentiometric microsensors, or conductance measuring microprobes have been used as measuring tips. SECM measurements showed details of topographic changes or gas exchange processes over living botanic samples. Metabolic activity of living individual cells or cell colonies could be studied without major invasion. Topographic changes of surface confined cells, transport of different materials through bio-layers could be assessed. Influence of chemical, radiation, or physical effects on the metabolic activity or surviving rate

L. Nagy and G. Nagy (✉)
Department for General and Physical Chemistry, Faculty of Sciences, University of Pécs, Ifjúság u. 6, 7624 Pécs, Hungary
e-mail: g-nagy@gamma.ttk.pte.hu

could be studied. The following chapter shortly summarizes the basics of the SECM and briefly introduces a few examples where the method was advantageously used in experiments of life sciences.

Keywords Ion selective micropipettes • Metabolic rate • Reactive oxygen species • Respiratory activity • Scanning Electrochemical Microscopy • Surviving rate • Transport through biomembranes • Voltammetric ultra-microelectrodes

Contents

Abbreviations

AFM	Atomic force microscopy
CV	Cyclic voltammetry
D	Diffusion coefficient
E	Electrode potential
EGFR	Epidermal growth factor receptor
FcCOOH	Ferrocene carboxylic acid
FcMeOH	Ferrocene methanol
GSH	Glutathione
GTC	Green tea catechin
HRP	Horseradish peroxidase
ITIES	Interface between two immiscible electrolyte solutions

ITO glass	Tin-doped indium oxide
MBP	Maltose-binding protein
NOEs	NAD(P)H-oxidizing enzymes
PMT	Photoelectron multiplier
PVDF	Polyvinylidene fluoride
RG value	Tip radius–measuring disc radius ratio
ROS	Reactive oxygen species
SECM	Scanning electrochemical microscopy
SG/TC	Substrate generating tip collecting mode
SICM	Scanning ion conductance microscopy
SNOM	Scanning near field optical microscopy
STA	Standing approach mode
STM	Scanning tunneling microscopy
TG/SC	Tip generating substrate collecting mode

1 Introduction

Scanning electrochemical microscopy (SECM) is a relatively new technique. The invention of it dates back to the second part of the eighties of the last century. In that time scanning tunneling microscopy (STM) and atomic force microscopy (AFM) with their enhanced resolution and simplicity have already revolutionized the tools of surface examinations. Miniaturization of electroanalytical sensors was also advancing. It was realized by several groups that the small electrode size provides several advances in basic electrochemistry as well as in chemical analysis. Research groups working in the field of experimental life sciences developed miniature electrochemical transducers. Using them they could measure with high spatial resolution the local concentration of different species in biological systems like animal tissue slices or in different body areas of anesthetized experimental animals, or in living plant tissues.

When reports, those we consider today as ground-braking steps in SECM [1–4], appeared many of us could not immediately see the power of the new technique. In those first papers we could read about application of carbon fiber or platinum microelectrodes with diameter of 10 μm or less for tracing concentration of ferrocyanide or ferricyanide ions inside diffusion profiles, or detecting the changes of amperometric current at the vicinity of surfaces. In those days neuroscience groups already used carbon fiber microelectrodes for detecting monoamine neurotransmitter related species in vivo (e.g., [5]). Submicrometer size ion selective electrodes were prepared and inserted inside living cells, from where ion activity data could be gathered (e.g., [6, 7]). The advantages of using miniaturized voltammetric electrodes in studying electrode reactions have been already discussed in broadscale.

Question can arise about the special features of the SECM that made it a new, well-known separate technique of electrochemistry. Trying to answer this, we need to consider the following:

- In earlier studies the positioned microelectrodes were just passive sensors. No interaction between the sample and the electrode was planned and used in evaluation. The smallest possible invasion on the investigated system was favored. In practice of SECM, however, often the sample system is tested through its interaction with the electrode process taking place at the positioned microelectrode. This opened new ways in characterizing local properties of microstructures. Selecting properly the electrode process new features like local catalytic activity, rate of surface reactions, transport characters of different species as well as viability or metabolic activity of living cells can be studied with SECM.
- Appearance of commercial instruments developed in cooperation with the pioneering research groups in the field made the technique easily accessible for other research groups not specifically interested in complex instrument developing research.
- Intensive work with the theory of SECM showed the potential and limits of its applications.

In our days the SECM is recognized as the member of numerous scanning probe microscopic techniques. Similarly to the other scanning probe microscopic methods, it employs a microsized measuring probe, three-dimensional positioning devices, computerized data collection, and evaluation. Special feature is, however, that in SECM electrochemical microprobes are used.

Up till now the SECM methods have been far from achieving the high spatial resolution provided by STM or AFM. However, the straightforward chemical information obtained makes SECM very attractive for researchers of different areas.

There are three different main directions of applications where the advantages of SECM have been proved:

- SECM can provide high resolution images with chemical information about a variety of samples. It can show concentration distribution of different species, spatial distribution of catalytic activity, or other kind of surface properties.
- SECM is a well applicable tool in measuring physicochemical properties. Among these measurements of diffusion coefficients of different species in different media, quantitative determination of reaction rate coefficient of heterogeneous reactions, transport properties through interfaces, or detecting metabolic activity of living cells or microbial objects can be mentioned.
- The SECM microtip can be used for delivering controlled microdoses of different reagents into different locations. This allows using it as a microtool in preparing fine structured objects, like microcavities, channels, micropolymer dots containing catalysts, etc. Furthermore microdoses of drugs or other reagents can be introduced with the positioned microtip for interacting with live objects.

From assorted perspective fields of applications of SECM methods different areas of biological sciences, like molecular biology, microbiology, biotechnology, cell physiology, etc., seem very promising. Right after the invention of the method, its power in imaging biologic objects has been tested [8]. As the method is getting more and more known and the number of laboratories equipped with electrochemical microscope is increasing, a growing number of papers dealing with application of SECM for investigation of biological processes are published.

There have already been published numerous review papers [9–20], a book [21], and several book chapters [22] about theory and applications of SECM. In this chapter we shortly describe the general principle of the technique. We deal with the special problems of different electrochemical detection methods used in SECM and introduce some specific microtips most often used in the practice of this microscopy.

In the second part of this chapter, examples showing the applicability of the technique for investigation of different biological objects, their function, and reactions are shown.

2 Methods of Electrochemistry Used in SECM Studies

Three major detecting methods of electrochemistry have been adapted for SECM studies. They are voltammetry, potentiometry, and conductometry. It must be mentioned here that scanning ion conductance microscopy (SICM) sometimes considered rather as an individual scanning probe microscopic technique than member of the SECM methods. Accordingly, we discuss shortly the SECM properties of the three detection techniques trying to show the major differences.

2.1 SECM with Voltammetric Detection

Originally SECM has been worked out for voltammetric detection. Ever since, in most of the electrochemical microscopic measurements amperometric data collection is employed. In amperometry an appropriate constant electrode potential is imposed on a working electrode and the current is followed in time. The current shows the rate of the overall electrode reaction. The transport of the electroactive species toward the electrode surface is the rate determining step of this reaction.

As it is well known from basic electrochemistry [23], if disc shaped ultramicro size working electrode is employed in quiescent electrolyte solution containing constant concentration of an electroactive species, then the diffusion controlled amperometric current achieves steady value in certain time. The time needed for a microelectrode for achieving this steady value has been discussed by Zoski et al. [24] (of course we exclude here electrode fouling, the very small sample

solution volume, etc.). Simple equation gives the steady state current ($i_{t\infty}$) when the electrode surface is in the bulk of electrolyte solution:

$$i_{t\infty} = 4nFDca$$

where D is the diffusion coefficient of the electroactive species reacting at the electrode, n is the number of electrons exchanged in electrode reaction, $\boldsymbol{F}$ is the Faraday, c is the concentration of the reacting species, and a is the radius of the disc shaped electrode.

The geometry of the electrode surface slightly affects $i_{t\infty}$ value. For taking into account of it a modified equation has been suggested [25]:

$$i_{t\infty} = 4nFDca\beta_{RG}$$

where the coefficient β_{RG} helps eliminating the discrepancy between theoretical current value and the one measured with a disc electrode of certain geometry. The coefficient β_{RG} depends on the RG value of the tip. The meaning of RG value needs explanation. The SECM measuring tip usually has a long conic body with a small, flat circular end plate. The actual electrode surface is a conductive disc in the center of this small circle embedded in supporting insulating shield. The RG value is the ratio of the total tip radius (shield + electrode) to electrode radius. Several numerically obtained equations have been published [25, 26] for calculation of appropriate value of β_{RG} from RG. One of them is shown below:

$$\beta_{RG} = 1 + \frac{0.23}{\left(RG^3 - 0.81\right)^{0.36}}$$

It can be seen that large value of $\mathrm{RG} > 50$ results in $\beta_{RG} \cong 1$ while $\mathrm{RG} \geq 10$ gives correction factor of about 2%. Application in SECM electrode with very thin shield like $\mathrm{RG} = 2$ is not usual in that case β_{RG} would be 1.11, that is, the measured $i_{t\infty}$ would be about 11% higher than the theoretical one.

If the electrode is brought to the close vicinity of an object, then presence of the object can change the diffusion flux of electroactive species toward the electrode. The current reflects this. If the electrode–object distance is smaller than the diffusion layer thickness, then the object hindering the mass flow can decrease the current. We call this negative feedback. Of course decrease of the current also shows up if the object acts as a local sink, decreasing the local concentration of electroactive species.

On the other hand the proximity of the object can result in current increase. Local releasing or forming the reacting species by the object results in current increase. This case is called substrate generating/tip collecting (SG/TC) mode. If the electrode reaction at the tip is reversible, then its product interacting with the near surface can be regenerated. The regenerated particles diffusing back through the narrow gap increase the flux to the electrode. This mechanism of current

increase is called positive feedback. The extent of this feedback depends on the rate of regeneration reaction as well as on the gap size and on diffusion coefficients.

Conductive surfaces are able to produce positive feedback, while insulator surfaces can just show negative feedback. The so-called approaching curves showing the dependence of the current on electrode–surface distance are used for characterizing these feedback effects. General forms for approximation of the normalized approaching curves for pure positive and pure negative feedback in case of disc shaped electrode have been calculated [27] and recalculated [28, 29]. The forms contain numerical parameters. Their value depends on the tip geometry that is on the RG value.

The general forms for positive and negative feedback curves are given in [21] together with tables containing the numerical parameters valid for different RG values.

Positive feedback approaching curve in case of fast regeneration process fits within 1% to the equation below if a shielded disc shaped electrode with RG value of 10.0 is used.

$$I_T(L) = \frac{I_L}{I_\infty} = 0.7449932 + \frac{0.7582943}{L} + 0.2353402 * e^{\frac{-1.683087}{L}}$$

I_L is the current measured at $L = d/a$ distance from the regenerating surface where d is the actual distance and a is the radius of the electrode. I_∞ is the current in the bulk. $I_T(L)$ is the normalized amperometric current.

When an SECM tip with RG value of 10.0 is approaching an insulating surface, then the reduced current–distance dependence fits well to the following expression as long as L is ranging between 0.04 and 10.

$$I_T(L) = \frac{I_L}{I_\infty} = \frac{1}{0.4571825 + \frac{1.4604238}{L} + 0.4312735 * e^{\frac{-2.35667}{L}}} - \frac{0.145437 * L}{5.5768952}$$

Since the negative feedback is caused by hindering the diffusion flux, it is more sensitive to the RG ratio. Bigger shield decreases more the current than small one.

The feedback effects give chemical information about the approached surface. It can show that it is isolating or conductive with high speed regenerating electrode process.

Figure 1 shows approaching curves with positive and negative feedback effects.

Negative feedback mode is often used for obtaining topographic image of different surfaces. In this case the tip is scanned close to the sample surface in the *XY* plane at constant *Z* coordinate (constant height scanning). Usually the measurement cell contains appropriate background electrolyte and electroactive species reacting on the tip at the employed electrode potential. Protruding areas on the surface decrease the amperometric current while pits and valleys allow higher diffusion flux. Fitting experimentally taken approaching curves to the negative feedback equation gives hand for *Z* direction tip–surface distance positioning.

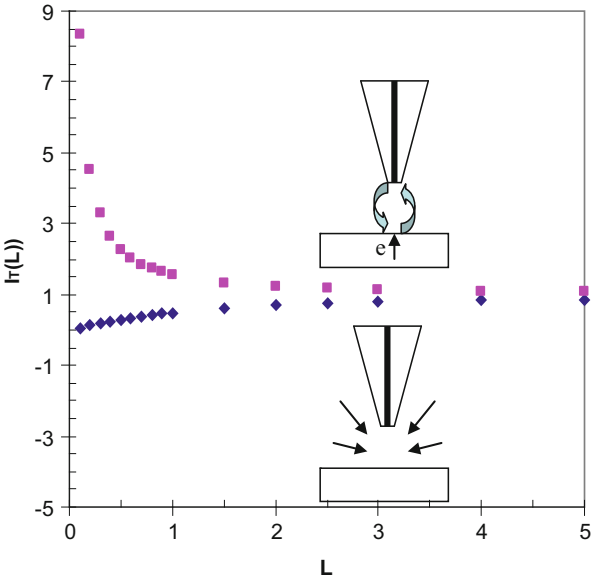

Fig. 1 Normalized current ($I_T(L) = {}^{i_L}/_{i_\infty}$) – normalized distance ($L = \frac{d}{a}$) for feedback responses at RG = 10 (The *curves* were obtained using the equations given above.) "Approaching" current–distance curves for positive (*pink markers*) and negative (*blue markers*) feedback. I_∞ is the current in the bulk, I_L is the current with L distance, d is the distance, and a is the diameter of the electrode disc

Positive feedback images obtained over conductive surface in presence of reversible redox mediators provide topographic image also. In that case higher current shows thinner gap, that means local protruding area. It is obvious, however, that if the scanned surface has both conductive and insulating areas, then the current values recorded at different tip locations cannot be simply transferred to images showing both the conductive/insulating nature and surface topology. Similarly if the mediator regeneration process is slow at different locations, then over those places the positive feedback contribution to the current is smaller. Deconvoluting the effect of mediator regeneration rate from the effect of topographic conditions cannot be done easily. Similarly, if local current values are collected aiming to get images of concentration distribution of certain species, then both the feedback and the concentration affect the current values. In order to separate these two, constant distance scanning is recommended that keeps feedback contribution constant. It can be done if appropriate surface–tip distance measuring method and controlling mechanism are available. As we can see it later, some of the advanced SECM apparatus are capable of doing constant distance scanning. Early chemical microscopes could only make constant height scanning on the *XY* sheet after adjusting the tip at constant *Z* height.

Figure 2 illustrates the constant height and the constant distance scanning techniques. Constant distance method can be used for obtaining chemical information free of influence of topographic conditions.

The SECM methods can be listed in two groups regarding the role of the tips. In the so-called active SECM mode the amperometric signal reflects the interaction of the tip reaction with the sampled object. When the tip just reports the concentration of a species at the sampled location, it can be considered as passive mode. It may

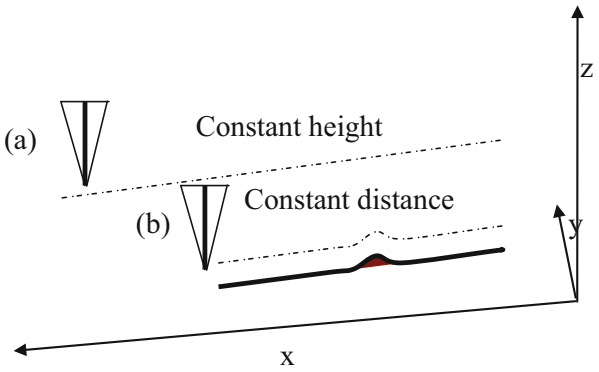

Fig. 2 Comparison of scanning at constant height and scanning at constant distance

worth mentioning here that in case of amperometric detection we can have as active mode the two feedback- and the tip generating–substrate collecting (TG/SC) manners.

2.1.1 SECM Tips Used in Voltammetric Mode

Different kinds of voltammetric microelectrodes have been used in electrochemical microscopy. Preparation procedures of them are well described in original papers and reviews [1, 30, 31].

Metal microelectrodes for amperometric SECM are made of noble metals like Pt, Au, and Pt-Ir alloys. Rarely mercury film coated metal or carbon fiber electrodes are also employed. The electrodes are usually made with circular glass body with pointy end. The small end plate contains in the center the imbedded measuring electrode disc. Regardless of the small size the amperometric tips are relatively robust tools. With special care they can last for years. Platinum and Pt-Ir microwires are commercially available with different diameter. Therefore very often scientists make their own SECM tips using quite straightforward, well described procedures. If a laser based micropipette puller (e.g., Sutter Instrument, type P2000) is under disposal, then platinum disc tips can easily be made with submicron size diameter just by pulling a quartz capillary with a platinum wire inserted inside. Sealing in Pt wire with conically etched end in glass micropipette, or employing silver coated platinum fiber, the so-called Wollaston wire in electrode fabrication can result also in ultramicro amperometric platinum tip. From Wollaston wire a hook is made and used to fix the wire inside glass capillary. The silver coating is etched from the lower end of the wire reaching close to the end. After washing and drying, this side of the capillary is heat sealed under vacuum. Careful sanding, beveling, polishing, and making electric connection from inside the lumen are needed to complete the electrode fabrication.

In amperometric SECM the tip–sample distance can be estimated by observing the feedback effect. This is the important advantage that often helps avoiding electrode crash or sample surface damage.

Au wires are also available. Owing to the different thermal expansion character however, more difficult is to make gold microelectrodes with glass electrode body. Their use is less frequent in SECM.

Carbon Microelectrodes

When electroactive organic molecules are oxidized on noble metal electrode then often happens that the product of the electrode process stays adsorbed on the surface forming an insulating film. This electrode fouling less frequently happens with carbon electrodes. Carbon fibers are used in industrial scale in composite materials. These fibers are available with diameters of 5–8 and 33 μm. They have been proven excellent material for microelectrode preparation. Buda and coworkers [32, 33] first employed electrochemically pretreated carbon fiber microelectrodes for in vivo measurements. SECM tips with carbon measuring surface can be easily made of carbon fibers embedding them in appropriate pointy bodies. In order to make ultramicro electrode the end of the fiber is chemically etched before embedding.

Usually small volume measurement cells are employed. The cell actually is part of the SECM microscope set. The object investigated usually is fixed onto the bottom of the cell. When the constant height mode is used then the cell bottom as well as the sample surface has to precisely set horizontally. Reference electrode that is most often a silver–silver chloride quasireference and the counter electrode in form of a platinum wire are fixed inside the cell.

2.2 SECM with Potentiometric Detection

As it is well known, potentiometry is the simplest and most often used electrometric measuring technique. In potentiometry the potential difference that is the electromotive force (often called open circuit potential) between the measuring and the reference electrodes is measured using a high resistance millivolt meter, like a pH meter. The concentration of the measured species is determined upon calibration.

The advantages and difficulties of application of potentiometric detection in SECM are obvious. It is an important advantage that potentiometric electrodes can selectively detect local concentration, correctly saying, activity of species not accessible with voltammetric methods. It is a further advantage that well described procedures are available for fabrication of ultramicro ion selective electrodes.

There are however serious drawbacks. As it is well known, the potentiometric electrode is a passive sensor. It just reports the concentration of the observed ion in

the solution, adjacent to the measuring surface. There is no feedback effect. Therefore for the estimation of the tip–sample distance a separate method is needed.

The other disadvantage can be the larger response time. If the tip response is slow, then only a small scanning rate can guarantee distortion free chemical images. Unfortunately, SECM needs relatively long data collecting time for imaging even in amperometric mode.

The dynamic behavior of selective potentiometric electrodes has been studied using different methods and conditions. It was found that in the dynamic concentration range, in absence of interfering ions two major factors determine the response time if no intensive convection is applied. These are the thin layer diffusion and the time constant of the measuring circuit.

The electrode potential at t time after concentration change (E_t) can be expressed if the response time is determined by the diffusion [34].

$$E_t = E_\infty + S_{\text{eff}}\left[\log 1 - \left(1 - \frac{a_i^0}{a_i^\infty}\right)e^{-\frac{t}{\tau}}\right]$$

$$\tau' \approx \frac{\delta^2}{2D'}$$

where E_∞ is the steady potential in new equilibrium at a_i^0 activity, S_{eff} is the slope of electrode function, a_i^0 and a_∞^0 are the activities of the detected ion in the bulk before and after the concentration change, respectively, δ is the thickness of the solution film adhering to the electrode surface, and D' is the diffusion coefficient of the detected species in the adhering film.

In case if the resistance (R) and capacity (C) of electrode and measuring circuit are controlling the response time, then the following form can be used for estimating E_t [35].

$$E_t = E_\infty - (E_\infty - E_0)e^{-\frac{t}{RC}}$$

When an ultramicro ion selective electrode is used, then the diffusion flux at the tip is hefty, therefore the contribution of the diffusion is smaller to the response time increase. However, the RC value can be very high. The smaller the tip the higher is the R. In case of ion selective micropipette electrodes the resistance can be in the $G\Omega$ range. The capacitance is originating from the double layers at interfaces, and from the electronic parts and wires. Commercial measuring instruments often contain capacitance compensating circuit. Homemade units with capacity compensating option have been put together, and used, e.g., [36]. Approximate value of the capacitance must be correctly guessed and set when capacitance compensation circuit is used, otherwise instead of elimination of the low pass filtering effect oscillating voltage signal can appear.

Among the drawbacks the high noise usually observed in potentiometric mode has to be also mentioned. The leads to the electrodes act as noise picking antennas. Therefore the possible shortest connecting wires between the preamplifier and the

cell should be applied. The shielding in case of potentiometric microscopy is essential if high resistance microelectrode tip is used.

2.2.1 Potentiometric Microelectrodes Used in SECM

The small size electrodes with perspective applicability as measuring tip in SECM can be listed in three categories. These are glass microelectrodes, metal based microelectrodes, and ion selective micropipettes.

Life scientists were the pioneers in preparing and using glass microelectrodes [37–43]. In practice of SECM, however, application of glass electrodes is scarce. Metal based microelectrodes and ion selective micropipettes became much more popular. Miniaturized version of silver electrodes could be prepared and used for measuring chloride or silver ion concentrations [44–46].

Metal oxide film coated metal electrodes can provide reliable potentiometric pH response. The miniaturized version of them gained application in potentiometric SECM. For example, a microdisc antimony pH electrode was used by Toth et al. [47] for investigating measuring function of silver iodide based ion selective cyanide electrode. Iridium oxide based microelectrode was applied by Wipf and coworkers [48] for pH imaging.

Ion Selective Micropipettes

Glass micropipettes with tip sizes down to nanometers and with different steepness are broadscale used tools in life science micromanipulations. From micropipettes, as it was shown by Walker [49], submicron sized ion selective microelectrodes can be prepared. For these the internal wall of the tip is silanized and hydrophobic cocktail plug that contains selective ionophore is introduced. As final step introduction of the internal filling solution and silver chloride coated silver wire serving for internal reference electrode follows.

The main advantages of ion selective micropipettes are their small size and the universal, easily attainable procedure of their fabrication [50]. The lifetime of these electrodes is not longer than a few days, therefore they need to be made just before their application.

Ion selective micropipettes have high resistance, and short lifetime. They are fragile tools. Regardless of these disadvantages, they are used in potentiometric SECM. Potassium micropipettes based on valinomycin or on BME 44 ionophores, nonactin based ammonium ion selective pipettes [51], or zinc [52] selective ones were proved well applicable for SECM imaging or line scanning over different targets.

Interestingly for pH microscopy often micropipette tips have been used [53], in spite of the existences of several different more stable, less fragile pH microelectrodes. Recently development of solid contact micropipettes of improved properties

has been reported [54–57]. These electrodes have reduced resistance and show improved lifetime.

2.3 SECM with Conductance Detection, SICM

Detecting ionic conductance with a traveling probe also can be used for obtaining information about topography of certain surfaces. The first report about taking advantage of this has been published by Hasma and coworkers [58]. The working principle of SICM easily can be understood considering the following. An open micropipette with a small orifice is used as scanned measuring probe. It is filled with electrolyte and contains a reference electrode, let say Ag/AgCl wire is inside. A same kind reference electrode is located in the bulk of the electrolyte solution inside the measuring cell, where the tip is moving. A bias voltage is applied from an outside source and the current is measured.

The following cathodic and anodic electrode processes take part at the surfaces of the two electrodes, respectively.

$$\underline{\mathrm{AgCl}} + \mathrm{e}^- \rightleftarrows \mathrm{Ag}^{\mathrm{o}} + \mathrm{Cl}^-$$

The current between these two electrodes is determined by the charge transfer resistances R_{ct} R'_{ct} and capacitances of the double layers at the two electrodes (C_{dl} and C'_{dl}) and the resistance of the solution. Figure 3 shows the connection of the resistances and capacitances in the conductivity cell. We suppose that the two electrodes have large surface area comparing to the aperture of the pipette and we suppose that the charge transfer process is fast. The ions carrying the charge have to pass through the small aperture of the pipette tip. In case of given voltage difference applied, the current is determined by the ionic fluxes through the narrow tip of the probe rather than the resistance in the bulk of the solutions (R_{sol}). That means the tip resistance (R_{tip}) controls the current (see Fig. 3), $R_{tip} \gg R_{sol}$.

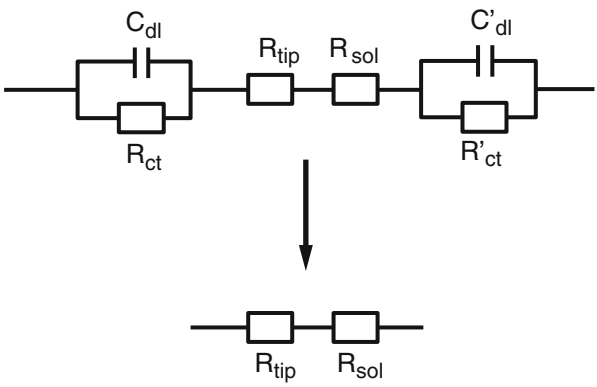

Fig. 3 Equivalent circuit of the conductivity cell for SICM

As long as the tip moves inside the bulk of the solution the current stays constant since $R_{tip} \gg R_{sol}$. However, if the tip approaches an obstacle that hinders the diffusion of the ions to the orifice, then part of R_{sol} between the tip and the obstacle surface increases. Its contribution to the total resistance depends on the thickness of the narrow gap that is on the distance between the tip and the surface.

The current change reflects the resistance change that is the distance between the obstacle and the tip (d).

We can write that

$$R_{sol,\infty}/R_{sol}(L) = i_T(L)/i_{T,\infty}$$

if L is the normalized distance in Z direction $L = d/a$, a is the tip orifice radius, R_{sol} (L) is the external solution resistance, $i_T(L)$ is the current at L distance, index ∞ indicates the values of i_T and R_{sol} when the tip is far from the obstacle.

Combining analytical consideration and numeric simulation an equation could be given [59] for describing the dependence of the resistance change,

$$\Delta R(L) = R_t(L) - R_{t,\infty} \text{ on } L$$

where t index indicates the total solution resistance. It is supposed that R_{tip} does not depend on L.

Therefore

$$R_t(L) - R_{t,\infty} = R_{sol}(L) - R_{sol,\infty} = \Delta R(L).$$

And the equation is

$$\frac{\Delta R(L)}{R_{sol,\infty}} = -0.708 + \frac{1.5151}{L} + 0.6553 \cdot e^{-2.435/L}$$

A more detailed theory of the SICM has been worked out by Unwin's group [60].

In practice constant height scanning or constant current scanning is applied over the XY plane. In constant current scanning the Z coordinate of the tip is changed to keep the current constant at each XY locations. In this case ΔZ displacement of the pipette normal to the surface shows the topography of the sample. The selection of d distance is critical. In case of large L the relative change of the gap will be small then no sharp topographic image can be obtained.

Hopping probe ion conductivity microscopy (HPICM) [61] is a new version of the SICM. In the working program of the HPICM the instrument at every location on the XY plane starts current measurements with pipette being far from the sample (reference current). Then the pipette approaches until the current is reduced by a predefined percentage, let say 1% of the reference. Those Z positions of the tip are used as Z coordinate for topographic imaging. Then the tip is withdrawn and moved laterally to the next imaging point on the XY sheet. By continuously updating the

reference current while the pipette is away from the surface, the method automatically adjusts for any changes.

Question can arise if the SICM can be considered as a chemical probe microscopy. While voltammetric and potentiometric probe microscopy methods give chemical information, about the samples, SICM provides only topographic images with high spatial resolution. Comparing with other methods its important advantage is that the probe does not touch the sample during line scan or image making.

3 Tip–Substrate Distance Determination and Control

In SECM the tip follows a predetermined travel program. It moves on the horizontal *XY* sheet step by step. The electrochemical instrument measures and records at each step the signal. Image or the line curve is made from the recorded signals and the corresponding *XY* tip location coordinates. The vertical, *Z* coordinate of the tip location is also an important feature. It must be adjusted before scanning, and that coordinate is an important parameter, needed to be given when presenting the SECM results. As it was mentioned before, two different scanning programs have been generally used concerning the vertical coordinate of tip location. One is the constant height method the other one is the constant distance method (see Fig. 2).

In constant height method the *Z* coordinate of the tip travel is kept constant (constant height), the tip travel is horizontal. In this case great care has to be taken for avoiding tilting of the substrate. The tip–sample distance is adjusted at an appropriate part of the sample surface, and that *Z* tip coordinate is kept constant for all the time of scanning. It is questionable how the distance can be measured and adjusted in the micrometer scale. When amperometric detection is used then feedback effect helps to determine tip–sample distance. From the current change resulted by the feedback the actual distance can be estimated knowing the radius and the RG value of the tip. That is, in practice the distance scale is attained by recording an approach curve, and fitting it to the appropriate feedback equation.

In case of passive tip, when feedback effect is not available other distance measuring method has to be selected. Double barrel tip, one barrel for imaging, the other one for distance measuring, has been successfully applied [51, 52]. In case of pH imaging double function antimony tip [62] could be used for both distance measurement (amperometric mode) and potentiometric mode (pH imaging). The constant height imaging mode is appropriate in case of thin film samples. It requires simpler apparatus.

For obtaining higher spatial resolution in SECM smaller and smaller tips have been fabricated and employed. When smaller electrodes are used in feedback effect based imaging then the tip needs to scan at smaller vertical distance from the substrate. The tip–substrate crash in this case easily can happen with tilted or rough surfaced samples. The other problem with constant height scanning in amperometric mode is that the signal obtained is contributed by two factors. On one hand the concentration of the observed species at the tip can be higher or

smaller depending on the nature and rate of the reaction taking part at the investigated surface. On the other one the tip–substrate distance or surface features seriously influence the local concentration of the diffusing species. The deconvolution of the convoluted image is not easy. Constant height imaging is advantageous in case of smooth, planar surfaces or if topographic image relying on negative feedback is planned to be made.

Scanning the tip at constant vertical distance from the substrate surface eliminates the effects of the surface topography. The image obtained reflects separately the surface processes without blurring caused by differences in diffusion layer thickness. Therefore constant distance imaging is advantageous specially, when submicron size electrode is used. Its application though requires more sophisticated apparatus and working programs.

Different methods have been worked out and used for distance checking, adjustment, and control. Shear force based distance control is getting broadscale applied in SECM. Actually, the nature of the shear force is still not clearly understood. It is a short range interaction between a thin vibrating probe and the surface. It is most likely contributed by the viscosity of the surface confined water, the van der Waals forces, or some kinds of near field atomic forces [63].

Shear force tip–substance distance control originally was introduced in scanning near field optical microscopy (SNOM) [64–66]. It is based on detecting the damping effects of the near surface force on vibration of a thin probe. The resonance of a vibrated thin probe changes upon approaching the sample. Either amplitude or phase of the vibration can be used as distance control parameter in the feedback system [67]. The reaching distance of the surface shear forces is very short. It is not longer than two hundred nanometers. However, below these the damping effect is very intensive. Therefore a given degree of damping of the bulk resonance amplitude indicates a very small tip–surface distance. It can be used as distance controlling signal in constant distance scanning.

The apparatus, being able implementing shear force distance control must be set with an actuator for providing the tip vibration and an amplitude detecting unit. Usually piezoelectric actuator is connected to the stem of the tip. It keeps it oscillating at resonance frequency. For detecting the amplitude different techniques are used. From the optical methods laser spot diffraction from the vibrating probe [54], or interferometric technique [68], has been successfully used for distance detection.

The other, frequently employed method for observing amplitude change relies in application of a quartz tuning fork interconnected between the probe and the piezo actuator. The quartz tuning forks are small, micro-machined electronic elements manufactured in different sizes. They are broadscale used in clocks and watches. Similarly to the optical tuning forks they have two prongs, with certain resonance vibration frequencies. Owing to the piezoelectric property of the matter they are made of, mechanical oscillation of the prongs induces surface charges. These are picked up through appropriate connecting pads as AC current. Therefore the tuning fork acts as a mechanical–electrical signal converter. Connected lock-in amplifier and electronic circuits can produce a signal reflecting the amplitude. When it is used

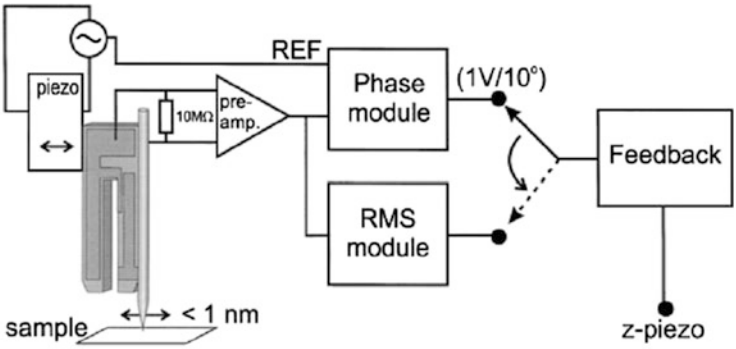

Fig. 4 Schematic design of tuning fork action based distance control unit. The figure was taken from [69]

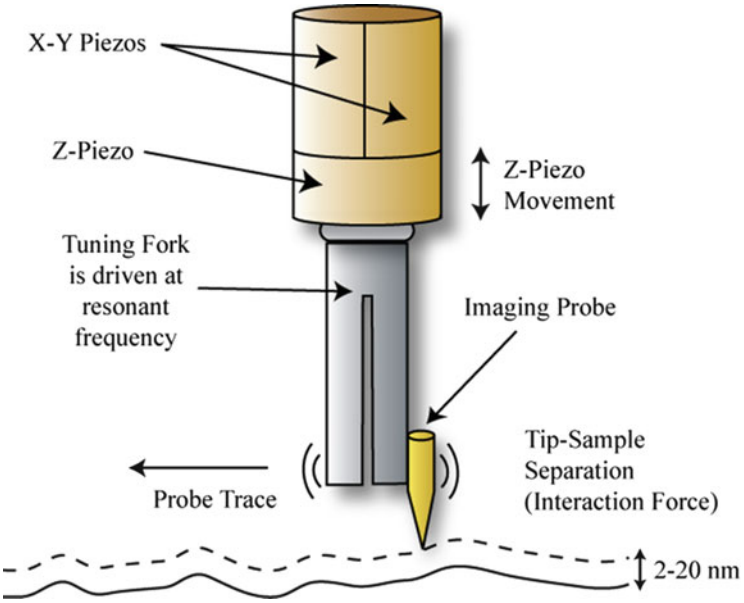

Fig. 5 Schematic design of the tuning fork applying distance control system. Figure was taken from [70]

in probe microscopy, the tuning fork is attached to a piezoelectric actuator that makes it vibrating at its resonance frequency. The ultramicro probe is glued onto one of its prongs, so it is also vibrated. The vibration is damped by the surface shear forces when the tip approaches very close to the surface. The amplitude change produces signal for the feedback loop that adjusts or controls the tip–surface distance. The schematic illustration is shown in Fig. 4 [69] (Fig. 5).

4 The Variety of SECM Measurements in Biologic Analysis

SECM measurements successfully were used in imaging or line scanning over high variety of different samples. Different species or effects were detected at different locations for obtaining information about different objects, about their local properties, or about different processes taking part at different locations.

Parts of these measurements have been using active tips. It was mentioned earlier that the positive and negative feedback based microscopy is done with active tips. Similar thing can be said about TG/SC mode [71, 72]. In this case when the generating tip is close to the sample surface then the concentration of the generated species is high at the vicinity of the substrate, therefore high signal is observed. Positive feedback is most often observed at metal surfaces [73] when reversible mediator is used. Positive feedback can also been obtained when testing biologic objects, like living cells, see later and [74]. The tip generated redox mediator passing through the cell membrane into the cytoplasm can be regenerated by an intracellular redox process [75]. As the regenerated mediator diffuses back into the extracellular space positive feedback, that means current increase can be obtained. Positive feedback also can be obtained if the cell membrane contains a redox active regenerating species. In some cases, the redox active species just selectively linked to the cell membrane as a label for SECM detection of a membrane component. Expression of certain membrane protein could be successfully detected using immunochemical redox enzyme labeling [76]. Figure 4 shows the two locations of mediator regeneration, one in the cytoplasm and the other at the surface by a surface confined species (Fig. 6).

Negative feedback mode available in voltammetric or conductometric imaging can be used for topographic imaging of cells, tissues, bio-layers; measuring of thickness, or volume of them, following their shrinking, growing, or proliferation in time (see later examples).

Passive SECM tips do not interact with the samples. They can be used for imaging local concentration profiles of different species. Living cells,

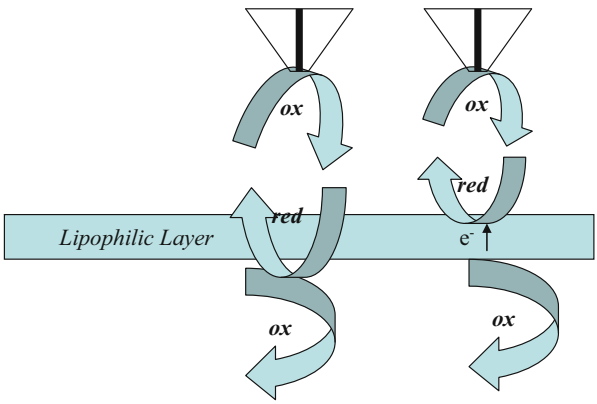

Fig. 6 Ways of obtaining positive feedback in biologic experiments

microorganisms, or tissues of metabolic activity create steady local concentration profiles in their environment. Local pH, and/or local oxygen concentration differences are generated by breathing or photosynthetic processes. Biological objects secrete or take in other electrochemically detectable species. This can be the result of passive diffusion transport through small openings like stomata on plants or through biomembranes. Sometimes carrier facilitated mechanism, sometimes active biochemical pump is involved in this transport. SECM therefore can be used for detecting metabolic activity of living species. As it is obvious enzymes confined to interfaces can also generate local concentration profiles. SECM can be a powerful tool in making chemical images that show map of local enzyme activity. Enzyme labeled histochemical imaging is also a very promising application field of SECM. (Examples are discussed below.)

5 Examples of Successful Application of SECM in Bioanalytical Experiments

In the following part of this chapter a few selected examples are introduced briefly, for showing examples of successful application of SECM in gathering valuable information about different biological objects.

5.1 SECM Experiments with Botanic Samples

SECM has been proved well applicable for investigating surface morphology of living botanic samples as well as their physiologic interaction with the environment. In certain measurements the studied object is immersed in appropriate buffer media. Redox mediator is added into the solution and the amperometric current is detected by the tip scanning in close vicinity of the surface. Microscopic image is made based on the negative feedback effect on the amperometric current. In the simplest cases the negative feedback image shows the surface topography. Since the oxygen is electroactive, another image showing the photosynthetic activity can be made detecting the local concentration of dissolved oxygen at the close vicinity of the sample. Interesting experiments can be made by changing the illumination, and by comparing the topographic and oxygen concentration images.

Yasukawa et al. [77] fabricated double disc measuring tip for SCEM measurements. They used it for characterizing both the shape and the photosynthetic activity of a single, living algal protoplast sample (radius 25 μm) obtained from marine alga *Bryopsis plumosa*. Two barrel theta (θ) glass capillary was used for making the microprobe. Platinum microwires with 0.5–4-μm radii were sealed into each barrel. Two images were used for characterization. Two images could be formed: one from the amperometric $K_4Fe(CN)_6$ mediator oxidation current data and another one from the local values of oxygen reduction current. The effect of

negative feedback on mediator oxidizing current showed the shape of the living sample, while the amperometric reduction current of oxygen produced upon light illumination showed the map of photosynthetic activity of the protoplast.

Application of SECM for topographic imaging of plant leafs and detecting photosynthetic activity of water plant was also reported by Bard's group [78] in a preliminary paper. They used 1 μm size platinum disc tip and 5 μm carbon fiber tip for making topographic image of grass (*Ligustrum sinense*) leaf surface showing the stomata structures. Potassium ferrocyanide ($K_4Fe(CN)_6$) mediator was used in these experiments. The photosynthetic oxygen production upon illumination of leaf of elodea, a well-known aquatic plant, was detected through CVs and SG/TC image production.

Brassica juncea (brown mustard) is a plant that accumulates heavy metals like cadmium in its roots. This metal accumulating habit can be used for removing heavy metals from polluted soils. Interesting question, how the Cd-induced stress influences the photosynthetic activity of this cadmium accumulating plant. SECM method allows measuring the immediate stress response at microscale, showing the change of stomata structure and photosynthetic activity.

Zhu and coworkers [79] investigated the stress response with platinum electrode made of Wollaston wire that contained Pt wire of diameter 2 μm coated with Ag to an overall diameter of 100 μm. The ratio of sheath diameter to that of the Pt disc (RG value) was 8 for their tip configuration. Figure 7 shows the experimental setup used for imaging the photosynthetic activity of brown mustard leaf, and a few obtained images.

As it can be seen the SECM experiments with this microtip have provided a simple and more immediate way to assess the net photosynthetic efficiency of

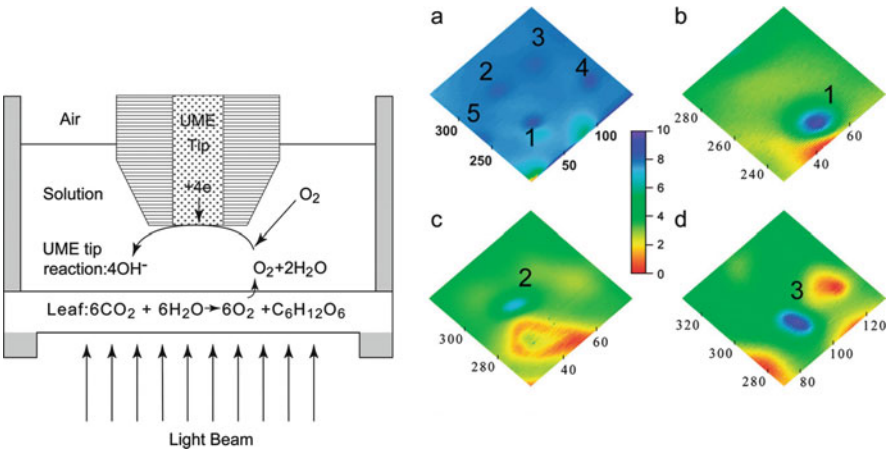

Fig. 7 The schematic view of the SECM cell used for imaging surface of *Brassica juncea* leaves (*left*) and images obtained (*right*). (**b–d**) Shows the individual stomata regions marked by numbers on (**a**). *Dark blue* indicates the high oxygen concentration. The sample extension is given in micrometer. Figure was obtained from [79]

individual stoma. The size of single stoma and stomata density on control plants and treated ones could be estimated based on in vivo recorded SECM images. Stomatal density and oxygen evolution were noticeably reduced in Cd-exposed leaves. A Cd-induced decrease in the size of the pore aperture and an increase in the overall stomatal complex have been observed.

Parthasarathy et al. [80] investigated the SECM behavior of seedling-derived peanut plants grown in test tube and grown in soil. Polarizing the platinum microelectrode to −0.5 V vs. Ag/AgCl, sat. KCl reference, the oxygen reduction current was detected. Difference could be observed between the evolved oxygen concentration detected over guard cells and over mesophyll cells. Images were recorded also with platinum tip polarized to 0 V. The electrochemical process that generated the images at this potential could not be clearly explained. It was believed that some unidentified electroactive component being on the leaf surface interacts with the tip. CVs recorded over aging leaves showed the presence of an adsorptive redox couple in the close vicinity of the surface.

Life wandering Jew (*Tradescantia fluminensis*) leafs were used as sample substrates in plant physiology studies of Tsinonsky et al. [81]. They used a carbon fiber microelectrode tip that was prepared by heat sealing carbon fiber (diameter 7 μm) into glass capillary and drawn down, sanded off the tip, and polished to expose a carbon disc in its center. Part of the apparatus was placed inside glove bag, in order to be able to lower background oxygen partial pressure when it was needed. Xenon lamp provided light for photosynthesis through the connected optical fiber. The leaf investigated was kept alive by keeping it attached to the plant. It was mounted into transparent bottom of the measuring cell of the SECM apparatus. The light guiding fiber illuminated the backside of the leaf through the bottom of the cell.

Topographic images about the leaf surface were made detecting the amperometric reduction current of oxygen in order to see the stomatal complexes. Negative feedback images were recorded in air saturated buffer solution in dark conditions where the possible interference of photosynthetic oxygen release was avoided. The obtained images clearly showed lower current regions (guard cells) around the higher current spots corresponding to the stomatal pores.

The approaching curves over green leaf areas showed negative feedback effect in dark, while positive feedback could be observed after turning on the light. The difference between currents measured in dark and in illuminated conditions showed up well when the oxygen concentration was reduced in bulk of the buffer.

The effect of light turn on and off was studied in SG/TC mode. The current change was quite extensive over green areas. However, the fluxes of oxygen from the white area located around the stomata were found extremely small. However, when the tip was positioned over those white areas the current increased turning the light on and decreased upon turning it off. This proved that the released oxygen is resulted also by photosynthetic process. The production in white area is small since in those areas the chloroplasts concentration is small.

Plants called halophytes are capable living in environment of high salinity. The salt tolerance is an important character. Agriculture production could be improved in salty areas, if cultivated plants could be furnished with this feature. Halophyte

plants upon exposing to high salinity respond with root growth and salt excretion in their leaves. It has been hypothesized that the salt excretion happens as a function of special excretion glands [82]. For obtaining proofs for existence and function of these salt glands Parthasarathy and coworkers [83] carried out extensive studies with SECM. They picked Bermuda grass (*Cynodon dactylon* L.) as sample, a salt tolerance plant that has been used in therapy of different diseases. The field collected explants were washed, sterilized, and inoculated in appropriate buffered media. Subcultured Bermuda grass leaf samples were fixed onto the bottom of the measuring cell and a 10 μm diameter Pt microelectrode (RG = 10) was used as SECM probe. Recording images following the amperometric oxidation current of ferrocyanide mediator over the adaxial and abaxial surfaces of the leaf, the negative feedback topography indicated the existence of the protruding gland cells. Imaging with electrode polarized to −0.8 V the local oxygen concentration was also detected. The photosynthetic process influencing the local oxygen concentration can interfere with the oxygen reduction based topographic images. Optical micrographs taken from the safranin stained tissue samples also proved the existence of the glands. Furthermore impedance measurements over the glands were also made. The overall results proved the applicability of SECM in studying plant physiologic tasks.

5.2 Topographic Imaging of Living Cells

In a collaborative work of Baur et al. [84] the applicability of negative feedback mode SECM for investigation of dynamic changes of living cells was tested. In their experiments PC12 dopamine-releasing immortal cell line established from rat adrenal glands was used as model. These cells upon exposed to nerve growth factor (NGF) can differentiate, and can grow neurite processes that make synaptic contacts with other cells. The authors tested several mediators previously used in SECM trying to find less toxic ones with no predictable short time effect on the physiology of the cells and having appropriate redox potential that avoids interaction with electroactive species like dopamine released by the cells and giving good electrochemical behavior on carbon fiber electrodes. Five of them: ascorbic acid, 1,4-benzochinone, $Ru(NH_3)_6^{3+}$, 4-amino TEMPO (4-amino-2,2,6,6-tetramethyl-piperidinyloxyl), and 4-hydroxy TEMPO (4-hydroxy-2,2,6,6-tetramethylpiperidine 1-oxyl) were selected for the work. Glass insulated and polymer insulated carbon fiber electrodes of different sizes were used. The applicability of the SECM for high resolution imaging of the PC12 cells was proved. Interestingly the neurites extended by the cell, not visible in optical microscope clearly showed up in SECM images. The method could be used for real-time observation of cell morphology changes. It was shown by exposing the cells to hypotonic and hypertonic extracellular conditions. Swelling and shrinking of the cells change the distance between the cell and the tip. This is reflected by the feedback current.

Razzaghi et al. [85] used SECM in studying the morphology and morphology changes of individual cells of EA.hy926 cell line (human umbilical vein cell line). This cell line was prepared by fusing of human umbilical vein endothelial cells (HUVEC) with permanent human cell line A549. Pt disc tip with a diameter of 10 μm and 5 mM $[Ru(NH_3)_6]Cl_3$ redox mediator in 0.1 M KCl have been used. Constant height scanning technique was employed. The current of $[Ru(NH_3)_6]^{3+}$ reduction was followed during scanning the tip over the immobilized living cells. The local values of feedback current could be used for image formation. The contrast of the images recorded over cells grown on classical 6 well plates was poor comparing it to images recorded over cells fixed on conductive ITO glass surface. The reason was obvious. Positive feedback over ITO glass increases the current while over the cells and plastic surface negative feedback dominates. The enhanced contrast provided by the conductive support helped in investigating the drug induced morphological changes of the cells. Submitting the living EA.hy926 cells to Combretastatin A4, antivascular drug, their original elongated shape considerable changed, they became round.

Recently Matysik and coworkers [86] demonstrated the applicability of SECM tip for treating individual cells. They used homemade ultramicro platinum electrodes with effective radii between 200 and 600 nm and nontoxic mediators like $[Ru(NH_3)_6]Cl_3$ and ferrocene methanol (FcMeOH) for SECM imaging. Monolayer of normal rat kidney epithelial cells was confined and cultured on microscope glass cover slips as sample surfaces. Parallel imaging with confocal laser microscope and SECM were performed. Owing to the small tip size high resolution images showing the individual cells could be obtained with constant height technique. The tip was used to attack individual cells with electrogenerated local pH shock. Necrosis of the selected individual cell was achieved. Morphological changes resulted by the cell necrosis could be detected with SECM imaging.

Imaging metabolic activity of a single cell is a challenging topic. Recently Matsue and coworkers [87] investigated the influence of tip reaction on the imaging of yeast cells in SG/TC mode. They detected activity of intracellular cytosolic and mitochondrial enzymes (NAD(P)H-oxidizing enzymes, NOEs) catalyzing electron transfer from NAD(P)H to quinone substrates. Dual mediator system, containing lipophilic menadione and hydrophilic ferricyanide $[Fe(CN)_6)]^{3-}$ provided increased current on nanosize platinum electrodes at the vicinity of single yeast cell with acceptable signal/noise ratio. The current increase resulted by the intra cellular redox reaction. The lipophilic menadione entering the cell interacts with the intracellular NOEs to form menadiol. It diffuses back into the extracellular solution where it reduces the ferricyanide. (Figure 9 shows the menadione/menadiol redox process.) The signal was generated by the amperometric oxidation of ferrocyanide $[Fe(CN)_6)]^{4-}$ at the tip. The tip acts as a sink for ferrocyanide, accordingly it influences the chemical environment of the cell. Different size platinum tips were used in order to check the extent of this. Electrode with tip diameter of 11.9-μm changed substantially the concentration at the cell environment influencing the intracellular processes, while electrode with 199-nm tip diameter produced very noisy signal.

For improving single cell level efficiency imaging of biological objects Takahashi et al. [88] fabricated double function probes with tip size in nanometer range. The probes could be used for both optical and electrochemical imaging. They were made of single mode optical fibers or glass capillaries. Steep conical ends of them were formed using puller apparatus. These optical microprobes could be used for topographic imaging. Conical electrodes were formed by sputtering their surface with Ti/Pt nanofilm, and subsequently insulating it with xylene polymer. The imaging was done with employing shear force method for sample–tip distance control. For this, the probe was attached to one of the prongs of a tuning fork and vibrated with a piezoelectric vibrator placed between the tip holder and the other prong of the tuning fork. Resonance frequency vibration of the probe was induced. The shear force changes generate signal for action of distance controller. Using the so-called standing approach (STA) tip–traveling data collecting mode high resolution images could be obtained from cells. The STA imaging is similar to tapping mode scanning used in other probe microscopies, like in AFM. Its data collecting program is the following: The tip follows a preset travel pattern in the horizontal *XY* plane at a relatively high distance from the surface. At every data collecting *XY* location it stops and the *Z* direction positioning motor is activated. The tip is approached to the sample surface in vertical (*Z*) direction and the shear force signal is continuously followed. The *Z* coordinate, where the shear force changing reaches a trace level is accepted as reference sample–tip distance. Upon reaching this distance the tip is detracted by a preset few micrometers and the electrochemical signal is recorded together with the tip coordinates. The tip is lifted up and the process repeated at the next *XY* spot.

Schuhmann's group recently proposed [89] a method for recording multiple constant distance images. The method that is called four-dimensional shear force based constant distance mode scanning electrochemical microscopy (4D SF/CD-SECM) allows taking several images at different preset tip–substrate distance at a relatively short time. An optically detected shear force distance controller unit helps to bring with *Z* direction approach the thin carbon disc electrode into the very close vicinity of the surface at every lateral *XY* grid points.

When inside the shear force regime, threshold amplitude, like 80% of the amplitude observed in the bulk is reached then the approaching and shear force detecting are stopped. The position, together with the corresponding tip current value, is stored in the computer memory. The *Z* coordinate taken at the threshold distance shows the topography at *XY* coordinate. After recording the closest distance values the tip is retracted in predetermined increments and at each positions the chemical tip signal is recorded. After recording the signal at each *Z* distances, the tip is moved to the next *XY* sampling grid point, the shear force detection and the approaching are started again and the previous measuring cycle is repeated. After each grid points were "visited" constant distance images could be extracted from the collected "4D" data fields relating to different constant distances. As indicated above, topologic image could be also prepared combining *Z* coordinate of the threshold reaching shear force signal with the *X* and *Y* coordinates of the tip location. The advantage of the proposed routine is the shorter scanning time in

making multiple constant distance imaging. Also this routine safely avoids tip crash even in large sampling areas.

An SECM method was worked out [90] for observing the morphological changes of a single live human bladder cancer cell (T24) in time. The cells were kept in transparent plate and inverse optical microscopic observation was employed parallel with the electrochemical measurements. A platinum microelectrode (diameter 5 μm) was positioned about 0.8 μm above the nucleus of the target cell and scans crossing the cell center in the *XY* plane were made recording the local current values. −0.5 V electrode potential has been selected for the studies. In the applied conditions the reduction of the dissolved oxygen gave the major component of the current. The negative feedback effect showed the topography that is the morphology of the cell. Small areas were scanned (80×60 μm or 80×80 μm) with 256×256 pixels. This provided short acquisition time of about 3 min for each image. Therefore real-time observation of morphological changes of the single live cells could be done with enhanced resolution. It is an important advantage of this SECM method that no external mediator or marker is needed. The authors visualize that with their method effect of different anticancer drugs on the cell physiology can be studied. Zhang and coworkers [91] using very similar SECM method investigated the evolution of reactive oxygen species (ROS) at single cell level. Similarly, live human bladder cancer cell (T24) fixed on the bottom of a Petri dish was imaged moving a platinum microdisc electrode (diameter 5 μm) in the *XY* plane at constant level horizontally. Probe approaching curves also were recorded over the cell and analyzed. −0.6 and −0.8 V electrode potentials were selected for the experiments. Negative feedback effect of the oxygen reduction competed with the positive feedback produced by the ROS release into the extracellular media. Apparent positive feedback indicated intensive ROS release. Relatively short time consecutive scans showed that ROS release has a cyclic timescale. Period of intensive ROS release is followed by period when the cell does not release it. The release in the active period has a steady rate. The authors investigated the effect of anticancer drug cisplatin on the ROS release intensity and kinetics. Cisplatin (*SP*-4-2)-diamminedichloroplatinum(II) is a broadscale used anticancer drug. Its therapeutic action is believed to rely on its triggering effect on programmed cell death (apoptosis). It was found that cisplatin significantly accelerated the periodicity of the ROS generation cycle of T24 cell. The observations also showed enhanced ROS productivity.

In a recent study the same authors [92] investigated further the influence of cisplatin on the physiology of T24 cancer cells with their SECM technique. They employed FcMeOH redox mediator. Quantitative time-course images were made and the topography and membrane permeability changes were observed. It was found that acute addition of cisplatin to the outer environment of T24 cells immediately induced membrane permeability change. The loosening of the cell membrane permeability was a quick process. After the short period no more continuous increase of the permeability could be seen. It could be concluded that the increase of the cell membrane permeability is involved in the apoptotic process

induced by cisplatin. The SECM measurement could give some insight into the anticancer action.

5.3 Imaging Metabolic Activity of Cells and Microorganisms

In vitro fertilization and embryogenesis is getting common in studying physiologic processes as well as in biotechnology, in infertility treatment programs, and in animal breeding practice. The oxygen consumption of embryos can give information on their vitality. Shiku and coworkers [93] investigated the applicability of SECM technique for invasion free measurement of this property using single bovine embryos obtained from in vitro fertilized oocytes. They kept the single embryo (morula) in a thermostatic microculture dish on the plate of an inverse microscope in water-saturated 5% CO_2 and 95% air gas atmosphere. Platinum disc working electrodes with 1.8–0.9 μm radius embedded in 4 μm glass shield radius, polarized to −0.6 V vs. Ag/AgCl were used for measuring the oxygen reduction current.

In estimation of the oxygen consumption it was assumed that the oxygen concentration at the spherical morula surface is uniform. Then the concentration at distance r, $C(r)$, can be expressed as

$$C(r) = \frac{(C_s - C^*)r_s}{r - r_s} + C^*$$

where r_s is the radius of the morula sample and C^* and C_s are the concentrations of oxygen in the bulk solution and at the sample. By plotting $C(r)$ against $r/(r - r_s)$ the authors could determine C^* from the intersection at $r/(r - r_s) = 1$. The oxygen consumption rate (F) was calculated as

$$F = 4\pi r_s D(C^* - C_s)$$

where D is the diffusion coefficient of oxygen in aqueous media at the temperature of the measurements (37°C). It was shown that the $\Delta C = (C^* - C_s)$ value is a significant indicator of viability and further developmental potential of an individual embryo.

A platform for SECM measurements on high number microtissue samples was prepared by Sridhar et al. [94]. They used hot embossing technique to stamp a microwell array in the bottom of polystyrene Petri dish. Array of 42 pits with 200 μm height, 400 μm diameter, and 800 μm spacing between them was made using polydimethylsiloxane stamp. Large scale microtissue samples of different cell lines were grown in the pits. The oxygen concentration in buffer media over the pits was detected with mercury coated 10 μm platinum SECM tip. Line scans, 15 μm over HeLa microtissue samples containing pits, were made for detecting the respiration rate. Figure 8 shows the experimental setup (scheme A) and the oxygen

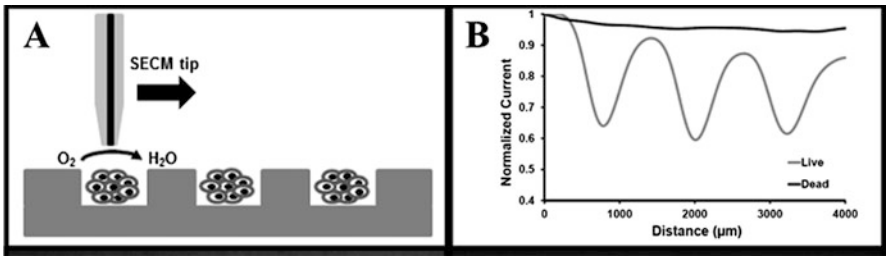

Fig. 8 SECM study of microtissue samples grown in array platform. Scheme showing the experimental SECM setup (**a**). Line scans over the tissue samples showing the oxygen reduction current before (*gray line*) and after treatment with 50% ethanol (*black line*). (**b**) Measurements were performed in HEPES buffer at −0.6 V vs. Ag/AgCl with a 10 μm Hg-coated Pt working electrode; scan rate of 10 μm/s. Figure was taken from [94]

reduction current (curve B) before treatment (gray line) and after treating the tissues with 50% ethanol for 45 min (black line). It can be seen that before exposing to ethanol the living tissue consumed oxygen. After exposure the oxygen concentration was practically constant along the line scan indicating that the microtissue samples were not viable any more.

Nagamine and coworkers [95] investigated the effect of osmotic stress on the bacterial response of glucose stimulated change of metabolic activity of *Staphylococcus aureus* pathogen bacteria. They positioned with a homemade SECM apparatus a platinum disc electrode of 10 μm radius over 50 μm distance from surface of collagen entrapped bacteria culture spots. Circular micropores with 300 μm diameter opening and 50 μm depths were etched on glass surface for using as microcontainer for the collagen–bacteria gel.

For measuring the respiratory activity of the bacteria they used 5.0 mM K3[Fe $(CN)_6$] hydrophilic mediator added to the PBS buffer electrolyte. The mediator after passing through the cell membrane could interfere with the respiration cycle and got reduced. As the formed $[Fe(CN)_6]^{4-}$ diffused back to the buffer through the gap, its mass flow could be detected recording the amperometric current at 0.6 V electrode potential. In this case the oxidative current depends on the transport and permeation rate of the mediator as well as on the metabolic activity of the culture.

Addition of 20 mM glucose was used to stimulate the metabolic activity. The behavior of Gram-negative *Escherichia coli* and the Gram-positive *S. aureus* cultures was compared.

Interestingly without osmotic stress high glucose response that means current change was obtained for *E. coli* culture and only marginal response for *S. aureus*. In presence of osmotic stress induced by 1.0 M Na_2SO_4 the glucose response of *E. coli* decreased, while for *S. aureus* it was quite big. It was expected that the hydrophilic $[Fe(CN)_6]^{3-}$ cannot easily penetrate into the Gram-positive species. Therefore the high glucose response of *S. aureus* in presence of osmotic stress could be resulted by change of diffusion character of the cell membrane. The respiration rate domination of the oxidation current change upon glucose addition in stress free

condition for *E. coli* could be proved with changing the mediator concentration. Using the SECM technique the accelerating effect of osmotic stress on respiration rate of *S. aureus* could also be proved. It was expected that using hydrophobic mediator, like menadione the effect would be more apparent.

The metabolic activity of *E. coli* bacteria culture entrapped in collagen gel was studied by Kaya et al. [96]. The cultures were immobilized in conic and cylindrical microwells etched on glass surfaces. Platinum microdisc electrodes were used as measuring tip. The bacteria culture obtained glucose as nutrient and potassium ferrocyanide ($K_4[Fe(CN)_6]$) was introduced into the buffer. Concentration profiles of oxygen and ferricyanide ($[Fe(CN)_6]^{3-}$) were recorded over the culture with SECM apparatus. The production rate of oxygen and ferricyanide ions could be estimated by measuring the concentration at different distances from the surface, and assuming hemispheric diffusion from the surface. The comparison indicated that the ferricyanide production rates were larger than the oxygen consumption rate. The authors explain the difference by the difference in the number of electron (s) required for the redox reactions. Pointing out that in the respiratory chain, oxygen is reduced to water via 4-electron reduction, whereas only one electron is involved in the ferricyanide/ferrocyanide redox process.

Micro-contact printing with poly(dimethyl siloxane) (PDMS) stamp was used for making a pattern on which HeLa cells from human cervix epithelial cell line were grown [97]. SECM imaging was used for investigating the respiration activity of the immobilized, patterned cells. In this work platinum disc tip, with 5 μm diameter, polarized to −0.5 V vs. Ag/AgCl electrode was used, so the local concentration of oxygen was detected through the amperometric current. The measured concentration values at certain distances allowed a rough estimation of the intake of oxygen by the cells.

Various types of genetically engineered microbial strains have been created by fusing a DNA damage-inducible gene with reporter genes, like β-galactosidase (β-Gal). β-Gal expression can be detected electrochemically using *p*-aminophenyl-β-D-galactopyranoside (PAPG) substrate. The β-Gal catalyzes the hydrolysis of PAPG that results in p-aminophenol (PAP) production. PAP is electroactive. It can be oxidized to p-iminoquinone at platinum electrode surface using a relative low electrode potential.

Matsui et al. [98] worked out a mutagen testing method using genetically engineered *Salmonella typhimurium* TA1535 strain with a plasmid pSK1002 carrying a umuC'–'lacZ fusion gene. In their work the cells were embedded in a microcavity (5 nL) on a glass substrate using collagen gel. The β-Gal expression on the microbial chip was electrochemically monitored as said before with the SECM apparatus. Upon treating with mutagens the UmuC'–'LacZ fusion protein was expressed from the pSK1002 plasmid showing β-Gal activity.

Detection of PAP by platinum microelectrode tip was used also for monitoring solubility of maltose-binding protein (MBP) in living *E. coli* DH5 entrapped in collagen matrix [99]. The bacteria cells had been transformed with specially constructed plasmid. They produced MBP target protein fused with β-Gal reporter. In SECM experiment PAPG was added into the buffer. In this way the PAP

concentration dependent amperometric current showed the β-Gal activity in the media that is the concentration of MBP.

An array of microwells filled with the bacteria gel was prepared. The PAP was detected in the wells. The release of PAP into the extracellular liquid indicated the β-Gal activity that is the solubility of the MBP. The authors used a Pt microdisc electrode (radius, 10 mm) as the probe set to 0.30 V vs. Ag/AgCl to record the oxidation current of PAP produced in βGal catalyzed hydrolysis of PAPG.

The reporter gene system is the most commonly used method for monitoring gene expression within cells. Several types of proteins have been employed as reporter. The secreted alkaline phosphatase (SEAP) could be also advantageously used because it is secreted into the culture medium and it also could be detected electrochemically. Torisawa et al. [100] have developed an electrochemical monitoring platform for SEAP reporter assays employing SECM. In their work genetically engineered SEAP producing cells in collagen matrix were immobilized in an array of pyramid like cavities on silicon substrate. SEAP expression of the cells could be triggered with exposing to α (TNFα) tumor necrosis factor. Cellular SEAP expression was detected by adding p-aminophenyl phosphate (PAPP) to the media. In the enzyme catalyzed hydrolysis PAP was formed that was electrochemically oxidized at the platinum SECM tip. The respiration activity of the immobilized cells was also checked by detecting the local oxygen concentration over the cell containing cavities with the SECM apparatus. The authors tested the SECM-based assay for in situ monitoring of cellular SEAP expression and found reliable. The feature allowing simultaneous measurements of cellular signal transduction and respiratory activity appeared as an important advantage.

One way is to use SCEM methods for estimation of intracellular redox activity of living cells without major interferences can be the measurement of transmembrane charge transfer rate with ultramicro electrode placed close to the cell surface. An appropriate redox mediator is added to the media and the reduction or oxidation current of it is recorded. If the mediator can pass through the membrane, then it can be regenerated by intracellular redox processes. Diffusing back to the electrode surface it can increase the current that means the redox activity is reflected by transmembrane positive feedback. The applicability of this method was tested by Mirkin's research group [101–103]. The redox activities of nonmetastatic and metastatic human breast cells were compared through the observed charge transfer (CT) rate. In these studies a two-electrode setup was used with either a 5.5-μm radius carbon fiber UME tip, a 5-μm Pt tip, or a 1-μm Pt tip. Different hydrophilic and hydrophobic mediators were employed in the media. The ultramicro electrode tip was positioned to the close vicinity of the cell surface. Using lipid-soluble mediators like menadione or 1,2-naphthoquinone significant difference was obtained between intracellular redox activity of nonmetastatic (MCF 10A), a non-tumorigenic epithelial cell line, and that of metastatic (MDA-MB-231), breast cancer cell line. The redox reactions involved in electrochemical reduction of menadione mediator and intercellular regeneration of it are shown in Fig. 9.

Spatially resolved redox activity map can be made by doing two-dimensional scanning over differently prepared individual live sample cells or tissues. The

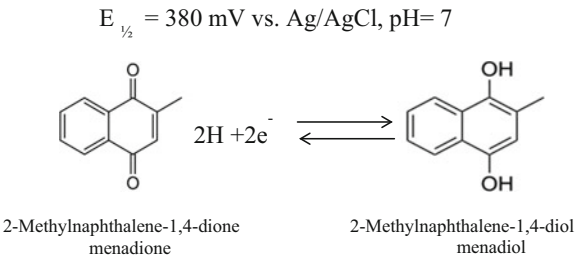

Fig. 9 Electrode reaction involved in SECM testing of redox activity of cultivated human breast cells. Dione is reduced to diol at the electrode, reoxidized inside the cell. Positive feedback is observed [102]

differences by redox activity can be used for distinguishing metastatic human breast cells from nontransformed ones. The authors predict [104] that in the future redox reactivity data collected by SECM measurements will be used successfully to predict breast cell metastatic potential.

Redox balance in a living cell is an important factor that affects proliferation, differentiation, and cell survival. Changes of it are believed to contribute to progression of diseases. It has been observed that the expression of oncogenes affects redox balance inside cells. The glutathione disulfide (GSSG)/glutathione (GSH) balance directly correlates to the overall cell redox balance. The cancer related alteration of the redox balance has been investigated in a work [105] recently published. The authors employed extracellular SECM method for assessing the GSSG/GSH balance being inside single cultured MCF10A cells. Normal and transformed/cancer cells were raised, and their features were compared.

A retroviral construct containing an oncogenic form of Ras (pBabeRasV12) infector was used for preparation of cancer sample cells and using the empty vector (pBabe) as infector for obtaining control cells. In the experiments FcMeOH redox mediator was added to the media. At the surface of the SECM tip the oxidized form of it ($FcMeOH^+$) has been generated. If the tip was close to the cell membrane, then considerable part of the oxidized mediator entered the cell, where depending on the redox balance it got reduced. As the regenerated FcMeOH diffused back to the electrode an increase of the current could be observed. The negative feedback effect was decreased or positive feedback could be seen. Measurements were performed in PBS containing 1 mM FcMeOH with a 10 μm Pt electrode polarized to 0.5 V vs. Ag/AgCl reference electrode. Constant height scans and tip approach curves were made. The faradaic current was significantly higher over the transformed cells. This indicates that the intracellular $FcMeOH^+$ reduction efficiency of the cancerous cells is higher than that of the normal ones.

In order to prove the diagnostic applicability of the method surgical samples from a patient affected by lung adenocarcinoma were taken. Primary tumor and normal cells were obtained by enzyme digestion of the tumor and of the normal tissue. The cells after cultivation were subjected to SECM experiments. SECM measurements were made with ferrocene carboxylic acid (FcCOOH) mediator to assess separately the negative feedback interaction. FcCOOH cannot permeate the cell membrane therefore it could show only the cell topography. The negative

feedback effects over the two different cells were almost identical. Using FcMeOH the intercellular mediator regeneration increased the current. An index of mediator regenerating activity (Ri) has been defined for comparison of character of different cells.

$$Ri = \frac{\int_{L=0}^{6} I_T - I_{\mathrm{NF}}}{\int_{L=0}^{6} I_{\mathrm{NF}}}$$

where I_T is the tip current with FcMeOH, I_{NF} is the negative feedback current, and L is d/a that is the ratio between the tip–surface distance and the measuring tip radius.

$Ri = 0.25$ value was obtained for the cancer cells while only $Ri = 0.05$ for the normal ones. The significant difference shows that the method provides a reliable cell level way for cancer diagnosis.

Drug resistance develops in certain cancer cells. It is assumed that action of MRP1 transmembrane protein helping to remove therapeutic agents from cancer cells can be responsible for drug resistance. In order to study this, single cell level comparative SECM experiments were carried out [106] with genetically modified HeLa cells and wild-type cells (HeLa-R) with overexpressing protein MRP1. A side-by-side co-culture pattern of HeLa cells and HeLa-R cells was fabricated and was subjected to SECM studies. FcMeOH mediator was used for imaging the redox activity of the cells. Measurements with hydrophilic $[Ru(NH_3)_6]^{3+}$ mediator were also made in order to deconvolute the topographic contribution from the redox activity signals. A heterogeneous rate constant of $FcMeOH^+$ reduction could be calculated. It was concluded that the mediator regenerating rate constant measured 12 μm above HeLa-R cells was about 2.4 times higher than over HeLa cells. The applicability of SECM in investigation of evolution of drug resistance process as well as detection of resistant cells could be foreseen.

Green tea catechins (GTCs) are considered as promising therapeutic substances in cancer treatment. One of the most studied GTCs is epigallocatechin gallate (EGCg) having the strongest antioxidant and preventive effect against chronic diseases like diabetes, neurogenerative disease, and cancer. In a recent study [107] living human adenocarcinoma cervical cancer cells (HeLa) were exposed to EGCg and the change of redox balance of the cells was tested using SECM. In the experiments the cells were grown on the bottom of Petri dish and platinum microelectrode polarized to 0.4 V was used making approach curves and line scans over the cell. The cell support media contained 1 mM FcMeOH redox mediator. The current increased as the tip was moved over the cell. This indicated that the cell interacted with the $FcMeOH^+$ produced at the electrode. The current increase shows the cell redox environment. The mechanism is the following: FcMeOH diffuses into the cell, where it promotes the intracellular generation of

GSH. The altered ratio of the redox couple GSH/GSSG results in an increase of GSH efflux from the cell. The GSH reduces $FcMeOH^+$.

After initial test the cell was incubated for 1 h in solution containing 25 mM EGCg. Next the GTC containing solution was replaced with cell supporting solution containing FcMeOH, and line scans were made 12 μm above the cells in different times. After exposure to EGCg the tip current over the cell increased, indicating a high $FcMeOH^+$ regenerating activity. However it decreased steadily in time. This proves that exposure to EGCg leads to increase of cellular GSH. Glutathione is trying to protect the cell from oxidation attract of the adsorbed aldehyde. When the time of exposure is too long or the concentration of the EGCg is too high, then the protective mechanism cannot cope and irreversible cell death takes place. The results that show the timescale of the change of cellular metabolic activity confirm the beneficial effect of EGCg on cancer cells and explain mechanism of its action.

Experiments for testing intracellular redox reactions were carried out [108] with *Rhodobacter sphaeroides* bacteria. In these works different hydrophobic and hydrophilic redox mediators were used for carrying the redox state between SECM microelectrode in solution and intracellular redox sites. The bacteria have two membranes, the outer cell membrane and the cytoplasmic membrane. Hydrophobic mediators are capable of permeating both. The effective rate constants of redox reactions of such mediators with intracellular redox moieties showed correlation with the formal potential of the mediator. Hydrophilic ionic species on the other hand can only cross the outer membrane of the bacteria and can react with redox centers in its periplasm. The relationship between reaction rate coefficient and formal potential of the hydrophilic mediator however is not linear.

Menadione (2-Methylnaphthalene-1,4-dione) is a cytotoxic compound, structure shown in Fig. 9. It easily can take part in a one-electron reduction too, resulting a semiquinone that easily gets reoxidized to quinone. In these redox reactions cell damaging reactive oxidizing species (ROS) are formed. Menadione is an amphiphilic molecule, water soluble enough to have relatively high concentration in aqueous media, but also can pass through lipophilic cell membranes. When entering in a living cell it reacts with intracellular GSH. The obtained S conjugate, thiodione (see Fig. 10), is more hydrophilic, therefore it cannot pass through the cell membrane with spontaneous passive transport. In living cell an ATP-dependent pump mechanism helps transferring this metabolite into the extracellular space. Extracellular thiodione is electroactive. It can be detected voltammetrically.

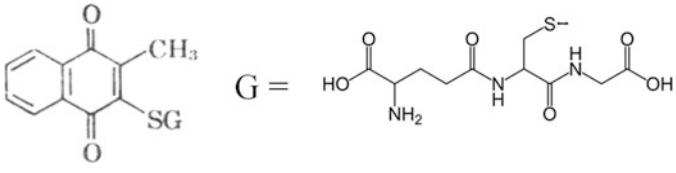

Fig. 10 Structure of (*thiodione*) 2-methyl-3-*S*-glutathionyl-1,4-naphthoquinone mediator

The outflux intensity of thiodione from a cell can characterize the viability of cells treated with menadione. The thiodione transport through life cell membranes was investigated by Bard's group [109] with SECM. They used malignant originate Hep G2 liver cells immobilized on inverse microscope plate as substrate and SG/TC measuring mode with a 10 μm platinum electrode. The SECM method allowed measuring the thiodione concentration at different distances from the biofilm at different menadione concentrations and incubation times. Using concentration value and constant flux model they could estimate the thiodione flux from a single cell. It was 1×10^{-17} mol s^{-1} per cell that corresponds to 6×10^{6} molecules released by each cell in a second.

There is another mechanism that protects the cells from toxic effects of quinones. It is the reaction catalyzed by the NAD(P)H:quinone oxidoreductase (NQO) (EC 1.6.5.2) enzyme. In this two-electron reduction the diol is formed. It can pass through the cell membrane. Getting to the extracellular space it can be detected amperometrically. The amperometric current in certain conditions reflects the NQO enzyme activity.

Matsumaea et al. [110] worked out an SECM method for detecting the intracellular NQO enzyme activity of a single cell. They employed menadione mediator for shuttling electrons through the cell membrane and ferricyanide as hydrophilic second mediator for increasing the electron exchange rate at the platinum surface of the microtip. In this study HeLa cells cultured on plastic Petri dish were tested and disc-type Pt electrode with a diameter of 20 μm (RG = 2) was used as SECM tip.

The principle of the double mediator mechanism used for intracellular NQO enzyme activity detection is shown in Fig. 11.

5.4 Investigation of Effects of Drugs on Metabolic Activity

Following directly the oxygen concentration through amperometry at the vicinity of cells is the most obvious SECM way for studying or checking the respiration activity of immobilized living cells. The observed decrease of amperometric current however is resulted by two effects. The proximity of the surface blocks the oxygen flux toward the working electrode that produces negative feedback (Δi_{p2}) and the oxygen consumption by the respiration (Δi_{p1}). Simple way of "deconvolution" was tested by Zhu et al. [111]. First they scanned with platinum tip of 5 μm polarized to −0.50 V and obtained an image resulted by the combination of the two effects ($\Delta i_{p1} + \Delta i_{p2}$). After the cells were sacrificed by exposing them to 1 mM KBr, NaN_3, or KCN a topographic image was recorded that showed separately the negative feedback (Δi_{p2}). For these studies human neutrophils immobilized in collagen matrix were studied on glass substrate of a Petri dish that served for measurement cell in SECM.

For many centuries the antimicrobial character of silver ions has been recognized and used. Silver dishes were employed for keeping drinks in or silver coins

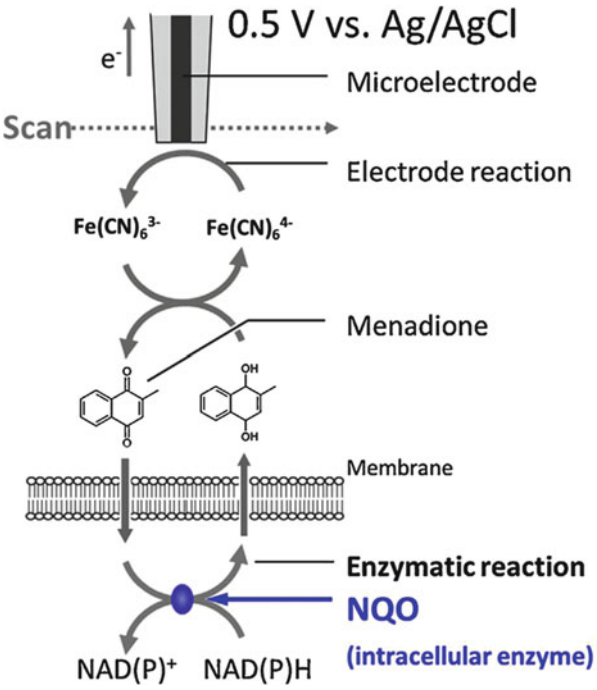

Fig. 11 The principle of the double mediator mechanism used for intracellular NQO enzyme activity. Figure was taken from the work of Matsumea et al. [110]

were added into water storage containers for avoiding contamination. In our days silver salts, silver zeolites, silver nanoparticles, or silver containing compounds are still used as additives in wound treating ointments, in endotracheal tubes, in surgical masks, in food packing foils, etc., to prevent microbial growth [112]. The SECM technique has been used in studying the toxicity of silver or silver ions, in exploring the nature of the interaction of them with living tissue, and the mechanism of antibacterial action.

Holt and Bard [113] studied the bactericide action of silver ions. In their work the oxygen concentration was followed in *E. coli* bacteria containing samples in presence of glucose. Two different measuring techniques were used. In part of the studies miniaturized Clark electrode was employed in small volume bacteria suspensions. While in other ones the oxygen concentration was detected with platinum microelectrode tip in SCEM system over immobilized bacteria cells. The changes of the respiration rate could be detected after administrating different amount of silver ions. Besides oxygen uptake the depletion of Ag^+ from the region above the immobilized cells could be followed using anodic stripping measuring method. The silver ion uptake of live cells was found significantly higher than that of the dead ones.

Bard's group investigated [114] further the toxicity of silver ions by SECM. In this work they detected the viability of single mouse embryo fibroblast cell that was grown on the bottom of Petri dish. They used three different mediators: FcMeOH, tris(bipyridine)cobalt(II) ions $[Co(bpy)_3]^{2+}$ and oxygen. SECM approach curves

and images were recorded over the cell with 10 μm platinum microdisc- and electrochemically prepared mercury hemispherical tip. The $FcMeOH^+$ generated at the tip could enter the cell where biochemical redox reactions in living fibroblast recycled it resulting in a slight positive feedback. This did not show up over dead cell. The ratio of the current measured at given distance over the cell and over a surface producing negative feedback could be used for characterization of the viability. The more hydrophilic $[Co(bpy)_3]^{3+}$ could not pass the cell membrane therefore it gave just negative feedback. The life cell consumes oxygen, therefore the amperometric current of oxygen reduction close to the cell was smaller than one could expect considering just the effect of diffusion shielding. The so-called consumptive feedback can be observed. The difference between the feedback and the consumption feedback currents could be used for expression of the cell viability. The decrease of consumptive feedback could be used for indication of the toxicity of silver ions.

Interesting observation was made studying the influences of silver ions on the SECM tip current when FcMeOH mediator was used. After exposing the fibroblast cell to silver ions, the positive feedback decreased indicating the toxicity that is the loss of cell viability. Complete ceasing however has not showed up. Furthermore the positive feedback recovered after long time exposure. This could not be explained by the increase of the viability. It was suggested for explanation that the silver ions taken up by the cells get reduced and form silver metal particles. As immobilized conductive metallic objects, they reduce the $FcMeOH^+$ that produces the positive feedback.

Kaya and coworkers [115] investigated the time courses of the cellular activity change of cultured HeLa cells affected by exposure of different chemicals like KCN, ethyl alcohol, and the antibiotic drug, Antimycin. They compared the SECM method with the conventional fluorescence cellular activity measurements. Immobilized HeLa S3 line cells, cultured on polystyrene or glass-bottom dishes were used as sample. The fluorescence method is based on addition of calcein-AM, a nonfluorescent aceto-methoxy derivate of calcein, to the cell culture. It can enter into the cells where it is converted by the cytoplasm esterase to calcein dye that emits fluorescence at 515 nm if excited at 490 nm. The calcein formed inside the cell is impermeable to the cell membrane, it stays inside. Therefore calcein-AM stained living cells emit fluorescence light. If the cellular membrane is seriously damaged, then calcein leaks out from the cell, and the intensity of the green fluorescence of the cells decreases.

In case of SECM measurement of the cell activity, the reduction current of oxygen was detected. The tip was a platinum microdisc electrode with diameter of 5 μm. It was positioned 25–30 μm over the cells. The SECM measurements show immediately the action of respiration activity halting species while the fading of the fluorescence intensity change reflects the increase of membrane permeability resulted by exposure to toxic chemical. The less invasive nature of the SECM makes it a well applicable tool for testing the effect of different species on the cellular respiration.

Interestingly, it was observed that after exposure to KCN the SECM measured respiration activity changed rapidly, while the change of fluorescence signal was

slow. It was in the opposite way when the cells were exposed to 50% ethyl alcohol. Then the luminescence decreased rapidly while the SECM signal change came later. These show that the SECM and fluorescence measurements afford different information about cellular activity at the single cell level.

The anticancer drug sensitivity of two kinds of cancer cells was investigated by Matsue's group [116] by detecting oxygen concentration over the collagen-embedded living cells. In their experiments an array of microholes prepared on a silicon wafer were used as platform for cell immobilization. Inside the pyramid like microholes living human erythroleukemia cell line (K562) and its Adriamycin drug-resistant subline (K562/ADM) cells containing collagen gel were applied. Scanning negatively polarized platinum microelectrode tip over the gel filled holes the obtained decrease of the oxygen reducing current indicated the respiration activity. The sensitivity of the cells to Adriamycin anticancer drug could be estimated from the SECM images and line scans. The SECM method with its noninvasive nature has advantage over the conventional colorimetric succinic dehydrogenase inhibition (SDI) assay [117], since it can be used for continuous monitoring of the response.

The sensitivity of tumor cells to anticancer drugs can be different. The success of chemotherapy depends on finding the effective drug species and dosing therapy for the individual patients. In vivo tests methods for anticancer sensitivity with involvements of experimental rats and mice have been worked out. In vitro assaying the drug sensitivity of tumor removed from individual patients effectively can be carried out [118] using collagen gel droplet embedded cell culture samples prepared from the tumor. Then these samples are treated with different drugs and the metabolic activity or the proliferation rate is monitored.

Torisawa et al. [119] worked out a method for following in vitro the respiratory activity of cultivated tumor cells with SECM. In their work mice were inoculated subcutaneously with human promyelocytic leukemia (HL-60) cells. After 31 days incubation the cells were taken from the animals and microsamples were prepared embedding the cells in small volume (18 nL) collagen gel matrix placed inside pyramid like cavities etched in silicon wafer. The decrease of amperometric reduction current of oxygen above the cell culture was used for indicating the respiration activity of the cell. The increase of the current upon addition of antitumor drugs showed the decrease of the oxygen intake. It indicated the extent of the anticancer effect of the drug.

SECM could be successfully employed for investigation of oxygen consumption and motion of beating cardiomyocytes. For these experiments, reported by Hirano and coworkers [120], primary cardiomyocytes were taken from neonatal rats, and seeded on collagen coated dishes. The cells were incubated in appropriate culture medium. Spontaneously beating cells were used for the SECM measurements. Platinum disc microelectrode with a radius of 5 μm was positioned over the beating cell in 9 μm distance. The oxidation current of ferrocyanide or reduction one of oxygen was followed. The current–time plot showed clearly the topography changes as the relaxation and contraction periods followed each other. The oxygen consumption also could be estimated. Effect of digoxin concentration or

temperature change on the beating amplitude and oxygen consumption could be studied. The success of the experiments predicts that system tested may become a powerful tool for studying pharmacological and toxicological effects in cardiomyocytes.

5.5 Imaging of Local Enzyme Activity

In biologic object the enzymes are often confined in certain structures, in membranes, in intracellular spots. The SECM is an excellent tool for detecting distribution and measuring activity of biocatalytic microsites, as well as changes of activity upon different treatments.

Wittstock [121] proposed a signal amplification method for imaging local enzyme activity spots with improved lateral resolution. The example shown employs microspots made of immobilized galactosidase (Gal) and pyrroloquinoline quinone (PQQ)-dependent glucose dehydrogenase (GDH) coated beads as sample. The PAPG and glucose are added to the solution. Gal enzyme catalyzes the hydrolysis of PAPG resulting PAP. An electrode potential is employed on the tip that results in electrooxidation of the PAP. At that potential the PAPG is not electroactive. The product of the electrode reaction of the PAP is p-quinoneimine (PQI). In presence of glucose the PQI is reduced to PAP in a redox reaction catalyzed by the GDH. This results in higher local PAP concentration. An amplified amperometric signal is obtained for marking the local Gal activity. As it is well known the PQQ-dependent GDH does not need the presence of NAD+/NADH cofactor. This kind of signal amplification has been successfully used in case of amperometric enzyme sensors earlier [122].

Diaphorase enzyme and diaphorase/albumine mixtures immobilized on the surface of a glass plate were imaged by Yamada [123] and coworkers using platinum disc tips. FcMeOH redox mediator and NADH reagent were used in these studies. The FcMeOH was oxidized at the platinum tip. The immobilized diaphorase catalyzed the oxidation of NADH by $FcMeOH^+$ the oxidized form of FcMeOH. So, if the tip was near to the catalytic surface, then the enzyme catalyzed reaction increased the local concentration of FcMeOH. That positive feedback generated increase of the current showed the active enzyme spots on the sample surface.

The authors connected tuning fork between the electrode and the holder and shear force based distance positioning and measuring technique was used. The close vicinity of the surface was detected by observing steep changing of the resonance amplitude of the vibrating electrode. The authors could image simultaneously topology and catalytic activity of the substrate surface. Special tip travel program, the so-called STA mode scanning pattern, mentioned earlier, was used. It employs shear force controlled approach and retracting steps at each laterally positioned measuring spot. STA scanning helps avoiding electrode–substrate crash.

Tyrosinase is an important enzyme that catalyzes the oxidation of phenolic compounds by oxygen. It has role in ripening different fruits and its action is responsible for pigmentation of fruit slices. Tyrosinase is considered [124] as autoantigen in developing vitiligo, an autoimmune skin disorder. Recently Girault's group [125] investigated the applicability of SECM for mapping immobilized micro-areas of tyrosinase activity and for obtaining information about the catalytic reaction. The samples for the measurements were prepared on porous and hydrophobic polyvinylidene fluoride (PVDF) membrane that has high protein binding capacity. Platinum microdisc electrode was used as SECM tip. Three different SECM experiments were implemented. In certain experiments the reduction current of oxygen was followed over protein treated PVDF surfaces. Tip current higher in the close vicinity of the surface than in the bulk indicated an open, air filled pore. Negative feedback current appeared over the pores blocked by adsorbed protein. In the other experiments L-3,4-dihydroxyphenylalanine (L-DOPA) was added to the media and its concentration was followed detecting the tip current upon polarizing the tip to 0.7 V vs. quasireference electrode. The tip was scanned horizontally close to the surface. It was expected that the current decreases over spots with tyrosinase activity, since there the enzyme catalyzed reaction decreases the L-DOPA concentration. Interestingly the opposite was observed. The current increase could be explained assuming that in the enzyme catalyzed reaction an electroactive species, probably 5,6-dihydroxyindole, is produced in a fast reaction. Therefore in the gap between the tyrosinase containing spot and the tip the overall concentration of electroactive matter that reacts on the electrode is higher than it would be without the enzymatic oxidation. Differential pulse voltammetric measurements proved this. The third type experiments used sandwich immunoassay style strategy. Primary tyrosinase antibody and horseradish peroxidase (HRP) labeled secondary antibody were employed for marking the spots on the PDVF surface containing adsorbed enzyme. The platinum tip was polarized to −0.15 V. 3,3′,5,5-′-tetramethylbenzidine (TMB_{red}) and hydrogen peroxide were added into the measuring cell and SECM imaging was carried out over the surface. The HRP catalyzes the oxidation of TMB_{red} to TMB_{ox}. The tip detects the concentration of the oxidized form. Therefore over the tyrosinase spots, higher reductive current showed up. The so-called coffee ring effect could be observed, that means the current was higher at the perimeter than in the center of the spot.

Sample surface containing both micro-contact-printed banana slice and spot with adsorbed tyrosinase side by side was imaged using the three SECM strategies. The result showed that SECM can be used for detecting enzyme activity distribution in micro-contact-printed samples, and for studying the changes created by different effects.

SECM with scanning electrochemically generated chemiluminescence (SCEL) was combined [126] for imaging local activity spots of enzyme embedded in polymer matrix. For these studies glucose oxidase (GOD) enzyme containing thin polymer spots was formed on hydrophobic glass slide surface. The experiments were carried out with an SECM that was built upon an inverted optical microscope. A photoelectron multiplier was installed for detecting the emitted light under the

cell holder of the microscope. The slide and buffer solution containing appropriate concentrations of glucose and luminol was introduced into the measuring cell. The detection was based on the well-known ECL principle [127]. The polarized SECM tip oxidized luminol producing anionic radical. This reacts with the hydrogen peroxide generated in enzyme catalyzed glucose oxidation. Excited state 3-aminophthalate is produced that emits light. As the tip moving in the XY plane approaches the bioactive surface spot the tip generated luminol radical meets higher concentration of H_2O_2 at that location. The higher reaction rate results in more intensive luminescence signal. Sinusoidal AC voltage was superimposed on the constant initial DC potential of the tip. The signal output of the PMT was connected to the signal input of a lock-in amplifier. In this way recovering signals by selective amplification at the modulation frequency allowed achieving higher signal/noise ratio. Naturally, SECM image of the bioactive spot could also be made with direct amperometric detection of H_2O_2.

100 μm thick surface confined enzyme microstructure lines were prepared [128] on gold coated glass slides using a microdispenser and cross linking with glutaraldehyde vapor. Line scans across GOD and of GOD –glutamate oxidase mixture containing lines were performed in presence of different concentrations of the substrates. The H_2O_2 was detected with an amperometric tip. The peak current over the stripes showed linear substrate concentration dependence.

Usually living organisms are trying to protect themselves against colonization by unwanted microorganisms. One way of this is the generation of oxidative stress conditions around them. Often hydrogen peroxide is produced in a biochemical process. Certain bacterial colonies however live in symbiosis with the host. Interesting question how can the bacteria resist the immune defense action of the host. Obvious answer can be the expression of catalase enzyme by the bacteria. Catalase – as it is well known – accelerates dramatically the decomposition of H_2O_2. Zoski's group [129] investigated the catalase activity in biofilms by SECM measuring the hydrogen peroxide decomposition rate over the biofilms. They picked bacterium *Vibrio fischeri* (*V. fischeri*), a bioluminescent strain for studying the bacterial defense mechanism against oxidative deterrence. These bacteria can live as a symbiotic strain in special light organ of bobtail squid mantle. The authors developed a method for assessing the H_2O_2 concentration over the colony. The SECM method allowed estimation of the catalase activity over the bacteria colony. Using it, they could get information about catalase activity at given location in a given time instant of bacterial film growth. It could be verified based on the results that catalase activity of the biofilm is an important factor for combatting oxidation stress imposed by the squid during colonization. Similar catalase activity was found in case of symbiotic and free growing bacteria. That indicates that high catalase activity may be equally important in maintaining the integrity of these biofilms.

Combined application of tapping mode AFM and SECM can have some advantages. The AFM can give a topographic image of very high lateral resolution. SECM cannot achieve resolution in that level, however, it provides chemical information about the sampled area. Double function tips for this combined application were prepared from original silicon nitride AFM cantilever using high tech

micromachining [130]. Actually chromium, gold, and finally silicon nitride layers were formed on the tip surface and focused ion beam (FIB) cutting technique was used for making the final form of the double function cantilever that had a very pointy tip for AFM and a thin ring of gold for SECM. The feasibility of the combined imaging technique for biochemical investigation was demonstrated [131] by imaging polymer entrapped spots of GOD.

5.6 Transport Through Bio-Layers

Dentine is a calcareous material sandwiched between the pulp and enamel of the teeth. One cm^2 of it contains 10^6–10^7 tubules with diameter of 1–2 μm. The movement of the dentinal fluid through dentine tubules is important factor in dental hygiene. Dentine hypersensitivity, for example, is caused by fluid movement within dentinal tubules thereby triggering sensitive nerves and eliciting a pain response. Unwin's group investigated [132, 133] the applicability of SECM for measuring transport of electroactive species through dentine slices. They used about 50 μm thick slices taken from human premolars as sample, and potassium ferrocyanide as transporting species. Moderate pressure could be applied for sustaining the flow. Transport through the dental tubules could be detected with the SECM technique applied, as well as topography of the slice. Mixture of calcium chloride and potassium oxalate was used as tubule blocking reagent. The thickness of the transport blocking calcium oxalate layer could be estimated using the results of the SECM measurements.

Recently preliminary level investigations [134] have been carried out for testing the applicability of SECM for tooth enamel corrosion studies. Smooth samples prepared from bovine tooth have been soaked in acidic solution and the consumption of hydrogen ions was detected at the sample surface amperometrically. Negatively polarized platinum disc electrode of 25 μm diameter was used in this work. The current decrease started much earlier in approaching to the surface than it could be expected in case of clear feedback effect. This indicated that the enamel dissolution rate in acidic corrosion could be detected, and SECM images taken reflected the extent of local corrosion. May be choosing potentiometric pH sensing tip with smaller size could have been more practical for these investigations.

Articular cartilage is a white layer covering the adjacent surfaces of joints of human and animal bodies. Its role is to protect the bones by keeping the surfaces of the bones apart from each other. Intercellular communication and the transport of nutrients and waste products must be effected by diffusion through this matrix. Knowledge of the transport of solutes through the cartilage matrix is therefore crucial in understanding the physiological functioning of the tissue, both in the healthy and diseased states. Therefore permeability of this layer for different species is in the focus of interest in physiology.

Unwin's group examined the permeability character of bovine articular cartilage with SECM technique. When the permeability for cationic methyl viologen (MV^{2+})

was studied [135], then negatively charged mediator ($Ru(CN)_6^{4-}$) that does not permeate into the negative cartilage matrix was used for taking the needed topology image. Constant height imaging with 5 μm platinum disc electrode was carried out. Sample was histologically stained to reveal the biochemical composition. The high MV^{2+} permeability is not coinciding with the collagen rich areas. Diffusion limited current map for oxygen reduction was also prepared [136]. Using earlier developed modeling method for taking into account the varying tip-substrate distances map of oxygen permeability in the cartilage was prepared. The map showed enhanced oxygen diffusion in areas that are low in collagen content.

The hydrophobic cell membranes are not permeable for hydrophilic species like $Ru(NH_3)_6^{2+}$, $Ru(NH_3)_6^{3+}$, $Fe(CN)_6^{4-}$, and $Fe(CN)_6^{3-}$. Surface active agents however can affect permeability. Koley and Bard [137] investigated with SECM the changes of cell membrane permeability by presence of Triton X-100 (TX100), a nonionic surfactant. They used individual HeLa cells (commonly used human cell lines) and HeLa cell cultures. Line scans at constant height and approach curves over the live cells were prepared using platinum electrode of 10 μm diameter, and potassium ferrocyanide mediator. The viability and morphology change at high surfactant concentration was also checked.

After soaking the cells in TX100 containing solution the permeability of their membrane changed. Quantitative data on the permeability of the cell membrane in the presence of TX100 could be estimated combining the SECM data and simulated functions. The permeability, P, was defined as $P = KD/L$ where D is the diffusion coefficient of the liquid, L is the thickness of the membrane, and K is the partition constant between the molecule and the membrane. When the concentration of TX100 was at or near 0.17 mM, the cells were able to recover upon removal of surfactant solution. The permeability was estimated to be $6.5 \pm 2.0 \times 10^{-6}$ m⁄s. The number of ferrocyanide molecules passed through single cell membrane after 32 min was calculated to be $1.06 \pm 0.54 \times 10^6$ in this case.

5.7 SECM Inside Living Cells

SECM inside living cells is a very challenging task. For this, electrode with submicron size tip diameter, special low current potentiostat, and appropriate shielding are needed. The obtained SECM signal is highly valuable from point of view of cell physiology if the measurement causes only minor invasion. It was shown [138] by trypan blue exclusion tests that MCF-10A breast cells can survive intracellular voltammetric experiments. The test is based on the dye out pumping property of the live cells [139]. That means if trypan blue dye is added (5 μM solution) to the immobilized cells, then after a few hours the dead cells appear blue but live cells appear uncolored.

Nanoprobes for intracellular voltammetry can be made with the commercially available sophisticated laser pullers. However, there are difficulties needed to be overcome. Like intracellular redox moieties are apparently localized and cannot

diffuse freely within the cell. Therefore addition of a redox mediator, with concentration as high as 1 mM, is recommended for obtaining appropriately high current signal. It is probably too high considering the invasion affected. To be able to probe enzymatic redox reactions, the mediator concentration must be in the micromolar range. That would produce current responses in femtoampere scale. The precise positioning of a nanoprobe inside the cell close to targeted organelles is also far from being solved.

Two interesting methods using intracellular voltammetry were worked out and tested by Mirkin's group [102]. One of them is the determination of the cell membrane potential. It is quite obvious that the difference between the half wave potentials ($\Delta E_{1/2}$) of the voltammograms of the same mediator measured extracellularly ($\Delta E_{1/2\ extr}$) and intracellularly ($\Delta E_{1/2intr}$) gives the cell membrane potential $\Delta E_{1/2cell} = (\Delta E_{1/2extr} - \Delta E_{1/2intr})$. For this it has to be assumed that the ohmic potential drop is negligible and that no biofilm is building up on the penetrated electrode surface before measurement.

The other intracellular voltammetric method worked out is applicable for measurement of transport rates across cell membranes. For this the cell is attached on gold substrate. The working electrode is positioned inside the cell over the section of the membrane which adheres to the gold surface. The regeneration of the mediator at the gold surface is faster and less complicated. Therefore the positive feedback current is less affected by a slow intracellular redox reaction that can be the case if the transport rate is tested by extracellular voltammetry.

5.8 Detection of Oligonucleotides or Hybridization

The adsorbed layer on conductive surfaces seriously can influence the positive feedback current. Coulombic interaction between the adsorbed layer and dissolved mediator can modulate the diffusion property of the latter. Schuhmann's group investigated the change of the feedback current over DNA-modified surface spots on gold surfaces [140]. For sample preparation spots of 20-base synthetic oligodeoxyribonucleotides with 150-μm diameter were immobilized on gold coated microscope slide. Platinum microdisc tip with 10-μm diameter was used in constant height SECM line scans. Scanning over the spots, a significant decrease of the feedback current was obtained in case of a negatively charged ferricyanide mediator, while with the positively charged $[Ru(NH3)6]^{3+}$ no noticeable change of the current could be observed. The decline of the feedback current could be explained by the electrostatic repulsion between the negative mediator ions and the phosphate groups in the backbone of the immobilized DNA strands. It slowed down the diffusion. Accordingly the recycling of tip generated $[Fe(CN)_6]^{4-}$ to $[Fe(CN)_6]^{3-}$ was slowed down. Hybridization of two oligodeoxyribonucleotides with increasing the density of the repulsive phosphate groups resulted in further decrease of feedback current. The hybridization could be detected without application of any labeling. This showed a perspective application field of feedback mode SECM.

Fortin and coworkers [141] reported about the successful dual application of SECM technique in oligonucleotide hybridization studies. They used SECM as tool preparing microspot array containing 15^{mer} oligonucleotide (ODN) strand on gold surface. The spots of the array were obtained by electropolymerization of pyrrol in ODN containing solution. Negative feedback obtained with appropriate mediator indicated the formation of the polymer spots. The complementary strain was labeled with HRP. In order to indicate the hybridization 4-chloro-1-naphthol and hydrogen peroxide were added to the media. The HRP label of the complementary strain catalyzed the oxidation of the 4-chloro-1-naphthol to insoluble 4-chloro-1-naphthon. The precipitate formed on the hybridized spots resulted in enhanced negative feedback effect. SECM line scans over the spots could be used for detecting the hybridization.

5.9 Imaging Enzyme Labeled Biocomplexes

Glycans attached to the cell membranes have important roles in different physiological happenings, like cell–cell communication, immune recognition or response, cancer metastasis, tumor progression, etc. Importance of methods capable in situ detection cell-glycan expression on living cell hardly can be questioned. The applicability of SECM in these experiments was tested by Xue and coworkers [142]. They used BGC-823 human gastric carcinoma cells as sample and 2 μm Pt disc tip in their experiments. The cells were confined in microwells. As it is well known, lectins have highly specific binding affinity to carbohydrates. Horseradish peroxidase (HRP) enzymes labeled lectins obtained from different sources were used for recognizing the cell attached carbohydrates. After incubation with HRP tagged lectin, and rinsing off the unbound reagent FcMeOH redox mediator and hydrogen peroxide was added to the media and the SECM imaging was carried out. The HRP attached to the cell-glycans through the lectin catalyzes the oxidation of the FcMeOH by the H_2O_2. An electrode potential needed for reduction of oxidized FcMeOH was applied on the tip. Depending on the tip–catalytic site distance and on the local catalytic activity, a current could be recorded, and used for imaging. Expression of different cell-glycan species tagged with different HRP labeled lectins could be imaged with individual cell level. The principle of the method is shown in Fig. 12.

Epidermal growth factor receptor (EGFR) is a membrane protein that exists on the cell surface. Mutations that lead to EGFR overexpression have been associated with different form of cancers. Information about EGFR expression level has important diagnostic value. The applicability of SECM for estimation of EGFR density on living cell surface has been tested [143]. In the experiments Chinese hamster ovary (CHO) cells and cells from human epidermoid carcinoma cell line A431 were applied as samples. The EGFR were linked to mouse anti-EGFR IgG primary antibodies and these were sandwiched to enzyme labeled antibodies.

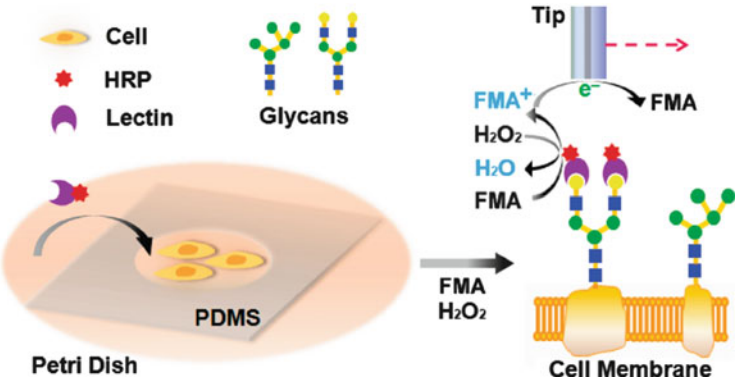

Fig. 12 Scheme of SECM imaging for cell-surface glycan expression using SG/TC mode. (*PDMS* poly(dimethylsiloxane) membrane). Taken from [142]

Alkaline phosphatase (ALP), diaphorase, and β-Gal enzyme labels were used. Both feedback mode and SG/TC mode were tested.

Best results were obtained with ALP labeled version. In that case PAPP containing buffer was added into the measuring cell. The ALP enzyme label on the EGFR of the membranes of the immobilized cells catalyzed the hydrolysis of the PAPP. The local concentration of the liberated PAP was detected with the scanning tip as it is shown in Fig. 13.

The worked out method could be used for single cell level imaging of the EGFR. This means that the SECM technique affords information on the expression state of cell membrane proteins at the single cell level. Figure 14 shows images recorded over single CHO cells with overexpressed EGFR (left image) and over a normal cell (right image). These experiments are an example showing the high potency of SECM in clinical diagnosis.

Another kind of sandwich type protein detection method was developed [144] using SECM in SG/TC mode. Thrombin as target protein and GOD as labeling enzyme were used for showing the feasibility of the method. Instead of two antibodies however, two specific aptamers that recognize different positions of thrombin were employed. One aptamer was linked onto the gold tip, the other was labeled with the enzyme. After formation of the thrombin–aptamer complex the H_2O_2 generated in enzyme catalyzed reaction in presence of glucose was detected as amperometric current.

5.10 Parallel Optical and Electrochemical Imaging

Matsue's team [145] used an optical fiber nanoelectrode probe with shear force distance controlling. The ring shaped microelectrode applied in this work was prepared with FIB technique. A tuning fork was interconnected between the cell and the probe

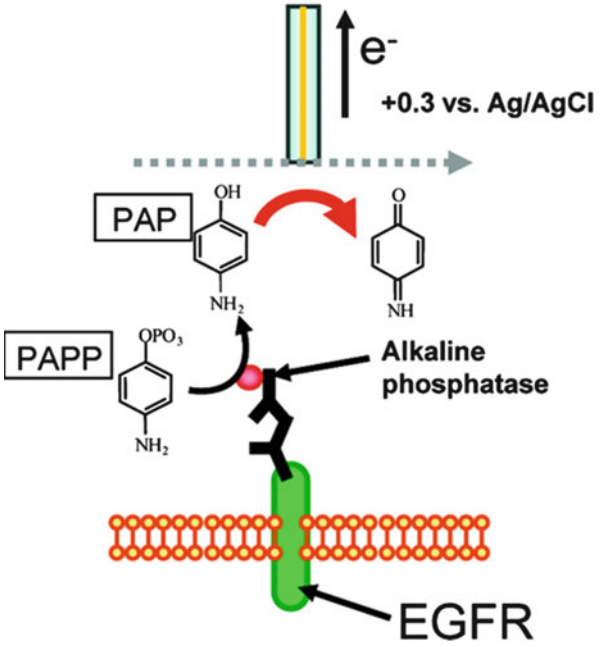

Fig. 13 The working principle of the SECM method used for single cell EGFR imaging. (*PAPP* *p*-aminophenylphosphate, *PAP* *p*-aminophenol) Figure was taken from [143]

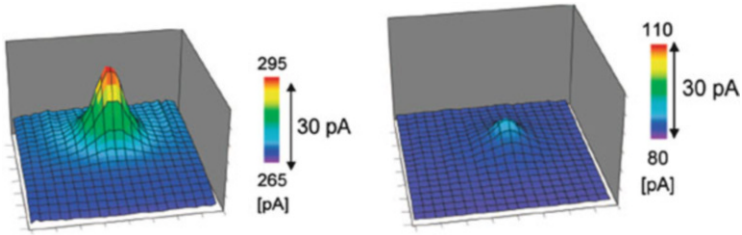

Fig. 14 Epidermal growth factor receptor (EGFR) image on single Chinese ovary (CHO) cell. Alkaline phosphatase was used as label in sandwich immune stile. PAP was detected in substrate generating tip collecting mode. Cell with EGRF (*left*), normal cell (*right*) [143]

holder. The distance between the living cell sample and the tip was controlled by detecting shear force. Simultaneously electrochemical and optical imaging could be performed over living HeLa cells obtained from a human cervix epithelial cell line.

A variety of STA mode was used in imaging. The piezoelectric tuning fork buzzler vibrated the probe at resonance frequency. The vibration signal from the tuning fork was followed by a lock-in amplifier. At every measuring spot in the XY plane a vertical approaching step was performed. Shear force induced change of the signal indicated the distance between the tip and sample. From that point the tip was

lifted up by a predetermined distance. At those elevated known distance points electrochemical and optical signals were simultaneously recorded. The quite slow STA mode imaging could be speeded up by a field-programmable gate arrays (FPGA) unit connected to the electronics that drastically increased the feedback speed and enhanced the accuracy and quality of the living cell images.

The sample HeLa cells were transfected with two expression vectors, namely with a green fluorescent protein GFP vector and SEAP control vector. *p*-aminophenylphosphate monosodium salt (PAPP) was added to the media. It was hydrolyzed by catalytic effect of the extracellular (SEAP). Electrochemical signal was obtained by oxidation of the PAP produced in the hydrolysis. A laser light beam (473 nm) was introduced through the optical fiber probe to excite GFP expressed inside the cell. Light emitted from the sample was collected by a photomultiplier tube (PMT) to obtain a fluorescent image. The authors could make simultaneous topography, fluorescent, and electrochemical images of transfected single HeLa cells in constant distance and constant height modes.

5.11 *Investigation of the Interaction of Different Bactrial Strains by SECM*

The SCEM technique was proved applicable for investigating the interaction of different bacteria strains in mixed culture biofilms. In a recent study of Bard's group [146] the distribution of bacterial produced hydrogen peroxide concentration was determined using SECM line scans over specially grown biofilms. In these experiments gold disc electrode with 25 μm diameter was used as measuring tip.

Streptococcus gordonii (Sp) and *Aggregatibacter actinomycetemcomitans* (Aa) strains grown in mixed biofilm were investigated. The streptococcus bacteria exist in human oral biofilms. They ferment glucose producing lactic acid and hydrogen peroxide. Their presence is beneficial from point of view of oral hygiene because they compete for nutrients with pathogen species limiting their escalation. Also the produced hydrogen peroxide inhibits the growth of other species. *A. actinomycetemcomitans* is a pathogen species. It is also found in oral cavity in case of severe infections. In co-culture with Sp, Aa can utilize lactic acid as nutrient. Its KatA enzyme can catalyze decomposition of hydrogen peroxide.

For the experiments biofilm from separately grown Sp and Aa strains was made on polycarbonate membrane. First the Sp biofilm was spread on the membrane and after a spot of the Aa culture was added. In this way a 25 μm diameter bacterial biofilm of Sg with a spot of 5–7 μm Aa in the middle was obtained as substrate for SECM studies. Two different strains of Aa were used – the Y4 and the Y4-katA – containing an insertion mutant of the catalase-encoding gene katA. It is Aa with higher tolerance to hydrogen peroxide toxicity.

The hydrogen peroxide concentration at different distances from different areas of the mixed colony could be measured with the SECM technique.

One-dimensional lateral scans showed the extent of catalytic decomposition of hydrogen peroxide over close vicinity of Aa with higher and lower catalase activity. The hydrogen peroxide flux at the biofilm surface could be estimated by employing digital stimulation and using the values of local hydrogen peroxide concentration measured at known distances. It was 1.0×10^{-11} mol cm^{-2} s^{-1}. Furthermore the authors could calculate the bacterial density $8.3 \times 10^{7}/cm^{2}$ and could guess 1.2×10^{-19} mol hydrogen peroxide outflux from a single bacterium at the film surface per second assuming that the average lateral dimension of the bacteria is 1.5 μm × 0.8 μm.

5.12 *Investigating of NO Outflux with Locally Prepared Chemically Modified Tip*

Nitric oxide (NO) is a gaseous messenger molecule that over its role in promoting smooth muscle relaxation is involved in many other physiological and pathological processes. Its detection and analysis are important tasks in physiological research. NO is not stable in physiologic conditions. Voltammetric methods and microelectrodes have been worked out for measuring NO selectively in biochemical, or physiological experiments (e.g., [147, 148]). However, when quantification of NO release from cell cultures, or tissue samples is attempted using a voltammetric microsensor, then it must be taken into account that the signal depends on the distance between the sensor and the source. A method using accurate electrode positioning with SECM and consequent chemical electrode modification needed for selective NO measurement has been worked out by Pailleret et al. [149]. As biologic NO releasing sample HUVEC cultured on the glass cover slip in RPM-1641 were used in the experiments.

The proposed method employs feedback curve based vertical distance positioning, that can be done with bare electrode. After an in situ chemical electrode modification follows before NO measurement. As first step a cover slip was introduced onto the microscope slide serving as measurement platform. A droplet of buffer solution was added over the slip surface. The electrodes were moved inside the droplet. Proper tip–sample vertical (Z) distance was set observing the amperometric reduction current of oxygen upon electrode approaching to the glass surface. The tip was a quite big (50 μm) bare platinum disc electrode.

After finding the distance the electrode was chemically modified in situ. First it was moved into nickel tetrasulfonated phthalocyanine tetrasodium salt (Na_4[NiTSPc]) containing solution droplet. Here electrodeposition of mediator layer was done. Other solution drops were visited by the chemically modified tip for rinsing and for checking its function. Finally the electrode was moved into the buffer droplet over the cell culture. The release of NO from the cell population was followed amperometrically. Bradykinin addition resulted in well detectable NO release.

Imaging the concentration of ROS over live macrophage cells (RAW264.7) was attempted by Zhao et al. [150]. They used constant distance scanning. The constant distance between the cell and the tip was provided by keeping a 20 kHz AC current constant. There was no external mediator added to the media.

5.13 Special Applications

5.13.1 Application of Amperometric Micropipette Electrodes

Ion selective micropipettes are usually employed in potentiometric measurements. Interestingly a micropipette type voltammetric silver ion concentration measuring tip was used in SECM studies investigating the Ag^+ ion uptake of living fibroblast cells [151]. The tip was prepared by introducing small volume of 1,2-dichloroethane solvent containing calixarene based silver ion ionophore and bis(triphenylphosphoranylidene) ammonium tetrakis(4-chlorophenyl)borate (BTPPATPBCl) as measuring cocktail and silver wire as internal electrode into appropriate prepared micropipette. Silver sulfate was added to the media and the tip was scanned over monolayer of fibroblast cells. When appropriate potential was employed between the internal electrode and the reference one, then the silver ions crossed through the interface between the two immiscible electrolyte solutions (ITIES) producing electric current signal. Imaging, one-dimensional scans, and approach curves were performed to investigate the interaction of the living cells with the silver ions in different times of soaking.

5.13.2 Application of SICM

Korchev and coworkers [152] demonstrated that the SICM can be well used for estimation of volume of living cells grown on microscope coverslips. In their work they used physiological media filled micropipette with opening diameter of about 50 nm. The resistance of the pipettes was about 500 MΩ.

Cells from single A6 cell line derived from *Xenopus laevis* renal tubular cells were grown on glass coverslip or on membrane filters. Using the constant current feedback mode of the SICM raster scanning was performed over the cells. Three-dimensional map was made from n raster points on the XY plane. The total cell volume (V_{cell}) was approached with the summed volumes of n rectangular raster prisms. The height of the cells at each raster prisms was determined by subtracting from the vertical tip positions (Z_{XY}) the reference Z coordinate value (Z_{ref}). Z_{ref} was measured above a naked slip area, see Fig. 15.

$$V_{\text{cell}} = \sum_{1}^{n} \left(Z_{XY} - Z_{\text{ref}}\right)\ dx\ dy$$

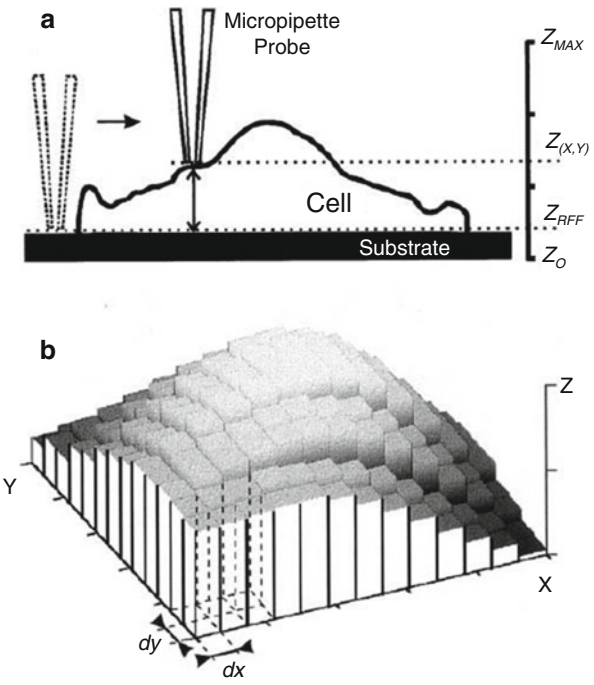

Fig. 15 Way of assessing the volume of a cell using constant current SICM method. The illustration of the measuring process (**b**). Approaching the cell volume with the sum of 13×13 rectangular prisms volumes of $Z_{XY} - Z_{ref}$. height. Figure is taken from [152]

Researchers of the same school studied the applicability of SECM for long time study of changes of living cells. According to the report of Korchev and coworkers [153] monolayer renal epithelia A6 living cells could be observed in physiological condition for long time. Images were acquired without any physical damage. Three-dimensional dynamic information about changes of surface anatomy could be obtained.

High resolution hopping probe ion conductance microscopy [154] was used for studying the phenotypic variants of living heterogeneous neuroblastomas. The existence of three different types of cells could be demonstrated. The volumes of the different cell types could be compared. The high resolution of the method makes it applicable for investigating the morphology and morphology changes of living different cell types in NB tumor.

5.13.3 Gas Phase Scanning Over Microbial Samples

CO_2 Investigation of Microorganism Produced by SECM

Up till now most of the SECM experiments have been carried out in liquid or gel phases. Biofilms, life tissues, microorganisms however often are confined on solid surfaces or forming thin floating films on air/water interfaces. For SECM investigation of the behavior of these samples without causing major invasion the

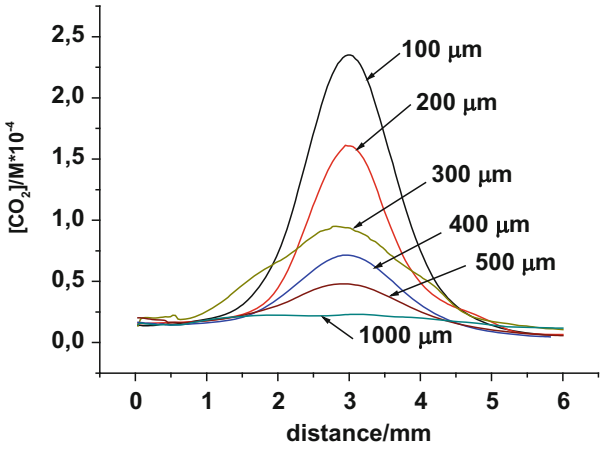

Fig. 16 One-dimensional carbon dioxide concentration–distance images obtained by scanning over the center of the circular yeast colony at different vertical (*Z* directional) distances

measuring probe cannot scan in liquid phase. In 2003 Carano et al. [155] tried to scan in air phase over a small hole with a microsize Clark oxygen probe for imaging the oxygen outflow through the hole. Most recently Kiss et al. [156] prepared a Severinghaus type carbon dioxide measuring microcell. For obtaining fast response, the gas permeable membrane of the Severinghaus sensor was substituted with an air gap. Using the tip in SECM apparatus line scans in the gas phase over small *Saccharomyces cerevisiae* cultures were successfully made. Line scans at different distances were made. The carbon dioxide concentration profiles were obtained upon using calibration curve. The extent of the outflow of carbon dioxide that indicates the vitality of the culture could be estimated without disturbing it using the measured data and diffusion coefficient. Figure 16 shows the CO_2 concentration–distance plots obtained by doing constant height line scans at different *Z* distances from the yeast culture.

5.13.4 Investigation of Quorum Sensing

Certain decisions of living objects are influenced by the population density of the colony they are member of. This means that changing some kind of behavior or physiologic condition depends on the number of individuals in the associations. The members can produce some kind of small effect and they have also receptors sensing the strength of this stimulus. They act uniformly upon the level of summed up stimulus that reaches a level higher than a trace. This mechanism is called quorum sensing (QS). Extensive literature deals with results achieved in investigation of this phenomenon. Examples of QS affecting the behavior of social colonies of high level decentralized animals like bees, ants, etc., are also discussed. Most of the experimental work studying QS however deal with communication among cells

in animal or human tissues and microorganisms inside their colony. Quorum sensing is used by colonies of bacteria [157] to regulate biochemical processes or synchronize population behavior. It is performed by a cell-density manner that means certain number of cells used is needed to initiate the action. In the bacterial mechanism of quorum sensing a relatively small autoinducer molecule is synthetized and if its amount is high enough then it is recognized by special receptors [158]. Quorum sensing has important roles in regulating cellular functions like biofilm formation [159], resistance against antibiotics, bioluminescence, gene expression, etc.

SECM method has already been applied for investigation of the quorum sensing mediated behavior synchronization in microorganism colonies. In that work [160] 3D printing technology was used for fabricating microtraps in which *Pseudomonas aeruginosa* bacteria aggregates were grown. The internal volume of these microtraps was 8pL. Their size was 20x20x20 μm surrounded by 8 μm thick walls and 3 μm thick roofs. The number of cells confined in the microtrap could be determined observing confocal microscopic image taken after appropriate staining. The *P. aeruginosa* bacteria secreted electroactive pyocyanin acting as QS inducer molecule was detected by the SECM tip over the roof of the microtraps. Interestingly it could be proved that colony of 500 cells confined in the same microtrap was numerous enough to produce detectable amount of pyocyanin. That means that an aggregate of a few hundred cells can show QS-dependent, synchronized behavior.

The 3D printing was used for position *P. aeruginosa* aggregates close to each other, in microtraps. The QS stimulation of neighboring aggregates confined in microtraps could be detected by positioning the SECM tip over the neighboring trap. It was observed that the number of bacteria higher than 2000 was needed to stimulate the neighboring colony confined in a microtrap being 8 μm away.

Acknowledgments The authors are grateful to the Hungarian National Research development and Innovation (NKFI), under grant OTKA: K 112699 CO_2 content selection of biogases and industrial waste gases" project.

References

1. Liu HY, Fan FRF, Lin CW, Bard AJ (1986) Scanning electrochemical and tunneling ultramicroelectrode microscope for high-resolution examination of electrode surfaces in solution. J Am Chem Soc 108:3838–3839
2. Engstrom RC, Weber M, Wunder DJ, Burgess R, Winquist S (1986) Measurements within the diffusion layer using a microelectrode probe. Anal Chem 58:844–848
3. Bard AJ, Fan FRF, Kwak J, Lev O (1989) Scanning electrochemical microscopy, Introduction and principles. Anal Chem 61:132–138
4. Kwak J, Bard AJ (1989) Scanning electrochemical microscopy. Theory of the feedback mode. Anal Chem 61:1221–1227
5. Gonon F, Buda M, Cespuglio R, Jouvet M, Pujol JF (1981) Voltammetry in the striatum of chronic freely moving rats: detection of catechols and ascorbic acid. Brain Res 223(1):69–80

6. Walker JL, Ladle RO (1973) Frog heart intracellular potassium activities measured with potassium microelectrodes. Am J Physiol 225:263–267
7. Thomas RC (1978) Ion-sensitive intracellular microelectrodes. Academic, New York
8. Wang J, Wu L-H, Li R (1989) Scanning electrochemical microscopy monitoring of biological processes. J Electroanal Chem 272:285–292
9. Barker AL, Gonsalves M, Macpherson JV, Slevin CJ, Unwin PR (1999) SECM, beyond the solid/liquid interface. Anal Chim Acta 385:223–240
10. Edvards MA, Martin S, Witworth AL, Macpherson JV, Unwin PR (2006) SECM: principles and applications to biophysical systems. Physiol Meas 27:R63–R108
11. Beaulieu I, Kuss S, Mauzeroll J, Geissler M (2011) Biological scanning electrochemical microscopy and its application to live cell studies, Progress in instrumental design continues to pave the way for high-resolution, real-time electrochemical measurements with living cells. Anal Chem 83:1485–1492
12. Gyurcsányi RE, Jágerszegi G, Kiss G, Tóth K (2004) Chemical imaging of biological systems with the scanning electrochemical microscope. Bioelectrochemistry 63:207–215
13. Nagy G, Nagy L (2000) Scanning electrochemical microscopy: a new way of making electrochemical experiments. Fresenius J Anal Chem 366:735–744
14. Lu X, Wang Q, Liu X (2007) Review: Recent applications of scanning electrochemical microscopy to the study of charge transfer kinetics. Anal Chim Acta 601:10–25
15. Bard AJ, Li X, Zhan W (2006) Chemically imaging living cells by scanning electrochemical microscopy. Biosens Bioelectron 22:461–472
16. Schuhmann W, Schulte A (2007) Scanning electrochemical miroscopy. Sigle-cell microelectrochemistry. Angew Chem Int Ed 46:8760–8777
17. Stoica L, Neugebauer S, Schuhmann W (2008) Scanning electrochemical microscopy (SECM) as a tool in biosensor research. Adv Biochem Eng Biotechnol 109:455–492
18. Wittstock G, Burchardt M, Pust SE, Shen Y, Zhao C (2007) Scanning electrochemical microscopy for direct imaging of reaction rates. Angew Chem Int Ed 46:1584–1617
19. Bergner S, Vatsyayan P, Matysik FM (2013) Recent advances in high resolution scanning electrochemical microscopy of living cells – a review. Anal Chim Acta 775:1–13
20. Amemiya S, Guo J, Xiong H, Gross DA (2006) Biological application of scanning electrochemical microscopy: chemical imaging of single living cells and beyond. Anal Bioanal Chem 386:458–471
21. Scanning electrochemical microscopy, Bard, A. J. and Mirkin, M. V., Eds., New York: Marcel Dekker, 2001
22. Schulte A, Schuhmann W (2007) Scanning electrochemical microscopy as tool in neuroscience (Chapter 17). In: Michael AC, Borlannd LM (eds) Electrochemical methods of neuroscience. CRC Press, Boca Baton
23. Wightman RM, Wipf DO (1988) In: Bard AJ (ed) Electroanalytical chemistry, vol 15. Marcel Dekker, New York, pp 267–353
24. Zoski CG, Bond AM, Allinson ET, Oldham KB (1990) How long does it take a microelectrode to reach a voltammetric steady state? Anal Chem 62:37–45
25. Lefrou C, Cornut R (2010) Analytical expressions for quantitative scanning electrochemical microscopy (SECM). Chemphyschem 11:547–556
26. Zoski CG, Mirkin MV (2002) Steady-state limiting currents at finite conical microelectrodes. Anal Chem 74:1986–1992
27. Mirkin MV, Fan FFR, Bard AJ (1992) Scanning electrochemical microscopy: 13. Evaluation of the tip shapes of nanometer size microelectrodes. J Electroanal Chem 328:47–62
28. Amphlett JL, Denuault GJ (1998) Scanning electrochemical microscopy (SECM): an investigation of the effects of tip geometry on amperometric tip response. J Phys Chem B 101:9946–9951
29. Shao Y, Mirkin MV (1998) Probing ion transfer at the liquid/liquid interface by SECM. J Phys Chem B 102:9915–9921

30. Ren F, Fan F, Demaille C (2001) The preparation of tips for SECM. In: Bard AJ, Mirkin MV (eds) Scanning electrochemical microscopy. Marcel Dekker, New York
31. Nagy G, Nagy L (2007) Electrochemical sensors developed for gathering microscale chemical information. Anal Lett 40:3–38
32. Gonon FG, Navarre F, Buda MJ (1984) In vivo monitoring of dopamine release in the rat brain with differential normal pulse voltammetry. Anal Chem 56:573–575
33. Buda M, De Simoni G, Gonon F, Pujol JF (1983) Catecholamine metabolism in the rat locus coeruleus as studied by in vivo differential pulse voltammetry. I. Nature and origin of contributors to the oxidation current at +0.1V. Brain Res 273:197–206
34. Morf WE, Lindner E, Simon W (1975) Theoretical treatment of the dynamic response of ion-selective membrane electrodes. Anal Chem 47:1596–1601
35. Morf WE, Simon W (1978) Ion-selective electrodes. In: Freiser H (ed) Analytical chemistry, vol I. Plenum, New York
36. McGillivray R, Wald R (1980) Dual-path capacitance compensation network for microelectrode recordings. Am J Physiol 238(6):H930–H931
37. Caldwell PC (1954) An investigation of the intracellular pH of crab muscle fibres by means of micro-glass and micro-tungsten electrodes. J Physiol 126:169–180
38. Hinke JAM (1959) Glass microelectrodes for measuring intracellular activities of sodium and potassium. Nature 184(16):1257–1258
39. Lev AA (1969) In: Lavalle M, Schanne OF, Hebert NC (eds) Glass microelectrodes. Wiley, New York
40. Thomas RC (1974) Intracellular pH of snail neurons measured with a new PH-sensitive glass microelectrode. J Physiol 238:159–180
41. Pucacco LR, Carter NW (1976) A glass membrane pH microelectrode. Anal Biochem 73:501–512
42. Levy S, Coles JA (1977) Intracellular pH of Limulus ventral photoreceptor measured with a double-barrelled pH microelectrode. Experientia 33:553–554
43. Yamaguchi H, Stephens NL (1977) A new method of fabricating recessed tip pH microelectrode. Fed Proc 36:499
44. Mauro A (1954) Electrochemical potential difference of chloride ion in the giant axonsea water system. Fed Proc 13:96
45. Kerkut GA, Meech RW (1966) The internal chloride concentration of H and D cells in the snail brain. Comp Biochem Physiol 19(4):819–832
46. Saunders JH, Brown HM (1977) Liquid and solid-state O-sensitive microelectrodes. J Gen Physiol 70:507–530
47. Tóth K, Nagy G, Horrocks BR, Bard AJ (1993) Investigation of iodide-based ion-selective membranes by scanning electrochemical microscopy. Anal Chim Acta 282:239–246
48. El-Deen E, El-Giar M, Wipf DO (2007) Microparticle-based iridium oxide ultramicroelectrodes for pH sensing and imaging. J Electroanal Chem 609:147–154
49. Walker JL (1971) Ion specific liquid ion exchanger microelectrodes. Anal Chem 43:89A–93A
50. Ammann D (1986) Ion-selective microelectrodes: principles, design and application. Springer, Heidelberg
51. Wei C, Bard AJ, Kapui I, Nagy G, Tóth K (1996) Scanning electrochemical microscopy, 32. Gallium ultramicroelectrodes and their application in ion selective probes. Anal Chem 68:2651–2656
52. Tóth K, Nagy G, Wei C, Bard AJ (1995) Novel application of potentiometric microelectrodes: scanning potentiometric microscopy. Electroanalysis 7:801–809
53. Klusmann E, Schultze JW (1997) pH microscopy – theoretical and experimental investigations. Electrochim Acta 42:3123–3134
54. Gyetvai G, Sundblom S, Nagy L, Ivaska A, Nagy G (2007) Solid contact micropipette ion selective electrode for potentiometric SECM. Electroanalysis 18:1116–1122

55. Gyetvai G, Nagy L, Ivaska A, Hernadi I, Nagy G (2009) Solid contact micropipette ion selective electrode II, potassium electrode for SECM and in vivo applications. Electroanalysis 21:1970–1976
56. Varga A, Nagy L, Izquierdo J, Bitter I, Souto RM, Nagy G (2011) Development of solid contact micropipette Zn ion selective electrode for corrosion studies. Anal Lett 44:2876–2886
57. Izquierdo J, Nagy L, Varga Á, Bitter I, Nagy G, Souto RM (2012) Scanning electrochemical microscopy for the investigation of corrosion processes: measurement of Zn^{2+} spatial distribution with ion selective microelectrodes. Electrochim Acta 59:398–403
58. Hasma PK, Dake B, Marti O, Gould SA, Prater CB (1989) The scanning ion conductance microscope. Science 243(4891):641–643
59. Wei C, Bard AJ, Nagy G, Tóth K (1995) Scanning ion selective potentiometric microscopy. Anal Chem 67:1346–1356
60. Edwards MA, Williams CG, Whitworth AL, Unwin PR (2009) Scanning ion condoctanc microscopy: a model for experimentally realistic conditions and image interpretation. Anal Chem 81:4482–4492
61. Yang X, Liu X, Zhang X, Lu H, Zhang J, Zhang Y (2011) Investigation of morphological and functional changes during neuronal differentiation of PC12 cells by combined Hopping probe ion conductance microscopy and patch-clamp technique. Ultramicroscopy 111:1417–1422
62. Horrocks BR, Mirkin MV, Pierce DT, Bard AJ, Nagy G, Tóth K (1993) Scanning electrochemical microscopy. 19. Ion selective potentiometric microscopy. Anal Chem 65:1213–1224
63. Karrai K, Tiemann I (2000) Interfacial shear force microscopy. Phys Rev B 62:13174–13181
64. Betzig E, Finn PL, Weiner JS (1992) Combined shear force and near-field scanning optical microscopy. Appl Phys Lett 60:2484–2488
65. Karraï K, Grober RD (1995) Piezoelectric tip–sample distance control for near-field optical microscopes. Appl Phys Lett 66:1842–1844
66. Hollricher O, Brunner R, Marti O (1998) Piezoelectrical shear-force distance control in near-field optical microscopy for biological applications. Ultramicroscopy 71:143–147
67. Ruiter AGT, Veerman JA, Van Der Werf KO, Van Hulst NF (1997) Dynamic behavior of tuning fork shear-force feedback. Appl Phys Lett 71:28–30
68. Toledo-Crow R, Yang PC, Chen Y, Vaez-Iravani M (1992) Near-field differential scanning optical microscope with atomic force regulation. Appl Phys Lett 60:2957–2959
69. Ruiter AGT, van der Werf KO, Veerman JA, Garcia-Parajo MF, Rensen WHJ, van Hulst NF (1998) Tuning fork shear-force feedback. Ultramicroscopy 71:149–157
70. Nowak DB (2010) The design of a novel tip enhanced near-field scanning probe microscope for ultra-high resolution optical imaging. PhD dissertation, Portland State University, UMI 3419910
71. Wang W, Zhang J, Han LH, Yang DZ, Zhan DP (2012) Generation/collection mode of SECM with combined probe. Chin Chem Lett 23:86–88
72. Lu G, Cooper JS, McGinn PJ (2007) SECM imaging of electrocatalytic activity for oxygen reduction reaction on thin film materials. Electrochim Acta 52(16):5172–5181
73. Cornut R, Griveau S, Lefrou C (2010) Accuracy study on fitting procedure of kinetics SECM feedback experiments. J Electroanal Chem 650:55–61
74. Mirkin MV, Liu B, Rotenberg SA (2002) Probing redox activity of human breast cells by scanning electrochemical microscopy. Methods Enzymol 352:112–124
75. Rapino S, Marcu R, Bigi A, Soldà A, Marcaccio M, Paolucci F, Pelicci PG, Giorgio M (2015) Scanning electro-chemical microscopy reveals cancer cell redox state. Electrochim Acta 179:65–73
76. Roberts WS, Davis F, Holmes JL, Collyer SD, Larcombe LD, Morgan SL, Higson SPJ (2013) Detection and imaging the expression of the trans-membrane protein CD44 in RT112 cells by use of enzyme-labeled antibodies and SECM. Biosens Bioelectron 41:282–288

77. Yasukawa T, Kaya T, Matsue T (1999) Dual imaging of topography and photosynthetic activity of a single protoplast by scanning electrochemical microscopy. Anal Chem 71:4637–4641
78. Lee C, Kwak J, Bard AJ (1990) Application of scanning electrochemical microscopy to biological samples. Proc Natl Acad Sci U S A 87:1740–1743
79. Zhu R, Macfie SM, Ding Z (2005) Cadmium-induced plant stress investigated by scanning electrochemical microscopy. J Exp Bot 56(421):2831–2838
80. Parthasarathy M, Singh S, Hazra S, Pillai VK (2008) Imaging the stomatal physiology of somatic embryo-derived peanut leaves by scanning electrochemical microscopy. Anal Bioanal Chem 391:2227–2233
81. Tsinonsky M, Cardon ZG, Bard AJ, Jacson RB (1997) Photosynthetic electron transport in single guard cells as measured by scanning electrochemical microscopy. Plant Physiol 113:895–901
82. Alshammary SF, Qian YL, Wallner SJ (2004) Growth response of four turfgrass species to salinity. Agric Water Manag 66:97–111
83. Parthasarathy M, Pemaiah B, Natesan R, Padmavathy SR, Pachiappan J (2015) Real-time mapping of salt glands on the leaf surface of Cynodon dactylon L. using scanning electrochemical microscopy. Bioelectrochemistry 101:159–164
84. Liebetrau JM, Miller HM, Baur JE, Takacs SA, Anupunpisit V, Garris PA, Wipf DO (2003) Scanning electrochemical microscopy of model neurons: imaging and real-time detection of morphological changes. Anal Chem 75:563–571
85. Razzaghi F, Seguin J, Amar A, Griveau S, Bedioui F (2015) Biological cell morphology studies by scanning electrochemical microscopy imagery at constant height: contrast enhancement using biocompatible conductive substrates. Electrochim Acta 157:95–100
86. Bergner S, Wegener J, Matysik FM (2011) Simultaneous imaging and chemical attack of a single living cell within a confluent cell. Monolayer by means of scanning electrochemical microscopy. Anal Chem 83:169–174
87. Nagamine K, Takahashi Y, Ino K, Shiku H, Matsue T (2011) Influence of tip size on single yeast cell imaging using scanning. Electrochem Microsc Electroanalysis 23:1168–1174
88. Takahashi Y, Hirano Y, Yasukawa T, Shiku H, Yamada H, Matsue T (2006) Topographic, electrochemical, and optical images captured using standing approach mode scanning electrochemical/optical microscopy. Langmuir 22:10299–10306
89. Nebel M, Eckhard K, Erichsen T, Schulte A, Schuhmann W (2010) 4D shearforce-based constant-distance mode scanning electrochemical microscopy. Anal Chem 82:7842–7848
90. Zhang MMN, Long YT, Ding Z (2012) Filming a live cell by scanning electrochemical microscopy: label-free imaging of the dynamic morphology in real time. Chem Cent J 6:20
91. Zhang MM, Long YT, Ding Z (2012) Cisplatin effects on evolution of reactive oxygen species from single human bladder cancer cells investigated by scanning electrochemical microscopy. J Inorg Biochem 108:115–122
92. Zhang MN, Ding Z, Long YT (2015) Sensing cisplatin-induced permeation of single live human bladder cancer cells by scanning electrochemical microscopy. Analyst 140:6054–6060
93. Shiku H, Shiraishi T, Ohya H, Matsue T, Abe H, Hoshi H, Kobayashi M (2001) Oxygen consumption of single bovine embryos probed by scanning electrochemical microscopy. Anal Chem 73(15):3751–3758
94. Sridhar A, de Boer HL, van den Berg A, Le Gac S (2014) Microstamped petri dishes for scanning electrochemical microscopy analysis of arrays of microtissues. PLoS One 9(4) e9361, 1-7
95. Nagamine K, Kaya T, Yasukawa T, Shiku H, Matsue T (2005) Application of microbial chip for amperometric detection of metabolic alteration in bacteria. Sens Actuat B 108:676–682
96. Kaya T, Numai D, Nagamine K, Aoyagi S, Shiku H, Matsue T (2004) Respiration activity of Escherichia coli entrapped in a cone-shaped microwell and cylindrical micropore monitored by scanning electrochemical microscopy (SECM). Analyst 129:529–534

97. Nishizawa M, Takoh K, Matsue T (2002) Micropatterning of HeLa cells on glass substrates and evaluation of respiratory activity using microelectrodes. Langmuir 18:3645–3649
98. Matsui N, Kaya T, Nagamine K, Yasukawa T, Shiku H, Matsue T (2006) Electrochemical mutagen screening using microbial chip. Biosens Bioelectron 21:1202–1209
99. Nagamine K, Onodera S, Kurihara A, Yasukawa T, Shiku H, Asano R, Kumagai I, Matsue T (2007) Electrochemical screening of recombinant protein solubility in Escherichia coli using scanning electrochemical microscopy (SECM). Biotechnol Bioeng 96:1008–1013
100. Torisawa YS, Ohara N, Nagamine K, Kasai S, Yasukawa T, Shiku H, Matsue T (2006) Electrochemical monitoring of cellular signal transduction with a secreted alkaline phosphatase reporter system. Anal Chem 78:7625–7631
101. Liu B, Rotenberg SA, Mirkin MV (2000) Scanning electrochemical microscopy of living cells: different redox activities of nonmetastatic and metastatic human breast cells. Proc Natl Acad Sci U S A 97:9855–9860
102. Liu B, Rotenberg SA, Mirkin MV (2002) Scanning electrochemical microscopy of living cells. 4. Mechanistic study of charge transfer reactions in human breast cells. Anal Chem 74:6340–6348
103. Feng W, Rotenberg SA, Mirkin MV (2003) Scanning electrochemical microscopy of living cells. 5. Imaging of fields of normal and metastatic human breast cells. Anal Chem 75:4148–4154
104. Rotenberg SA, Mirkin MV (2004) Scanning electrochemical microscopy: detection of human breast cancer cells by redox environment. J Mammary Gland Biol Neoplasia 9:375–382
105. Rapino S, Marcu R, Bigi A, Soldà A, Marcaccio M, Paolucci F, Pelicci PG, Giorgio M (2015) Scanning electro-chemical microscopy reveals cancer cell redox state. Electrochim Acta (in press). Corrected. doi:10.1016/j.electacta.2015.04.053
106. Kuss S, Polcari D, Geissler M, Brassard D, Mauzeroll J (2013) Assessment of multidrug resistance on cell co-culture patterns using scanning electrochemical microscopy. Proc Natl Acad Sci U S A 110:9249–9254
107. Kuss S, Trinh D, Mauzeroll J (2015) High-speed scanning electrochemical microscopy method for substrate kinetic determination: application to live cell imaging in human cancer. Anal Chem 87:2102–2106
108. Cai C, Liu B, Mirkin MV (2002) Scanning electrochemical microscopy of living cells. 3. Rhodobacter sphaeroides. Anal Chem 74:114–119
109. Mauzeroll J, Bard AJ, Owhadian O, Monks TJ (2004) Menadione metabolism to thiodione in hepatoblastoma by scanning electrochemical microscopy. Proc Natl Acad Sci U S A 101:17582–17587
110. Matsumaea Y, Takahashi Y, Ino K, Shiku H, Matsue T (2014) Electrochemical monitoring of intracellular enzyme activity of single living mammalian cells by using a double-mediator system. Anal Chim Acta 842:20–26
111. Zhu L, Gao N, Zhang X, Jin W (2008) Accurately measuring respiratory activity of single living cells by scanning electrochemical microscopy. Talanta 77:804–808
112. Monteiro DR, Gorup LF, Takamiya AS, Ruvollo-Filho AC, de Camargo ER, Barbosa DB (2009) The growing importance of materials that prevent microbial adhesion: antimicrobial effect of medical devices containing silver. Int J Antimicrobial Agents 34(2):103–110
113. Holt KB, Bard AJ (2005) The interaction of silver (I) ions with the respiratory chain of Escherichia coli: an electrochemical and scanning electrochemical microscopy study of the antimicrobial mechanism of micromolar Ag+. Biochemistry 44:13214–13223
114. Zhan D, Li X, Nepomnyashchii AB, Alpuche-Aviles MA, Fan F-RF, Bard AJ (2013) Characterization of Ag^{+} toxicity on living fibroblast cells by the ferrocenemethanol and oxygen response with the scanning electrochemical microscope. J Electroanal Chem 688:61–68
115. Kaya T, Torisawa YS, Oyamatsu D, Nishizawa M, Matsue T (2003) Monitoring the cellular activity of a cultured single cell by scanning electrochemical microscopy (SECM). A comparison with fluorescence viability monitoring. Biosens Bioelectron 18:1379–1383

116. Torisawa YS, Kaya T, Takii Y, Oyamatsu D, Nishizawa M, Matsue T (2003) Scanning electrochemical microscopy-based drug sensitivity test for a cell culture integrated in silicon microstructures. Anal Chem 75:2154–2158
117. Okuyama T, Maehara Y, Endo K, Baba H, Adachi Y, Kuwano M, Sugimachi K (1994) Expression of glutathione S-transferase-pi and sensitivity of human gastric cancer cells to cisplatin. Cancer 74(4):1230–1236
118. Takamura Y, Kobayashi H, Taguchi T, Motomura K, Inaji H, Noguchi S (2002) Prediction of chemotherapeutic response by collagen gel droplet embedded culture-drug sensitivity test in human breast cancers. Int J Cancer 98:450–455
119. Torisawa YS, Shiku H, Kasai S, Nishizawa M, Matsue T (2004) Proliferation assay on a silicon chip applicable for tumors extirpated from mammalians. Int J Cancer 109:302–308
120. Hirano Y, Kodama M, Shibuya M, Maki Y, Komatsu Y (2014) Analysis of beat fluctuations and oxygen consumption in cardiomyocytes by scanning electrochemical microscopy. Anal Biochem 447:39–42
121. Zhao C, Wittstock G (2004) An SECM detection scheme with improved sensitivity and lateral resolution: detection of galactosidase activity with signal amplification by glucose dehydrogenase. Angew Chem Int Ed 43:4170–4172
122. Schubert F, Kirstein D, Schröder KL, Scheller FW (1985) Enzyme electrodes with substrate and co-enzyme amplification. Anal Chim Acta 169:391–396
123. Yamada H, Fukumoto H, Yokoyama T, Koike T (2005) Immobilized diaphorase surfaces observed by scanning electrochemical microscope with shear force based tip-substrate positioning. Anal Chem 77:1785–1790
124. Baharav E, Merimski O, Shoenfeld Y, Zigelman R, Gilbrud B, Yecheskel G, Youinou P, Fishman P (1996) Tyrosinase as an autoantigen in patients with vitiligo. Clin Exp Immunol 105:84–88
125. Lin T-E, Cortés-Salazar F, Lesch A, Qiao L, Bondarenko A, Girault HH (2015) Multiple scanning electrochemical microscopy mapping of tyrosinase micro-contact printed fruit samples on polyvinylidene fluoride membrane. Electrochim Acta. 179:57–64. doi:10.1016/j.electacta.2015.03.224
126. Lei R, Stratmann L, Schafer D, Erichsen T, Neugebauer S, Li N, Schuhmann W (2009) Imaging biocatalytic activity of enzyme-polymer spots by means of combined scanning electrochemical microscopy/electrogenerated chemiluminescence. Anal Chem 81:5070–5074
127. Cui H, Zou GZ, Lin XQ (2003) Electrochemiluminescence of luminol in alkaline solution at a paraffin-impregnated graphite electrode. Anal Chem 75:324–331
128. Mureşan L, Nistor M, Gáspár S, Popescu IC, Csöregi E (2009) Monitoring of glucose and glutamate using enzyme microstructures and scanning electrochemical microscopy. Bioelectrochemistry 76:81–86
129. Abucayon E, Ke N, Cornut R, Patelunas A, Miller D, Nishiguchi MK, Zoski CG (2014) Investigating catalase activity through hydrogen peroxide decomposition by bacteria biofilms in real time using scanning electrochemical microscopy. Anal Chem 86:498–505
130. Kranz C, Friedbacher G, Mizaikoff B, Lugstein A, Smoliner J, Bertagnolli E (2001) Integrating an ultramicroelectrode in an AFM cantilever: combined technology for enhanced information. Anal Chem 73:2491–2500
131. Kueng A, Kranz C, Lugstein A, Bertagnolli E, Mizaikoff B (2003) Integrated AFM–SECM in tapping mode: simultaneous topographical and electrochemical imaging of enzyme activity. Angew Chem Int Ed 42:3237–3240
132. MacPherson JV, Beeston MA, Unwin PR, Hughes NP, Littlewood D (1995) Scanning electrochemical microscopy as a probe of local fluid flow through porous solids. J Chem Soc Faraday Trans 91:1407–1410
133. Macpherson JV, Beeston MA, Unwin PR (1995) Imaging the action of fluid flow blocking agents on dentinal surfaces using a scanning electrochemical microscope. Langmuir 11:3959–3963

134. Castro PS, Lima AS, Ferreira TL, Bertotti M (2011) Scanning electrochemical microscopy as a tool for the characterization of dental erosion. Int J Electrochem. doi:10.4061/2011/952470
135. Gonsalves M, Macpherson JV, O'Hare D, Winlove CP, Unwin PR (2000) High resolution imaging of the distribution and permeability of methyl viologen dication in bovine articular cartilage using scanning electrochemical microscopy. Biochim Biophys Acta 1524:66–74
136. Gonsalves M, Barker AL, Macpherson JV, Unwin PR, O'Hare D, Winlove CP (2000) Scanning electrochemical microscopy as a local probe of oxygen permeability in cartilage. Biophys J 78:1578–1588
137. Koley D, Bard AJ (2010) Triton X-100 concentration effects on membrane permeability of a single HeLa cell by scanning electrochemical microscopy (SECM). Proc Natl Acad Sci 107 (39):16783–16787
138. Sun P, Laforge FO, Abeyweera TP, Rotenberg SA, Carpino J, Mirkin MV (2008) Nanoelectrochemistry of mammalian cells. Proc Natl Acad Sci U S A 105(2):443–448
139. Altman SA, Randers L, Rao G (1993) Comparison of trypan blue dye exclusion and fluorometric assays for mammalian cell viability determinations. Biotechnol Prog 9 (6):671–674
140. Turcu F, Schulte A, Hartwich G, Schuhmann W (2004) Label-free electrochemical recognition of DNA hybridization by means of modulation of the feedback current in SECM. Angew Chem Int Ed 43:43482–43485
141. Fortin E, Mailley P, Lacroixa L, Szunerits S (2006) Imaging of DNA hybridization on microscopic polypyrrole patterns using scanning electrochemical microscopy (SECM): the HRP bio-catalyzed oxidation of 4-chloro-1-naphthol. Analyst 131:186–193
142. Xue Y, Ding L, Lei J, Yan F, Ju H (2010) In situ electrochemical imaging of membrane glycan expression on micropatterned adherent single cells. Anal Chem 82:7112–7118
143. Takahashi Y, Miyamoto T, Shiku H, Asano R, Yasukawa T, Kumagai I, Matsue T (2009) Electrochemical detection of epidermal growth factor receptors on a single living cell surface by scanning electrochemical microscopy. Anal Chem 81:2785–2790
144. Park K, Kwon D, Kwak J (2011) Aptamer based electrochemical sensor system for protein using the generation/collection mode of scanning electrochemical microscope (SECM). J Nanosci Nanotechnol 11:4305–4311
145. Takahashi Y, Shiku H, Murata T, Yasukawa T, Matsue T (2009) Transfected single-cell imaging by scanning electrochemical optical microscopy with shear force feedback regulation. Anal Chem 81:9674–9681
146. Liu X, Ramsey MM, Chen X, Koley D, Whiteley M, Bard AJ (2011) Real-time mapping of a hydrogen peroxide concentration profile across a polymicrobial bacterial biofilm using scanning electrochemical microscopy. Proc Natl Acad Sci U S A 108:2668–2673
147. Katrlik J, Zalesakova P (2002) Nitric oxide determination by amperometric carbon fiber microelectrode. Bioelectrochemistry 56:73–76
148. Bedioui F, Villeneuve N (2003) Electrochemical nitric oxide sensors for biological samples – principle, selected examples and applications. Electroanalysis 15:5–18
149. Pailleret A, Oni J, Reiter S, Isik S, Etienne M, Bedioui F, Schuhmann W (2003) In situ formation and scanning electrochemical microscopy assisted positioning of NO-sensors above human umbilical vein endothelial cells for the detection of nitric oxide release. Electrochem Commun 5:847–852
150. Zhao X, Diakowski PM, Ding Z (2010) Deconvoluting topography and spatial physiological activity of live macrophage cells by scanning electrochemical microscopy in constant-distance mode. Anal Chem 82:8371–8373
151. Zhan D, Li X, Zhan W, Fan FRF, Bard AJ (2007) Scanning electrochemical microscopy. 58. Application of a micropipet-supported ITIES tip to detect Ag^+ and study its effect on fibroblast cells. Anal Chem 79:5225–5231
152. Korchev YE, Gorelik J, Lab MJ, Sviderskaya EV, Johnston CL, Coombes CR, Vodyanoy I, Edwards CRW (2000) Cell volume measurement using scanning ion conductance microscopy. Biophys J 78:451–457

153. Gorelik J, Zhang Y, Shevchuk AI, Frolenkov GI, Sánchez D, Lab MJ, Vodyanoy I, Edwards CRW, Klenerman D, Korchev YE (2004) The use of scanning ion conductance microscopy to image A6 cells. Mol Cell Endocrinol 217:101–108
154. Liu X, Yang X, Zhang B, Zhang X, Lu H, Zhang J, Zhang Y (2011) High-resolution morphological identification and characterization of living neuroblastoma SK-N-SH cells by hopping probe ion conductance microscopy. Brain Res 1386:35–40
155. Canaro M, Holt KB, Bard AJ (2003) Gas-phase scanning electrochemical microscopy. Measurements with a clark oxygen ultramicroelectrode. Anal Chem 75:5071–5079
156. Kiss A, Kiss L, Kovács B, Nagy G (2011) Air gap microcell for scanning electrochemical microscopic imaging of carbon dioxide output. Model calculation and gas phase SECM measurements for estimation of carbon dioxide producing activity of microbial sources. Electroanalysis 23:2257–2497
157. Sifri CD (2008) Quorum sensing: bacteria talk sense healthcare. Epidemiology 48:1070–1076
158. De Kievit TR, Iglewski BH (2000) Bacterial quorum sensing in pathogenic relationships. Infect Immun 68:4839–4849
159. Parsek MR, Greenberg EP (2005) Sociomicrobiology: the connections between quorum sensing and biofilms. Trends Microbiol 13(1):27–33
160. Connell JL, Jiyeon K, Jason BS, Bard AJ, Whiteley M (2014) Real-time monitoring of quorum sensing in 3D-printed bacterial aggregates using scanning electrochemical microscopy. Proc Natl Acad Sci U S A 111:18255–18260

Index